GEOCHEMISTRY OF THE LATE DEVONIAN 'PUNCTATA' EVENT IN THE WESTERN CANADA SEDIMENTARY BASIN

By

Maciej Grzegorz Śliwiński

RECOMMENDED:

Thomas. P. Trainor

Kenneth P. Severin

Michael T. Whalen, Advisory Committee Chair

Rainer J. Newberry, Advisory Committee Co-Chair

Michael T. Whalen, Chair, Department of Geology

APPROVED:

Paul W. Layer, Dean, College of Natural Science and Mathematics

Lawrence K. Duffy, Dean of the Graduate School

April 5, 2012

Date

GEOCHEMISTRY OF THE LATE DEVONIAN 'PUNCTATA' EVENT IN THE WESTERN CANADA SEDIMENTARY BASIN

A

THESIS

Presented to the Faculty

of the University of Alaska Fairbanks

in Partial Fulfillment of the Requirements

for the Degree of

DOCTOR OF PHILOSOPHY

By

Maciej Grzegorz Śliwiński, B.S.

Fairbanks, Alaska

May 2012

Abstract

Carbonate deposits straddling the Early-Middle Frasnian (Late Devonian) transitional interval at the isolated Miette carbonate platform in the Western Canada Sedimentary Basin were studied geochemically to better understand the paleoceanographic changes that had taken place regionally during the global '*punctata* Event' Earth-system perturbation, characterized by the short-term (<0.5 M.y.) yet wide-spread eutrophication of epeiric environments and the deposition of organic carbon-rich facies. This event occurred while the evolution of terrestrial forests entered a rapid, near exponential phase of diversification and expansion, thus altering nutrient-cycling between the terrestrial and marine realms through a transient increase in the intensity of pedogenic weathering. I've attempted a reconstruction of the chemostratigraphic variance of (1) bioproductivity, paleoredox and detrital elemental proxies, of (2) isotopic records ($\delta^{13}C_{(carb\ \&\ org)}$; $\delta^{15}N_{org}$), and of (3) related parameters, including TOC, magnetic susceptibility (MS) and the abundance and mineralogy of acid-insoluble carbonate residues, and interpreted these within the context of regional sequence stratigraphy and paleogeography against the background of global geobiological events. Analytical methods and standards were developed for measuring low (<10 ppm) concentrations of crucial proxies in carbonates (down to 1-2 ppm) by WD-XRF, and were verified by a diversity of statistical tests and analyses. Evaluation of chemostatigraphic trends revealed that eutrophication and geochemical anomalies associate strongly with a 3rd-order transgression (IIc1) and increased detrital input in the lower *punctata* Zone. Factor analyses were thus applied to constrain the influence of 1) siliciclastic input vs. 2) the development of benthic anoxia (explaining 55 and 35% of total variance, respectively) on trace element excursions, but also to 3) assess the extent to which MS records within the stratigraphy track the clastic input. Mineralogical controls on MS variance were determined by XRD analyses of acid-insoluble limestone residues, and a multivariate linear regression model was found to account for 97.7 % of total variance as a function of variable admixing of illite, pyrite, quartz and feldspars, in turn variably diluted by the total carbonate content.

Dedication

To B. Charlotte Schreiber,

for years of mentoring, caring support, and friendship

Table of Contents

Page

Page

Page

List of Figures

Page

Page

Page

Page

List of Tables

Page

Page

Page

List of Appendices

Page

Acknowledgments

I warmly thank B.C. Schreiber for years of caring support and help with navigating through academia (especially its unpleasant aspects), as well as help in establishing working relationships with her research groups abroad that resulted in collaborative work and publications that go beyond this thesis. I am especially grateful for continued work with Prof. Maciej Bąbel and friends at the University of Warsaw.

I thank my committee – Mike Whalen, Rainer Newberry, Ken Severin and Tom Trainor - for their input and guidance over the years, which has helped shape my various research projects. I especially thank Rainer for being a fellow conspirator and friend at nearly all hours of each day during the crazy, intense and inspiring last three and a half years.

I very warmly thank Jessica Larsen for employing me to work on her Okmok Volcano 2008 eruption project; this work provided a very much needed patch in my funding quilt while providing a valuable learning experience by allowing me to part take in an exceptionally interesting Fourier Transform Infrared (FTIR) spectormetry methods development project, resulting in a joint publication and others planned.

I thank all of those with whom I worked over the years for their help with various aspects of my projects and for sharing their expertise: Karen Spaleta and Franz Meyer, with whom I had the pleasure and fun of developing analytical methods and testing their validity by searching out suitable statistical methods; Dr. Jason Addison, for countless thoughtful discussions on various aspects of paleoceanography and for bringing together a phenomenal research group together with Sarah Hayes that resulted in a successful joint proposal that recently allowed us to begin work at the Stanford Synchrotron Radiation Lightsource, offering exciting new research prospects for the years to come; Franta Majs and Suzanna Salazaar for much help and collaboration with capillary XRF methods; Jeff Benowitz and Paul Layer for collaboration on our joint geochronological project with Maciej Bąbel (University of Warsaw) and B.C. Schreiber (University of Washington) concerning the evaporite sequence of the Badenian Salinity Crisis in the Carpathian Foredeep; Tim Howe and Norma Haubenstock of the Alaska Stable Isotope Facility for their help with isotopic analyses; Ellen and June in the Geology Dept. Office for their help in avoiding various bureaucratic pitfalls; and Andy Krumhardt for her help with work in the Pollen Lab. I warmly thank all my friends for their caring support over the years, especially Suzanna Salazaar, Susi Tomsisch and Dave McAlpin.

I thank the American Association of Petroleum Geologists, British Petroleum and the Geological Society of American for grants that helped partially offset the costs of analytical work, and very kindly thank the University of Alaska Fairbanks Graduate School for funding in the form of a Thesis Completion Grant that allowed me to focus this year on finishing my dissertation.

1. Introduction

1.1. A word about organization

The chapters of this work are concerned with changes in the geochemical properties of carbonate sequences deposited during the Frasnian (383.6-376.7 Ma; De Vleeschouwer et al., 2012) epoch of the Late Devonian in the tropical epicontinental seaway of the Western Canada Sedimentary Basin (WCSB), during a peculiar episode of paleoceanographic perturbations known in the literature as the *'punctata* Event'. Stratigraphic variations in 1) trace element distributions and 2) in the extent of fractionations of C and N isotopes contained within fossil organic matter and of the C and O isotopes bound within the hosting carbonate sediment are used as proxies for reconstructing changes in oceanic and climatic conditions and changes in biogeochemical cycling throughout the duration of this relatively short-term, < 0.5 m.y. event.

The intention of this general introduction is to provide a broader context for Late Devonian paleoceanographic studies within the framework of Earth's unfolding geobiological evolution. Further, it is to emphasize the relevance of studying unusual events of rapid ecosystem changes in the geologic past as a means of understanding Earth system responses and how these will relate to the evolution of human societies as they continue to alter global biogeochemical cycles.

This work is a collection of four individual manuscripts arranged chronologically in the order in which they evolved. The exception is Chapter 2 which focuses on the development of X-ray fluorescence spectroscopic (XRF) methods for measuring low abundances (0-100 ppm) of various trace element proxies in carbonate lithologies, for which certified standard reference materials from institutions such as the USGS and NIST are lacking. These methods have been improved upon following the initial trace element study on the *punctata* Event in the WCSB presented in Chapter 3 (Śliwiński et al., 2010) through the use of synthetic, *in-house* carbonate trace element standards and refinements of the original XRF calibrations. The acquisition by University of Alaska Fairbanks' (UAF) *Advanced Instrumentation Laboratory (AIL)* of PANalytical's PROTrace XRF trace element standards and analytical software (UAF Technology Advisory Board grant to Śliwiński and Severin, April 2011) has further facilitated refinements and verifications of preexisting methods (Śliwiński et al., 2012). In order to not disrupt the flow of the *punctata* Event story in Chapters 3, 4 and 5, I've placed this chapter on methods development at the onset of the compilation (Chapter 2).

Variations in the minor and trace element geochemistry of marine sedimentary strata are interpreted as proxies for changes in 1) oceanic bioproductivity (*e.g.* Ni, Cu, P, Ba, Zn), 2) relative influxes of terrigenous siliciclastics into depositional basins (*e.g.* Al, Si, Ti, K, Cr, Zr, Co), and 3) for changes in the dominant benthic redox conditions (*e.g.* U, Mo, V, Ni/Co, U/Th, V/Cr, V/(V+Ni);

Hatch and Leventhal, 1992; Calvert and Pedersen, 1993; Jones and Manning, 1994; Rimmer, 2004; Rimmer et al., 2004; Riquier et al., 2006; Tribovillard et al., 2006; Algeo and Maynard, 2008; Piper and Calvert, 2009). Measurements of trace element abundances and interpretations of their chemostratigraphic trends in core and outcrop aid paleoceanographic inferences regarding redox conditions within the depositional environment based on observable sedimentary features and characteristic fossil/trace fossil assemblages (*e.g.* ichnofacies indices of Droser and Bottjer, 1986; see also Boyer and Droser, 2009). At times such geochemical records necessitate a re-evaluation of prior depositional models and of taphonomic conditions, as in the recent reexamination of the Cambrian Burgess Shale *Lagerstätten* (Powell, 2003, 2009). Importantly, however, trace element trends also provide information which exists only at the chemical level, such as the characteristic 'chemical fingerprints' that develop within the sediment profile when the circulation of basinal waters becomes restricted, causing differential draw-down of redox sensitive trace metals with differing oceanic residence times (*cf.* Algeo and Maynard, 2008).

Existing also primarily at the chemical level in the form of biologically-induced fractionations of C and N isotopes are accounts of dynamic changes in the mode and intensity of primary production at sea throughout geologic time which speak to broader changes in regional and global biogeochemical cycles (Popp et al., 1997; Galbraith et al., 2008). These are the topics of Chapters 3, 4 and 5 as they pertain to the unfolding of the *punctata* Event in the WCSB. Chapter 5 additionally presents an attempt at statistically decoupling, through the use of factor analyses, 1) the influence and relative importance of detrital siliciclastic input vs. benthic anoxia on producing the trace element anomalies and accumulations of organic matter (OM)-rich horizons observed in the *punctata* Event stratigraphy in the WCSB, and at 2) assessing the extent to which magnetic susceptibility (MS) records within the basin, reported extensively on by Whalen and Day (2008, 2010), track changes in detrital input and nutrient delivery to the oceans. Methods for better understanding the mineralogical controls on MS variance are aided by transmission X-ray diffraction analyses in glass capillaries to overcome the analytical problems posed by the generally low content of acid-insoluble impurities within carbonate lithologies.

The initial trace element study on the *punctata* Event in the WCSB presented in Chapter 3 is followed by an appendix in which I revisit certain aspects of the observed trace element excursions originally discussed in Śliwiński et al. (2010). Of interest here are Mn enrichments that correspond to intervals within the stratigraphy that are best interpreted as representing anoxic events, and are in contradiction with the model of Mn cycling across redox gradients commonly cited in the literature (Tribovillard et al., 2006) and with the use of this element as a proxy for deposition under oxic benthic conditions (*e.g.* Sageman et al., 2003). Studies in the literature using trace elements proxies are predominately focused on shale systems (Schultz and Rimmer,

2004). In depositional environments where carbonate sediment dominates, however, the use of certain proxies, such as the Mn example herein, may need to be reconsidered in terms of the information they provide about depositional processes. Recent geochemical analyses of other Late Devonian profiles confirm this alternate behavior of Mn in carbonate systems (Racka et al., 2010) and are the subject of the brief addendum following Chapter 3. The Chapter 3 appendix further presents a reanalysis of an expanded sample dataset from the *punctata* zone stratigraphy in the WCSB using trace element calibrations based on AIL's recently acquired PROTrace standard suite, which routinely and efficiently measures 43 trace elements with detection limits at the 0-5 ppm level. It thus offers information about the chemostratigraphic distributions of additional redox-sensitive trace metals which help strengthen interpretations of changing benthic redox conditions throughout the *punctata* interval as discussed in Chapters 3, 4 and 5.

1.2. The uniqueness of the Late Devonian within the context of Earth's geobiological evolution

The Earth is a complex, continuously evolving system of intricate geobiological interactions. Pre-Holocene sediments and sedimentary rocks form a carapace that covers 66% of the Earth's surface (Blatt and Jones, 1975) and record the evolution of marine and terrestrial environments from back as far as Early Archean times (~3.8 Ga). Fossils - whether in the form of physical bodily remains, microbially induced sedimentary structures or chemical evidence for biological activity - contained within sedimentary sequences record the first appearance and subsequent evolution of life, of which the earliest, readily observable evidence remains preserved as stromatolitic structures that date back to 3.47 Ga (North Pole, Australia, Fig. 1.1). These are layered mounds of sediment accreted through the growth of microbial mats and cemented by precipitates formed by metabolism-induced changes in the surrounding chemical environment (Buick, 2003). Chemical evidence of life in the form of biological fractionations of carbon isotopes recorded by kerogen (fossil organic matter) and its hosting carbonate sediment dates back somewhat further to 3.52 Ga (Coonterunah Group of NW Australia; Buick, 2003).

Evolutionary milestones in microbial metabolic pathways and the development of microbially-mitigated global biogeochemical cycles that allowed for the establishment of planetary homeostasis and for the rise of metazoans characterize different intervals of geologic time (Schopf and Klein (1992); The Proterozoic Bioshpere, a multidisciplinary study). Not the least of these were the two major Earth-surface oxidation events dated at around 2.2 and 0.6 Ga, mediated by both microbial and by more complex planktonic (algal) oxygenic photosynthesizers (Holland, 2006). Presumably, photosynthetic marine plankton was already common in the Late Archean (2.5-2.8 billion years ago) given the common occurrences of shales (fine grained,

sedimentary rocks, commonly marine) with a high abundance of organic carbon (kerogen; Buick, 2003). Recent findings of 3.2 Ga acritarchs (organic microfossils with uncertain biological affinities) in the Moodies Group of South Africa, at present the oldest *certain* microfossils (Javaux et al., 2010), supports this inference. It may not be a coincidence in timing that the later of these oxygenation events at 0.6 Ga was soon followed by the rapid rise and diversification of metazoans during the Cambrian Explosion at the base of the Phanerozoic (~540 million years ago; Sepkoski, 1995, 1997; Butterfield, 2003).

The history of Phanerozoic evolutionary faunas - that is the characteristic *Cambrian, Paleozoic* and *Modern* taxonomic assemblages recognized and defined by Sepkoski (1978, 1979, 1984, 1990) - throughout Phanerozoic time defines the Modern oceanic biosphere. The geologic record of marine strata indicates, however, that this history was at times turbulent and punctuated by episodic mass extinction events that attest to perturbations of the Earth system, commonly resulting in climatic instability on timescales sufficiently short to outpace evolution's 'buffering capacity' (Sepkoski, 1978, 1979, 1984, 1990). The deposition of OM-rich sediments, *e.g.* black shales, sapropels and bituminous carbonates that are commonly associated with economically important hydrocarbon energy resources, appears to be a common outcome of such events, as are widespread geochemical anomalies (Fig. 1.2; House, 2002; Negri et al., 2006). Within the time span of the Late Devonian alone (383.7 ± 3.1 Ma to 360.7 ± 2.7 Ma; Kaufmann, 2006), at least twenty anomalous black shale and/or biotic crises have been recognized (House, 2002) and are the subject of on-going research that seeks to resolve 'cause and effect' mechanisms on increasingly finer time scales (< 0.6 m.y., the average duration of Late Devonian conodont-based biostratigraphic zones; Racki, 2005; Kaufman, 2006). Particular scrutiny has recently been directed toward reconstructing high-resolution climatic, biotic and geochemical records of the Late Devonian '*punctata* Event' (Early-Middle Frasnian transition), which holds an account of geologically rapid eutrophication events that affected shallow tropical seas and coastal marine environments of the time and which are in large part attributed to increased nutrient loading resulting from the initial pulses of terrestrial afforestation by deeply rooted vascular land plants of tree stature and the concomitant evolution of complex soil profiles (*cf.* the models of Algeo et al., 1995 and Algeo and Scheckler, 1998, 2010; see special issue of *Acta Palaeontologica Polonica* edited by Balinski et al. (2006) that documents the Early-Middle Frasnian transition and biotic responses to a major perturbation of the global carbon cycle; Pisarzowska et al., 2006; Yans et al., 2007; da Silva and Boulvain, 2008; John et al., 2008; Ma et al., 2008; Marynowski et al., 2008; Pisarzowska, 2008; Racki et al., 2008; Morrow et al., 2009; Śliwiński et al., 2010, 2011; Pisarzowska et al., unpublished). Within the context of the 23.0 ± 4.1 m.y. duration of the Late Devonian (Kaufmann, 2006), this event provides an unprecedented account of rapid ecosystem

stresses and Earth-system responses on a timescale of less than 0.6 m.y.. By scrutinizing preexisting long-terms records of the unique changes that transformed Late Devonian marine and terrestrial ecosystems, we are increasingly better able to understand how the Earth responds to rapid stresses and changes in nutrient cycling and to relate such events to the relevant timescale of human evolution and interactions, all too often detrimental (IPCC, 2007), with the surrounding environment.

Unprecedented evolutionary changes transformed the character of the Late Devonian biosphere and of its interactions with the surrounding geological environment, through increases in the biodiversity of terrestrial habitats and in the rates of their colonization by metazoans and plants (Milner, 1990; Edwards and Burgess, 1990, 2001; Selden, 1990, 2001; Coates, 2001). Particularly noteworthy was the diversification and geographic expansion of deeply-rooted vascular land floras and their influence on the evolution of deeply weathered soils; the evolution of the latter increased the environmental abundances and fluxes to the marine realm of readily available trace element micronutrients which, together with the major algal nutrients C, N, P, and Si, limit oceanic bioproductivity (Algeo et al., 1995; Algeo and Scheckler, 1998, 2010; House, 2002; Falkowski, 2004; Morel et al., 2004). Current interpretations thus suggest that the common occurrences of oceanic anoxia during the Late Devonian and the associated deposition of OM-rich sediments were intimately related to eutrophication through the impacts of terrestrial afforestation on terrestrial-marine nutrient cycling (Algeo and Scheckler, 1998, 2010; Racki, 1998, 2005). The efficient weathering of mountain ranges rising in near-equatorial latitudes during pulses of the Eovariscan and Ellesmerican orogenies (Fig. 1.3) likely further increased nutrient fluxes to the oceans and contributed to the eutrophication of epeiric seas environments (Tribovillard et al., 2004; John et al., 2008). A warming Frasnian 'greenhouse' climate and rising sea level (2nd order) were conducive to the development of such vast epeiric waterways and extensive reef complexes, such as those of the WCSB and the Devonian "Great Barrier Reef" of Western Australia (Fig. 1.3; Playford et al., 1984; Geldsetzer, 1989; Mountjoy, 1989; Mossop and Shetsen, 1994; Kiessling et al., 1999). However climatic conditions shifted towards an 'icehouse' mode near the Frasnian-Famennian (F/F) boundary interval, culminating in end Devonian glaciations (Brzezinski et al., 2008; Caputo et al., 2008). Through the combined effects of these ecosystem changes and other geological stresses – among them multiple meteor impacts, extensive flood basalt volcanism on the Siberian platform and fluctuations of sea level – the biosphere experienced one of the most severe biotic crises, since the radiation of metazoans during the Cambrian explosion, near the close of the Devonian period (Sepkoski 1984; House, 2002; Racki, 2005). However, approximately twenty relatively 'short-term' geobiological 'events' precede the terminal Devonian extinctions at the F/F boundary and across the Devonian-

Carboniferous boundary transition. It's been recognized that some of these events are characterized by 1) relatively discrete faunal perturbations, 2) deposition of black shales and other OM-rich facies, but also 3) by major excursions or permanent shifts of various geochemical records (Algeo et al., 1995; House, 2002). The geochemical histories of most, however, are yet to be written and it is unlikely that any one of these events will comprehensively clarify the global ecosystem and environmental changes of the Late Devonian time interval (House, 2002).

1.3. Eutrophication, reef-building, and exceptional organic matter-rich deposits of the Phanerozoic: the Late Devonian within a broader geobiological context

1.3.1. Eutrophication

Throughout this work, eutrophication events in the geological record of epeiric seaways are defined as episodes of increased nutrient loadings that resulted in 1) phytoplankton and algal blooms, 2) likely changes in the species composition of the dominant primary producers (see Section 1.3.6.), 3) shoaling of the euphotic zone by reductions in water transparency and hence the effective penetration depth of sunlight that fuels photosynthesis among oceanic primary producers, 4) diminished carbonate production and 5) other trophic changes that favored lower biodiversities and taxonomic assemblages dominated by generalists and opportunistic species (*c.f.* Hallock, 1988a,b; Hallock and Schlager, 1986; Wood, 1993; Brasier, 1995; Whalen et al., 2002). Examples of eutrophication and its adverse effects on modern reef systems and carbonate environments include but are by no means limited to the Great Barrier Reef tract, reefs of the Caribbean and those off the Brazilian coast (Bell, 1992; Hallock, 1988b; Costa Jr. et al., 2008; see Section 1.3.7.).

Eutrophication in marine environments is a symptom of high nutrient loadings which, if persistent, lead to the formation of oxygen-deprived (hypoxic-anoxic) waters and to general benthic ecosystem stagnation (Diaz, 2001; Rabalais et al., 2010; Wood, 1993). Eutrophication stimulates primary production in the euphotic zone and increases the export of OM to the sediment-water interface, where its aerobic respiration by heterotrophic microbes consumes oxygen dissolved in benthic waters. Depending on the balance between sedimentary OM fluxes and the rates of benthic water ventilation, dissolved O_2 concentrations can become severely depleted. At less than approx. 30% saturation (< 2 mg O_2 per L), waters become hypoxic and generally inhospitable to marine life except to select organisms which have coevolved with persistent, naturally occurring hypoxic systems, such as coastal upwelling and oceanic oxygen minimum zones (OMZs)(Rabalais et al., 2010). High respiratory oxygen demands can, however, exhaust dissolved O_2 concentrations completely, thus rendering the benthic environment anoxic

and inhospitable except to a successive progression of microbial communities which continue to thrive by respiring OM first by denitrification (by stripping oxygen bound within dissolved NO_3^{2-}), followed by the reduction of Mn and Fe-oxides, and finally dissolved sulfate (SO_4^{2-}; this progression is dictated thermodynamically by the amount of energy released during carbon oxidation using the different oxygen doners; see Table 2 in Tribovillard et al., 2006).

1.3.2. Proneness of marine systems to eutrophication: hydrogeomorphology, climate, and basinal circulation patterns

Marine systems especially prone to the development of hypoxic or anoxic conditions resulting from eutrophication include continental margins that experience upwelling of nutrient-rich deep-waters (eastern boundary currents, at present along the coasts of South, Central and North America, south- and northwestern Africa and the Arabian Sea; Rabalais et al., 2010) and systems 1) with otherwise restricted to semi-restricted circulation patterns and communication with the global ocean which 2) become prone to thermohaline stratification which restricts the ventilation of benthic waters through vertical mixing. These include, for example, both silled and unsilled marginal basins, sub-basins and fjords (*e.g.* the Cariaco Basin off the Venezuelan Coast; Framvaren Fjord in Norway, Saanich Inlet of British Columbia, Canada; Rabalais et al., 2010), inland seas (*e.g.* the Black Sea) and epicontinental seas (*e.g.* the Baltic Sea and Hudson Bay; Witzke, 1987). The inferred circulation dynamics within the vast tropical to sub-tropical epicontinental seaways of the geologic past, for which no Modern analogues exist, indicate they were especially prone to water column stratification and eutrophication (Witzke, 1987). The stratigraphic covariance of trace metals with differing oceanic residence times is increasingly being used as a guide to reconstructing circulation patterns and water-mass redox conditions within such paleosystems (*cf.* Algeo and Maynard, 2008).

Two end-member circulation models have been developed for the vast epicontinental seaways that have inundated extensive portions of the continents for broad intervals of Phanerozoic time (Witzke, 1987): 1) the quasiestuarine (QEC) and 2) the antiestuarine circulation models (AEC). In concert with hydrogeomorphic features such as sills or other physical barriers that impeded water flow - including extensive and intricate reef structures - both circulation systems establish the important requisite conditions of watermass stratification (thermohaline) that allows the benthic environments of such seaways to become OM traps. The basin thus becomes prone to eutrophication and to the development of benthic hypoxia or anoxia (Witzke, 1987). In broad terms, a basin's geographic location and predominant climatic conditions control the balance of the water budget, which is a function of fluxes associated with 1) surface water evaporation, 2) freshwater inflow from continental discharge and rainfall, and the 3) inflow and 4)

outflow of oceanic waters, where the interplay of the first two flux conditions dictates the dominant circulation pattern (Witzke, 1987). QEC conditions (Fig. 1 in Witzke, 1987) predominate in humid climatic settings where the net freshwater influx exceeds water loss by evaporation. Surface waters become less saline and less dense, and tend to move offshore; to maintain mass balance, oceanic waters inflow as bottom currents. Conversely, AEC conditions (Fig. 2 in Witzke, 1987) characterize arid climates where net evaporation exceeds freshwater influx. As surface waters undergo evaporation, they become denser and more saline and thus sink to the benthic realm to eventually outflow, if unrestricted, to the open ocean as bottom currents; to maintain mass balance, oceanic waters inflow as surface currents. If conditions are suitable for extensive evaporite deposition (see Schreiber and Hsü, 1980), oceanic water movements may be unidirectional into the basin with no outflow necessary (B.C. Schreiber, personal communication). At any given time and place, a basin develops its own unique variant composed of these end-members through the action of regional tidal effects, wind patterns and associated currents, storm activity, climatic oscillations and global eustacy. Further, those epeiric seas of the geologic past that extended over broad expanses of latitude and longitude and thus across climatic gradients were likely characterized by a continuum of circulation patterns between the two end-member types (Witzke, 1987).

1.3.2.1. Proneness of the Western Canada Sedimentary Basin to eutrophication during Late Devonian time

The Late Devonian *punctata* Event occurred during the Early-Middle Frasnian transition. The Western Canada Sedimentary Basin was at that time situated at near-equatorial latitudes on the western margin of the Laurussian landmass (Figs. 1.3, 1.4 and 1.5). During much of the Frasnian, the basin was the site of extensive reef development characterized by a system of isolated and attached platforms, commonly known as the 'Leduc interval' of the Woodbend Group (Fig. 1.6). The Leduc Formation in places exceeds 275 m in thickness and acts as a reservoir for significant accumulations of economic hydrocarbon pools (roughly 1/3 the initially estimated resourced within the basin) sourced from the highly prolific source rocks of the surrounding shale basins (Creaney et al., 1994) . These include the Duvernay Fm. in the subsurface of Central Alberta and the equivalent Perdrix Fm. exposed in the fold and thrust belt of the Canadian Rockies; it is the Perdrix Formation (Fm.) around the isolated Miette carbonate platform complex that was sampled for the purpose of reconstructing the geochemical history of the *punctata* Event anomaly (Figs. 1.4 and 1.6).

Given the general prevalence of evaporite deposits throughout the Leduc stratigraphy (Fig. 1.5), the antiestuarine circulation model (Witzke, 1987) is seemingly appropriate to

characterize the regional movements of waters throughout the WCSB. Hypersaline and evaporitic facies are the telltale evidence of such a circulation system (Witzke, 1987), as they require warm and arid climatic settings with a negative water balance for their genesis. At present, such conditions are generally met between 15 and 45° north and south of the equator (Warren, 1989). This is, however, in contrast, but is not incompatible, with the quasiestuarine circulation model proposed for the deposition of the Middle and Upper Frasnian (Late Devonian) black shale sequence in the epeiric seaway of the U.S. Midcontinent (Witzke, 1987). Witzke (1987) cites numerous studies that have recognized the need for significant density stratification as a requisite for the sequence's formation, and proposes, based on the evolution of facies types and predominant lack of extensive evaporite deposits, that such conditions would have been met by freshwater runoff from the Acadian orogen. Runoff would have promoted the formation of less saline and less dense surface waters, leading to water column stratification and hence reduced benthic water ventilation. In a manner analogous to modern stratified epicontinental seas (*e.g.* the Baltic Sea), such conditions would have rendered the benthic environment susceptible to eutrophication in the presence of increased nutrient loadings (see also Algeo and Maynard's (2008) description of conditions in the Devonian-Mississippian Appalachian Sea, Fig. 4B therein).

A single circulation model, however, does not necessarily suffice for epicontinental seaways vast enough to have existed across climatic gradients (Witzke, 1987). Quasiestuarine circulation systems similar to that of the Midcontinent Sea thus likely also existed elsewhere within the Late Devonian epeiric sea system, where conditions for evaporite formation similar to those in the WCSB did not prevail. Speculatively, such conditions may have existed further to the north of the reef system, nearer the Ellesmerian orogen (Fig. 1.4). Perhaps in a manner analogous to the draining of the Acadian uplift into the Midcontinent sea, which not only helped establish water column stratification but also supplied the requisite nutrients for eutrophication (Algeo and Maynard, 2008 and references therein), runoff from the Ellesmerian uplift may have induced similar effects. Much of the nutrients that episodically promoted eutrophication within the Leduc reef system were likely associated with the influx of basin-filling sediments within the WCSB, which are probably in large part of Ellesmerian Fold Belt provenance (Oliver and Cowper, 1963, Stoakes, 1980). Stoakes (1980) proposed that the infilling of the intra-Leduc reef shale basins (Fig. 1.4) progressed from a generally N-NW direction towards the S-SE, thus delimiting the predominant pattern of oceanic water movements into and within the basin. The general distribution of evaporite facies throughout the Devonian of the WCSB can be interpreted to be supportive of such a generalized trend in basin circulation (Schreiber and Hsü, 1980; Fig. 32 in Warren, 2010), where increasingly saline facies occur towards SE Alberta, S-SW Saskatchewan, north Central Montana and NW North Dakota, delineating the evaporitic concentration and

evolution of normal marine waters likely inflowing predominantly from the N-NW. The evaporitic concentration would have promoted the formation of a stratified water column, rendereing it susceptible to become a stagnant nutrient trap, especially if circulation around the reef complexes was indeed 'sluggish,' as suggested by Stoakes (1980). Stratification was likely most intense near the evaporitic depocenters and substantially less so on the peripheries of the Leduc reef system to the west, as for example near the isolated Miette carbonate platform (Fig. 1.4), of which the SE margin was sampled for the geochemical analyses reported herein. While surrounding waters may have been stratified and thus more prone to eutrophication, an examination of the relevant stratigraphic intervals indicates that the platform slope was generally hospitable to benthic faunas outside the occurrence of anoxic events (*e.g.* Whalen et al., 2000; Śliwiński et al., 2011).

1.3.3. Sources of nutrients that drive eutrophication

Seawater is an extreme environment in terms of its low abundances of bioavailable trace metals that are essential to primary production (Bruland and Lohan, 2004; Falkowski, 2004; Morel et al., 2004). Increased nutrient loadings and eutrophication events in the geological past are usually interpreted from one of two or a combination of both types of general models used to explain the (bio)physical mechanisms responsible for nutrient delivery to marine basins:

1. Models that explore the advent of novel styles of geobiological interactions within the Earth system through time, commonly associated with the evolutionary rise of organisms capable of interacting with their surrounding environment in unprecedented ways. An example is the Devonian *terrestrial-marine teleconnections model* of Algeo and Scheckler (1998, 2010; see also Algeo et al., 1995), which focuses on the relatively rapid evolutionary rise, diversification and expansion of the first terrestrial forests and complex soils and the effects this had on perturbing nutrient fluxes from the continents to the oceans.

2. Models that focus more on the temporal associations of eutrophication events in the geological record with climatically-driven changes in the intensity of chemical weathering and continental run-off as a means of transiently loading the oceans with nutrients (*e.g.* Meyers, 2006). These models extensively consider the weathering of rising orogens under different climatic regimes and the impacts of enhanced continental weathering on global climate through draw-down of atmospheric CO_2 levels (Raymo et al., 1988; Raymo and Ruddiman, 1992; Berner, 1993; Tribovillard et al., 2004; Averbuch et al., 2005). The

effects of orbital cyclicities on modulating climatic oscillations are an integral part of these models.

1.3.4. The influence of nutrient regimes on reef-building

Nutrient regimes, ranging from oligotrophic (low nutrient availability) through mesotrophic to eutrophic (high nutrient availability), are important factors that 1) control the distribution of carbonate-forming organisms in the modern tropical and sub-tropical shallow seas (*e.g.* Hallock and Schlager, 1986) and 2) affect ecosystem/environmental stability (*e.g.* Hallock and Schlager, 1986). Increasingly oligotrophic conditions are favorable to the expansion of the euphotic zone (controlled by water clarity), to overall ecosystem stability, and to larger expanses of habitable space for highly diverse and complex reef-building taxonomic assemblages (see Table 1 in Wood, 1993). Changes in nutrient regimes have exerted an important control on the history of Phanerozoic reef-building (Wood, 1993). Oligotrophic time intervals (*sensu* Wood, 1993) favored the development of aerially extensive, highly evolved reef complexes and climax-stage autotrophic communities such as those of the Devonian, although these were not the norm throughout the Phanerozoic as they dominated for only some 25-35% of its duration, and only for 16-25% during the combined time span of the Paleozoic and Mesozoic (Wood, 1993). Rather, extended periods of meso-eutrophic conditions characterized by benthic communities consisting of algal assemblages and soft-substrate inhabiting, opportunistic heterotrophs (detrital grazer and consumers of planktonic primary producers) tended to dominate, as for example during the early Carboniferous, Permian and mid- to late Cretaceous (Wood, 1993).

Some of the most extensive reef complexes known from the geologic record thrived during Late Devonian time (Fig. 1.3). Six major centers of reef development have been recognized (Figs. 1.5 and 1.6 in Kiessling et al., 1999). These include 1 & 2) the Siberian platform and the Timan Pechora province in Russia, 3) the Western Canada Sedimentary Basin, 4) central Europe, 5) Morocco, and 6) South China. More than 30% of these reef occurrences are either producing hydrocarbon reservoirs or are of reservoir quality, with major sites of hydrocarbon production located in the WCSB and in western Russia (the Volga Urals and the Timan-Pechora province; Kiessling et al., 1999). These extensive reefs experienced drastic declines through a series of seemingly pulsed eutrophication and extinction events/biotic crises (House, 2002) that appear to have been a prelude to the meso-eutrophy and icehouse climatic conditions of the Late Devonian and Early Carboniferous. These events are in large part ascribed to changes in terrestrial-marine interactions and nutrient cycling related to the rapid evolutionary diversification and expansion of terrestrial forests and the development of deeply weathered soils (Algeo et al., 1995; Algeo and Scheckler, 1998, 2010).

1.3.5. Exceptional OM-rich deposits of the Phanerozoic

The widespread deposition of organic matter-rich sediments (up to 30 wt.% *total organic carbon - TOC*) has occurred periodically throughout the Phanerozoic (Fig. 1.2). Remarkable is the fact that such deposits form when only some 10% or less of the organic matter produced in the ocean's euphotic zone escapes recycling within the water column and later at the seabed to become part of the sedimentary record (Tribovillard et al., 2006). Notable examples of such deposits include the Pliocene-Holocene sapropels of the Mediterranean region and the mid-Cretaceous black shales that formed during relatively discrete, short-term marine 'anoxic' events related to climate-enhanced oceanic bioproductivity paced principally by the Earth's orbital cycles (Negri et al., 2006). Processional minima, characterized by increased seasonality, appear to have been conducive to warmer and wetter climatic conditions and hence to episodes of increased continental run-off and nutrient delivery to marginal seas (Meyers, 2006). Collectively, some of these anoxic organic carbon burial events characterize longer intervals of geologic time. An example is the ~5 m.y. time interval of the Plio-Pleistocene during which the numerous sapropels of the Mediterranean region formed; each sapropelic event unfolded over a span of only several thousand years and occurred repetitively, apparently paced by orbital cyclicites at ~21 k.y. intervals (corresponding to precessional minima; Meyers, 2006). Orbital cyclicites are evident also in distribution of TOC maxima in the black shales of the Cretaceous *Oceanic Anoxic Events (OAE)*, although these episodes were generally longer in duration (*e.g.* OAE '1b' = approx. 42 k.y.; Meyers, 2006). The extent to which orbital cyclicities and resulting climatic shifts paced the twenty-some Late Devonian black shale events (House, 2002) over the course of the 23.0 ± 4.1 m.y. of its duration (Kaufmann, 2006) remains unknown, as the resolution of orbital signals in Late Devonian sedimentary deposits has only very recently been attempted (De Vleeschouwer et al., 2012). Further research might reveal, however, that the maxima of the numerous eutrophication pulses and black shale events, elegantly related to the greening and afforestation of the Late Devonian (Algeo and Scheckler, 1998, 2010), might have been in large part driven by orbitally induced warmer and wetter climatic episodes that helped flush readily available bionutrients from the then evolving deeply weathered soils into the oceans.

1.3.6. Reconstructing paleoceanographic conditions and events using geochemical methods

The formation of black shales and sapropels seems to be associated with unusually eutrophic, nitrate-limited, 'greenwater' oceanic conditions (*sensu* Brasier, 1995) and faunal variations during which primary production shifts to otherwise marginal species of planktic/benthic

algae and other microbial organisms (N is one of the four major algal nutrients: C, N, P and Si; Falkowski, 2004; Morel et al., 2004). Significant geochemical anomalies in the form of chemostratigraphic accumulations of redox-sensitive *(e.g.* Mo, V and U) and sulfide-forming *(e.g.* Ni, Cu, Zn; see Tribovillard et al., 2006) trace metals are a common feature of black shales and sapropels; common also are excursions in the isotopic composition of C and N in sedimentary OM and of C and O in carbonate sediment. Such geochemical anomalies attest to changing conditions in the water column and to the generally inhospitable stagnation that enveloped portions of the benthic realm, at times encroaching also into the photic zone, during the course of black shale and sapropel deposition (Murphy et al., 2000; Schultz and Rimmer, 2004; Meyers, 2006; Negri et al., 2006; Racki et al., 2008; Wagreich et al., 2011). Recently increasing interest in the nitrogen isotope dynamics ($\delta^{15}N$) of sedimentary OM, for example, adds an intriguing aspect to the uniqueness and scale of such events, which cannot be compared in terms of their areal extent nor in terms of the exceptional organic richness of their facies to even the most productive upwelling regions of the Modern Ocean (Meyers, 1997, 2006, Rabalais et al., 2010). Although still limited compared to the widespread use and reporting of $\delta^{13}C_{(organic\ and\ carbonate)}$ records, studies that examine the stratigraphic variance of $\delta^{15}N$ in OM from Late Devonian (Calvert et al., 1996; Caplan et al., 1996; Levman and von Bitter, 2002; de la Rue et al., 2007; Śliwiński et al., 2011) and mid-Cretaceous (*e.g.* Rau et al., 1987; Kuypers et al., 2004a,b; Junium and Arthur, 2007) black shales and the Mediterranean sapropels (Calvert et al., 1992; Struck et al., 2001; Arnaboldi and Meyers, 2006; Meyers, 2006;) consistently suggest that primary production dominated by diazotrophs (N_2-fixing autotrophs, especially cyanobacteria) might be particularly characteristic of such events of widespread oceanic anoxia and OM production/preservation *(e.g.* Kuypers et al., 2004b). Changes in the community composition of primary producers are a characteristic of environmental eutrophication; associated changes in nutrient ratios, especially decreases of N:P under anoxic conditions that enhance bioavailable N loss to denitrification, *are* (Diaz and Rosenberg, 2008, Rabalais et al., 2010; Vahtera et al., 2007) and apparently *were* in the geologic past (*e.g.* Kuypers et al., 2004b) ecologically advantageous to the proliferation of diazotrophs (especially cyanobacteria) because of their unique ability among microbes to utilize dissolved N_2 gas to sustain their metabolic N requirements (Altabet, 2006; Galloway, 2003; Montoya et al., 2004). Cyanobacteria likely constitute a significant if not a major fraction of the export biomass during such oceanographic events, inducing the uniquely low $\delta^{15}N$ values in sedimentary OM (~0‰ or less) that are distinctly lower than typical marine OM $\delta^{15}N$ at ~5‰ (Fig. 1.7; Galbraith et al., 2008; Meyers, 2006). Low $\delta^{15}N$ values and elevated C/N ratios (above the normal marine level of ~6-8) always characterize the OM within the facies deposited during such episodes throughout the Phanerozoic and are not readily explained away as mere artifacts of diagenetic

processes (Fig. 1.8; Junium and Arthur, 2007). This is in part the subject of Chapter 4 of the present work, which explores $\delta^{15}N$ records of sedimentary OM deposited during the Late Devonian *punctata* Event at the isolated Miette carbonate platform in the WCSB. Within the context of the 'multiproxy approach' towards understanding geobiological events and perturbations, the observed $\delta^{15}N$ records imply a prominent role of nitrogen-fixing microbes in sustaining high levels of primary production following the initial eutrophication pulses and benthic stagnation at the onset of the *punctata* Event paleoceanographic anomalies. These observations suggests parallels, at least in terms of ecosystem responses to eutrophication, with the OAEs and associated black shales of the Mesozoic and Mediterranean sapropels (Junium and Arthur, 2007; Meyers, 2006), and are not unlike some of the symptoms of the currently on-going eutrophication of coastal waters by anthropogenic nutrient loading, as for example in the Baltic Sea and Scandinavian waters, in the Gulf of Mexico, the East China Sea or the Northwestern Shelf of the Black Sea (Rabalais et al., 2010).

1.3.7. Anthropogenic eutrophication of water bodies and the spread of hypoxic-anoxic zones: the relevance of paleoceanographic studies

Eutrophication and the evolution of hypoxic-anoxic oceanic water masses on a scale large enough to rank as a 'global event' are not phenomenon that unfold solely on geologic timescales (see Fig. 1.5 in Rabalais et al., 2010). Through increased nutrient loadings since the beginning of the Anthropocene, the spread of hypoxia and anoxia in estuarine and marine environments has developed into a major global environmental problem (Diaz and Rosenberg, 2008). In their review of over 400 hypoxic-anoxic systems worldwide (Fig. 1.9), Diaz and Rosenberg (2008; pg. 929) conclude that "the weight of evidence indicates that in pre-industrialized times, most coastal and offshore ecosystems never became hypoxic except in natural upwellings" (Fig. 1.9). The quoted number of affected systems, however, is more than likely an underestimation given the general lack of scientific reporting from the Southern Hemisphere (Diaz and Rosenberg, 2008). Importantly, much of the hypoxia and anoxia in shallow coastal marine areas has developed only within the last 50 years of increased industrial fertilizer use, attesting to the ability of human societies to perturb the Earth system on a global scale within a time interval that is geologically near instantaneous. As stated in the assessment of Diaz and Rosenberg (2008), "there is no other variable of such ecological importance to coastal marine ecosystems that has changed so drastically over such a short time as dissolved oxygen [levels]." The dynamics of anthropogenic eutrophication and the spread of hypoxic/anoxic zones, the ecosystem changes and responses, economic impacts and mitigation measures are extensively documented (*e.g.* Joyce, 2000; Diaz, 2001; Prepas and Charette, 2004; Diaz and Rosenberg,

2008; Rabalais et al., 2009, 2010; Howarth et al., 2011; see also the National Centers for Coastal Ocean Science's *Gulf of Mexico Hypoxia Assessment).*

It is interesting to note that assessments of eutrophication and spreading hypoxic-anoxic 'dead zones' focus primarily on the nitrate and phosphate components of the nutrient fluxes from agricultural and waste-water run-off. The rapid erosion of soils driven by modern agricultural practices (Montgomery, 2007), however, also contributes to the nutrient fluxes by supplying the trace elements that are essential to the biochemical machinery of marine primary production for utilizing the major algal nutrients (Bruland and Lohan, 2004; Falkowski, 2004; Morel et al., 2004). Further, although speculatively, the volume of water that is redirected for agricultural irrigation and flushed through soil systems is undoubtedly far in excess of the amount that any given cubic meter of farm land would otherwise receive per unit time from rainfall; such 'excess flushing' may be considered a form of accelerated chemical erosion and likely amounts to an additional elevation of trace element fluxes to the oceans.

Thus the ultimate relevance of committing time and resources toward developing analytical methods and approaches for studying unusual events of rapid ecosystem change in the geologic past, especially outside the immediate 'tangibility' of the Holocene/Anthropocene, lies in learning to understand the full range of Earth system responses to induced environmental stresses and evolving to find a balanced existence for human societies within their ecosystem.

1.3.8. References:

Algeo, T.J., Berner, R.A., Maynard, J.B. and Scheckler, S.E., 1995. Late Devonian oceanic anoxic events and biotic crises: "rooted" in the evolution of vascular land plants? *GSA Today*, **5**, 1-66

Algeo, T.J. and Maynard, J.B., 2008. Trace-metal covariation as a guide to water-mass conditions in ancient anoxic marine environments. *Geosphere*, **4**, 872-887

Algeo, T.J. and Scheckler, S.E., 1998. Terrestrial-marine teleconnections in the Devonian: links between the evolution of land plants, weathering processes, and marine anoxic events. *Philosophical Transactions of the Royal Society B-Biological Sciences*, **353**, 113-128

Algeo, T.J. and Scheckler, S.E., 2010. Land plant evolution and weathering rate changes in the Devonian. *Journal of Earth Science,* **21,** 75-78

Altabet, M.A., 2006. Isotopic tracers of the marine nitrogen cycle: present and past. *In*: Handbook of Environmental Chemistry Volume 2 Part N, 251-293

Arnaboldi, M. and Meyers, P.A., 2006. Patterns of organic carbon and nitrogen isotopic compositions of latest Pliocene sapropels from six locations across the Mediterranean Sea. *Palaeogeography, Palaeoclimatology, Palaeoecology*, **235**, 149-167

Averbuch, O., Tribovillard, N., Devleeschouwer, X., Riquier, L., Mistiaen, B. and Van Vliet-Lanoe, B., 2005. Mountain building-enhanced continental weathering and organic carbon burial as major causes for climatic cooling at the Frasnian- Famennian boundary (c. 376 Ma)? *Terra Nova*, **17**, 25-34

Balinski, A., Olempska, E. and Racki, G., 2006. Early-Middle Frasnian transition: Biotic response to a major perturbation of the global carbon budget *Acta Palaeontologica Polonica*, **51**, 606-608.

Bell, P.R.F. 1992. Eutrophication and coral reefs – some examples in the Great Barrier Reef Lagoon. *Water Research*, **26**(5), 553-568

Berner, R.A., 1993. Weathering and its effect on atmospheric CO_2 over Phanerozoic time. *Chemical Geology*, **107**, 373-374

Blatt, H. and Jones, R.L., 1975. Proportions of exposed igneous, metamorphic, and sedimentary rocks. *Geological Society of America Bulletin*, **81**, 255-262

Boyer, D.L. and Droser, M.L., 2009. Palaeoecological patterns within the dysaerobic biofacies: Examples from Devonian black shales of New York state. *Palaeogeography, Palaeoclimatology, Palaeoecology*, **276**, 206-216

Brasier, M.D., 1995. Fossil indicators of nutrient levels. 1: Eutrophication and climate change. *In:* Bosence, D.W.J. and Allison, P.A. (Eds.), Marine palaeoenvironmental analysis from fossils. *Geological Society [London] Special Publication*, **83**, 133- 132

Bruland, K.W., and Lohan, M.C., 2004. Controls of Trace Metals in Seawater. *In:* The Oceans and Marine Geochemistry, Treatise on Geochemistry Volume 6, Elderfield, H., Holland, H. D. and Turekian, K. K. (Eds.), Elsevier, Amsterdam, Heidelberg, 23-47

Brzezinski, D.K., Cecil, C.B., Skema, V.W. and Stamm, R., 2008. Late Devonian glacial deposits from the eastern United States signal an end of the mid-Paleozoic warm period: *Palaeogeography, Palaeoclimatology, Palaeoecology*, **268**, 143–151.

Buick, R. 2003. Life in the Archaean. *In:* Briggs, D.E.G. and Crowther, P.R. (Eds.), Palaeobiology II. Blackwell Science, Oxford

Butterfield, N.J., 2003. Exceptional fossil preservation and the Cambrian Explosion. *Integrative and Comparative Biology*, **43**, 166-177

Calvert, S.E., Bustin, R.M. and Ingal, E.D., 1996. Influence of water column anoxia and sediment supply on the burial and preservation of organic carbon in marine shales. *Geochimica et Cosmochimica Acta*, **60**, 1577-1593

Calvert, S.E., Nielsen, B. and Fontugne, M.R., 1992. Evidence from nitrogen isotope ratios for enhanced productivity during formation of eastern Mediterranean sapropels. *Nature*, **359**, 223-225

Calvert, S.E. and Pedersen, T.F., 1993. Geochemistry of recent oxic and anoxic marine sediments - implications for the geological record. *Marine Geology*, **113**(1-2), 67- 88

Caplan, M.L., Bustin, R.M. and Grimm, K.A., 1996. Demise of a Devonian- Carboniferous carbonate ramp by eutrophication. *Geology,* **24**(8), 715-718

Caputo, M.V., 2008. Late Devonian and Early Carboniferous glacial records of South America. *Geological Society of America Special Papers*, **441**, 161-173

Coates, M.I., 2001. Major Events in the History of Life: Palaeozoic Events: Origin of Tetrapods. *In:* Briggs, D.E.G. and Crowther, P.R. (Eds.), Palaeobiology II. Blackwell Science, Oxford. 74-79

Costa, Jr., O.S., Nimmo, M. and Attrill, M.J., 2008. Coastal nitrification in Brazil: a review of the role of nutrient excess on coral reef demise. *Journal of South American Earth Science,* **25**, 257-270

Creaney, S., Allan, J., Cole, K.S., Fowler, M.G., Brooks, P.W., Osadetz, K.G., Macqueen, R.W., Snowdon, L.R. and Riediger, C.L., 1994. Ch. 31: Petroleum generation and migration in the Western Canada Sedimentary Basin. *In*: Mossop, G.D. and Shetsen, I (Eds.) Geological atlas of the Western Canada Sedimentary Basin; Canadian Society of Petroleum Geologists and Alberta Research Council, Special Report 4, URL: http://www.ags.gov.ab.ca/publications/wcsb_atlas/atlas.htmlN, [December 17, 2011].

da Silva, A.C. and Boulvain, F., 2008. Carbon isotope lateral variability in a Middle Frasnian carbonate platform (Belgium): significance of facies, diagenesis and sea- level history. *Palaeogeography, Palaeoclimatology, Palaeoecology,* **269**, 189–204

de la Rue, S., Rowe, H.D., Rimmer, S.M., 2007. Palynological and bulk geochemical constraints on the paleoceanographic conditions across the Frasnian-Famennian boundary, New Albany Shale, Indiana. International Journal of Coal Geology, **71**, 72-84

De Vleeschouwer, D., Whalen, M.T., Day, J.E., Philippe, C., 2012. Cyclostratigraphic calibration of the Frasnian (Late Devonian) time-scale (western Alberta, Canada). *The Geological Society of America Bulletin*. doi:10.1130/B30547.1

Diaz, R.J. 2001. Overview of hypoxia around the world. Journal of Environmental Quality, **30**, 275-281

Diaz, R.J. and Rosenberg, R., 2008. Spreading dead zones and consequences for marine ecosystems. *Science*, **321,** 926-929

Droser, M.L. And Bottjer, D.J., 1986. A semiquantitative field classification of ichnofabric. *Journal of Sedimentary Research,* **56,** 558-559

Edwards, D., and Burgess, N.D., 1990. Major Events in the History of Life: Terrestrialization: Plants. *In:* Briggs, D.E.G. and Crowther, P.R. (Eds.), Palaeobiology. Blackwell Science, Oxford. 60-64

Edwards, D., and Burgess, N.D., 2001. Major Events in the History of Life: Palaeozoic Events: Early Land Plants. *In:* Briggs, D.E.G. and Crowther, P.R. (Eds.), Palaeobiology II. Blackwell Science, Oxford. 63-67

Falkowski, P.G., 2004. Biogeochemistry of Primary Production in the Sea. *In:* Biogeochemistry, Treatise on Geochemistry Volume 8, Elderfield, H., Holland, H. D. and Turekian, K. K. (Eds.), Elsevier, Amsterdam, Heidelberg, 185-213

Galbraith, E. D., Sigman, D.M., Robinson, R. S. and Pedersen, T. F.. 2008. "Nitrogen in Past Marine Environments," *In:* Nitrogen in the Marine Environment (2^{nd} edition), Capone, D.G., Bronk, D.A., Mulholland, M. R. and Carpenter, E. J. (Eds.), Chapter 34, 1497-1535, Academic Press

Galloway, J.N., 2003. 8.12. The Global Nitrogen Cycle. *In:* Biogeochemistry, Treatise on Geochemistry Volume 8, Elderfield, H., Holland, H. D. and Turekian, K. K. (Eds.), Elsevier, Amsterdam, Heidelberg, 557-583

Geldsetzer, H.H.J., 1989. Ancient Wall reef complex, Frasnian age, Alberta, *In:* Geldsetzer, H.H.J., James, N.P. and Tebbutt, G.E. (Eds.), Reefs, Canada and Adjacent Areas, *Canadian Society of Petroleum Geologists, Memoir,* **13**, 431-439

Hallock, P., 1988a. The role of nutrient availability in bioerosion: consequences to carbonate buildups. *Palaeogeography, Palaeoclimatology, Palaeoecology,* **63**, 275-291

Hallock, P., 1988b. Platforms of the Nicaraguan Rise: examples of the sensitivity of carbonate sedimentation to excess trophic resources. *Geology,* **16**, 1104-1107

Hallock, P., and Schlager, W., 1986. Nutrient excess and the demise of coral reefs and carbonate platforms. *Palaios*, **1,** 389-398

Hatch, J.R. and Leventhal, J.S., 1992. Relationship between inferred redox potential of the depositional environment and geochemistry of the Upper Pennsylvanian (Missourian) Stark Shale Member of the Dennis Limestone, Wabaunsee Country, Kansas, U.S.A. *Chemical Geology*, **99**, 65-82

Holland, H.D. 2006. The oxygenation of the atmosphere and oceans. *Philosophical Transactions of the Royal Society B*, **361,** 903-915

House, M.R., 2002. Strength, timing, setting and cause of mid-Palaeozoic extinctions. *Palaeogeography, Palaeoclimatology, Palaeoecology*, **181**, 5-25.

Howarth, R., Chan, F., Conley, D.J., Garnier, J., Doney, S.C., Marino, R. and Billen, G., 2011. Coupled biogeochemical cycles: eutrophication and hypoxia in temperate estuaries and coastal marine ecosystems. *Frontiers in Ecology*, **9**(1), 18-26

Intergovernmental Panel on Climate Change (IPCC). 2007. Climate Change 2007 - Impacts, Adaptation and Vulnerability. Contribution of Working Group II to the Fourth Assessment Report of the Intergovernmental Panel on Climate Change. (Parry, M.I., Canziani, O.F., Patulikof, J.P., van der Linder, P.J. and Nanson, C.E., Eds). Cambridge University Press, Cambride, Uk. 976 pp.

Javaux, E.J., Marshall, C.P. and Bekker. A., 2010. Organic-walled microfossils in 3.2- billion-year-old shallow-marine siliciclastic deposits. *Nature,* **463**, 934-938

John, E.H., Cliff, R. and Wignall, P.B., 2008. A positive trend in seawater Sr-87/Sr-86 values over the Early-Middle Frasnian boundary (Late Devonian) recorded in well-preserved conodont elements from the Holy Cross Mountains, Poland. *Palaeogeography Palaeoclimatology Palaeoecology*, **269**, 166-175

Jones, B. and Manning, D.A.C., 1994. Comparison of geochemical indices used for the interpretation of paleoredox conditions in ancient mudstone. *Chemical Geology*, **111**, 111-129

Joyce, S., 2000. The dead zones: oxygen-starved coastal water. *Environmental Health Perspectives*, **108**(3), A121-125

Junium, C.K. and Arthur, M.A., 2007. Nitrogen cycling during the Cretaceous, Cenomanian-Turonian Oceanic Anoxic Event II. *Geochemistry, Geophysics,Geosystems,* **8**(3), 1-18

Kaufmann, B., 2006. Calibrating the Devonian time scale: A synthesis of U-Pb ID-TIMS ages and conodont stratigraphy. *Earth-Science Reviews*, **76**, 175-190.

Kiessling, W., Flügel, E. and Golonka, J. 1999. Paleoreef maps: evaluation of a comprehensive database on Phanerozoic reefs. *AAPG Bulletin*, **83** (10), 1552- 1587

Kump, L.R., and Arthur, M.A., 1999. Interpreting carbon-isotope excursions: carbonates and organic matter. *Chemical Geology*, **161**, 181-198

Kuypers, M.M.M., van Breugel, Y., Schouten, S., Erba, E. and Damste, J.S.S. 2004a. N_2- fixing cyanobacteria supplied nutrient N for Cretaceous oceanic anoxic events. *Geology*, **32**(10), 853-856

Kuypers, M.M.M, van Breugel, Y., Schouten, S., Erba, E. and Sinninghe Damsté. 2004b. N_2-fixing cyanobacteria supplied nutrient N for Cretaceous oceanic anoxic events. *Geology,* **32**(10), 853-856

Levman, B.G. and von Bitter, P.H., 2002. The Rasnian-Famennian (mid-Late Devonian) boundary in the type section of the Long Rapids Formation, James Bay Lowlands, northern Ontario, Canada. *Canadian Journal of Earth Sciences*, **39**, 1795-1818

Ma, X.P., Wang, C.Y., Racki, G. and Racka, M., 2008. Facies and geochemistry across the Early-Middle Frasnian transition (Late Devonian) on South China carbonate shelf: Comparison with the Polish reference succession. *Palaeogeography Palaeoclimatology Palaeoecology*, **269**, 130-151

Marynowski, L., Filipiak, P. and Pisarzowska, A., 2008. Organic geochemistry and palynofacies of the Early-Middle Frasnian transition (Late Devonian) of the Holy Cross Mountains, Southern Poland. *Palaeogeography, Palaeoclimatology, Palaeoecology*, **269**, 152-165

Meyers, P.A., 1997. Organic geochemical proxies of paleoceanographic, paleolimnologic, and paleoclimatic processes, *Organic Geochemistry,* **27,** 213-250

Meyers, P. A., 2006. Paleoceanographic and paleoclimatic similarities between Mediterranean sapropels and Cretaceous black shales. *Palaeogeography, Palaeoclimatology, Palaeoecologhy*, **235**, 305-320

Milner, A.C., 1990. Major Events in the History of Life: Terrestrialization: Vertebrates. *In:* Briggs, D.E.G. and Crowther, P.R. (Eds.), Palaeobiology. Blackwell Science, Oxford. 68-72

Montgomery, D.R., 2007. Dirt: The erosion of civilizations. University of California Press

Montoya, J.P., Holl, C.M., Zehr, J.P., hansen, A., Villareal, T.A. and Capone, D.G., 2004. High rates of N_2 fixation by unicellular diazotrophs in the oligotrophic Pacific Ocean. *Nature,* **430,** 1027-1031

Morel, F.M.M., Milligan, A.J. and Saito, M.A. 2004. Marine bioinorganic chemistry: The role of trace metals in the oceanic cycles of major nutrients, *In:* The Oceans and Marine Geochemistry, Treatise on geochemistry Volume 6, Elderfield, H., Holland, H. D. and Turekian, K. K., (Eds.), Elsevier, Amsterdam, Heidelberg, 113–143

Morrow, J.R., Sandberg, C.A., Malkowski, K., Joachimski, M.M., 2009. Carbon isotope chemostratigraphy and precise dating of middle Frasnian (lower Upper Devonian) Alamo Breccia, Nevada, USA. *Palaeogeography, Palaeoclimatology, Palaeoecology*, **282**, 105-118

Mossop, G.D. and Shetsen, I (comp.) (1994): Geological atlas of the Western Canada Sedimentary Basin; Canadian Society of Petroleum Geologists and Alberta Research Council, Special Report 4, URL <http://www.ags.gov.ab.ca/publications/wcsb_atlas/atlas.html>, [April, 2012]

Mountjoy, E.W., 1989. Miette Reef Complex (Frasnian), Jasper National Park, Alberta. *Memoirs of the Canadian Society of Petroleum Geologists*, **13**, 497-505

Murphy, A.E., Sageman, B.B., Hollander, D.J., Lyons, D.J., and Brett, C.E., 2000. Black shale deposition and faunal overturn in the Devonian Appalachian basin: Clastic starvation, seasonal water-column mixing, and efficient biolimiting nutrient recycling. *Paleoceanography*, **15**, 280-291

Negri, A., Wagner, T. and Meyers, P.A., 2006. Introduction to 'Causes and consequences of organic carbon burial through time." *Palaeogeography, Palaeoclimatology, Palaeoecology*, **235**, 1-7

Oliver, T.A. and Cowper, N.W., 1963. Depositional environments of the Ireton Formation, central Alberta. *Bulletin of Canadian Petroleum Geology*, **11**, 183-202

Peterhänsel A. and Pratt, B.R., 2001. Nutrient-triggered bioerosion on a giant carbonate platform masking the post extinction Famennian benthic community. *Geology*, **29**, 1079-1082

Piper, D.Z. and Calvert, S.E., 2009. A marine biogeochemical perspective on black shale deposition. *Earth-Science Reviews*, **95**, 63-96

Pisarzowska, A., 2008. Geochemia stabilnych izotopów węgla i tlenu na pograniczu dolnego i śrdokowego franu (dewon górny) na obszarze południowego szelfu Laurussi. PhD. Thesis, Silesian University, Sosnowiec, Poland.

Pisarzowska, A., Sobstel, M., Racki., G., 2006. Conodont-based event stratigraphy of the Early-Middle Frasnian transition on the South Polish carbonate shelf. *Acta Palaeontologica Polonica*, **51**(4), 609-646.

Playford, P.E., McClaren, D.J., Orth, C.J., Gilmore, J.S., and Goodfellow, W.D., 1984. Iridium anomaly in the upper Devonian of the Canning basin, Western Australia. *Science*, **226**, 437-439

Popp, B.N., Parekh, P., Tilbrook, B., Bidigare, R.R., and Laws, E.A., 1997. Organic carbon $\delta^{13}C$ variations in sedimentary rocks as chemostratigraphic and paleoenvironmental tools. *Palaeogeography, Palaeoclimatology, Palaeoecology*, **132**, 119-132

Powell, W.G., 2009. Comparison of geochemical and distinctive mineralogical features associated with the Kinzers and Burgess Shale formations and their units. *Palaeogeography, Palaeoclimatology, Palaeoecology*, **277**, 127-140

Powell, W.G., 2003. Greenshist-facies metamorphism of the Burgess Shale and its implications for models of fossil formation and preservation. *Canadian Journal of Earth Sciences,* **40**, 13-724

Prepas, E.E. and Charette, T. 2004. Worldwide eutrophication of water bodies: Causes, concerns, controls. *In*: Environmental Geochemistry, Treatise on Geochemistry Volume 9, Elderfield, H., Holland, H. D. and Turekian, K. K. (Eds.), Elsevier, Amsterdam, Heidelberg, 311-331

Rabalais, N.N., Turner, R.E., Diaz, R.J. and Justić, D., 2009. Global change and eutrophication of coastal waters. *ICES Journal of Marine Science*, **66**, 1528-1537

Rabalais, N.N., Diaz, R.J., Levin, L.A., Turner, R.E., Gilbert, D. and Zhang, J., 2010. Dynamics and distribution of natural and human-caused hypoxia. *Biogeosciences*, **7**, 585-619

Racka, M., Marynowski, L., Filipiak, P. and Sobstel, M., 2010. Anoxic Annulata Events in the Late Famennian of the Holy Cross Mountains (Southern Poland): Geochemical and palaeontological record. *Palaeogeography, Palaeoclimatology, Palaeoecology*, **297**, 549-575

Racki, G., 1998. Frasnian-Famennian biotic crisis: undervalued tectonic control? *Palaeogeography, Palaeoclimatology, Palaeoecology*, **141**, 177-198

Racki, G., 2005. Toward understanding Late Devonian global events: few answers, many questions. *In:* Understanding Late Devonian and Permian-Triassic biotic and climatic events: Towards an integrated approach. Over, D.J., Morrow, J.R., Wignall, P.B. (Eds.), Elsevier, B.V.,Chapter 2, 5-36

Racki, G., Joachimski, M.M. & Morrow, J.R., 2008. A major perturbation of the global carbon budget in the Early-Middle Frasnian transition (Late Devonian) – Preface. *Palaeogeography Palaeoclimatology Palaeoecology*, **269**, 127-129.

Rau, G.H., Arthur, M., and Dean, W.E., 1987. $^{15}N/^{14}N$ variations in Cretaceous Atlantic sedimentary sequences: implication for past changes in marine nitrogen biogeochemistry. *Earth and Planetary Science Letters*, **82**, 269-279

Raymo, M.E. And Ruddiman, W.F., 1992. Tectonic forcing of late Cenozoic climate. *Nature,* **359,** 117-122

Raymo, M.E., Ruddiman, W.F. And Froelich, P.N., 1988. Influence of late Cenozoic mountain building on ocean geochemical cycles. *Geology,* **16,** 649-653

Rimmer, S.M., 2004. Geochemical paleoredox indicators in Devonian-Mississippian black shales, central Appalachian basin (USA). *Chemical Geology*, **206**, 373-391

Rimmer, S.M., Thompson, J.A., Goodnight, S.A. and Robl, T.L., 2004. Multiple controls on the preservation of organic matter in Devonian-Mississippian marine black shales: geochemical and petrographic evidence. *Palaeogeography Palaeoclimatology Palaeoecology*, **215**, 125-154

Riquier, L., Tribovillard, N., Averbuch, O., Devleeschouwer, X. and Riboulleau, A.., 2006. The Late Frasnian Kellwasser horizons of the Harz Mountains (Germany): Two oxygen-deficient periods resulting from different mechanisms. *Chemical Geology*, **233**, 137-155

Sageman B.B., Murphy, A.E., Werne, J.P., Ver Straeten, C.A., Hollander, D.J., Lyons, T.W., 2003.A tale of shales: the relative roles of production, decomposition, and dilution in the accumulation of organic-rich strata, Middle–Upper Devonian, Appalachian basin. *Chemical Geology*, **195**, 229– 273

Schreiber, B.C. and Hsü, K.J. 1980. Evaporites. *In:* Developments in Petroleum Geology, v.2. G.D. Hobson (Ed.), Applied Science Publishers, London, 87-138

Schopf, J.W. and Klein, C., 1992. The Proterozoic Biosphere:, a multidisciplinary study. Cambridge University Press

Schultz, R.B. and Rimmer, S.M. 2004. Geochemistry of organic-rich shales: new perspectives. *Chemical Geology*, **206**, 163-165

Selden, P.A., 1990. Major Events in the History of Life: Terrestrialization: Invertebrates. *In:* Briggs, D.E.G. and Crowther, P.R. (Eds.), Palaeobiology. Blackwell Science, Oxford. 64-68

Selden, P.A., 2001. Major Events in the History of Life: Palaeozoic Events: Terrestrialization of Animals. *In:* Briggs, D.E.G. and Crowther, P.R. (Eds.), Palaeobiology II. Blackwell Science, Oxford, 71-74

Sepkoski, J.J., Jr., 1978. A kinetic model of Phanerozoic taxonomic diversity I. Analysis of marine orders, *Paleobiology*, **4**(3), 223-251

Sepkoski, J.J., Jr., 1979. A kinetic model of Phanerozoic taxonomic diversity II. Early Phanerozoic families and multiple equilibria, *Paleobiology*, **5**(3), 222-251

Sepkoski, J.J., Jr., 1984. A kinetic model of Phanerozoic taxonomic diversity III. Post- Paleozoic families and mass extinctions, *Paleobiology*, 10(2), 246-267

Sepkoski, J.J., Jr., 1990. Evolutionary Faunas. Chapter 1.6 in *Paleobiology*, Briggs et al. 1990. 37-41

Sepkoski, J.J., Jr., 1995. Proterozoic-Early Cambrian Diversification of Metazoans and Metaphytes. Section 11.4, *In*: Schopf, J.W. and Klein, C. (eds.), *The Proterozoic Biosphere*: A Multidisciplinary Study, Cambridge University Press, 553-565

Sepkoski, J.J., Jr., 1997. Biodiversity: Past, Present, and Future. *Journal of Paleontology*, **71(4)**, 533-539

Śliwiński, M.G., Whalen, M.T., and Day, J., 2010, Trace element variations in the Middle Frasnian punctata zone (Late Devonian) in the western Canada sedimentary basin - changes in oceanic bioproductivity and paleoredox spurred by a pulse of terrestrial afforestation? *Geologica Belgica*, **4**, 459–482

Śliwiński, M.G., Whalen, M.T., Newberry, R.J., Payne, J., and Day, J., 2011. Stable Isotope ($\delta^{13}C_{carb\ \&\ org}$, $\delta^{15}N_{org}$) and Trace Element Anomalies during the Late Devonian '*punctata* Event' in the Western Canada Sedimentary Basin. *Palaeogeography, Palaeoclimatology, Palaeoecology*, **307**, 245–271

Śliwiński, M.G., Whalen, M.T., Meyer, F.J. and Majs, F., 2012. Using factor analysis and transmission XRD in capillary to constrain the influence of clastic input on magnetic susceptibility and trace element anomalies during the Late Devonian *punctata* Event in the Western Canada Sedimentary Basin. doi: 10.1111/j.1365-3121.2012.01063.x

Śliwiński, M.G., Spaleta, K.J., Meyer, F.J., Hutton, E.M., Newberry, R.J., Trainor, T.P., Severin, K.P. and Whalen, M.T, 2012. Making low concentration *in- house* pressed pellet trace element standards for carbonate rock analyses by WD-XRF. *Chemical Geology,* **298-299,** 97-115

Stoakes, F.A., 1980. Nature and control of shale basin fill and its effect on reef growth and termination: Upper Devonian Duvernay and Ireton Formations of Alberta, Canada. *Bulletin of Canadian Petroleum Geology,* **28**, 345-410

Struck, U., Emeis, K.C., Voss, M., Krom, M.D., and Rau, G.H., 2001. Biological productivity during sapropel S5 formation in the Eastern Mediterranean Sea: Evidence from stable isotopes of nitrogen and carbon. *Geochimica et Cosmochimca Acta*, **65**(19), 3249-3266

Switzer, S.B., Holland, W.G., Christie, D.S., Graf, G.C., Hedinger, A.S., McAuley, R.J., Wierzbicki, R.A. And Packard, J.J., 1994. Chapter 12 Devonian Woodbend- Winterburn strata of the Western Canada Sedimentary Basin. *In*: Mossop, G.D. and Shetsen, I (Eds.) Geological atlas of the Western Canada Sedimentary Basin; Canadian Society of Petroleum Geologists and Alberta Research Council, Special Report 4, URL: http://www.ags.gov.ab.ca/publications/wcsb_atlas/atlas.htmlN, [December 17, 2011].

Tribovillard, N., Averbuch, O., Devleeschouwer, X., Racki, G. and Riboulleau, A., 2004. Deep-water anoxia over the Frasnian-Famennian boundary (La Serre, France): a tectonically induced oceanic anoxic event? *Terra Nova*, **16**, 288-295

Tribovillard, N., Algeo, T.J., Lyons, T. and Riboulleau, A., 2006. Trace metals as paleoredox and paleoproductivity proxies: An update. *Chemical Geology*, **232**, 12- 32

Tucker, M.E., 2001. Sedimentary Petrology. Blackwell Science, Oxford.

Vahtera, E., Conley, D.J., Gustafsson, B.G., Kuosa, H., Pitkänen, H., Savchuk, O.P., Tamminen, T., Viitasalo, M., Voss, M., Wasmund, N. and Wulff, F., 2007. Internal ecosystem feedbacks enhance nitrogen fixing cyanobacteria blooms and complicate management in the Baltic Sea, *AMBIO,* **36**(2), 186-194

Veizer, J., 1983. Trace elements and isotopes in sedimentary carbonates. *Reviews in Mineralogy: Carbonates: Mineralogy and Chemistry*, **11**, 265-299

Wagreich, M., Hu, X. and Sageman, B. 2011. Causes of oxic-anoxic changes in Cretaceous marine environments and their implications for Earth systems - An introduction. *Sedimentary Geology,* **235,** 1-4

Warren, J.W. 1989. Evaporite Sedimentology: Importance in hydrocarbon accumulation. Prentice Hall, Englewood Cliffs, New Jersey

Warren, J.W., 2010. Evaporites through time: Tectonic, climatic and eustatic controls in marine and nonmarine deposits. *Earth-Science Reviews,* **98,** 217–268

Whalen, M.T., Eberli, G.P., Van Buchem, F.S.P., Mountjoy, E.W. and Homewood, P.W., 2000. Bypass margins, basin-restricted wedges, and platform-to-basin correlation, Upper Devonian, Canadian Rocky Mountains: Implications for sequence stratigraphy of carbonate platform systems. *Journal of Sedimentary Research*, **70**, 913-936

Whalen, M.T., Day, J., Eberli, G.P., Homewood, P.W., 2002. Microbial carbonates as indicators of environmental change and biotic crises in carbonate systems: examples from the Late Devonian, Alberta basin, Canada. *Palaeogeography, Palaeoclimatology, Palaeoecology*, **18**,127-151

Whalen, M.T. and Day, J.E., 2008. Magnetic susceptibility, biostratigraphy, and sequence stratigraphy: insights into Devonian carbonate platform development and basin infilling, western Alberta, Canada. *Society for Sedimentary Geology*, **89**, 291-314

Whalen, M.T. and Day, J.E., 2010. Cross-basin variations in magnetic susceptibility influenced by changing sea level, paleogeography and climate, Upper Devonian Western Canada Sedimentary Basin. *Journal of Sedimentary Research*, **80**, 1109- 1127

Witzke, B.J., 1987. Models for circulation patterns in epicontinental seas applied to paleozoic facies of north america craton. *Paleoceanography*, **2**(2), 229-248

Wood, R., 1993. Nutrients, predation and the history of reef-building. *Palaios*, **8**, 526-543

Yans, J., Corfield, R.M., Racki, G. and Preat, A., 2007. Evidence for perturbation of the carbon cycle in the Middle Frasnian punctata Zone (Late Devonian). *Geological Magazine*, **144**, 263-270

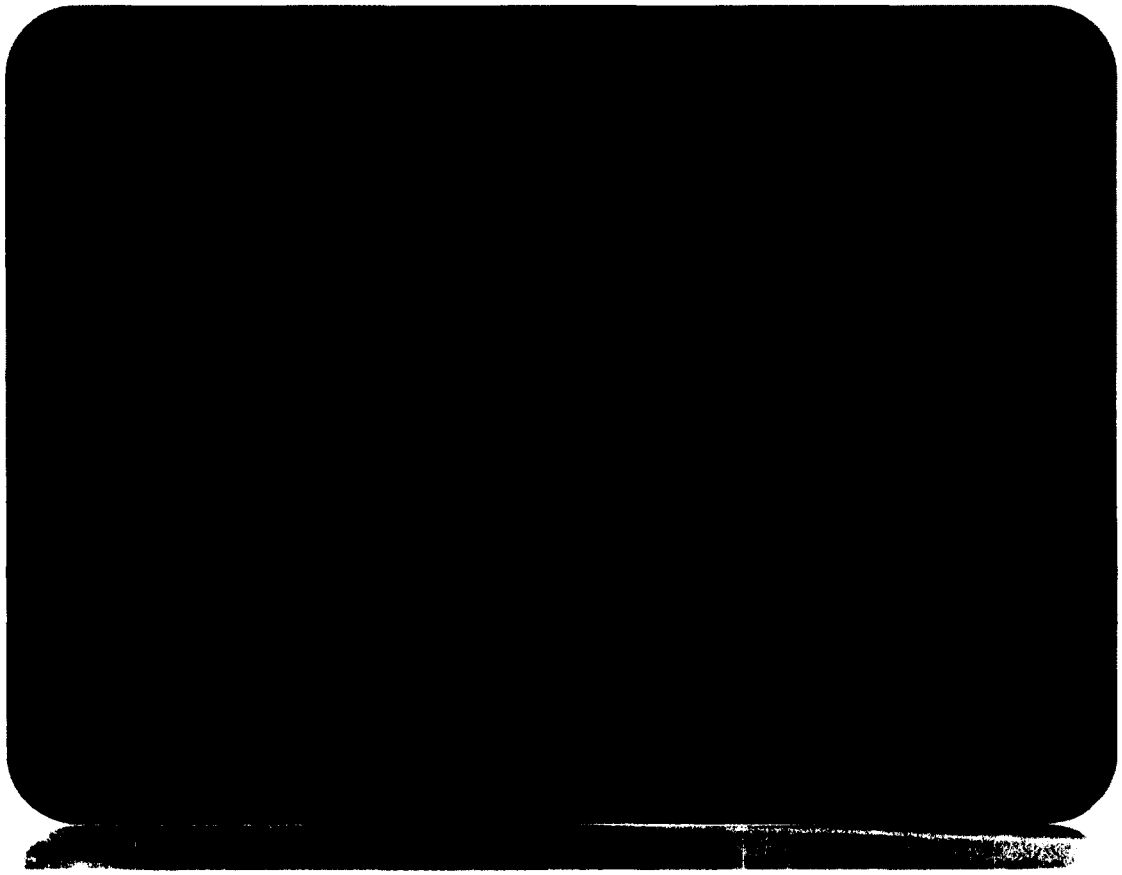

Fig. 1.1. Oldest known stromatolite dated at 3.47 Ga, North Pole, Australia. This stromatolitic structure was produced by the growth and metabolism of mat forming microbial communities and constitutes the oldest certain, indirect fossil evidence of life on the early Earth. Courtesy of R.Buick, Dept. of Earth and Space Science, University of Washington (Buick, 2003).

GEOBIOLOGICAL 'EVENTS' AND OCCURRENCES OF SAPROPELS AND BLACK SHALES THROUGHOUT THE PHANEROZOIC

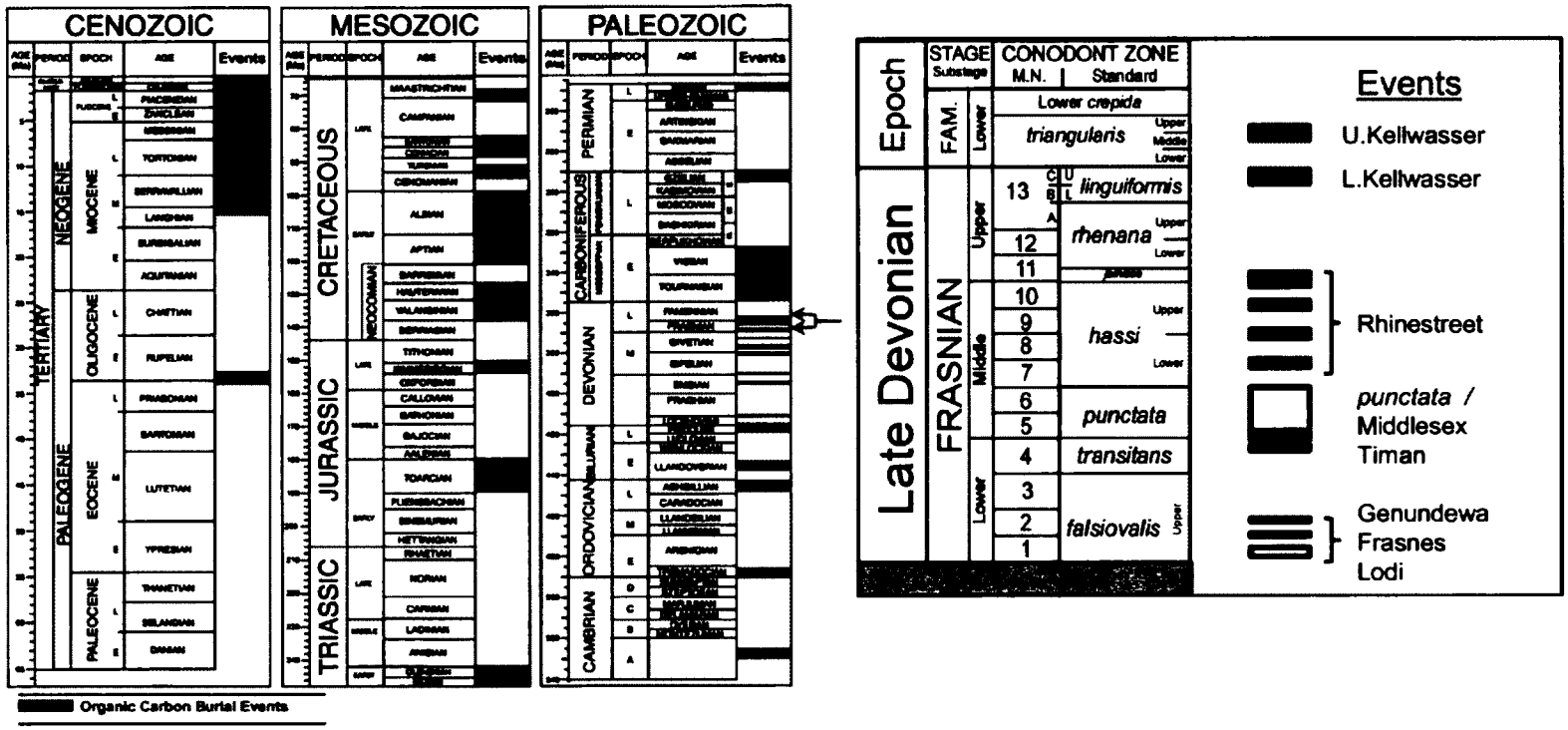

Fig. 1.2. Phanerozoic occurrences of organic matter-rich facies deposition and global geobiological perturbations of the Earth system. Modified after Negri et al., 2006 and House, 2002.

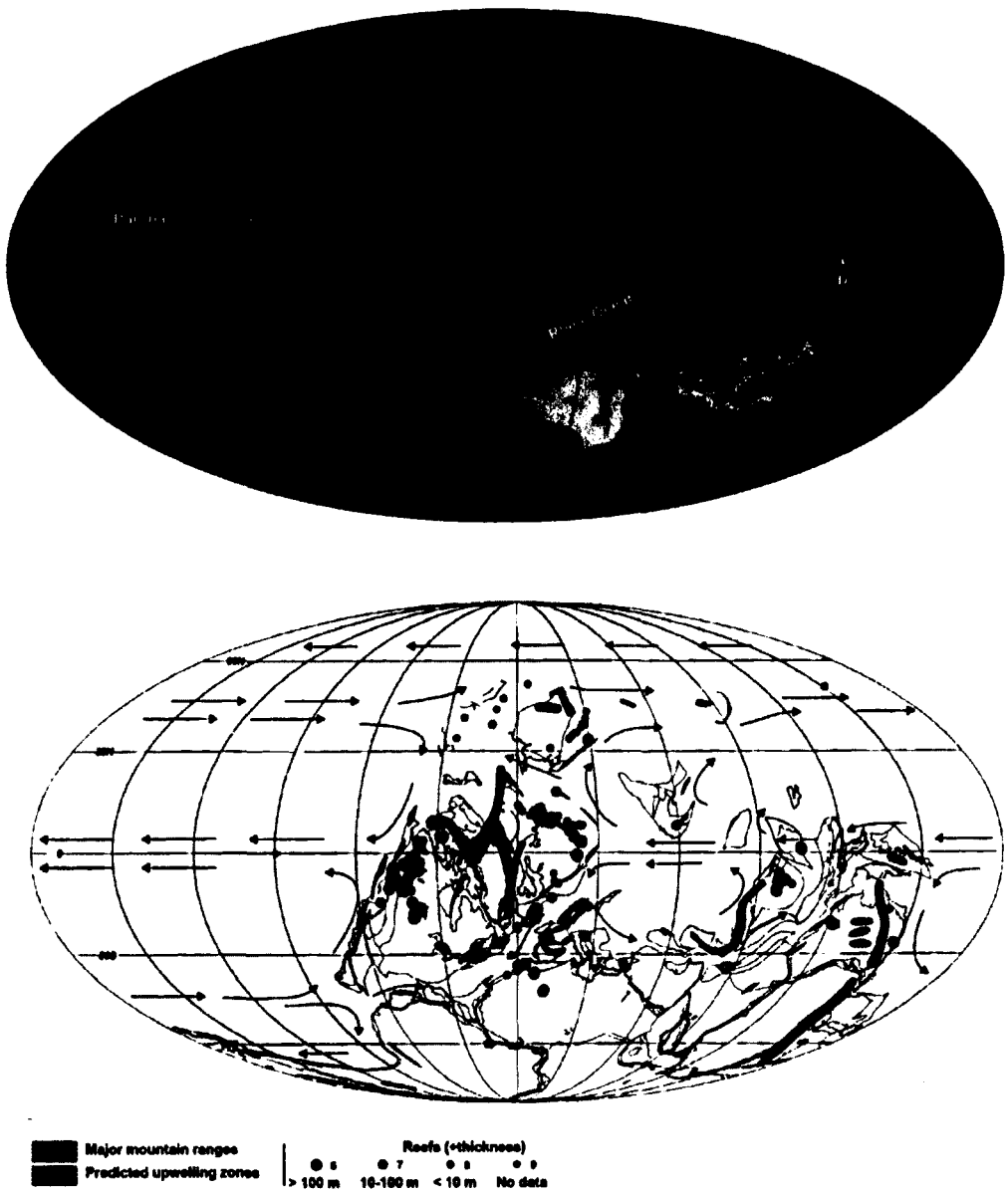

Fig. 1.3. Late Devonian paleogeography. Top: modified after R. Blakey, Northern Arizona University. Source: http://cpgeosystems.com/mollglobe.html. Bottom: Distribution of reef during the Givetian-Frasnian time interval. Modified after Kiessling et al., 1999.

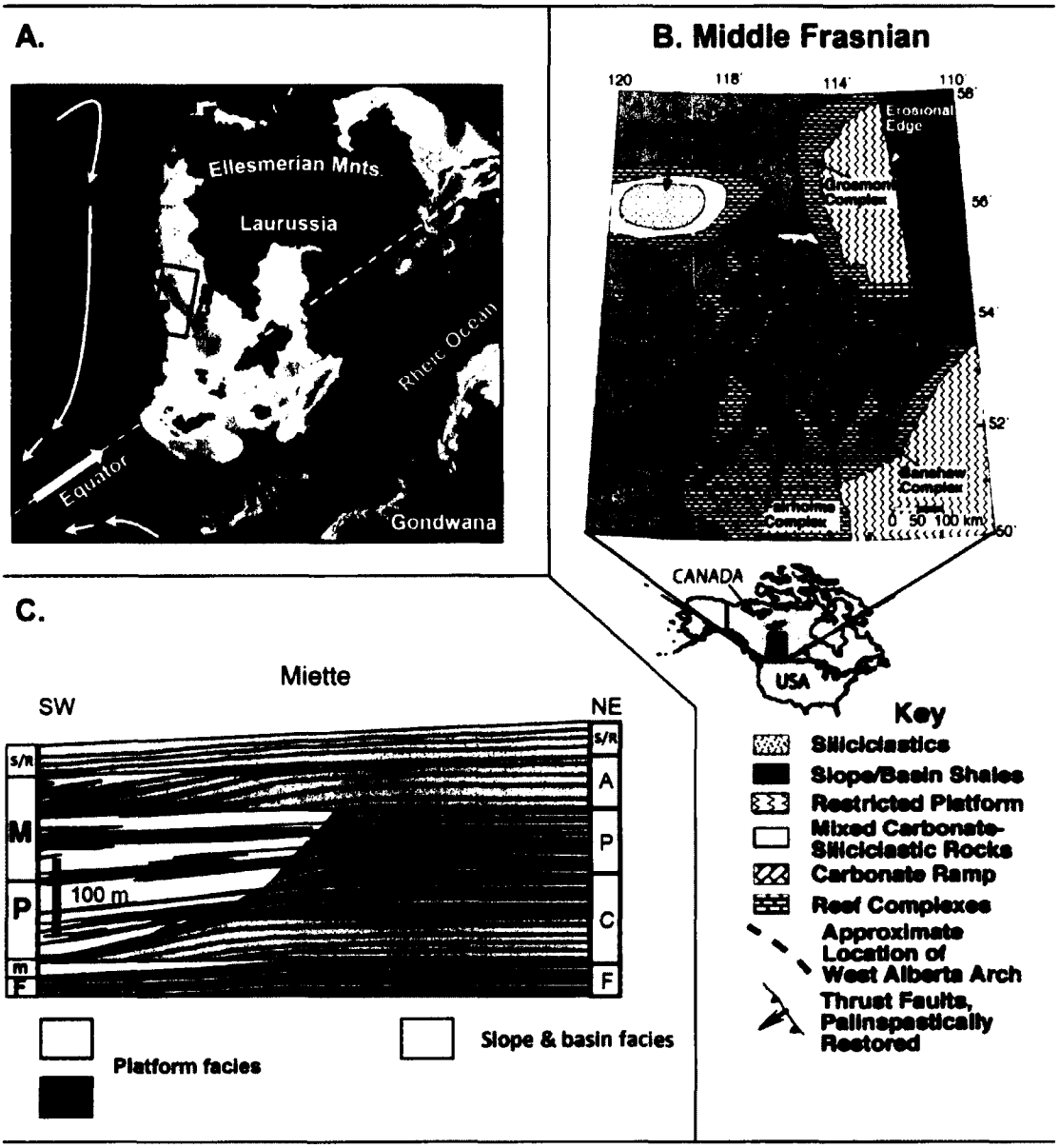

Fig. 1.4. Study area in the WCSB. **A:** Late Devonian paleogeography of North America (basemap modified after R.Blakey, Colorado Plateau Geosystems, Inc.). Circulation patterns after Kiessling et al. (1999). Thick white arrow = equatorial undercurrent. Dot indicates location of the Miette carbonate platform. **B:** Paleogeographic map of the WBSB during Middle Frasnian times. **C:** Cross section of the Miette platform (after Whalen et al., 2000). Key to platform unit abbreviations: F = Flume Fm., C = Cairn, Fm. P = Peechee Mb, A = Arcs Mb., R = Ronde Mb., S = Simla Mb., Southesk Fm. The corresponding slope and basin units are the m - Maligne, P - Perdrix and M- Mt. Hawk formations.

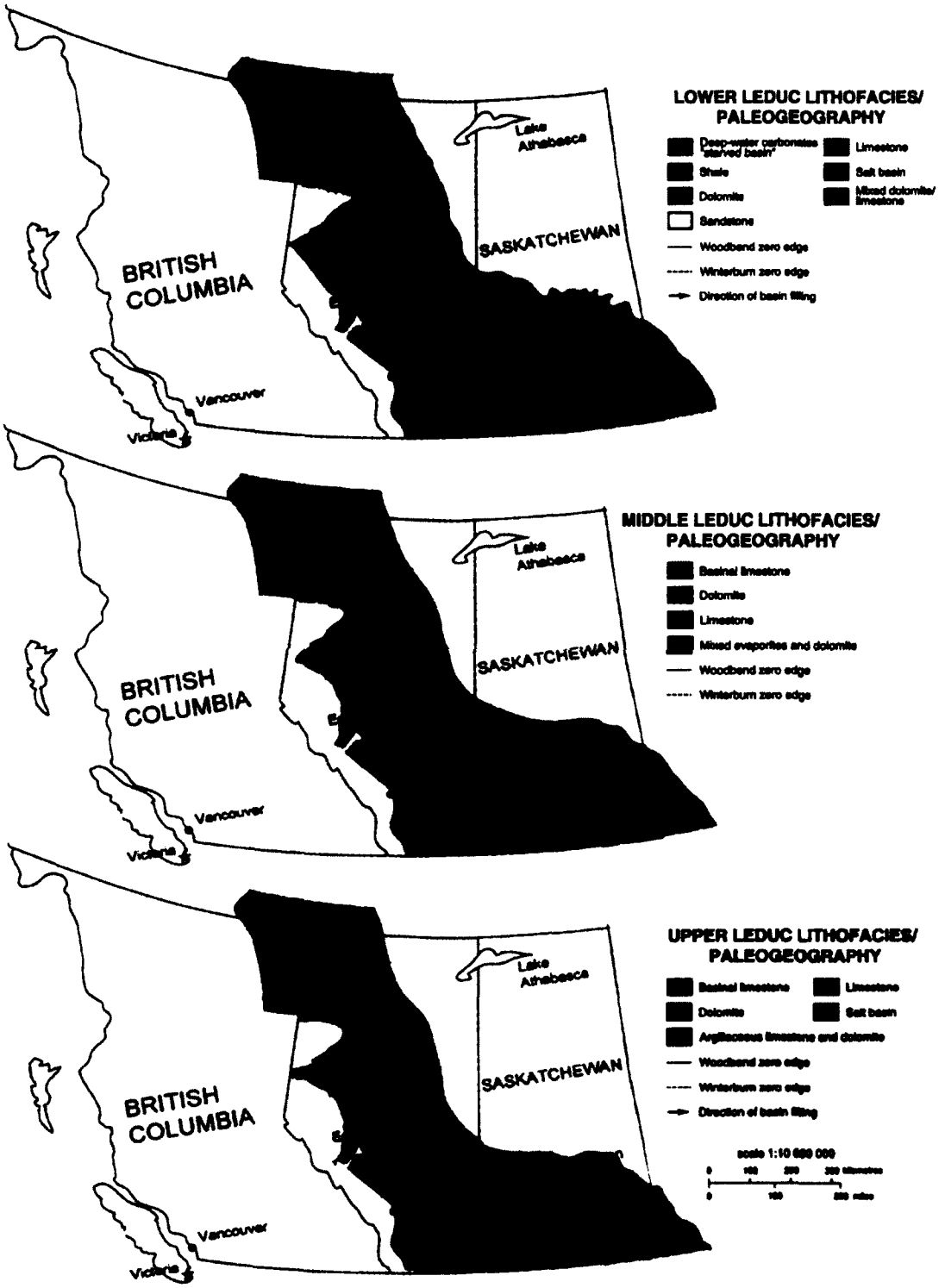

Fig. 1.5. Facies distribution throughout the Late Devonian 'Leduc' time interval in the WCSB during which thick and extensive reef complex developed. Modified after Fig. 12.22 in Switzer et al., (1994).

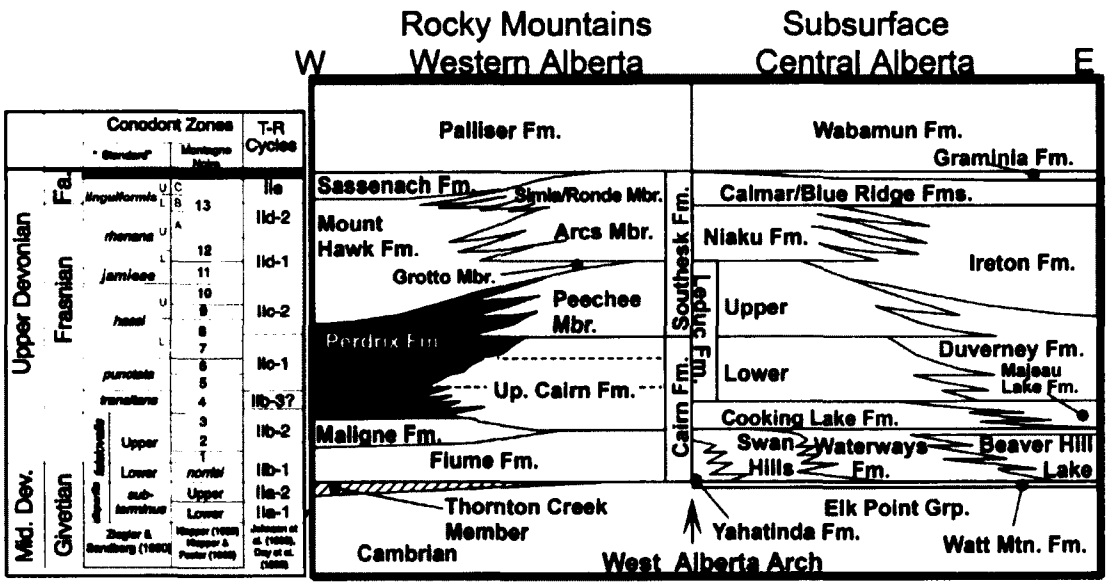

Fig. 1.6. Late Devonian stratigraphy of the Western Canada Sedimentary Basin: Alberta. The lithologies sampled for reconstructing the geochemical record of the *punctata* Event within this basin are the slope/basinal shales and shaley-carbonates of the Perdrix Formation exposed in the Canadian Rockies of Western Alberta. Emphasized are the stratigraphic correlations of the sampled strata in outcrop with the subsurface 'Leduc' buildups elsewhere within the basin. Modified after Whalen et al., 2000.

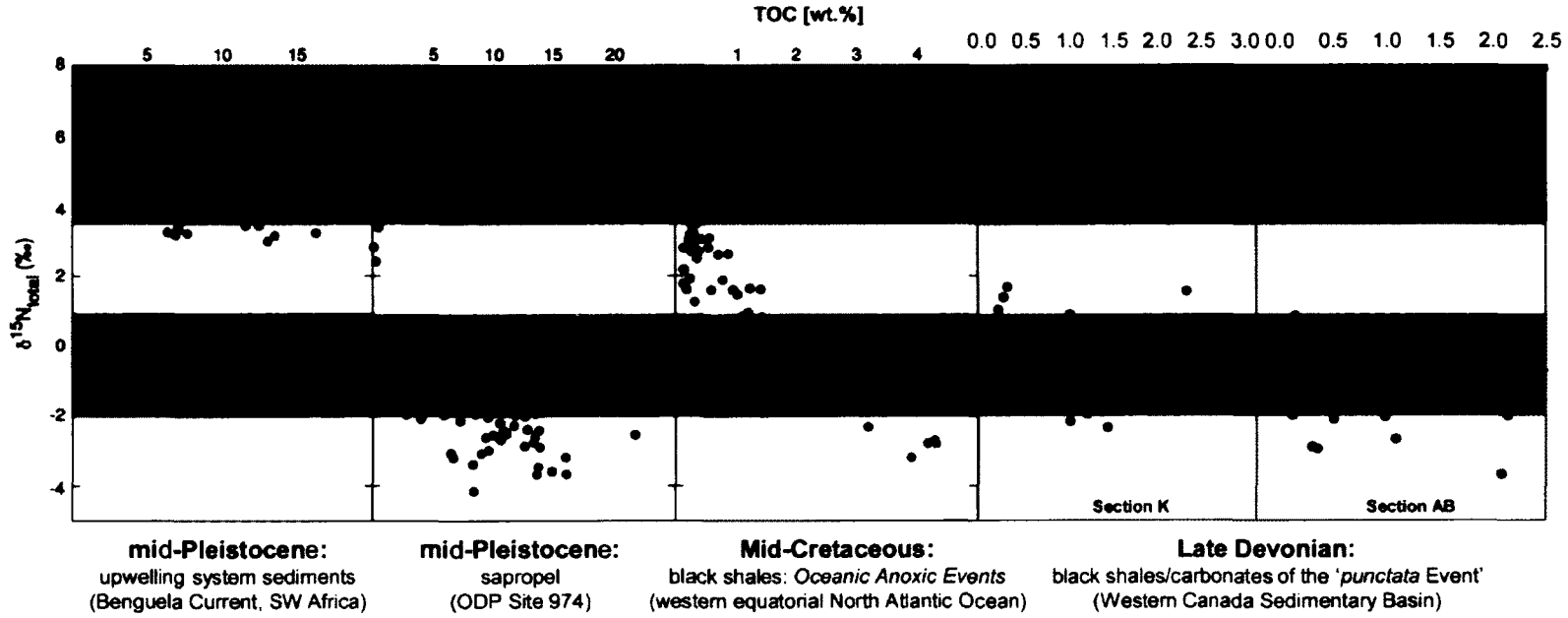

Fig. 1.7. The apparent importance of cyanobacterial nitrogen fixation during times of black shale and sapropel deposition throughout Phanerozoic time. A cross-plot of TOC vs. $\delta^{15}N$ values of sapropels (B.) and black shales/carbonates (C-E) compared against sediments from the most productive regions of the modern ocean - coastal upwelling zones (A.). Datasets presented in (D.) and (E.) are the subject of the present study (Chapter 3) on the geochemistry of the Late Devonian *punctata* Event in the Western Canada Sedimentary Basin. Modified after Fig. 2 in Meyers (2006).

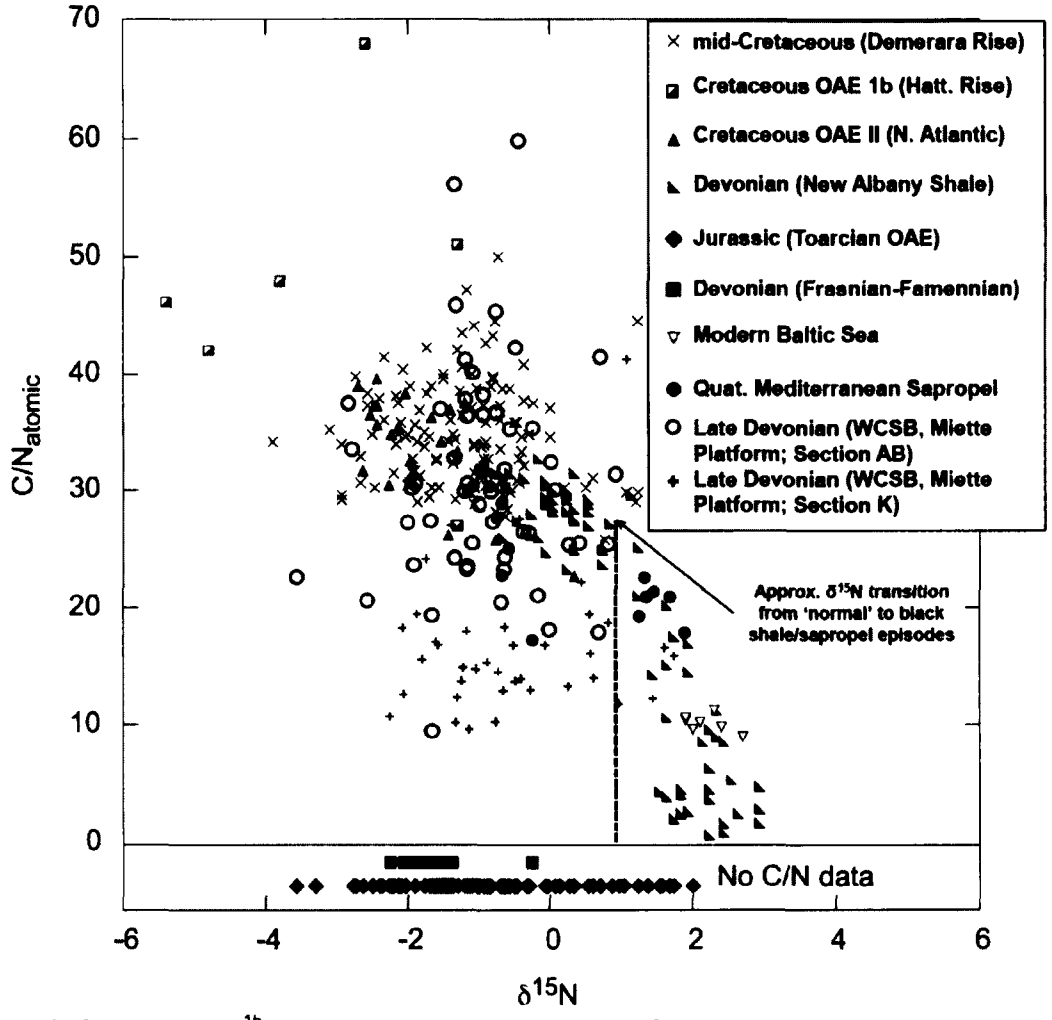

Fig. 1.8. Cross-plot of $\delta^{15}N$ vs. C/N ratios during episodes of black shale and sapropel deposition throughout the Phanerozoic. Such facies always share the following in common: C/N ratios are elevated above normal marine OM (~6-8), whereas $\delta^{15}N$ values are distinctly lower ($\sim \leq 0‰$) than marine OM at (~5‰). Figure modified after Junium and Arthur (2007). Note that the Late Devonian data reported on herein (Miette Platform, Sections AB and K) plot in agreement with 'similar' episodes throughout the Phanerozoic. Dashed vertical line denotes approximate boundary between 'normal' vs. anoxic shale/sapropel intervals in the cited datasets.

Fig. 1.9. Global distribution of over 400 coastal deadzones related to anthropogenic eutrophication. Data compiled by Prof. R.J. Diaz of the Virginia Institute of Marine Science (VIMS) and R.Rosenberg of the Dept. of Marine Ecology, University of Gothenburg, Sweden. Solid white lines denote zones of upwelling.

Sources: Modifed after http://www.vims.edu/research/topics/dead_zones/index.php, Diaz and Rosenberg (2008) and Rabalais et al. (2010).

2. Making low concentration *in-house* pressed pellet trace element standards for carbonate rock analyses by WD-XRF[1]

Abstract

We describe a simple method for making *in-house,* low concentration (0-100 ppm) pressed pellet standards for analyzing Ni, Cu, Mo, V and U in carbonate lithologies by *wavelength dispersive x-ray fluorescence* (WD-XRF) spectrometry. This method can easily be modified to include other elements of interest and to encompass a different range of concentrations. The purpose here was to circumvent the general lack of adequate geological *certified reference materials* (CRMs) having the necessary concentrations of the above five elements that are commonly used in paleoceanographic studies as proxies for changes in bioproductivity and paleoredox conditions in the water column and near the sediment-water interface. Standards were prepared by spiking 99.999% pure calcium carbonate powder with single element, *inductively coupled plasma mass spectrometry* (ICP-MS) standard stock solutions to yield final multi-element mixtures containing 0, 1, 2, 5, 10, 20, 50 and 100 ppm of Ni, Cu, Mo, V and U, independently verified using acid digestion ICP-MS and PROTrace XRF trace element analyses. The level of *in-house* standard homogeneity was determined statistically using ANOVA tests *(analyses of variance)* on count rate data generated for each analyte from three surface transects (50 x 500 µm) ablated on each standard using laser-ablation ICP-MS, demonstrating that all are statistically distinguishable and sufficiently homogenous for the intended purposes of larger spatial scale XRF measurements. The *in-house* standards were then used to refine preexisting XRF calibrations based on a broad suite of non-carbonate geological CRMs. The refined calibrations yield close agreement with ICP-MS and PROTrace XRF-derived values for the suite of *in-house* standards when analyzed repeatedly as 'unknown samples' by the XRF analytical protocol. The precision of sample preparation and analysis was assessed statistically by ANOVA tests on the results of repeated analyses of analyte concentrations for replicate XRF samples prepared from a representative carbonate sample, yielding reproducibility on the order of 1) < 2.5% at the 50-100 ppm level, 2) within ± 5-10% or better at the 10-20 ppm level, 3) within ± 5-15% at the 5 ppm level, and 4) ± 10-55% at the 1-2 ppm level which approaches analytical detection limits. Analytical detection limits and residual calibration backgrounds of the XRF protocol were constrained empirically by repeated analyses of ultrapure calcite blanks.

---

[1] Śliwiński, M.G., Spaleta, K.J., Meyer, F.J., Hutton, E.M., Newberry, R.J., Trainor, T.P., Severin, K.P. and Whalen, M.T., 2012. Making low concentration in-house pressed briquette trace element standards for carbonate rock analyses by WD-XRF. *Chemical Geology,* **298-299,** 97-115

2.1. Introduction

X-ray fluorescence spectroscopy (XRF) is an analytical technique commonly used for quantitatively determining the chemical composition of rocks, soils and sediments. It is based on exciting samples, commonly in the form or finely ground pressed powders (< 63 μm particle size), with X-ray radiation and measuring the intensity of the fluorescent spectrum, within which intensity peaks in discrete regions of energy (keV) / wavelength (Å) characterize the abundances of the elements present (*Goldstein et al., 2003; Potts, 1987; Revenko, 2002; Rose et al., 1986*). It is a comparative analytical technique in which X-ray intensities emitted from a sample are converted to element concentrations via calibrations of measured intensities from materials of known composition (*Potts, 1987*). There is however a general lack of certified reference materials suitable for analyzing the diversity of trace elements that are commonly hosted by carbonate lithologies (*Veizer, 1983; Revenko, 2002*). Our emphasis here is on Ni, Cu, Mo, V and U, which are proxies commonly and reliably used in paleoceanographic studies to trace changes in 1) surface water bioproductivity (Ni, Cu) and 2) redox conditions near the sediment water interface (U, Mo, V) (*e.g. Algeo and Maynard, 2008; Calvert and Pedersen, 1993; Hatch and Leventhal, 1992; Jones and Manning, 1994; Piper and Calvert, 2009; Rimmer, 2004; Rimmer et al., 2004; Riquier et al., 2006; Tribovillard et al., 2006*). Within our samples suites however, these elements frequently occur in concentrations of only several parts per million (ppm) and are thus difficult to measure both accurately and precisely using wavelength dispersive (WD)-XRF in the absence of suitable standards (*Śliwiński et al., 2010, Śliwiński et al., 2011*).

We modified and expanded on the prior methods of *Pearce et al. (1992)* and describe a simple procedure for inexpensively making matrix-matched, *in-house*, low-concentration pressed pellet trace element standards by spiking 99.999% pure calcium carbonate powder with single element ICP-MS (*inductively coupled plasma mass spectrometry*) standard 1000 ppm stock solutions (see also *Craig et al., 2000; Hathorne et al., 2003; Perkins et al., 1991, 1997; Tanaka et al., 2007; Ulens et al., 1994*). Standard compositions were independently verified by acid-digestion ICP-MS and by XRF using PANalytical's PROTrace trace element standard suite, whereas their homogeneity and suitability for XRF use were assessed statistically through analyses of variance on count rate data collected on the surface of each standard for each of the five analytes using laser-ablation(LA)-ICP-MS. The suite of compositionally cross-checked *in-house* standards was then used to verify and refine preexisting XRF trace element analytical protocols that were originally calibrated against siliciclastic geologic standards whose trace element abundances and bulk sample matrices differ from those of carbonate lithologies *(Veizer, 1983; Tables 7-2, 7-3 in Brownlow, 1996; Table 4.5 in Faure, 1998)*. To account for these obvious discrepancies, we relied heavily on 1) careful element by element standard selection and 2)

corrections for the matrix miss-matches between samples and standards based on the rhodium-Compton scatter method of ratioing measured x-ray intensities (*Potts, 1987*).

2.2. Methods

2.2.1. Preparing *in-house* carbonate trace element powders and pressed pellets

In-house trace element standards were prepared using 99.999% pure $CaCO_3$ powder as a matrix (Surepure Chemetals, C.A.S. number: 471-34-1). Trace impurities were determined by the manufacturer using ICP-MS and include Ni, Mo and V from among the analytes of interest, although only at the < 1 ppm level (Table 2.1). For each of the desired final concentrations of 0, 1, 2, 5, 10, 20, 50 and 100 ppm, 10.000 grams of calcite powder were spiked with the needed volumes of single element, 1000 µg/g (ppm) ICP-MS standard stock solutions (Ni: ICP-028, Cu: ICP-029, Mo: ICP-042, V: ICP-023; JT Baker U: 5788-04; matrix solution: 2% HNO_3 acid), closely approximated using the relationship $V_s = C_{dM}/100$, where V_s = µL of single element standard stock solution needed to produce desired final concentration C_d (in ppm) of added element M. Stock solutions were added to calcite powders held in Teflon beakers using high-precision, gravimetrically calibrated micropipettes. The largest total volume of liquid added was the 5 mL needed to make the 100 ppm [Ni, Cu, Mo, V, U]-standard. The acidic matrix solution of the ICP-MS standards caused a brief reaction with the carbonate, inducing a progressively larger, although negligible, loss of calcite with increasing total volume of solution added (5 mL of 2% HNO_3 can only react away approx. 1% of the total 10 g of calcite powder used). The mixtures were oven-dried at 110 °C for about 1 hr to evaporate off excess moisture, and subsequently homogenized in a corundum mortar and pestle. A similar procedure was previously reported by *Pearce et al. (1992)* for making *in-house* carbonate standards for laser ablation ICP-MS analyses.

A 6.5 gram split of each trace element-spiked carbonate powder was mixed with 6 drops of 5% (wt./wt.) polyvinyl alcohol (PVA) binder and pressed under 10 metric tons of pressure into 35 mm diameter, 5 mm thick pellet XRF standards. Another 1 gram split was mixed with two drops of PVA and pressed into 13 mm diameter, 3 mm thick pellets for laser ablation ICP-MS analyses. Lastly, an additional gram was set aside for determining trace element concentrations by acid-digestion ICP-MS. Stock solution additions, powder homogenization and pelletizing was done in order of increasing concentration to minimize cross-contamination.

Two ultrapure $CaCO_3$ pressed pellet blanks were additionally prepared to constrain 1) the level of analytical noise during routine XRF analyses and 2) the level of contamination introduced during sample grinding using SPEX Hardened Steel Vials (99.999% $CaCO_3$, C.A.S. No. 471-34-1, certified to contain impurities only at the sub ppm level; Table 2.1). The first blank was prepared by mixing ~7g of powder with ~7 drops of PVA binder, homogenizing in a quartz-sand

prescrubbed and subsequently 2N HCl washed corundum mortar and pestle, and pressing under 10 tons of pressure. The other was prepared by grinding approx. 10 g of the calcite powder in quartz-sand pre-cleaned (10 minutes of grinding) SPEX Hardened Steel Vials for 6 minutes before mixing with PVA and pressing.

2.2.2. Methods of compositional analysis using liquid digestion ICP-MS

Following the method in *Robinson et al. (2007),* 18 mg of each 1 gram split reserved from each *in-house* standard mixture for liquid digestion was weighed out into acid washed teflon beakers. 0.4 ml of 50% OmniTrace Ultra (EMD Millipore) nitric acid was added to each powder and allowed to sit for two hours to ensure complete digestion of the carbonate. The samples were then diluted with 8.6 ml of Milli-Q water to reach a concentration of approximately 800 ppm Ca, and 2% nitric acid. The samples were diluted further with 2% OmniTrace Ultra nitric acid for a final volume of 36 ml and a Ca concentration of 200 ppm, resulting in a 2000 fold final dilution.

The samples were then analyzed on an *Agilent 7500ce Inductively Coupled Plasma Mass Spectrometer* (ICP-MS) at the University of Alaska Fairbanks *Advanced Instrumentation Laboratory (AIL)* using the operating conditions specified in Table 2.2. Multi-element calibration standards in 2% v/v HNO_3 were prepared for Mg, V, Ni, Cu, Mo and U from ICP-MS standard stock solutions listed previously, covering the concentration range of 0 to 50 ppb. Internal standards of Sc and Ge were added online to standards and samples. Data was collected for 95Mo and 238U in no gas mode; 24Mg, 51V, 58Ni, 60Ni, 63Cu, and 65Cu in Helium gas mode; and for 51C, 58Ni, 60Ni, 63Cu, and 65Cu in Hydrogen gas mode. Dwell times for each isotope were 0.3 seconds except for 51V, 58Ni, 60Ni and 63Cu which were 1.5 seconds. The measurement of each sample was replicated three times in quantitative mode.

2.2.3. Laser Ablation ICP-MS analyses

Laser ablation ICP-MS analyses werer performed using a *New Wave UP213* Nd:YAG laser coupled to an Agilent 7500ce ICP-MS also at AIL. The Agilent 7500ce was operated in normal mode without the use of the reaction cell, with operating parameters as listed in Table 2.2 Ablations were performed in an argon atmosphere. Data was acquired using time resolved analysis mode on the isotopes 26Mg, 34S, 35Cl, 42Ca, 43Ca, 51V, 58Ni, 60Ni, 62Ni, 62Ni, 63Cu, 64Ni, 65Cu, 95Mo, and 238U with dwell times of 0.1 seconds per isotope. Each ablated transect was preceded by a thirty second warm-up period of the laser, operated using the conditions listed in Table 2.2. No preablation of the sample was performed.

2.2.4. X-ray fluorescence analyses

The lithologies we commonly sample come from the Late Devonian of the Western Canada Sedimentary Basin. They consist mostly of carbonate mudstones-wackstones with a total carbonate content of > 90 wt.%, but also of more shaly intervals with a siliciclastic content as high as approx. 50 wt. % *(Whalen et al., 2000)*. Elemental abundances in these lithologies are measured using a *PANalytical Axios wavelength-dispersive x-ray fluorescence spectrometer* (WD-XRF) at AIL. Custom trace element analytical routines were developed and were optimized to 1) detect low concentrations (~0-100 ppm) of various trace elements, Ni, Cu, Mo, V and U among them, and 2) to resolve concentration differences among samples down to the ~0.5-1 ppm level. Calibrations were performed relative to certified geologic standard reference materials (*e.g. United States Geological Survey*, *United States National Institute of Standards and Technology*) and refined using the carbonate matrix-matched *in-house* suite reported on herein. Not all standards were always used in establishing a calibration for each element, usually on account of difficult to resolve spectral line overlaps caused by excessively high concentrations of an interfering element. The accuracy of calibration lines relative to standards is commonly better than 10%, whereas empirically determined detection limits for Ni, Cu, Mo, V and U are on the order of 0.5-1.5 ppm (Table 2.3). Replicate measurements of multiple pressed pellets prepared from a representative carbonate sample constrain the analytical precision for these analytes at 0.3-0.5 ppm (Table 2.3). Samples are prepared by powdering using an aluminosilicate puck mill from SPEX CertiPrep Group and pelletizing as described above.

An alternative method made only recently available in our lab specifically for quantifying trace element abundances in geologic materials using our WD-XRF makes use of PANalytical's PROTrace trace element standard suite and SuperQ software expansion. Routine PROTrace analyses were calibrated to quantify 43 trace elements with detection limits near the 0.5-2 ppm level for the analytes in question (Table 2.3), and serve here as an alternate independent measure (alongside liquid digestion ICP-MS) of *in-house* standard composition.

2.2.5. Statistical analyses

The homogeneity of the *in-house* standards and the precision achieved with ICP-MS and XRF analyses were assessed by ANOVA statistics (*analyses of variance; Davis, 2002*) using measured count rates and derived concentrations using SPSS software. Histograms and one-sample Kolmogorov-Smirnov (K-S) tests (*Davis, 2002*) were used to assess the normalcy of data distributions required by ANOVA tests, which in some cases needed to be adjusted for unequal sample variances as shown by the use of the Levene statistic *(Davis, 2002)*. Log transforms were performed as needed, and subsequent K-S tests were used to verify distribution normalcy.

2.3. Results and interpretations of *in-house* standard analyses

Concentrations of Ni, Cu, Mo, V and U measured by acid digestion ICP-MS (Table 2.4) for each of the *in-house* standards fall along well-defined linear trends (R^2: 0.09889-0.9982; Fig. 2.1 A and B) which reflect internal consistency and a systematic increase in analyte concentrations across the calibration range (R^2 = 0.9998-1.0000 for the set of solution ICP-MS calibration standards). Note however that regression slope values differ to within ± 5-25 % of an ideal 1:1 correspondence (slope = b = 1) between concentrations measured by solution ICP-MS and those expected based on the volumes of spike solutions added (Fig. 2.1 A and B). We emphasize, however, that the objective of this work was to create an internally consistent, highly correlated set of *in-house* standards with analyte concentrations *approximately* near those expected.

The abundances of each trace metal within the *in-house* standards were also determined independently of solution ICP-MS by using an XRF analytical protocol calibrated against PANalytical's suite of PROTrace element standards (Fig. 2.1 A and B, Table 2.5). Measurements again fall along well-defined linear trends (R^2: 0.9930-0.9995; Fig. 2.1 A and B) while deviations from an ideal 1:1 correspondence (slope = b = 1) with the values expected measure to within only ± 4.5-13% and are smaller than those associated with the ICP-MS analyses. Nonetheless, results of both sets of analyses correlate strongly (R^2: 0.9796-0.9971; Fig. 2.1 C) and provide two independent measures of trace metal concentrations within the *in-house* standards. One-sample t-tests indicate, however, that 1) the slopes values of linear regressions fitted to the cross-plots of PROTrace XRF vs. ICP-MS measurements (Fig. 2.1 C) are significantly different at the 99.9% level from an ideal 1:1 correspondence (b =1) for all analytes with the exception of and V and Ni

2.3.1. Assessment of *in-house* standard homogeneity by LA-ICP-MS

The laser ablation ICP-MS analyses, testing for *in-house* standard homogeneity, contain several layers of information requiring a statistical approach to effectively determine their results and implications. Three laser transects, each measuring 50 x 500 µm, were ablated on three spatially random locations on each of the eight standards. Data are presented for the isotopes Ni-58, Cu-65, Mo-95, V-51 and U-238 as the logarithm (base 10) of count rates on those portions of the laser ablation profiles that form a 'mesa' (or a plateau that is above the analytical background beginning at around t = 20 sec.; Appendix A). Count rates were corrected for the average analytical background by subtraction, and subsequently normalized to the count rate of the Ca-42 internal standard to account for instrumental drift and to thus allow comparisons among replicate analyses (Fig. 2.2). Because almost all count rate distributions were log-normal, a log transform was applied to satisfy the normal distribution criterion required by subsequent ANOVA statistics;

K-S tests confirm the normalcy of the transformed distributions for 115/120 cases at the 95% confidence level (failing cases: Mo95-20ppm, Mo95-100 ppm, U238-1ppm, Fig. 2.2), and for 118/120 cases if the 99% level is considered (failing cases: V51-10ppm and U238-Blank, Fig. 2.2). Count rates rather than concentrations are presented for two reason: 1) there is a general lack of suitable, matrix-matched LA-ICP-MS carbonate standards for the trace elements of interest *(see Pearce et al., 1992; Craig et al., 2000; Perkins et al., 1991, 1997)*, and 2) count rate data undergoes less processing and manipulation, and thus seems more appropriate for statistical purposes as a means of assessing the variability of sample response during analysis. The data was analyzed from the following statistical perspectives, revealing information on several levels.

2.3.2.1. Analysis of spatial homogeneity of each *in-house* standard

An ANOVA analysis, adjusted for inequality of variances where necessary, was performed to determine if the mean analyte count rates measured on each of the three laser transects per standard are statistically distinguishable (Fig. 2.2, Appendix A). At the 95% confidence level (a=5%) the ANOVA tests revealed no significant differences between the mean plateau count rates measured by the three ablation profiles for 21 of the 40 cases. When a confidence level of 99% was considered, eight additional observations (total 29/40) showed an equality of means in the ANOVA analysis. For the remaining 11 cases a statistically significant inhomogeneity could be determined. However, three of these cases represent standard blanks with several outlying noisy points which likely account for the fact that the ANOVA analyses identified at least one of the three transects as statistically different from the others (Ni-58-Blank, Cu-65-Blank and U-238-Blank, Fig. 2.2). Five additional cases represent the distribution of Mo, which is much more uniform for the 1, 5 and 10 ppm standards than it is for the other elements (Mo-95-1ppm, 5, and 10 ppm standards; Appendix A). This allows for a statistical resolution of smaller differences among mean values, leading to a comparatively inappropriate rejection by ANOVA tests (possibly also for Cu65-2ppm and V51-20ppm). At the 20 and 50 ppm levels, one of the three Mo ablation profiles show deflections in narrow regions above the otherwise generally uniform trends, allowing ANOVA statistics to identify one transect as different from the others (Mo95-20ppm and 50ppm). The same appears to be true for Ni-58 at the 50 ppm level.

The dominant pattern in the laser ablation analyses is one that trends strongly towards standard homogeneity across each of three measured transects. 37/40 cases can be presumed to be sufficiently homogenous. It is noteworthy however to emphasize the scale of the LA-ICP-MS analyses compared to the ultimate intended scale of analysis using the suite of *in-house* standards for XRF spectroscopy. The total area sampled with the laser transects on each

standard measures approx. 75,000 μm^2, a mere 0.013% of the total area analyzed with a 27mm collimator on the XRF spectrometer (5.72×10^8 μm^2; integration down to the penetration depth of both the laser and the incident X-ray beam have been omitted here for simplicity). The above observed level of homogeneity was achieved using only a mortar and pestle. It is interesting to consider whether an alternative mixing scheme, *e.g.* using methacrylate vials and balls to minimize metal contamination (available from SPEX), would result in a higher degree of powder uniformity across only three spatially random, 50 x 500 µm ablation transects. While we consider these *in-house* standards sufficiently homogenous for the intended XRF use, we would opt for such an alternate mixing method and for a more extensive assessment of surface homogeneity if they were to be used as calibration standards for LA-ICP-MS (*e.g.* by sampling a larger surface area with additional transects, either on replicate pellets or alternatively on both sides of each single pellet prepared).

2.3.2.2. Statistical analysis of count rate differences among standards with increasing analyte concentrations

After it was determined in the previous test that the count rates measured from the three LA-ICP-MS transects per standard are sufficiently similar for all cases, data from each set of replicate transects were sorted and pooled into one of five larger populations representing each of the five analytes measured (Ni, Cu, Mo, V, U). This was done to assess whether the overall mean count rate for each element in each standard is statistically distinguishable from all others throughout the suite representing the 0-100 ppm concentration range. Log-transformed data was used as a basis. An unequal variances ANOVA (robust test of equality of mean using Welch statistics) and post hoc tests (Tamhane's T2 conservative pairwise, t-test based comparisons) confirmed significant differences for all analytes and all standards at the > 99.9% confidence level, with the single exception of the V-51 blank and 1 ppm standards, between which the difference of means is not significant at the 95% level.

2.4. Discussion: applications of the *in-house* standards in refining preexisting XRF trace element analytical protocols

The following discussion focuses on the refinement of our preexisting XRF calibrations intended for analyzing the carbonate lithologies we commonly sample by 1) incorporating the suite of *in-house* standards, 2) evaluating the agreement between these modified calibrations and the results of the ICP-MS and PROTrace XRF analyses, 3) empirically constraining the absolute backgrounds and detection limits that our calibrations afford using ultrapure calcite blanks, and

finally 4) statistically evaluating the analytical precision of replicate measurements made on replicate samples.

2.4.1. Refining XRF trace element analytical routines using the *in-house* standards

Preexisting XRF trace element calibrations for Ni, Cu, Mo, V and U based on various non-carbonate geologic CRMs were refined by the addition of the suite of matrix-matched and ICP-MS/PROTRrace XRF cross-checked *in-house* standards. Slopes and intercepts of fitted linear regressions where readjusted for Mo, V and U to accommodate the additional standards which effectively expanded the original calibration ranges through to approx. the 100 ppm level. The original calibration windows for Cu and Ni, however, extended from 0 to ~250 ppm, and the set of 0-100 ppm *in-house* standards are seen to plot agreeably within them (Fig. 2.3). Each *in-house* standard was assigned the Ni, Cu, Mo, V and U concentrations measured by ICP-MS and each was then analyzed three times consecutively as an 'unknown sample' to gauge the level of agreement relative to the ICP-MS/PROTrace XRF results, but also to determine the level of analytical precision with increasing trace metal abundance across the calibration range (Figs. 2.4 and 2.5, Table 2.6). Standard deviations, listed as a percentage of the mean values measured for each element in each standard by XRF are 1) < 2.5% at the 50-100 ppm analyte concentration level, 2) within ± 5-10% at the 10-20 ppm level, 3) within ± 5-15% at the 5 ppm level, and 4) decrease to ± 10-55% at the 1-2 ppm level which begins to overlap with analytical detection limits (Tables 2.3 and 2.6). Cross-plotting results obtained for each of the five analytes in the suite of *in-house* standards by ICP-MS and the XRF routine, the latter calibrated against both *in-house* and various certified geologic standards, yields a near 1:1 correspondence for Cu, Mo, and U (slope values between b = 0.9903 and 1.0243; R^2: 0.9944-0.9986), a -12% deviation in slope from the ideal b = 1 for Ni (b = 0.8786; R^2: 0.9918) and a -6% deviation in slope from an ideal correspondence for V (b = 0.9396, R^2: 0.9930; Fig. 2.5 A). One sample t-tests show that 1) the slope values of linear regressions fitted to cross-plots of measurements by ICP-MS and the XRF routine are statistically different from b = 1 at the 95% confidence level for the analytes Ni, Cu and V. Cross-plotting results obtained by PROTrace XRF and the XRF routine calibrated against both *in-house* and certified geologic standards yields deviations from an ideal 1:1 correspondence that measure within ± 4.5-22% of b = 1 (Fig. 2.5 B). To again statistically confirm the correspondence of both sets of measurements, the calculated regression slopes were tested against the expectation of b = 1 using one-sample t-tests. At the 95% confidence level, the difference in slope from b = 1 was shown to be significant for all five analytes. This partially reflects the ± 12-26% discrepancies from an ideal correspondence noted between *in-house*

standard values determined by PROTrace XRF and ICP-MS for Cu, Mo and U (Fig. 2.1 C) and the 1-1.5% discrepancies for Ni and V.

2.4.2. Empirically determined lowest levels of detection (LLDs) and absolute backgrounds in the XRF analytical protocol

Analytical detection limits and absolute calibration backgrounds of the XRF analytical protocol were determined by noting the apparent concentrations and associated uncertainties measured on each analyte's spectral peak position on the zero-concentration blanks (Fig. 2.6). Backgrounds arise as a result of the X-ray continuum spectrum generated during sample excitation (*bremsstrahlung* (breaking) radiation), with energies ranging from zero keV up through the operating potential of the X-ray tube (*Potts, 1987*). The X-ray count rate generated at each analyte's peak position is converted to a concentration via *intensity vs. concentration* calibrations (commonly linear regressions) defined using a carefully chosen set of CRMs. However, in cases where the calibration regression does not intercept the origin of *intensity vs. concentration* plots, an apparent small positive or small negative concentration value is necessarily assigned for an analyte in the zero-concentration standard. This calibration artifact is corrected for by either adding or subtracting its apparent value when it is respectively negative or positive, from all subsequently measured samples. Small positive backgrounds were noted for the calibrations of Ni, Cu, Mo, V and U after analyzing the ultrapure blanks 24 times consecutively (Fig. 2.6), and range from a mere 0.4 ppm (U) to 2.3 ppm (Ni; Table 2.6). The first set of 12 analyses (Run #s 1-12, Fig. 2.6) were performed on the ultrapure calcite blank prepared with no prior grinding in the commonly used SPEX hardened steel vials, whereas the latter 12 analyses (Run #s 13-24) were performed on the blank prepared after six minutes of grinding. No apparent differences are noted between the two sets of analyses for all five analytes (Fig. 2.6), implying only a negligible contribution of Ni, Cu, Mo, V and U impurities introduced from the grinding equipment. Lowest levels of analytical detection were defined as three standard deviations (3σ) of the pooled average of all 24 analyses and fall within the 0.5-1.5 ppm range (Table 2.6).

2.4.3. Constraining analytical uncertainties in the XRF analytical protocol: precision in sample preparation and analysis

The precision (reproducibility) of results obtained by our XRF analytical protocol and sample preparation procedure was evaluated by replicate analyses (18 total) of a set of three pressed pellets prepared from the same representative carbonate sample.

Several different factors contribute to analytical uncertainties in XRF measurements. These include 1) counting statistical errors (CSEs) which reflect the certainty to which the

measured X-ray intensity (the count rate) is determined for a given experimental setup; 2) calibration errors, which reflect the accuracy of the protocol relative to calibration standards; 3) the uncertainties associated with reported concentrations for CRMs; and 4) inconsistencies in sample preparation, including inadequate sample homogeneity. These sources of analytical uncertainty become increasingly important as analyte abundances approach analytical detection limits (*Potts, 1987*).

2.4.3.1. Replicate analyses of individual XRF samples

The precision of individual sample analyses was assessed on both 1) the set of eight *in-house* standards, each of which was analyzed 3x as an unknown (Table 2.6, Figs. 2.4 and 2.7), and 2) on three XRF pellets prepared from a representative carbonate sample and analyzed 6x each (Table 2.7). Replicate measurements of Ni, Cu, V, Mo, U abundances indicate that the analytical precision, expressed as a percentage of the calculated average, is: 1) < 2.5% at the 50-100 ppm level, 2) within ± 5-10% in the 10-20 ppm range, 3) within ± 5-15% at the 5 ppm level, and 4) decreases to ± 10-50% at the 1-2 ppm level which begins to overlap with detection limits (Tables 2.6 and 2.7; note the apparent random error in one of the three V analyses in Table 2.6 (20ppm Syn.Carb.std) which increases the uncertainty to 11.0% of the calculated average. In contrast, the precision is at the ± 4% level for the next lower concentration standard (10ppm Syn.Carb.std), and is an average of 3.4% for the set of three replicate samples with a measured V concentration of ~15 ppm; Table 2.7).

2.4.3.2. Replicate analyses of replicate XRF samples

Results of multiple analyses of three replicate XRF samples (6x each) were used to statistically demonstrate the consistency of the sample preparation procedure and of the analytical protocol using an analysis of variance on three populations of observations (Table 2.7, Fig. 2.8). An ANOVA test, however, requires that three conditions be met for its output to be statistically sound: 1) each group of analyses whose calculated averages are compared must represent random samples from distinct populations; 2) each sample's parent population must be normally distributed; and 3) each parent population must have the same variance. Conditions 1) and 3) are met by the nature of the fact that three pressed pellets were prepared from one sample and analyzed multiple times (hence 3 groups of analyses representing the three replicate samples, analyzed 6 times). Condition 2) is more difficult to satisfy because of the cost associated with generating a sufficiently large number of observations per sample to demonstrate the normalcy of distribution of the parent population. However, an alternative set of analyses is of help here. An independent set of XRF analyses were used to determine the X-ray intensity of only

the Rh-Compton spectral peak position as scattered from three different metal standards a total of 100 times each (Ti, Ag and Brass discs; 40 sec. on peak, 10 sec. on each of two backgrounds). One sample K-S tests (*Davis, 2002)* were applied to the raw X-ray intensity data to assess distribution normalcy (Fig. 2.9); as the significance values of all tests is larger than the chosen alpha level of a=5%, we can assume that the data follows a normal distribution in each case (Fig. 2.9). This result is consistent with the commonly used approximation in which X-ray intensities are modeled using normal distributions for large numbers of X-ray counts measured *(Goldstein et al., 2003, pg. 440; Potts, 1987)*. It is thus assumed that each set of six analyses per each of the three replicate samples prepared represents a subsample of a likewise normally distributed parent population and allows for the use of an ANOVA to cross-compare population means. A test of the homogeneity of variances for each of the three groups shows no significant differences at the 95% confidence level, allowing for the use of a simple 'equal variances ANOVA' test, which demonstrates that no significant differences exists at this same level of certainty in the mean measured concentrations of each element among the three samples.

2.5. Conclusions

-Low concentration (0-100 ppm) carbonate trace element standards can be readily prepared *in-house* by: 1) spiking ultrapure calcite powders (99.999% $CaCO_3$) with variable volumes of single element, standard 1000 ppm ICP-MS stock solutions, 2) drying and homogenizing, 3) verifying compositions by acid digestion ICP-MS and *e.g.* PROTrace XRF, and 3) pressing into pellets of desired size for use as *in-house* standards in XRF calibrations or, as previously demonstrated by *Pearce et al.* (1992) for use in laser ablation ICP-MS analyses.

-This method is inexpensive, straightforward to carry out in the laboratory, and can help circumvent the general lack of certified standards suitable for the analysis of various trace elements that are commonly measured in carbonate lithologies and used as proxies of paleoceanographic changes. Further, it is easily tailored to 1) only those elements of interest, 2) to the specific calibration range desired, and 3) can help improve XRF calibrations set against other certified geologic standards that may not be optimally matched to the samples of interest.

-Laser-ablation-ICP-MS and analyses of variance (ANOVA, 95% confidence level) tests of the *in-house* standards show a sufficient level of count rate homogeneity across each of three random spatial transects measured (50 x 500 µm each), which collectively account for only 0.013% of the total surface area analyzed with the intended use in XRF calibrations. With the single exception of the V-51-blank and V-51 1 ppm preparations, all standards are statistically distinguishable from each other at the 95% confidence level (0, 1, 2, 5, 10, 20, 50, 100 ppm-Ni, Cu, Mo, V, U).

-Cross-plotting the concentrations of Ni, Cu, Mo, V and U measured in each of the *in-house* standards by our XRF protocol (calibrated against both these and other certified geologic standards) against the independent compositional analyses using acid digestion ICP-MS and PROTrace XRF yields overall good agreement (R^2 values > 0.99) indicating that concentrations of each analyte can be reliably measured in the 0-100 ppm range typical of the lithologies we commonly sample.

-The precision of the XRF sample preparation procedure and analytical protocol was evaluated by replicate analyses (6x) of three pressed pellets prepared from the same representative carbonate sample. Analyses of variance reveal no significant differences at the 95% confidence level among the calculated average concentrations of Ni, Cu, Mo, V and U. The precision, expressed as a percentage of the mean, is on the order of 1) < 2.5% at the 50-100 ppm concentration level, 2) better than ± 5-10% at the 10-20 ppm level, 3) ± 5-15% near the 5 ppm level, and 4) decreases to ± 10-55% at the 1-2 ppm level which begins to overlap with analytical detection limits.

Acknowledgments

This work was performed using the analytical instrumentation and resources of the *Advanced Instrumentation Laboratory* (AIL), University of Alaska Fairbanks. We kindly thank UAF Vice Chancellor of Research for additional funding that made this work possible as well as the UAF Technology Advisory Board for a grant that helped AIL outfit the XRF lab with the latest trace element analytical capabilities (2011, Śliwiński and Severin)

2.6. References:

Algeo, T.J. and Maynard, J.B., 2008. Trace-metal covariation as a guide to water-mass conditions in ancient anoxic marine environments. *Geosph.*, **4**, 872-887

Brownlow, A.H. 1996. Geochemistry (2nd Edition). Prentice Hall.

Calvert, S.E. and Pedersen, T.F., 1993. Geochemistry of recent oxic and anoxic marine sediments - implications for the geological record. *Mar. Geol.*, **113**(1-2), 67-88

Craig, C-A., Jarvis, K.E. and Clarke, L.J., 2000. An assessment of calibration strategies for the quantitative and semi-quantitative analysis of calcium carbonate matrices by laser ablation-inductively coupled plasma-mass spectrometry (LA-ICP-MS). *J. Anal. At. Spectrom.,* **15,** 1001-1008

Davis, J.C., 2002. Statistics and Data Analysis in Geology (3rd ed.). New York: John Wiley & Sons, 656 p.

Faure, G., 1998. *Principles and Applications of Geochemistry (2nd Edition).* Prentice Hall, Upper Saddle River

Goldstein, J., Newbury, D., Joy, D., Lyman, C., Echlin, P., Lifshin, E., Sawyer, L., and Michael, J., 2003. Scanning Electron Microscopy and X-ray Microanalysis (3rd edition.). Springer.

Hatch, J.R. and Leventhal, J.S., 1992. Relationship between inferred redox potential of the depositional environment and geochemistry of the Upper Pennsylvanian (Missourian) Stark Shale Member of the Dennis Limestone, Wabaunsee Country, Kansas, U.S.A. *Chem. Geol.*, **99**, 65-82

Hathorne, E.C., Alard, O., James, R.H. and Rogers, N.W. 2003. Determination of intratest variability of trace elements in foraminifera by laser ablation inductively coupled plasma-mass spectrometry. *Geochem. Geophy. Geosy.*, **12**(4), 1-14

Jones, B. and Manning, D.A.C., 1994. Comparison of geochemical indices used for the interpretation of paleoredox conditions in ancient mudstone. *Chem. Geol.*, **111**, 111-129

Pearce, N.J.G., Perkins, W.T., and Fuge, R., 1992. Developments in the quantitative and semiquantitative determination of trace elements in carbonates by laser ablation inductively coupled plasma mass spectrometry. *J. Anal. Atom. Spectrom.,* 7, 595- 598

Perkins, W.T., Fuge, R. and Pearce, N.J.G., 1991. Quantitative analysis of trace elements in carbonates using laser ablation inductively coupled plasma mass spectrometry. *J. Anal. Atom. Spectrom.,* **6,** 445-449

Perkins, W.T., Pearce, N.J.G. and Westgate, J.A., 1997. The development of laser ablation ICP-MS and calibration strategies: examples from the analysis of trace elements in volcanic glass shards and sulfide minerals. *Geostandard Newslett.*, **21,** 175-190

Piper, D.Z. and Calvert, S.E., 2009. A marine biogeochemical perspective on black shale deposition. *Earth Sci. Rev.*, **95**, 63-96

Potts, P.J. 1987. A Handbook of Silicate Rock Analysis. Blackie Academic & Professional.

Revenko, A.G., 2002. X-ray fluorescence analysis of rocks, soils and sediments. *X-ray Spectrosc.*, **31**, 264-273

Rimmer, S.M., 2004. Geochemical paleoredox indicators in Devonian-Mississippian black shales, central Appalachian basin (USA). *Chem. Geol.*, **206**, 373-391

Rimmer, S.M., Thompson, J.A., Goodnight, S.A. and Robl, T.L., 2004. Multiple controls on the preservation of organic matter in Devonian-Mississippian marine black shales: geochemical and petrographic evidence. *Palaeogeo. Palaeoclim. Palaeoecol.*, **215**, 125-154

Riquier, L., Tribovillard, N., Averbuch, O., Devleeschouwer, X. and Riboulleau, A., 2006. The Late Frasnian Kellwasser horizons of the Harz Mountains (Germany): Two oxygen-deficient periods resulting from different mechanisms. *Chem. Geol.*, **233**, 137-155

Robinson, C. D., Devalla, S., Rompais, M., and Davies, I. M., 2009. Solution-based determination of trace elements in biogenic carbonates: comparison of two sample introduction systems for use in flow injection ICPMS analysis. *J. Anal. At. Spectrom*, **24**, 939-943

Rose, W.I., Bornhorst, T.J. and Sivonent, S.J. 1986. Rapid, high-quality major and trace element analysis of powdered rock by X-ray fluorescence spectrometry. *X-ray Spec.*, **24,** 939-943

Śliwiński, M.G., Whalen, M.T., and Day, J., 2010, Trace element variations in the Middle Frasnian punctata zone (Late Devonian) in the western Canada sedimentary basin -changes in oceanic bioproductivity and paleoredox spurred by a pulse of terrestrial afforestation? *Geologica Belgica*, **4**, 459–482

Śliwiński, M.G., Whalen, M.T., Newberry, R.J., Payne, J., and Day, J., 2011. Stable Isotope ($\delta^{13}C_{carb\ \&\ org}$, $\delta^{15}N_{org}$) and Trace Element Anomalies during the Late Devonian '*punctata* Event' in the Western Canada Sedimentary Basin. *Palaeogeo. Palaeoclim. Palaeoecol*, **307**, 245–271

Tanaka, K., Takahashi, Y. and Shimizu, H., 2007. Determination of rare earth element in carbonate using laser-ablation inductively-coupled plasma mass spectrometry: an examination of the influence of the matrix on laser-ablation inductively-coupled plasma mass spectrometry analysis. *Anal. Chim. Acta,* **583,** 303-309

Tribovillard, N., Algeo, T.J., Lyons, T. and Riboulleau, A., 2006. Trace metals as paleoredox and paleoproductivity proxies: An update. *Chem. Geol*, **232**, 12-32

Tribovillard, N., Averbuch, O., Devleeschouwer, X., Racki, G. and Riboulleau, A., 2004. Deep-water anoxia over the Frasnian-Famennian boundary (La Serre, France): a tectonically induced oceanic anoxic event? *Terr. Nova*, **16**, 288-295

Ulens, K., Moens, L. and Dams, R., 1994. Study of element distributions in weathered marble crusts using laser ablation inductively coupled plasma mass spectrometry. *J. Anal. Atom. Spectrom.,* 9, 1243-1248

Veizer, J., 1983. Trace elements and isotopes in sedimentary carbonates, Reviews in Mineralogy: Carbonates: Mineralogy and Chemistry, **11**, 265-299

Whalen, M.T., Eberli, G.P., Van Buchem, F.S.P., Mountjoy, E.W. and Homewood, P.W., 2000. Bypass margins, basin-restricted wedges, and platform-to-basin correlation, Upper Devonian, Canadian Rocky Mountains: Implications for sequence stratigraphy of carbonate platform systems. *J. Sediment. Res.*, **70**, 913-936

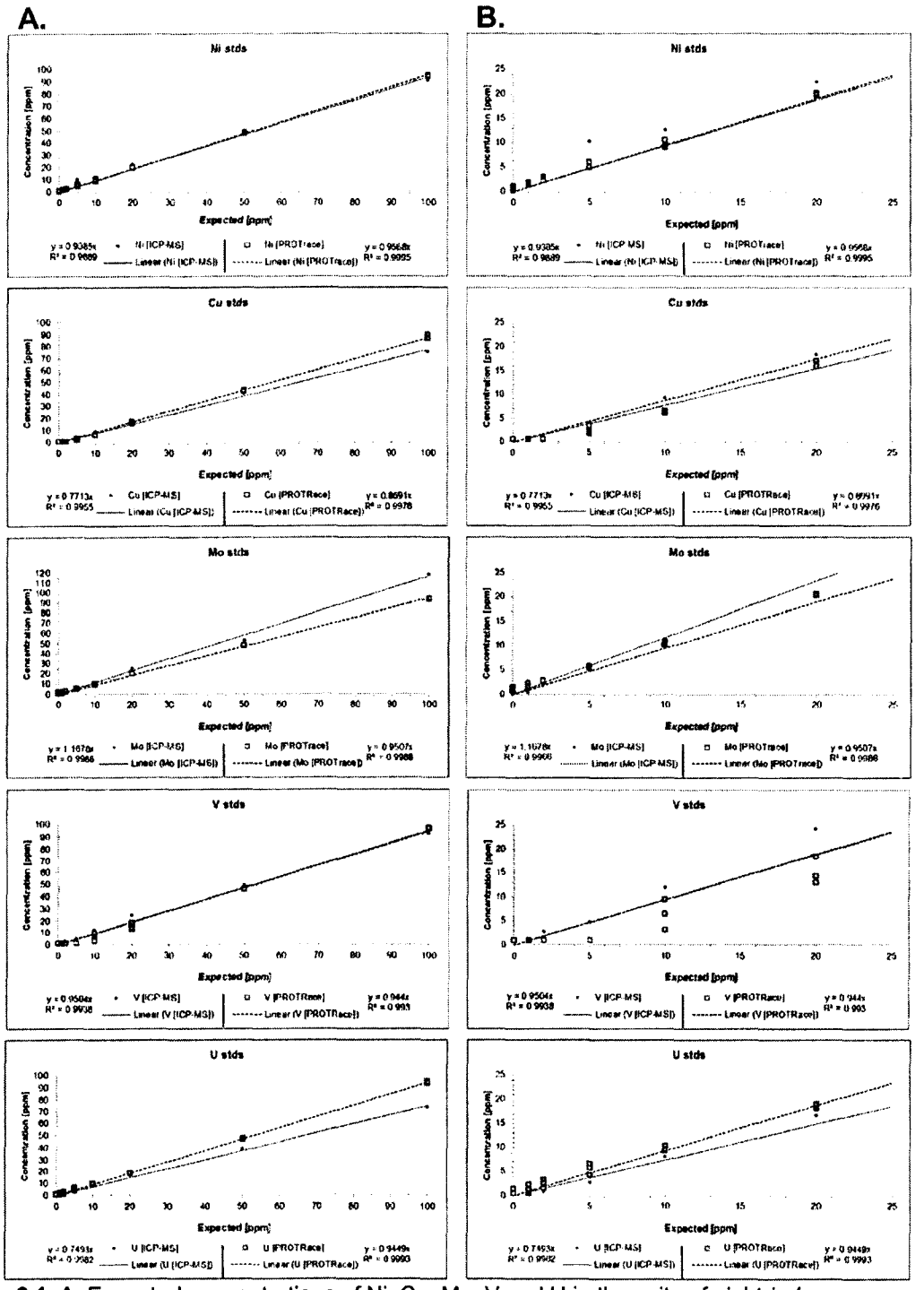

Fig. 2.1. A. Expected concentrations of Ni, Cu, Mo, V and U in the suite of eight *in-house* carbonate trace element standards plotted against values measured independently by acid digestion ICP-MS and PROTrace XRF trace element analysis. B. Close-up of (A.) showing the 0-25 ppm concentration range.

C.

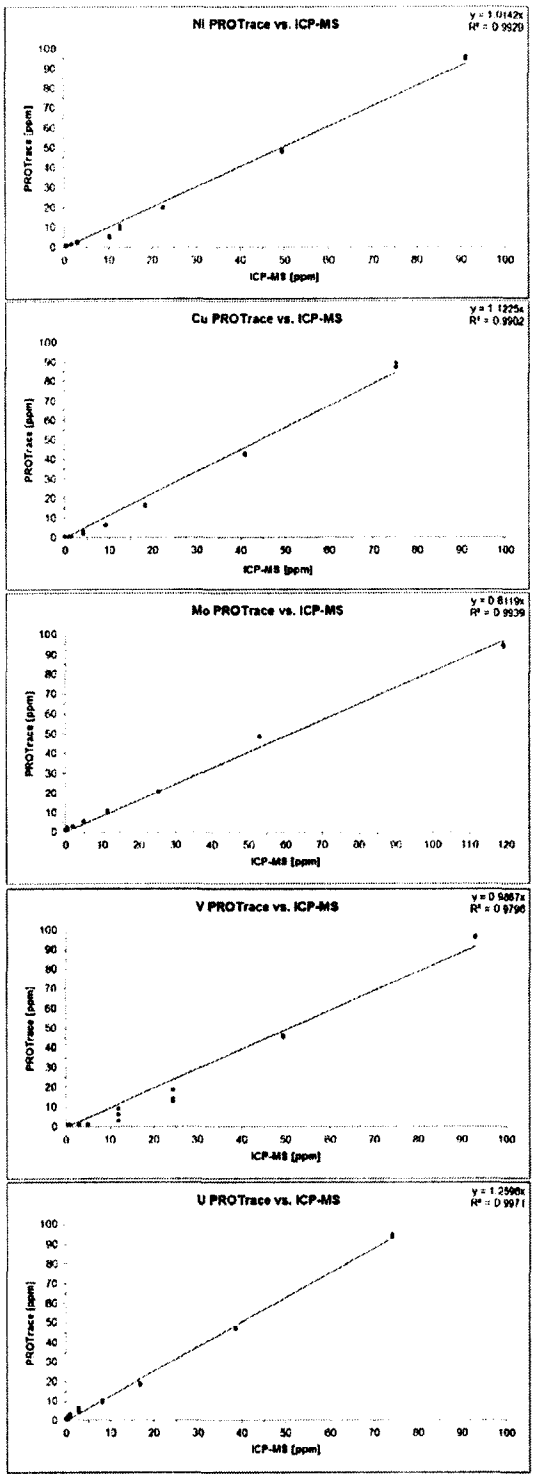

Fig. 2.1. C. Cross-plot of analyte concentrations determined by solution ICP-MS and PROTrace XRF

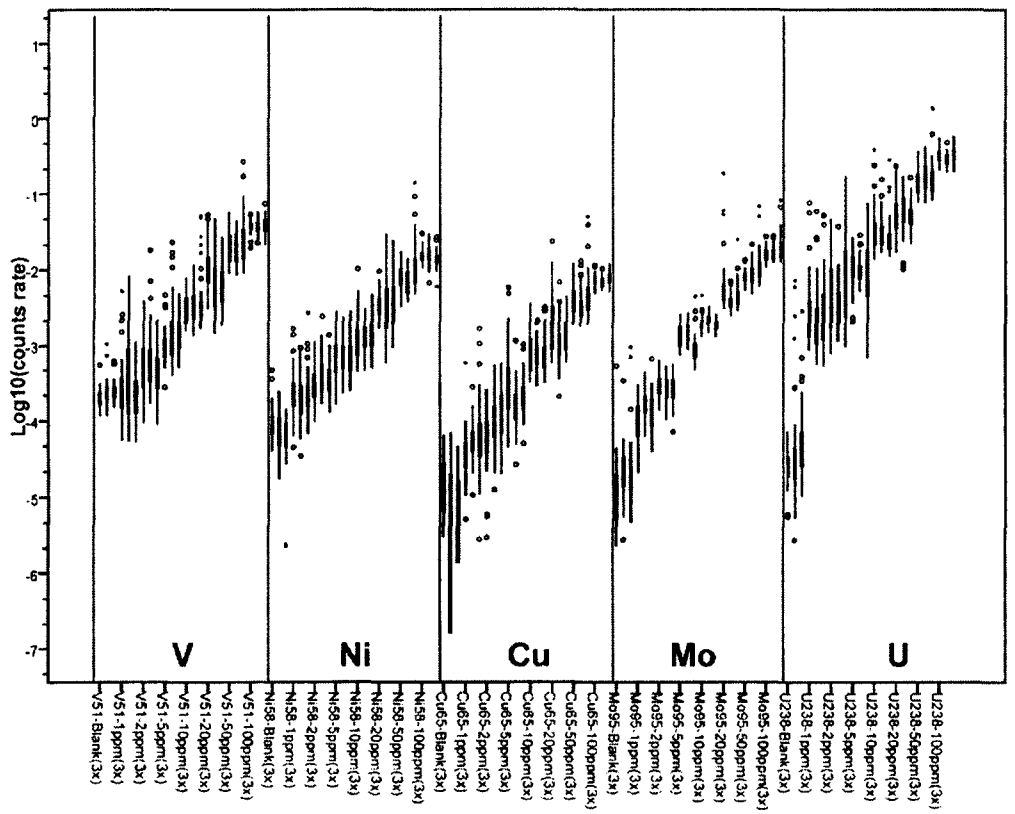

Fig. 2.2. Internal standard (Ca-42)-normalized and log-transformed count rates for NI, Cu, Mo, V and U measured in each *in-house* standard by three LA-ICP-MS transects, showing a progressive count rate increase with increasing analyte concentrations. Circles and stars denote statistical outliers.

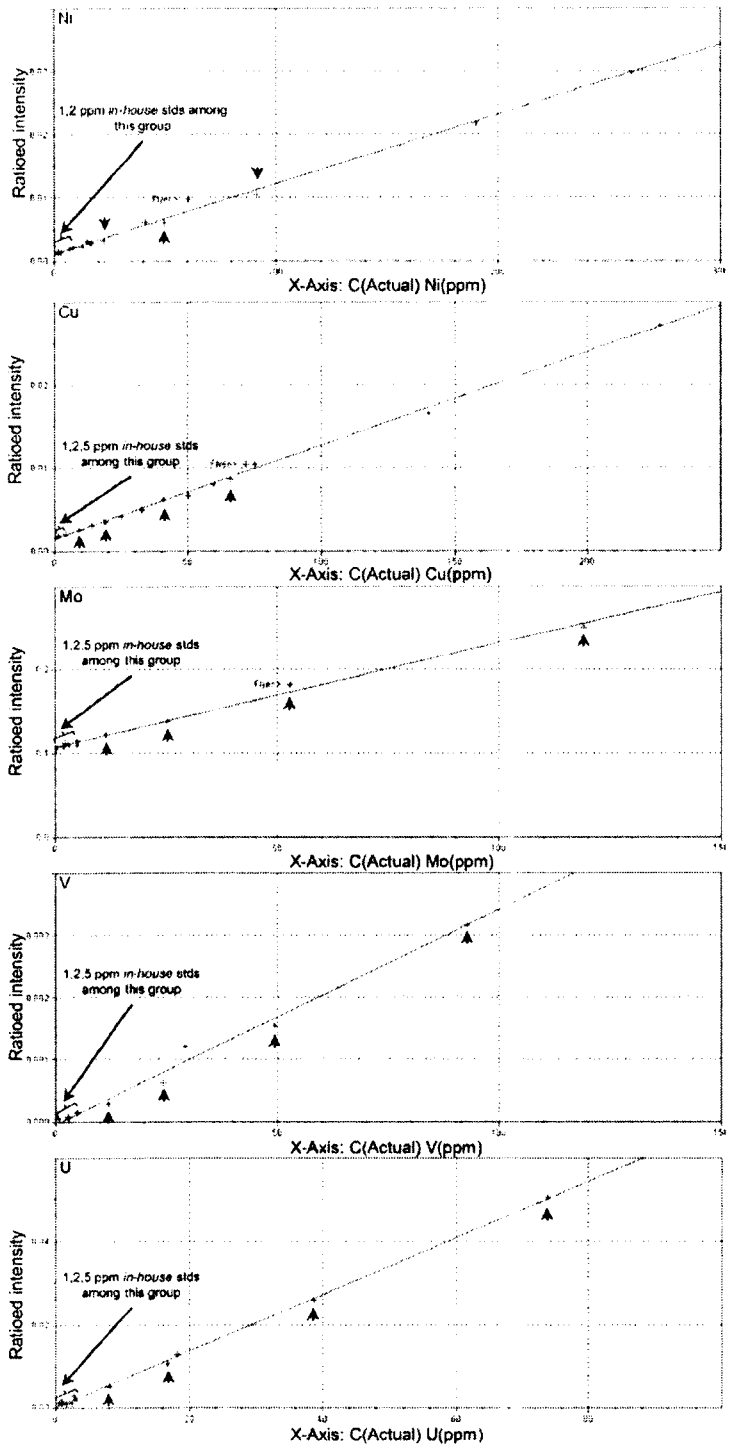

Fig. 2.3. Calibration lines for Ni, Cu, Mo, V and U in our XRF analytical protocol that uses both the low-concentration *in-house* carbonate standards reported on herein and other certified geologic standards. Arrows denote in-house standards.

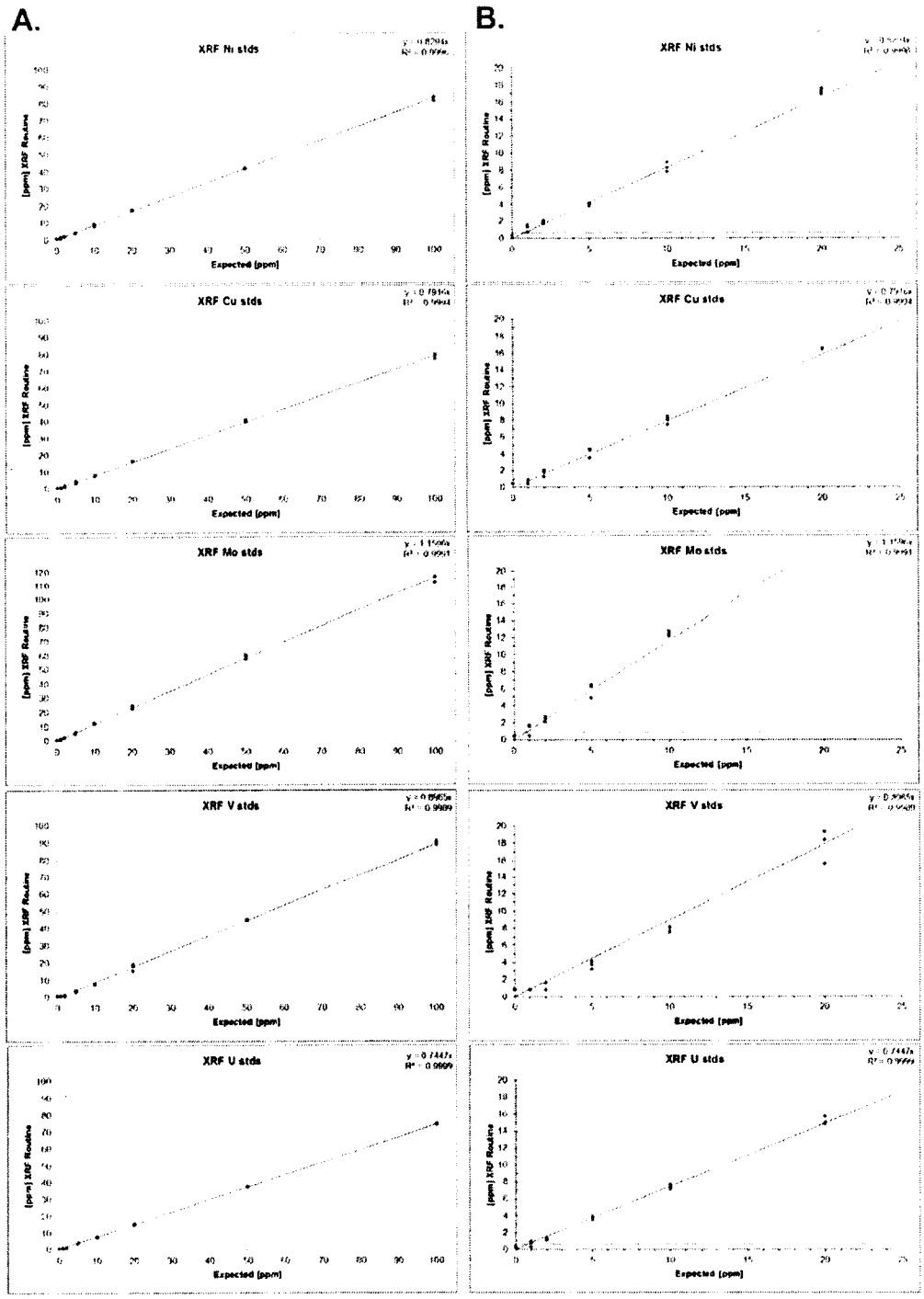

Fig. 2.4. Concentrations of Ni, Cu, Mo, V and U measured in each of the *in-house* carbonate standards by our XRF analytical protocol, calibrated against both *in-house* and certified geologic standards. A. Full range of data; B. Close-up of (A) showing the 0-25 ppm concentration range. Dashed horizontal lines indicate empirically determined detection limits measured on ultrapure calcite blanks.

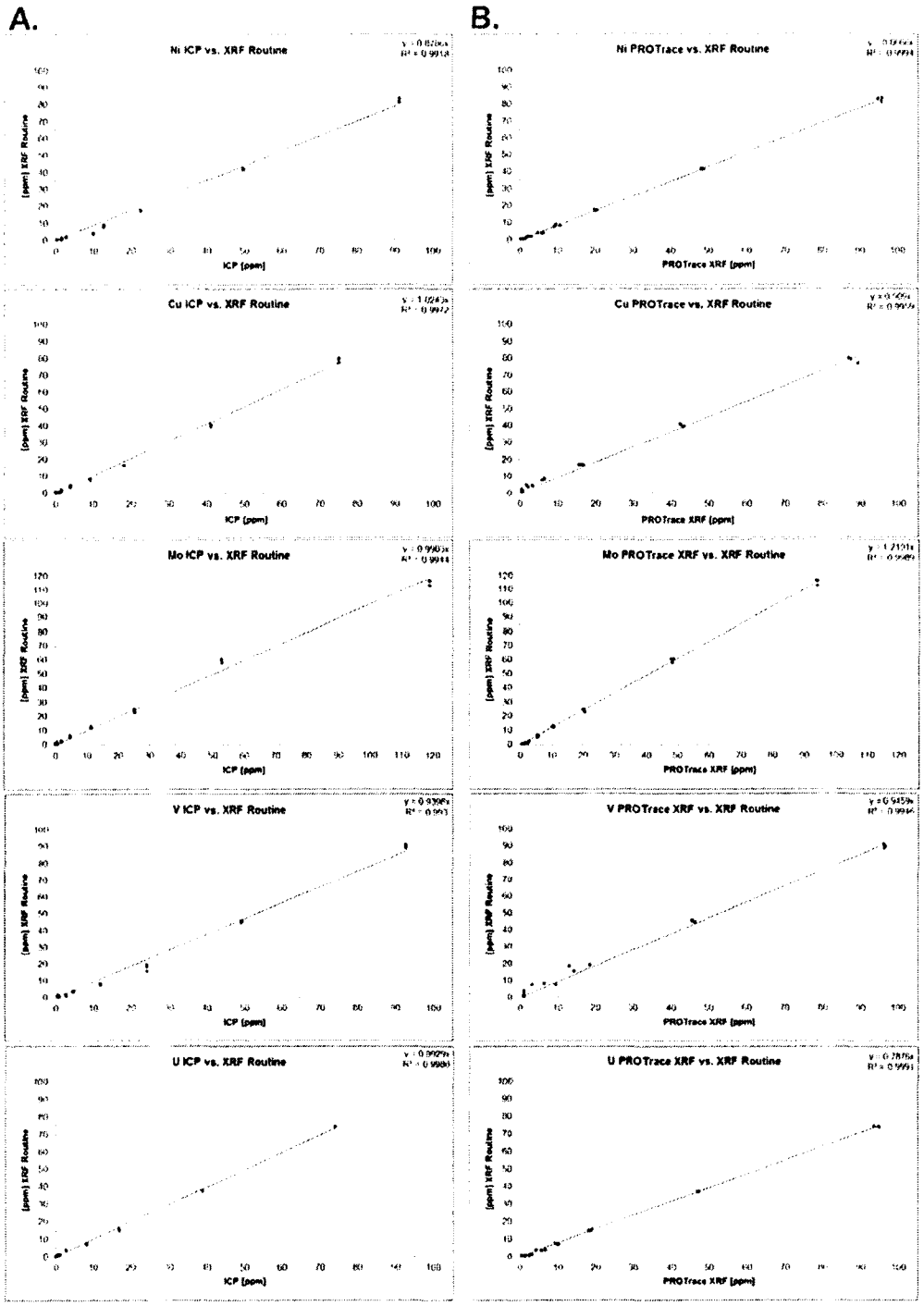

Fig. 2.5. A. Cross-plots of Ni, Cu, Mo, V and U concentrations measured in the *in-house* standards by acid-digestion ICP-MS and our XRF analytical protocol, the latter calibrated against both *in-house* standards and certified geologic standard reference materials. B. Cross-plots of analyte concentrations measured in the *in-house* standards by PROTrace XRF trace element analyses and our XRF protocol.

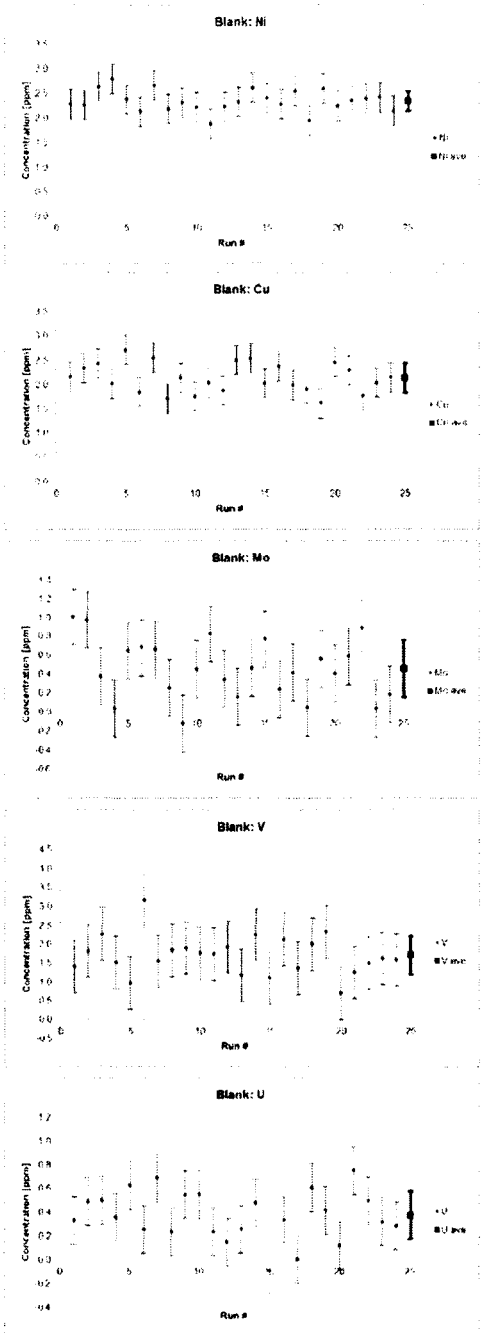

Fig. 2.6 Replicate XRF analyses of ultrapure (zero-concentration) calcite standards (2 pellets, analyzed 12x each) used to determine 1) calibration backgrounds in our XRF protocol for Ni, Cu, Mo, V and U, defined as the average concentration measured on each analyte's spectral peak position, and 2) the lowest levels of detection (LLDs), in turn defined as 3σ of the average apparent concentration measured. Error bars on individual measurements denote the *counting statistical errors* (CSE) associated with the number of X-ray counts detected, while bold squares denote the *average* ± *1σ* of each set of 24 measurements.

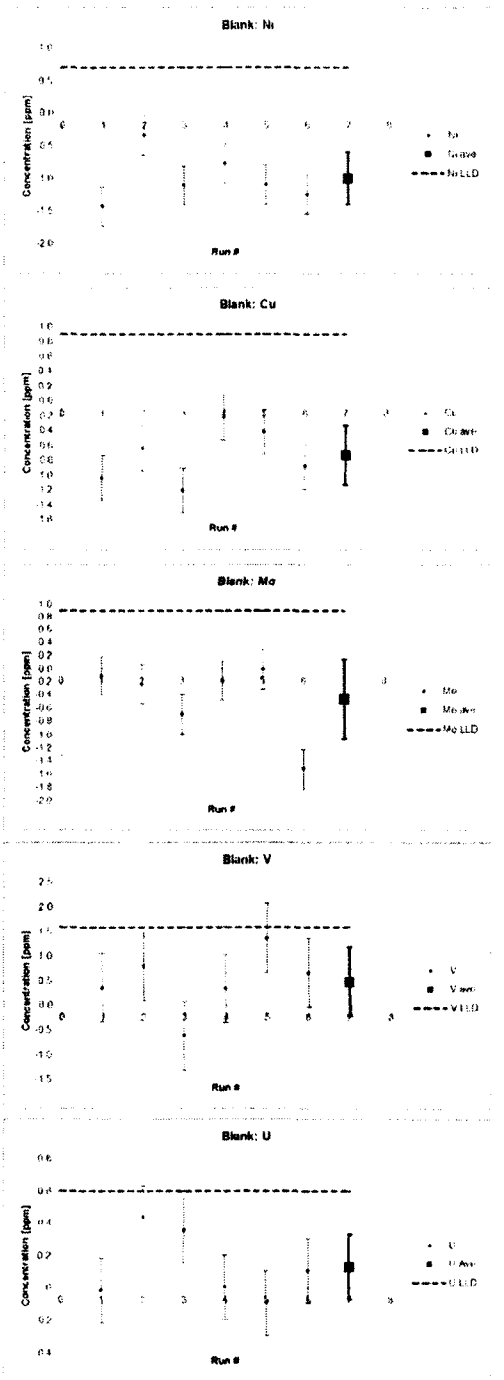

Fig. 2.7. Replicate XRF analyses by our analytical protocol of a blank prepared alongside the set of *in-house* standards as a control on laboratory contamination. Dashed horizontal lines indicate empirically determined detection limits. Bold squares denote the *average* ± *1σ* of each set of six measurements per element. Error bars on individual measurements denote the *counting statistical errors* (CSE) associated with the number of X-ray counts detected during analysis.

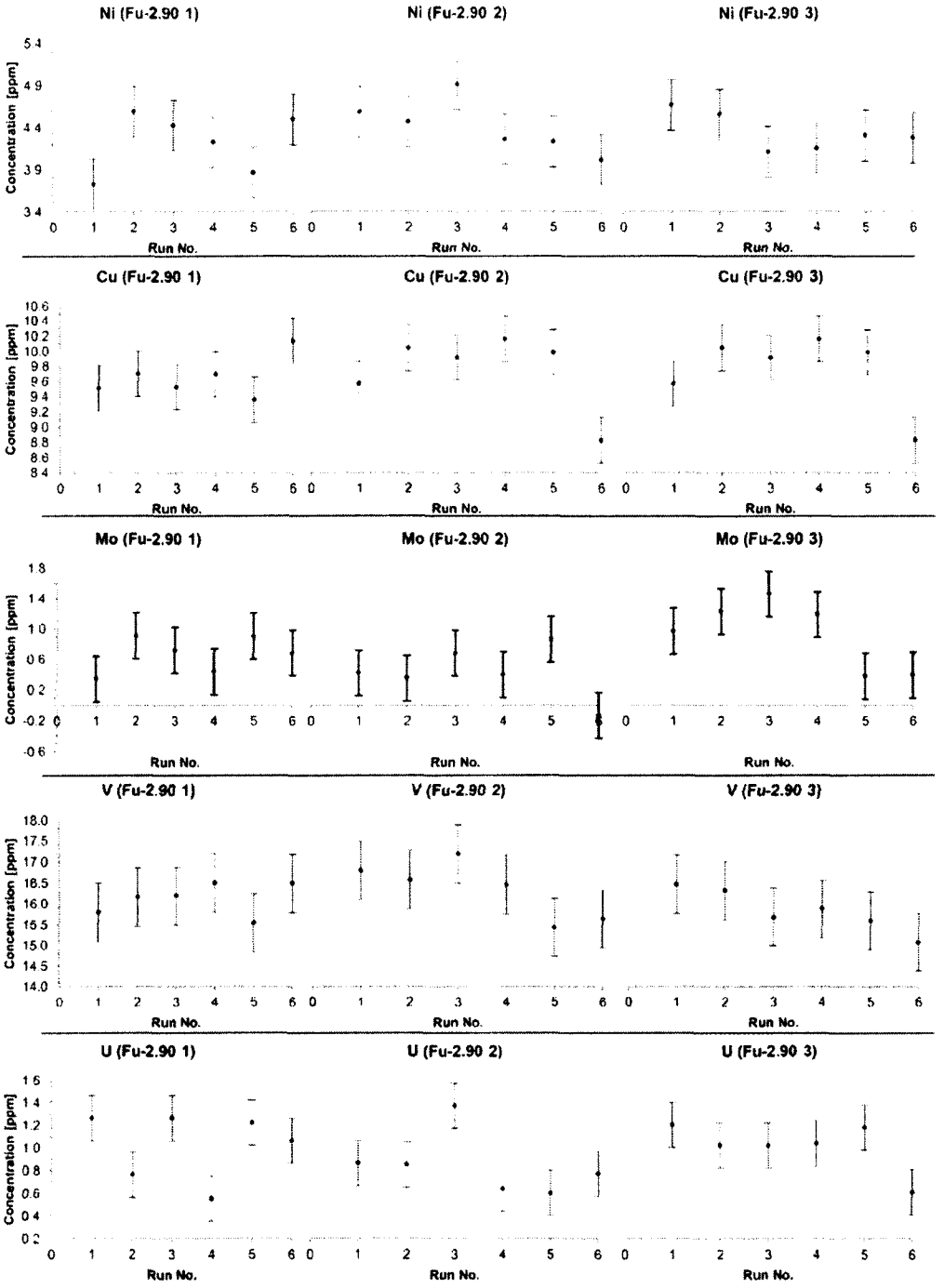

Fig. 2.8. Replicate XRF analyses of three pressed pellets (3 x 6x) prepared from the same representative powdered carbonate sample, used to assess the precision of sample preparation and analyses. Concentrations not corrected for calibration backgrounds or detection limits. Error bars on individual measurements denote the *counting statistical errors* (CSE) associated with the number of X-ray counts detected. Dashed horizontal lines indicate empirically determined detection limits.

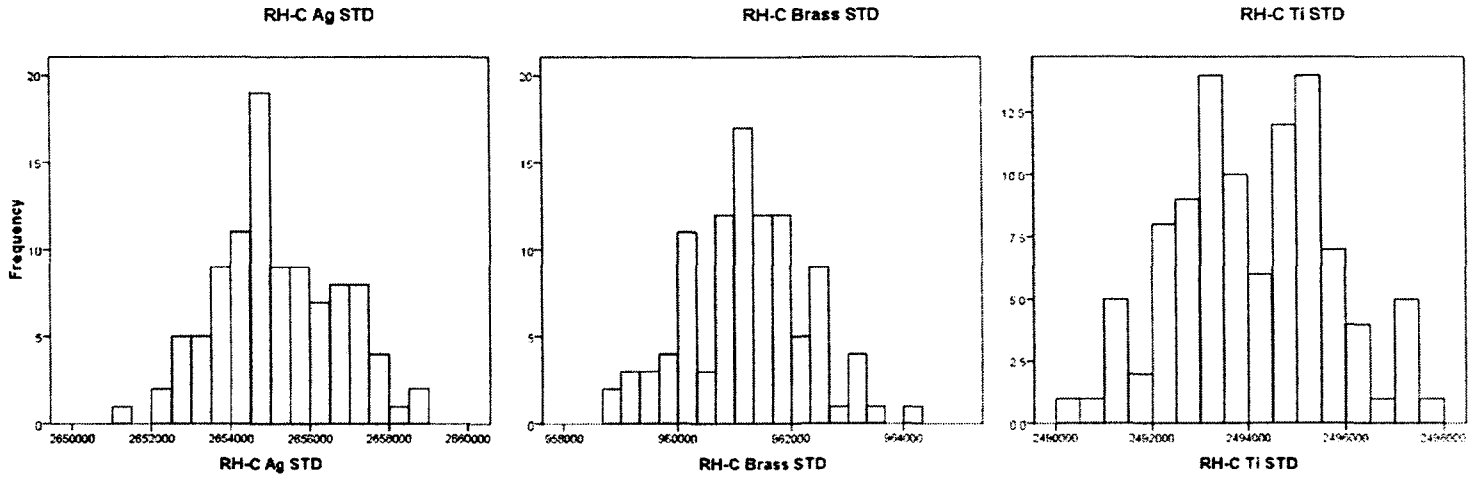

		RH-C Ag STD	RH-C Brass STD	RH-C Ti STD
N		100	100	100
Normal Parameters[a,b]	Mean	2655183.24	961221.84	2494096.64
	Std. Deviation	1563.845	1066.863	1622.559
Most Extreme Differences	Absolute	.087	.093	.073
	Positive	.087	.046	.073
	Negative	-.047	-.093	-.058
Kolmogorov-Smirnov Z		.873	.930	.727
Asymp. Sig. (2-tailed)		.431	.352	.665

a. Test distribution is Normal.

b. Calculated from data.

Test distribution is Normal if 'Asymp. Sig. (2-tailed) > 0.05.

Fig. 2.9. Replicate XRF measurements (100x) of the Rh-Compton analytical line from Ag, Ti and Brass standards, used to demonstrate that large numbers of X-ray observations follow a normal distribution. A one-sample Kolmogorov-Smirnov test confirms distribution normalcy.

Table 2.1. Trace element impurities in the 99.999% ultrapure calcite powder used to prepare in-house carbonate trace element standards [C.A.S. No. 471-34-1]; determined by ICP-MS.

Trace Impurities																	
Al	**As**	**Ba**	**Be**	**Cd**	**Ce**	**Co**	**Cr**	**Cu**	**Fe**	**Ga**	**Ge**	**Hf**	**In**	**K**	**Li**	**Mg**	**Mn**
< 1	< 1	< 1	< 1	< 1	< 2	< 1	< 1	< 1	3	< 1	< 1	< 1	< 2	< 1	< 3	< 1	< 1
Mo	**Na**	**Ni**	**Pb**	**Re**	**Rh**	**Ru**	**Sb**	**Sc**	**Se**	**Sn**	**Sr**	**Ta**	**Tl**	**V**	**W**	**Zn**	**Zr**
< 1	< 1	< 1	< 2	< 2	< 1	< 1	< 1	< 1	< 2	1	5	< 1	< 2	< 1	< 1	< 1	1

Table 2.2. ICP-MS operating conditions for liquid digestion and laser ablation analyses.

ICP-MS Conditions:	Liquid Analysis		Laser Analysis	
RF Power	1500	**W**	1200	**W**
RF Matching	1.68	**V**	1.58	**V**
Sample depth	8.9	**mm**	5	**mm**
Carrier gas	0.9	**L/min**	1.2	**L/min**
Makeup gas	0.17	**L/min**	N/A	N/A
Extract 1	4.1	**V**	4.5	**V**
Extract 2	-139	**V**	-138.5	**V**
Scan speed		-	10	**µm sec^{-1}**
Focal depth		-	5	**µm**
Power		-	80	**%**
Pulse rate		-	10	**Hz**
Spot size		-	25	**µm**

Table 2.3. Representative analytical precisions, detection limits and absolute calibration backgrounds of our XRF analytical protocol for the analytes Ni, Cu, Mo, V and U, as well as the detection limits afforded by PROTrace XRF trace element calibrations.

In-house XRF Routine:	Ni	Cu	Mo	V	U
Ave. background [ppm] *	2.3	2.1	0.5	1.7	0.4
Empirical LLD [ppm] **	0.7	0.9	0.9	1.6	0.6
Ave. precision [ppm] ***	0.3	0.3	0.4	0.5	0.3

PANalytical's PROTrace XRF Routine	Ni	Cu	Mo	V	U
LLD [ppm]	0.6	1.1	0.4	1.9	0.9

* = average concentration of 12 measurements on each of two 99.999% pure $CaCO_3$ pressed pellets

** = 3σ of 24 measurements on 99.999% pure $CaCO_3$ pressed pellets

*** = average of 6 replicate measurements on three replicate samples of a representative carbonate lithology commonly sampled

Table 2.4. Concentrations of Ni, Cu, Mo, V and U measured in each of the in-house standards using acid digestion ICP-MS.

Expected [ppm]	Measured concentration:				
	V-51	Ni-58	Cu-63	Mo-95	U-238
100 ppm	92.84	91.16	75.16	119.2	73.92
50 ppm	49.3	49.58	41.04	52.94	38.76
20 ppm	24.26	22.46	18.28	25.3	16.766
10 ppm	11.926	12.668	9.178	11.434	8.182
5 ppm	4.846	10.184	4.078	4.858	2.754
2 ppm	2.82	2.88	1.4108	1.9156	0.8664
1 ppm	0.836	1.61	0.8202	0.5412	0.4748
Blank	0.6028	0.4206	0.02623	0.001622	3.808E-05

Table 2.5. Concentrations of Ni, Cu, Mo, V and U measured in each of the in-house standards using PROTrace XRF.

Expected [ppm]	Measured concentration:				
	V	Ni	Cu	Mo	U
100 ppm	96.19	94.61	87.01	93.92	94.76
100 ppm	96.65	95.72	87.39	94.24	95.09
100 ppm	96.30	95.59	89.32	94.35	93.62
Average:	**96.38**	**95.31**	**87.91**	**94.17**	**94.49**
1σ	**0.24**	**0.60**	**1.24**	**0.23**	**0.77**
50 ppm	45.48	47.81	42.18	48.74	47.24
50 ppm	45.47	48.60	42.37	48.14	46.99
50 ppm	46.20	47.97	43.21	48.37	47.19
Average:	**45.72**	**48.13**	**42.59**	**48.42**	**47.14**
1σ	**0.42**	**0.41**	**0.55**	**0.30**	**0.13**
20 ppm	18.52	19.71	16.31	20.37	19.10
20 ppm	12.97	20.23	15.80	20.29	18.26
20 ppm	14.32	19.87	16.97	20.72	18.87
Average:	**15.27**	**19.94**	**16.36**	**20.46**	**18.74**
1σ	**2.90**	**0.26**	**0.58**	**0.23**	**0.43**
10 ppm	3.16	9.41	6.47	10.57	9.63
10 ppm	6.42	9.06	6.34	10.28	9.40
10 ppm	9.41	10.57	5.96	10.82	10.30
Average:	**6.33**	**9.68**	**6.26**	**10.56**	**9.77**
1σ	**3.12**	**0.79**	**0.27**	**0.27**	**0.47**
5 ppm	0.95	5.86	3.38	5.39	4.33
5 ppm	0.95	4.80	1.74	5.76	6.74
5 ppm	0.95	6.15	2.14	5.52	5.75
Average:	**0.95**	**5.61**	**2.42**	**5.56**	**5.60**
1σ	**0.00**	**0.71**	**0.85**	**0.19**	**1.21**
2 ppm	0.95	2.15	0.55	2.84	2.62
2 ppm	0.95	2.23	0.55	2.78	1.51
2 ppm	0.95	2.97	0.55	2.79	3.28
Average:	**0.95**	**2.45**	**0.55**	**2.80**	**2.47**
1σ	**0.00**	**0.45**	**0.00**	**0.03**	**0.89**
1 ppm	0.95	1.88	0.55	1.53	1.16
1 ppm	0.95	1.58	0.55	1.78	2.35
1 ppm	0.95	1.45	0.55	2.33	0.44
Average:	**0.95**	**1.64**	**0.55**	**1.88**	**1.31**
1σ	**0.00**	**0.22**	**0.00**	**0.41**	**0.96**
0 ppm	0.95	0.31	0.55	0.71	1.42
0 ppm	0.95	1.02	0.55	1.23	0.44
0 ppm	0.95	0.64	0.55	1.53	1.34
Average:	**0.95**	**0.66**	**0.55**	**1.16**	**1.07**
1σ	**0.00**	**0.35**	**0.00**	**0.41**	**0.54**

Table 2.6. Replicate *in-house* standard analyses by our XRF analytical protocol.

Analyte [ppm]	V	Ni	Cu	Mo	U
100ppm Syn.Carb.std	90.8	83.3	79.8	116.6	74.5
100ppm Syn.Carb.std	89.5	83.4	79.3	116.2	74.2
100ppm Syn.Carb.std	88.7	81.3	77.1	112.4	74.7
Mean:	**89.7**	**82.7**	**78.7**	**115.1**	**74.4**
1σ	1.1	1.2	1.4	2.3	0.2
1σ as % of mean	**1.2%**	**1.5%**	**1.8%**	**2.0%**	**0.3%**
50ppm Syn.Carb.std	45.4	42.2	40.7	60.2	37.3
50ppm Syn.Carb.std	45.5	41.6	40.3	59.9	37.4
50ppm Syn.Carb.std	44.7	41.4	39.5	57.6	37.0
Mean:	**45.2**	**41.7**	**40.2**	**59.2**	**37.2**
1σ	0.5	0.4	0.6	1.4	0.2
1σ as % of mean	**1.1%**	**0.9%**	**1.4%**	**2.4%**	**0.6%**
20ppm Syn.Carb.std	19.3	17.5	16.5	24.8	15.6
20ppm Syn.Carb.std	18.4	17.2	16.5	24.8	14.9
20ppm Syn.Carb.std	15.6	16.9	16.5	22.5	14.8
Mean:	**17.7**	**17.2**	**16.5**	**24.0**	**15.1**
1σ	1.9	0.3	0.0	1.3	0.4
1σ as % of mean	**10.9%**	**1.7%**	**0.1%**	**5.5%**	**3.0%**
10ppm Syn.Carb.std	7.7	8.9	8.4	12.8	7.3
10ppm Syn.Carb.std	8.1	7.8	8.1	12.4	7.7
10ppm Syn.Carb.std	7.5	8.3	7.5	12.2	7.1
Mean:	**7.8**	**8.3**	**8.0**	**12.5**	**7.4**
1σ	0.3	0.5	0.5	0.3	0.3
1σ as % of mean	**4.0%**	**6.6%**	**5.8%**	**2.4%**	**4.1%**
5ppm Syn.Carb.std	3.7	3.8	4.4	6.5	3.9
5ppm Syn.Carb.std	4.1	4.1	4.6	6.2	3.9
5ppm Syn.Carb.std	3.2	4.0	3.5	4.9	3.5
Mean:	**3.7**	**4.0**	**4.2**	**5.8**	**3.8**
1σ	0.5	0.2	0.6	0.9	0.2
1σ as % of mean	**12.5%**	**4.4%**	**13.6%**	**14.8%**	**5.5%**
2ppm Syn.Carb.std	1.0	1.8	2.0	2.1	1.1
2ppm Syn.Carb.std	1.0	2.1	1.9	2.7	1.1
2ppm Syn.Carb.std	1.6	1.7	1.3	2.5	1.3
Mean:	**1.2**	**1.9**	**1.7**	**2.4**	**1.1**
1σ	0.3	0.2	0.4	0.3	0.1
1σ as % of mean	**27.3%**	**10.1%**	**23.8%**	**12.1%**	**8.9%**
1ppm Syn.Carb.std	0.8	1.6	0.9	1.6	0.8
1ppm Syn.Carb.std	0.8	1.4	0.5	1.7	0.3
1ppm Syn.Carb.std	0.8	0.7	0.5	0.5	0.9
Mean:	**0.8**	**1.2**	**0.6**	**1.2**	**0.7**
1σ	0.0	0.5	0.3	0.7	0.3
1σ as % of mean	**0.0%**	**37.6%**	**42.4%**	**55.1%**	**49.6%**
Blank Syn.carb.std	0.8	0.4	0.5	0.5	0.3
Blank Syn.carb.std	0.8	0.4	0.5	0.5	0.3
Blank Syn.carb.std	0.8	0.4	0.5	0.5	0.3
Blank Syn.carb.std	0.8	0.4	0.5	0.5	0.3
Blank Syn.carb.std	0.8	0.4	0.5	0.5	0.3
Blank Syn.carb.std	0.8	0.4	0.5	0.5	0.3
Mean:	**0.8**	**0.4**	**0.5**	**0.5**	**0.3**
1σ	0.0	0.0	0.0	0.0	0.0
1σ as % of mean	**0.0%**	**0.0%**	**0.0%**	**0.0%**	**0.0%**

All values corrected for absolute calibration backgrounds and LLDs

All values of standards in the 1 to 100 ppm range corrected for the average value of the blank for each analyte

Table 2.7. Replicate XRF analyses of Ni, Cu, Mo, V and U in three pressed pellets (3 x 6x) prepared from the same representative powdered carbonate sample, used to assess the precision of sample preparation and analyses. Measured concentrations not corrected for absolute backgrounds and detection limits. An ANOVA test demonstrates no significant differences at the 95% confidence level in the mean concentrations of all analytes among the three pellets. CSE = counting statistical error associated with detecting X-rays.

Sample Fu 2.90 (representative carbonate material)

Analyte:	V	Ni	Cu	Mo	U
Pressed Pellet 3					
Ave. [ppm]; N=6*	**16.1**	**4.2**	**9.7**	**0.7**	**1.0**
1σ [ppm]	0.4	0.4	0.3	0.2	0.3
1σ as % of mean	2.4%	8.3%	2.8%	35.1%	29.3%
Pressed Pellet 2					
Ave. [ppm]; N=6*	**16.3**	**4.4**	**9.7**	**0.4**	**0.8**
1σ [ppm]	0.7	0.3	0.5	0.3	0.3
1σ as % of mean	4.2%	7.1%	5.1%	79.2%	32.6%
Pressed Pellet 1					
Ave. [ppm]; N=6*	**15.8**	**4.3**	**9.9**	**0.9**	**1.0**
1σ [ppm]	0.5	0.2	0.1	0.5	0.2
1σ as % of mean	3.2%	5.1%	1.5%	48.5%	21.0%
Counting Statistical Error					
Ave. CSE (3); N=6	0.7	0.3	0.3	0.3	0.2
Ave. CSE (2); N=6	0.7	0.3	0.3	0.3	0.2
Ave. CSE (1); N=6	0.7	0.3	0.3	0.3	0.2
Summary Statistics					
Ave. [ppm]; N=18	**16.1**	**4.3**	**9.8**	**0.7**	**1.0**
1σ [ppm]; N=18	**0.5**	**0.3**	**0.3**	**0.4**	**0.3**
1σ as % of mean	**3.4%**	**6.8%**	**3.4%**	**58.4%**	**27.3%**
Overall ave. CSE	0.7	0.3	0.3	0.3	0.2
Detection Limit (LLD)	1.6	0.7	0.9	0.9	0.6

*Values not corrected for residual calibration backgrounds and detection limits.

Appendix 2A

Appendix to Śliwiński et al., (Chemical Geology, in press).

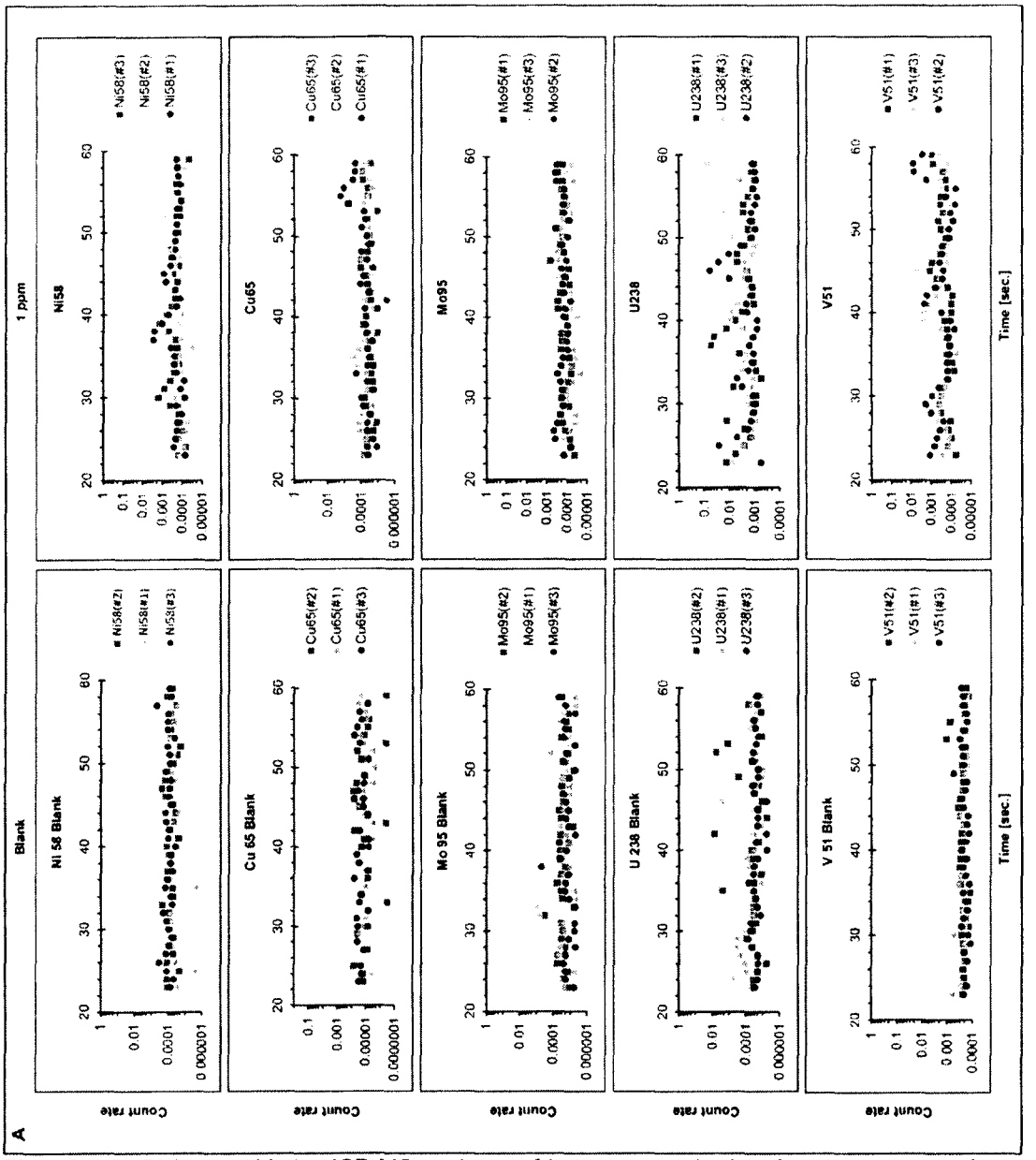

Fig. 2A-1 (A-D) Laser Ablation ICP-MS analyses of *in-house* standard surface homogeneity for the analytes Ni, Cu, Mo, V and U. A subsample of each *in-house* standard was pressed into a standard LA-ICP-MS pellet and three transects measuring 50 x 500 µm were ablated on each (denoted as '#1, 2 & 3;' numbers following each element's periodic symbol denote the particular isotope measured). Count rates were corrected for background, normalized to the Ca-42 internal standard and log-transformed for the purposes of calculating ANOVA statistics.

Fig. 2A-1 (A-D) continued.

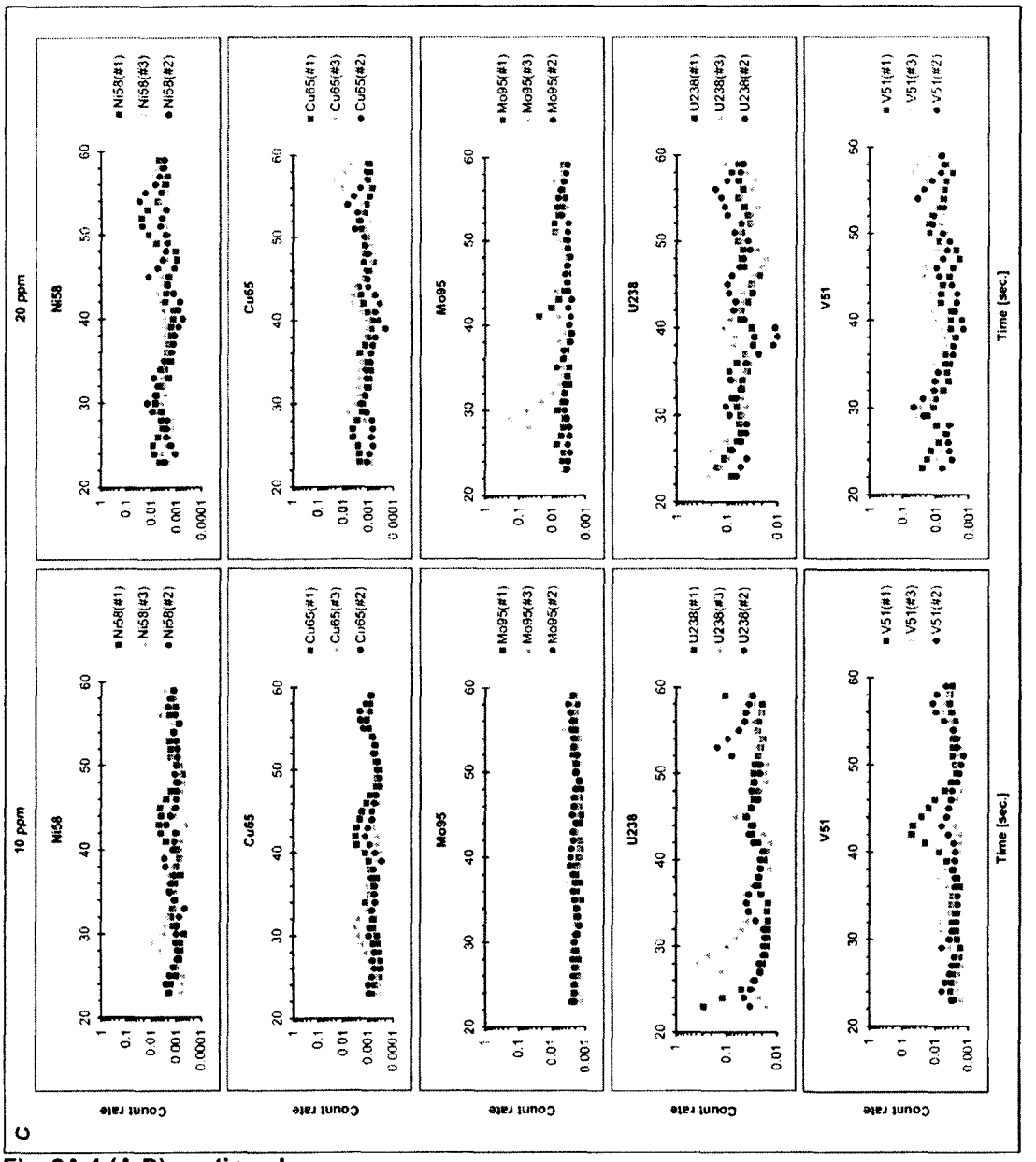

Fig. 2A-1 (A-D) continued.

Fig. 2A-1 (A-D) continued.

Table. 2A-1. PANalytical Axios XRF operating conditions for our analytical protocol.

PANalytical Axios Wave-length Dispersive X-ray Flourescence Spectrometer (WD-XRF) operating conditions

Channel	Type	Line	X-tal	Collimator	Detector	Tube filter	kV	mA	Angle (°2T)	Offset Bg1 (°2T)	Offset Bg2 (°2T)
Ti	Gonio	KA	LiF 200	300 µm	Flow*	None	42	95	86.1878		
V	Gonio	KA	LiF 200	300 µm	Flow*	None	47	85	76.9382	-0.7452	1.169
Ni	Gonio	KA	LiF 200	300 µm	Flow*	None	60	66	48.675	-1.7826	1.1832
Cu	Gonio	KA	LiF 200	300 µm	Flow*	None	60	66	45.0266	-0.942	0.7056
Mo	Gonio	KA	LiF 200	300 µm	Scint.**	None	60	66	20.2812	-0.6108	0.5746
Ba	Gonio	LA	LiF 200	300 µm	Scint.**	None	42	95	87.2202	-1.9132	1.016
Rh1	Gonio	KA-C	LiF 200	300 µm	Scint.**	None	60	66	18.437	-0.531	1.2346
Rb	Gonio	KA	LiF 220	150 µm	Scint.**	None	60	66	37.9588		
U	Gonio	LA	LiF 220	150 µm	Scint.**	None	60	66	37.2858	-0.3634	

***Flow proportional detector; **Scintillation detector.**

Calibration details:

	D	E	K	Bg	Bg1	Bg2	Ratio channel	Lo(C) Ti	Lo(C) Ba	Lo(C) Rb	Lo(C) U
Ti [ppm]	-35.55	170.55	0.01045	Yes	Yes	Yes			-0.01456		
V [ppm]	1.43	28870.55	0.00126	Yes	Yes	Yes	Rh1	0.01887			
Ni [ppm]	-10.26	9061.20	0.00162	Yes	Yes	Yes	Rh1				
Cu [ppm]	-12.85	8875.95	0.00102	Yes	Yes	Yes	Rh1				
Mo [ppm]	-85.58	800.99	0.00093	Yes	No	Yes	Rh1				
Ba [ppm]	-1.19	822.27	0.00673	Yes	Yes	Yes		-0.00146			
Rb [ppm]	0.83	747.46	0.00120	Yes	Yes	Yes	Rh1				-0.4058
U [ppm]	-0.11	1475.91	0.00030	Yes	Yes	Yes	Rh1			0.0003	

Regression model: C=D+E.R.M.; Error weighting: Sq. root; Weighting constant: 1000

D: The intercept of the regression line; E: The slope of the regression line

K: The 'K-factor' indicating the goodness of the regression for Sq. Error Weighting.

Lo(C) of Xx: The concentration based line overlap correction factor for compound Xx.

Appendix 2B

Supplementary Data to Śliwiński et al., (Chemical Geology, in press).

Table 2B-1. Ca-42-normalized (internal standard) and log-transformed count rate data for the analytes Ni, Cu, Mo, V and U measured in each *in-house* carbonate standard by three LA-ICP-MS transects. Kolmogorov-Smirnov (K-S) tests of distribution normalcy indicate that only 5/120 cases do not satisfy this condition at the 95% confidence level (indicated by circled 'x's), while only 2 cases fail at the 99% level.

One-Sample Kolmogorov-Smirnov Test (N=37)

	V51-Blank	**V51-Blank**	**V51-Blank**	**V51-1ppm**	**V51-1ppm**
K-S 'Z'	.613	.997	.678	1.078	.730
Sig.*	.847	.274	.747	.195	.661
	V51-1ppm	**V51-2ppm**	**V51-2ppm**	**V51-2ppm**	**V51-5ppm**
K-S 'Z'	.538	1.065	1.324	.694	.808
Sig.*	.935	.207	.060	.722	.531
	V51-5ppm	**V51-5ppm**	**V51-10ppm**	**V51-10ppm**	**V51-10ppm**
K-S 'Z'	1.012	.674	.885	.826	1.836
Sig.*	.257	.754	.414	.503	.002
	V51-20ppm	**V51-20ppm**	**V51-20ppm**	**V51-50ppm**	**V51-50ppm**
K-S 'Z'	.782	.607	.522	.440	.858
Sig.*	.574	.855	.948	.990	.453
	V51-50ppm	**V51-100ppm**	**V51-100ppm**	**V51-100ppm**	**Ni58-Blank**
K-S 'Z'	.846	.922	.614	.421	.662
Sig.*	.472	.363	.846	.994	.774
	Ni58-Blank	**Ni58-Blank**	**Ni58-1ppm**	**Ni58-1ppm**	**Ni58-1ppm**
K-S 'Z'	.437	1.199	.979	.778	1.236
Sig.*	.991	.113	.293	.580	.094
	Ni58-2ppm	**Ni58-2ppm**	**Ni58-2ppm**	**Ni58-5ppm**	**Ni58-5ppm**
K-S 'Z'	.704	.902	.585	.445	.657
Sig.*	.704	.390	.884	.989	.781
	Ni58-5ppm	**Ni58-10ppm**	**Ni58-10ppm**	**Ni58-10ppm**	**Ni58-20ppm**
K-S 'Z'	.504	.999	.779	.634	.474
Sig.*	.961	.271	.579	.816	.978
	Ni58-20ppm	**Ni58-20ppm**	**Ni58-50ppm**	**Ni58-50ppm**	**Ni58-50ppm**
K-S 'Z'	.631	.543	.507	.630	1.267
Sig.*	.820	.930	.959	.822	.081
	Ni58-100ppm	**Ni58-100ppm**	**Ni58-100ppm**	**Cu65-Blank**	**Cu65-Blank**
K-S 'Z'	.880	.778	.878	1.919	1.219
Sig.*	.421	.580	.424	.001	.103
	Cu65-Blank	**Cu65-1ppm**	**Cu65-1ppm**	**Cu65-1ppm**	**Cu65-2ppm**
K-S 'Z'	1.646	2.082	1.999	.910	2.095
Sig.*	.009	.000	.001	.379	.000
	Cu65-2ppm	**Cu65-2ppm**	**Cu65-5ppm**	**Cu65-5ppm**	**Cu65-5ppm**
K-S 'Z'	.601	.507	1.128	.581	.694
Sig.*	.863	.959	.157	.888	.721

*** Asymp. Sig. (2-tailed)**

Table 2B-1 continued.

One-Sample Kolmogorov-Smirnov Test (N=37)

	Cu65-10ppm(3x)	Cu65-10ppm	Cu65-10ppm	Cu65-20ppm	Cu65-20ppm
K-S 'Z'	.892	.761	.753	.729	.752
Sig.*	.404	.609	.623	.663	.624
	Cu65-20ppm(3x)	Cu65-50ppm	Cu65-50ppm	Cu65-50ppm	Cu65-100ppm
K-S 'Z'	.696	.888	1.157	1.103	.737
Sig.*	.717	.410	.137	.176	.649
	Cu65-100ppm(3x)	Cu65-100ppm	Mo95-Blank	Mo95-Blank	Mo95-Blank
K-S 'Z'	.584	.577	2.081	2.192	1.196
Sig.*	.885	.894	.000	.000	.114
	Mo95-1ppm(3x)	Mo95-1ppm	Mo95-1ppm	Mo95-2ppm	Mo95-2ppm
K-S 'Z'	.569	.652	.598	.495	.810
Sig.*	.902	.788	.867	.967	.528
	Mo95-2ppm(3x)	Mo95-5ppm	Mo95-5ppm	Mo95-5ppm	Mo95-10ppm
K-S 'Z'	.744	.584	.703	1.328	.941
Sig.*	.637	.885	.706	.059	.339
	Mo95-10ppm(3x)	Mo95-10ppm	Mo95-20ppm	Mo95-20ppm	Mo95-20ppm
K-S 'Z'	.478	.903	1.624	.902	1.210
Sig.*	.977	.389	.010	.389	.107
	Mo95-50ppm(3x)	Mo95-50ppm	Mo95-50ppm	Mo95-100ppm	Mo95-100ppm
K-S 'Z'	.687	.694	1.179	.726	1.216
Sig.*	.733	.722	.124	.668	.104
	Mo95-100ppm(3x)	U238-Blank	U238-Blank	U238-Blank	U238-1ppm
K-S 'Z'	1.470	1.168	2.026	1.125	1.112
Sig.*	.027	.131	.001	.159	.169
	U238-1ppm(3x)	U238-1ppm	U238-2ppm	U238-2ppm	U238-2ppm
K-S 'Z'	1.433	.848	.982	1.076	.628
Sig.*	.033	.468	.289	.197	.826
	U238-5ppm(3x)	U238-5ppm	U238-5ppm	U238-10ppm	U238-10ppm
K-S 'Z'	.798	.847	.741	1.047	.788
Sig.*	.547	.470	.643	.223	.563
	U238-10ppm(3x)	U238-20ppm	U238-20ppm	U238-20ppm	U238-50ppm
K-S 'Z'	1.340	.821	.905	.790	.720
Sig.*	.055	.510	.386	.561	.677
	U238-50ppm(3x)	U238-50ppm	U238-100ppm	U238-100ppm	U238-100ppm
K-S 'Z'	1.017	1.041	.446	.648	.445
Sig.*	.252	.229	.989	.794	.989

* Asymp. Sig. (2-tailed)

Table 2B-2. Analysis of variance (ANOVA) tests for each set of 3 laser transects ablated on each of the *in-house* standards (analyte count rates normalized to Ca-42 internal standard and log-transformed). A) ANOVA output assuming equal variances among each group of observations. As shown in (B), not all groups satisfy this assumption (sig. < 0.01), necessitating (C) an adjusted ANOVA for several observations (adjusted degrees of freedom and critical statistic values). Significant differences (sig. < 0.01) in the mean count rates are noted for 5/40 cases.

		ANOVA					Test of Homogeneity of Variances				Robust Tests of Equality of Means				Pass at:
Variance		SS	df	MS	F	Sig.	LS	df1	df2	Sig.	WS	df1	df2	Sig.	
(3x) V51-Blank	B.G.	.128	2	.064	3.104	**.049**	413	2	108	**.663**					
	W.G	2.233	108	.021											2σ
	Tot.	2.361	110												
(3x) V51-1ppm	B.G.	.958	2	.479	2.390	**.096**	5.475	2	108	**.005**	2.546	2	68.896	**.086**	
	W.G	21.639	108	.200											1σ
	Tot.	22.596	110												
(3x) V51-2ppm	B.G.	.563	2	.282	1.960	**.146**	2.144	2	108	**.122**					
	W.G	15.516	108	.144											1σ
	Tot.	16.079	110												
(3x) V51-5ppm	B.G.	.554	2	.277	2.548	**.083**	6.088	2	108	**.003**	3.540	2	68.590	**.034**	
	W.G	11.748	108	.109											1σ
	Tot.	12.302	110												
(3x) V51-10ppm	B.G.	.333	2	.166	2.109	**.126**	3.897	2	108	**.023**	1.713	2	68.840	**.188**	
	W.G	8.515	108	.079											1σ
	Tot.	8.847	110												
(3x) V51-20ppm	B.G.	1.421	2	.710	7.178	**.001**	1.112	2	108	**.333**					
	W.G	10.688	108	.099											**Fails at 2σ**
	Tot.	12.109	110												
(3x) V51-50ppm	B.G.	.237	2	.118	1.806	**.169**	2.062	2	108	**.132**					
	W.G	7.078	108	.066											1σ
	Tot.	7.315	110												
(3x) V51-100ppm	B.G.	.025	2	.013	1.456	**.238**	1.552	2	108	**.216**					
	W.G	.941	108	.009											1σ
	Tot.	.966	110												
(3x) NI58-Blank	B.G.	1.009	2	.505	5.716	**.004**	1.456	2	108	**.238**					
	W.G	9.532	108	.088											**Fails at 2σ**
	Tot.	10.542	110												
(3x) NI58-1ppm	B.G.	.292	2	.146	1.307	**.275**	.139	2	108	**.871**					
	W.G	12.061	108	.112											1σ
	Tot.	12.353	110												
(3x) NI58-2ppm	B.G.	.217	2	.108	1.805	**.169**	.352	2	108	**.704**					
	W.G	6.478	108	.060											1σ
	Tot.	6.695	110												
(3x) NI58-5ppm	B.G.	.032	2	.016	.289	**.750**	.614	2	108	**.543**					
	W.G	6.016	108	.056											1σ
	Tot.	6.048	110												
(3x) NI58-10ppm	B.G.	.026	2	.013	.208	**.812**	3.150	2	108	**.047**	.275	2	68.436	**.760**	
	W.G	6.619	108	.061											1σ
	Tot.	6.644	110												
(3x) NI58-20ppm	B.G.	.055	2	.028	.265	**.767**	8.523	2	108	**.000**	.193	2	62.541	**.825**	
	W.G	11.287	108	.105											1σ
	Tot.	11.343	110												

B.G. = Between Group Variance; W.G. =Within Group Variance; SS = Sum of Squares; MS = Mean Square; LS = Leven Statistic; WS = *Welch Statistic*

Table 2B-2 continued.

		ANOVA					Test of Homogeneity of Variances				Robust Tests of Equality of Means				Pass at:
	Variance	SS	df	MS	F	Sig.	LS	df1	df2	Sig.	WS	df1	df2	Sig.	
(3x) Ni58-50ppm	B.G.	.721	2	.360	6.562	.002	7.160	2	108	.001	5.901	2	67.717	.004	Fails at 2σ
	W.G	5.929	108	.055											
	Tot.	6.650	110												
(3x) Ni58-100ppm	B.G.	.047	2	.023	1.623	.202	2.047	2	108	.134					1σ
	W.G	1.549	108	.014											
	Tot.	1.596	110												
(3x) Cu65-Blank	B.G.	7.054	2	3.527	7.213	.001	41.703	2	108	.000	9.389	2	66.576	.000	Fails at 2σ
	W.G	52.809	108	.489											
	Tot.	59.863	110												
(3x) Cu65-1ppm	B.G.	1.200	2	.600	3.679	.028	3.117	2	108	.048	4.054	2	69.009	.022	2σ
	W.G	17.608	108	.163											
	Tot.	18.807	110												
(3x) Cu65-2ppm	B.G.	2.258	2	1.129	8.269	.000	.055	2	108	.947					Fails at 2σ
	W.G	14.745	108	.137											
	Tot.	17.002	110												
(3x) Cu65-5ppm	B.G.	1.228	2	.614	4.566	.012	4.510	2	108	.013	3.969	2	68.949	.023	2σ
	W.G	14.527	108	.135											
	Tot.	15.756	110												
(3x) Cu65-10ppm	B.G.	.050	2	.025	.397	.673	3.299	2	108	.041	.466	2	69.795	.630	1σ
	W.G	6.764	108	.063											
	Tot.	6.814	110												
(3x) Cu65-20ppm	B.G.	1.133	2	.567	5.935	.004	4.463	2	108	.014	4.710	2	68.636	.012	2σ
	W.G	10.312	108	.095											
	Tot.	11.445	110												
(3x) Cu65-50ppm	B.G.	.411	2	.206	3.334	.039	1.348	2	108	.264					2σ
	W.G	6.662	108	.062											
	Tot.	7.074	110												
(3x) Cu65-100ppm	B.G.	.042	2	.021	3.624	.030	.831	2	108	.438					2σ
	W.G	.632	108	.006											
	Tot.	.675	110												
(3x) Mo95-Blank	B.G.	1.135	2	.568	2.980	.055	.249	2	108	.780					1σ
	W.G	20.577	108	.191											
	Tot	21.712	110												
(3x) Mo95-1ppm	B.G.	1.034	2	.517	8.401	.000	2.020	2	108	.138					Fails at 2σ
	W.G	6.645	108	.062											
	Tot.	7.679	110												
(3x) Mo95-2ppm	B.G.	.077	2	.039	1.255	.289	.888	2	108	.415					1σ
	W.G	3.314	108	.031											
	Tot.	3.391	110												
(3x) Mo95-5ppm	B.G.	.855	2	.428	13.564	.000	2.125	2	108	.124					Fails at 2σ
	W.G	3.404	108	.032											
	Tot.	4.260	110												

B.G. = Between Group Variance; W.G. =Within Group Variance; SS = Sum of Squares; MS = Mean Square; LS = Leven Statistic; WS = Welch Statistic

Table 2B-2 continued.

		ANOVA					Test of Homogeneity of Variances				Robust Tests of Equality of Means				Pass at:
Variance		SS	df	MS	F	Sig.	LS	df1	df2	Sig.	WS	df1	df2	Sig.	
(3x) Mo95-10ppm	B.G.	.129	2	.064	9.550	.000	.764	2	108	.468					Fails at 2σ
	W.G	.727	108	.007											
	Tot.	.855	110												
(3x) Mo95-20ppm	B.G.	.907	2	.453	6.949	.001	7.104	2	108	.001	8.496	2	62.557	.001	Fails at 2σ
	W.G	7.046	108	.065											
	Tot.	7.953	110												
(3x) Mo95-50ppm	B.G.	.364	2	.182	7.336	.001	3.540	2	108	.032	5.856	2	66.657	.005	Fails at 2σ
	W.G	2.678	108	.025											
	Tot.	3.042	110												
(3x) Mo95-100ppm	B.G.	.174	2	.087	5.082	.008	6.005	2	108	.003	3.577	2	68.100	.033	2σ
	W.G	1.848	108	.017											
	Tot.	2.022	110												
(3x) U238-Blank	B.G.	2.040	2	1.020	3.352	.039	5.195	2	108	.007	6.417	2	60.640	.003	2σ
	W.G	32.867	108	.304											
	Tot.	34.907	110												
(3x) U238-1ppm	B.G.	.347	2	.174	.789	.457	.021	2	108	.980					1σ
	W.G	23.762	108	.220											
	Tot.	24.109	110												
(3x) U238-2ppm	B.G.	2.274	2	1.137	4.824	.010	8.724	2	108	.000	4.942	2	67.566	.010	2σ
	W.G	25.462	108	.236											
	Tot.	27.736	110												
(3x) U238-5ppm	B.G.	.014	2	.007	.070	.933	13.951	2	108	.000	.049	2	63.522	.952	1σ
	W.G	10.738	108	.099											
	Tot.	10.752	110												
(3x) U238-10ppm	B.G.	.186	2	.093	1.284	.281	1.717	2	108	.185					1σ
	W.G	7.807	108	.072											
	Tot.	7.992	110												
(3x) U238-20ppm	B.G.	.024	2	.012	.207	.813	2.667	2	108	.074					1σ
	W.G	6.213	108	.058											
	Tot.	6.237	110												
(3x) U238-50ppm	B.G.	.095	2	.048	.948	.391	3.363	2	108	.038	1.360	2	68.057	.264	1σ
	W.G	5.433	108	050											
	Tot.	5.529	110												
(3x) U238-100ppm	B.G.	.047	2	.023	2.609	.078	1.096	2	108	.338					1σ
	W.G	.970	108	.009											
	Tot.	1.017	110												

B.G. = Between Group Variance; W.G. =Within Group Variance; SS = Sum of Squares; MS = Mean Square; LS = Leven Statistic; WS = Welch Statistic

Table 2B-3. ANOVA tests for all elements routinely measured, calculated for three replicate XRF pressed pellets prepared from the same representative sample (Fu 2.90) and analyzed 6x each. **A)** ANOVA tests assuming equal variances and **(B)** tests of variance homogeneity showing that adjusted ANOVA statistics **(C)** are required for some cases. Concentration differences among the three pellets are significant at the 95% confidence level if the 'Sig.' parameter in Column A is <0.05. If the 'Sig.' parameter in Column B is also <0.05, refer to the adjusted ANOVA in Column C.

A. **B.** **C.**

		ANOVA					Test of Homogeneity of Variances				Robst Tests of Equality of Means (Welch)			
		Sum of Squares	df	Mean Square	F	Sig.	Levene Statistic	df1	df2	Sig.	Stat.[a]	df1	df2	Sig.
Na	Between Groups	.000	2	.000	74.817	.000	1.529	2	15	.249	97.479	2	9.702	.000
	Within Groups	.000	15	.000										
	Total	.000	17											
Mg	Between Groups	.000	2	.000	58.900	.000	.280	2	15	.760	67.485	2	9.580	.000
	Within Groups	.000	15	.000										
	Total	.000	17											
Al	Between Groups	.000	2	.000	22.890	.000	1.607	2	15	.233	26.500	2	9.541	.000
	Within Groups	.000	15	.000										
	Total	.000	17											
Si	Between Groups	.000	2	.000	5.482	.016	1.176	2	15	.335	7.343	2	9.191	.012
	Within Groups	.001	15	.000										
	Total	.001	17											
P	Between Groups	.000	2	.000	.929	.417	.590	2	15	.567	.951	2	9.837	.419
	Within Groups	.000	15	.000										
	Total	.000	17											
S	Between Groups	.000	2	.000	66.286	.000	3.803	2	15	.046	41.622	2	9.448	.000
	Within Groups	.000	15	.000										
	Total	.000	17											
K	Between Groups	.000	2	.000	1.387	.280	.205	2	15	.817	1.218	2	9.817	.337
	Within Groups	.000	15	.000										
	Total	.000	17											
Ti	Between Groups	9.759	2	4.880	8.448	.003	.794	2	15	.470	12.871	2	9.558	.002
	Within Groups	8.664	15	.578										
	Total	18.423	17											
V	Between Groups	.781	2	.391	1.352	.289	1.200	2	15	.328	1.088	2	9.511	.375
	Within Groups	4.334	15	.289										
	Total	5.115	17											
Cr	Between Groups	2.953	2	1.476	7.156	.007	1.006	2	15	.389	6.362	2	9.535	.018
	Within Groups	3.095	15	.206										
	Total	6.047	17											
Mn	Between Groups	14.664	2	7.332	2.451	.120	3.211	2	15	.069	1.584	2	8.240	.262
	Within Groups	44.877	15	2.992										
	Total	59.540	17											
Fe	Between Groups	3433.725	2	1716.863	8.054	.004	1.746	2	15	.208	18.171	2	8.767	.001
	Within Groups	3197.588	15	213.173										
	Total	6631.313	17											
Co	Between Groups	.183	2	.091	.299	.746	3.534	2	15	.055	.278	2	8.880	.764
	Within Groups	4.577	15	.305										
	Total	4.760	17											

a. Asymptotically F distributed.

Table 2B-3 continued.

A.

		ANOVA				
		Sum of Squares	df	Mean Square	F	Sig.
Ni	Between Groups	.107	2	.054	.590	.567
	Within Groups	1.364	15	.091		
	Total	1.471	17			
Cu	Between Groups	.198	2	.099	.877	.436
	Within Groups	1.691	15	.113		
	Total	1.889	17			
Zn	Between Groups	.250	2	.125	1.408	.275
	Within Groups	1.330	15	.089		
	Total	1.580	17			
Sr	Between Groups	11.227	2	5.613	1.367	.285
	Within Groups	61.612	15	4.107		
	Total	72.838	17			
Zr	Between Groups	.571	2	.285	2.854	.089
	Within Groups	1.499	15	.100		
	Total	2.070	17			
Mo	Between Groups	.769	2	.384	3.088	.075
	Within Groups	1.867	15	.124		
	Total	2.636	17			
Ba	Between Groups	15.785	2	7.892	1.538	.247
	Within Groups	76.964	15	5.131		
	Total	92.748	17			
Ca	Between Groups	.025	2	.013	3.205	.069
	Within Groups	.059	15	.004		
	Total	.085	17			
Rb	Between Groups	.090	2	.045	.666	.528
	Within Groups	1.014	15	.068		
	Total	1.104	17			
Pb	Between Groups	.791	2	.396	5.027	.021
	Within Groups	1.180	15	.079		
	Total	1.971	17			
Th	Between Groups	.703	2	.352	3.178	.071
	Within Groups	1.659	15	.111		
	Total	2.363	17			
U	Between Groups	.111	2	.056	.791	.471
	Within Groups	1.055	15	.070		
	Total	1.166	17			

B.

	Test of Homogeneity of Variances			
	Levene Statistic	df1	df2	Sig.
Ni	.741	2	15	.493
Cu	2.504	2	15	.115
Zn	2.061	2	15	.162
Sr	1.674	2	15	.221
Zr	.233	2	15	.795
Mo	1.465	2	15	.262
Ba	.167	2	15	.848
Ca	9.428	2	15	.002
Rb	.791	2	15	.471
Pb	1.344	2	15	.290
Th	.146	2	15	.866
U	.660	2	15	.531

C.

	Robst Tests of Equality of Means (Welch)			
	Stat.[a]	df1	df2	Sig.
Ni	.444	2	9.587	.654
Cu	2.020	2	8.486	.192
Zn	2.287	2	9.341	.155
Sr	.796	2	8.978	.480
Zr	2.372	2	9.931	.144
Mo	2.312	2	9.337	.153
Ba	1.436	2	9.968	.283
Ca	1.668	2	8.368	.246
Rb	.611	2	9.355	.563
Pb	6.537	2	9.558	.016
Th	3.424	2	9.646	.075
U	.723	2	9.768	.510

a. Asymptotically F distributed.

Table 2B-3 continued. D. Post hoc tests assuming unequal variances and demonstrating which specific cases are alike or different (denoted by '*').

D.

Multiple Comparisons

Post Hoc Tests: Tamha

Dependent Variable	(I) Run	(J) Run	Mean Difference (I-J)	Std. Error	Sig.	95% Confidence Interval Lower Bound	95% Confidence Interval Upper Bound
Na	1	2	-.001167	.000601	.233	-.00293	.00059
		3	.005167*	.000582	.000	.00344	.00690
	2	1	.001167	.000601	.233	-.00059	.00293
		3	.006333*	.000459	.000	.00502	.00765
	3	1	-.005167*	.000582	.000	-.00690	-.00344
		2	-.006333*	.000459	.000	-.00765	-.00502
Mg	1	2	.001167	.000477	.102	-.00021	.00254
		3	.004500*	.000428	.000	.00322	.00578
	2	1	-.001167	.000477	.102	-.00254	.00021
		3	.003333*	.000380	.000	.00223	.00444
	3	1	-.004500*	.000428	.000	-.00578	-.00322
		2	-.003333*	.000380	.000	-.00444	-.00223
Al	1	2	-.004167*	.000703	.001	-.00630	-.00203
		3	-.001167	.000703	.358	-.00330	.00097
	2	1	.004167*	.000703	.001	.00203	.00630
		3	.003000*	.000471	.000	.00165	.00435
	3	1	.001167	.000703	.358	-.00097	.00330
		2	-.003000*	.000471	.000	-.00435	-.00165
Si	1	2	-.007167	.003317	.182	-.01729	.00295
		3	.004000	.003893	.698	-.00718	.01518
	2	1	.007167	.003317	.182	-.00295	.01729
		3	.011167*	.002979	.016	.00227	.02006
	3	1	-.004000	.003893	.698	-.01518	.00718
		2	-.011167*	.002979	.016	-.02006	-.00227
P	1	2	-.000667	.000527	.557	-.00220	.00087
		3	-.000167	.000543	.987	-.00174	.00140
	2	1	.000667	.000527	.557	-.00087	.00220
		3	.000500	.000453	.651	-.00080	.00180
	3	1	.000167	.000543	.987	-.00140	.00174
		2	-.000500	.000453	.651	-.00180	.00080
S	1	2	.009167*	.000980	.000	.00614	.01219
		3	.008167*	.000980	.000	.00514	.01119
	2	1	-.009167*	.000980	.000	-.01219	-.00614
		3	-.001000	.000606	.341	-.00273	.00073
	3	1	-.008167*	.000980	.000	-.01119	-.00514
		2	.001000	.000606	.341	-.00073	.00273
K	1	2	.000333	.001261	.992	-.00333	.00400
		3	.002000	.001386	.448	-.00197	.00597
	2	1	-.000333	.001261	.992	-.00400	.00333
		3	.001667	.001206	.486	-.00182	.00515
	3	1	-.002000	.001386	.448	-.00597	.00197
		2	-.001667	.001206	.486	-.00515	.00182
Tl	1	2	-.7563	.4710	.383	-2.186	.673
		3	1.0398	.4885	.181	-.411	2.491
	2	1	.7563	.4710	.383	-.673	2.186
		3	1.7962*	.3423	.001	.813	2.779
	3	1	-1.0398	.4885	.181	-2.491	.411
		2	-1.7962*	.3423	.001	-2.779	-.813
V	1	2	-.5097	.3468	.438	-1.517	.498
		3	-.2757	.2592	.678	-1.028	.477
	2	1	.5097	.3468	.438	-.498	1.517
		3	.2340	.3186	.863	-.728	1.196
	3	1	.2757	.2592	.678	-.477	1.028
		2	-.2340	.3186	.863	-1.196	.728

*. The mean difference is significant at the 0.05 level.

Table 2B-3 continued. D. Post hoc tests assuming unequal variances and demonstrating which specific cases are alike or different (denoted by '*').

D.

Multiple Comparisons

Post Hoc Tests: Tamha

Dependent Variable	(I) Run	(J) Run	Mean Difference (I-J)	Std. Error	Sig.	95% Confidence Interval Lower Bound	95% Confidence Interval Upper Bound
Cr	1	2	-.6025	.2117	.053	-1.214	.009
		3	-.9838*	.2927	.026	-1.843	-.125
	2	1	.6025	.2117	.053	-.009	1.214
		3	-.3813	.2754	.497	-1.216	.453
	3	1	.9838*	.2927	.026	.125	1.843
		2	.3813	.2754	.497	-.453	1.216
Mn	1	2	2.1453	1.1813	.273	-1.263	5.554
		3	.6100	.8059	.855	-1.926	3.146
	2	1	-2.1453	1.1813	.273	-5.554	1.263
		3	-1.5353	.9731	.416	-4.690	1.620
	3	1	-.6100	.8059	.855	-3.146	1.926
		2	1.5353	.9731	.416	-1.620	4.690
Fe	1	2	2.2320	9.9464	.995	-28.464	32.928
		3	30.3512*	5.1510	.001	15.092	45.610
	2	1	-2.2320	9.9464	.995	-32.928	28.464
		3	28.1192	9.3653	.071	-2.637	58.875
	3	1	-30.3512*	5.1510	.001	-45.610	-15.092
		2	-28.1192	9.3653	.071	-58.875	2.637
Co	1	2	.0645	.2694	.994	-.753	.882
		3	.2385	.3106	.849	-.730	1.207
	2	1	-.0645	.2694	.994	-.882	.753
		3	.1740	.3689	.956	-.887	1.235
	3	1	-.2385	.3106	.849	-1.207	.730
		2	-.1740	.3689	.956	-1.235	.887
Ni	1	2	-.0655	.1573	.969	-.525	.394
		3	.1208	.1702	.873	-.384	.626
	2	1	.0655	.1573	.969	-.394	.525
		3	.1863	.1929	.734	-.367	.739
	3	1	-.1208	.1702	.873	-.626	.384
		2	-.1863	.1929	.734	-.739	.367
Cu	1	2	.1613	.2105	.854	-.533	.856
		3	.2537	.1251	.217	-.126	.633
	2	1	-.1613	.2105	.854	-.856	.533
		3	.0923	.2298	.973	-.604	.789
	3	1	-.2537	.1251	.217	-.633	.126
		2	-.0923	.2298	.973	-.789	.604
Zn	1	2	.0165	.1895	1.000	-.577	.610
		3	.2577	.1193	.161	-.086	.601
	2	1	-.0165	.1895	1.000	-.610	.577
		3	.2412	.1963	.588	-.357	.839
	3	1	-.2577	.1193	.161	-.601	.086
		2	-.2412	.1963	.588	-.839	.357
Sr	1	2	1.7972	1.3745	.548	-2.498	6.093
		3	.2787	.6926	.972	-1.741	2.298
	2	1	-1.7972	1.3745	.548	-6.093	2.498
		3	-1.5185	1.3185	.647	-5.827	2.790
	3	1	-.2787	.6926	.972	-2.298	1.741
		2	1.5185	1.3185	.647	-2.790	5.827
Zr	1	2	-.3973	.1879	.174	-.939	.144
		3	-.3543	.1890	.250	-.898	.190
	2	1	.3973	.1879	.174	-.144	.939
		3	.0430	.1700	.993	-.443	.529
	3	1	.3543	.1890	.250	-.190	.898
		2	-.0430	.1700	.993	-.529	.443

*. The mean difference is significant at the 0.05 level.

Table 2B-3 continued. D. Post hoc tests assuming unequal variances and demonstrating which specific cases are alike or different (denoted by '*').

D.

Multiple Comparisons

Post Hoc Tests: Tamha

Dependent Variable	(I) Run	(J) Run	Mean Difference (I-J)	Std. Error	Sig.	95% Confidence Interval Lower Bound	95% Confidence Interval Upper Bound
Mo	1	2	.5058	.2306	.156	-.164	1.176
		3	.2693	.2078	.550	-.366	.905
	2	1	-.5058	.2306	.156	-1.176	.164
		3	-.2365	.1676	.473	-.728	.255
	3	1	-.2693	.2078	.550	-.905	.366
		2	.2365	.1676	.473	-.255	.728
Ba	1	2	-2.1618	1.3474	.364	-6.022	1.699
		3	-.4168	1.3204	.986	-4.208	3.374
	2	1	2.1618	1.3474	.364	-1.699	6.022
		3	1.7450	1.2537	.477	-1.842	5.332
	3	1	.4168	1.3204	.986	-3.374	4.208
		2	-1.7450	1.2537	.477	-5.332	1.842
Ca	1	2	.0757	.0424	.343	-.069	.221
		3	.0832	.0438	.286	-.060	.226
	2	1	-.0757	.0424	.343	-.221	.069
		3	.0075	.0156	.955	-.039	.054
	3	1	-.0832	.0438	.286	-.226	.060
		2	-.0075	.0156	.955	-.054	.039
Rb	1	2	.1483	.1692	.785	-.336	.633
		3	.1517	.1367	.655	-.255	.558
	2	1	-.1483	.1692	.785	-.633	.336
		3	.0033	.1423	1.000	-.423	.430
	3	1	-.1517	.1367	.655	-.558	.255
		2	-.0033	.1423	1.000	-.430	.423
Pb	1	2	.4717	.1758	.084	-.062	1.006
		3	.4117*	.1239	.023	.057	.767
	2	1	-.4717	.1758	.084	-1.006	.062
		3	-.0600	.1801	.984	-.599	.479
	3	1	-.4117*	.1239	.023	-.767	-.057
		2	.0600	.1801	.984	-.479	.599
Th	1	2	-.0617	.2023	.988	-.667	.544
		3	-.4467	.2114	.180	-1.066	.173
	2	1	.0617	.2023	.988	-.544	.667
		3	-.3850	.1581	.103	-.839	.069
	3	1	.4467	.2114	.180	-.173	1.066
		2	.3850	.1581	.103	-.069	.839
U	1	2	.1633	.1425	.827	-.250	.576
		3	-.0067	.1496	1.000	-.444	.430
	2	1	-.1633	.1425	.627	-.576	.250
		3	-.1700	.1662	.700	-.646	.306
	3	1	.0067	.1496	1.000	-.430	.444
		2	.1700	.1662	.700	-.306	.646

*. The mean difference is significant at the 0.05 level.

Table 2B-4. Replicate XRF analyses of all elements routinely measured. Three pressed pellets (3 x 6x) were prepared from the same representative powdered carbonate sample, and were used to assess the precision of sample preparation and analyses. Measured concentrations are not corrected for absolute calibration backgrounds and LLDs.

Three replicate briquettes of a representative carbonate sample analyzed 6x each by XRF.

Sample		Na	Mg	Al	Si	P	S	K	Ti	V	Cr	Mn	Fe	Co	Ni	Cu	Zn	Sr	Zr	Mo	Ba	Ca (wt.%)	Rb	Pb	Th	U
		[wt.%]							[ppm]																	
Fu 2.90 3	Conc.	0.006	0.226	0.188	1.683	0.079	0.106	0.181	45.0	15.8	-20.1	275.3	2382.3	-1.8	3.7	9.5	12.7	293.6	10.0	0.3	9.4	37.39	8.8	0.3	3.0	1.3
	CSE [ppm]	0.001	0.001	0.001	0.002	0.000	0.001	0.001	0.9	0.7	0.7	1.4	1.6	0.4	0.3	0.3	0.3	0.4	0.3	0.3	2.3	0.03	0.2	0.3	0.3	0.2
Fu 2.90 3	Conc.	0.007	0.226	0.190	1.666	0.077	0.105	0.186	44.4	16.2	-19.8	274.9	2382.3	-2.2	4.6	9.7	12.9	292.8	10.4	0.9	7.1	37.40	8.7	0.6	3.0	0.8
	CSE [ppm]	0.001	0.001	0.001	0.002	0.000	0.001	0.001	0.9	0.7	0.7	1.4	1.6	0.4	0.3	0.3	0.3	0.4	0.3	0.3	2.3	0.03	0.2	0.3	0.3	0.2
Fu 2.90 3	Conc.	0.008	0.227	0.188	1.679	0.077	0.104	0.183	44.7	16.2	-21.0	275.0	2375.7	-0.9	4.4	9.5	13.3	292.7	9.9	0.7	7.9	37.33	8.8	0.5	2.6	1.3
	CSE [ppm]	0.001	0.001	0.001	0.002	0.000	0.001	0.001	0.9	0.7	0.7	1.4	1.6	0.4	0.3	0.3	0.3	0.4	0.3	0.3	2.3	0.03	0.2	0.3	0.3	0.2
Fu 2.90 3	Conc.	0.007	0.226	0.189	1.671	0.078	0.104	0.184	45.9	16.5	-20.5	274.7	2383.5	-0.9	4.2	9.7	12.8	292.7	10.3	0.4	8.8	37.37	8.4	0.5	2.2	0.6
	CSE [ppm]	0.001	0.001	0.001	0.002	0.000	0.001	0.001	0.9	0.7	0.7	1.4	1.6	0.4	0.3	0.3	0.3	0.4	0.3	0.3	2.3	0.03	0.2	0.3	0.3	0.2
Fu 2.90 3	Conc.	0.008	0.227	0.188	1.670	0.077	0.103	0.180	44.2	15.5	-21.4	274.4	2379.5	-1.5	3.9	9.4	12.9	291.7	10.7	0.9	9.1	37.42	8.8	0.4	2.9	1.2
	CSE [ppm]	0.001	0.001	0.001	0.002	0.000	0.001	0.001	0.9	0.7	0.7	1.4	1.6	0.4	0.3	0.3	0.3	0.4	0.3	0.3	2.3	0.03	0.2	0.3	0.3	0.2
Fu 2.90 3	Conc.	0.007	0.227	0.189	1.673	0.078	0.105	0.185	44.3	16.5	-20.4	273.1	2365.5	-0.3	4.5	10.1	12.9	290.8	10.3	0.7	3.7	37.36	8.9	0.1	2.8	1.1
	CSE [ppm]	0.001	0.001	0.001	0.002	0.000	0.001	0.001	0.9	0.7	0.7	1.4	1.6	0.4	0.3	0.3	0.3	0.4	0.3	0.3	2.3	0.03	0.2	0.3	0.3	0.2
Fu 2.90 2	Conc.	0.014	0.230	0.191	1.683	0.078	0.105	0.187	45.8	16.8	-21.1	273.3	2419.0	-0.9	4.6	9.6	13.7	292.4	10.6	0.4	5.6	37.37	8.5	0.6	2.7	0.9
	CSE [ppm]	0.001	0.001	0.001	0.002	0.000	0.001	0.001	0.9	0.7	0.7	1.4	1.6	0.4	0.3	0.3	0.3	0.4	0.3	0.3	2.3	0.03	0.2	0.3	0.3	0.2
Fu 2.90 2	Conc.	0.014	0.230	0.191	1.681	0.078	0.104	0.184	47.0	16.6	-20.7	275.1	2417.6	-1.7	4.5	10.0	13.1	292.6	10.0	0.4	10.0	37.40	8.8	0.5	2.2	0.9
	CSE [ppm]	0.001	0.001	0.001	0.002	0.000	0.001	0.001	0.9	0.7	0.7	1.4	1.6	0.4	0.3	0.3	0.3	0.4	0.3	0.3	2.3	0.03	0.2	0.3	0.3	0.2
Fu 2.90 2	Conc.	0.014	0.231	0.192	1.684	0.078	0.103	0.183	45.8	17.2	-20.9	274.2	2414.4	-1.5	4.9	9.9	12.9	292.2	10.6	0.7	9.7	37.37	9.3	0.9	2.2	1.4
	CSE [ppm]	0.001	0.001	0.001	0.002	0.000	0.001	0.001	0.9	0.7	0.7	1.4	1.6	0.4	0.3	0.3	0.3	0.4	0.3	0.3	2.3	0.03	0.2	0.3	0.3	0.2
Fu 2.90 2	Conc.	0.014	0.230	0.193	1.689	0.079	0.104	0.185	46.9	16.5	-21.5	274.9	2412.7	-0.5	4.3	10.2	12.5	291.7	10.2	0.4	8.7	37.37	8.7	-0.2	2.2	0.6
	CSE [ppm]	0.001	0.001	0.001	0.002	0.000	0.001	0.001	0.9	0.7	0.7	1.4	1.6	0.4	0.3	0.3	0.3	0.4	0.3	0.3	2.3	0.03	0.2	0.3	0.3	0.2
Fu 2.90 2	Conc.	0.013	0.229	0.192	1.682	0.079	0.102	0.187	46.8	15.4	-20.6	271.5	2412.0	-1.5	4.2	10.0	13.6	291.7	10.0	0.9	12.4	37.41	8.7	0.4	2.7	0.6
	CSE [ppm]	0.001	0.001	0.001	0.002	0.000	0.001	0.001	0.9	0.7	0.7	1.4	1.6	0.4	0.3	0.3	0.3	0.4	0.3	0.3	2.3	0.03	0.2	0.3	0.3	0.2
Fu 2.90 2	Conc.	0.012	0.229	0.191	1.690	0.077	0.103	0.183	46.9	15.6	-21.0	269.3	2391.9	-0.4	4.0	8.8	13.1	284.6	10.4	-0.1	9.9	37.41	8.4	0.2	2.1	0.8
	CSE [ppm]	0.001	0.001	0.001	0.002	0.000	0.001	0.001	0.9	0.7	0.7	1.4	1.5	0.4	0.3	0.3	0.3	0.4	0.3	0.3	2.3	0.03	0.2	0.3	0.3	0.2
Fu 2.90	Conc.	0.011	0.232	0.187	1.685	0.079	0.115	0.184	46.6	16.5	-21.8	276.3	2416.7	1.1	4.7	10.0	13.0	292.9	10.4	1.0	10.3	37.55	9.3	0.7	3.1	1.2
	CSE [ppm]	0.001	0.001	0.001	0.002	0.000	0.001	0.001	0.9	0.7	0.7	1.4	1.6	0.4	0.3	0.3	0.3	0.4	0.3	0.3	2.3	0.03	0.2	0.3	0.3	0.2
Fu 2.90	Conc.	0.014	0.232	0.189	1.677	0.078	0.114	0.182	45.6	16.3	-21.0	276.0	2414.8	-1.1	4.6	9.8	13.3	294.2	9.5	1.2	8.1	37.46	8.9	1.0	2.3	1.0
	CSE [ppm]	0.001	0.001	0.001	0.002	0.000	0.001	0.001	0.9	0.7	0.7	1.4	1.6	0.4	0.3	0.3	0.3	0.4	0.3	0.3	2.3	0.03	0.2	0.3	0.3	0.2
Fu 2.90	Conc.	0.012	0.231	0.189	1.679	0.078	0.114	0.187	46.4	15.7	-21.6	273.9	2411.9	-1.4	4.1	10.1	12.9	293.5	9.8	1.5	8.4	37.56	8.7	0.8	2.2	1.0
	CSE [ppm]	0.001	0.001	0.001	0.002	0.000	0.001	0.001	0.9	0.7	0.7	1.4	1.6	0.4	0.3	0.3	0.3	0.4	0.3	0.3	2.3	0.03	0.2	0.3	0.3	0.2
Fu 2.90	Conc.	0.011	0.231	0.188	1.686	0.077	0.113	0.189	46.6	15.9	-21.7	277.6	2417.6	-0.5	4.1	9.8	13.3	293.5	9.6	1.2	7.8	37.53	9.1	0.7	2.3	1.0
	CSE [ppm]	0.001	0.001	0.001	0.002	0.000	0.001	0.001	0.9	0.7	0.7	1.4	1.6	0.4	0.3	0.3	0.3	0.4	0.3	0.3	2.3	0.03	0.2	0.3	0.3	0.2
Fu 2.90	Conc.	0.013	0.230	0.187	1.669	0.076	0.110	0.184	45.6	15.6	-21.1	272.6	2394.6	-0.9	4.3	9.8	13.2	291.3	10.2	0.4	5.3	37.36	8.8	1.2	1.8	1.2
	CSE [ppm]	0.001	0.001	0.001	0.002	0.000	0.001	0.001	0.9	0.7	0.7	1.4	1.6	0.4	0.3	0.3	0.3	0.4	0.3	0.3	2.3	0.03	0.2	0.3	0.3	0.2
Fu 2.90	Conc.	0.013	0.230	0.185	1.670	0.077	0.110	0.185	43.9	15.1	-22.0	274.6	2395.4	-1.2	4.3	10.0	13.3	290.7	9.8	0.4	3.5	37.32	8.5	0.8	2.0	0.6
	CSE [ppm]	0.001	0.001	0.001	0.002	0.000	0.001	0.001	0.9	0.7	0.7	1.4	1.6	0.4	0.3	0.3	0.3	0.4	0.3	0.3	2.3	0.03	0.2	0.3	0.3	0.2

Table 2B-4 continued.

Three replicate briquettes of a representative carbonate sample analyzed 6x each by XRF.

Sample	Na	Mg	Al	Si	P	S	K	Ti	V	Cr	Mn	Fe	Co	Ni	Cu	Zn	Sr	Zr	Mo	Ba	Ca (%)	Rb	Pb	Th	U
	[wt.%]							[ppm]																	
Ave. conc. Run3	**0.007**	**0.227**	**0.189**	**1.674**	**0.078**	**0.105**	**0.183**	**44.7**	**16.1**	**-20.5**	**274.6**	**2378.1**	**-1.3**	**4.2**	**9.7**	**12.9**	**292.4**	**10.3**	**0.7**	**7.6**	**37.38**	**8.7**	**0.4**	**2.7**	**1.0**
1σ	0.001	0.001	0.001	0.006	0.001	0.001	0.002	0.6	0.4	0.6	0.8	6.8	0.7	0.4	0.3	0.2	1.0	0.3	0.2	2.1	0.0	0.2	0.2	0.3	0.3
1σ as % of mean	10.5%	0.2%	0.4%	0.4%	1.1%	1.0%	1.3%	1.4%	2.4%	-2.9%	0.3%	0.3%	-56.1%	8.3%	2.8%	1.7%	0.3%	2.9%	35.1%	27.7%	0.1%	2.0%	50.5%	10.7%	29.3%
Ave. conc. Run2	**0.014**	**0.230**	**0.192**	**1.685**	**0.078**	**0.104**	**0.185**	**46.5**	**16.3**	**-20.9**	**273.0**	**2406.3**	**-1.1**	**4.4**	**9.7**	**13.2**	**290.9**	**10.3**	**0.4**	**9.4**	**37.39**	**8.7**	**0.4**	**2.4**	**0.8**
1σ	0.001	0.001	0.001	0.004	0.001	0.001	0.002	0.5	0.7	0.3	2.3	21.9	0.6	0.3	0.5	0.4	3.1	0.3	0.3	2.2	0.0	0.3	0.4	0.3	0.3
1σ as % of mean	6.2%	0.3%	0.4%	0.2%	1.0%	1.0%	1.0%	1.2%	4.2%	-1.5%	0.8%	0.9%	53.5%	7.1%	5.1%	3.2%	1.1%	2.8%	79.2%	23.6%	0.1%	3.5%	98.5%	10.7%	32.6%
Ave. conc. Run1	**0.012**	**0.231**	**0.188**	**1.678**	**0.078**	**0.113**	**0.185**	**45.8**	**15.8**	**-21.5**	**275.2**	**2408.5**	**-1.0**	**4.3**	**9.9**	**13.2**	**292.7**	**9.9**	**0.9**	**7.2**	**37.46**	**8.9**	**0.9**	**2.3**	**1.0**
1σ	0.001	0.001	0.002	0.007	0.001	0.002	0.002	1.0	0.5	0.4	1.6	15.6	0.3	0.2	0.1	0.2	1.4	0.4	0.5	2.4	0.1	0.3	0.2	0.4	0.2
1σ as % of mean	9.8%	0.4%	0.8%	0.4%	1.4%	1.9%	1.3%	2.2%	3.2%	-1.9%	0.7%	0.4%	-30.9%	5.1%	1.5%	1.4%	0.5%	3.6%	48.5%	33.8%	0.3%	3.2%	23.8%	19.6%	21.0%
Ave. CSE Run3	0.001	0.001	0.001	0.002	0.000	0.001	0.001	0.9	0.7	0.7	1.4	1.6	0.4	0.3	0.3	0.3	0.4	0.3	0.3	2.3	0.03	0.2	0.3	0.3	0.2
Ave. CSE Run2	0.001	0.001	0.001	0.002	0.000	0.001	0.001	0.9	0.7	0.7	1.4	1.6	0.4	0.3	0.3	0.3	0.4	0.3	0.3	2.3	0.03	0.2	0.3	0.3	0.2
Ave. CSE Run1	0.001	0.001	0.001	0.002	0.000	0.001	0.001	0.9	0.7	0.7	1.4	1.6	0.4	0.3	0.3	0.3	0.4	0.3	0.3	2.3	0.03	0.2	0.3	0.3	0.2
Overall average	**0.011**	**0.229**	**0.189**	**1.679**	**0.078**	**0.107**	**0.184**	**45.7**	**16.1**	**-21.0**	**274.3**	**2397.6**	**-1.1**	**4.3**	**9.8**	**13.1**	**292.0**	**10.2**	**0.7**	**8.1**	**37.4**	**8.8**	**0.6**	**2.5**	**1.0**
Overall precision (1σ)	**0.003**	**0.002**	**0.002**	**0.007**	**0.001**	**0.004**	**0.002**	**1.0**	**0.5**	**0.6**	**1.9**	**19.8**	**0.5**	**0.3**	**0.3**	**0.3**	**2.1**	**0.3**	**0.4**	**2.3**	**0.1**	**0.3**	**0.3**	**0.4**	**0.3**
1σ as % of mean	**27.0%**	**0.9%**	**1.1%**	**0.4%**	**1.1%**	**4.2%**	**1.2%**	**2.3%**	**3.4%**	**-2.8%**	**0.7%**	**0.8%**	**-47.2%**	**6.8%**	**3.4%**	**2.3%**	**0.7%**	**3.4%**	**58.4%**	**28.9%**	**0.2%**	**2.9%**	**60.6%**	**15.1%**	**27.3%**
Overall ave. CSE	**0.001**	**0.001**	**0.001**	**0.002**	**0.000**	**0.001**	**0.001**	**0.9**	**0.7**	**0.7**	**1.4**	**1.6**	**0.4**	**0.3**	**0.3**	**0.3**	**0.4**	**0.3**	**0.3**	**2.3**	**0.0**	**0.2**	**0.3**	**0.3**	**0.2**
Ave. LLD*	0.0060	0.0015	0.0327	0.0075	0.0000	0.0020	0.0022	2.0	1.6	2.0	2.9	2.0	1.4	0.7	0.9	1.0	2.4	1.3	0.9	7.5	0.14(wt.%)	0.6	1.0	0.7	0.6

* = 3σ of 12 measurements on 99.999% pure CaCO3 pressed pellets

Table 2B-5. WD-XRF analytical routine calibration details for all elements analyzed.

Calibration details for 'CarbTraceMaj' analytical routine

Analyte	D	E	K	Bg	Bg1	Bg2	Ratio channel	Lo(C) Ti	Lo(C) Sr	Lo(C) Ba
Na [%]	0.00	0.06	0.11309	Yes	Yes	Yes				
Mg [%]	-0.09	0.02	0.17859	Yes	No	Yes				
Al [%]	-0.01	0.06	0.10316	Yes	Yes	No				
Si [%]	0.32	0.07	0.14906	Yes	Yes	Yes				
P [%]	0.01	0.01	0.03777	Yes	Yes	Yes				
S [%]	0.00	0.03	0.01717	Yes	Yes	Yes				
K [ppm]	-0.01	0.02	0.08055	Yes	Yes	Yes				
Ti [ppm]	-35.55	170.55	0.01045	Yes	Yes	Yes				-0.01456
V [ppm]	1.43	28870.55	0.00126	Yes	Yes	Yes	**Rh1**	0.01887		
Cr [ppm]	-26.02	16389.23	0.02942	Yes	Yes	Yes	**Rh1**			
Mn [ppm]	88.33	11190.65	0.02809	Yes	Yes	Yes	**Rh1**			
Fe [ppm]	160.97	14078.97	0.06051	Yes	Yes	Yes	**Rh1**			
Co [ppm]	5.56	25502.15	0.00060	Yes	Yes	Yes	**Rh1**			
Ni [ppm]	-10.26	9061.20	0.00162	Yes	Yes	Yes	**Rh1**			
Cu [ppm]	-12.85	8875.95	0.00102	Yes	Yes	Yes	**Rh1**			
Zn [ppm]	-0.21	3254.60	0.00269	Yes	Yes	Yes	**Rh1**			
Sr [ppm]	1.59	976.10	0.00220	Yes	Yes	Yes	**Rh1**			
Zr [ppm]	11.36	802.46	0.00379	Yes	Yes	Yes	**Rh1**		0.09141	
Mo [ppm]	-85.58	800.99	0.00093	Yes	No	Yes	**Rh1**			
Ba [ppm]	-1.19	822.27	0.00673	Yes	Yes	Yes		-0.00146		
Ca [wt.%]	0.17	0.18	0.15833	Yes	Yes	Yes				

Calibration details for 'MgSliwUThRbPb' analytical routine

Analyte	D	E	K	Bg	Bg1	Bg2	Ratio channel	Lo(C) Rb	Lo(C) U
Rb [ppm]	0.83	747.46	0.00120	Yes	Yes	Yes	**Rh**		-0.40580
Pb [ppm]	-0.34	1403.23	0.00698	Yes	Yes	Yes	**Rh**		
Th [ppm]	3.66	85.16	0.00025	Yes	Yes	Yes		0.03298	
U [ppm]	-0.11	1475.91	0.00030	Yes	Yes	Yes	**Rh**	0.00030	

Regression model: C=D+E.R.M.; Error weighting: Sq. root; Weighting constant: 1000 for all elements except Na, Mg, Al, Si, P, S, K, for which weighing constant = 0.1

D: The intercept of the regression line; E: The slope of the regression line

K: The 'K-factor' indicating the goodness of the regression for Sq. Error Weighting.

Lo(C) of Xx: The concentration based line overlap correction factor for compound Xx.

Table 2B-5 continued.

PANalytical Axios Wave-length Dispersive X-ray Flourescence Spectrometer (WD-XRF) operating conditions

Channel	Type	Line	X-tal	Collimator	Detector	Tube filter	kV	mA	Angle (°2T)	Offset Bg1 (°2T)	Offset Bg2 (°2T)
Calibration details for 'CarbTraceMaj' analytical routine											
Na	Gonio	KA	PX1	700 µm	Flow*	None	32	125	27.0788	-1.4564	1.2508
Mg	Gonio	KA	PX1	700 µm	Flow*	None	32	125	22.411	-2.6422	2.732
Al	Gonio	KA	PE 002	300 µm	Flow*	None	32	125	144.9454	-1.0386	
Si	Gonio	KA	PE 002	300 µm	Flow*	None	32	125	109.153	-3.9356	6.1148
P	Gonio	KA	Ge 111	300 µm	Flow*	None	32	125	140.959	-3.4944	2.7938
S	Gonio	KA	Ge 111	300 µm	Flow*	None	32	125	110.6454	-1.5506	1.9962
K	Gonio	KA	LiF 200	300 µm	Flow*	None	32	125	136.7376	-0.9894	1.537
Ti	Gonio	KA	LiF 200	300 µm	Flow*	None	42	95	86.1878		
V	Gonio	KA	LiF 200	300 µm	Flow*	None	47	85	76.9382	-0.7452	1.169
Cr	Gonio	KA	LiF 200	300 µm	Flow*	None	57	70	69.3628	-0.603	1.1064
Mn	Gonio	KA	LiF 200	300 µm	Flow*	None	57	70	62.9978	-0.9428	1.6314
Fe	Gonio	KA	LiF 200	300 µm	Flow*	None	60	66	57.5336	-1.4124	1.202
Co	Gonio	KA	LiF 220	150 µm	Flow*	None	60	66	77.897	-3.5332	1.4096
Ni	Gonio	KA	LiF 200	300 µm	Flow*	None	60	66	48.675	-1.7826	1.1832
Cu	Gonio	KA	LiF 200	300 µm	Flow*	None	60	66	45.0266	-0.942	0.7056
Zn	Gonio	KA	LiF 200	300 µm	Scint. **	None	60	66	41.7736	-1.7828	0.6704
Sr	Gonio	KA	LiF 200	300 µm	Scint. **	None	60	66	25.1138	-0.6378	0.5612
Zr	Gonio	KA	LiF 200	300 µm	Scint. **	None	60	66	22.508	-0.4188	0.5424
Mo	Gonio	KA	LiF 200	300 µm	Scint. **	None	60	66	20.2812	-0.6108	0.5746
Ba	Gonio	LA	LiF 200	300 µm	Scint. **	None	42	95	87.2202	-1.9132	1.016
Rh1	Gonio	KA-C	LiF 200	300 µm	Scint. **	None	60	66	18.437	-0.531	1.2346
Ca	Gonio	KA	LiF 200	300 µm	Flow*	Al (200 µm)	32	125	113.1542	-2.4266	2.7542
Calibration details for 'MgSiIwUThRbPb' analytical routine											
Rb	Gonio	KA	LiF 220	150 µm	Scint. **	None	60	66	37.9588		
Pb	Gonio	LA	LiF 220	150 µm	Scint. **	None	60	66	48.7654	-0.4976	0.952
Th	Gonio	LA	LiF 220	150 µm	Scint. **	None	60	66	39.199		0.7896
U	Gonio	LA	LiF 220	150 µm	Scint. **	None	60	66	37.2858	-0.3634	
Rh	Gonio	KA-C	LiF 220	150 µm	Scint. **	None	60	66	26.1488	-0.8788	1.8534

*Flow proportional detector; **Scintillation detector.

Fig. 2B-1. Calibration plots of all analytes measured using the CarbTraceMaj and MgSliwUThRbPb WD-XRF analytical routines.

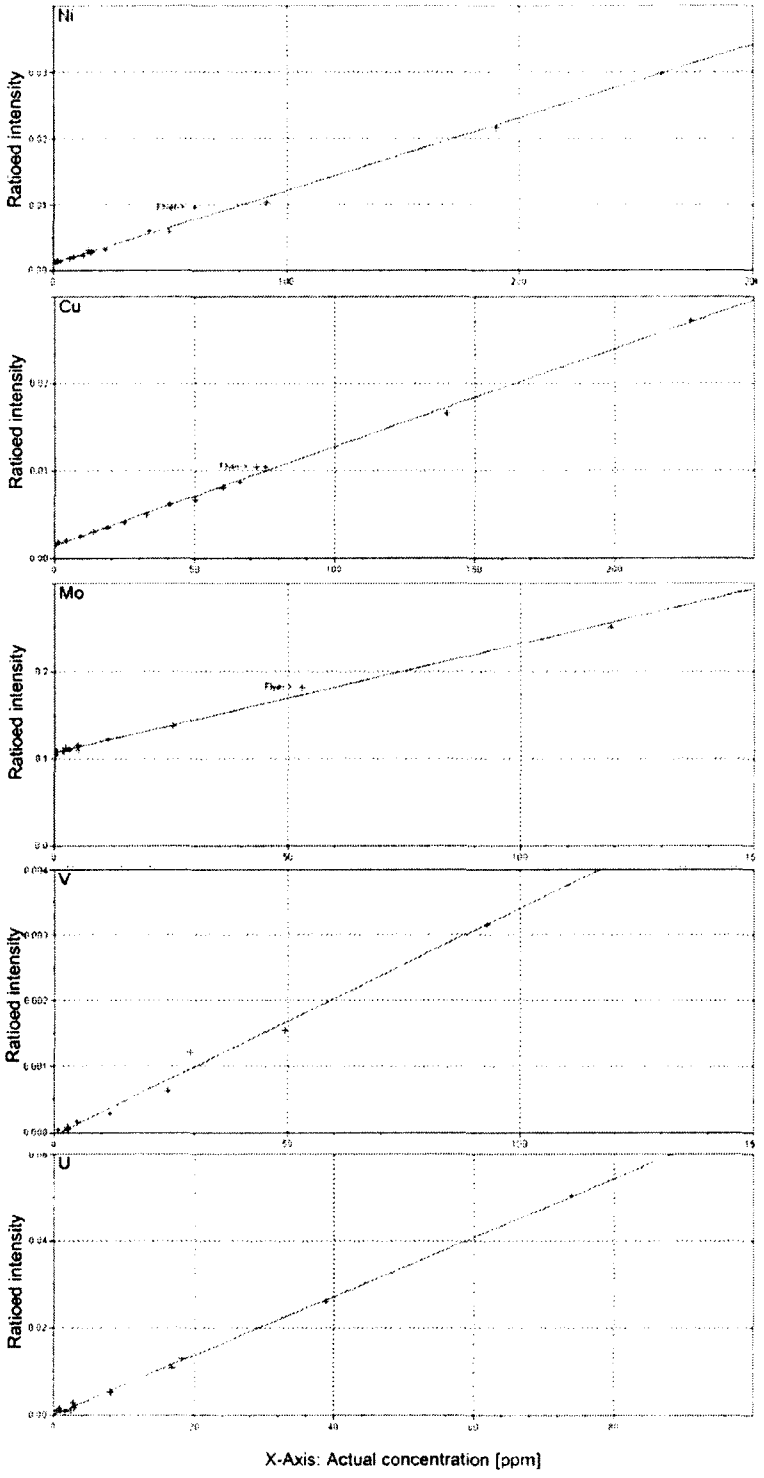

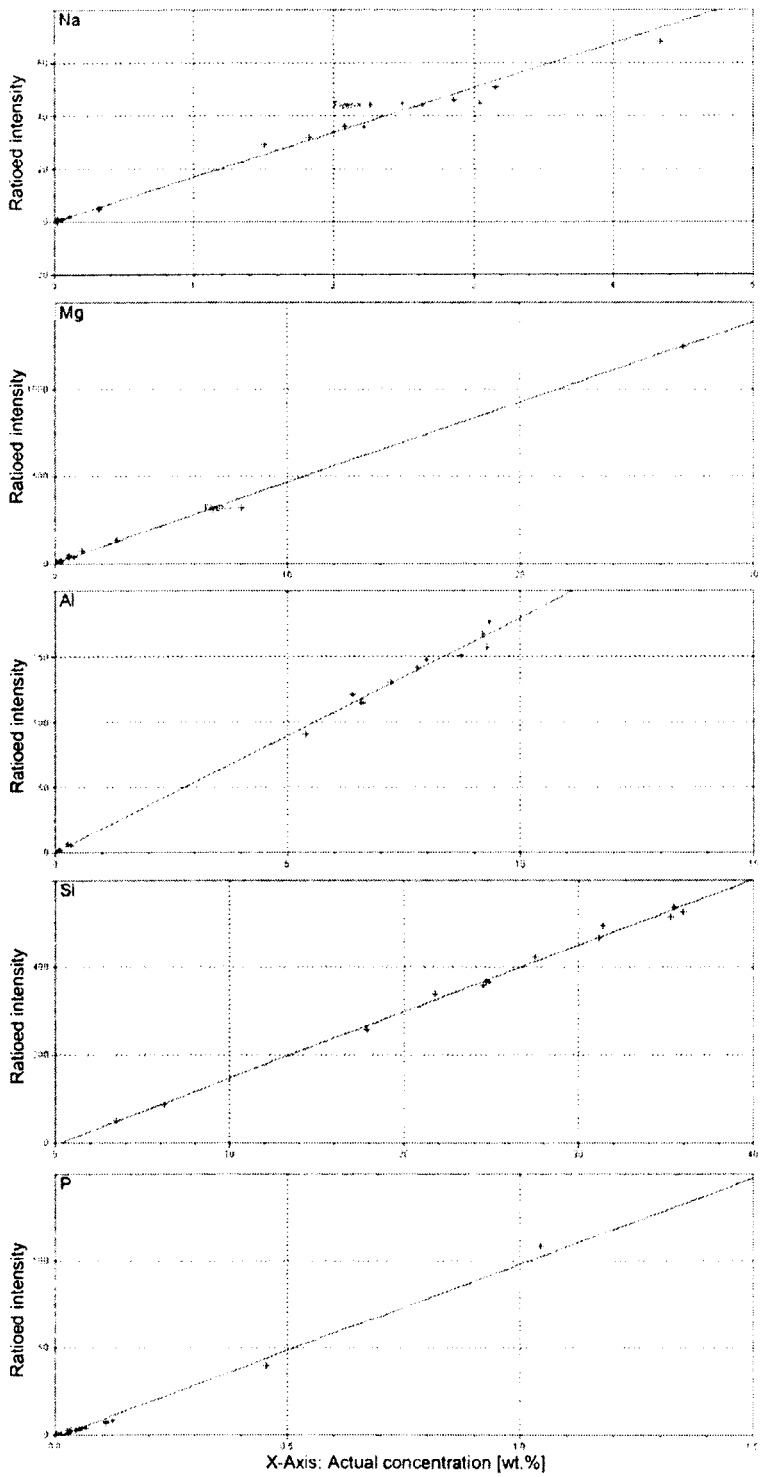

Fig. 2B-1 continued.

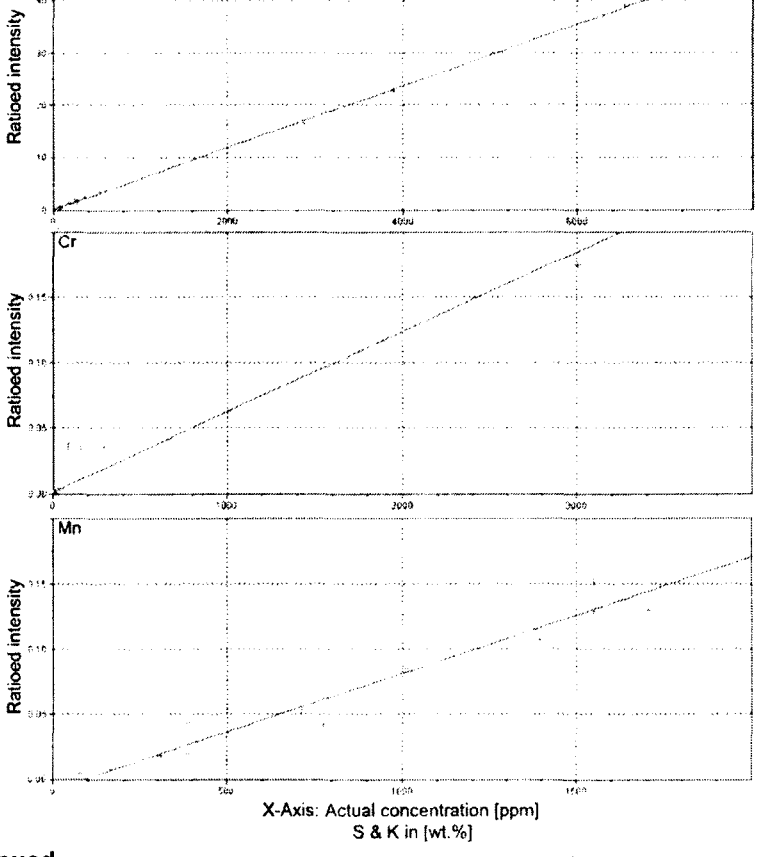

Fig. 2B-1 continued.

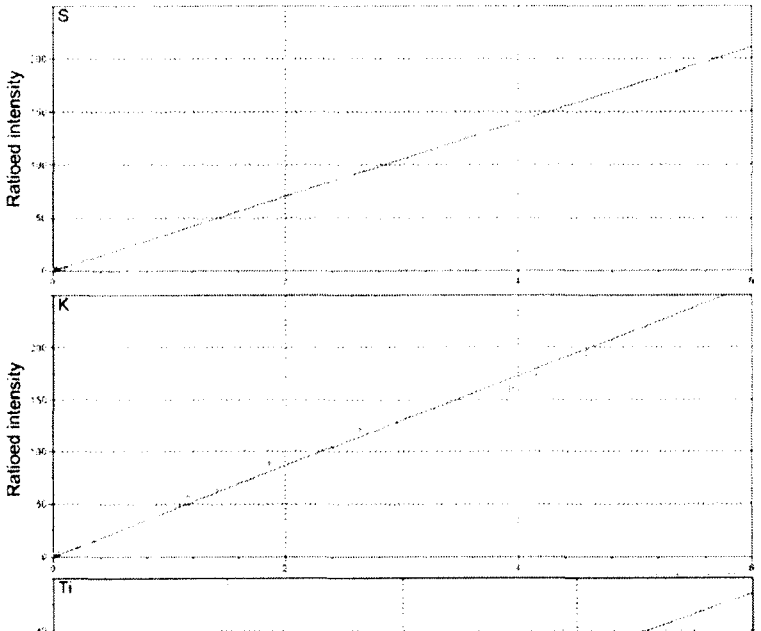
S
Ratioed intensity
K
Ratioed intensity
Ti

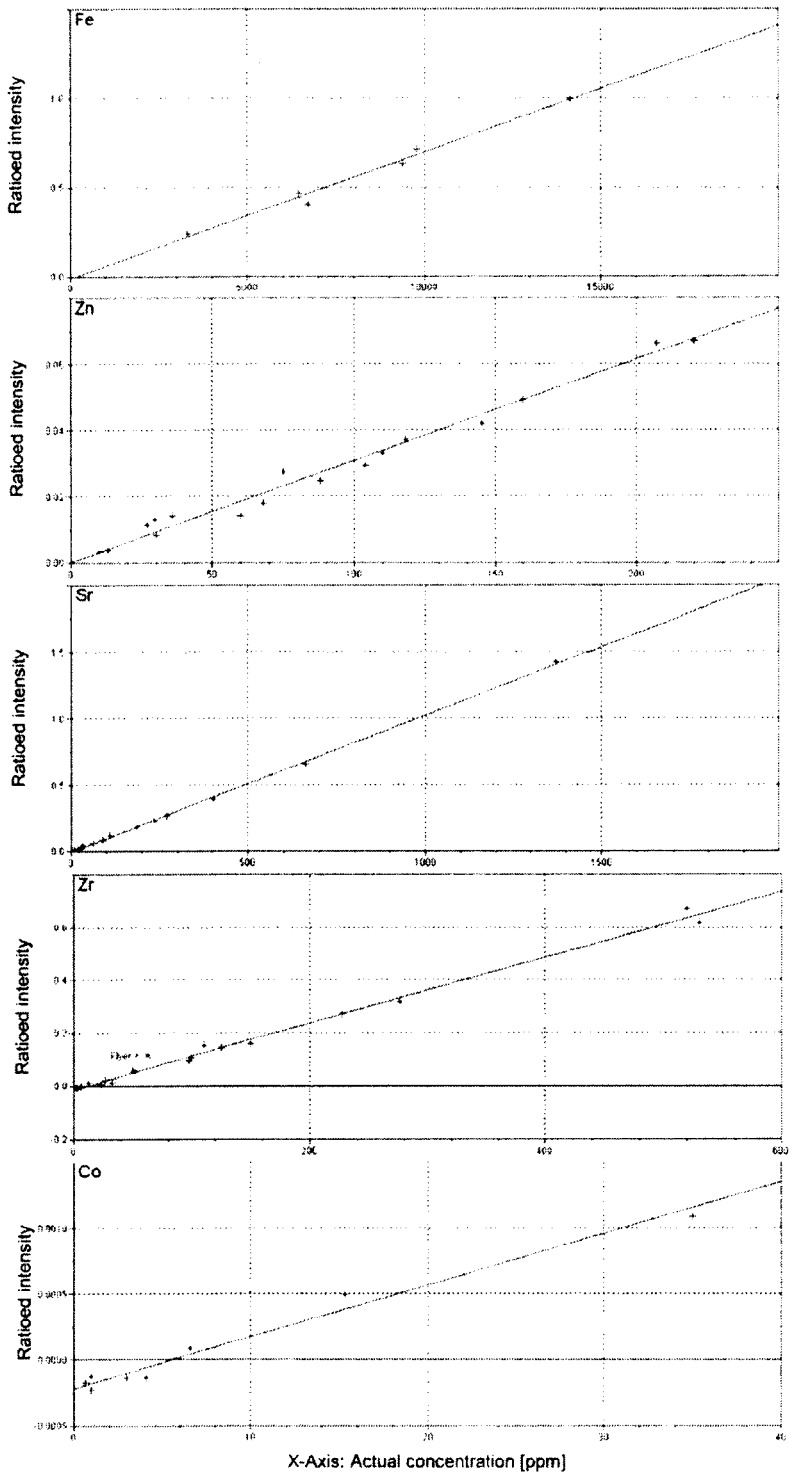

Fig. 2B-1 continued.

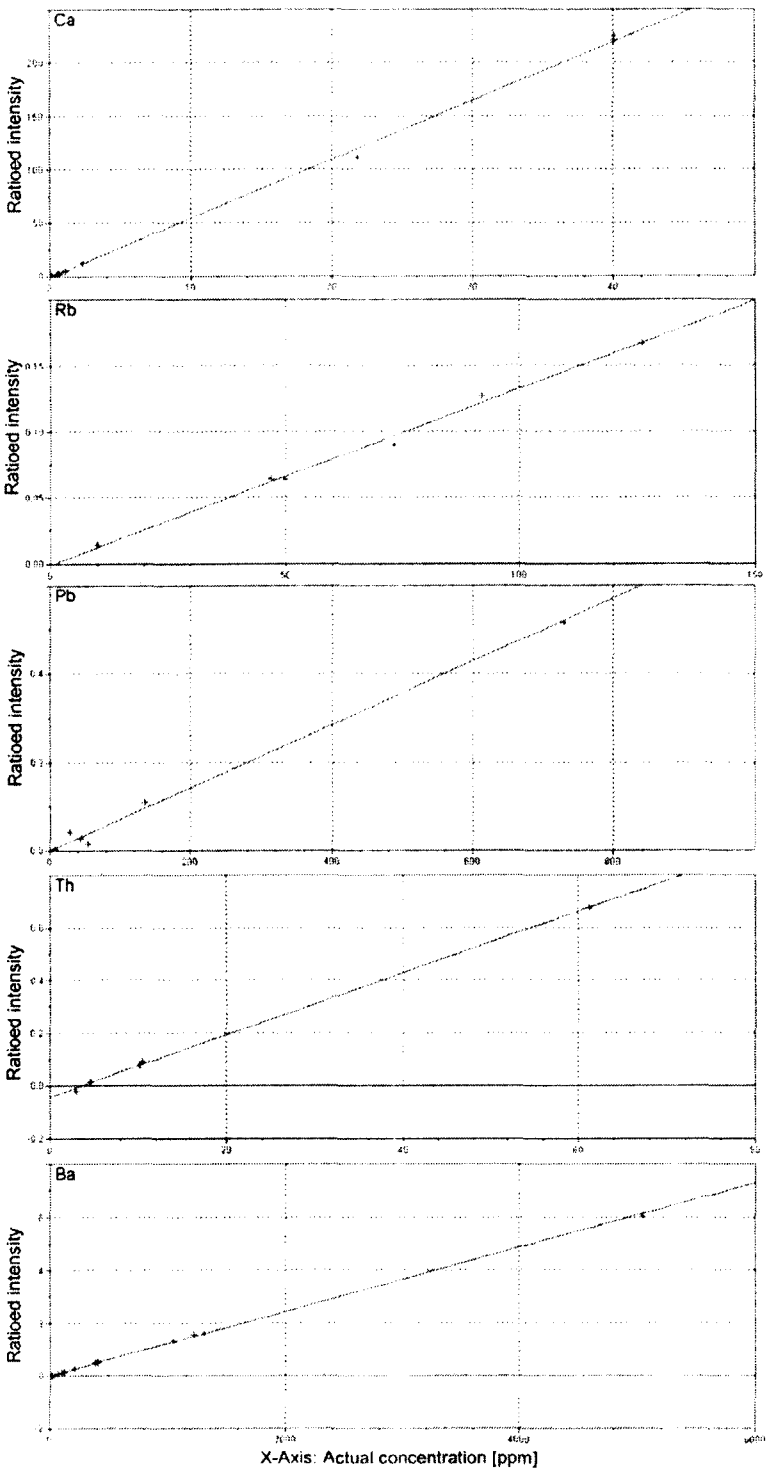

Fig. 2B-1 continued.

Table 2B-6. Table of standards used for establishing analyte calibrations in the WD-XRF analytical protocol.

Standard name		Na (%)	Mg (%)	Al (%)	Si (%)	P (%)	S (%)	K (%)	Ti (ppm)	V (ppm)	Cr (ppm)	Mn (ppm)	Fe (ppm)	Co (ppm)
NIM-S	Incl/Excl				X		X	X		X	X			
	C(Calc)	0.291	0.267	9.327	31.601	0.046	0.003	11.757	221.7	13.6	-3.7	132.0	10249.7	2.0
	C(Chem)	0.319	0.277	9.177	29.745	0.052	---	0.037	263.8	10	12	77.4	9792.11	3
	Diff(C)	0.0	0.0	0.2	1.9	0.0	---	11.7	-42.1	3.6	-15.7	54.6	457.6	-1.0
	Rel.err.(%)	-8.8%	-3.6%	1.6%	6.2%	-11.5%	---	31675.7%	-16.0%	36.4%	-131.0%	70.5%	4.7%	-32.9%
BR	Incl/Excl						X		X	X	X		X	X
	C(Calc)	2.614	6.814	5.079	17.338	0.414	0.064	1.325	14312.8	640.2	399.7	1532.1	123860.8	50.3
	C(Chem)	2.263	8.009	5.398	17.857	0.454	0.039	1.162	15587	235	380	1548.9	90087.41	52
	Diff(C)	0.4	-1.2	-0.3	-0.5	0.0	0.0	0.2	-1274.2	405.2	19.7	-16.8	33773.4	-1.7
	Rel.err.(%)	15.5%	-14.9%	-5.9%	-2.9%	-8.8%	64.1%	14.0%	-8.2%	172.4%	5.2%	-1.1%	37.5%	-3.2%
JB-2	Incl/Excl		X						X	X	X		X	X
	C(Calc)	1.723	1.704	7.894	24.382	0.037	0.007	0.365	6865.6	1071.9	66.0	1786.9	148579.7	50.6
	C(Chem)	1.506	2.81	7.764	24.869	0.044	0.009	0.349	7134	575	28.1	1548.9	100299.2	39.8
	Diff(C)	0.2	-1.1	0.1	-0.5	0.0	0.0	0.0	-268.4	496.9	37.9	238.0	48280.5	10.8
	Rel.err.(%)	14.4%	-39.4%	1.7%	-2.0%	-15.9%	-22.2%	4.6%	-3.8%	86.4%	134.8%	15.4%	48.1%	27.2%
DR-N	Incl/Excl									X			X	
	C(Calc)	2.118	2.792	8.765	24.495	0.084	0 039	1.489	6613.5	371.9	34.0	1537.0	87005.4	33.2
	C(Chem)	2.218	2.654	9.272	24.706	0.109	0.035	1.411	6534.5	220	42	1703.8	67845.34	35
	Diff(C)	-0.1	0.1	-0.5	-0.2	0.0	0.0	0.1	79.0	151.9	-8.0	-166.8	19160.1	-1.8
	Rel.err.(%)	-4.5%	5.2%	-5.5%	-0.9%	-22.9%	11.4%	5.5%	1.2%	69.0%	-19.0%	-9.8%	28.2%	-5.2%
NIM-N	Incl/Excl		X		X		X		X	X	X		X	X
	C(Calc)	1.898	3.262	8.387	21.682	0.017	0.004	0.22	1036.4	284.7	32.0	1290.9	81899.1	38.4
	C(Chem)	1.825	4.523	8.732	24.607	0.013	---	0.208	1199	220	30	1394	62319.79	58
	Diff(C)	0.1	-1.3	-0.3	-2.9	0.0	---	0.0	-162.6	64.7	2.0	-103.1	19579.3	-19.6
	Rel.err.(%)	4.0%	-27.9%	-4.0%	-11.9%	30.8%	---	5.8%	-13.6%	29.4%	6.7%	-7.4%	31.4%	-33.9%
NIM-L	Incl/Excl	X								X	X	X	X	X
	C(Calc)	5.858	0.098	7.27	23.966	0.019	0.088	4.457	2798.6	258.1	43.7	8144.0	141726.9	30.9
	C(Chem)	6.209	0.169	7.219	24.495	0.026	0.1	4.574	2877.6	81	9	5963.3	69663.87	2.3
	Diff(C)	-0.4	-0.1	0.1	-0.5	0.0	0.0	-0.1	-79.0	177.1	34.7	2180.7	72063.0	28.6
	Rel.err.(%)	-5.7%	-42.0%	0.7%	-2.2%	-26.9%	-12.0%	-2.6%	-2.7%	218.6%	385.7%	36.6%	103.4%	1242.3%
AGV-1	Incl/Excl		X	X		X				X			X	
	C(Calc)	3.023	0.656	8.349	28.209	0.148	0.007	2.425	6289.6	203.7	-7.4	683.0	56003.4	18.2
	C(Chem)	3.16	0.9227	3.16	27.482	0.214	0.005	2.416	6294.7	121	10.1	712.5	47281.9	15.3
	Diff(C)	-0.1	-0.3	5.2	0.7	-0.1	0.0	0.0	-5.1	82.7	-17.5	-29.5	8721.5	2.9
	Rel.err.(%)	-4.3%	-28.9%	164.2%	2.6%	-30.8%	40.0%	0.4%	-0.1%	68.4%	-173.3%	-4.1%	18.4%	19.0%

Table 2B-6 continued.

Standard name		Na (%)	Mg (%)	Al (%)	Si (%)	P (%)	S (%)	K (%)	Ti (ppm)	V (ppm)	Cr (ppm)	Mn (ppm)	Fe (ppm)	Co (ppm)
BX-N	Incl/Excl	X		X			X	X	X	X			X	X
	C(Calc)	0.087	0.109	26.349	3.582	0.052	0.038	0.071	20397.4	1477.1	563.5	578.4	311761.8	98.2
	C(Chem)	0.03	0.066	28.689	3.459	0.057	---	0.042	14208.1	310	290	387.2	162059.4	35
	Diff(C)	0.1	0.0	-2.3	0.1	0.0	---	0.0	6189.3	1167.1	273.5	191.2	149702.4	63.2
	Rel.err.(%)	190.0%	65.2%	-8.2%	3.6%	-8.8%	---	69.0%	43.6%	376.5%	94.3%	49.4%	92.4%	180.6%
GSP-1	Incl/Excl									X			X	
	C(Calc)	2.148	0.671	8.221	33.047	0.096	0.026	4.561	3824.7	78.1	-9.2	295.2	30787.0	7.7
	C(Chem)	2.077	0.579	7.991	31.39	0.122	0.032	4.574	3896.7	53	13	309.8	30005.82	6.6
	Diff(C)	0.1	0.1	0.2	1.7	0.0	0.0	0.0	-72.0	25.1	-22.2	-14.6	781.2	1.1
	Rel.err.(%)	3.4%	15.9%	2.9%	5.3%	-21.3%	-18.8%	-0.3%	-1.8%	47.4%	-171.0%	-4.7%	2.6%	17.0%
JP-1	Incl/Excl				X	X			X				X	X
	C(Calc)	-0.007	26.908	0.283	17.315	0.014	0.005	-0.001	27.2	36.3	2837.6	898.4	79425.4	61.2
	C(Chem)	0.016	26.97	0.328	19.816	---	0.003	0.003	---	29	3010	929.3	58333	7
	Diff(C)	0.0	-0.1	0.0	-2.5	---	0.0	0.0	---	7.3	-172.4	-30.9	21092.4	54.2
	Rel.err.(%)	-143.8%	-0.2%	-13.7%	-12.6%	---	66.7%	-133.3%	---	25.1%	-5.7%	-3.3%	36.2%	774.2%
FER-1	Incl/Excl				X		X	X		X	X	X	X	X
	C(Calc)	0.062	0.184	0.328	12.731	1.103	0.545	0.025	205.2	709.1	134.7	6634.9	824029.8	498.2
	C(Chem)	0.022	0.181	0.275	7.924	1.043	0.26	0.017	179.8	100	7	1703.8	530592.5	12
	Diff(C)	0.0	0.0	0.1	4.8	0.1	0.3	0.0	25.4	609.1	127.7	4931.1	293437.3	486.2
	Rel.err.(%)	181.8%	1.7%	19.3%	60.7%	5.8%	109.6%	47.1%	14.1%	609.1%	1823.9%	289.4%	55.3%	4051.9%
FER-3	Incl/Excl				X					X	X	X	X	X
	C(Calc)	0.003	0.902	0.05	35.272	0.039	0.019	0.012	13.7	28.0	53.3	1490.8	702375.3	168.8
	C(Chem)	0.022	0.615	0.048	25.061	0.031	0.03	0.025	59.9	8	6	619.6	311249.2	2
	Diff(C)	0.0	0.3	0.0	10.2	0.0	0.0	0.0	-46.2	20.0	47.3	871.2	391126.1	166.8
	Rel.err.(%)	-86.4%	46.7%	4.2%	40.7%	25.8%	-36.7%	-52.0%	-77.1%	249.7%	788.4%	140.6%	125.7%	8339.2%
IF-G	Incl/Excl				X					X	X	X	X	X
	C(Calc)	0.019	1.481	0.076	23.722	0.038	0.074	0.002	45.6	12.3	9.1	905.2	568673.8	328.2
	C(Chem)	0.024	1.14	0.079	19.26	0.027	0.07	0.01	83.9	4	10	325.3	390635.3	29
	Diff(C)	0.0	0.3	0.0	4.5	0.0	0.0	0.0	-38.3	8.3	-0.9	579.9	178038.5	299.2
	Rel.err.(%)	-20.8%	29.9%	-3.8%	23.2%	40.7%	5.7%	-80.0%	-45.7%	206.5%	-8.7%	178.3%	45.6%	1031.8%
GXR-1	Incl/Excl			X	X		X			X	X	X	X	X
	C(Calc)	0.06	0.18	2.343	22.219	0.051	0.828	0.046	398.3	317.6	38.4	1996.0	668488.2	162.2
	C(Chem)	0.052	0.217	3.509	22.681	0.065	0.257	0.05	359.7	80	12	851.9	249978.6	8
	Diff(C)	0.0	0.0	-1.2	-0.5	0.0	0.6	0.0	38.6	237.6	26.4	1144.1	418509.6	154.2
	Rel.err.(%)	15.4%	-17.1%	-33.2%	-2.0%	-21.5%	222.2%	-8.0%	10.7%	297.0%	220.0%	134.3%	167.4%	1927.0%

Table 2B-6 continued.

Standard name		Na (%)	Mg (%)	Al (%)	Si (%)	P (%)	S (%)	K (%)	Ti (ppm)	V (ppm)	Cr (ppm)	Mn (ppm)	Fe (ppm)	Co (ppm)
GXR-6	Incl/Excl			X					X	X	X		X	X
	C(Calc)	0.101	0.776	16.272	22.684	0.038	0.022	2.053	6708.5	351.4	88.2	1043.4	76081.0	22.3
	C(Chem)	0.104	0.609	17.697	21.803	0.035	0.016	1.868	4975.8	186	96	1006.8	55815.03	13.8
	Diff(C)	0.0	0.2	-1.4	0.9	0.0	0.0	0.2	1732.7	165.4	-7.8	36.6	20266.0	8.5
	Rel.err.(%)	-2.9%	27.4%	-8.1%	4.0%	8.6%	37.5%	9.9%	34.8%	88.9%	-8.1%	3.6%	36.3%	61.7%
GH	Incl/Excl									X				
	C(Calc)	2.734	-0.004	6.395	35.712	0.015	0.006	3.729	467.2	1.8	-19.1	309.7	9066.0	2.4
	C(Chem)	2.856	0.018	6.615	35.434	0.004	0.007	3.951	479.6	5	6	387.2	9372.45	1
	Diff(C)	-0.1	0.0	-0.2	0.3	0.0	0.0	-0.2	-12.4	-3.2	-25.1	-77.5	-306.5	1.4
	Rel.err.(%)	-4.3%	-122.2%	-3.3%	0.8%	275.0%	-14.3%	-5.6%	-2.6%	-64.5%	-418.5%	-20.0%	-3.3%	136.9%
JR-1	Incl/Excl			X				X		X				
	C(Calc)	2.653	0.027	6.067	34.274	0.017	0.006	3.282	624.5	6.3	-23.1	556.6	5868.6	1.2
	C(Chem)	3.042	0.054	6.822	35.252	0.009	0.0009	3.661	599.5	0	1	774.5	6714.59	0.654
	Diff(C)	-0.4	0.0	-0.8	-1.0	0.0	0.0	-0.4	25.0	6.3	-24.1	-217.9	-846.0	0.6
	Rel.err.(%)	-12.8%	-50.0%	-11.1%	-2.8%	88.9%	566.7%	-10.4%	4.2%	---	-2405.2%	-28.1%	-12.6%	89.1%
JG-2	Incl/Excl													
	C(Calc)	2.628	0.006	6.412	34.991	0.016	0.007	3.681	279.5	3.0	-22.2	170.1	6727.0	2.1
	C(Chem)	2.634	0.024	6.568	35.971	0.001	0.0009	3.918	239.8	3	2	116.2	6434.82	4.1
	Diff(C)	0.0	0.0	-0.2	-1.0	0.0	0.0	-0.2	39.7	0.0	-24.2	53.9	292.2	-2.0
	Rel.err.(%)	-0.2%	-75.0%	-2.4%	-2.7%	1500.0%	677.8%	-6.0%	16.5%	0.0%	-1207.7%	46.4%	4.5%	-49.6%
MA-N	Incl/Excl					X				X				
	C(Calc)	4.032	0.03	9.815	31.1	0.382	0.006	2.824	72.2	11.7	-21.2	278.8	3530.1	-0.1
	C(Chem)	4.332	0.024	9.325	31.133	0.607	0.01	2.64	60	5	3	309.8	3287.35	1
	Diff(C)	-0.3	0.0	0.5	0.0	-0.2	0.0	0.2	12.2	6.7	-24.2	-31.0	242.7	-1.1
	Rel.err.(%)	-6.9%	25.0%	5.3%	-0.1%	-37.1%	-40.0%	7.0%	20.3%	134.9%	-805.3%	-10.0%	7.4%	-114.7%
GXR-3	Incl/Excl	X		X			X	X		X	X	X	X	X
	C(Calc)	0.706	0.695	3.846	6.068	0.088	0.681	0.933	1041.5	192.6	34.7	37693.5	451227.8	120.0
	C(Chem)	0.838	0.808	6.398	6.241	0.109	0.232	0.731	1019.1	42	19	22304.4	189966.9	46
	Diff(C)	-0.1	-0.1	-2.6	-0.2	0.0	0.4	0.2	22.4	150.6	15.7	15389.1	261260.8	74.0
	Rel.err.(%)	-15.8%	-14.0%	-39.9%	-2.8%	-19.3%	193.5%	27.6%	2.2%	358.7%	82.4%	69.0%	137.5%	160.8%
NIM-G	Incl/Excl				X		X			X				X
	C(Calc)	2.66	0.006	6.744	37.854	0.014	0.009	4.024	579.8	3.3	-13.3	173.9	14142.1	2.8
	C(Chem)	2.493	0.036	6.393	35.387	0.004	---	4.142	540	2	12	162.6	14128.62	0.3
	Diff(C)	0.2	0.0	0.4	2.5	0.0	---	-0.1	39.8	1.3	-25.3	11.3	13.5	2.5
	Rel.err.(%)	6.7%	-83.3%	5.5%	7.0%	250.0%	---	-2.8%	7.4%	66.5%	-210.5%	6.9%	0.1%	827.7%

Table 2B-6 continued.

Standard name		Na (%)	Mg (%)	Al (%)	Si (%)	P (%)	S (%)	K (%)	Ti (ppm)	V (ppm)	Cr (ppm)	Mn (ppm)	Fe (ppm)	Co (ppm)
NBS 88 CaCO3 cali	Incl/Excl													
	C(Calc)	---	---	---	---	---	---	---	---	---	---	---	---	---
	C(Chem)	---	---	---	---	---	---	---	---	---	---	---	---	---
	Diff(C)	---	---	---	---	---	---	---	---	---	---	---	---	---
	Rel.err.(%)	---	---	---	---	---	---	---	---	---	---	---	---	---
1ppm Syn.Carb.std	Incl/Excl													
	C(Calc)	---	---	---	---	---	---	---	---	2.5	---	---	---	---
	C(Chem)	---	---	---	---	---	---	---	---	0.836	---	---	---	---
	Diff(C)	---	---	---	---	---	---	---	---	1.6	---	---	---	---
	Rel.err.(%)	---	---	---	---	---	---	---	---	196.7%	---	---	---	---
2ppm Syn.Carb.std	Incl/Excl													
	C(Calc)	---	---	---	---	---	---	---	---	3.7	---	---	---	---
	C(Chem)	---	---	---	---	---	---	---	---	2.82	---	---	---	---
	Diff(C)	---	---	---	---	---	---	---	---	0.8	---	---	---	---
	Rel.err.(%)	---	---	---	---	---	---	---	---	29.8%	---	---	---	---
5ppm Syn.Carb.std	Incl/Excl													
	C(Calc)	---	---	---	---	---	---	---	---	5.6	---	---	---	---
	C(Chem)	---	---	---	---	---	---	---	---	4.846	---	---	---	---
	Diff(C)	---	---	---	---	---	---	---	---	0.8	---	---	---	---
	Rel.err.(%)	---	---	---	---	---	---	---	---	15.8%	---	---	---	---
10ppm Syn.Carb.std	Incl/Excl													
	C(Calc)	---	---	---	---	---	---	---	---	9.7	---	---	---	---
	C(Chem)	---	---	---	---	---	---	---	---	11.93	---	---	---	---
	Diff(C)	---	---	---	---	---	---	---	---	-2.3	---	---	---	---
	Rel.err.(%)	---	---	---	---	---	---	---	---	-18.9%	---	---	---	---
20ppm Syn.Carb.std	Incl/Excl													
	C(Calc)	---	---	---	---	---	---	---	---	19.3	---	---	---	---
	C(Chem)	---	---	---	---	---	---	---	---	24.26	---	---	---	---
	Diff(C)	---	---	---	---	---	---	---	---	-4.9	---	---	---	---
	Rel.err.(%)	---	---	---	---	---	---	---	---	-20.3%	---	---	---	---
50ppm Syn.Carb.std	Incl/Excl													
	C(Calc)	---	---	---	---	---	---	---	---	45.9	---	---	---	---
	C(Chem)	---	---	---	---	---	---	---	---	49.3	---	---	---	---
	Diff(C)	---	---	---	---	---	---	---	---	-3.4	---	---	---	---
	Rel.err.(%)	---	---	---	---	---	---	---	---	-6.8%	---	---	---	---

Table 2B-6 continued.

Standard name		Na (%)	Mg (%)	Al (%)	Si (%)	P (%)	S (%)	K (%)	Ti (ppm)	V (ppm)	Cr (ppm)	Mn (ppm)	Fe (ppm)	Co (ppm)
100ppm Syn.Carb.std	Incl/Excl													
	C(Calc)	---	---	---	---	---	---	---	---	92.8	---	---	---	---
	C(Chem)	---	---	---	---	---	---	---	---	92.84	---	---	---	---
	Diff(C)	---	---	---	---	---	---	---	---	-0.1	---	---	---	---
	Rel.err.(%)	---	---	---	---	---	---	---	---	-0.1%	---	---	---	---
SGR-1-S-1.53%	Incl/Excl													
	C(Calc)	---	---	---	---	---	1.556	---	---	---	---	---	---	---
	C(Chem)	---	---	---	---	---	1.53	---	---	---	---	---	---	---
	Diff(C)	---	---	---	---	---	0.0	---	---	---	---	---	---	---
	Rel.err.(%)	---	---	---	---	---	1.7%	---	---	---	---	---	---	---
SDO-1-S-5.35%	Incl/Excl													
	C(Calc)	---	---	---	---	---	5.328	---	---	---	---	---	---	---
	C(Chem)	---	---	---	---	---	5.35	---	---	---	---	---	---	---
	Diff(C)	---	---	---	---	---	0.0	---	---	---	---	---	---	---
	Rel.err.(%)	---	---	---	---	---	-0.4%	---	---	---	---	---	---	---
BE-N	Incl/Excl													
	C(Calc)	---	---	---	---	---	---	---	---	---	---	---	---	---
	C(Chem)	---	---	---	---	---	---	---	---	---	---	---	---	---
	Diff(C)	---	---	---	---	---	---	---	---	---	---	---	---	---
	Rel.err.(%)	---	---	---	---	---	---	---	---	---	---	---	---	---

Table 2B-6 continued.

Standard name		Ni (ppm)	Cu (ppm)	Zn (ppm)	Sr (ppm)	Zr (ppm)	Mo (ppm)	Ba (ppm)	Ca (%)	Rb (ppm)	Pb (ppm)	Th (ppm)	U (ppm)
NIM-S	Incl/Excl						X	X					
	C(Calc)	6.8	18.3	10.3	60.7	20.0	0.4	2274.0	0.3	---	---	---	---
	C(Chem)	7	19	10	62	33	---	2400	0.486	---	---	---	---
	Diff(C)	-0.2	-0.7	0.3	-1.3	-13.0	---	-126.0	-0.1	---	---	---	---
	Rel.err.(%)	-2.7%	-3.9%	3.1%	-2.0%	-39.5%	---	-5.2%	-28.6%	---	---	---	---
BR	Incl/Excl					X	X		X				
	C(Calc)	260.0	79.9	160.1	1387.3	275.8	22.7	1080.8	5.9	48.9	3.2	10.3	1.4
	C(Chem)	260	72	160	1370	250	2.4	1050	9.863	47	8	10.19	2.5
	Diff(C)	0.0	7.9	0.1	17.3	25.8	20.3	30.8	-4.0	1.9	-4.8	0.1	-1.1
	Rel.err.(%)	0.0%	11.0%	0.1%	1.3%	10.3%	846.6%	2.9%	-40.6%	3.9%	-59.8%	1.0%	-43.2%
JB-2	Incl/Excl						X		X				
	C(Calc)	15.8	228.6	107.7	188.1	53.3	8.1	225.8	4.1	---	---	---	---
	C(Chem)	16.6	227	110	185	51.2	1.1	208	7.068	---	---	---	---
	Diff(C)	-0.8	1.6	-2.3	3.1	2.1	7.0	17.8	-3.0	---	---	---	---
	Rel.err.(%)	-5.1%	0.7%	-2.1%	1.7%	4.1%	632.5%	8.5%	-42.3%	---	---	---	---
DR-N	Incl/Excl						X		X				
	C(Calc)	17.2	45.9	136.4	387.8	125.0	6.3	400.2	2.8	68.0	21.1	4.9	1.2
	C(Chem)	15	50	145	400	125	---	385	5.039	73	55	4.66	1.63
	Diff(C)	2.2	-4.1	-8.6	-12.2	0.0	---	15.2	-2.3	-5.0	-33.9	0.3	-0.4
	Rel.err.(%)	14.9%	-8.3%	-5.9%	-3.1%	0.0%	---	3.9%	-44.7%	-6.8%	-61.7%	6.0%	-25.2%
NIM-N	Incl/Excl	X							X				
	C(Calc)	108.2	14.0	57.9	261.6	16.2	2.1	94.0	4.6	---	---	---	---
	C(Chem)	120	14	68	269	23	5	100	8.219	---	---	---	---
	Diff(C)	-11.8	0.0	-10.1	-7.4	-6.8	-2.9	-6.0	-3.6	---	---	---	---
	Rel.err.(%)	-9.9%	0.3%	-14.8%	-2.7%	-29.4%	-57.6%	-6.0%	-44.0%	---	---	---	---
NIM-L	Incl/Excl	X	X	X	X	X	X		X	X			
	C(Calc)	16.4	30.3	604.6	6756.2	24462.7	894.0	415.6	1.3	345.7	38.6	61.0	18.9
	C(Chem)	11	---	424	4770	11300	4	409	2.301	197	43	61.2	18.3
	Diff(C)	5.4	---	180.6	1986.2	13162.7	890.0	6.6	-1.0	148.7	-4.4	-0.2	0.6
	Rel.err.(%)	48.8%	---	42.6%	41.6%	116.5%	22250.2%	1.6%	-44.3%	75.5%	-10.2%	-0.3%	3.4%
AGV-1	Incl/Excl						X		X				
	C(Calc)	14.6	57.8	80.4	646.9	228.9	13.4	1273.9	1.9	---	---	---	---
	C(Chem)	16	60	88	662	227	2.7	1226	3.531	---	---	---	---
	Diff(C)	-1.4	-2.2	-7.6	-15.1	1.9	10.7	47.9	-1.6	---	---	---	---
	Rel.err.(%)	-8.7%	-3.7%	-8.7%	-2.3%	0.8%	396.5%	3.9%	-46.2%	---	---	---	---

Table 2B-6 continued.

Standard name		Ni (ppm)	Cu (ppm)	Zn (ppm)	Sr (ppm)	Zr (ppm)	Mo (ppm)	Ba (ppm)	Ca (%)	Rb (ppm)	Pb (ppm)	Th (ppm)	U (ppm)
BX-N	Incl/Excl		X				X					X	
	C(Calc)	186.7	39.5	88.5	122.1	547.3	39.7	-8.4	0.3	11.3	153.3	49.7	7.8
	C(Chem)	190	18	75	110	520	7.7	34	0.121	10	135	55	8
	Diff(C)	-3.3	21.5	13.5	12.1	27.3	32.0	-42.4	0.1	1.3	18.3	-5.3	-0.2
	Rel.err.(%)	-1.7%	119.5%	18.0%	11.0%	5.2%	415.7%	-124.7%	108.3%	12.9%	13.5%	-9.7%	-3.1%
GSP-1	Incl/Excl						X		X				
	C(Calc)	8.8	30.6	95.3	227.5	505.9	26.6	1340.3	0.8	---	---	---	---
	C(Chem)	8.8	33	104	234	530	---	1310	1.479	---	---	---	---
	Diff(C)	0.0	-2.4	-8.7	-6.5	-24.1	---	30.3	-0.6	---	---	---	---
	Rel.err.(%)	0.1%	-7.4%	-8.4%	-2.8%	-4.5%	---	2.3%	-43.4%	---	---	---	---
JP-1	Incl/Excl	X	X				X						
	C(Calc)	2176.0	-28.9	42.6	2.0	11.7	-3.8	14.3	0.4	---	---	---	---
	C(Chem)	2460	5.7	29.5	0	6	---	17	0.4	---	---	---	---
	Diff(C)	-284.0	-34.6	13.1	2.0	5.7	---	-2.7	0.0	---	---	---	---
	Rel.err.(%)	-11.5%	-607.6%	44.3%	---	95.5%	---	-15.7%	1.0%	---	---	---	---
FER-1	Incl/Excl	X	X	X	X		X	X					
	C(Calc)	38.2	198.4	5689.6	130.6	20.9	51.3	1209.5	2.4	---	---	---	---
	C(Chem)	8	100	3600	90	13	---	1000	2.351	---	---	---	---
	Diff(C)	30.2	98.4	2089.6	40.6	7.9	---	209.5	0.0	---	---	---	---
	Rel.err.(%)	377.5%	98.4%	58.0%	45.1%	60.8%	---	21.0%	0.6%	---	---	---	---
FER-3	Incl/Excl	X	X				X						
	C(Calc)	20.9	20.4	45.5	40.8	7.6	19.5	13.8	0.7	---	---	---	---
	C(Chem)	10	6	36	31	2	---	11	0.6	---	---	---	---
	Diff(C)	10.9	14.4	9.5	9.8	5.6	---	2.8	0.1	---	---	---	---
	Rel.err.(%)	109.4%	239.9%	26.4%	31.6%	280.9%	---	25.4%	12.5%	---	---	---	---
IF-G	Incl/Excl	X	X				X						
	C(Calc)	35.0	44.9	36.8	6.6	5.3	29.4	-1.1	1.1	---	---	---	---
	C(Chem)	22.5	13	27	3	2.4	1	2	1.108	---	---	---	---
	Diff(C)	12.5	31.9	9.8	3.6	2.9	28.4	-3.1	0.0	---	---	---	---
	Rel.err.(%)	55.5%	245.7%	36.2%	119.1%	119.1%	2842.0%	-157.0%	-2.7%	---	---	---	---
GXR-1	Incl/Excl		X	X	X		X	X		X		X	X
	C(Calc)	45.0	1246.0	858.6	325.4	56.5	39.5	926.6	1.0	36.5	721.8	401.1	23.2
	C(Chem)	41	1110	760	275	50	18	750	0.958	14	730	2.44	35
	Diff(C)	4.0	136.0	98.6	50.4	6.5	21.5	176.6	0.0	22.5	-8.2	398.7	-11.8
	Rel.err.(%)	9.6%	12.3%	13.0%	18.3%	13.1%	119.6%	23.5%	5.2%	160.9%	-1.1%	16340.2%	-33.8%

Table 2B-6 continued.

Standard name		Ni (ppm)	Cu (ppm)	Zn (ppm)	Sr (ppm)	Zr (ppm)	Mo (ppm)	Ba (ppm)	Ca (%)	Rb (ppm)	Pb (ppm)	Th (ppm)	U (ppm)
GXR-6	Incl/Excl	X						X					
	C(Calc)	22.0	63.7	120.8	36.9	132.9	4.2	1597.2	0.3	---	---	---	---
	C(Chem)	27	66	118	35	110	2.4	1300	0.179	---	---	---	---
	Diff(C)	-5.0	-2.3	2.8	1.9	22.9	1.8	297.2	0.1	---	---	---	---
	Rel.err.(%)	-18.4%	-3.4%	2.4%	5.6%	20.8%	75.1%	22.9%	42.5%	---	---	---	---
GH	Incl/Excl		X	X									
	C(Calc)	2.7	19.0	53.6	9.1	135.8	1.3	15.4	0.4	---	---	---	---
	C(Chem)	3	14	85	10	150	2	20	0.493	---	---	---	---
	Diff(C)	-0.3	5.0	-31.4	-0.9	-14.2	-0.7	-4.6	-0.1	---	---	---	---
	Rel.err.(%)	-9.3%	35.5%	-37.0%	-8.9%	-9.5%	-34.6%	-23.2%	-14.8%	---	---	---	---
JR-1	Incl/Excl		X					X					
	C(Calc)	1.6	22.3	26.5	27.2	95.8	1.9	55.1	0.4	---	---	---	---
	C(Chem)	0.66	1.4	30	29.1	99.9	3.2	40	0.45	---	---	---	---
	Diff(C)	0.9	20.8	-3.5	-1.9	-4.1	-1.3	15.1	-0.1	---	---	---	---
	Rel.err.(%)	140.2%	1489.3%	-11.6%	-6.4%	-4.1%	-39.6%	37.7%	-14.0%	---	---	---	---
JG-2	Incl/Excl		X										
	C(Calc)	2.3	6.5	12.0	16.0	85.6	-2.1	61.9	0.4	---	---	---	---
	C(Chem)	2.1	0.4	13	18	98	0.2	67	0.572	---	---	---	---
	Diff(C)	0.2	6.1	-1.0	-2.0	-12.0	-2.3	-5.1	-0.2	---	---	---	---
	Rel.err.(%)	8.9%	1531.5%	-8.0%	-11.3%	-12.6%	-1155.0%	-7.7%	-29.5%	---	---	---	---
MA-N	Incl/Excl	X					X	X					
	C(Calc)	9.1	133.8	217.7	85.8	27.8	-4.3	68.7	0.4	---	---	---	---
	C(Chem)	3	140	220	90	27	---	42	0.422	---	---	---	---
	Diff(C)	6.1	-6.2	-2.3	-4.2	0.8	---	26.7	0.0	---	---	---	---
	Rel.err.(%)	204.9%	-4.4%	-1.1%	-4.7%	3.0%	---	63.6%	-10.0%	---	---	---	---
GXR-3	Incl/Excl				X		X		X		X		
	C(Calc)	77.3	23.7	215.4	1142.8	102.4	35.1	4965.2	9.9	95.8	3999.5	1.9	2.4
	C(Chem)	60	25	207	950	-63	6.5	5050	13.601	92	15	2.94	3
	Diff(C)	17.3	-1.3	8.4	192.8	39.4	28.6	-84.8	-3.7	3.8	3984.5	-1.0	-0.6
	Rel.err.(%)	28.9%	-5.0%	4.1%	20.3%	-262.6%	440.3%	-1.7%	-27.4%	4.1%	26563.5%	-35.7%	-20.3%
NIM-G	Incl/Excl	X	X				X						
	C(Calc)	4.9	8.3	45.6	10.8	264.5	10.4	112.0	0.4	---	---	---	---
	C(Chem)	8	12	60	10	276	3	120	0.557	---	---	---	---
	Diff(C)	-3.1	-3.7	-14.4	0.8	-11.5	7.4	-8.0	-0.1	---	---	---	---
	Rel.err.(%)	-38.6%	-30.8%	-24.1%	8.2%	-4.2%	245.4%	-6.7%	-19.7%	---	---	---	---

Table 2B-6 continued.

Standard name		Ni (ppm)	Cu (ppm)	Zn (ppm)	Sr (ppm)	Zr (ppm)	Mo (ppm)	Ba (ppm)	Ca (%)	Rb (ppm)	Pb (ppm)	Th (ppm)	U (ppm)
NBS 88 CaCO3 call	Incl/Excl												
	C(Calc)	---	---	---	---	---	---	---	20.3	---	---	---	---
	C(Chem)	---	---	---	---	---	---	---	21.812	---	---	---	---
	Diff(C)	---	---	---	---	---	---	---	-1.5	---	---	---	---
	Rel.err.(%)	---	---	---	---	---	---	---	-6.7%	---	---	---	---
1ppm Syn.Carb.std	Incl/Excl												
	C(Calc)	2.3	1.9	---	---	---	0.9	---	---	---	---	---	1.2
	C(Chem)	1.61	0.036	---	---	---	0.541	---	---	---	---	---	0.475
	Diff(C)	0.7	1.9	---	---	---	0.4	---	---	---	---	---	0.8
	Rel.err.(%)	43.9%	5236.1%	---	---	---	70.1%	---	---	---	---	---	158.9%
2ppm Syn.Carb.std	Incl/Excl												
	C(Calc)	2.7	3.3	---	---	---	1.8	---	41.1	---	---	---	2.2
	C(Chem)	2.88	1.411	---	---	---	1.916	---	40.05	---	---	---	0.866
	Diff(C)	-0.2	1.9	---	---	---	-0.1	---	1.0	---	---	---	1.3
	Rel.err.(%)	-7.6%	131.8%	---	---	---	-4.2%	---	2.6%	---	---	---	152.9%
5ppm Syn.Carb.std	Incl/Excl	X											
	C(Calc)	5.1	4.9	---	---	---	6.4	---	---	---	---	---	4.1
	C(Chem)	10.18	4.078	---	---	---	4.858	---	---	---	---	---	2.754
	Diff(C)	-5.0	0.9	---	---	---	1.5	---	---	---	---	---	1.3
	Rel.err.(%)	-49.4%	21.3%	---	---	---	31.9%	---	---	---	---	---	47.8%
10ppm Syn.Carb.std	Incl/Excl												
	C(Calc)	10.1	9.1	---	---	---	12.4	---	---	---	---	---	7.5
	C(Chem)	12.67	9.178	---	---	---	11.43	---	---	---	---	---	8.182
	Diff(C)	-2.6	-0.1	---	---	---	1.0	---	---	---	---	---	-0.7
	Rel.err.(%)	-20.5%	-0.9%	---	---	---	8.6%	---	---	---	---	---	-8.1%
20ppm Syn.Carb.std	Incl/Excl												
	C(Calc)	19.0	17.8	---	---	---	24.6	---	---	---	---	---	15.6
	C(Chem)	22.46	18.28	---	---	---	25.3	---	---	---	---	---	16.77
	Diff(C)	-3.5	-0.5	---	---	---	-0.7	---	---	---	---	---	-1.2
	Rel.err.(%)	-15.5%	-2.8%	---	---	---	-2.7%	---	---	---	---	---	-6.9%
50ppm Syn.Carb.std	Incl/Excl												
	C(Calc)	43.8	41.7	---	---	---	60.1	---	---	---	---	---	38.0
	C(Chem)	49.58	41.04	---	---	---	52.94	---	---	---	---	---	38.76
	Diff(C)	-5.8	0.7	---	---	---	7.2	---	---	---	---	---	-0.7
	Rel.err.(%)	-11.7%	1.7%	---	---	---	13.5%	---	---	---	---	---	-1.9%

Table 2B-6 continued.

Standard name		Ni (ppm)	Cu (ppm)	Zn (ppm)	Sr (ppm)	Zr (ppm)	Mo (ppm)	Ba (ppm)	Ca (%)	Rb (ppm)	Pb (ppm)	Th (ppm)	U (ppm)
100ppm Syn.Carb.std	Incl/Excl												
	C(Calc)	83.5	80.0	---	---	---	115.1	---	40.4	---	---	---	74.4
	C(Chem)	91.16	75.16	---	---	---	119.2	---	40.03	---	---	---	73.92
	Diff(C)	-7.6	4.9	---	---	---	-4.1	---	0.3	---	---	---	0 5
	Rel.err.(%)	-8.4%	6.5%	---	---	---	-3.4%	---	0.9%	---	---	---	0.6%
SGR-1-S-1.53%	Incl/Excl												
	C(Calc)	---	---	---	---	---	---	---	---	---	---	---	---
	C(Chem)	---	---	---	---	---	---	---	---	---	---	---	---
	Diff(C)	---	---	---	---	---	---	---	---	---	---	---	---
	Rel.err.(%)	---	---	---	---	---	---	---	---	---	---	---	---
SDO-1-S-5.35%	Incl/Excl												X
	C(Calc)	---	---	---	---	---	---	---	---	125.6	59.6	11.3	36.4
	C(Chem)	---	---	---	---	---	---	---	---	126	28	10.5	48.8
	Diff(C)	---	---	---	---	---	---	---	---	-0.4	31.6	0.8	-12.4
	Rel.err.(%)	---	---	---	---	---	---	---	---	-0.3%	112.7%	7.8%	-25.4%
BE-N	Incl/Excl												
	C(Calc)	---	---	---	---	---	---	---	---	48.4	3.1	10.3	1.4
	C(Chem)	---	---	---	---	---	---	---	---	50	4	10.23	1
	Diff(C)	---	---	---	---	---	---	---	---	-1.6	-0.9	0.0	0 4
	Rel.err.(%)	---	---	---	---	---	---	---	---	-3.2%	-23.5%	0.2%	40.0%

Table 2B-7. Results of repeated XRF measurements (12x) on 99.999% pure calcite zero-concentration pressed pellet standards used to determine absolute calibration backgrounds and lowest levels of detection (defined as 3σ of the analyte spectral peak count rate, background corrected).

XRF Applications used: CarbTraceMaj & MgSliwUThRbPb

Units:	WT.%	WT.%	WT.%	WT.%	WT.%	WT.%	WT.%	[PPM]	[PPM]	[PPM]	[PPM]	[PPM]	[PPM]
Sample name	**Na**	**Mg**	**Al**	**Si**	**P**	**S**	**K**	**Ti**	**V**	**Cr**	**Mn**	**Fe*****	**Co**
Ultrapure calcite ground in Spex Hardened Steel for 6 min.													
99.999%CALCITE after 6 min. of grinding*	0.055	-0.061	0.011	0.332	0.014	0.003	-0.005	-5.7	1.4	-22.3	90.4	211.6	-2.4
99.999%CALCITE after 6 min. of grinding*	0.054	-0.061	0.011	0.332	0.014	0.004	-0.005	-5.6	1.8	-22.7	89.3	212.2	-3.0
99.999%CALCITE after 6 min. of grinding*	0.054	-0.060	0.011	0.332	0.014	0.004	-0.005	-5.3	2.3	-24.0	89.7	211.2	-1.8
99.999%CALCITE after 6 min. of grinding*	0.053	-0.061	0.010	0.332	0.014	0.004	-0.006	-5.4	1.5	-22.5	89.5	212.2	-2.0
99.999%CALCITE after 6 min. of grinding*	0.055	-0.061	0.010	0.332	0.014	0.003	-0.005	-6.2	1.0	-23.1	90.2	210.6	-2.7
99.999%CALCITE after 6 min. of grinding*	0.055	-0.061	0.011	0.331	0.014	0.003	-0.005	-5.5	3.2	-22.3	88.6	211.3	-2.6
Ave:	**0.054**	**-0.061**	**0.011**	**0.332**	**0.014**	**0.004**	**-0.005**	**-5.6**	**1.9**	**-22.8**	**89.6**	**211.5**	**-2.4**
SD	0.001	0.000	0.001	0.000	0.000	0.001	0.000	0.3	0.8	0.7	0.7	0.6	0.4
Empirical LLD (3x SD)	**0.002**	**0.001**	**0.002**	**0.001**	**0.000**	**0.002**	**0.001**	**0.9**	**2.3**	**2.0**	**2.0**	**1.8**	**1.3**

*Ground using SPEX Hardened Steel Vials

***Corr. for 3ppm Fe in calcite pellet

Sample name	**Na**	**Mg**	**Al**	**Si**	**P**	**S**	**K**	**Ti**	**V**	**Cr**	**Mn**	**Fe*****	**Co**
99.999%CALCITE PURE	0.049	-0.060	-0.010	0.328	0.014	0.004	-0.007	-5.8	1.5	-22.2	88.2	179.4	-2.7
99.999%CALCITE PURE	0.051	-0.060	-0.010	0.327	0.014	0.005	-0.006	-6.0	1.8	-22.9	88.0	179.5	-2.3
99.999%CALCITE PURE	0.050	-0.060	-0.010	0.327	0.014	0.004	-0.007	-5.9	1.9	-23.1	90.1	179.0	-2.4
99.999%CALCITE PURE	0.050	-0.060	-0.010	0.327	0.014	0.004	-0.006	-4.7	1.8	-23.1	88.0	178.3	-1.8
99.999%CALCITE PURE	0.049	-0.060	-0.010	0.327	0.014	0.004	-0.007	-6.3	1.7	-22.1	89.9	178.2	-2.0
99.999%CALCITE PURE	0.049	-0.061	-0.010	0.327	0.014	0.004	-0.006	-5.4	1.9	-22.6	89.7	178.0	-3.0
Ave:	**0.050**	**-0.060**	**-0.010**	**0.327**	**0.014**	**0.004**	**-0.007**	**-5.7**	**1.8**	**-22.7**	**89.0**	**178.7**	**-2.4**
SD	0.001	0.000	0.000	0.000	0.000	0.000	0.001	0.6	0.1	0.5	1.0	0.7	0.4
Empirical LLD (3x SD)	**0.002**	**0.001**	**0.000**	**0.001**	**0.000**	**0.001**	**0.002**	**1.7**	**0.4**	**1.4**	**3.0**	**2.0**	**1.3**

Absolute background	**0.052**	**-0.061**	**0.000**	**0.330**	**0.014**	**0.004**	**-0.006**	**-5.7**	**1.8**	**-22.7**	**89**	**195**	**-2.4**
Ave. LLD	**0.008**	**0.002**	**0.03**	**0.01**	**0.000**	**0.002**	**0.003**	**2.4**	**1.6**	**2**	**3**	**2**	**1**

Table 2B-7 continued.

XRF Applications used: CarbTraceMaj & MgSliwUThRbPb

Units:	[PPM]	[PPM]	[PPM]	[PPM]	[PPM]	[PPM]	[PPM]	WT.%	[PPM]	[PPM]	[PPM]	[PPM]
Sample name	**Ni**	**Cu**	**Zn**	**Sr****	**Zr**	**Mo**	**Ba**	**Ca**	**Rb**	**Pb**	**Th**	**U**
Ultrapure calcite ground in Spex Hardened Steel for 6 min.												
99.999%CALCITE after 6 min. of grinding*	2.3	2.2	4.2	2.7	8.7	1.0	-3.2	42.19	6.3	0.1	3.6	0.3
99.999%CALCITE after 6 min. of grinding*	2.3	2.3	5.0	1.7	8.8	1.0	0.4	42.18	6.3	-0.6	3.0	0.5
99.999%CALCITE after 6 min. of grinding*	2.6	2.4	4.4	2.1	8.7	0.4	-1.4	42.13	6.0	-0.4	2.9	0.5
99.999%CALCITE after 6 min. of grinding*	2.8	2.0	4.5	1.5	8.5	0.0	2.2	42.18	6.2	-0.7	3.2	0.4
99.999%CALCITE after 6 min. of grinding*	2.4	2.7	4.8	2.4	8.8	0.7	-1.5	42.17	5.9	0.0	3.0	0.6
99.999%CALCITE after 6 min. of grinding*	2.1	1.8	4.4	-0.9	7.8	0.7	-0.7	42.23	6.1	-0.3	2.8	0.3
Ave:	**2.4**	**2.2**	**4.6**	**1.6**	**8.6**	**0.6**	**-0.7**	**42.18**	**6.1**	**-0.3**	**3.1**	**0.4**
SD	0.2	0.3	0.3	1.3	0.4	0.4	1.8	0.03	0.1	0.3	0.3	0.1
Empirical LLD (3x SD)	**0.7**	**0.9**	**0.9**	**3.8**	**1.2**	**1.1**	**5.5**	**0.09**	**0.4**	**0.9**	**0.8**	**0.4**

*Ground using SPEX Hardened Steel Vials

**Corr. for 5ppm Sr in calcite pellet

Sample name	**Ni**	**Cu**	**Zn**	**Sr****	**Zr**	**Mo**	**Ba**	**Ca**	**Rb**	**Pb**	**Th**	**U**
99.999%CALCITE PURE	2.7	2.6	4.1	-1.5	7.7	0.7	-0.2	42.28	5.9	-0.6	3.0	0.7
99.999%CALCITE PURE	2.2	1.7	4.7	2.6	8.9	0.3	3.5	42.28	6.2	-0.7	3.0	0.2
99.999%CALCITE PURE	2.3	2.1	4.1	2.3	8.9	-0.1	-2.2	42.22	6.0	-0.4	2.9	0.6
99.999%CALCITE PURE	2.2	1.8	4.4	2.2	8.9	0.4	1.6	42.26	6.1	0.3	3.5	0.6
99.999%CALCITE PURE	1.9	2.0	4.3	2.3	8.8	0.8	-1.0	42.31	5.8	-0.1	3.2	0.2
99.999%CALCITE PURE	2.2	1.9	4.7	2.4	9.0	0.3	4.9	42.28	5.6	-0.6	3.2	0.2
Ave:	**2.2**	**2.0**	**4.4**	**1.7**	**8.7**	**0.4**	**1.1**	**42.27**	**5.9**	**-0.4**	**3.1**	**0.4**
SD	0.3	0.3	0.3	1.6	0.5	0.3	2.7	0.03	0.2	0.4	0.2	0.2
Empirical LLD (3x SD)	**0.8**	**0.9**	**0.9**	**4.7**	**1.4**	**1.0**	**8.2**	**0.09**	**0.7**	**1.1**	**0.6**	**0.7**

Absolute background	**2.3**	**2**	**4**	**2**	**8.6**	**0.5**	**0.2**	**42.2**	**6.0**	**-0.3**	**3**	**0.4**
Ave. LLD	**0.8**	**1**	**1**	**3**	**1.3**	**1.1**	**7**	**0.2**	**0.6**	**1.0**	**1**	**0.5**

Table 2B-8. Results of repeated XRF measurements (12x) on 99.999% pure calcite zero-concentration pressed pellet standards used to determine absolute calibration backgrounds and lowest levels of detection (defined as 3σ of the analyte spectral peak count rate, background corrected).

XRF Applications used: CarbTraceMaj & MgSliwUThRbPb

Duplicate set of analyses

Units:	WT.%	WT.%	WT.%	WT.%	WT.%	WT.%	WT.%	[PPM]	[PPM]	[PPM]	[PPM]	[PPM]	[PPM]
Sample name	**Na**	**Mg**	**Al**	**Si**	**P**	**S**	**K**	**Ti**	**V**	**Cr**	**Mn**	**Fe*****	**Co**
Ultrapure calcite ground in Spex Hardened Steel for 6 min.													
99.999%CALCITE after 6 min. of grinding*	0.054	-0.061	0.012	0.331	0.014	0.002	-0.005	-6.2	1.2	-21.8	89.7	211.1	-2.0
99.999%CALCITE after 6 min. of grinding*	0.053	-0.061	0.011	0.331	0.014	0.002	-0.005	-5.9	2.2	-22.6	90.8	212.1	-2.6
99.999%CALCITE after 6 min. of grinding*	0.055	-0.060	0.011	0.331	0.014	0.001	-0.006	-5.8	1.1	-22.5	87.9	211.1	-2.4
99.999%CALCITE after 6 min. of grinding*	0.054	-0.060	0.011	0.331	0.014	0.001	-0.005	-6.0	2.1	-23.3	90.6	211.0	-2.8
99.999%CALCITE after 6 min. of grinding*	0.055	-0.061	0.011	0.330	0.014	0.000	-0.005	-5.8	1.4	-22.1	91.1	210.4	-3.0
99.999%CALCITE after 6 min. of grinding*	0.055	-0.060	0.010	0.330	0.014	0.000	-0.005	-6.4	2.0	-22.4	90.3	210.6	-2.2
Ave:	**0.054**	**-0.061**	**0.011**	**0.331**	**0.014**	**0.001**	**-0.005**	**-6.0**	**1.7**	**-22.4**	**90.1**	**211.0**	**-2.5**
SD	0.001	0.001	0.001	0.001	0.000	0.001	0.000	0.3	0.5	0.5	1.1	0.6	0.3
Empirical LLD (3x SD)	**0.002**	**0.002**	**0.002**	**0.002**	**0.000**	**0.003**	**0.001**	**0.8**	**1.5**	**1.5**	**3.4**	**1.8**	**1.0**

*Ground using SPEX Hardened Steel Vials

***Corr. for 3ppm Fe in calcite pellet

Sample name	**Na**	**Mg**	**Al**	**Si**	**P**	**S**	**K**	**Ti**	**V**	**Cr**	**Mn**	**Fe*****	**Co**
99.999%CALCITE PURE	0.053	-0.061	-0.010	0.326	0.014	0.002	-0.006	-5.3	2.3	-24.3	88.3	178.2	-2.7
99.999%CALCITE PURE	0.052	-0.061	-0.010	0.326	0.014	0.001	-0.006	-5.8	0.7	-22.3	89.7	179.3	-2.2
99.999%CALCITE PURE	0.053	-0.061	-0.010	0.326	0.014	0.001	-0.006	-5.9	1.2	-22.3	89.0	177.9	-2.8
99.999%CALCITE PURE	0.051	-0.061	-0.010	0.326	0.014	0.001	-0.006	-6.0	1.5	-24.2	88.8	178.4	-3.5
99.999%CALCITE PURE	0.051	-0.061	-0.010	0.326	0.014	0.001	-0.007	-6.4	1.6	-23.3	90.4	178.4	-1.8
99.999%CALCITE PURE	0.052	-0.060	-0.010	0.325	0.014	0.000	-0.006	-7.5	1.6	-23.6	88.2	177.9	-1.8
Ave:	**0.052**	**-0.061**	**-0.010**	**0.326**	**0.014**	**0.001**	**-0.006**	**-6.1**	**1.5**	**-23.3**	**89.1**	**178.3**	**-2.5**
SD	0.001	0.000	0.000	0.000	0.000	0.001	0.000	0.8	0.5	0.9	0.8	0.5	0.6
Empirical LLD (3x SD)	**0.003**	**0.001**	**0.000**	**0.001**	**0.000**	**0.002**	**0.001**	**2.3**	**1.6**	**2.6**	**2.5**	**1.5**	**1.9**

Absolute background	**0.053**	**-0.061**	**0.000**	**0.328**	**0.014**	**0.001**	**-0.006**	**-6.1**	**1.6**	**-22.9**	**90**	**195**	**-2.5**
Ave. LLD	**0.004**	**0.001**	**0.03**	**0.01**	**0.000**	**0.002**	**0.002**	**1.6**	**1.5**	**2**	**3**	**2**	**1**

Table 2B-8 continued.

XRF Applications used: CarbTraceMaj & MgSliwUThRbPb

Duplicate set of analyses

Units:	[PPM]	[PPM]	[PPM]	[PPM]	[PPM]	[PPM]	[PPM]	WT.%	[PPM]	[PPM]	[PPM]	[PPM]
Sample name	**Ni**	**Cu**	**Zn**	**Sr****	**Zr**	**Mo**	**Ba**	**Ca**	**Rb**	**Pb**	**Th**	**U**
Ultrapure calcite ground in Spex Hardened Steel for 6 min.												
99.999%CALCITE after 6 min. of grinding*	2.3	2.5	4.7	2.3	9.3	0.2	-5.6	42.25	6.2	-0.6	3.2	0.3
99.999%CALCITE after 6 min. of grinding*	2.6	2.5	4.2	2.0	8.8	0.5	0.3	42.23	6.5	-0.5	3.0	0.5
99.999%CALCITE after 6 min. of grinding*	2.4	2.0	4.5	2.0	9.0	0.8	4.4	42.29	6.0	-1.0	3.2	-0.1
99.999%CALCITE after 6 min. of grinding*	2.3	2.4	4.7	2.1	8.7	0.2	2.0	42.27	6.3	-0.4	2.7	0.3
99.999%CALCITE after 6 min. of grinding*	2.5	2.0	4.5	2.4	8.7	0.4	-2.4	42.24	6.2	0.3	2.6	0.0
99.999%CALCITE after 6 min. of grinding*	1.9	1.9	4.6	1.8	8.2	0.0	1.3	42.27	6.5	0.0	3.2	0.6
Ave:	**2.3**	**2.2**	**4.5**	**2.1**	**8.8**	**0.3**	**0.0**	**42.26**	**6.3**	**-0.4**	**3.0**	**0.3**
SD	0.2	0.3	0.2	0.2	0.4	0.3	3.5	0.02	0.2	0.4	0.2	0.3
Empirical LLD (3x SD)	**0.7**	**0.8**	**0.5**	**0.7**	**1.1**	**0.8**	**10.6**	**0.07**	**0.6**	**1.3**	**0.7**	**0.8**

*Ground using SPEX Hardened Steel Vials

**Corr. for 5ppm Sr in calcite pellet

Sample name	**Ni**	**Cu**	**Zn**	**Sr****	**Zr**	**Mo**	**Ba**	**Ca**	**Rb**	**Pb**	**Th**	**U**
99.999%CALCITE PURE	2.6	1.6	4.7	2.3	7.8	0.6	-1.5	42.31	6.1	-0.8	3.2	0.4
99.999%CALCITE PURE	2.2	2.5	3.9	2.1	8.3	0.4	-1.5	42.30	5.9	-0.5	2.6	0.1
99.999%CALCITE PURE	2.3	2.3	4.2	2.7	8.3	0.6	-1.0	42.32	6.5	-0.6	2.6	0.8
99.999%CALCITE PURE	2.4	1.8	4.9	1.7	7.9	0.9	2.5	42.21	6.4	-0.6	3.1	0.5
99.999%CALCITE PURE	2.4	2.0	5.1	0.3	7.9	0.0	1.0	42.32	6.2	-0.6	2.9	0.3
99.999%CALCITE PURE	2.1	2.1	4.8	2.2	8.5	0.2	0.7	42.29	5.9	-0.2	2.7	0.3
Ave:	**2.3**	**2.0**	**4.6**	**1.9**	**8.1**	**0.4**	**0.1**	**42.29**	**6.2**	**-0.6**	**2.8**	**0.4**
SD	0.2	0.3	0.5	0.9	0.3	0.3	1.6	0.04	0.2	0.2	0.3	0.2
Empirical LLD (3x SD)	**0.5**	**1.0**	**1.4**	**2.6**	**0.8**	**0.9**	**4.9**	**0.13**	**0.7**	**0.5**	**0.8**	**0.6**

Absolute background	**2.3**	**2**	**5**	**2**	**8.4**	**0.4**	**0.0**	**42.3**	**6.2**	**-0.5**	**3**	**0.3**
Ave. LLD	**0.6**	**1**	**1**	**2**	**1.4**	**0.8**	**8**	**0.1**	**0.7**	**1.0**	**1**	**0.7**

3. Trace element variations in the Middle Frasnian *punctata* Zone (Late Devonian) in the Western Canada Sedimentary Basin – changes in oceanic bioproductivity and paleoredox spurred by a pulse of terrestrial afforestation?[1]

Abstract: The '*punctata* Event' (Early–Middle Frasnian transition , Late Devonian) was recently recognized as yet another episode of major geochemical perturbations associated with the Middle-Late Devonian ecosystem readjustments which culminated in the Frasnian-Fammenian (F/F) mass extinction event, one of five largest of the Phanerozoic. We report variations in total organic carbon (TOC), magnetic susceptibility (MS), major, minor and trace element proxies (for changes in detrital input, bioproductivity and redox conditions) across the *P.punctata* conodont biozone in the Western Canada Sedimentary Basin (Western Laurussia). Geochemical proxies and MS display similar trends, suggesting an intimate interdependence. The data is thus evaluated within 1) a regional sequence stratigraphic perspective and 2) the *marine-terrestrial teleconnections* model *(Algeo & Sheckler, 1998)*, whereby the rise and expansion of arborescent vascular land plants (the first 'true' forests) results in a transient increase in pedogenesis and solute delivery (hence biolimiting micronutrients) to the oceans. The *punctata* Event approximately coincides temporally with the advent of archaeopterid forest expansion and rise to dominance in the Frasnian-Fammenian age. This evolutionary event is speculated to have amplified the detrital influx which was likely already elevated by conditions of sea level lowstand, early transgression, episodes of mountain building and increased weathering during Frasnian warming. Statistical correlations among proxies suggest that changes in detrital input were the main driver of a bioproductivity increase. Elevated organic matter export from the photic zone likely led to the deposition and later preservation of organic-carbon rich facies under facilitated conditions of bottom water oxygen depletion. This paper is intended to supplement the growing body of work aimed at elucidating the causes of the *punctata* Event and documenting ecosystem responses to major perturbations of the global carbon cycle.

3.1. Introduction

In this contribution we report changes in the geochemistry (major [>1%], minor [<1%] and trace [ppm] elements), magnetic susceptibility (MS) and total organic carbon (TOC) recorded in

---

[1] Śliwiński, M.G. Whalen, M.T. and Day, J., 2010. Trace element variations in the Middle Frasnian *punctata* Zone (Late Devonian) in the Western Canada Sedimentary Basin – changes in oceanic bioproductivity and paleoredox spurred by a pulse of terrestrial afforestation? *Geologica Belgica,* **13**(4), 459-482

the basinal limestones of the Miette carbonate platform during the early Late Devonian *punctata* Event (early Middle Frasnian [E-MF] transition) in the Western Canada Sedimentary Basin. This event, occuring within and named after the *Palmatolepis punctata* conodont biostratigraphic zone, is characterized by one of the larger positive carbon isotope ($\delta^{13}C$) excursions know to date in the Phanerozoic (a shift of up to ~6-7 ‰ in the $\delta^{13}C$ reservoir [*Yans et al., 2007*], although more commonly reported as 4-5‰, occurring in four distinct steps described by *Racki et al., 2008; Pisarzowska et al., 2006; Pisarzowska, 2008*). It has been recognized as a *global* perturbation (or reorganization) of the carbon cycle *(Yans et al., 2007; Racki et al., 2008)* and its particular geochemical signatures have been found in multiple localities around the world - most notably in Belgium *(Yans et al., 2007)*, the Holy Cross Mountains of Poland *(Racki et al., 2008; Pisarzowska et al., 2006; Pisarzowksa, 2008)*, South and Central-West China *(Ma et al., 2008),* Nevada in the western USA *(Morrow et al., 2009),* and also in the Western Canada Sedimentary Basin *(Holmden et al., 2006; this study)*. The triggering mechanism(s) that caused this event are not yet satisfactorily explained. *Racki et al. (2008, p. 127)* observed that no major sea level change nor any primary climatic or evolutionary turning point is associated with this large-scale perturbation. While the *punctata* Event does not culminate in a major extinction episode, it could be argued that the rapid and unprecedented evolution and expansion of archaeopterid forests in the mid-Frasnian could be viewed as a evolutionary turning point (*Kasig & Wilder, 1983; Wilder, 1994*; *Algeo & Sheckler, 1998). Algeo & Scheckler's (1998)* terrestrial-marine teleconnections model provides an intricate contextual framework for understanding the major ecosystem adjustments of the Devonian. Close temporal associations exists between Late Devonian marine anoxic events, pulses of extinction, major excursions in various geochemical records and paleobotanical developments in the terrestrial realm *(Algeo et al., 1995; Racki, 2005)*. The rise of vascular plants and the resulting impact to the Devonian global ecosystem has also been assayed by *Wright (1990), Berner (1997, 1998), Scheckler (2001), Beerling & Berner (2005),* and an attempt to quantify the effect of vascular plants on weathering has been reported by *Moulton & Berner (1998)* for a field study in Iceland. The strength, timing, setting and causes of various mid-Palaeozoic extinctions associated with the many geochemical disturbances observed in this time period were reviewed by *House (2002)*. Twenty 'short-term' events were recognized, each characterized by a distinctive 'brief' sedimentary and/or faunal perturbation (an interesting discussion on the meaning of 'abruptness' with increasing age in the geological record was discussed by *van Loon, 1999)*.

The Late Devonian was a period of rapid and major changes in the biospheres of both the terrestrial and marine realms *(Algeo et al., 1995; Algeo & Scheckler, 1998; House, 2002; Streel et al., 2000; Racki, 2005; Joachimski et al., 2009)*. The *punctata* Event may represent a

pulse of change in response to terrestrial afforestation, superimposed on the 'extensive adjustments' which were taking place within the Devonian ecosystem, among them the progressive colonization of terrestrial habitats by both metazoans and plants, a shift from greenhouse to icehouse climatic conditions together with pulses of Eovariscan and Ellesmerian orogenic activity *(Caputo, 1985; Tait et al., 1997; Savoy et al., 2000; Stevenson et al., 2000; Streel et al., 2000, Matte 2001, Echarfaoui et al. 2002, Tribovillard et al., 2004; Caputo, 2008; Racki et al., 2008; Joachimski et al., 2009; Elrick et al., 2009)*. The current state of research on this global geochemical perturbation (*Yans et al., 2007*) and the associated biotic response is brought together in a collection of publications edited by *Baliński et al. (2006)* and *Racki et al. (2008)*. These include studies of $\delta^{13}C$ variations, seawater $^{87}Sr/^{86}Sr$ trends, magnetic susceptibility (MS), and trace element variations as tracers of oceanic bioproductivity and paleoredox conditions. Of all the geochemical records compiled thus far, however, only the carbon isotope excursions are documented *globally*. The geographic extent of supporting geochemical studies is not yet sufficient nor comprehensive enough to cross-compare records from the various localities where the *punctata* Event $\delta^{13}C$ excursion has been recognized. Most of these, thus far, have focused on the stratigraphic sections of the Holy Cross Mountains (Poland) *(John et al., 2008, Marynowski et al., 2008, Nawrocki et al., 2008)*. A common problem of Late Devonian (bio)geochemical studies is a lack of refined trends at the inter-basinal scale (*Racki, 2005*). Thus here we present supporting data from the distant Western Canada Sedimentary Basin. Supporting trace element trends for the *punctata* interval have been published for a stratigraphic section in the South China Basin, but hydrothermal overprinting of those geochemical signatures severely complicates their interpretation (*Ma et al., 2008*). The trace element data presented here is believed to represent a near-primary record across the E-MF, and will contribute to the existing body of work on this 'brief' time period (0.5-1.0 Ma) of pronounced but poorly understood change.

3.2. Geological background

For this study we examined a portion of the Miette carbonate platform margin stratigraphic profile (Section AB, *Whalen & Day, 2008)* containing the *Palmatolepis punctata* conodont biozone and portions of the underlying *P.transitans* and overlying *P.hassi* zones, encompassing the topmost Malige and lower Perdrix formations (Fig. 3.1). This platform is located in the Western Canada Sedimentary Basin, which, during the Late Devonian, was situated at near-equatorial latitudes on the western coast of the Laurussian continent (Fig. 3.2). With an areal extent of ~165 km^2 and a thickness of 400-500 m *(Geldsetzer, 1989; Mountjoy, 1989)*, it was one of a system of attached and isolated platforms that developed during the

Frasnian age atop a preexisting carbonate ramp which had formed across an extensive subaerial unconformity during the Middle and Late Devonian transgressions. Platform growth kept pace with a 2nd order sea level rise (Fig. 3.3) and rates of platform sedimentation surpassed those of the associated basins (*Whalen et al., 2000*). These basins are filled with platform-derived carbonate material variably mixed with fine-grained siliciclastic sediment, likely of Ellesmerian Fold Belt (Canadian Arctic Archipelago) or continental Larussian provenance *(Oliver & Cowper 1963; Stoakes, 1980; Switzer et al., 1994; Whalen & Day, 2008)*. Extensive reef development ceased in this region following the Frasnian-Fammenian mass extinction event which exterminated the stromatoporoid-coral frame-building fauna *(McLaren, 1982; McLaren & Goodfellow, 1990; Stearn, 1987)*. The development of the Miette platform was subdivided into four phases, detailed in *Whalen et al. (2000)*. A current total of nine 3rd order sea level change depositional sequences characterize these four phases which span the Late Givetian to Early Fammenian *(Whalen & Day, 2008)*. Strata containing evidence of the *punctata* Event are situated across and just above the boundary of Sequences 4 & 5 of *Whalen & Day (2008)*, which was a time period of rimmed platform progradation (Seq. 4) followed by backstepping and aggradation of a relatively flat-topped, isolated platform with a bypass margin (Seq. 5 & 6) *(Whalen et al., 2000)*.

The biostratigraphy and sequence stratigraphy for the Section AB profile was established within the context of recent work by *Whalen et al. (2000), Whalen & Day (2008) and Whalen & Day (in review)*. A rigorous biostratigraphy based on recovered conodonts could not be established for the upper portion of the profile because those samples did not yield sufficient fossils. The biostratigraphy is reinforced based on correlations with an equivalent section in an adjacent thrust sheet (Section K), for which firm biostratigraphic constraints have been established (*Whalen & Day, 2008, p. 304)*. Variations and correlations of the magnetic susceptibility (MS) signature of Section AB and other stratigraphic profiles in the study area were used to establish its sequence stratigraphy and to further reinforce the sparse biostratigraphic constraints *(Whalen & Day, 2008; Whalen & Day, in review)*.

The sampled interval (67 m; Fig. 3.2) encompasses the topmost portion of *P.transitans* conodont biozone (upper Montagne Noire Zone 4 of *Klapper, 1989*) and most of the *P.punctata* zone (Montagne Noire Zones 5 and 6 of *Klapper, 1989*). The exact stratigraphic position of the *P.punctata* and overlying *P.hassi* zonal boundary (above the observed trace element excursions – Sec. 4) could not, however, be precisely located. MS and biostratigraphic correlations with adjacent sections suggest it is situated within a 28 m covered interval which sits almost 20 m above the sampled horizons. According to the recalibrated Devonian time scale of *Kaufmann (2006)*, conodont zonal resolution averages 0.6 Ma in the highly resolved part of the time scale

(mid-Eifelian to the Devonian-Carboniferous boundary). The *punctata* Event may thus be limited to a time period of less tha 600 k.y. (taken together, all 57 Devonian conodont zones give an average duration of about 1 Ma).

The stratigraphic profile consists of stark alternations of organic-rich carbonate mudstones and coarser carbonate lithologies redeposited from upslope, mostly floatstones and rudstones. Some basinal facies horizons within the region are bioturbated, while others lack benthic fauna, are laminated and contain framboidal pyrite, indicating changes from oxygenated to oxygen-depleted bottom water conditions *(Whalen et al., 2000)*. Detailed facies descriptions of the Miette carbonate platform were previously reported by *Whalen et al. (2000)* and facies descriptions of the broader Western Canada Sedimentary Basin have been provided by *Klovan (1964), Stoakes (1980)* and *van Buchem et al. (1996)*, among others. *Stoakes (1980)* reports that the chief minerals present in the basin filling facies are calcite, dolomite, illite and fine-grained quartz. This is consistent with our unpublished observations of x-ray diffraction patterns of Section AB lithologies. Only the mudstones-wackstones were sampled (n = 43) for analyses so as to avoid any potential biases associated with facies redeposited from up-slope.

3.3. Methods

3.3.1 Geochemical proxies from XRF, TOC, and MS analyses

Minor and trace element abundances in the rock record provide insight into prevailing oceanic paleobioproductivity (Ni, Cu, P, Ba, Zn), indicate changes in the relative influx of terrigenous siliciclastic material into depositional basins (Al, Si, Ti, K, Cr, Zr, Co), and record the redox conditions near the sediment-water interface (U, Mo, V) (*Calvert & Pedersen, 1993; Tribovillard et al., 2006; Algeo & Maynard, 2008; Piper & Calvert, 2009*). Various other elements were previously measured and different ratios employed to further interpret conditions in the depositional environment. For example, redox-sensitive trace element ratios (Ni/Co, U/Th, V/Cr, V/(V+Ni)) were used by various authors (e.g. *Hatch & Leventhal, 1992; Jones & Manning, 1994; Rimmer, 2004; Rimmer et al., 2004; Riquier et al., 2006; Algeo & Maynard, 2008*) as indicators of bottom water oxygen levels. *Riquier et al. (2006)* additionally measured Mn to further infer whether the boundary between oxidizing and reducing conditions resided within the water column or near the sediment-water interface. Lead, Fe, Zn and the Fe/S ratio were applied as proxies for pyrite, hence as supplementary indicators of sulfate reducing conditions (*Riquier et al., 2006*). A Fe-S crossplot with a slope of 1.15 – that of stoichiometric pyrite – assumes all Fe is secured as this sulfide (*Riquier et al., 2006; Rimmer, 2004*). Ratios of detrital proxy elements were also evaluated and interpreted in terms of changes in relative sedimentation rates (Ti/Al – *Bertrand et al., 1996; Murphy et al., 2000;* Zr/Al – *Piper & Calvert, 2009*).

It is common practice to normalize trace element abundances in marine sedimentary rocks (especially shales) to the Al content as a means of decoupling the *detrital* trace element contribution from the overall signal *(Calvert & Pedersen, 1993; van der Weijden, 2002; Rimmer, 2004; Rimmer et al., 2004; Riquier et al., 2006; Ma et al. 2008)*. Al is cited as being 'overwhelmingly of detrital origin' (*Riquier et al., 2006; Tribovillard et al.,* 2006). More intricate ways of manipulating and presenting trace element data are discussed by *Algeo & Maynard (2008)*. It seems questionable whether this practice, as applied to *shales,* is equally applicable to carbonate lithologies. The seawater trace element signal recorded in a shale lithology is severely masked behind the stronger signal of trace element concentrations in the siliciclastic fraction of the rock. Shales also contain variable amounts of opal and carbonate, both of which act as 'dilutants' of the authigenic trace element signature. This necessitates a 'signal decoupling procedure' such as Al-normalization. The mechanism of trace element enrichment is however different for carbonate lithologies. Minor (Mg, Sr) and trace elements (commonly Cd, Mn, Fe, Co, Zn, Ni, Pb, Ba, Eu, K) are incorporated via 1) substitution for the Ca^{2+} cation in the $CaCO_3$ crystal structure, 2) inclusion between crystallographic planes, 3) incorporation into defected, empty lattice positions and 4) via surface adsorption *(Veizer, 1983)*. They also reside within a limestone's siliciclastic fraction.

Such methods of data manipulation as Al-normalization and enrichment factor calculations were critically evaluated by *van der Weijden (2002)* with surprising results. Using Al (or another element) as a common divisor, uncorrelated variables can acquire false correlations. Preexisting interrelationships between variables may be enhanced, distorted, changed from positive to negative (and vice versa) or may be destroyed altogether. This is especially so if the *coefficient of variance* of the devisor (standard deviation divided by the mean) is high. Theses effects are minimized or do not occur altogether when the *coefficient of variance* is small. But if such is the case, a normalization procedure is unnecessary altogether (*van der Weijden, 2002).*We thus present an unmodified trace element dataset for a suite of samples consisting of a near-constant carbonate mudstone lithology.

The major, minor and trace element data was generated using a PANalytical Axios wavelength-dispersive x-ray fluorescence spectrometer (XRF) at the University of Alaska Fairbanks *Advanced Instrumentation Laboratory*. A custom pressed-pellet trace element analytical routine specific to this particular carbonate lithology was developed. A major focus of routine development was to be able to detect single digit concentrations of certain trace elements and to obtain an analytical resolution capable of distinguishing concentration differences across samples down to 1 ppm (parts per million). The routine quantifies Al, Si, P, S, K, Ti, V, Cr, Mn, Fe, Co, Ni, Cu, Zn, Sr, Zr, Mo, Ba, U, Th, Rb and Pb in a dominantly carbonate matrix. Each analyte

was calibrated against 'in-house' and certified standard reference materials (available from the *United States Geological Survey* and the *United States National Institute of Standards and Technology*). The analytical accuracy based on calibrations relative to standard reference materials is within 10%. The reproducibility of results is to within several tens of parts per million for those elements present in concentrations of several hundred to several thousand ppm, and is around one-tenth of a ppm for those elements generally present in concentrations below 100 ppm. Calculated lowest levels of detection for each analyte along with representative analytical precisions are summarized in Table 3.1.

Samples were pulverized using hardened steel vials from SPEX CertiPrep Group. Because of the relative softness of the lithology, a 5 minute crushing time was sufficient to produce a homogenous powder. Each sample was subsequently made into a 35 mm diameter pressed pellet using polyvinyl alcohol as a binder.

3.3.2 Total Organic Carbon (TOC) determination

TOC was determined using a ECS 4010 Elemental Combustion System at the *Alaska Stable Isotope Facility* (University of Alaska Fairbanks) during $\delta^{13}C_{org}$, $\delta^{13}C_{carb}$, $\delta^{18}O_{carb}$ and $\delta^{15}N_{org}$ data generation (not reported here). TOC concentrations present in the acid-insoluble residue following carbonate acidification were used to calculate the TOC for the bulk rock based on the initial mass measured before processing. The analytical precision and accuracy associated with the TOC analysis is within 2% and 10% of the reported values.

3.3.3 Magnetic susceptibility determinations

Samples for magnetic susceptibility measurements were weighed to within 0.001 g and measured on a KLY-3 Kappa bridge magnetic-susceptibility meter at Brooks Ellwood's lab (Louisiana State University). MS values represent an average of three measurements of mass-normalized bulk magnetic susceptibility (with units of m^3/kg), taken on each sample. Previous work by *Whalen & Day (2008)* indicates that the MS is dominated by the paramagnetic component.

3.4. Results

Prominent trace element variations are observed within the *P.punctata* conodont biozone and correspond to the large, globally distributed, $\delta^{13}C$ excursion *(Racki, 2004, 2005; Holmden et al., 2006; Pisarzowska et al., 2006; Yans et al., 2007; Ma et al., 2008; Racki et al., 2008; Morrow et al., 2009)*. MS variability and geochemical proxies for changes in detrital input (Figs. 3.4 & 3.5), bioproductivity (Fig. 3.6), oceanic paleoredox conditions (Fig. 3.6) during the *punctata* Event

display similar trends, indicating that these proxies and MS are inherently linked. The stratigraphic distribution of proxies reveals a first-order enrichment in the 50-75 m interval of the profile, which can be subdivided into two excursions (at around 64 m and 72.5 m in profile) separated by a trough (at around 65-70 m in profile) where trace element values return to 'background' levels. Both excursions are generally characterized by at least a two-fold increase in trace element concentrations above stratigraphic background, and bulk-rock TOC is elevated from an average of 0.2 [wt.%] to 2.5 [wt.%] and 1.0 [wt.%] during the lower and higher peaks, respectively (Fig. 3.6).

Correlation coefficients (*Person's r* and *Spearman's rho*) (*Davis, 2002)* were calculated among the elements (Tables 3.3 & 3.4), and significant correlations were found to exist (the raw geochemical dataset is in Appendix A). The observed interdependence between bioproductivity and detrital input proxies and MS implies that primary production increases during the *punctata* Event were driven largely by changes in detrital supply and associated nutrients. Similar overall trends in, and correlations between, paleoredox proxies and TOC (Fig. 3.6, Tables 3.3 & 3.4) suggest that low bottom water oxygen conditions were responsible for the preservation of organic matter (OM) produced during detrital-driven high productivity. Evaluation of the data from a sequence stratigraphic perspective implies that trends are likely influenced by relative sea level change. Most proxies display an initial increase during 3rd order sea level lowstand and early transgression (transition between Sequences 4-5), and eventually return to 'background' levels during sea level highstand.

Following the approach of *Bertrand et al. (1996)* and *Piper & Calvert (2009)*, the Ti/Al and Zr/Al ratios were employed as proxies for changes in relative sedimentation rates and plotted against both MS and the speculative *quasi*-proxies for continental weathering – Rb and Sr (Fig. 3.5). Increasing Ti/Al and Zr/Al ratios of marine sediments correlate with increasing grain size of mud-dominated facies. This observation was used by *Murphy et al. (2000)* to demonstrate changes in sedimentation rates during the deposition of Devonian black shales in the Appalachian Basin, and *Piper & Calvert (2009)* interpreted trends in Zr/Al values in a similar manner. Both Ti and Zr reside in the heavy mineral fraction of sediments, sequestered in rutile and ziron mineral phases, respectively. Given their high specific gravities compared to quartz (rutile: specific gravity (G) = 4.23-5.5, zircon: G=4.68, quartz: G=2.65), both minerals tend to be deposited with a coarser sand fraction (hydraulic equivalence: silt-sized zircons and rutile are approximately equivalent to sand-sized quartz) *(Tucker, 2001)*. While both ratios follow the general trend of MS variation (corroborating hypotheses about MS and detrital input – *Ellwood et al., 1999)*, the Zr/Al trend displays an inverse relationship, which may be an artifact of dividing Ti and Zr concentrations by Al contents (in essence a Al-normalization of the sort discussed by *van*

der Weijden, 2002). Notice, for example, that the unnormalized Zr profile faithfully mimics the MS trend (compare Figs. 3.4 & 3.5). The increases of Sr and Rb concentrations throughout the interval are observed to coincide with elevated levels of other detrital proxies and MS, possibly further supporting the notion of increased land-derived siliciclastic delivery to ocean basins. Both elements could be regarded as speculative *quasi*-proxies of continental weathering. *John et al. (2008)* observed a pulsed increase in seawater $^{87}Sr/^{86}Sr$ ratios during the onset of the *punctata* Event - an isotopic shift that should also manifest itself as a rise in the absolute concentration of Sr in seawater given that the residence time of this element in the oceans (>4 Myr) is longer than oceanic mixing rates (~10^3 yr) *(Veizer, 1989)*. During fractional crystallization, both Sr and Rb are concentrated into the melt, which effectively enriches both elements in continental crust *(Veizer, 1989)*. Uplift and increased weathering of crystalline rocks, especially in humid, warm tropical/equatorial regions will increase the flux of both elements into the oceans via riverine discharge.

The calculated redox element ratios - Ni/Co, V/Cr, V/(V+Ni) and U/Th (Fig. 3.7) – were assigned the oxic-dysoxic-anoxic threshold values of *Jones & Manning (1994)* and *Hatch & Leventhal (1992)* (Table 3.2), although these calculations ought to be viewed only relatively (see discussion in *Rimmer, 2004; see also Riquier et al., 2006*). Applying a set of absolute threshold values to these ratios based either on contemporary dysoxic-anoxic basin analogues or thresholds developed for a specific paleobasin may not be appropriate for depositional environments of a different age, a different paleogeographic setting, or supplied with detritus of a different provenance. These redox indices are suggested to be used *collectively* to interpret the degree of anoxia based on *relative* variations (*Rimmer, 2004*). Absolute thresholds established in previous studies ought not to be applied *strictly (Rimmer, 2004)*. The calculated indices (Fig. 3.7) reveal oscillations which suggest changes in the oxygenation level of bottom waters from dominantly dysoxic-anoxic to intermittently oxic conditions (note that no threshold values were assigned to the U/Th redox index. The highest observed value is near 0.04 - much lower than the cutoffs determined by *Jones & Manning, 1994;* [Table 3.2]). Dominantly reducing conditions may also be inferred from the observed enrichments of the sulfide-forming (excluding Mn) supporting proxies (Zn, Pb, Fe, S - Fig. 3.8) and a S/Fe ratio near that of stoichiometric pyrite (Fig. 3.9).

3.5. Discussion: TOC and Trace element enrichments: Implications for detrital input, paleobioproductivity, and redox conditions

3.5.1 Changes in detrital input and MS before and during the punctata Event

The growth and development of the Miette carbonate platform kept pace with a 2nd order sea level rise, superimposed on which are nine 3rd order transgressive-regressive cycles (T-R) *(Whalen et al., 2000; Whalen & Day, 2008)*. The observed geochemical excursions of the *punctata* Event occur during sea level lowstand and early transgression of 3rd order transgressive pulse IIc1 (Fig. 3.3) (pulse IIc1 coincides with the onset of the *punctata* zone and continues into the overlying *P.hassi* zone). The IIc T-R event was identified by *Johnson et al. (1985)*, further refined by *Day (1996), Johnson et al. (1996), and Sandberg et al. (2002)*, and subdivided into two events – IIc1 and IIc2 – in western Canada by *Whalen & Day (2008, Fig. 6)*. Within the framework of the four-step $\delta^{13}C$ perturbation which characterizes the *punctata* Event (see Fig. 3.18 in *Pisarzowska et al., 2006* and Fig. 1 in *Racki et al., 2008)*, the trace element enrichments correspond to the major positive isotopic shift (step III in *Pisarzowska et al., 2006*). The concentrations of detrital proxies (Al, Si, K, Ti, Cr, Zr and Co) increases prominently across the *P.transitans-P.punctata* zonal boundary and into the *punctata* zone itself. This corresponds well with magnetic susceptibility increases following a MS low during eustatic sea level highstand in the mid-*transitans* zone *(cf. Whalen & Day, 2008)* (Fig. 3.4). Ti/Al and Zr/Al ratios (Fig. 3.5) are interpreted to record relative variations in the sedimentation rate during this time, and record oscillations throughout the sampled interval in tandem with MS. The Zr/Al ratio shows an inversed trend, and the use of both the Ti/Al and the Zr/Al proxies is thus inconclusive in this study. However, graphic correlation of MS trends from Section AB with three other stratigraphic profiles in the basin reveals a thicker package of sediment deposited during the *punctata* interval at Section AB, interpreted by *Whalen & Day (in review)* to indicate higher rates of sedimentation. The observed trace element enrichments are interpreted in part as an increase in the amount of terrigenous siliciclastic material delivered to the depositional basin during a transient intensification of continental weathering *(cf. John et al., 2008; Racki et al., 2008 and others therein)*. It must also be noted, however, that this detrital signal may have been amplified in part by the 3rd order scale relationships between sea level and MS developed by *Whalen & Day (in review)* for the Western Canada Sedimentary Basin. MS highs are observed during late highstand, lowstand and early transgression. *Whalen & Day (in review)* observe that because early transgressive systems commonly rework siliciclastic material originally deposited during sea level lowstands, early transgressive facies may similarly inherit higher MS signatures. In concordance with this observation, MS signatures recorded in the stratigraphic profile are seen to

be high during late highstand of Sequence 4 (late *P.transitans* zone), lowstand at the Sequence 4-5 boundary (*P.transitans-P.punctata* zonal boundary) and during early transgressive pulse IIc1 of Sequence 5 (early *P.punctata* zone). While relative MS highs are thus expected in accordance with the observations of *Whalen & Day (2008, in review)* and *Ellwood et al. (1999)* for the study area, it is also conceivable that the amount of siliciclastic material available for deposition during lowstand and reworking during early transgression was significantly increased during this period of enhanced continental weathering and paleobotanical developments taking place on land during the *punctata* Event.

Two corresponding *punctata* Event sections in Poland (Holy Cross Mountains) record two distinct pulses of increased clastic detritus delivery to the ocean basins of Central Europe *(Nawrocki et al., 2008)*. These pulses mark the beginning and the end phases of a broad MS low which spans the *punctata* zone. Generally, eustatic sea level *rises* correspond to low MS values, and sea level *falls* are associated with increased detrital fluxes and higher MS because more continental land is exposed and subject to erosion *(Ellwood et al., 1999, 2000; Whalen & Day, 2008)*. *Nawrocki et al. (2008)* thus interpreted the MS variation as a record of a general transition from relatively high to low sea-level stands near the *P.punctata-P.hassi* zonal boundary. Further, they suggested that pulses of Eovariscan tectonic uplift and erosion have enhanced the MS record they observed. The basinal facies of the Miette carbonate platform in Western Alberta record an increase in MS throughout the lower *punctata* zone. Recognizing any potential MS high at the top of this zone, as observed in Central Europe, is precluded by the covered portion of the outcrop that contains the *P.punctata-P.hassi* zonal boundary. We interpret the MS elevation in the lower *punctata* zone in part as an increase in the amount of terrigenous siliciclastic material delivered to the basin, in correspondence with sea-level lowstand at the end of T-R cycle IIb3 and early transgression of T-R cycle IIc1. MS signatures from marine sediments have been proposed for use in regional and supraregional stratigraphic correlations *(Ellwood et al., 2000; Whalen & Day, 2008, Nawrocki et al., 2008 and references therein)*. Long-term, high magnitude and low-frequency MS events correspond to supraregional erosion associated with geographically extensive orogenic events *(Ellwood et al., 1999; Nawrocki et al., 2008; Whalen & Day, 2008)*. Conversely, short-term, low-magnitude, high-frequency MS oscillations correspond to *regional* sediment shedding and may reflect climatic signatures and relative changes in sea level *(Ellwood et al., 1999; Nawrocki et al., 2008; Whalen & Day, 2008)*. Concerning the Early to Middle Frasnian, various authors have noted and interpreted a general long-term decrease of MS magnitude as indicative of worldwide sea level transgressions and the associated decrease in detrital input *(see references in Nawrocki et al., 2008)*. This long-term trend is also observed in

the Western Canada Sedimentary Basin *(Whalen & Day, 2008)*, superimposed on top of which are the likely regional oscillations of the *punctata* Event.

The two MS pulses in the *P.punctata* zone recorded in the Holy Cross Mountains (Poland) were interpreted to represent initial pulses of the Variscan orogeny, which uplifted the Mid-German Crystalline High *(Nawrocki et al., 2008)*. The beginning of synorogenic sedimentation is thought to have taken place near the E-MF Frasnian transition – i.e. temporally near the beginning of the *P.punctata* conodont biozone. This interpretation is supported by a pulsed increase in the seawater $^{87}Sr/^{86}Sr$ ratio throughout the *punctata* Event *(John et al., 2008)*. While the overall Sr isotope ratio of seawater increased throughout the Middle and Late Devonian, the superimposed 'pulsed increase' within the *punctata* zone may reflect a transient increase in continental weathering associated with the initial phases of Eovariscan orogenic uplift *(John et al., 2008)*. It is noteworthy to point out that during Middle to Late Devonian times, all the thus-far studied *punctata* Event sections, including those in the Western Canada Sedimentary Basin, were located in the equatorial paleolatitudes, where denundation of uplifted areas and rates of chemical weathering, associated with the spread of forests and advent of intense pedogenesis, would have been relatively high (*cf. John et al., 2008)*. Our geochemical dataset displays a prominent increase in the absolute concentrations of both Rb and Sr throughout the *punctata* disturbance (Fig. 3.5). Sr concentrations generally increase steadily up-section, with a superimposed 'pulse,' corresponding to all other trace element enrichments (Figs. 3.4-3.6). *John et al. (2008)* demonstrated that uniformity of $^{87}Sr/^{86}Sr$ values across all oceans of the Frasnian age is to be expected, given that the residence time of Sr in oceans is, and likely has been in past periods of geologic time, longer than oceanic mixing rates. This was evidenced by comparing values from Central European basins and those of palaeogeograhpically distant locations in South China. Thus a rapid weathering-related flux of Sr into the oceans at one locality (i.e. the Central Europeans basins) would be recorded globally (both as an increase in the $^{87}Sr/^{86}Sr$ ratio, but also as an increase in absolute Sr concentrations). The basinal carbonates of Western Alberta could thus have recorded a mixed signal indicating regional weathering of uplifted lands but also weathering of distant orogens, such as those of Central Europe and northern Canada.

Previous work in the Alberta subsurface documented the progressive east-to-west infilling of the Western Canada Sedimentary Basin from the Late Givetian through the Fammenian *(Stoakes, 1980)*. Frasnian siliciclastics consist of clay and silt partially derived from the Ellesmerian fold belt provenance in the Canadian Arctic Archipelago but a component of this sediment was probably eolian transported from the Laurussian continental interior *(Whalen & Day, 2008)*. *Stevenson et al. (2000)* argued, based on Sm-Nd isotopic data, that the detrital provenance did not change to the westerly Antler orogeny related source areas until the

Fammenian. Thus the observed increases in MS and detrital influx during the *punctata* Event cannot be explained directly by regional pulses of orogenic activity in the immediate vicinity of the depositional basin (as was done by *Nawrocki et al., 2008* for the basins of Central Europe). But perhaps an intensification of weathering, in the northerly Ellesmerian Fold Belt region and the continental interior, caused by a pulse of forest expansion and a warming climate can be implicated. The advent and spread of vascular land plants of tree stature would have profoundly altered the hydrologic cycle and the course of soil development *(Algeo & Scheckler, 1998)*. Intimate interactions of vegetation with atmospheric water would have begun altering the land surface albedo and increased precipitation while weathering substrates more thoroughly and intensely than non-vascular vegetation of the pre-Middle-Late Devonian *(Algeo & Scheckler, 1998 and references therein)*. Weathering rates would have been all the more accelerated in wet, warm near-equatorial regions (*White & Blum, 1995)* and further amplified by a Frasnian climatic warming trend reconstructed using conodont apatite $\delta^{18}O$ signatures (*Joachimski et al., 2009*) and palynomorph assemblages *(Streel et al., 2000)* (however, see Fig. 1 in *Racki et al. 2008* showing a reconstructed Frasnian *cooling* trend based on conodont apatite and *Pisarzowska, 2008* for the original isotopic study).

3.5.2 Bioproductivity proxy trends

The *punctata* Event $\delta^{13}C$ excursion was interpreted by *Ma et al. (2008, p. 144)* using supporting trace element geochemistry as an indicator of enhanced bioproductivity and organic matter burial during the early-Middle Frasnian transition within the South China basin. Trace element records from the Western Canada Sedimentary Basin are consistent with this interpretation, as are changes in TOC (both for the studied stratigraphic profile (Fig. 3.6) but also for a correlative section in an adjacent thrust sheet - Section K; Fig. 7 in *Whalen et al., 2000*). Both Cu and Ni, which have been used as direct proxies for oceanic bioproductivity *(i.e. Piper & Perkins, 2004; Riquier et al., 2006; Ma et al., 2008; Perkins et al., 2008; Piper & Calvert, 2009)*, are appreciably enriched. Both elements behave as micronutrients (although Cu to a lesser extent than Ni) in oxic marine environments and are delivered to the sediment via complexations with OM but are also enriched via the redox cycling of Fe-Mn oxyhydroxides *(Calvert & Pedersen, 1993; Tribovillard et al., 2006)*. Sediments with high OM fluxes are a significant sink for these metals (and also for Cd, Zn, Cr, V, Re, Mo and U). Zn also behaves as a micronutrient and is removed form surface waters by plankton growth. Its enrichment in the profile supports what is inferred from the elevated levels of Cu and Ni.

Within the context of the *Algeo & Sheckler (1998)* model, a transient intensification of pedogenesis and increased delivery of biolimiting nutrients (Ni, Cu, Zn, P) to the oceans may

have stimulated a temporary elevation of primary productivity. High correlations between the MS, TOC, bioproductivity and detrital influx proxies (Tables 3.3 & 3.4) suggest that enhanced primary production was mainly detrital-driven. Organic matter enrichments are interpreted as a mixed signal of both increased productivity *and* preservation under at least intermittently reducing bottom water conditions *(cf. Murphy et al., 2000)*, given that strong correlations exist between TOC and the redox sensitive proxies (Tables 3.3 & 3.4). *Rimmer (2004, p. 388)* suggests that "different relationships between C_{org} and a redox-sensitive element in adjacent units, units that most likely have experienced similar tectonic and basinal fluid influences, may suggest differing roles of anoxia during OM accumulation." Without a suitable point of comparison, however, we are at present unable to describe the relative importance of anoxia in OM accumulation. The strong correlations only confirm the intimate relationship between C_{org} preservation and bottom water oxygen deficiency, but are not adequate to discern whether enhanced preservation or a greater flux of OM to the sediment was responsible for the observed organic enrichments.

Sedimentary phosphorus enrichments, as discerned in the geochemical trends (Fig. 3.6), are unfortunately not necessarily directly indicative of enhanced primary productivity *(Tribovillard et al., 2006)*. Dissolved phosphate is immobilized in the sediment when the surface layer is oxic, and sequestration occurs via bioaccumulation (active phosphorus storage by microorganisms) and Fe-oxyhydroxide precipitation (which prevents P escape to the water column because of a large sorption capacity *(van Cappellen & Ingall, 1994))*. If the overlying water layer becomes oxygen-depleted, P is released and may diffuse back to the photic zone where it can again be utilized by the planktonic biomass. In the context of the other productivity proxies, the observed P enrichment and correlation with TOC (Tables 3.3 & 3.4) suggests increased OM fluxes to the sediment preserved during intermittently oxic bottom water conditions which favor P retention, and possible trapping in an apatite mineral phase. While the redox proxies imply dominantly suboxic-anoxic conditions during the *punctata* Event, periodic oxia is supported by petrographic evidence – mainly bioturbation observed within some sedimentary horizons but not in others (*Whalen et al., 2000*).

Together with Ni, Cu and P, Ba levels are also elevated at the base of the *punctata* biozone. The enrichment is an order of magnitude higher than 'background' values in the chemostratigraphic profile, the peaks and troughs of which correspond to those of the other trace element proxies (even though these peaks and troughs are obscured by the magnitude of the Ba peak). This may be a mixed signal of Ba accumulation in a sedimentary horizon as a result of cycling across redox gradients (barium 'fronts,' as described in *Dickens et al., 2003; Tribovillard et al., 2006)* and increased riverine delivery of Ba to the oceans. Correlations with the detrital proxies are high (although not with MS – Tables 3.3 & 3.4), suggesting increased weathering in

the sediment source areas as a partial mechanism of increased Ba delivery. The flux of Ba to oceanic surface waters is substantial *(Dickens et al., 2003)*, and presumably would have been augmented significantly during the initial phases of terrestrial afforestation and intensification of pedogenetic processes. Once in solution, Ba precipitates within microenvironments surrounding decaying and sinking OM *(Dickens et al., 2003)*. Increased OM and Ba levels in the euphotic zone during the *punctata* Event could have resulted in a greater export of this element to the sediment-water interface. While difficult to use as a direct bioproductivity indicator (because of it mobility under varying redox conditions; *Tribovillard et al., 2006*), the Ba signal, when set within the context of the other geochemical proxies, seems consistent with both an increased riverine delivery of this element and increases in primary production and export productivity (suggested by Ni, Cu and P enrichments) which may have effectively transferred inflowing Ba from the water column to the sediment.

3.5.3 Paleoredox proxy trends

Oceanic bottom water anoxia and changes in primary productivity have been traditionally regarded as distinct processes which control the formation of organic-carbon rich sediments and sedimentary rocks *(Pedersen & Calvert 1990; Canfield, 1994)*. Early work on ancient black shales tended to prefer one process over the other to explain the origin of such facies, whereas more recently, enhanced OM preservation under anoxic conditions and enhanced bioproductivity are viewed as two endmembers of a continuum *(Murphy et al., 2000)*. Within a given depositional basin, the degree of influence of either end-member may shift along this continuum as time passes and oceanographic conditions change. The C_{org}-rich slope and basinal mudstones of the Miette carbonate platform are thus interpreted as a product of both increased primary productivity during the *punctata* Event, as indicated by enrichments of bioproductivity tracers and TOC, but also of enhanced OM preservation driven by bottom water oxygen depletion and the prevalence of reducing conditions, as evidenced by coeval enrichments of paleoredox tracers (Mo, U, V; Fig. 3.6). Using first order trends observed in the stratigraphic distribution of each redox index (Ni/Co, U/Th, V/Cr, V/(V+Ni)) (Fig. 3.7), and following the precautions outlined in *Rimmer (2004)*, we collectively and relatively interpret these indices as further indicating dominantly suboxic-anoxic conditions throughout the *punctata* Event. *Rimmer (2004)* found 'fairly good agreement' when interpreting redox conditions using the threshold values for Ni/Co and V/Cr established by *Jones & Manning (1994)*. In the present study, we found reasonable agreement likewise with the Ni/Co threshold of those same authors, and the V/(V+Ni) cutoff values of *Hatch & Leventhal (1992)*. The V/Cr and U/Th ratios, however, despite showing prominent enrichments within the *punctata* zone consistent with the other indices, fall below the established oxic-dysoxic boundaries of the above

cited studies (Fig. 3.7, Table 3.2). Our observations strengthen the arguments of *Rimmer (2004)* concerning strict definitions and applications of these ratio indices.

Dominantly reducing conditions in the depositional basin likely developed in the presence of sedimentary OM (high correlations of TOC and redox tracers – Tables 3.3 & 3.4). But can a distinction between water-column and sediment pore-water anoxia be made? Second-order oscillations of the redox index trends (Fig. 3.7) seem to indicate intermittently oxic bottom water conditions at the sediment-water interface, allowing for the accumulation of P (and in agreement with the aforementioned petrographic evidence) (via P-trapping under oxic conditions; *Ingall & Jahnke, 1994, van Cappellen & Ingall, 1994, 1996; Lenton & Watson, 2000; Wallmann, 2003; Tribovillard et al., 2006)*. Intermittent oxygenation may have been caused by some degree of water column mixing associated with the well documented gravity flow deposits prevalent within the stratigraphic profile *(Whalen et al., 2000)*. Following the interpretation of *Riquier et al. (2006)*, the observed Mn enrichment (Fig. 3.8) can further aid the distinction between water-column and sediment pore-water anoxia. Mn and redox-sensitive, sulphide-forming element enrichments *in tandem* could indicate that at times the boundary between oxidizing and reducing conditions was 'pushed down' from an otherwise stratified water column to the sediment-water interface, or below it - allowing for Mn fixation (in either rhodochrosite [$MnCO_3$] or kutnahorite [$Ca(Mn,Mg,Fe)(CO_3)_2$]).

3.5.4 The punctata Event within the context of the Algeo & Sheckler (1998) model

The *Devonian marine-terrestrial teleconnections model* of *Algeo & Scheckler (1998)* provides a theoretical framework within which the geochemical trends of the *punctata* Event may be interpreted. At the core of this model is the soil, which behaves as a geochemical interface between the lithosphere, the atmosphere and the hydrosphere. The Middle-Late Devonian is characterized by widespread oceanic bottom water anoxia, increased organic carbon burial rates and a prolonged biotic crisis that culminates in the Frasnian-Famennian mass extinction (*Racki, 2005*). The rapid evolution and geographically vast expansion of soils during this time period may be the link which connects such marine events to developments in the terrestrial realm - mainly the rise, rapid diversification and expansion of vascular plants, but archaeopterid forests in particular *(Algeo et al., 1995; Algeo & Scheckler, 1998)*. Prior to the Late Devonian, terrestrial plants were small, at most shallowly-rooted and their geographic extent was limited to moist lowland habitats by their reproductive mode *(Gensel & Andrews, 1984, 1987; Thomas & Spicer, 1987)*. By Late Devonian time, vascular land plants (which evolved and began diversifying in the Late Silurian-Early Devonian) became arborescent (achieved tree stature) and evolved the seed habit, which allowed them to expand geographically into previously inaccessible upland habitats

(Thomas & Spicer, 1987). Archaeopterids, which grew to more than 30 meters in height, achieved trunk diameters of more than 1.5 meters *(Beck, 1981)* and were significantly more deeply rooted than any prior plant, may have comprised monotaxic forests in floodplain habitats during the Middle to Late Frasnian. Soil penetration depths by root systems increased to 80-100 cm by the Frasnian-Fammenian, resulting in intensified pedogenesis and pedoturbation *(Beck, 1967; Snigirevskaya 1984, 1995; Retallack, 1985).*

The occurrence of deeply rooted palaeosols and in particular soil types associated mainly with temperate-zone forests increases in frequency during the Devonian, and has been interpreted as a reflection of forest expansion beyond floodplain habitats *(Allen, 1986; Driese & Mora, 1993; Retallack, 1986, 1990, 1992)*. But how rapid could afforestation have been? *Burnham (2008)* reviewed certain aspects of the plant fossil record and contemporary plant ecology (especially records of invasive plant species spread, recolonization of volcanic areas and otherwise disturbed habitats, but also historical plant migration patterns) in an attempt to answer the following question: how rapidly do newly evolved and reasonably successful plant species increase in abundance from a few individuals to a biomass sufficiently large so as to have a high probability of representation in the fossil record? *Burnham (2008)* concluded that this time interval is geologically short (ca. 2000 years), and for rocks of Devonian age can be thought of as instantaneous. *Algeo et al. (1995, p. 64)* note that the Frasnian-Famennian (F/F) boundary Kellwasser events occurred 'within the mid-Frasnian to mid-Famennian interval of archaeopterid dominance and might represent the rapid spread of this genus." While it may be nearly impossible to *tightly* constrain and correlate the timing of archaeopterid forest expansion (perhaps in multiple pulses?) with marine events in the geological record (because of a lack of suitable datable materials in Devonian non-marine successions), we can speculate that the *punctata* Event, temporally near the onset of archaeopterid rise to dominance, may record the geochemical consequence of a initial pulse of afforestation.

The *Algeo and Scheckler (1998)* model and related studies (*Wright, 1990; Berner, 1997, 1998; Scheckler, 2001; Beerling & Berner, 2005*) further propose that the diversification and expansion of vascular land plants altered the nature of continental weathering via the evolution of deeply rooted palaeosols. In essence, more thorough weathering of the bedrock was initiated within the microenvironments created around the root systems of arborescent taxa. While overall sediment yields may have decreased, the landscape stabilizing properties of vegetative cover had the net result of increasing the residence time of sediment within the weathering zone, where it could be more thoroughly decomposed. This in turn would have increased the flux of readily available micronutrients delivered to the shallow oceans by riverine discharge. Such a flux of

biolimiting nutrients would stimulate primary production, lead to increased burial of organic matter and thus contribute to water-column stratification via bottom water oxygen depletion.

A fundamental characteristic of this model, however, is that it very eloquently describes the *dynamic* but *transient* response of the lithosphere-atmosphere-ocean system to a rapid and aerially expansive diversification of a terrestrial biomass capable of interacting in a unprecedented way with its substrate. The large atmospheric CO_2 reservoir of the pre-Devonian (4-20 PAL [present atmospheric level], *Berner, 1994, 2006; Berner et al., 2007)* likely allowed for a rapid but pulsed diversification and expansion of forests. 'Excess' atmospheric CO_2 (that amount which was in excess of that supplied by fluxes into the atmosphere-ocean system by volcanic and metamorphic degassing) was consumed for increasing the terrestrial biomass and actively pumped into soils, where it stimulated a transient increase in silicate weathering (pedogenesis). Steady-state was eventually achieved with lower overall atmospheric CO_2 concentrations (pCO_2) (mid-Carboniferous pCO_2 around 1 PAL, *Berner, 1994, 2006; Berner et al., 2007*) maintained by active pumping by terrestrial vegetation and a return of silicate weathering rates to those of the pre-Devonian. It is within the context of this working model that we interpret the geochemical signatures of the *punctata* Event recorded in the basinal carbonate mudstones in Western Canada Sedimentary Basin.

3.6. Summary

-The *punctata* Event records one of the larger $\delta^{13}C$ excursions found to date in the rock record of the Phanerozoic. This perturbation of the global carbon cycle is accompanied by geochemical excursions, among them the suites of trace elements used as proxies for changes in detrital input, bioproductivity, and oceanic bottom water redox conditions. This event was set within the context of the rapidly changing Late Devonian world, where ecosystem readjustments eventually culminated in the Frasnian-Fammenian mass extinction, one of the five largest since the base of the Cambrian. Yet despite this apparently severe environmental perturbation, no major biotic crisis was found to be associated with the *punctata* Event.

-Among other localities worldwide, a record of this geochemical event was found in the basinal facies of the Miette carbonate platform in the Western Canada Sedimentary Basin. Using trace element proxies, MS variability and TOC determinations, we interpreted the *punctata* Event within 1) a regional sequence stratigraphic context and 2) within the framework of concurrent global changes of the Frasnian age. This dataset is intended to complement the growing body of work (summarized in *Yans et al., 2007; Racki et al., 2008; Morrow et al., 2009)* aimed at elucidating the causes and understanding the effects of terrestrial and marine events of the

P.punctata biozone and, more broadly, at understanding the Earth-system changes of the Late Devonian leading up to the F/F boundary.

-The stratigraphic distribution of bioproductivity, paleoredox and detrital influx proxies reveals a prominent enrichment near the onset of the *punctata* Event, beginning across the *P.transitans-P.punctata* zonal boundary and continuing above it. It coincides also with the transition between 3rd order sea level sequences 4 & 5 (*Whalen & Day, 2008).* The proxy suites co-vary with MS, suggesting an inherent interdependence and changes in detrital input as the main driver of the oceanographic changes which produced the observed geochemical excursions. Such covariance trends are consistent with recently developed models of MS variation during the different phases of T-R cycles within this region *(Whalen & Day, in review).*

-The bioproductivity proxies and TOC excursions suggest that a prominent but transient increase of the planktonic biomass occurred during the *punctata* Event, allowing for the development of dominantly dysoxic to anoxic bottom water conditions (punctuated by intermittent oxia, likely associated with water column mixing during the deposition of the numerous gravity flow deposits). Given that significant statistical correlations were found among all suites of geochemical proxies, TOC and MS, this biomass growth was likely detrital-driven. While a higher influx of terrigenous siliciclastics is expected to enter the depositional basin during conditions of sea level lowstand and early transgression (during which the observed geochemical excursions took place), coeval developments on land may have amplified the oceanographic changes observed during the *punctata* Event. The climatic warming trend of the Frasnian (*Joachimski et al.,* 2009) may have intensified the weathering of uplifted lands in the Ellesmerian fold belt (Canadian Arctic Archipelago) – a partial sediment source for the Alberta Basin. Potentially more influential, however, was the rapid rise and expansion of the first terrestrial forests (archaeopterid forests) and the evolution of complex paleosols, beginning in the mid-Frasnian. The rise of vascular, arborescent land plants would have had a profound effect on the interactions between the lithosphere, hydrosphere and the atmosphere increasing weathering rates not only in uplands but also in any forested continental area. The *Algeo & Sheckler (1998) terrestrial-marine teleconnections* model provides an intricate contextual framework for explaining marine events of the Late Devonian (mainly widespread bottom water anoxia and enhanced rates of organic carbon burial) by observing changes (primarily paleobotanical) taking place on the continents. The expansion of forests was accompanied by the concurrent evolution of deeply weathered and aerially expansive soils that altered solute fluxes (among them biolimiting nutrients) to the oceans via riverine discharge, allowing for increases of the planktonic biomass. While tight time constraints and correlations between the *punctata* Event and the onset of terrestrial afforestation

will likely remain elusive, we can speculate that this mid-Frasnian evolutionary event contributed substantially to the observed geochemical perturbation.

Acknowledgments

This work is dedicated to Prof. B.C. Schreiber, for years of support. The authors would like to thank K. Severin and R. Newberry for constructive discussions and instrumental help in developing the specialized XRF analytical protocols used for generating the trace element data for this study. The authors would also like to thank J. Addison for insightful discussions on interpreting trace element proxies in light of near-contemporary oceanography .

3.7. References

Algeo, T.J., Berner, R.A., Maynard, J.B. and Scheckler, S.E., 1995. Late Devonain oceanic anoxic events and biotic crises: "rooted" in the evolution of vascular land plants? *GSA Today*, **5**, 1-66.

Algeo, T.J. & Maynard, J.B., 2008. Trace-metal covariation as a guide to water-mass conditions in ancient anoxic marine environments. *Geosphere*, **4**, 872-887.

Algeo, T.J. & Scheckler, S.E., 1998. Terrestrial-marine teleconnections in the Devonian: links between the evolution of land plants, weathering processes, and marine anoxic events. *Philosophical Transactions of the Royal Society B-Biological Sciences*, **353**, 113-128.

Allen, J.R.L., 1986. Pedogenic calcretes in the Old Red Sandstone facies (Late Silurian – Early Carboniferous) of the Anglo-Welsh area, southern Britain. *In* Wright, V.P. (ed.) *Paleosols: their recognition and interpretation.* Oxford: Blackwell, 58-86.

Baliński, A., Olempska, E. & Racki, G., 2006. Early-Middle Frasnian transition: Biotic response to a major perturbation of the global carbon budget *Acta Palaeontologica Polonia*, **51**, 606-608.

Beck, C.B., 1967. *Eddya sullivanensis,* gen. et sp. nov., a plant of gymnospermic morphology from the Upper Devonian of New York. *Paleontographics* B **121**, 1- 22.

Beck, C.B., 1981. Archaeopteris and its role in vascular plant evolution. *In* Niklas, K.J., (ed.) *Paleobotany, paleoecology, and evolution, vol. 1.* Praeger, New York.

Beerling, D.J. & Berner, R.A., 2005. Feedbacks and the coevolution of plants and atmospheric CO_2. *Proceedings of the National Academy of Sciences of the United States of America*, **102**, 1302-1305.

Berner, E.K., Berner, R.A., and Moulton, K.L., 2007. Plants and mineral weathering: Present and past. *In Treatise on Geochemistry,* Chapter 5.06, 169-188.

Berner, R.A., 1994. 3GEOCARB-II - A revised model of atmospheric CO_2 over Phanerozoic time. *American Journal of Science*, **294**, 56-91.

Berner, R.A., 1997. Paleoclimate - The rise of plants and their effect on weathering and atmospheric CO_2. *Science*, **276**, 544-546.

Berner, R.A., 1998. The carbon cycle and CO_2 over Phanerozoic time: the role of land plants *Philosophical Transactions of the Royal Society of London Series B- Biological Sciences*, **353**, 75-81.

Berner, R.A., 2006. GEOCARBSULF: A combined model for Phanerozoic atmospheric O_2 and CO_2. *Geochimica et Comochimica Acta*, **70**(23), 5653-5664.

Bertrand, P., Shimmield, G., Martinez, P., Grousset, F., Jorissen, F., Paterne, M., Pujol, C., Bouloubassi, I., Buat Menard, P., Peypouquet, J.-P., Beaufort, L., Sicre, M.-A., Lallier-Verges, E., Foster, J.M., Ternois, Y. and et al., 1996. The glacial ocean productivity hypothesis: The importance of regional temporal and spatial studies. *Marine Geology*, **130**, 1-9.

Burnham, R.J., 2008. Hide and go seek: What does presence mean in the fossil record? *Annals of the Missouri Botanical Garden*, **95**, 51-71.

Calvert, S.E. & Pedersen, T.F., 1993. Geochemistry of recent oxic and anoxic marine sediments - implications for the geological record. *Marine Geology,* **113**(1-2), 67- 88

Canfield, D.E., 1994. Factors influencing organic-carbon preservation in marine sediments. *Chemical Geology*, **114**(3-4), 315-329

Caputo, M.V., 1985. Late Devonian glaciation in South America. *Palaeogeography Palaeoclimatology Palaeoecology*, **51**, 291-317.

Caputo, M.V., 2008. Late Devonian and Early Carboniferous glacial records of South America. *Geological Society of America Special Papers*, **441**, 161-173.

Davis, J.C., 2002. Statistics and Data Analysis in Geology (3rd ed.). New York: John Wiley & Sons.

Day, J., 1996. Faunal signatures of Middle-Upper Devonian depositional sequences and sea level fluctuations in the Iowa Basin: US mid-continent. *Geological Society of America Special Papers*, **306**, 277-300.

Dickens, G.R., Thomas, E. & Bralower, T.J., 2003. Excess barite accumulation during the Paleocene-Eocene Thermal Maximum: Massive input of dissolved barium from seafloor gas hydrate reservoirs. *Geological Society of America Special Papers*, **369**, 11-23.

Driese, S.G. & Mora, C.I., 1993. Physico-chemical environment of pedogenic carbonate formation in Devonian vertic palaeosols, central Appalachians, USA. *Sedimentology* **40,** 199-216.

Echarfaoui, H., Hafid, M. & Salem, A.A., 2002. Seismic structure of the Doukkala basin, Palaeozoic basement, western Morocco: a hint for an Eovariscan fold-and-thrust belt. *Comptes Rendus Geoscience*, **334**, 13-20.

Ellwood, B.B., Crick, R.E., El Hassani, A., 1999. The magneto-susceptibility event and cyclostratigraphy (MSEC) method used in geological correlation of Devonian rocks from Anti-Atlas Morroco. *American Association of Petroleum Geologists Bulletin,* **83**, 1119-1134.

Ellwood, B.B., Crick, R.E., El Hassani, A., Benoist, S.L., & Young, R.H., 2000. Magnetosusceptibility event and cyclostratigraphy method applied to marine rocks: Detrital input versus carbonate productivity. *Geology*, **28**, 1135-1138.

Elrick, M., Berkyova, S., Klapper, G., Sharp, Z., Joachimski, M., & Fryda, J., 2009. Stratigraphic and oxygen isotope evidence for My-scale glaciation driving eustasy in the Early-Middle Devonian greenhouse world. *Palaeogeography Palaeoclimatology Palaeoecology*, **276**, 170-181.

Geldsetzer, H.H.J., 1989. Ancient Wall reef complex, Frasnian age, Alberta, *In* Geldsetzer, H.H.J., James, N.P. & Tebbutt, G.E. (eds.), *Reefs, Canada and Adjacent Areas, Canadian Society of Petroleum Geologists, Memoir,* **13,** 431-439.

Gensel, P.G. & Andrews, H.N., 1984. Plant life in the Devonian. New York: Praeger.

Gensel, P.G. & Andrews, H.N., 1987. The evolution of early land plants. *American Scientist,* **75,** 478-489.

Hatch, J.R. & Leventhal, J.S., 1992. Relationship between inferred redox potential of the depositional environment and geochemistry of the Upper Pennsylvanian (Missourian) Stark Shale Member of the Dennis Limestone, Wabaunsee Country, Kansas, U.S.A. *Chemical Geology*, **99**, 65-82.

Holmden, C., Braun, W.K., Patterson, W.P., Eglington, B.M., Prokopiuk, T.C., & Whittaker, S., 2006. Carbon isotope chemostratigraphy of Frasnian sequences in Western Canada. *Saskatchewan Geological Survery, Summary of Investigration*, **1**, 1-6.

House, M.R., 2002. Strength, timing, setting and cause of mid-Palaeozoic extinctions. *Palaeogeography Palaeoclimatology Palaeoecology*, **181**, 5-25.

Ingall, E. & Jahnke, R., 1994. Evidence for enhanced phosphorus regeneration from marine sediments overlain by oxygen depleted waters. *Geochimica Et Cosmochimica Acta*, **58**, 2571-2575.

Joachimski, M.M., Breisig, S., Buggisch, W., Talent, J.A., Mawson, R., Gereke, M., Morrow, J.R., Day, J., & Weddige, K., 2009. Devonian climate and reef evolution: Insights from oxygen isotopes in apatite. *Earth and Planetary Science Letters*, **284**, 599-609.

John, E.H., Cliff, R. & Wignall, P.B., 2008. A positive trend in seawater Sr-87/Sr-86 values over the Early-Middle Frasnian boundary (Late Devonian) recorded in well-preserved conodont elements from the Holy Cross Mountains, Poland. *Palaeogeography Palaeoclimatology Palaeoecology*, **269**, 166-175.

Johnson, J.G., Klapper, G. & Sandberg, C.A., 1985. Devonian eustatic fluctuations in Euramerica. *Geological Society of America Bulletin*, **96**, 567-587.

Johnson, J.G., Klapper, G. & Elrick, M., 1996. Devonian transgressive-regressive cycles and biostratigraphy, northern Antelope Range, Nevada: Establishment of reference horizons for global cycles. *Palaios*, **11**, 3-14.

Jones, B. & Manning, D.A.C., 1994. Comparison of geochemical indices used for the interpretation of paleoredox conditions in ancient mudstone. *Chemical Geology*, **111**, 111-129.

Kasig, W., and Wilder, H., 1983. The sedimentary development of the Western Rheinisches Schiefergebirge and the Ardennes (Germany/Belgium). *In* Martin, H., Eder, F.W. (eds.) *Intercontinental Fold Belts*. Springer, Berlin. 185-209.

Kaufmann, B., 2006. Calibrating the Devonian time scale: A synthesis of U-PbID-TIMS ages and conodont stratigraphy. *Earth-Science Reviews*, **76**, 175-190.

Klapper, G., 1989. The Montagne Noire Frasnian (Upper Devonian) conodont succession. *Memoirs of the Canadian Society of Petroleum Geologists*, **14**, 449- 459

Klovan, J.E., 1964. Facies analysis of the Redwater reef complex, Alberta. Canada *Bulletin of Canadian Petroleum Geology*, **12**, 1-100.

Lenton, T.M. & Watson, A.J., 2000. Redfield revisited 1. Regulation of nitrate, phosphate, and oxygen in the ocean. *Global Biogeochemical Cycles*, **14**, 225-248.

Ma, X.P., Wang, C.Y., Racki, G. & Racka, M., 2008. Facies and geochemistry across the Early-Middle Frasnian transition (Late Devonian) on South China carbonate shelf: Comparison with the Polish reference succession. *Palaeogeography Palaeoclimatology Palaeoecology*, **269**, 130-151.

Marynowski, L., Filipiak, P. & Pisarzowska, A., 2008. Organic geochemistry and palynofacies of the Early-Middle Frasnian transition (Late Devonian) of the Holy Cross Mountains, Southern Poland. *Palaeogeography Palaeoclimatology Palaeoecology*, **269**, 152-165.

Matte, P., 2001. The Variscan collage and orogeny (480-290 Ma) and the tectonic definition of the Armorica microplate: a review. *Terra Nova*, **13**, 122-128.

McLaren, D.J., 1982. Frasnian-Famennian extinction. *Geological Society of America Special Papers*, **190**, 477-484.

McLaren, D.J. & Goodfellow, W.D., 1990. Geological and biological consequences of giant impacts. *Annual Review of Earth and Planetary Sciences*, **18**, 123-171.

Morrow, J.R., Sandberg, C.A., Malkowski, K., Joachimski, M.M., 2009. Carbon isotope chemostratigraphy and precise dating of middle Frasnian (lower Upper Devonian) Alamo Breccia, Nevada, USA. *Palaeogeography, Palaeoclimatology, Palaeoecology*, **282**, 105-118.

Moulton, K.L. & Berner, R.A., 1998. Quantification of the effect of plants on weathering: Studies in Iceland. *Geology*, **26**, 895-898.

Mountjoy, E.W., 1989. Miette Reef Complex (Frasnian), Jasper National Park, Alberta. *Memoirs of the Canadian Society of Petroleum Geologists*, **13**, 497-505.

Murphy, A.E., Sageman, B.B., Hollander, D.J., Lyons, D.J., & Brett, C.E., 2000. Black shale deposition and faunal overturn in the Devonian Appalachian basin: Clastic starvation, seasonal water-column mixing, and efficient biolimiting nutrient recycling. *Paleoceanography*, **15**, 280-291.

Nawrocki, J., Polechonska, O. & Werner, T., 2008. Magnetic susceptibility and selected geochemical-mineralogical data as proxies for Early to Middle Frasnian (Late Devoni an) carbonate depositional settings in the Holy Cross Mountains, southern Poland. *Palaeogeography Palaeoclimatology Palaeoecology*, **269**, 176-188.

Oliver, T.A. & Cowper, N.W., 1963. Depositional environments of the Ireton Formation, central Alberta. *Bulletin of Canadian Petroleum Geology*, **11**, 183-202.

Pedersen, T.F. & Calvert, S.E., 1990. Anoxia vs productivity - what controls the formation of organic-carbon-rich sediments and sedimentary rocks? *AAPG Bulletin-American Association of Petroleum Geologists*, 74, 454-466.

Perkins, R.B., Piper, D.Z. & Mason, C.E., 2008. Trace-element budgets in the Ohio/Sunbury shales of Kentucky: Constraints on ocean circulation and primary productivity in the Devonian-Mississippian Appalachian Basin. *Palaeogeography Palaeoclimatology Palaeoecology*, **265**, 14-29.

Piper, D.Z. & Calvert, S.E., 2009. A marine biogeochemical perspective on black shale deposition *Earth-Science Reviews*, **95**, 63-96.

Piper, D.Z. & Perkins, R.B., 2004. A modem vs. Permian black shale - the hydrography, primary productivity, and water-column chemistry of deposition. *Chemical Geolog y*, **206**, 177-197

Pisarzowska, A., 2008. Geochemia stabilnych izotopów węgla i tlenu na pograniczu dolnego i śrdokowego franu (dewon górny) na obszarze południowego szelfu Laurussi. PhD. Thesis, Silesian University, Sosnowiec, Poland.

Pisarzowska, A., Sobstel, M., Racki., G., 2006. Conodont-based event stratigraphy of the Early-Middle Frasnian transition on the South Polish carbonate shelf. *Acta Palaeontologica Polonica*, **51**(4), 609-646.

Racki, G., 2004. Geochemical and ecological aspects of lower Frasnian pyrite-ammonoid level at Kostomłoty (Holy Cross Mountains, Poland). *Geological Quarterly*, **48**(3), 267-282.

Racki, G., 2005. Toward understanding Late Devonian global events: few answers, many questions. *In* Over, D.J., Morrow, J.R., Wignall, P.B. (eds.) *Understanding Late Devonian and Permian-Triassic biotic and climatic events: Towards an integrated approach.* Elsevier, B.V.,Chapter 2, 5-36

Racki, G., Joachimski, M.M. & Morrow, J.R., 2008. A major perturbation of the global carbon budget in the Early-Middle Frasnian transition (Late Devonian) – Preface. *Palaeogeography Palaeoclimatology Palaeoecology*, **269**, 127-129.

Retallack, G.J., 1985. Fossil soils as grounds for interpreting the advent of large plants and animals on land. *Philosophical Transactions of the Royal Society of London B,* **309,** 105-142.

Retallack, G.J., 1986. The fossil record of soils. *In* Wright, V.P., (ed.) *Paleosols: their recognition and interpretation,* Princeton University Press, 1-57.

Retallack, G.J., 1990. Soils of the past. London: Unwin-Hyman

Retallack, G.J., 1992. Paleozoic paleosols. *In* Martini, I.P. & Chesworth, W. (eds.) *Weathering, soils and paleosols,* Amsterdam: Elsevier B.V., 543-564.

Rimmer, S.M., 2004. Geochemical paleoredox indicators in Devonian-Mississippian black shales, central Appalachian basin (USA). *Chemical Geology*, **206**, 373-391.

Rimmer, S.M., Thompson, J.A., Goodnight, S.A. & Robl, T.L., 2004. Multiple controls on the preservation of organic matter in Devonian-Mississippian marine black shales: geochemical and petrographic evidence. *Palaeogeography Palaeoclimatology Palaeoecology*, **215**, 125-154.

Riquier, L., Tribovillard, N., Averbuch, O., Devleeschouwer, X. and Riboulleau, A., 2006. The Late Frasnian Kellwasser horizons of the Harz Mountains (Germany): Two oxygen-deficient periods resulting from different mechanisms. *Chemical Geology*, **233**, 137-155.

Sandberg, C.A., Morrow, J.R., Ziegler, W., 2002. Late Devonian sea-level changes, catastrophic events, and mass extinctions. *Geological Society of America Special Papers*, **356**, 473-487

Savoy, L.E., Stevenson, R.K. and Mountjoy, E.W., 2000. Provenance of Upper Devonian- Lower Carboniferous miogeoclinal strata, southeastern Canadian Cordillera: Link between tectonics and sedimentation. *Journal of Sedimentary Research*, **70**, 181- 193.

Scheckler, S.E., 2001. Major Events in the History of Life: Palaeozoic Events: Afforestation - the First Forests. *In* Briggs, D.E.G. & Crowther, P.R. (eds.) *Palaeobiology II*, Blackwell Science, Oxford.

Snigirevskaya, N.S., 1984. Root system of archaeopterids from the Upper Devonian od Donetz Basin (In Russian). *Annual Report All-Union Paleontology Society* (Academy of Sciences, USSR) 27, 28-41

Snigirevskaya, N.S., 1995. Archaeopterids and their role in the land plant cover evolution. (In Russian). *Botanicheskii Zhournal,* **80**, 70-75.

Steam, C.W., 1987. Effect of the Frasnian-Famennian extinction event on the stromatoporoids, *Geology*, **15**, 677-679.

Stevenson, R.K., Whittaker, S. & Mountjoy, E.W., 2000. Geochemical and Nd isotopic evidence for sedimentary-source changes in the Devonian miogeocline of the southern Canadian Cordillera. *Geological Society of America Bulletin*, **112**, 531- 539.

Stoakes, F.A., 1980. Nature and control of shale basin fill and its effect on reef growth and termination: Upper Devonian Duvernay and Ireton Formations of Alberta, Canada. *Bulletin of Canadian Petroleum Geology,* **28**, 345-410.

Streel, M., Caputo, M.V., Loboziak, S. & Melo, J.H.G., 2000. Late Frasnian-Famennian climates based on palynomorph analyses and the question of the Late Devonian glaciations. *Earth-Science Reviews*, **52**, 121-173.

Switzer, S.B., Holland, W.G., Christie, G.S., Graf, G.C., Hedinger, A.S., McAuley, R.J., Wierzbicki, R.A., & Packard, J.J., 1994. Devonian Woodben-Winterburn strata of the western Canada sedimentary basin. *In* Mossop, G. & Shetsen, I. (eds.) *Geological Atlas of the Western Canada Sedimentary Basin: Canadian Society of Petroleum Geologists and Alberta Research Council*, 165-202

Tait, J.A., Bachtadse, V., Franke, W. & Soffel, H.C., 1997. Geodynamic evolution of the European Variscan fold belt: palaeomagnetic and geological constraints. *Geologische Rundschau*, **86**, 585-598.

Thomas, B.A. & Spicer, R.A., 1987. The evolution and paleobiology of land plants. London: Croom Helm.

Tribovillard, N., Algeo, T.J., Lyons, T. & Riboulleau, A., 2006. Trace metals as paleoredox and paleoproductivity proxies: An update. *Chemical Geology*, **232**, 12- 32.

Tribovillard, N., Averbuch, O., Devleeschouwer, X., Racki, G. & Riboulleau, A., 2004. Deep-water anoxia over the Frasnian-Famennian boundary (La Serre, France): a tectonically induced oceanic anoxic event? *Terra Nova*, **16**, 288-295.

Tucker, M.E., 2001. *Sedimentary Petrology*. Blackwell Science, Oxford.

van Buchem, F.S.P., Eberli, G.P., Whalen, M.T., Mountjoy, E.W., & Homewood, P.W., 1996. The basinal geochemical signature and platform margin geometries in the Upper Devonian mixed carbonate-siliciclastic system of western Canada. *Bulletin De La Societe Geologique De France*, **167**, 685-699.

van Cappellen, P. & Ingall, E.D., 1994. Benthic phosphorus regeneration, net primary production, and ocean anoxia - a model of the coupled marine biogeochemical cycles of carbon and phosphorus, *Paleoceanography*, **9**, 677-692.

van Cappellen, P. & Ingall, E.D., 1996. Redox stabilization of the atmosphere and oceans by phosphorus-limited marine productivity, *Science*, **271**, 493-496.

van der Weijden, C.H., 2002. Pitfalls of normalization of marine geochemical data using a common divisor, *Marine Geology*, **184**, 167-187.

van Loon, A.J., 1999. The meaning of 'abruptness' in the geological past, *Earth-Science Reviews*, **45**, 209-214.

Veizer, J., 1983. Trace elements and isotopes in sedimentary carbonates, *Reviews in Mineralogy: Carbonates: Mineralogy and Chemistry*, **11**, 265-299.

Veizer, J., 1989. Strontium isotopes in seawater through time, *Annual Review of Earth and Planetary Sciences*, **17**, 141-167.

Wallmann, K., 2003. Feedbacks between oceanic redox states and marine productivity: A model perspective focused on benthic phosphorus cycling. *Global Biogeochemical Cycles*, **17**, 18.

Whalen, M.T. & Day, J.E., 2008. Magnetic susceptibility, biostratigraphy, and sequence stratigraphy: insights into Devonian carbonate platform development and basin infilling, western Alberta, Canada. *Society for Sedimentary Geology*, **89**, 291-314.

Whalen, M.T. & Day, J.E., *In review*. Cross-basin variations in magnetic susceptibility influenced by changing sea level, paleogeography and climate, Upper Devonian Western Canada Sedimentary Basin.

Whalen, M.T., Eberli, G.P., Van Buchem, F.S.P., et al., 2000. Bypass margins, basin- restricted wedges, and platform-to-basin correlation, Upper Devonian, Canadian Rocky Mountains: Implications for sequence stratigraphy of carbonate platform systems. *Journal of Sedimentary Research*, **70**, 913-936.

White, A.F. & Blum, A.E., 1995. Effects of climate on chemical-weathering in watersheds. *Geochimica Et Cosmochimica Acta*, **59**, 1729-1747.

Wilder, H., 1994. Death of Devonian reefs – implications and further investigations. *Courier Forschungsinstitut Senckenberg,* **172,** 241-247.

Wright, V.P., 1990. Major Events in the History of Life: Terrestrialization: Soils. *In* Briggs, D.E.G. & Crowther, P.R. (eds.), *Palaeobiology*. Blackwell Science, Oxford. 57-59

Yans, J., Corfield, R.M., Racki, G. & Preat, A., 2007. Evidence for perturbation of the carbon cycle in the Middle Frasnian punctata Zone (Late Devonian). *Geological Magazine*, **144**, 263-270.

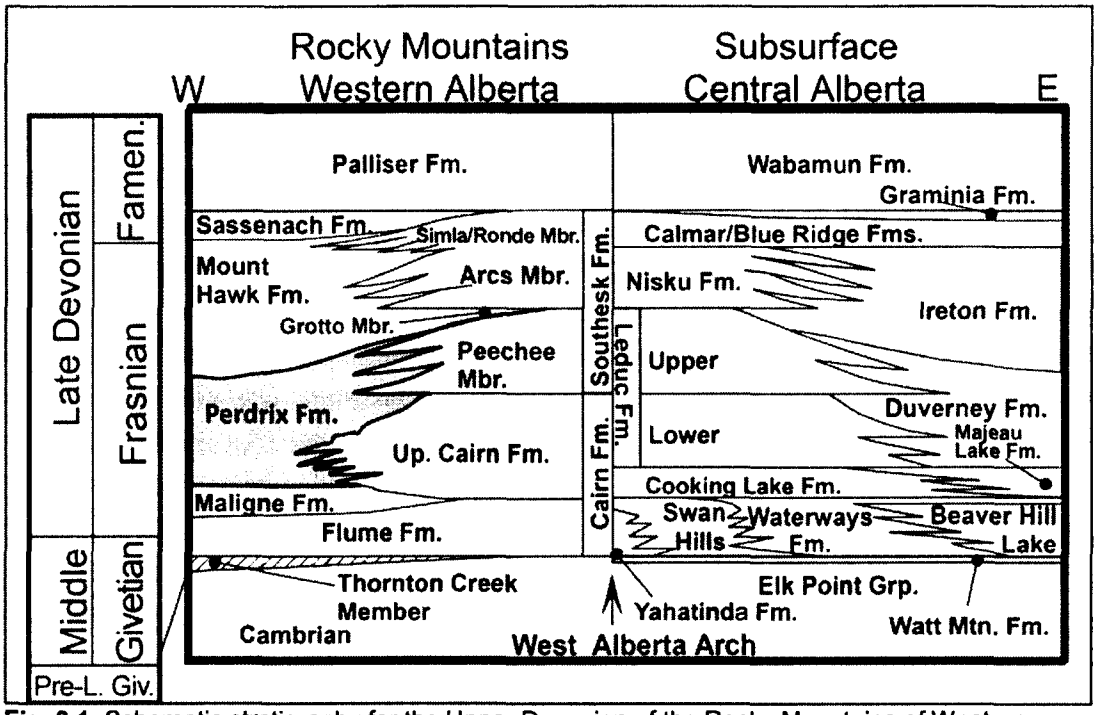

Fig. 3.1. Schematic stratigraphy for the Upper Devonian of the Rocky Mountains of Western Alberta and the central Alberta subsurface, for which an independent stratigraphic nomenclature was developed (figure modified from *Whalen et al., 2000*).

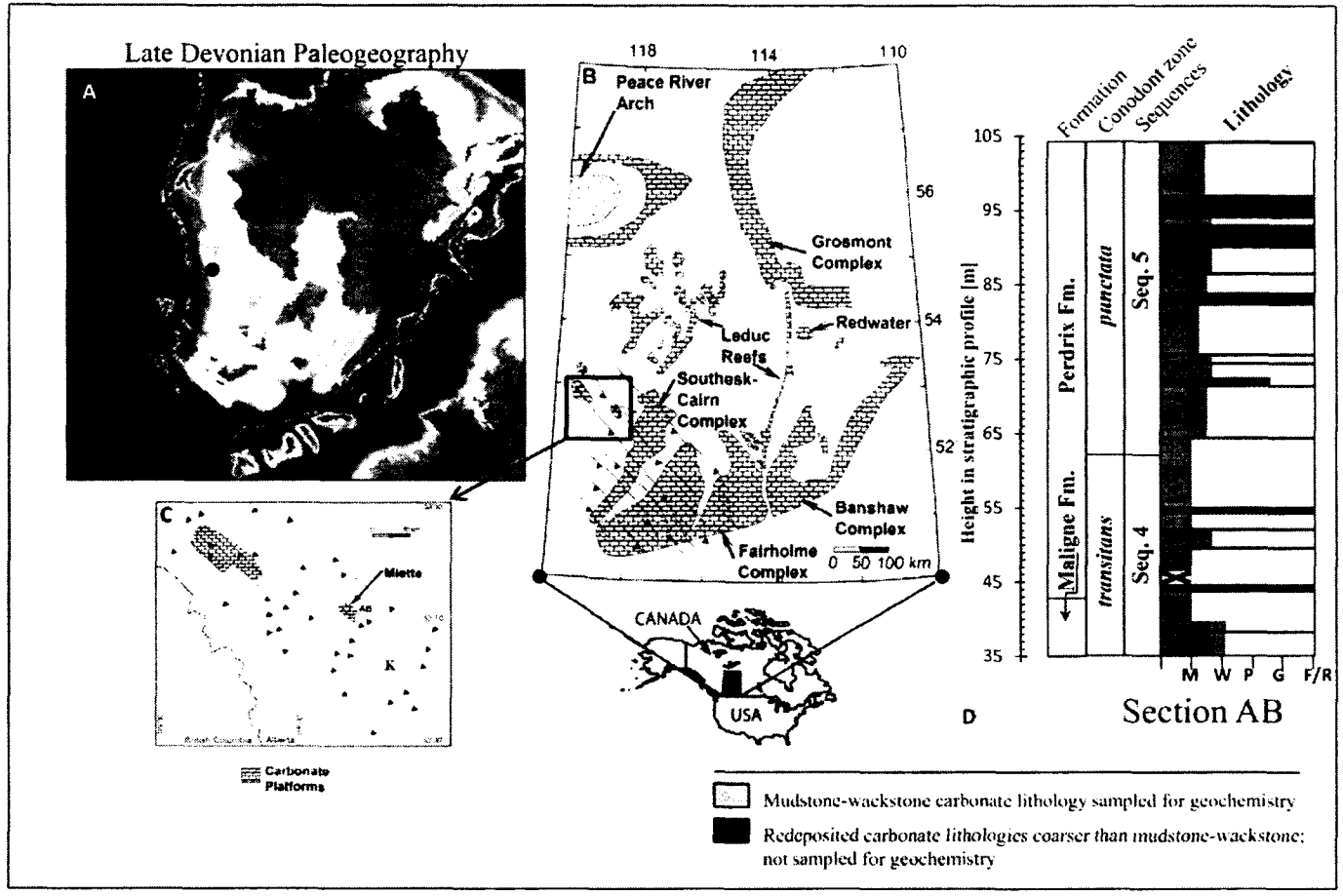

Fig. 3.2. A. Study area. Paleogeographic reconstruction of Ron Blakey (Northern Arizona University, Geology) of Late Devonian North America. Black dot indicates the paleolocality of the study area. **B.** Location of the Miette carbonate platform within the greater Western Canada Sedimentary Basin. **C.** Location of the Miette platform within the thrust belts of Western Alberta. 'AB' denotes the location of stratigraphic Section AB investigated in this study. 'K' denotes the location of Section K, a correlatable section in an adjacent thrust sheet. (Insets B and C modified from *Whalen et al., 2000*). **D.** Generalized lithostratigraphic profile for Section AB.

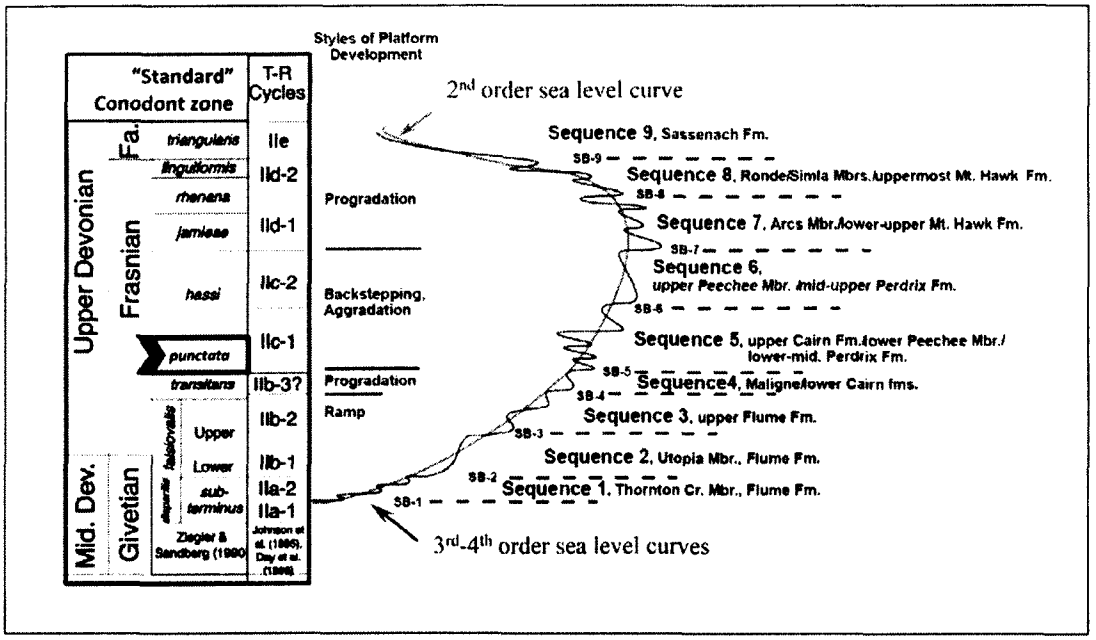

Fig. 3.3. Sequence stratigraphy, conodont zonations and interpreted sea level curve developed for the study area. Figure modified from *Whalen et al. (2000)*. The geochemical perturbation of the *punctata* Event coincides with the late sea level highstand of Sequence 4, lowstand at the boundary between Sequences 4 and 5 and with early transgressive pulse IIc1 of Sequence 5, during a period of carbonate platform backstepping and aggradation.

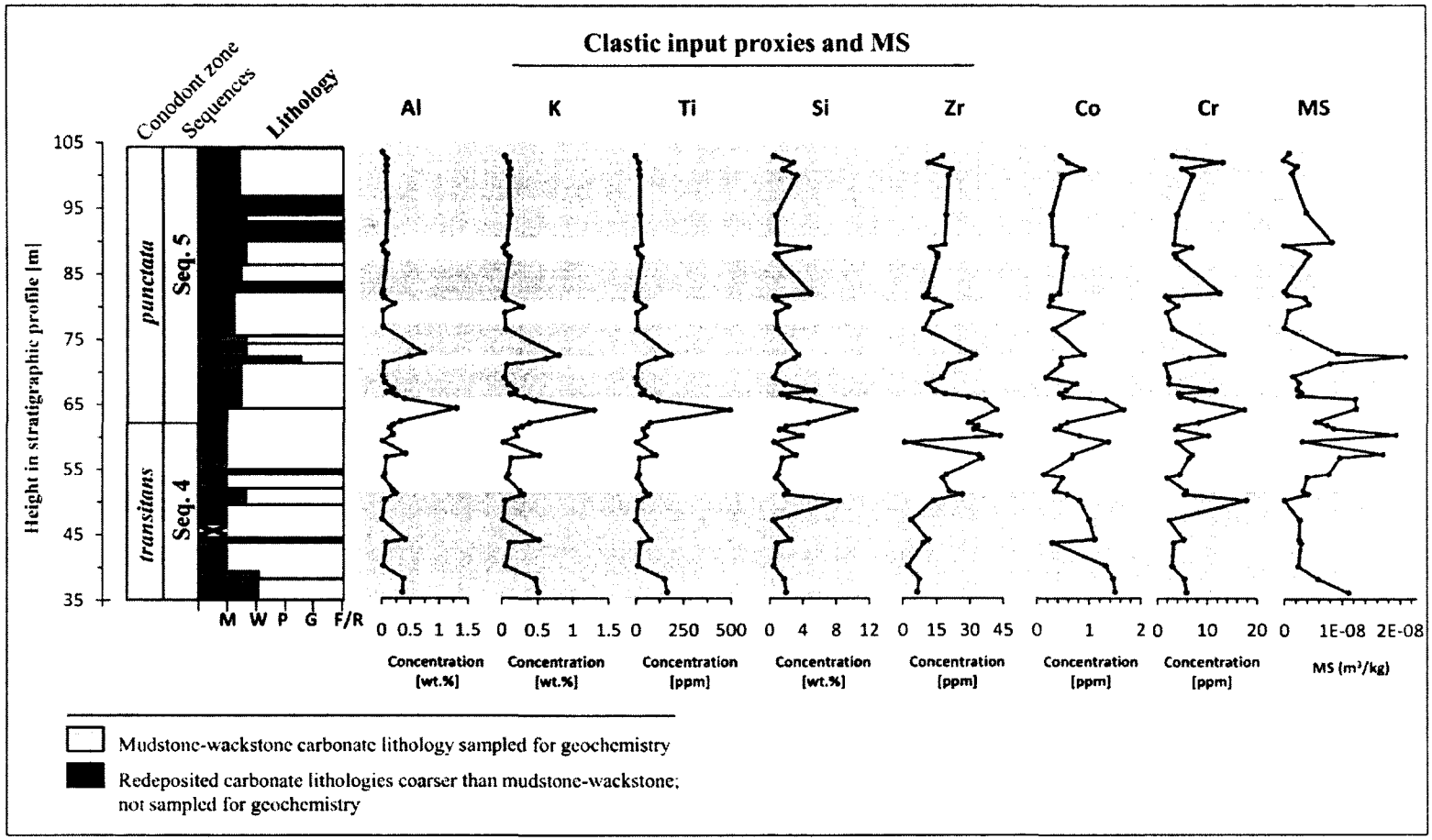

Fig. 3.4. Chemostratigraphic profiles of elements used as proxies for terrigenous clastic influxes into marine depositional basins. Plotted also is the corresponding magnetic susceptibility (MS) profile. Shaded areas are meant to help visualize common trends.

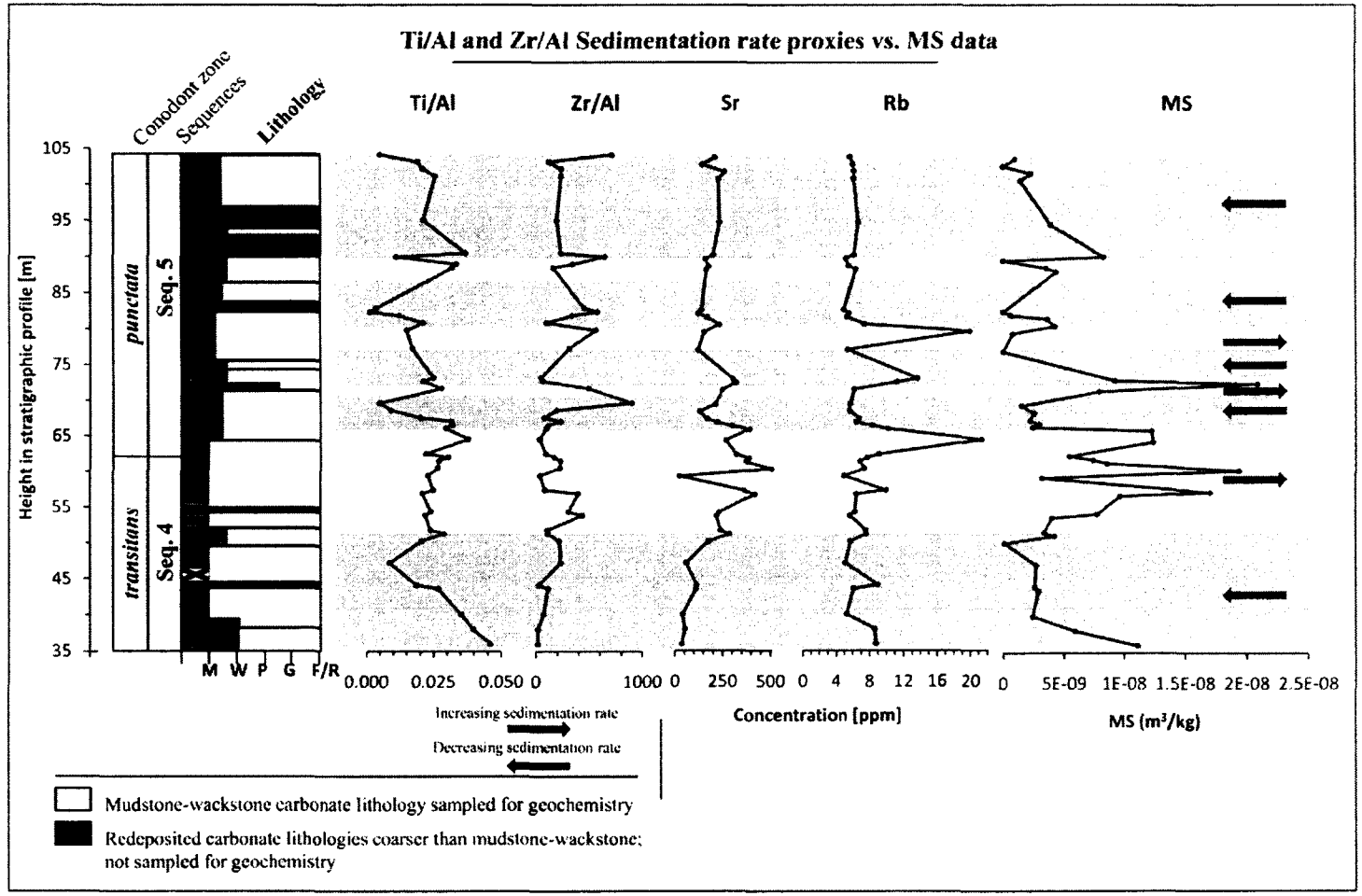

Fig. 3.5. The Ti/Al and Zr/Al ratios plotted against the magnetic susceptibility (MS) profile for stratigraphic Section AB. Plotted also are the quasi-proxies for continental weathering – Rb & Sr. Shaded areas are meant to help visualize common trends.

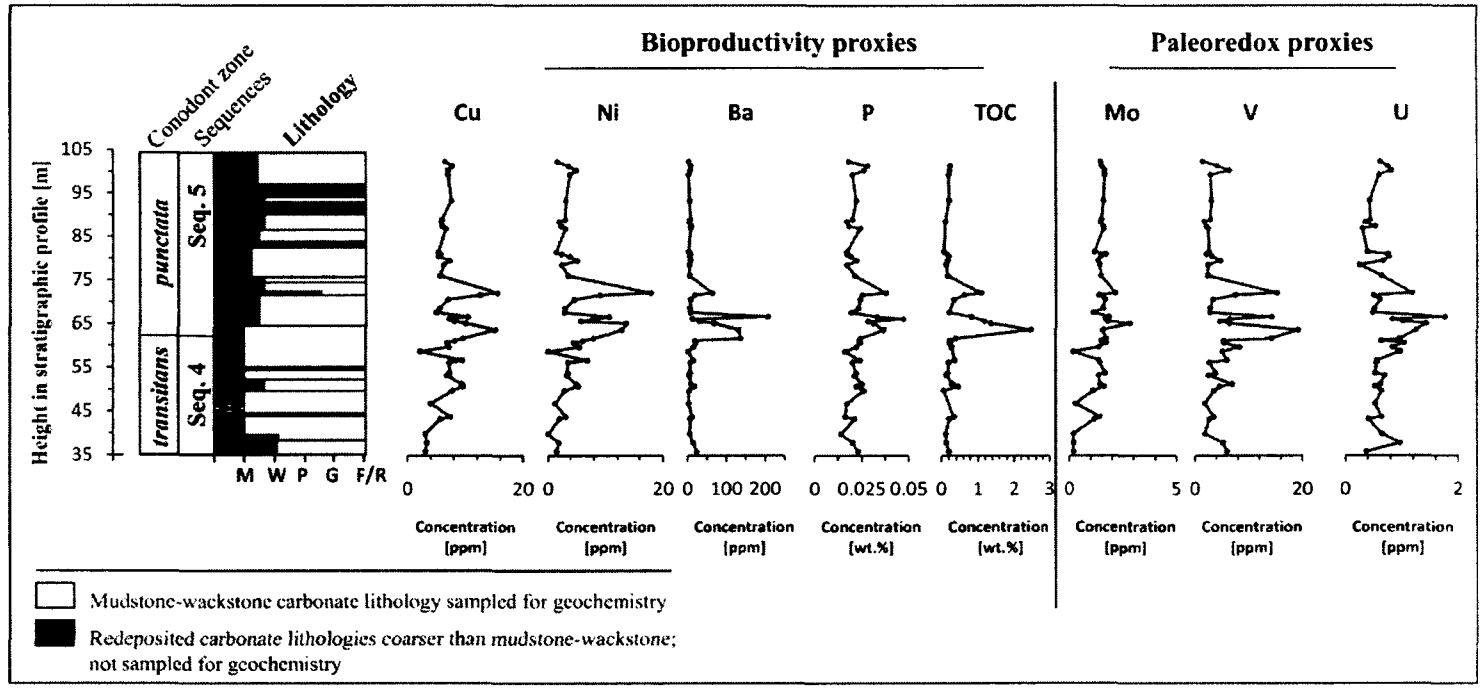

Fig. 3.6. Chemostratigraphic profiles of bioproductivity and paleoredox proxies and the stratigraphic distribution of total organic carbon (TOC).

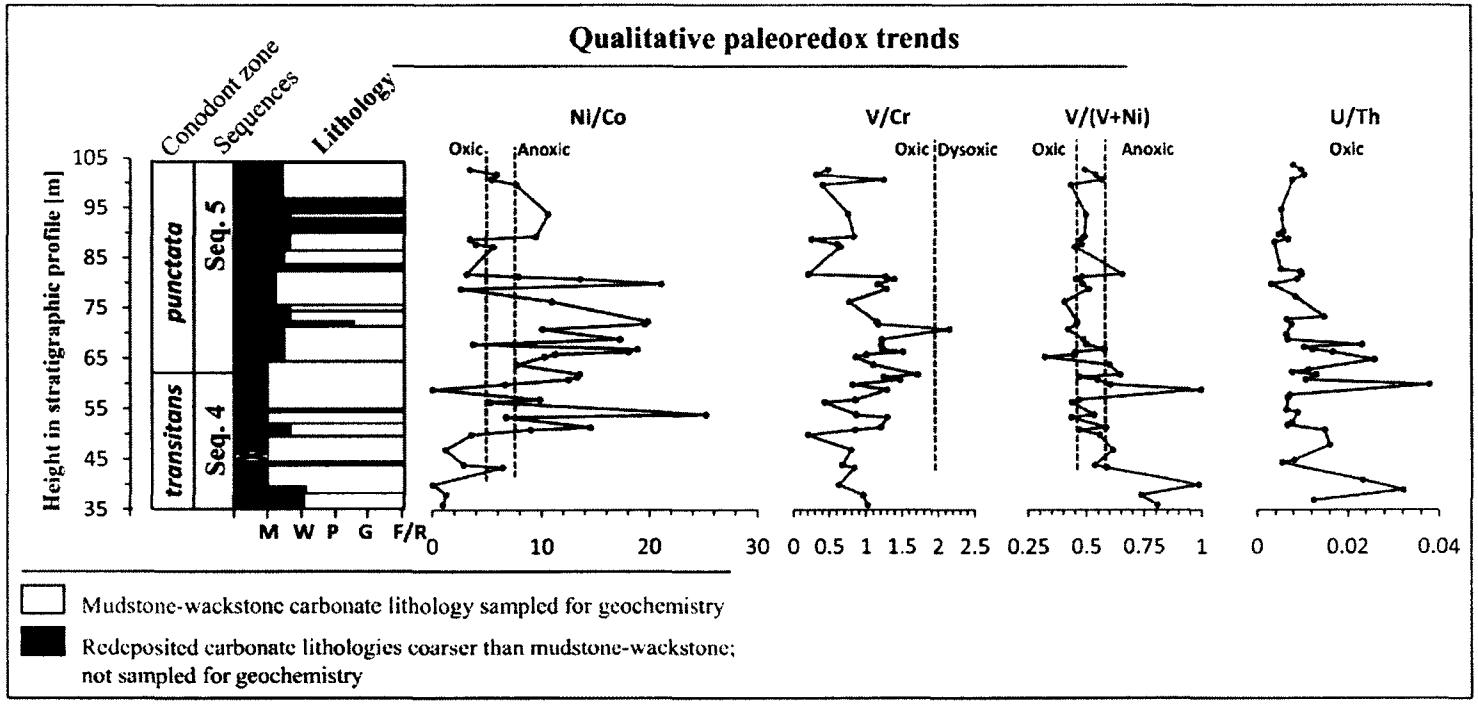

Fig. 3.7. Chemostratigraphic profiles of elemental ratios used as proxies for bottom water redox conditions. Taken *collectively* and interpreted *relatively*, these indices suggest dominantly dysoxic-anoxic bottom water conditions prevailing during the *punctata* Event. Shaded area highlights the horizon of trace element enrichment.

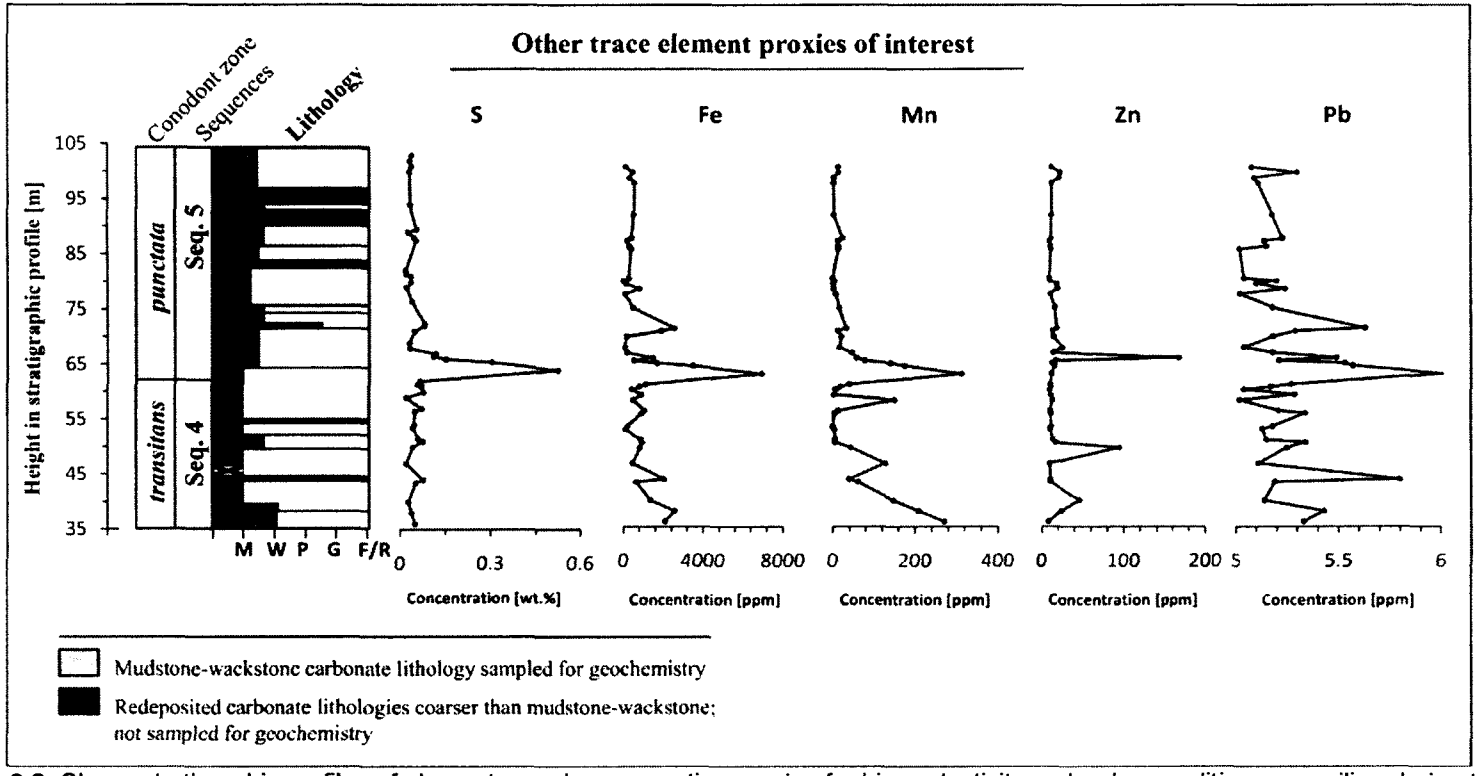

Fig. 3.8. Chemostratigraphic profiles of elements used as supporting proxies for bioproductivity and redox conditions prevailing during the *punctata* Event.

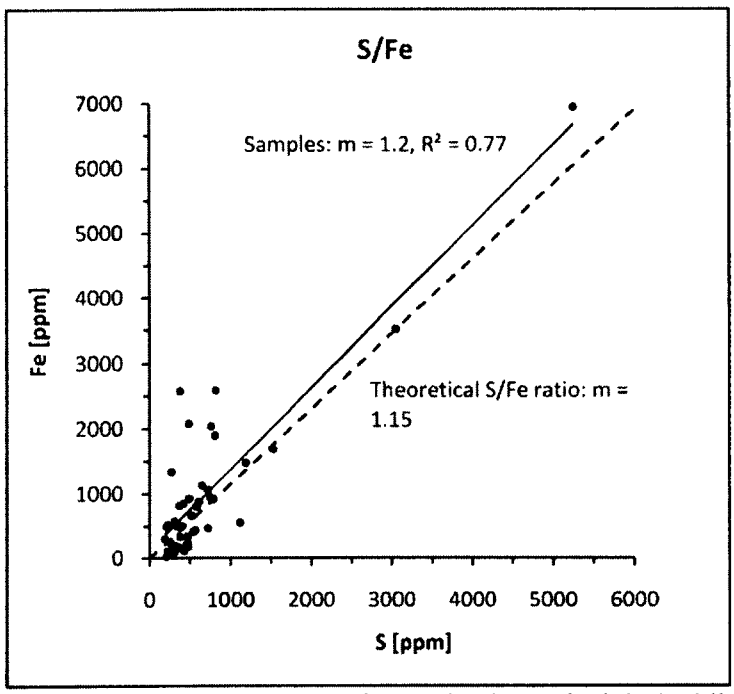

Fig. 3.9. Crossplot of S versus Fe concentrations. The theoretical dashed line with a slope of 1.15 indicates that all Fe is sequestered in a pyritic phase *(see discussion in Rimmer, 2004).*

Table 3.1. Lowest levels of detection and representative analytical precisions for each minor and trace element analyzed based on calibrations of the custom x-ray fluorescence (XRF) analytical routine developed for this study.

Element	**Al**	**Si**	**P**	**S**	**Ti**	**V**	**Cr**	**Mn**	**Fe**	**Co**
Analyte measured in units of:	(%)	(%)	(%)	(%)	(ppm)	(ppm)	(ppm)	(ppm)	(ppm)	(ppm)
Lowest level of detection (LLD) for typical analysis of this lithology [ppm]	N/A because analyte is measured in wt.%				1.4	0.6	1.4	1.7	2.3	0.3
Representative analytical precision [ppm]	4.1	33.4	0.0	0.0	0.6	0.2	0.1	0.8	0.2	0.2
Element	**Ni**	**Cu**	**Zn**	**Sr**	**Zr**	**Mo**	**Ba**	**K**	**Rb**	**Pb**
Analyte measured in units of:	(ppm)	(ppm)	(ppm)	(ppm)	(ppm)	(ppm)	(ppm)	(ppm)	(ppm)	(ppm)
Lowest level of detection (LLD) for typical analysis of this lithology [ppm]	0.7	0.7	0.6	0.6	0.5	0.3	4.7	3.7	0.2	0.2
Representative analytical precision [ppm]	0.1	0.4	0.2	1.0	0.3	0.1	1.1	0.0	0.0	0.1
Element	**Th**	**U**								
Analyte measured in units of:	(ppm)	(ppm)								
Lowest level of detection (LLD) for typical analysis of this lithology [ppm]	0.1	0.2								
Representative analytical precision [ppm]	0.4	0.0								

Table 3.2. Redox sensitive trace element ratio thresholds indicative of oxic, dysoxic and anoxic bottom water conditions *(Jones & Manning, 1994; Hatch & Leventhal, 1992).*

Water column oxgenation conditions:			
	Oxic	**Dysoxic**	**Anoxic**
Ni/Co[a]	< 5.00	5.00-7.00	> 7.00
V/Cr[a]	< 2.00	2.00-4.25	> 4.25
V/(V+Ni)[b]	< 0.46	0.46-0.60	0.54-0.82
U/Th[b]	< 0.75	0.75-1.25	> 1.25

[a] Jones and Manning (1994)

[b] Hatch and Leventhal (1992)

Table 3.3. Matrix showing *Person's r* correlations among the variables in the geochemical dataset (correlations calculated using the SPSS statistical software).

	MS	Al	Si	K	Ti	Zr	Cr	Ni	Cu	Ba	P	TOC	Mo	V	U	Fe	S	Pb	Zn	Mn	Co	Th	Sr	Rb
MS	1.000	.533**	.166	.580**	.474**	.697**	.138	.474**	.431**	.149	.338*	.363*	.091	.412*	.161	.425*	.374*	.285	-.218	.213	.252	.015	.628**	.356*
Al	.533**	1.000	.582**	.990**	.965**	.523**	.511**	.713**	.725**	.518**	.665**	.839**	.138	.795**	.450**	.922**	.797**	.819**	-.077	.609**	.571**	-.213	.235	.739**
Si	.166	.582**	1.000	.517**	.584**	.352*	.882**	.480**	.542**	.552**	.548**	.600**	.185	.613**	.414*	.623**	.648**	.536**	.350*	.379*	.398*	-.211	.181	.383*
K	.580**	.990**	.517**	1.000	.946**	.519**	.449**	.695**	.693**	.478**	.632**	.795**	.104	.760**	.413*	.902**	.749**	.803**	-.118	.611**	.573**	-.214	.242	.719**
Ti	.474**	.965**	.584**	.946**	1.000	.450**	.488**	.592**	.590**	.485**	.619**	.834**	.026	.738**	.413*	.943**	.837**	.778**	-.092	.739**	.638**	-.350*	.144	.729**
Zr	.697**	.523**	.352*	.519**	.450**	1.000	.294	.671**	.694**	.294	.550**	.554**	.566**	.533**	.371*	.404*	.541**	.341*	-.211	.002	.046	.417*	.946**	.396*
Cr	.138	.511**	.882**	.449**	.488**	.294	1.000	.464**	.544**	.457**	.603**	.466**	.124	.596**	.384*	.512**	.448**	.488**	.387*	.253	.343*	-.220	.156	.288
Ni	.474**	.713**	.480**	.695**	.592**	.671**	.464**	1.000	.895**	.652**	.863**	.778**	.647**	.809**	.701**	.616**	.635**	.607**	.157	.197	.210	.262	.528**	.528**
Cu	.431**	.725**	.542**	.693**	.590**	.694**	.544**	.895**	1.000	.556**	.804**	.743**	.618**	.767**	.490**	.566**	.611**	.581**	.112	.044	.065	.329	.546**	.571**
Ba	.149	.518**	.552**	.478**	.485**	.294	.457**	.652**	.556**	1.000	.640**	.633**	.329	.836**	.779**	.538**	.567**	.546**	.555**	.366*	.251	.009	.155	.368*
P	.338*	.665**	.548**	.632**	.619**	.550**	.603**	.863**	.804**	.640**	1.000	.768**	.503**	.796**	.705**	.610**	.645**	.587**	.299	.331	.224	.082	.390*	.442**
TOC	.363*	.839**	.600**	.795**	.834**	.554**	.466**	.778**	.743**	.633**	.768**	1.000	.438**	.734**	.638**	.874**	.942**	.802**	.071	.596**	.442**	-.017	.300	.657**
Mo	.091	.138	.185	.104	.026	.566**	.124	.647**	.618**	.329	.503**	.438**	1.000	.290	.456**	.077	.360*	.210	-.008	-.310	-.308	.788**	.595**	.162
V	.412*	.795**	.613**	.760**	.738**	.533**	.596**	.809**	.767**	.836**	.796**	.734**	.290	1.000	.686**	.694**	.643**	.628**	.267	.385*	.353*	-.038	.330	.573**
U	.161	.450**	.414*	.413*	.413*	.371*	.384*	.701**	.490**	.779**	.705**	.638**	.456**	.686**	1.000	.529**	.573**	.564**	.503**	.346*	.271	.026	.269	.197
Fe	.425*	.922**	.623**	.902**	.943**	.404*	.512**	.616**	.566**	.538**	.610**	.874**	.077	.694**	.529**	1.000	.889**	.862**	.038	.799**	.717**	-.378*	.114	.672**
S	.374*	.797**	.648**	.749**	.837**	.541**	.448**	.635**	.611**	.567**	.645**	.942**	.360*	.643**	.573**	.889**	1.000	.750**	.024	.651**	.502**	-.096	.290	.626**
Pb	.285	.819**	.536**	.803**	.778**	.341*	.488**	.607**	.581**	.546**	.587**	.802**	.210	.628**	.564**	.862**	.750**	1.000	.132	.609**	.580**	-.172	.099	.523**
Zn	-.218	-.077	.350*	-.118	-.092	-.211	.387*	.157	.112	.555**	.299	.071	-.008	.267	.503**	.038	.024	.132	1.000	.050	.051	-.223	-.191	-.134
Mn	.213	.609**	.379*	.611**	.739**	.002	.253	.197	.044	.366*	.331	.596**	-.310	.385*	.346*	.799**	.651**	.609**	.050	1.000	.800**	-.699**	-.249	.432**
Co	.252	.571**	.398*	.573**	.638**	.046	.343*	.210	.065	.251	.224	.442**	-.308	.353*	.271	.717**	.502**	.580**	.051	.800**	1.000	-.671**	-.157	.503**
Th	.015	-.213	-.211	-.214	-.350*	.417*	-.220	.262	.329	.009	.082	-.017	.788**	-.038	.026	-.378*	-.096	-.172	-.223	-.699**	-.671**	1.000	.563**	-.092
Sr	.628**	.235	.181	.242	.144	.946**	.156	.528**	.546**	.155	.390*	.300	.595**	.330	.269	.114	.290	.099	-.191	-.249	-.157	.563**	1.000	.166
Rb	.356*	.739**	.383*	.719**	.729**	.396*	.288	.528**	.571**	.368*	.442**	.657**	.162	.573**	.197	.672**	.626**	.523**	-.134	.432**	.503**	-.092	.166	1.000

**. Correlation is significant at the 0.01 level (2-tailed).

*. Correlation is significant at the 0.05 level (2-tailed).

Table 3.4. Matrix showing *Spearman's rho* correlations among the variables in the geochemical dataset (correlations calculated using the SPSS statistical software).

	MS	Al	Si	K	Ti	Zr	Cr	Ni	Cu	Ba	P	TOC	Mo	V	U	Fe	S	Pb	Zn	Mn	Co	Th	Sr	Rb
MS	1.000	.673**	.107	.712**	.670**	.638**	.132	.502**	.366*	.585**	.358*	.539**	.048	.605**	.181	.488**	.638**	.387*	-.161	.134	.198	.327	.608**	.637**
Al	.673**	1.000	.490**	.986**	.973**	.547**	.503**	.646**	.658**	.787**	.595**	.758**	.156	.830**	.385*	.848**	.778**	.713**	.081	.387*	.405*	.214	.452**	.832**
Si	.107	.490**	1.000	.410*	.445**	.394*	.888**	.479**	.567**	.372*	.495**	.392*	.131	.559**	.248	.520**	.430**	.456**	.025	.234	.344*	-.092	.316	.313
K	.712**	.986**	.410*	1.000	.969**	.545**	.419*	.630**	.605**	.794**	.547**	.760**	.145	.803**	.348*	.826**	.789**	.678**	.006	.384*	.393*	.236	.450**	.842**
Ti	.670**	.973**	.445**	.969**	1.000	.492**	.480**	.589**	.589**	.782**	.589**	.726**	.148	.807**	.389*	.880**	.782**	.696**	.061	.467**	.440**	.179	.398*	.825**
Zr	.638**	.547**	.394*	.545**	.492**	1.000	.367*	.842**	.724**	.483**	.576**	.638**	.472**	.618**	.363*	.315	.640**	.242	-.067	-.153	.069	.615**	.972**	.545**
Cr	.132	.503**	.888**	.419*	.480**	.367*	1.000	.393*	.565**	.341*	.510**	.346*	.111	.562**	.231	.591**	.391*	.493**	.080	.178	.422*	-.086	.297	.303
Ni	.502**	.646**	.479**	.630**	.589**	.842**	.393*	1.000	.849**	.667**	.759**	.827**	.611**	.767**	.559**	.433**	.751**	.414*	.200	.053	.049	.504**	.789**	.588**
Cu	.366*	.658**	.567**	.605**	.589**	.724**	.565**	.849**	1.000	.579**	.746**	.758**	.529**	.683**	.363*	.515**	.711**	.532**	.176	.111	.088	.501**	.673**	.622**
Ba	.585**	.787**	.372*	.794**	.782**	.483**	.341*	.667**	.579**	1.000	.619**	.836**	.416*	.792**	.544**	.683**	.805**	.691**	.006	.508**	.323	.308	.448**	.712**
P	.358*	.595**	.495**	.547**	.589**	.576**	.510**	.759**	.746**	.619**	1.000	.718**	.491**	.794**	.516**	.459**	.675**	.445**	.306	.297	.153	.287	.545**	.491**
TOC	.539**	.758**	.392*	.760**	.726**	.638**	.346*	.827**	.758**	.836**	.718**	1.000	.549**	.754**	.444**	.589**	.863**	.614**	.093	.344*	.211	.469**	.580**	.667**
Mo	.048	.156	.131	.145	.148	.472**	.111	.611**	.529**	.416*	.491**	.549**	1.000	.322	.497**	.019	.370*	.165	.066	-.088	-.183	.643**	.489**	.219
V	.605**	.830**	.559**	.803**	.807**	.618**	.562**	.767**	.683**	.792**	.794**	.754**	.322	1.000	.533**	.644**	.752**	.509**	.175	.235	.304	.230	.552**	.706**
U	.181	.385*	.248	.348*	.389*	.363*	.231	.559**	.363*	.544**	.516**	.444**	.497**	.533**	1.000	.374*	.474**	.393*	.388*	.252	.211	.143	.315	.227
Fe	.488**	.848**	.520**	.826**	.880**	.315	.591**	.433**	.515**	.683**	.459**	.589**	.019	.644**	.374*	1.000	.698**	.788**	.206	.613**	.574**	-.033	.224	.663**
S	.638**	.778**	.430**	.789**	.782**	.640**	.391*	.751**	.711**	.805**	.675**	.863**	.370*	.752**	.474**	.698**	1.000	.667**	.030	.412*	.257	.379*	.581**	.679**
Pb	.387*	.713**	.456**	.678**	.696**	.242	.493**	.414*	.532**	.691**	.445**	.614**	.165	.509**	.393*	.788**	.667**	1.000	.236	.562**	.441**	.032	.163	.552**
Zn	-.161	.081	.025	.006	.061	-.067	.080	.200	.176	.006	.306	.093	.066	.175	.388*	.206	.030	.236	1.000	.156	.138	-.212	-.090	-.063
Mn	.134	.387*	.234	.384*	.467**	-.153	.178	.053	.111	.508**	.297	.344*	-.088	.235	.252	.613**	.412*	.562**	.156	1.000	.602**	-.248	-.197	.356*
Co	.198	.405*	.344*	.393*	.440**	.069	.422*	.049	.088	.323	.153	.211	-.183	.304	.211	.574**	.257	.441**	.138	.602**	1.000	-.237	-.013	.424*
Th	.327	.214	-.092	.236	.179	.615**	-.086	.504**	.501**	.308	.287	.469**	.643**	.230	.143	-.033	.379*	.032	-.212	-.248	-.237	1.000	.694**	.359*
Sr	.608**	.452**	.316	.450**	.398*	.972**	.297	.789**	.673**	.448**	.545**	.580**	.489**	.552**	.315	.224	.581**	.163	-.090	-.197	-.013	.694**	1.000	.459**
Rb	.637**	.832**	.313	.842**	.825**	.545**	.303	.588**	.622**	.712**	.491**	.667**	.219	.706**	.227	.663**	.679**	.552**	-.063	.356*	.424*	.359*	.459**	1.000

**. Correlation is significant at the 0.01 level (2-tailed).

*. Correlation is significant at the 0.05 level (2-tailed).

Appendix 3A

Geochemical Dataset accompanying Śliwiński et al., 2010 (Chapter 3).

Table 3A-1. Major and trace element abundances for stratigraphic SectionAB generated using XRF (*punctata* Event, Early-Middle Frasnian Transition, Late Devonian, Western Canada Sedimentary Basin, Western Alberta, Canada).

Sample	Na (%)	Mg (%)	Al (%)	Si (%)	P (%)	S (%)	K (%)	Ti (ppm)	V (ppm)
pE 103.0	0.036	0.151	0.025	0.673	0.018	0.039	0.051	1.3	1.6
pE 102.0	0.032	0.625	0.097	2.918	0.028	0.033	0.104	18.6	4.2
pE 101.0	0.039	0.183	0.092	1.730	0.026	0.038	0.123	19.4	6.4
pE 100.0	0.036	0.198	0.087	3.354	0.020	0.031	0.110	22.3	3.0
pE 94.0	0.052	0.227	0.102	0.887	0.022	0.033	0.120	21.6	3.1
pE 89.5	0.044	0.229	0.081	0.983	0.020	0.056	0.078	29.9	2.9
pE 89.0	0.037	0.424	0.019	4.786	0.017	0.027	0.028	2.1	1.8
pE 88.0	0.037	0.238	0.044	0.748	0.018	0.047	0.060	14.8	2.1
pE 87.5	0.036	0.313	0.094	1.009	0.024	0.054	0.112	30.2	2.5
pE 82.0	0.035	0.267	0.024	4.956	0.017	0.019	0.040	0.9	2.6
pE 81.5	0.034	0.112	0.016	0.610	0.017	0.021	0.027	0.2	2.1
pE 81.0	0.035	0.184	0.042	0.876	0.019	0.037	0.067	5.2	3.2
pE 80.0	0.036	0.225	0.216	2.290	0.022	0.037	0.290	45.6	4.8
pE 79.0	0.033	0.125	0.023	0.826	0.017	0.022	0.041	3.5	2.4
pE 76.5	0.034	1.550	0.030	0.972	0.021	0.040	0.060	5.1	2.4
pE 72.5	0.052	0.279	0.734	3.463	0.038	0.082	0.795	183.2	15.3
pE 72.0	0.051	0.280	0.493	2.957	0.025	0.081	0.621	104.6	7.5
pE 71.0	0.057	0.203	0.041	1.126	0.024	0.048	0.072	11.5	3.3
pE 69.0	0.038	0.124	0.019	0.564	0.023	0.031	0.037	1.0	2.8
pE 68.0	0.036	1.218	0.056	1.863	0.019	0.033	0.090	5.1	2.8
pE 67.0	0.044	0.649	0.191	5.355	0.033	0.119	0.196	38.6	14.3
pE 66.5	0.035	0.155	0.081	1.425	0.047	0.112	0.121	25.6	6.5
pE 66.0	0.041	0.252	0.254	2.241	0.028	0.153	0.319	81.2	4.6
pE 65.5	0.047	0.463	0.390	4.929	0.031	0.305	0.465	115.6	6.4
pE 64.0	0.069	1.414	1.303	10.359	0.037	0.525	1.291	493.3	19.2
pE 62.0	0.041	0.276	0.327	4.616	0.024	0.065	0.379	72.3	14.3
pE 61.5	0.044	0.454	0.200	2.109	0.024	0.058	0.291	61.0	5.4
pE 61.0	0.042	0.316	0.142	1.289	0.024	0.072	0.197	38.1	5.5
pE 60.0	0.040	0.334	0.198	3.964	0.022	0.079	0.223	52.3	8.4
pE 59.0	0.042	12.595	0.023	0.649	0.016	0.022	0.027	5.3	5.1
pE 57.0	0.042	0.547	0.424	3.209	0.024	0.072	0.524	105.4	6.0
pE 56.5	0.037	0.256	0.088	1.592	0.020	0.049	0.137	18.5	2.7
pE 54.0	0.037	0.333	0.064	1.073	0.022	0.047	0.097	15.4	3.9
pE 53.5	0.037	0.481	0.040	0.829	0.021	0.043	0.076	8.8	2.6
pE 51.5	0.035	0.280	0.196	2.215	0.025	0.061	0.257	46.8	7.0
pE 51.0	0.036	0.288	0.243	1.846	0.022	0.075	0.306	70.5	4.6
pE 50.0	0.041	0.758	0.063	8.381	0.026	0.042	0.052	12.9	3.6
pE 47.0	0.068	6.788	0.016	0.484	0.017	0.021	0.028	1.4*	1.9
pE 44.0	0.034	0.142	0.411	2.530	0.016	0.076	0.516	76.5	3.6
pE 43.5	0.038	1.166	0.084	0.951	0.021	0.052	0.116	22.3	2.7
pE 40.0	0.048	12.889	0.033	0.533	0.014	0.027	0.057	11.7	1.8
pE 38.0	0.050	11.337	0.378	1.791	0.020	0.038	0.466	150.2	5.2
pE 36.0	0.035	12.195	0.356	2.029	0.023	0.049	0.512	163.6	6.0

Table 3A-1 continued.

Sample	Cr (ppm)	Mn (ppm)	Fe (ppm)	Co (ppm)	Ni (ppm)	Cu (ppm)	Zn (ppm)	Sr (ppm)	Zr (ppm)
pE 103.0	3.2	13.3	160.5	0.5	1.6	6.5	12.5	214.5	17.9
pE 102.0	13.3	14.4	505.9	0.6	3.6	7.7	22.9	147.4	11.8
pE 101.0	5.2	3.4	338.8	0.9	5.0	7.0	22.0	264.0	22.1
pE 100.0	7.3	2.2	574.4	0.5	3.9	7.0	12.6	231.4	20.7
pE 94.0	4.1	3.9	553.8	0.3	3.1	7.6	12.6	234.4	19.7
pE 89.5	3.5	23.9	439.4	0.3	3.0	5.9	12.1	202.8	18.8
pE 89.0	6.9	13.4	223.6	0.6	2.0	5.8	10.3	164.5	12.4
pE 88.0	3.4	14.1	335.9	0.6	2.3	5.9	11.2	181.1	15.5
pE 87.5	3.8	13.7	415.6	0.5	3.0	6.6	11.8	168.1	15.4
pE 82.0	12.5	0.4	300.5	0.4	1.4	5.3	9.8	143.1	11.0
pE 81.5	1.7	4.1	26.1	0.3	2.3	5.7	10.9	128.0	9.3
pE 81.0	2.3	-0.5	165.8	0.3	3.8	5.4	18.7	173.6	14.3
pE 80.0	4.1	2.9	813.9	0.2	5.1	7.2	19.4	233.6	21.4
pE 79.0	1.9	7.8	105.1	0.9	2.3	6.2	11.1	156.8	13.0
pE 76.5	3.1	15.0	502.0	0.3	3.5	5.6	16.3	125.1	9.5
pE 72.5	13.3	32.3	2584.9	0.9	17.9	15.5	18.7	306.2	32.3
pE 72.0	6.4	12.3	1894.1	0.5	9.0	12.5	13.6	322.9	30.2
pE 71.0	1.6	20.3	181.2	0.5	4.6	7.0	14.8	250.3	20.4
pE 69.0	2.3	15.6	91.9	0.2	2.9	5.5	25.4	213.5	17.2
pE 68.0	2.3	45.7	190.6	0.8	2.8	4.9	14.5	133.1	10.7
pE 67.0	11.7	57.0	1479.4	0.6	10.5	10.4	168.3	170.1	14.1
pE 66.5	4.3	78.5	555.2	0.4	7.8	7.1	17.2	222.9	18.8
pE 66.0	4.6	141.2	1683.7	0.5	5.7	8.0	12.7	303.3	29.2
pE 65.5	7.4	175.9	3516.0	1.3	13.6	10.0	15.6	392.9	36.7
pE 64.0	17.4	312.7	6942.3	1.7	12.9	15.2	12.4	269.0	42.1
pE 62.0	8.3	39.9	1126.1	0.6	7.8	9.6	10.4	322.9	29.4
pE 61.5	4.3	16.8	801.3	0.5	6.1	8.3	10.9	389.5	33.7
pE 61.0	3.7	7.7	468.7	0.4	4.5	6.9	10.4	375.4	32.0
pE 60.0	10.3	3.7	919.9	0.8	5.5	7.2	11.5	505.9	43.8
pE 59.0	4.0	151.7	519.4	1.4	0.0	2.2	13.4	27.4	0.9
pE 57.0	7.1	13.6	1062.1	0.7	6.9	9.5	10.6	369.5	34.2
pE 56.5	6.4	5.0	925.6	0.7	3.5	7.2	11.4	422.0	35.4
pE 54.0	4.5	0.1	234.1	0.1	3.5	7.3	11.7	233.4	19.5
pE 53.5	2.0	4.2	113.3	0.5	3.3	6.8	10.5	219.9	17.6
pE 51.5	5.8	5.9	877.6	0.3	5.0	9.3	14.1	240.3	20.8
pE 51.0	5.5	5.9	945.9	0.6	5.3	9.6	17.1	286.8	26.4
pE 50.0	17.9	44.0	844.7	0.8	2.9	7.7	95.0	177.2	13.7
pE 47.0	2.4	128.4	488.1	1.0	1.2	4.0	10.0	61.3	3.7
pE 44.0	5.3	39.3	2037.4	1.1	3.1	7.4	11.0	115.6	11.3
pE 43.5	3.3	61.3	663.0	0.3	1.9	5.7	11.0	112.8	9.3
pE 40.0	3.0	148.0	1342.2	1.3	0.0	3.1	45.9	41.1	2.2
pE 38.0	5.4	208.6	2575.0	1.5	1.9	3.3	24.3	52.9	7.2
pE 36.0	5.9	270.8	2076.6	1.5	1.4	3.1	8.4	36.7	6.3

Table 3A-1 continued.

Sample	Mo (ppm)	Ba (ppm)	Ca (%)	Rb (ppm)	Pb (ppm)	Th (ppm)	U (ppm)
pE 103.0	1.5	3.0	76.9	5.7	5.1	78.2	0.6
pE 102.0	1.5	8.7	69.5	6.1	5.3	77.2	0.8
pE 101.0	1.7	6.5	73.5	6.2	5.1	78.7	0.8
pE 100.0	1.7	2.5	69.1	6.2	5.1	77.2	0.6
pE 94.0	1.6	5.5	76.1	6.7	5.2	82.0	0.4
pE 89.5	1.5	6.2	75.2	6.1	5.2	77.3	0.4
pE 89.0	1.5	3.9	65.3	5.3	5.1	75.7	0.4
pE 88.0	1.6	9.0	76.4	5.6	5.2	77.6	0.5
pE 87.5	1.6	7.5	75.0	6.4	5.0	78.9	0.3
pE 82.0	1.2	2.2	64.6	5.0	5.0	74.7	0.4
pE 81.5	1.7	7.4	78.0	5.6	5.2	78.2	0.8
pE 81.0	1.5	5.6	75.9	5.4	5.1	78.3	0.8
pE 80.0	1.3	7.1	70.7	7.5	5.2	75.9	0.7
pE 79.0	1.4	4.3	77.0	20.0	5.0	79.2	0.3*
pE 76.5	1.5	5.2	70.5	5.4	5.2	75.2	0.6
pE 72.5	2.1	63.2	65.2	13.7	5.6	80.0	1.2
pE 72.0	1.4	18.4	66.3	11.3	5.3	76.8	0.5
pE 71.0	1.7	7.2	75.8	6.2	5.2	81.3	0.6
pE 69.0	1.6	5.6	77.9	5.7	5.0	80.2	0.5
pE 68.0	1.1	7.3	68.5	5.7	5.2	72.5	0.5
pE 67.0	1.8	207.0	61.7	6.7	5.5	76.4	1.8
pE 66.5	1.7	12.7	73.5	6.4	5.2	80.3	0.8
pE 66.0	1.8	31.1	70.0	8.4	5.5	83.0	1.0
pE 65.5	2.8	67.8	61.4	10.2	5.6	85.9	1.4
pE 64.0	1.6	131.7	42.5	21.3	6.0	48.4	1.3
pE 62.0	1.7	137.4	65.4	9.1	5.3	85.6	1.0
pE 61.5	1.5	19.2	70.4	7.7	5.2	83.8	0.6
pE 61.0	1.7	21.8	73.6	6.8	5.0	81.2	1.1
pE 60.0	1.4	15.8	65.6	7.3	5.3	78.3	0.8
pE 59.0	0.2*	1.7	37.9	5.0	5.0	25.7	1.0
pE 57.0	1.4	15.6	66.1	10.0	5.2	80.1	0.6
pE 56.5	1.4	7.4	73.1	6.4	5.3	82.7	0.6
pE 54.0	1.7	6.0	75.3	6.2	5.2	83.1	0.5
pE 53.5	1.4	3.8	74.7	5.7	5.1	78.8	0.7
pE 51.5	1.4	9.6	70.9	7.5	5.2	81.3	0.6
pE 51.0	1.6	17.1	71.5	7.6	5.3	80.6	0.5
pE 50.0	1.1	3.5	55.0	5.8	5.3	43.2	0.6
pE 47.0	0.3	2.6	53.0	5.2	5.1	33.3	0.5
pE 44.0	1.4	12.2	69.8	9.0	5.8	78.9	0.6
pE 43.5	1.2	6.6	71.2	6.1	5.2	76.0	0.4
pE 40.0	0.2*	5.4	38.1	5.3	5.1	28.0	0.7
pE 38.0	0.2*	14.3	37.4	8.6	5.4	30.3	1.0
pE 36.0	0.2*	23.2	35.8	8.8	5.3	29.6	0.4

* For values with a *, the lowest detection limit for the given analyte was substitued for the original analysis value, which fell below the lowest level of detection.

Table 3A-1 continued.

Sample	U/Th (x 10^{-2})	Ni/Co	V/Cr	V/(V+Ni)
pE 103.0	0.8	3.4	0.5	0.5
pE 102.0	1.0	5.9	0.3	0.5
pE 101.0	1.0	5.4	1.2	0.6
pE 100.0	0.8	7.7	0.4	0.4
pE 94.0	0.5	10.6	0.7	0.5
pE 89.5	0.6	9.5	0.8	0.5
pE 89.0	0.5	3.5	0.3	0.5
pE 88.0	0.7	4.0	0.6	0.5
pE 87.5	0.4	5.6	0.6	0.5
pE 82.0	0.5	3.1	0.2	0.7
pE 81.5	1.0	7.9	1.3	0.5
pE 81.0	1.0	13.6	1.4	0.5
pE 80.0	0.9	21.1	1.2	0.5
pE 79.0	0.3	2.6	1.3	0.5
pE 76.5	0.9	11.0	0.8	0.4
pE 72.5	1.5	19.8	1.1	0.5
pE 72.0	0.7	19.6	1.2	0.5
pE 71.0	0.8	10.1	2.1	0.4
pE 69.0	0.6	17.3	1.2	0.5
pE 68.0	0.7	3.7	1.2	0.5
pE 67.0	2.3	18.9	1.2	0.6
pE 66.5	1.0	18.1	1.5	0.5
pE 66.0	1.2	11.2	1.0	0.4
pE 65.5	1.7	10.3	0.9	0.3
pE 64.0	2.6	7.7	1.1	0.6
pE 62.0	1.1	13.5	1.7	0.6
pE 61.5	0.8	13.4	1.2	0.5
pE 61.0	1.3	12.5	1.5	0.5
pE 60.0	1.1	6.6	0.8	0.6
pE 59.0	3.8	0.0	1.3	1.0
pE 57.0	0.7	9.8	0.8	0.5
pE 56.5	0.7	5.3	0.4	0.4
pE 54.0	0.6	25.2	0.9	0.5
pE 53.5	0.9	6.7	1.3	0.4
pE 51.5	0.8	14.5	1.2	0.6
pE 51.0	0.7	9.0	0.8	0.5
pE 50.0	1.5	3.5	0.2	0.6
pE 47.0	1.6	1.2	0.8	0.6
pE 44.0	0.8	2.8	0.7	0.5
pE 43.5	0.5	6.4	0.8	0.6
pE 40.0	2.3	0.0	0.6	1.0
pE 38.0	3.2	1.3	1.0	0.7
pE 36.0	1.3	1.0	1.0	0.8

Appendix 3B

Expanded geochemical dataset for Section AB

This appendix contains:

1. **Table 3B-1:** An expanded trace element dataset over that initially published in Śliwiński et al., (2010) (Chapter 3), consisting of i) additional samples that allow for better resolution of trace element variability throughout the *punctata* Event (Chapters 4 and 5) stratigraphy at the Miette carbonate platform and of ii) data for additional elements measured using PROTrace XRF calibrations (43 trace elements in total, see discussion in Section 1.1.). All data are corrected for calibration backgrounds and analytical detection limits determined empirically (Chapter 2).
2. **Table 3B-1:** An expanded and recalibrated XRF dataset (generated using my own analytical protocols) for the light major elements Na, Mg, Al, Si, P, S, K, and Ca, which again allows for better resolution of geochemical variability in the *punctata* Event stratigraphy.
3. **Table 3B-1:** Calculated redox indices: Ni/Co, V/Cr, V/(V+Ni), V/Sc (data generated using PROTRace XRF calibrations)
4. **Table 3B-1:** Other parameters broadly related to changes in the detrital input throughout the stratigraphic profile, including the ratios Ti/Al and Zr/Al, magnetic susceptibility measurements (MS), and the abundances of i) total carbonate, ii) TOC and of iii) acid insoluble residues determined by bulk sample acidification.
5. **Table 3B-2:** An expanded and recalibrated XRF trace element dataset through the *punctata* Event stratigraphy at the Miette carbonate platform in the WCSB generated using my analytical protocol (Chapter 2).
6. **Figs. 3B1-5:** Expanded chemostratigraphic profiles.
7. **Table 3B-3 and Fig. 3B-6:** Select bioproductivity (P, Ni, Cu) and paleoredox (Mo, V, U) proxies throughout the *punctate* Event stratigraphy plotted against stratigraphic Al abundances and against the values in the North American Shale Composite / Upper Continental Crust, used to assess the expected trace element contribution from the detrital fraction of the sediment.

Table 3B-1. Geochemical dataset: Section AB (WCSB).

Sample	Sc (ppm)	TiO2 (ppm)	Ti (ppm)	V (ppm)	Cr (ppm)	Mn (ppm)	Fe2O3 (ppm)	Fe [wt.%]	Fe [ppm]	Co (ppm)	Ni (ppm)	Cu (ppm)
114.0	60.7	241.1	144.5	40.4	14.9	80.1	2327.7	0.16	1628.1	0.7	11.6	4.4
112.0	65.7	455.0	272.7	39.8	15.2	78.6	7830.9	0.55	5477.3	1.5	13.5	8.1
111.0	71.8	154.5	92.6	17.2	12.3	64.3	3062.8	0.21	2142.3	2.2	8.8	0.6
110.0	78.6	41.8	25.1	1.0	4.5	37.2	536.4	0.04	375.2	1.6	1.4	0.6
109.5	63.3	64.3	38.5	7.9	19.2	45.6	1266.7	0.09	886.0	1.7	3.7	0.6
108.5	75.6	73.8	44.2	1.0	7.1	30.0	967.4	0.07	676.6	2.8	3.4	0.6
107.0	77.2	27.1	16.2	1.0	5.8	58.1	329.2	0.02	230.3	2.9	1.3	0.6
106.5	73.2	56.5	33.9	1.0	5.7	64.5	507.1	0.04	354.7	2.0	1.3	0.6
105.5	71.6	60.6	36.3	1.0	7.4	72.5	644.5	0.05	450.8	1.7	2.5	0.8
105.0	75.7	49.5	29.7	1.0	7.1	68.3	453.0	0.03	316.8	2.9	1.6	0.6
104.0	78.6	22.8	13.6	1.0	5.0	58.9	359.1	0.03	251.2	2.2	0.3	0.6
103.5	62.4	131.7	78.9	1.0	8.9	99.5	1503.7	0.11	1051.7	2.6	3.1	0.6
102.5	74.9	60.0	36.0	2.8	6.6	60.2	711.8	0.05	497.8	2.3	2.4	0.6
102.0	72.6	76.9	46.1	4.0	21.5	55.6	875.1	0.06	612.1	2.5	3.0	0.6
101.5	67.9	61.3	36.8	6.5	7.3	59.6	724.2	0.05	506.6	0.7	3.8	0.6
101.0	74.2	76.3	45.7	8.0	8.9	44.1	610.6	0.04	427.1	3.1	3.1	0.6
100.0	71.9	88.3	52.9	1.0	12.3	40.2	952.6	0.07	666.3	1.4	2.4	0.6
94.0	76.6	91.3	54.7	1.0	7.1	38.6	924.9	0.06	646.9	2.1	2.7	0.6
89.5	77.3	109.6	65.7	1.0	9.0	76.9	842.3	0.06	589.2	2.7	2.0	0.6
89.0	70.2	33.1	19.8	1.0	7.1	58.1	454.4	0.03	317.8	1.9	1.1	0.6
88.0	78.0	66.5	39.9	1.0	4.7	55.7	698.4	0.05	488.5	1.7	1.1	0.6
87.5	78.6	106.6	63.9	1.0	7.5	57.9	726.2	0.05	507.9	1.7	1.8	0.6
82.0	68.1	26.3	15.7	1.0	16.6	31.1	610.7	0.04	427.1	2.5	1.2	0.6
81.0	76.9	41.3	24.8	1.0	6.9	33.5	371.7	0.03	260.0	2.7	1.8	0.6
80.0	73.8	160.3	96.1	1.0	11.1	37.4	1309.1	0.09	915.6	2.7	5.6	0.6
79.0	75.7	34.2	20.5	1.0	5.0	47.7	283.0	0.02	198.0	2.3	1.5	0.6
76.5	70.6	38.2	22.9	1.0	2.4	59.8	853.7	0.06	597.1	2.7	3.2	0.6
72.5	75.1	539.0	323.1	23.0	16.9	96.8	3824.7	0.27	2675.1	2.2	19.4	10.7
72.0	72.8	329.6	197.6	10.0	8.4	58.7	2875.4	0.20	2011.2	2.7	7.4	8.0
71.0	76.7	57.8	34.6	1.0	6.3	70.7	391.5	0.03	273.9	1.5	3.4	0.6
69.0	78.1	28.1	16.9	1.0	6.8	60.5	260.5	0.02	182.2	2.1	2.5	0.6
68.0	74.8	36.9	22.1	1.0	7.5	109.5	422.6	0.03	295.6	2.4	2.0	0.8
66.5	71.9	99.6	59.7	7.8	5.5	174.0	926.8	0.06	648.3	0.7	7.8	0.6
66.0	72.8	255.1	152.9	3.1	9.4	292.2	2562.1	0.18	1792.0	2.5	4.8	0.6
65.5	68.6	361.4	216.6	8.9	8.9	347.6	5217.0	0.36	3649.0	4.7	14.6	2.8
65.0	53.3	1762.4	1056.4	30.2	31.7	495.8	22023.7	1.54	15404.3	5.0	16.0	14.8
64.5	56.7	960.5	575.7	24.3	22.0	500.8	8692.1	0.61	6079.6	4.1	15.0	11.5
64.0	52.8	1250.4	749.5	24.2	21.3	528.4	10253.0	0.72	7171.4	3.6	13.2	9.2
63.5	49.8	2328.1	1395.4	47.8	47.7	490.0	18263.9	1.28	12774.5	6.6	34.1	27.4
63.0	63.4	595.1	356.7	21.5	13.8	205.8	4160.0	0.29	2909.7	3.5	9.4	7.3
62.5	60.6	1089.5	653.1	133.8	25.0	138.1	8374.7	0.59	5857.6	3.2	30.0	26.4
62.0	70.3	239.1	143.3	24.3	8.9	109.9	1749.6	0.12	1223.8	3.8	7.7	3.9
61.5	72.9	201.7	120.9	3.8	9.7	67.5	1281.2	0.09	896.1	4.3	4.8	0.6
61.0	74.5	133.4	80.0	8.7	6.4	47.9	808.1	0.06	565.2	2.4	5.0	0.6
60.0	72.2	179.0	107.3	9.0	14.5	43.8	1490.0	0.10	1042.2	3.0	5.2	1.3
59.0	41.4	27.6	16.6	4.8	5.2	207.7	919.0	0.06	642.8	0.7	2.0	0.6
57.0	69.6	327.5	196.3	3.6	13.6	54.1	1643.7	0.11	1149.6	1.9	5.9	3.7
56.5	78.9	86.0	51.5	1.0	6.8	41.6	1453.8	0.10	1016.8	3.1	1.9	0.6
54.0	76.7	67.9	40.7	1.0	6.7	34.2	472.2	0.03	330.3	3.4	1.4	0.6
53.5	74.2	44.5	26.7	1.0	6.9	37.4	297.2	0.02	207.9	2.4	1.9	0.6
51.5	76.6	164.8	98.6	11.6	13.3	41.0	1385.9	0.10	969.3	1.9	4.6	1.3
51.0	68.4	229.6	137.6	2.9	9.6	42.0	1490.6	0.10	1042.6	1.6	4.5	2.2
44.0	72.5	251.8	150.9	1.0	7.9	104.3	3055.5	0.21	2137.2	3.8	2.7	0.6
43.5	71.2	93.0	55.7	1.0	6.1	143.7	1084.9	0.08	758.8	2.6	2.0	0.6
40.0	40.6	41.1	24.7	1.0	3.5	202.3	2129.0	0.15	1489.1	0.7	0.3	0.6
38.0	42.2	316.8	189.9	1.0	9.2	285.7	3919.7	0.27	2741.6	0.7	3.0	0.6
36.0	38.5	335.8	201.3	4.2	7.4	361.7	3181.3	0.22	2225.1	0.7	3.2	0.6

Table 3B-1 continued.

Sample	Zn (ppm)	Ga (ppm)	Ge (ppm)	As (ppm)	Se (ppm)	Br (ppm)	Rb (ppm)	Sr (ppm)	Y (ppm)	Zr (ppm)	Nb (ppm)	Mo (ppm)
114.0	9.6	0.4	0.3	2.0	0.4	1.8	6.8	239.7	14.2	5.0	0.6	3.3
112.0	3.7	0.9	0.3	2.0	0.4	2.1	12.3	234.6	9.5	7.7	0.9	3.2
111.0	7.5	0.4	0.3	2.0	0.4	1.0	3.7	225.2	7.0	3.1	0.4	3.9
110.0	11.9	0.4	0.3	2.0	0.8	0.8	2.3	313.2	3.5	1.8	0.1	1.3
109.5	4.1	0.4	0.3	2.0	0.4	1.4	1.9	197.9	4.5	1.5	0.1	1.8
108.5	12.3	0.4	0.3	2.0	0.4	1.5	2.6	254.0	3.1	1.8	0.1	1.6
107.0	2.2	0.4	0.3	2.0	0.4	0.7	1.6	229.5	2.7	1.4	0.1	1.1
106.5	3.9	0.4	0.3	2.0	0.4	0.8	2.0	149.8	4.3	1.8	0.3	1.9
105.5	7.1	0.4	0.3	2.0	0.4	1.2	1.9	131.6	3.6	1.7	0.1	1.4
105.0	5.3	0.4	0.3	2.0	0.4	0.7	1.9	136.6	3.4	1.6	0.1	1.2
104.0	2.3	0.4	0.3	2.0	0.4	0.8	1.4	159.8	2.8	1.2	0.4	1.4
103.5	3.2	0.4	0.3	2.0	0.4	0.9	2.8	113.2	3.9	3.1	0.7	1.6
102.5	8.4	0.4	0.3	2.0	0.4	1.3	1.9	184.8	5.3	2.1	0.1	1.6
102.0	16.2	0.4	0.3	2.0	0.4	0.2	2.6	155.0	5.5	2.5	0.5	1.7
101.5	14.4	0.4	0.3	2.0	0.4	1.5	2.2	154.7	6.2	2.0	0.1	1.4
101.0	15.1	0.4	0.3	2.0	0.4	0.6	2.7	280.3	6.4	2.9	0.5	1.7
100.0	3.7	0.4	0.3	2.0	0.4	1.1	2.5	237.2	3.3	2.3	0.3	1.9
94.0	3.3	0.4	0.3	2.0	0.4	1.7	2.8	244.3	3.1	2.2	0.3	1.0
89.5	3.7	0.4	0.3	2.0	0.4	1.7	2.4	214.5	5.2	4.0	0.4	1.8
89.0	2.6	0.4	0.3	2.0	0.4	1.5	1.1	170.6	1.4	1.1	0.1	1.2
88.0	1.8	0.4	0.3	4.8	0.4	1.3	1.6	185.6	3.2	2.5	0.1	1.2
87.5	3.7	0.4	0.3	2.0	0.4	1.1	2.4	171.8	3.8	3.1	0.1	1.3
82.0	1.2	0.4	0.3	2.0	0.4	0.2	1.5	150.4	0.9	1.6	0.1	1.3
81.0	10.5	0.4	0.3	2.0	0.4	1.2	1.4	179.2	3.8	2.0	0.5	1.3
80.0	12.9	0.4	0.3	2.0	0.4	0.8	4.2	248.7	5.0	3.6	0.3	1.4
79.0	3.0	0.4	0.3	2.0	0.4	1.1	1.5	159.5	3.1	1.4	0.1	0.9
76.5	8.5	0.4	0.3	2.0	0.4	0.2	1.0	127.5	4.6	1.0	0.1	1.3
72.5	11.5	1.2	0.3	2.0	0.9	2.4	11.7	323.2	17.7	9.9	0.9	3.1
72.0	5.6	0.4	0.3	2.0	0.4	1.6	9.3	343.6	6.3	5.7	0.8	1.3
71.0	6.1	0.4	0.3	2.0	0.4	2.6	2.7	262.9	4.9	1.7	0.1	0.8
69.0	18.4	0.4	0.3	2.0	0.4	2.0	1.6	224.0	3.8	1.3	0.3	1.0
68.0	6.3	0.4	0.3	2.0	0.4	1.3	1.8	134.6	5.7	1.5	0.4	1.2
66.5	10.2	0.4	0.3	2.0	0.4	1.3	2.7	235.9	9.2	2.4	0.1	2.0
66.0	4.8	0.4	0.3	2.0	1.0	1.5	6.0	316.0	8.1	5.4	0.7	1.9
65.5	8.1	0.4	0.3	6.2	0.8	1.9	8.2	417.0	9.0	7.0	0.4	5.3
65.0	6.5	0.4	0.3	2.0	0.4	1.2	27.0	355.4	10.4	31.8	2.3	3.1
64.5	4.6	1.8	0.3	2.0	0.4	2.0	16.8	282.0	9.6	17.1	1.5	3.0
64.0	4.4	2.8	0.3	2.0	0.4	1.3	21.0	287.2	9.1	23.8	1.8	2.5
63.5	9.3	4.8	0.3	5.7	1.2	1.7	38.2	285.8	13.3	39.6	2.9	6.1
63.0	2.7	1.6	0.3	2.0	1.2	1.5	12.1	316.2	8.6	9.2	0.7	2.6
62.5	5.5	2.3	0.3	2.0	1.1	2.2	22.8	360.5	15.3	17.1	1.3	9.2
62.0	2.3	0.4	0.3	2.0	0.4	1.7	6.5	342.3	10.8	4.9	0.5	1.7
61.5	2.1	0.4	0.3	2.0	0.4	1.7	5.3	412.6	7.3	4.1	0.5	1.4
61.0	1.0	0.4	0.3	2.0	0.4	2.8	4.2	399.2	6.4	3.3	0.1	1.3
60.0	2.6	0.4	0.3	2.0	0.4	1.4	6.4	550.2	4.0	3.7	0.1	1.6
59.0	7.2	0.4	0.3	2.0	0.4	1.4	0.4	30.0	5.0	1.0	0.1	0.8
57.0	1.3	0.9	0.3	2.0	0.4	2.1	8.3	392.8	7.1	5.4	0.5	1.1
56.5	2.5	0.4	0.3	4.4	0.4	2.2	3.9	447.9	4.1	2.1	0.1	1.2
54.0	3.3	0.4	0.3	2.0	0.4	2.3	2.6	243.6	4.0	2.2	0.1	1.1
53.5	2.5	0.4	0.3	2.0	0.4	2.8	1.6	231.5	3.8	1.9	0.3	0.7
51.5	5.7	0.4	0.3	2.0	0.4	1.0	4.0	255.6	3.7	2.7	0.1	1.4
51.0	9.5	0.4	0.3	2.0	0.4	1.8	5.0	302.7	6.0	4.2	0.3	1.3
44.0	2.8	0.4	0.3	2.0	0.4	0.2	5.5	121.4	6.6	4.6	0.6	1.4
43.5	2.0	0.4	0.3	2.0	0.4	0.2	1.6	115.3	7.2	2.1	0.7	1.1
40.0	46.3	0.4	0.3	2.0	0.4	1.8	0.6	45.0	1.7	0.8	0.1	1.0
38.0	19.4	0.4	0.3	2.0	0.4	1.9	5.2	57.6	3.1	5.8	0.3	0.7
36.0	1.0	0.4	0.3	2.0	0.4	1.1	5.3	39.8	1.9	6.7	0.7	0.9

Table 3B-1 continued.

Sample	Ag (ppm)	Cd (ppm)	Sn (ppm)	Sb (ppm)	Te (ppm)	I (ppm)	Cs (ppm)	Ba (ppm)	La (ppm)	Ce (ppm)	Nd (ppm)	Sm (ppm)
114.0	2.0	2.0	1.2	2.6	2.7	2.8	11.0	2.3	4.4	21.5	12.5	2.7
112.0	2.0	2.0	1.2	2.6	2.7	2.8	2.4	12.2	10.2	24.1	10.1	2.7
111.0	2.0	2.0	1.2	2.6	2.7	2.8	12.4	2.3	4.4	18.1	2.9	2.7
110.0	2.0	2.0	1.2	2.6	2.7	2.8	8.6	2.3	4.4	15.4	2.9	2.7
109.5	2.0	2.0	1.2	2.6	2.7	2.8	10.3	2.3	20.9	28.3	13.5	2.7
108.5	2.0	2.0	2.5	2.6	2.7	2.8	7.6	2.3	11.4	18.5	8.5	2.7
107.0	2.0	2.0	3.4	2.6	2.7	2.8	2.4	2.3	17.5	19.1	11.4	2.7
106.5	2.0	2.0	3.6	2.6	2.7	2.8	8.6	2.3	14.3	4.6	2.9	2.7
105.5	2.0	2.0	1.2	2.6	2.7	2.8	15.5	2.3	4.4	18.7	2.9	2.7
105.0	2.0	2.0	1.2	2.6	2.7	2.8	12.0	2.3	16.7	6.3	2.9	8.6
104.0	2.0	2.0	1.2	2.6	2.7	2.8	9.1	2.3	4.4	16.3	2.9	2.7
103.5	2.0	2.0	3.4	2.6	2.7	2.8	2.4	2.3	4.4	9.4	2.9	2.7
102.5	2.0	2.0	1.2	2.6	2.7	2.8	6.4	2.3	14.7	12.6	2.9	2.7
102.0	2.0	2.0	1.2	2.6	2.7	2.8	5.5	2.3	4.4	4.9	2.9	2.7
101.5	2.0	2.0	1.2	2.6	2.7	2.8	2.4	2.3	18.5	16.7	2.9	2.7
101.0	2.0	2.0	1.2	2.6	2.7	2.8	6.8	2.3	4.4	20.5	2.9	2.7
100.0	2.0	2.0	1.2	2.6	2.7	2.8	5.4	2.3	4.4	20.4	2.9	2.7
94.0	2.0	2.0	1.2	2.6	2.7	2.8	6.9	2.3	14.1	12.5	2.9	2.7
89.5	2.0	2.0	1.2	2.6	2.7	2.8	10.8	2.3	9.9	20.9	11.1	2.7
89.0	2.0	2.0	1.2	2.6	2.7	2.8	20.4	2.3	4.4	11.2	2.9	2.7
88.0	2.0	2.0	1.2	2.6	2.7	2.8	2.4	2.3	9.5	25.2	7.3	6.1
87.5	2.0	2.0	1.2	2.6	2.7	2.8	7.2	2.3	4.4	23.0	2.9	8.3
82.0	2.0	2.0	1.2	2.6	2.7	2.8	2.4	2.3	4.4	16.7	2.9	2.7
81.0	2.0	2.0	1.2	2.6	2.7	2.8	5.0	2.3	4.4	22.3	2.9	2.7
80.0	2.0	2.0	1.2	2.6	2.7	2.8	14.7	2.3	9.0	17.0	10.5	2.7
79.0	2.0	2.0	1.2	2.6	2.7	2.8	20.7	2.3	4.4	21.2	10.3	2.7
76.5	2.0	2.0	1.2	2.6	2.7	2.8	10.1	2.3	4.4	26.5	2.9	2.7
72.5	2.0	2.0	1.2	2.6	2.7	2.8	7.3	63.1	4.4	31.1	17.1	7.2
72.0	2.0	2.0	1.2	2.6	2.7	2.8	14.2	2.3	4.4	31.4	12.8	2.7
71.0	2.0	2.0	1.2	2.6	2.7	2.8	2.4	2.3	4.4	24.0	2.9	2.7
69.0	2.0	2.0	1.2	2.6	2.7	5.9	9.8	2.3	4.4	23.5	9.1	2.7
68.0	2.0	2.0	1.2	2.6	2.7	2.8	6.5	2.3	4.4	28.2	7.7	2.7
66.5	2.0	2.0	2.4	2.6	2.7	2.8	2.4	2.3	9.3	24.7	6.2	2.7
66.0	2.0	2.0	1.2	2.6	2.7	2.8	2.4	14.1	4.4	26.7	2.9	2.7
65.5	2.0	2.0	1.2	2.6	2.7	2.8	4.9	84.0	12.8	23.2	14.8	2.7
65.0	2.0	6.4	14.3	2.6	2.7	2.8	2.4	6263.2	9.8	1.7	2.9	2.7
64.5	2.0	2.0	1.2	2.6	2.7	2.8	10.4	97.4	17.0	35.9	13.0	10.5
64.0	2.0	2.0	1.2	2.6	2.7	2.8	2.4	169.2	22.6	35.2	10.9	2.7
63.5	2.0	2.0	1.2	2.6	2.7	2.8	2.4	274.9	10.1	43.0	10.3	2.7
63.0	2.0	2.0	1.2	2.6	2.7	2.8	2.4	25.9	4.4	18.2	8.5	2.7
62.5	2.0	2.0	2.5	2.6	2.7	2.8	5.5	170.5	17.4	26.4	16.7	10.0
62.0	2.0	2.0	1.2	7.8	2.7	2.8	2.4	187.4	9.6	29.5	11.0	2.7
61.5	2.0	2.0	1.2	2.6	2.7	7.2	2.4	2.3	4.4	16.4	7.4	10.9
61.0	2.0	2.0	1.2	2.6	2.7	8.4	6.5	2.3	4.4	22.4	2.9	5.9
60.0	2.0	2.0	1.2	2.6	2.7	2.8	6.4	2.3	10.0	18.7	2.9	2.7
59.0	2.0	2.0	1.2	2.6	2.7	2.8	2.4	2.3	9.1	4.1	2.9	2.7
57.0	2.0	2.0	1.2	2.6	2.7	2.8	6.7	2.3	12.3	20.7	2.9	2.7
56.5	2.0	2.0	1.2	2.6	2.7	2.8	16.6	2.3	4.4	18.1	2.9	2.7
54.0	2.0	2.0	1.2	2.6	2.7	2.8	12.5	2.3	4.4	18.7	8.7	10.6
53.5	2.0	2.0	1.2	2.6	2.7	2.8	2.4	2.3	16.3	23.5	10.3	2.7
51.5	2.0	2.0	1.2	2.6	2.7	2.8	5.8	2.3	9.6	20.1	7.8	2.7
51.0	2.0	2.0	1.2	2.6	2.7	2.8	16.8	2.3	4.4	17.8	6.1	2.7
44.0	2.0	2.0	1.2	2.6	2.7	2.8	7.4	2.3	9.4	40.8	16.7	7.6
43.5	2.0	2.0	1.2	2.6	2.7	2.8	7.2	2.3	4.4	20.3	6.5	2.7
40.0	2.0	2.0	1.2	2.6	2.7	2.8	8.1	2.3	4.4	12.1	2.9	2.7
38.0	2.0	2.0	1.2	2.6	2.7	2.8	12.1	5.7	4.4	10.2	6.7	2.7
36.0	2.0	2.0	1.2	2.6	2.7	2.8	2.4	9.5	4.4	13.4	2.9	2.7

Table 3B-1 continued.

Sample	Yb (ppm)	Hf (ppm)	Ta (ppm)	W (ppm)	Hg (ppm)	Tl (ppm)	Pb (ppm)	Bi (ppm)	Th (ppm)	U (ppm)
114.0	1.0	1.4	1.0	0.8	1.8	1.0	0.5	0.5	2.1	3.1
112.0	1.0	1.4	1.0	2.3	1.8	1.0	2.0	0.5	1.3	3.1
111.0	1.0	1.4	1.0	0.8	1.8	1.0	0.5	0.5	0.5	4.6
110.0	1.0	1.4	2.4	0.8	1.8	1.0	0.5	0.5	2.7	3.9
109.5	1.0	1.4	1.0	0.8	1.8	1.0	0.5	0.5	0.5	2.9
108.5	1.0	1.4	1.0	0.8	1.8	1.0	0.5	0.5	2.2	2.4
107.0	1.0	1.4	2.0	0.8	1.8	1.0	0.5	0.5	2.1	1.1
106.5	1.0	1.4	1.0	0.8	1.8	1.0	0.5	0.5	1.9	1.8
105.5	1.0	1.4	1.0	0.8	1.8	1.0	0.5	0.5	1.9	1.1
105.0	1.0	1.4	1.0	0.8	1.8	1.0	0.5	0.5	1.3	2.6
104.0	1.0	1.4	1.0	0.8	1.8	1.0	0.5	0.5	1.6	1.9
103.5	1.0	1.4	1.0	0.8	1.8	1.0	0.5	0.5	1.7	1.9
102.5	1.0	1.4	1.0	0.8	1.8	1.0	0.5	0.5	1.2	3.3
102.0	1.0	1.4	1.0	0.8	1.8	1.0	0.5	0.5	2.6	2.3
101.5	1.0	1.4	1.0	0.8	1.8	1.0	0.5	0.5	0.5	3.0
101.0	1.0	1.4	1.0	0.8	1.8	1.0	0.5	0.5	2.7	2.6
100.0	1.0	1.4	1.0	0.8	1.8	1.0	0.5	0.5	1.3	1.6
94.0	1.0	1.4	2.2	0.8	1.8	1.0	0.5	0.5	1.6	1.2
89.5	1.0	1.4	1.0	0.8	1.8	1.0	0.5	0.5	2.3	1.3
89.0	1.0	1.4	1.0	0.8	1.8	1.0	0.5	2.5	2.6	1.3
88.0	1.0	1.4	1.0	0.8	1.8	1.0	0.5	1.3	2.0	2.4
87.5	1.0	1.4	1.0	0.8	1.8	1.0	0.5	1.1	1.9	2.2
82.0	1.0	1.4	1.0	0.8	1.8	1.0	0.5	0.5	1.9	1.1
81.0	1.0	3.3	1.0	0.8	1.8	1.0	0.5	1.9	2.2	3.2
80.0	1.0	1.4	1.0	0.8	1.8	1.0	1.4	1.2	1.5	3.1
79.0	1.0	1.4	1.0	0.8	1.8	1.0	0.5	2.0	1.3	1.5
76.5	1.0	1.4	1.0	0.8	1.8	1.0	0.5	0.5	0.5	2.2
72.5	1.0	1.4	1.0	0.8	1.8	1.0	1.9	0.5	2.7	5.0
72.0	1.0	1.4	1.0	1.8	1.8	1.0	2.5	0.5	2.7	2.5
71.0	1.0	1.4	1.0	0.8	1.8	1.0	0.5	0.5	0.5	3.5
69.0	1.0	1.4	1.0	0.8	1.8	1.0	0.5	0.5	2.4	2.4
68.0	1.0	1.4	1.0	0.8	1.8	1.0	0.5	0.5	1.5	0.4
66.5	1.0	1.4	1.0	0.8	1.8	1.0	0.5	0.5	0.5	3.0
66.0	1.0	1.4	1.0	0.8	1.8	1.0	0.5	0.5	2.0	4.2
65.5	1.0	1.4	1.0	0.8	1.8	1.0	1.3	1.0	1.4	5.9
65.0	1.0	3.7	1.0	7.8	1.8	1.0	5.2	0.5	3.3	4.2
64.5	1.0	1.4	1.0	2.8	1.8	1.0	3.5	0.5	2.4	3.0
64.0	1.0	1.4	1.0	3.1	1.8	1.0	3.4	0.5	4.0	3.0
63.5	1.0	1.4	1.0	10.1	1.8	1.0	5.1	0.5	3.4	3.9
63.0	1.0	1.4	1.0	0.8	1.8	1.0	1.9	0.5	1.4	1.8
62.5	1.0	1.4	1.0	2.1	1.8	1.0	7.3	1.4	2.6	4.9
62.0	1.0	1.4	1.0	0.8	1.8	1.0	0.5	0.5	2.7	4.5
61.5	1.0	1.4	2.1	1.7	1.8	1.0	0.5	0.5	2.3	3.6
61.0	1.0	1.4	1.0	0.8	1.8	1.0	0.5	1.2	1.1	3.1
60.0	1.0	1.4	1.0	0.8	1.8	1.0	0.5	0.5	2.0	4.8
59.0	1.0	1.4	2.1	0.8	1.8	1.0	0.5	0.5	1.6	0.4
57.0	1.0	1.4	1.0	0.8	1.8	1.0	0.5	0.5	2.0	3.0
56.5	1.0	1.4	1.0	0.8	1.8	1.0	0.5	2.3	1.7	3.4
54.0	1.0	1.4	1.0	0.8	1.8	1.0	0.5	2.2	1.4	1.9
53.5	1.0	1.4	1.0	0.8	1.8	1.0	1.0	1.9	2.1	2.5
51.5	1.0	1.4	1.0	0.8	1.8	1.0	0.5	0.5	1.5	0.4
51.0	1.0	1.4	1.0	0.8	1.8	1.0	1.8	0.5	2.6	2.3
44.0	1.0	1.4	1.0	0.8	1.8	1.0	4.0	0.5	2.2	0.4
43.5	1.0	1.4	2.1	0.8	1.8	1.0	0.5	0.5	2.1	0.4
40.0	1.0	1.4	1.0	0.8	1.6	1.0	1.9	0.5	1.4	0.4
38.0	1.0	3.5	1.0	0.8	1.8	1.0	1.5	0.5	1.1	0.4
36.0	1.0	1.4	1.0	0.8	1.8	1.0	1.7	0.5	1.4	0.4

Table 3B-1 continued.

Sample	Ni/Co -	V/Cr -	V/V+Ni -	U/Th -	V/Sc -	Ti/Al -	Zr/Al -	MSraw [kg/m³]	MSE10 [kg/m³]
114.0	17.5	2.7	0.8	1.5	0.67	413.3	14.3	1.6E-08	159.0
112.0	8.8	2.6	0.7	2.4	0.61	408.6	11.6	3.0E-08	298.0
111.0	4.0	1.4	0.7	8.3	0.24	562.6	19.0	1.0E-08	101.0
110.0	0.9	0.2	0.4	1.4	0.01	1534.9	112.2	3.9E-09	39.4
109.5	2.2	0.4	0.7	5.3	0.12	615.8	24.6	3.4E-09	34.4
108.5	1.2	0.1	0.2	1.1	0.01	685.0	27.8	7.1E-09	70.7
107.0	0.4	0.2	0.4	0.5	0.01	994.6	85.2	2.1E-09	20.7
106.5	0.6	0.2	0.4	1.0	0.01	643.9	34.2	2.3E-09	22.7
105.5	1.5	0.1	0.3	0.5	0.01	642.3	30.1	2.9E-09	29.2
105.0	0.5	0.1	0.4	1.9	0.01	750.1	40.5	1.5E-09	15.4
104.0	0.1	0.2	0.8	1.2	0.01	835.5	74.2	1.0E-11	0.1
103.5	1.2	0.1	0.2	1.1	0.02	623.4	24.4	5.9E-10	5.9
102.5	1.1	0.4	0.5	2.8	0.04	684.4	39.9	7.6E-10	7.6
102.0	1.2	0.2	0.6	0.9	0.05	477.3	25.7	1.0E-11	0.1
101.5	5.8	0.9	0.6	5.4	0.10	506.5	27.0	8.1E-10	8.1
101.0	1.0	0.9	0.7	1.0	0.11	499.4	31.9	2.3E-09	22.8
100.0	1.8	0.1	0.3	1.2	0.01	611.2	26.1	1.5E-09	14.5
94.0	1.3	0.1	0.3	0.7	0.01	538.5	21.6	3.9E-09	39.0
89.5	0.8	0.1	0.3	0.6	0.01	905.3	54.5	8.3E-09	83.4
89.0	0.6	0.1	0.5	0.5	0.01	1214.1	65.1	1.0E-11	0.1
88.0	0.7	0.2	0.5	1.2	0.01	1033.5	65.6	3.6E-09	35.7
87.5	1.0	0.1	0.4	1.2	0.01	682.6	32.8	4.4E-09	44.1
82.0	0.5	0.1	0.5	0.6	0.01	963.7	97.5	1.0E-11	0.1
81.0	0.7	0.1	0.3	1.4	0.01	595.5	48.2	3.6E-09	36.4
80.0	2.1	0.1	0.1	2.1	0.01	445.7	16.7	4.3E-09	42.9
79.0	0.7	0.2	0.4	1.1	0.01	1254.5	87.4	7.6E-10	7.6
76.5	1.2	0.4	0.2	4.0	0.01	1403.3	58.4	1.0E-11	0.1
72.5	8.7	1.4	0.5	1.8	0.31	440.4	13.5	9.3E-09	92.8
72.0	2.7	1.2	0.6	0.9	0.14	401.1	11.6	2.1E-08	208.7
71.0	2.3	0.2	0.2	6.5	0.01	853.7	42.3	7.9E-09	79.3
69.0	1.2	0.1	0.3	1.0	0.01	1032.3	78.3	1.5E-09	15.2
68.0	0.8	0.1	0.3	0.3	0.01	398.0	27.9	2.5E-09	25.3
66.5	11.8	1.4	0.5	5.6	0.11	740.5	29.5	2.9E-09	29.4
66.0	1.9	0.3	0.4	2.1	0.04	602.9	21.4	2.4E-09	24.4
65.5	3.1	1.0	0.4	4.3	0.13	556.0	17.9	1.2E-08	122.7
65.0	3.2	1.0	0.7	1.3	0.57	662.9	19.9	1.2E-08	124.4
64.5	3.7	1.1	0.6	1.2	0.43	610.1	18.1	1.3E-08	133.2
64.0	3.7	1.1	0.6	0.7	0.46	575.4	18.3	1.2E-08	123.9
63.5	5.2	1.0	0.6	1.2	0.96	593.4	16.8	1.3E-08	129.2
63.0	2.7	1.6	0.7	1.3	0.34	551.7	14.2	1.1E-08	109.4
62.5	9.3	5.4	0.8	1.9	2.21	489.3	12.8	6.8E-09	67.7
62.0	2.0	2.7	0.8	1.7	0.35	438.8	15.0	5.4E-09	54.2
61.5	1.1	0.4	0.4	1.6	0.05	605.7	20.3	7.4E-09	74.2
61.0	2.1	1.4	0.6	2.8	0.12	564.8	23.3	8.6E-09	85.9
60.0	1.7	0.6	0.6	2.4	0.12	543.0	18.5	1.9E-08	193.6
59.0	3.0	0.9	0.7	0.3	0.12	1014.2	58.9	3.2E-09	31.8
57.0	3.0	0.3	0.4	1.4	0.05	463.4	12.7	1.7E-08	170.5
56.5	0.6	0.1	0.3	2.1	0.01	588.5	23.7	9.7E-09	96.8
54.0	0.4	0.1	0.4	1.4	0.01	639.7	34.3	7.8E-09	77.8
53.5	0.8	0.1	0.3	1.2	0.01	673.8	46.9	4.0E-09	40.3
51.5	2.4	0.9	0.7	0.3	0.15	504.3	13.9	3.3E-09	33.3
51.0	2.9	0.3	0.4	0.9	0.04	567.3	17.4	4.2E-09	42.1
44.0	0.7	0.1	0.3	0.2	0.01	367.6	11.3	2.6E-09	26.1
43.5	0.8	0.2	0.3	0.2	0.01	666.8	24.6	2.9E-09	29.0
40.0	0.5	0.3	0.8	0.3	0.02	1510.1	50.9	2.4E-09	24.4
38.0	4.5	0.1	0.2	0.4	0.02	502.9	15.4	5.9E-09	59.0
36.0	4.8	0.6	0.6	0.3	0.11	566.0	18.8	1.1E-08	111.2

Table 3B-1 continued.

Sample	Na [wt.%]	Mg [wt.%]	Al [wt.%]	Si [wt.%]	P [wt.%]	S [wt.%]	K [wt.%]	Ca [wt.%]	TOC [wt.%]	Tot. Carb. [wt.%]	Acid Insolubles [wt.%]
114.0	0.003	0.214	0.350	7.604	0.014	0.160	0.391	29.866	0.76	83.6	15.68
112.0	0.003	0.287	0.668	6.601	0.012	0.205	0.798	30.253	0.68	85.8	13.48
111.0	0.003	0.280	0.165	5.245	0.011	0.186	0.191	32.99	0.51	89.1	10.37
110.0	0.003	0.230	0.016	0.671	0.006	0.042	0.060	39.827	0.11	98.1	1.74
109.5	0.003	0.209	0.063	6.256	0.006	0.105	0.083	31.775	0.29	84.8	14.91
108.5	0.003	0.227	0.065	1.108	0.003	0.087	0.104	39.051	0.21	97.4	2.40
107.0	0.003	0.178	0.016	0.521	0.003	0.042	0.039	40.243	0.10	98.5	1.40
106.5	0.003	0.712	0.053	1.918	0.005	0.058	0.089	36.835	0.16	96.4	3.42
105.5	0.003	1.269	0.057	0.997	0.005	0.059	0.096	36.556	0.23	97.3	2.51
105.0	0.003	0.955	0.040	0.823	0.004	0.054	0.070	37.864	0.17	98.1	1.73
104.0	0.003	0.168	0.016	0.194	0.004	0.044	0.031	40.707	0.10	99.2	0.70
103.5	0.003	3.424	0.127	1.157	0.009	0.140	0.184	31.384	0.53	96.2	3.23
102.5	0.003	0.226	0.053	0.790	0.006	0.042	0.113	39.635	0.11	97.8	2.13
102.0	0.003	0.676	0.097	2.564	0.014	0.066	0.114	37.98	0.23	95.0	4.79
101.5	0.003	0.702	0.073	3.142	0.008	0.096	0.102	35.27	0.38	93.9	5.69
101.0	0.003	0.234	0.092	1.361	0.012	0.081	0.136	40.1615	0.21	96.7	3.11
100.0	0.003	0.249	0.087	3.005	0.006	0.057	0.121	36.905	0.12	92.3	7.54
94.0	0.003	0.278	0.102	0.506	0.008	0.068	0.132	41.594	0.23	97.4	2.33
89.5	0.003	0.253	0.073	0.569	0.006	0.132	0.084	40.4855	0.18	98.0	1.80
89.0	0.003	0.475	0.016	4.453	0.003	0.049	0.026	35.742	0.14	88.1	11.76
88.0	0.003	0.258	0.039	0.327	0.003	0.104	0.064	40.7665	0.15	98.7	1.15
87.5	0.003	0.364	0.094	0.630	0.010	0.129	0.123	41.027	0.31	97.6	2.12
82.0	0.003	0.331	0.016	4.140	0.003	0.026	0.036	34.709	0.08	86.6	13.33
81.0	0.003	0.235	0.042	0.496	0.005	0.078	0.071	41.511	0.19	98.5	1.35
80.0	0.003	0.276	0.216	1.928	0.008	0.078	0.326	38.633	0.16	96.7	3.15
79.0	0.003	0.176	0.016	0.444	0.003	0.036	0.042	42.069	0.12	98.3	1.61
76.5	0.003	1.601	0.016	0.593	0.007	0.087	0.063	38.55	0.16	98.1	1.78
72.5	0.003	0.330	0.734	3.115	0.024	0.210	0.884	35.665	1.09	88.0	10.91
72.0	0.003	0.331	0.493	2.604	0.011	0.207	0.695	36.257	0.63	92.1	7.23
71.0	0.003	0.254	0.041	0.749	0.010	0.111	0.077	41.452	0.33	96.6	3.05
69.0	0.003	0.175	0.016	0.179	0.009	0.062	0.036	42.578	0.30	98.2	1.49
68.0	0.003	1.269	0.056	1.496	0.005	0.067	0.098	37.471	0.20	95.8	3.98
66.5	0.003	0.206	0.081	1.052	0.033	0.296	0.134	40.174	0.74	95.5	3.73
66.0	0.003	0.303	0.254	1.879	0.014	0.414	0.359	38.291	1.17	92.1	6.73
65.5	0.003	0.514	0.390	4.597	0.017	0.857	0.522	33.568	1.36	87.1	11.49
65.0	0.039	2.242	1.594	8.381	0.025	2.553	1.771	19.863	1.95	72.0	26.08
64.5	0.007	0.660	0.944	9.559	0.021	0.884	1.095	24.736	2.14	76.0	21.90
64.0	0.003	1.465	1.303	10.067	0.023	1.495	1.408	23.277	2.46	73.6	23.98
63.5	0.007	1.633	2.352	11.390	0.036	1.949	2.362	18.039	2.07	67.5	30.47
63.0	0.003	0.444	0.647	8.202	0.014	0.225	0.801	28.625	0.51	83.7	15.81
62.5	0.003	0.389	1.335	10.481	0.030	0.611	1.508	24.338	0.99	76.5	22.54
62.0	0.003	0.327	0.327	4.281	0.010	0.162	0.426	35.747	0.38	92.2	7.38
61.5	0.003	0.505	0.200	1.745	0.010	0.139	0.328	38.502	0.23	95.0	4.73
61.0	0.003	0.367	0.142	0.914	0.010	0.180	0.220	40.239	0.22	97.4	2.39
60.0	0.003	0.385	0.198	3.622	0.008	0.201	0.250	35.9	0.27	91.6	8.10
59.0	0.003	12.646	0.016	0.265	0.002	0.037	0.025	20.783	0.23	98.2	1.60
57.0	0.003	0.598	0.424	2.858	0.010	0.181	0.588	36.143	0.35	93.1	6.54
56.5	0.003	0.307	0.088	1.221	0.006	0.113	0.151	39.979	0.20	96.5	3.34
54.0	0.003	0.384	0.064	0.695	0.008	0.109	0.106	41.185	0.17	98.2	1.63
53.5	0.003	0.532	0.040	0.448	0.007	0.096	0.082	40.82	0.13	98.8	1.09
51.5	0.003	0.331	0.196	1.852	0.011	0.148	0.288	38.767	0.29	94.9	4.80
51.0	0.003	0.339	0.243	1.478	0.008	0.188	0.345	39.119	0.46	94.8	4.77
44.0	0.003	0.193	0.411	2.171	0.002	0.191	0.579	38.193			
43.5	0.003	1.217	0.084	0.571	0.007	0.122	0.128	38.914			
40.0	0.003	12.940	0.016	0.148	0.000	0.050	0.060	20.909	0.15	99.1	0.71
38.0	0.003	11.388	0.378	1.423	0.006	0.081	0.523	20.523	0.13	95.4	4.45
36.0	0.003	12.246	0.356	1.664	0.009	0.113	0.574	19.624	0.20	95.2	4.65

Table 3B-2. Geochemical dataset: Section AB (WCSB). Generated using my own XRF analytical protocols (Chapter 2).

Sample	Ti (ppm)	V (ppm)	Cr (ppm)	Mn (ppm)	Fe (ppm)	Co (ppm)	Ni (ppm)	Cu (ppm)	Zn (ppm)	Sr (ppm)	Zr (ppm)
114.0	83.2	40.3	10.2	42.6	1508.9	0.7	8.9	3.3	6.6	224.7	1.9
112.0	156.7	44.1	10.7	42.1	5124.4	1.7	9.5	8.2	1.5	219.8	4.6
111.0	49.2	19.5	3.7	29.5	1972.4	0.7	6.2	1.9	4.2	208.8	0.7
110.0	8.0	2.5	1.0	19.4	343.6	0.7	0.3	0.5	9.7	292.1	0.7
109.5	16.7	11.5	11.9	23.7	815.5	0.7	2.5	0.5	1.8	184.7	0.7
108.5	20.6	4.0	1.0	17.7	627.1	0.7	0.3	0.5	9.8	236.3	0.7
107.0	5.3	1.8	1.0	29.4	212.4	0.7	0.3	0.5	1.2	215.6	0.7
106.5	15.7	4.6	2.4	35.9	324.2	0.7	0.3	0.5	2.2	141.5	0.7
105.5	19.5	4.6	2.3	36.4	401.7	0.7	0.3	0.5	4.4	120.5	0.7
105.0	13.4	3.6	1.0	36.5	283.2	0.7	0.3	0.5	3.1	128.5	0.7
104.0	3.6	0.8	1.0	30.8	227.2	0.7	0.3	0.5	0.5	147.2	0.7
103.5	44.9	6.5	4.8	49.0	958.7	0.7	0.3	0.5	0.5	104.4	0.7
102.5	17.0	6.7	1.0	29.2	449.4	0.7	1.2	0.5	5.5	169.3	0.7
102.0	25.0	6.6	11.0	30.1	554.1	0.7	1.3	2.6	13.0	145.6	0.7
101.5	17.4	10.4	3.9	28.2	457.3	0.7	1.7	0.5	10.8	142.4	0.7
101.0	24.9	12.6	3.6	20.5	398.1	0.7	2.5	2.0	12.1	262.3	0.7
100.0	26.3	3.3	5.8	18.7	606.2	0.7	1.3	1.1	1.9	222.1	0.7
94.0	27.9	4.0	2.7	21.1	598.6	0.7	0.9	2.5	2.5	232.6	0.7
89.5	33.3	2.8	2.6	39.6	546.9	0.7	0.8	0.5	1.5	200.2	0.7
89.0	8.6	0.8	5.2	28.3	292.1	0.7	0.3	0.5	0.5	162.6	0.7
88.0	19.2	1.6	1.0	29.8	445.3	0.7	0.3	0.5	0.5	174.5	0.7
87.5	36.3	2.2	2.4	30.2	470.2	0.7	0.8	1.5	1.7	166.3	0.7
82.0	5.7	2.7	7.5	16.1	379.9	0.7	0.3	0.5	0.5	139.6	0.7
81.0	11.7	4.5	1.0	16.8	238.5	0.7	1.5	0.5	8.7	171.8	0.7
80.0	51.5	7.8	2.7	19.8	840.7	0.7	2.8	2.2	9.4	231.7	0.7
79.0	10.0	2.6	1.0	24.9	182.3	0.7	0.3	1.1	1.0	155.0	0.7
76.5	11.6	2.3	1.0	30.1	550.4	0.7	1.2	0.5	6.3	123.3	0.7
72.5	188.9	31.2	11.4	47.3	2506.8	1.6	15.8	10.6	8.7	304.4	6.0
72.0	109.9	13.6	4.9	28.5	1853.4	0.7	6.6	7.5	3.5	321.0	2.4
71.0	17.9	4.8	1.0	37.0	252.8	0.7	2.3	1.9	4.8	248.5	0.7
69.0	7.5	3.6	1.0	32.6	170.1	0.7	0.7	0.5	15.5	211.6	0.7
68.0	11.7	3.3	1.0	57.9	261.5	0.7	0.3	0.5	4.5	131.3	0.7
66.5	32.1	12.4	2.9	92.0	599.9	0.7	5.5	2.1	7.2	221.1	0.7
66.0	87.3	6.7	3.2	151.1	1655.5	0.7	3.4	3.0	2.6	301.5	3.0
65.5	122.4	10.2	5.8	179.6	3395.4	2.5	11.3	5.1	5.6	391.1	3.1
66.0	730.9	50.3	26.6	266.7	15257.7	5.4	13.3	14.1	5.2	338.5	25.6
64.5	354.9	30.5	15.0	261.9	5675.7	2.6	11.5	11.6	2.2	260.4	12.8
64.0	496.4	31.3	15.3	278.5	6736.9	3.4	10.7	10.2	2.3	267.2	19.4
63.5	920.8	59.4	37.8	261.8	12239.0	5.0	27.9	24.0	6.6	263.3	33.7
63.0	209.0	26.9	8.9	107.0	2702.4	2.1	7.2	8.5	1.0	294.5	6.5
62.5	398.1	130.8	24.1	71.3	5535.9	2.4	25.2	24.7	3.6	335.9	13.1
62.0	82.3	30.3	6.7	54.3	1132.3	0.7	5.5	4.5	0.5	321.1	1.5
61.5	67.1	9.1	2.9	33.0	829.0	0.7	3.8	3.2	0.5	387.7	0.7
61.0	44.6	9.8	2.4	24.6	519.5	0.7	2.3	1.8	0.5	373.6	0.7
60.0	58.4	16.3	8.4	20.1	939.7	0.7	3.2	2.1	1.4	504.1	0.7
59.0	11.7	6.0	2.6	105.3	566.7	2.3	0.3	0.5	3.4	25.5	0.7
57.0	110.7	9.6	5.4	29.5	1072.4	0.7	4.5	4.4	0.5	367.6	2.4
56.5	24.8	3.1	4.8	22.0	945.0	0.7	1.3	2.2	1.4	420.2	0.7
54.0	21.7	6.1	3.1	17.3	301.8	0.7	1.2	2.2	1.6	231.6	0.7
53.5	15.2	2.8	1.0	21.1	189.9	0.7	1.1	1.7	0.5	218.1	0.7
51.5	52.7	13.4	4.3	22.6	900.2	0.7	2.7	4.3	4.1	238.5	0.7
51.0	76.3	7.0	4.0	22.8	963.9	0.7	3.0	4.5	7.1	285.0	1.6
44.0	82.1	4.2	3.8	54.8	1988.5	1.9	0.9	2.3	1.0	113.8	1.4
43.5	28.6	2.9	1.0	73.5	700.3	0.7	0.3	0.5	0.5	110.9	0.7
40.0	18.1	0.8	1.0	103.7	1334.8	2.3	0.3	0.5	36.2	39.3	0.7
38.0	154.7	3.9	3.9	147.0	2498.0	2.6	0.3	0.5	14.4	51.0	2.8
36.0	168.2	4.7	4.3	182.3	2026.2	2.7	0.3	0.5	0.5	34.9	3.4

Table 3B-2 continued.

Sample	Mo (ppm)	Ba (ppm)	Ca (ppm)	Rb (ppm)	Pb (ppm)	Th (ppm)	U (ppm)	Ni/Co -	U/Th -	V/Cr -	V/(V+Ni) -
114.0	1.2	20.0	29.9	4.5	0.5	0.4	1.4	13.1	3.7	3.9	0.8
112.0	1.6	21.6	30.3	9.2	2.0	0.4	1.0	5.5	2.6	4.1	0.8
111.0	2.0	18.8	33.0	2.3	1.9	0.4	2.0	9.1	5.3	5.3	0.8
110.0	0.5	7.7	39.8	0.3	0.5	0.4	0.3	0.5	0.9	2.5	0.9
109.5	0.5	3.8	31.8	0.3	1.1	0.4	0.3	3.6	0.9	1.0	0.8
108.5	0.5	3.8	39.1	0.8	0.5	0.4	0.3	0.5	0.9	3.9	0.9
107.0	0.5	3.8	40.2	0.3	0.5	0.4	0.3	0.5	0.9	1.7	0.8
106.5	0.5	9.7	36.8	0.3	0.5	0.4	0.3	0.5	0.9	1.9	0.9
105.5	0.5	8.3	36.6	0.8	1.2	0.4	0.3	0.5	0.9	2.0	0.9
105.0	0.5	3.8	37.9	0.3	0.5	0.4	0.3	0.5	0.9	3.5	0.9
104.0	0.5	3.8	40.7	0.3	0.5	0.4	0.3	0.5	0.9	0.8	0.7
103.5	0.5	3.8	31.4	1.5	1.0	0.4	0.8	0.5	2.3	1.3	1.0
102.5	0.5	3.8	39.6	1.0	0.5	0.4	0.7	1.7	2.0	6.6	0.9
102.0	0.5	8.6	38.0	0.3	0.5	0.4	0.8	1.9	2.1	0.6	0.8
101.5	0.5	9.9	35.3	1.1	0.5	0.4	0.3	2.5	0.9	2.7	0.9
101.0	0.5	3.8	40.2	0.8	0.5	0.4	1.1	3.7	2.9	3.5	0.8
100.0	0.5	3.8	36.9	0.3	0.5	0.4	0.3	1.9	0.9	0.6	0.7
94.0	0.5	3.8	41.6	0.8	0.5	0.4	0.3	1.3	0.9	1.5	0.8
89.5	0.5	3.8	40.5	0.7	0.5	0.4	0.3	1.1	0.9	1.1	0.8
89.0	0.5	3.8	35.7	0.3	0.5	0.4	0.3	0.5	0.9	0.1	0.7
88.0	0.5	3.8	40.8	0.3	1.9	0.4	0.3	0.5	0.9	1.6	0.8
87.5	0.5	3.8	41.0	0.3	0.5	0.4	0.3	1.1	0.9	0.9	0.7
82.0	0.5	3.8	34.7	0.3	0.5	0.4	0.3	0.5	0.9	0.4	0.9
81.0	0.5	3.8	41.5	0.3	0.5	0.4	0.8	2.2	2.1	4.4	0.7
80.0	0.5	3.8	38.6	1.7	0.5	0.4	0.3	4.0	0.9	2.9	0.7
79.0	0.5	3.8	42.1	0.3	0.5	0.4	0.3	0.5	0.9	2.6	0.9
76.5	0.5	3.8	38.6	0.3	0.5	0.4	0.3	1.8	0.9	2.3	0.7
72.5	1.6	63.1	35.7	8.2	2.2	0.4	1.5	9.9	4.2	2.7	0.7
72.0	0.5	18.3	36.3	5.4	0.5	0.4	0.3	9.7	0.9	2.8	0.7
71.0	0.5	3.8	41.5	0.3	0.5	0.4	0.3	3.4	0.9	4.7	0.7
69.0	0.5	3.8	42.6	0.3	0.5	0.4	0.3	1.0	0.9	3.5	0.8
68.0	0.5	3.8	37.5	0.3	0.5	0.4	0.3	0.5	0.9	3.3	0.9
66.5	0.5	12.6	40.2	0.7	0.5	0.4	0.9	8.0	2.5	4.3	0.7
66.0	0.5	31.0	38.3	2.8	1.9	0.4	1.3	5.0	3.5	2.1	0.7
65.5	4.2	67.7	33.6	4.9	2.0	0.4	2.1	4.6	5.9	1.8	0.5
65.0	4.5	4328.9	19.9	21.8	7.1	0.9	1.6	2.4	1.9	1.9	0.8
64.5	0.5	83.3	24.7	12.9	2.6	0.4	1.5	4.5	4.0	2.0	0.7
64.0	0.5	131.6	23.3	15.5	3.6	1.0	1.0	3.1	1.0	2.0	0.7
63.5	5.6	203.5	18.0	30.9	6.9	0.8	2.1	5.5	2.7	1.6	0.7
63.0	1.4	39.8	28.6	9.0	2.0	0.4	1.0	3.5	2.6	3.0	0.8
62.5	8.6	130.9	24.3	18.0	5.7	0.4	2.4	10.5	6.7	5.4	0.8
62.0	0.5	137.3	35.7	3.5	0.5	0.4	1.3	8.1	3.5	4.5	0.8
61.5	0.5	19.1	38.5	2.0	0.5	0.4	0.3	5.6	0.9	3.1	0.7
61.0	0.5	21.7	40.2	1.2	0.5	0.4	1.3	3.3	3.6	4.1	0.8
60.0	0.5	15.7	35.9	1.6	0.5	0.4	0.9	4.7	2.5	1.9	0.8
59.0	0.5	3.8	20.8	0.3	0.5	0.4	0.3	0.1	0.9	2.3	0.9
57.0	0.5	15.5	36.1	4.2	0.5	0.4	0.3	6.6	0.9	1.8	0.7
56.5	0.5	3.8	40.0	0.3	1.1	0.4	0.3	1.9	0.9	0.7	0.7
54.0	0.5	3.8	41.2	0.3	0.5	0.4	0.3	1.7	0.9	2.0	0.8
53.5	0.5	3.8	40.8	0.3	0.5	0.4	0.7	1.6	1.8	2.8	0.7
51.5	0.5	9.5	38.8	1.8	0.5	0.8	0.3	4.0	0.4	3.1	0.8
51.0	0.5	17.0	39.1	1.8	1.1	0.4	0.3	4.4	0.9	1.8	0.7
44.0	0.5	12.1	38.2	3.2	2.8	0.4	0.3	0.5	0.9	1.1	0.8
43.5	0.5	3.8	38.9	0.3	0.5	0.4	0.3	0.5	0.9	2.8	0.9
40.0	0.5	3.8	20.9	0.3	0.5	0.4	0.3	0.1	0.9	0.8	0.7
38.0	0.5	14.2	20.5	2.6	1.5	0.4	0.3	0.1	0.9	1.0	0.9
36.0	0.5	23.1	19.6	2.8	1.1	0.4	0.3	0.1	0.9	1.1	0.9

Table 3B-2 continued.

Sample	Na [wt.%]	Mg [wt.%]	Al [wt.%]	Si [wt.%]	P [wt.%]	S [wt.%]	K [wt.%]	Ca [wt.%]	TOC [wt.%]	Tot. Carb. [wt.%]
114.0	0.003	0.214	0.350	7.604	0.014	0.160	0.391	29.866	0.76	83.6
112.0	0.003	0.287	0.668	6.601	0.012	0.205	0.798	30.253	0.68	85.8
111.0	0.003	0.280	0.165	5.245	0.011	0.186	0.191	32.99	0.51	89.1
110.0	0.003	0.230	0.016	0.671	0.006	0.042	0.060	39.827	0.11	98.1
109.5	0.003	0.209	0.063	6.256	0.006	0.105	0.083	31.775	0.29	84.8
108.5	0.003	0.227	0.065	1.108	0.003	0.087	0.104	39.051	0.21	97.4
107.0	0.003	0.178	0.016	0.521	0.003	0.042	0.039	40.243	0.10	98.5
106.5	0.003	0.712	0.053	1.918	0.005	0.058	0.089	36.835	0.16	96.4
105.5	0.003	1.269	0.057	0.997	0.005	0.059	0.096	36.556	0.23	97.3
105.0	0.003	0.955	0.040	0.823	0.004	0.054	0.070	37.864	0.17	98.1
104.0	0.003	0.168	0.016	0.194	0.004	0.044	0.031	40.707	0.10	99.2
103.5	0.003	3.424	0.127	1.157	0.009	0.140	0.184	31.384	0.53	96.2
102.5	0.003	0.226	0.053	0.790	0.006	0.042	0.113	39.635	0.11	97.8
102.0	0.003	0.676	0.097	2.564	0.014	0.066	0.114	37.98	0.23	95.0
101.5	0.003	0.702	0.073	3.142	0.008	0.096	0.102	35.27	0.38	93.9
101.0	0.003	0.234	0.092	1.361	0.012	0.081	0.136	40.1615	0.21	96.7
100.0	0.003	0.249	0.087	3.005	0.006	0.057	0.121	36.905	0.12	92.3
94.0	0.003	0.278	0.102	0.506	0.008	0.068	0.132	41.594	0.23	97.4
89.5	0.003	0.253	0.073	0.569	0.006	0.132	0.084	40.4855	0.18	98.0
89.0	0.003	0.475	0.016	4.453	0.003	0.049	0.026	35.742	0.14	88.1
88.0	0.003	0.258	0.039	0.327	0.003	0.104	0.064	40.7665	0.15	98.7
87.5	0.003	0.364	0.094	0.630	0.010	0.129	0.123	41.027	0.31	97.6
82.0	0.003	0.331	0.016	4.140	0.003	0.026	0.036	34.709	0.08	86.6
81.0	0.003	0.235	0.042	0.496	0.005	0.078	0.071	41.511	0.19	98.5
80.0	0.003	0.276	0.216	1.928	0.008	0.078	0.326	38.633	0.16	96.7
79.0	0.003	0.176	0.016	0.444	0.003	0.036	0.042	42.069	0.12	98.3
76.5	0.003	1.601	0.016	0.593	0.007	0.087	0.063	38.55	0.16	98.1
72.5	0.003	0.330	0.734	3.115	0.024	0.210	0.884	35.665	1.09	88.0
72.0	0.003	0.331	0.493	2.604	0.011	0.207	0.695	36.257	0.63	92.1
71.0	0.003	0.254	0.041	0.749	0.010	0.111	0.077	41.452	0.33	96.6
69.0	0.003	0.175	0.016	0.179	0.009	0.062	0.036	42.578	0.30	98.2
68.0	0.003	1.269	0.056	1.496	0.005	0.067	0.098	37.471	0.20	95.8
66.5	0.003	0.206	0.081	1.052	0.033	0.296	0.134	40.174	0.74	95.5
66.0	0.003	0.303	0.254	1.879	0.014	0.414	0.359	38.291	1.17	92.1
65.5	0.003	0.514	0.390	4.597	0.017	0.857	0.522	33.568	1.36	87.1
65.0	0.039	2.242	1.594	8.381	0.025	2.553	1.771	19.863	1.95	72.0
64.5	0.007	0.660	0.944	9.559	0.021	0.884	1.095	24.736	2.14	76.0
64.0	0.003	1.465	1.303	10.067	0.023	1.495	1.408	23.277	2.46	73.6
63.5	0.007	1.633	2.352	11.390	0.036	1.949	2.362	18.039	2.07	67.5
63.0	0.003	0.444	0.647	8.202	0.014	0.225	0.801	28.625	0.51	83.7
62.5	0.003	0.389	1.335	10.481	0.030	0.611	1.508	24.338	0.99	76.5
62.0	0.003	0.327	0.327	4.281	0.010	0.162	0.426	35.747	0.38	92.2
61.5	0.003	0.505	0.200	1.745	0.010	0.139	0.328	38.502	0.23	95.0
61.0	0.003	0.367	0.142	0.914	0.010	0.180	0.220	40.239	0.22	97.4
60.0	0.003	0.385	0.198	3.622	0.008	0.201	0.250	35.9	0.27	91.6
59.0	0.003	12.646	0.016	0.265	0.002	0.037	0.025	20.783	0.23	98.2
57.0	0.003	0.598	0.424	2.858	0.010	0.181	0.588	36.143	0.35	93.1
56.5	0.003	0.307	0.088	1.221	0.006	0.113	0.151	39.979	0.20	96.5
54.0	0.003	0.384	0.064	0.695	0.008	0.109	0.106	41.185	0.17	98.2
53.5	0.003	0.532	0.040	0.448	0.007	0.096	0.082	40.82	0.13	98.8
51.5	0.003	0.331	0.196	1.852	0.011	0.148	0.288	38.767	0.29	94.9
51.0	0.003	0.339	0.243	1.478	0.008	0.188	0.345	39.119	0.46	94.8
44.0	0.003	0.193	0.411	2.171	0.002	0.191	0.579	38.193		
43.5	0.003	1.217	0.084	0.571	0.007	0.122	0.128	38.914		
40.0	0.003	12.940	0.016	0.148	0.000	0.050	0.060	20.909	0.15	99.1
38.0	0.003	11.388	0.378	1.423	0.006	0.081	0.523	20.523	0.13	95.4
36.0	0.003	12.246	0.356	1.664	0.009	0.113	0.574	19.624	0.20	95.2

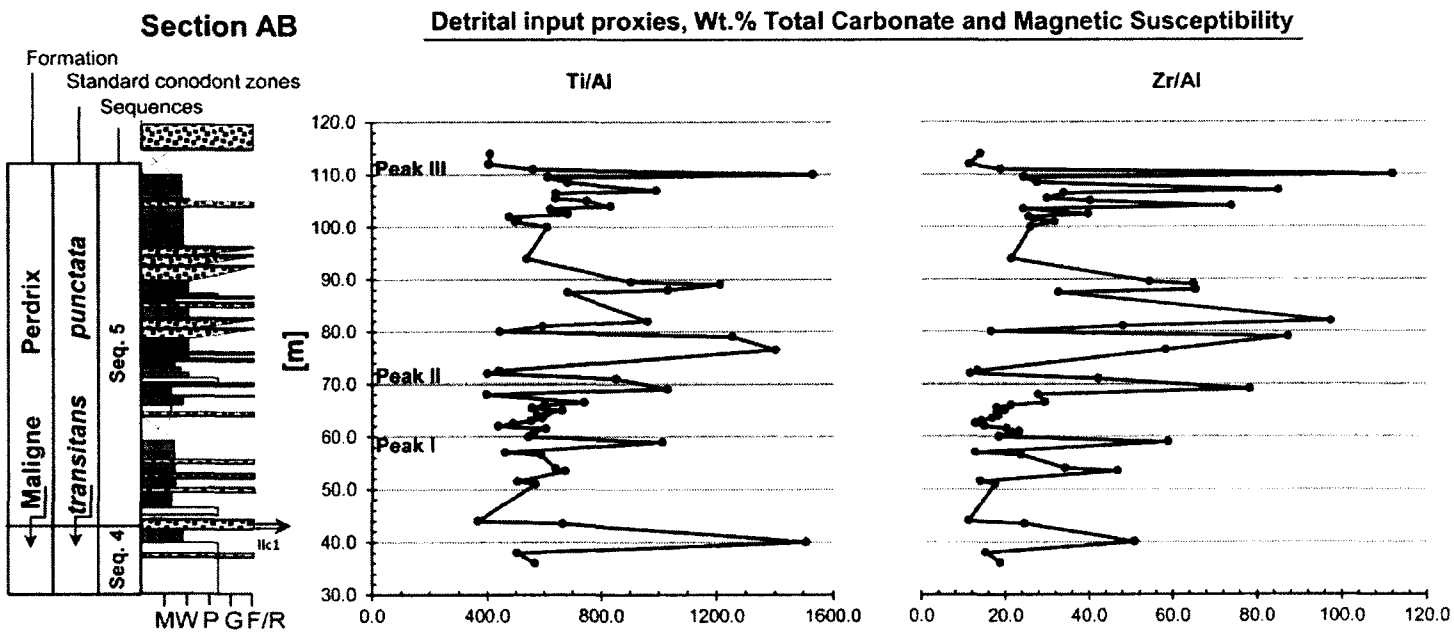

Fig. 3B-1. Expanded and refined version of chemostratigraphic trends in the Ti/Al and Zr/Al ratios originally presented in Fig. 3.5 in Śliwiński et al. (2010). Ti and Zr data generated using PROTrace XRF calibrations; Al data generated using my protocols.

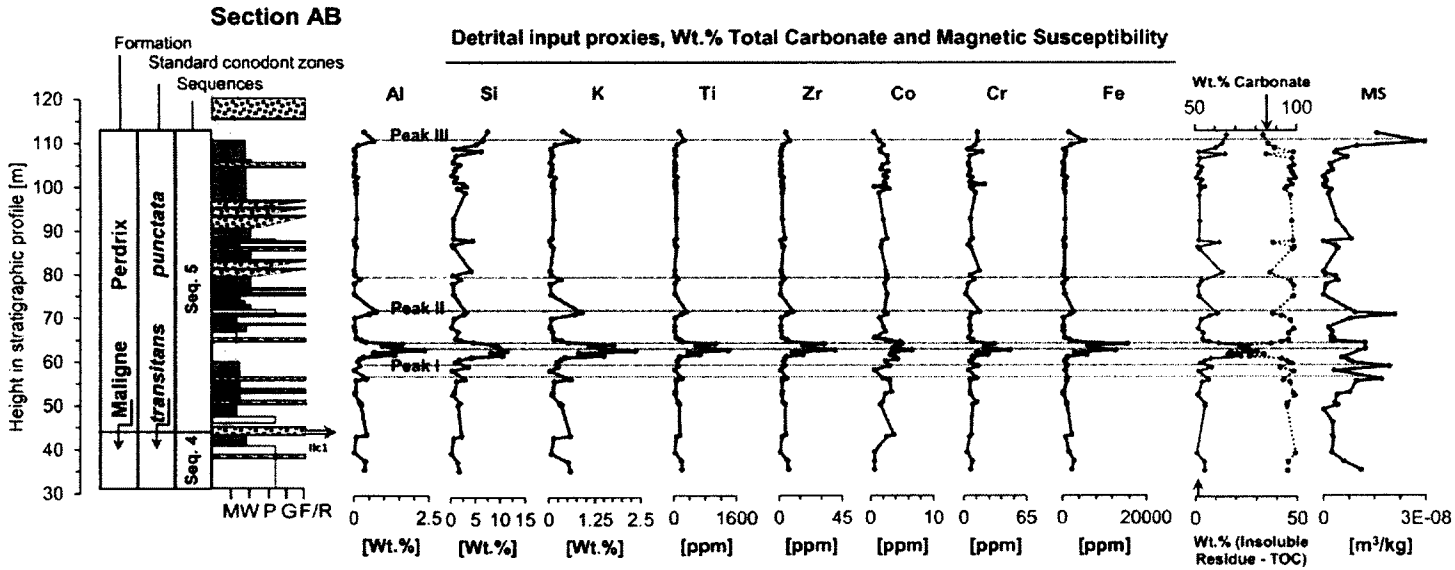

Fig. 3B-2. The MS profile throughout the *punctata* Zone in the WCSB plotted against the stratigraphic distributions of clastic proxies and acid insoluble limestone residues. Circled crosses denoted samples whose acid insoluble mineralogy was determined by capillary XRD analyses (Chapter 5). Pulses of increased clastic input (Peaks I-III) correspond to excursions of bioproductivity and paleoredox proxies (Śliwiński *et al.*, 2011). Gray stripped area indicates the lowest possible but also the most probable position of the *punctata-hassi* zonal boundary, which is situated within a 28 m covered interval (Whalen and Day, 2008, 2010). Al, Si and K data generated using my analytical protocol; trace elements determined using PROTrace XRF calibrations.

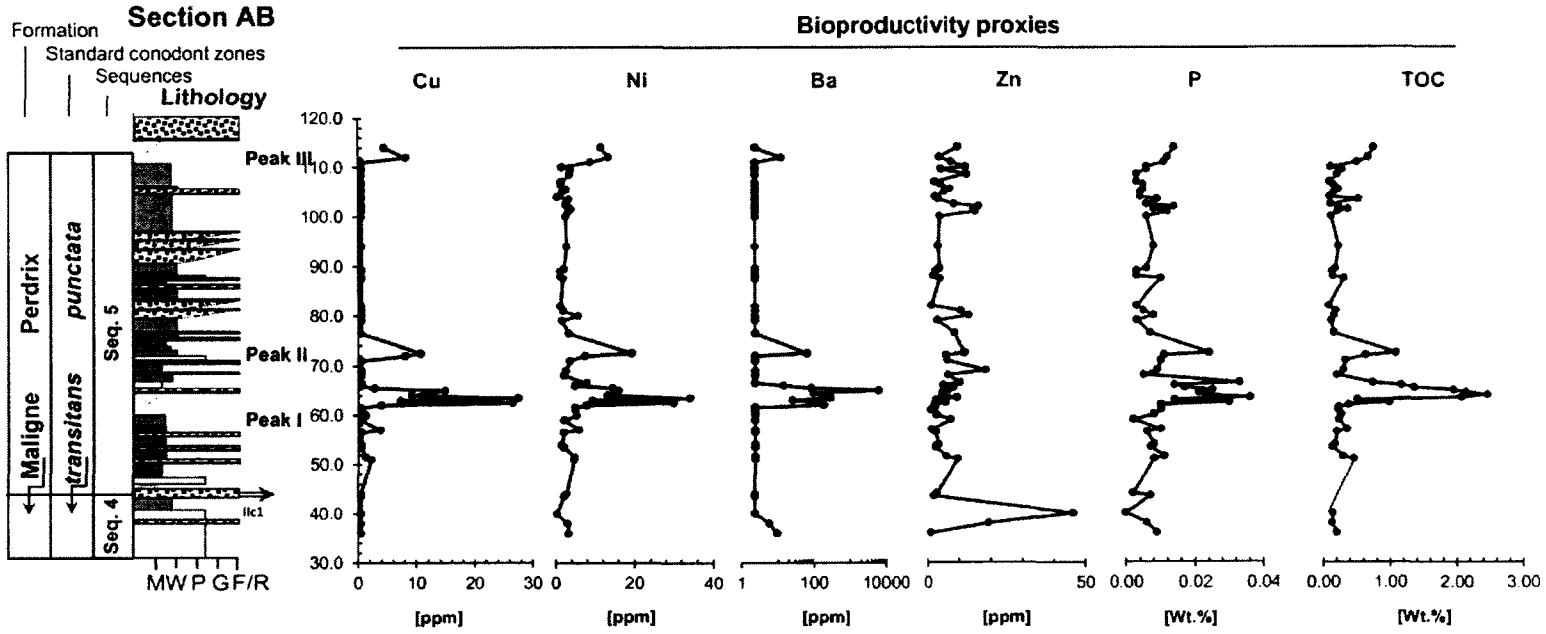

Fig. 3B-3. Refined and expanded chemostratigraphic distributions of paleoproductiv proxies. Trace element data generated using PROTrace XRF calibrations.

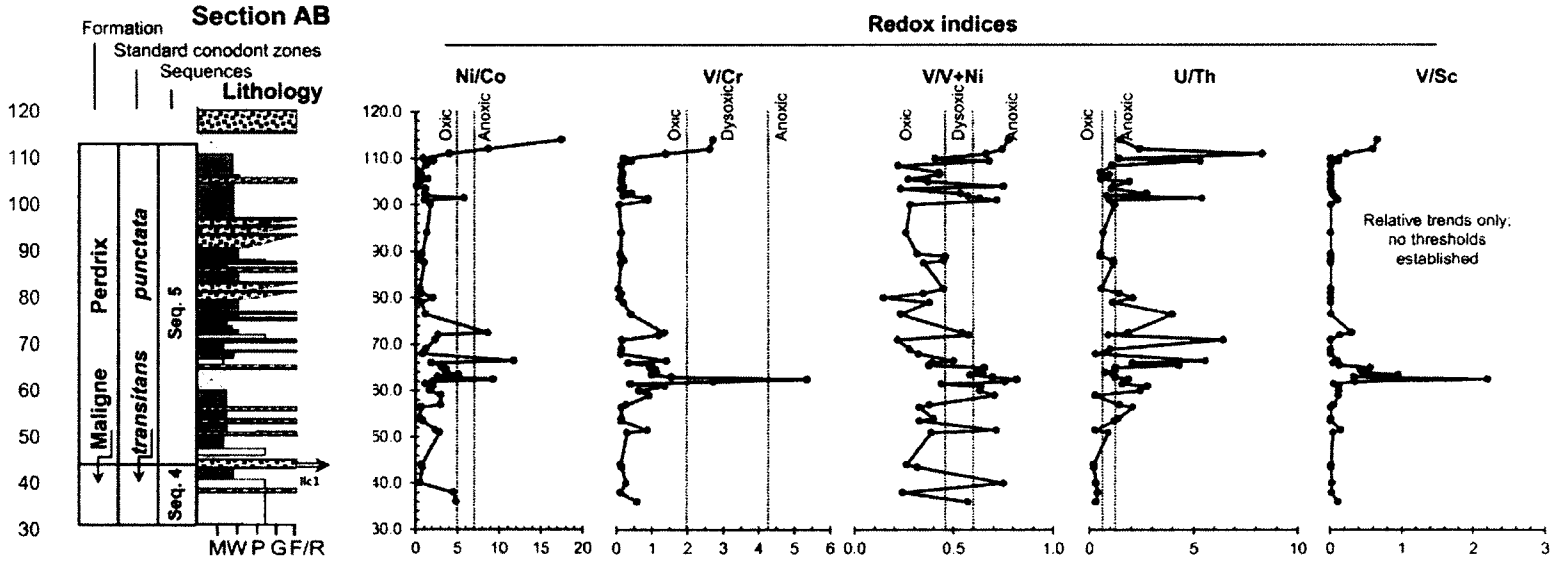

Fig. 3B-4. Refined and expanded chemostratigraphic distributions of paleoredox indicies (see Table 3.2). V/Sc: see Powell, W.G., 2009. Comparison of geochemical and distinctive mineralogical features associated with the Kinzers and Burgess Shale formations and their units. *Palaeogeography, Palaeoclimatology, Palaeoecology*, **277,** 127-140. Data generated using PROTrace XRF calibrations.

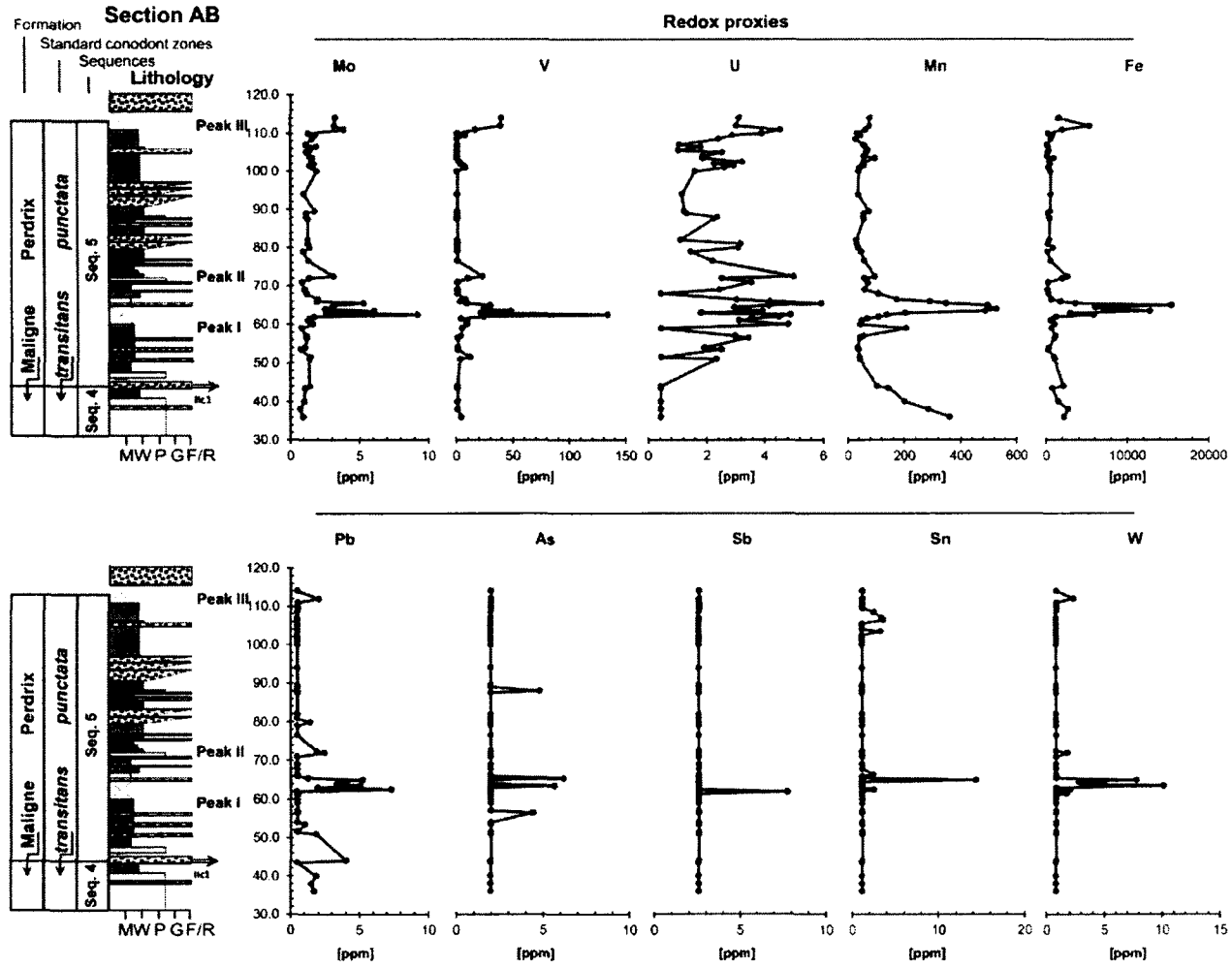

Fig. 3B-5. Refined and expanded chemostratigraphic distributions of paleoredox proxies (Tribovillard et al., 2006). Data generated using PROTrace XRF calibrations.

Table 3B-3. Upper Continental Crust and North American Shale Composite values for P, Ni, Cu, V, Mo, U and Al. The average expected detrital contribution to a sample's minor and trace element abundance can be assessed based on a given sample's Al abundance (Tribovillard et al., 2006). Chemostratigraphic enrichments of bioproductivity and redox-sensitive proxies above UCC/NASC levels can be used to infer the presence of oceanographic conditions favorable to their accumulation. See Fig. 3B-6.

Upper Continental Crust (UCC): Rudnick and Gao (2004).							
	P	**V**	**Ni**	**Cu**	**Mo**	**U**	**Al**
	0.0655	97	47	28	1.1	2.7	8.15
North American Shale Composite (NASC): Gromet et al. (1984)							
	P	**V***	**Ni**	**Cu***	**Mo***	**U**	**Al**
	0.065	**97**	**58**	**28**	**1.1**	**2.66**	**9.02**
D.F.		**UCC used**		**UCC used**	**UCC used**		
0	**0**	**0**	**0**	**0**	**0**	**0**	**0**
0.1	**0.0065**	**9.7**	**5.8**	**2.8**	**0.11**	**0.266**	**0.902**
0.25	**0.01625**	**24.25**	**14.5**	**7**	**0.275**	**0.665**	**2.255**
0.5	**0.0325**	**48.5**	**29**	**14**	**0.55**	**1.33**	**4.51**
1	**0.065**	**97**	**58**	**28**	**1.1**	**2.66**	**9.02**

D.F. = concentration factor used to calculate the detrital contribution to a sample's minor and trace element abundances based on it Al content. Al is considered to be almost entirely of detrital origin (Tribovillard et al., 2006).

* UCC values used if NASC value not available.

Rudnick, R.L. and Gao, S. 2004. Composition of the Continental Crust. *In:* Treatise on Geochemistry, Vol. 3 (Rudnick, R.L., Ed.), 1-64.

Gromet, L.P., Dymek, R.F., Haskin, L.A. and Korotev, R.L., 1984. The 'North American shale composite' - Its compilation, major and trace element characterstic. *Geochimica et Cosmochimica Acta,* **48**, 2469-2482

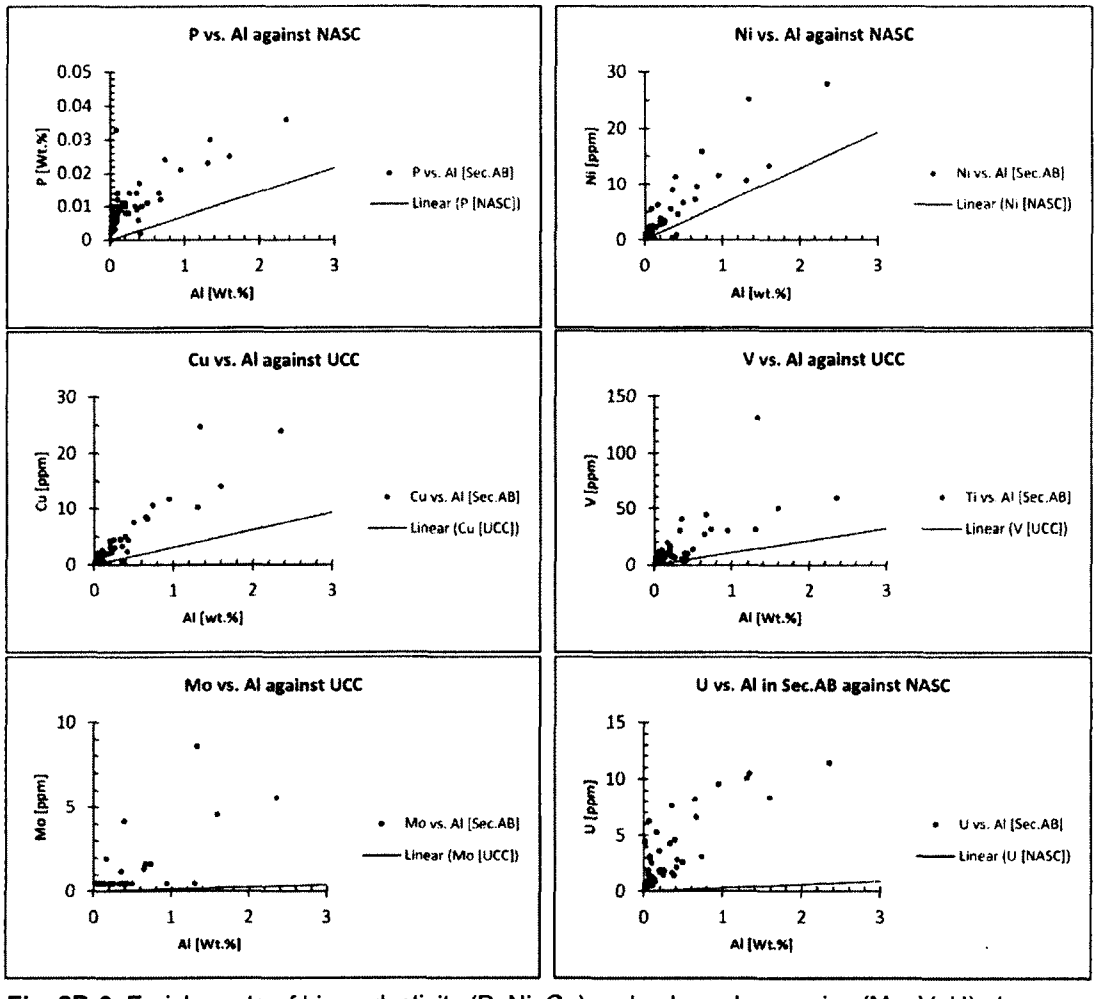

Fig. 3B-6. Enrichments of bioproductivity (P, Ni, Cu) and paleoredox proxies (Mo, V, U) above North American Shale Composite levels throughout the *punctate* Event stratigraphy at the Miette carbonate platform in the WCSB. In the absence of a NASC value, minor and trace element concentrations in UCC were used (Table 3B-3). Enrichments of all proxies above NASC/UCC levels supports the idea that physical processes other than changes in the detrital input were responsible for the trace element excursions noted throughout the *punctate* Zone (see also the use of factor analyses in Chapter 5). Elevated levels of Mo, U and V support the notion of anoxia near the sediment-water interface, allowing for the preservation of OM and it's proxies.

Appendix 3C.
Geochemistry of Mn in the *punctata* Event stratigraphy

3C.1. Introduction

In this appendix I revisit the question of the stratigraphic Mn enrichment associated with the most prominent of the three trace element excursions (Peak I of III, Fig. 3B-1) of the *punctata* Event in the Western Canada Sedimentary Basin (WCSB). This accumulation of Mn corresponds to an interval within the stratigraphy that is best interpreted as an episode of eutrophication-induced benthic anoxia in a carbonate depositional environment (Chapters 3, 4 and 5), and seems to constitute a variant of Mn-trapping that is not explicitly considered in the reviews of trace metal use as proxies for paleoredox and paleoproductivity conditions outlined by Calvert and Pedersen (1993) and updated by Tribovillard et al. (2006).

The use of trace metal proxies in paleoceanography seems to focus predominately on shale systems (Schultz and Rimmer, 2004), in which Mn trends have been used to distinguish between anoxia below the sediment-water interface versus anoxia in the overlying water column (*e.g.* Sageman et al., 2003; Riquier et al., 2006). In depositional environments where carbonate sediment dominates, however, the use of Mn as a proxy may need to be reconsidered in terms of the information it provides about depositional processes. While Tribovillard et al. (2006) conclude that Mn is of limited use as a redox proxy because of its exceptional mobility across redox gradients, its apparent trapping in carbonate systems through incorporation into carbonate minerals during diagenesis under anoxic conditions in organic matter (OM)-rich sediments indicates some utility; recent geochemical analyses of other Late Devonian profiles seem to confirm this alternate behavior of Mn in carbonate systems (Racka et al., 2010). Both Mn-carbonates ***and*** MnS form readily in the anoxic sapropels of the Landsort Deep sub-basin of the Baltic Sea, and their genesis has been ascribed to changes in the alkalinity of pore waters within OM-rich sediments under sulfate-reducing conditions (Suess, 1979; Lepland and Stevens, 1998). Preliminary data using synchrotron-based μ-XRF mapping of elemental proxy distributions indicates that MnS may be the predominant host phase of the Mn enrichment observed in the one of the most OM-rich horizons associated with the *punctata* Event in the WCSB, but may exist also in solid solution with the surrounding carbonate sediment.

3C.2. Mn accumulation in the *punctata* Event stratigraphy in the WCSB

3C.2.1. Chemostratigraphic distribution of Mn

The chemostratigraphic distribution of Mn in the *punctata* biozone stratigraphy at the Miette platform (Section AB) reveals two prominent enrichment zones:

1) Between 36.0 and 44.0 m in profile (Section AB, Fig. 3B-1), a dolomitized interval is enriched in Mn by a factor of 3 above stratigraphic background levels (~80ppm), and is probably hosted in solid solution with the disordered, non-stoichiometric, calcian dolomites described by Melim et al. (2000) at the Miette carbonate platform (see Chapter 4). In its reduced state, Mn^{2+} readily substitutes for the Ca^{2+} cations within carbonate minerals (Veizer, 1983). Because this enrichment interval is confined to a narrow dolomitzed zone within the stratigraphy, it is omitted from the statistical considerations (factor analyses) described below.

2) Between 59.0 and 68.0 m in profile (Section AB, 3B-1), Mn is enriched by a factor of 4 above stratigraphic background levels (~80ppm). This excursion corresponds to the most prominent trace element anomaly of the *punctata* Event (Chapter, 3, Peak I of III at 61.5-66.5 m in profile as described in Chapter 4), which is best interpreted as an episode of regional eutrophication and subsequent benthic anoxia on the basis of sedimentary OM accumulation (TOC up to 2.46 wt.%), redox-sensitve trace metal enrichments, sedimentary characteristics (laminated sediment), and changes in the regional C and N cycling recorded by excursions of isotopic proxies (Chapter 4). Significantly, the highest observed Mn concentrations within the stratigraphy correspond to the highest observed TOC contents (at 63.5 m in profile: Mn = 490.0 ppm, TOC = 2.07 wt.%; 64.0 m, Mn = 528.4 ppm, TOC = 2.56 wt.%; 64.5 m, Mn = 500.8 ppm, TOC = 2.14 wt.%; 65.0 m, Mn = 495.8 ppm, TOC = 1.95 wt.%; stratigraphic background: Mn = 80 ppm, TOC = 0.3 wt.%) while the total carbonate content of the sediment remains high (67.5-72.0 wt.%), indicating that changes in the sediment pore water chemistry during OM decomposition under sulfate reducing conditions may have spurred conditions favorable to Mn trapping in diagenetic carbonate or sulfide mineral phases (*cf.* Suess, 1979; Lepland and Stevens, 1998).

3C.2.2. Decoupling authigenic Mn enrichments from the siliciclastic input through statistical factor analysis

3C.2.2.1. *General considerations*

Is the Mn enrichment within the *punctata* Event stratigraphy a mere artifact of the lithological change associated with the main trace element excursion (Peak I, Chpater 4), mainly a decrease in the total carbonate content (down to 67.5-72.0 wt.%) and an increase in the abundance of acid-insoluble siliciclastics (up to 30.5 wt.%) that are the dominant carrier phase of trace elements in marine depositional environments (van der Weijden, 2002; Tribovillard et al., 2006)? Marine sediments are composed of some or all of the following 'phases': 1) detrital minerals (*e.g.* quartz, feldspars, clays, etc.), 2) carbonate minerals (primary and diagenetic), 3) biogenic silica, 4) organic matter, 5) authigenic clay minerals, 6) hydrogenous phases such as Fe and Ms oxides, and 7) authigenic sulfides (*e.g.* van der Weijden, 2002). Trace elements can be hosted and associated in variable proportions with any of these phases, and thus the total sedimentary trace element content is calculated by summing the elemental concentrations associated with each extant phase, weighted to reflect its overall contribution to the sedimentary makeup. This can be expressed mathematically as a closed-sum problem taking the form:

(Eq. 3B.1) $$M_{tot} = aM_{detrital\ fraction} + bM_{carbonates} + cM_{clays} + dM_{organic\ matter} + eM_{authigenic\ phases} + fM_{silica}$$

where 'M' is the concentration of any given trace element and 'a-f' are weight fractions of each respective phase that makes up the sediment. Considering the carbonate system at the Miette platform, this equation can be simplified to:

(Eq. 3B.2) $$M_{tot} = aM_{detrital\ fraction\ +\ clays} + bM_{carbonates} + cM_{organic\ matter} + eM_{authigenic\ phases}$$

As Al is considered to be primarily of detrital origin (Tribovillard et al., 2006), its abundance measured within bulk samples is often used as a means of decomposing the overall trace element signal of any element that can be associated with the siliciclastic fraction into 1) the dominant clastic-hosted/adsorbed contribution and 2) the lesser contributions from other possible carrier phases (OM, authigenic phases, etc.); in shale systems especially, the magnitude of the clastic contribution easily overshadows all others, and requires additional recourse to calculations of enrichment and depletion factors relative to 'reference shales.' However these methods are plagued with serious pitfalls if applied carelessly (see van der Weijden, 2002). A severe limitation in their application in the geochemisty of carbonate lithologies relates especially to the degree of

uncertainty associated with accurately and precisely determining the often very low Al abundances (< 0.1 wt.%, as noted in the Section AB stratigraphic profile). Using Al as a common divisor in such a case increases the potential for creating spurious correlations, *c.f.* those discussed by van der Weijden (2002). Ti and Zr can also be used for this purpose, and have the advantage of posing less analytical difficulties by X-ray fluorescence spectroscopy (XRF, Chapter 2). Both elements are strongly enriched in association with most prominent trace element anomaly of the *punctata* Event (Chapters 4 and 5; Peak I of III at 61.5-66.5 m in profile), indicating that a substantial portion of the trace element excursions is likely related to the increased clastic loading; the magnitude of this effect is assessed below via the use of a simple factor analysis.

3C.2.2.2. Statistical methods

Factor analyses (Davis, 2002) were performed using the SPSS statistical package and the geochemical dataset in Appendix 3A; PROTrace XRF data was used as an input for the trace element variables. The variables considered are: Ti, Zr, Al (clastic proxies), Fe, S, and the pyrite abundance of a sample subset (Chpater 5), Mo, V, U (redox proxies), TOC, P (bioproductivity proxies), the total carbonate content within the stratigraphy, and Mn (excluding the datapoints lying within the dolomitized interval; see detailed discussion in Chapter 5, which focuses on the statistical associations of redox and paleoproductivity proxies with changes in the detrital input and magnetic susceptibility). Log-transforms were applied before higher-level data analysis to normalize data distributions if the original distribution failed a one-sample Kolomogrovo-Smirnov (K-S) test of distribution normalcy. Based on a principal component analysis, relevant factors were extracted for further analysis by identifying those factors with eigenvalues greater > 1.0. This approach retains all factors that contain greater variance than the original standardized variables and was found to be a useful approach if the original variables are highly correlated (Davis, 2002). Subsequent to factor selection, a factor rotation was applied using Kaiser's varimax scheme to optimize the factor position and support factor interpretation.

3C.2.2.3. Factor analysis outcomes

Two components were extracted in the factor analysis and collectively explain 86.6% of total dataset variance (Fig. 3B-2, Table 3B-1). The choice of the number of components to extract is driven by 1) considering only those factors that show eigenvalues > 1, thus accounting for more of the total variance than explained by any of the original input variables, 2) by extracting as many factors as necessary to account for at least 75% of total dataset variance, or 3) by extracting as many factors as the theory considered demands (Davis, 2002). In this particular scenario I was

interested in observing how the multivariate geochemical dataset partitions among only two components that represent 1) the suite of physical processes responsible for fluvial and eolian clastic delivery to the WCSB ('detrital input,' Fig. 3B-2) and 2) the development of benthic anoxia, which is conducive to the excess accumulation of OM and its proxies (TOC, P), redox-sensitive trace metals (U, Mo, V) and authigenic sulfide formation within the sediment. The properties of the first two components extracted satisfy all three of the conditions stated above (Fig. 3B-2, Table 3B-1) and allow for determining 1) the extent to which Mn associates with the redox-sensitive and bioproductivity proxies considered (Mo, V, U, Fe, S, Pyrite, TOC, P) and 2) to what extent the variance in stratigraphic distribution of Mn and of the redox sensitive proxies is controlled by changes in the detrital input. Component 1, which explains 45% of total variance, most readily represents the detrital input as it received heavy loadings from Ti, Zr and Al (r = 0.972-0.938; Table 3B-1). Predictably, the total carbonate content is inversely related to the clastic content, and is anti-correlated with Component 1 (r = -0.456; Table 3B-1). Component 2 accounts for an additional 41.5% of total variance and received heavy loadings from Mn and all redox-sensitive proxies (r = 0.972-0.762; Table 3B-1). These two components allow for a clear distinction between the accumulation of redox-sensitive proxies resulting solely from increases in the clastic content of the carbonates in question vs. accumulation associated with anoxic scavenging from the water column and sulfide authigenesis within the sediment (*e.g.* pyrite and probably MnS discussed below). Importantly, the chemostratigraphic distribution of Mn shows a clear association with excursions of the redox proxies and essentially no association with the increased detrital input observed throughout the most prominent trace element anomaly of the *punctata* Event (Peak I, Fig. 3B-2), indicating that the anoxic conditions interpreted for that stratigraphic interval may be especially important for Mn trapping in this carbonate depositional system.

3C.2.3. Mapping Fe and Mn distributions using synchrotron μ-XRF: Preliminary results

3C.2.3.1. Samples and methods

The anoxic interval within the lower *punctata* Zone at the Miette platform (Peak I, Fig. 3B-1) was sub-sampled, in part for mapping the spatial distributions of Fe and Mn using micro-focused X-ray fluorescence spectroscopy. The chosen sample at 63.5 meters in profile (Section AB, Fig. 3B-1) was prepared into a doubly-polished (0.25 μm), 30 μm petrographic thin section, mounted on a quartz slide which contains less impurities than standard glass backings. Measurements were performed at the Stanford Synchrotron Radiation Lightsource (SSRL) using the μ-XRF capabilities of Beamline 10-2. Synchrotron radiation at this beamline is generated by

bending the flight path of relativistic electrons in a 30-pole, 1.45-Tesla Wiggler (Sham and Rivers, 2002; Sutton et al., 2002), which allows for a focused energy range between 4.5 and 30 keV. The experimental setup is depicted in Fig. 3B-3. Synchrotron radiation from the SSRL storage rings enters the experimental hutch and is attenuated as needed by variably thick Al-metal absorbers and passes through a monochromator which consists of a Si diffracting crystal (Si 111) that transmits only a single desired X-ray energy from among the broad continuum of energies of the primary white synchrotron light (Sutton et al., 2002). The beam then passes through collimating slits and an ion chamber that measures its intensity. A capillary then micro-focuses the beam and the beam spot size on the sample is controlled by moving the sample stage closer to, or farther away, from the capillary (beam size used: ~50 μm^2, ~20 μm^2). The beam then strikes the sample mounted on a xyz stage (air atmosphere) at a 45° angle; fluorescent radiation is detected by an energy-dispersive Ge-array detector (capable of measuring eight (8) energy channels simultaneously) positioned at 90° to the incident beam and at 45° to the sample surface to ensure optimal background reduction (Sutton et al., 2002).

Spatial distributions of Fe, Mn and Ca were mapped by collecting line scans using a ~50 µm spot size and a 25 ms dwell time; the incident (excitation) beam energy was kept at 9 keV and 350 mA. An additional Fe map was collected using a higher excitation energy of 13 keV, a ~20 µm spot size and a 75 ms dwell time.

3C.2.3.2. Fe-Mn distributions and probable Mn-trapping mechanisms

Spatial mapping of element distributions indicates that both Fe and Mn are contained predominantly within the authigenic sulfides noted in thin section (sample 63.5; Figs. 3B-4, 5 and 6), which are in turn associated with patches of OM (Fig. 3B-7). Because Mn does not exist in solid solution within pyrite, it is probably present as its own sulfide. It is expected that Mn trapping within carbonate sediments under near-normal marine conditions will most likely occur through 1) co-precipitation in solid solution with calcium carbonates, 2) precipitation of the manganoan carbonates kutnahorite ($Ca(Mn,Mg,Fe)(CO_3)_2$) or rhodocrostie ($MnCO_3$) or 3) precipitation as a sulfide if H_2S is present within pore waters. Based on thermodynamic considerations, Mn in oxic seawater should exist primarily as Mn-oxides and hydroxides (MnO_2 or MnOOH), although because of slow oxidation kinetics, the reduced form seems to predominate along with $MnCl^+$ (Calvert and Pedersen, 1993 and Tribovillard et al., 2006). Under reducing conditions, such as those common in organic-rich sediments, Mn preferentially exists as the Mn^{2+} cation, and the dissolution of Mn-oxide particles that settle out an oxic water column provides a source of 'excess' benthic Mn (Tribovillard et al., 2006).

Manganese is predominantly supplied to the oceans in the form of coatings on aeolian and riverine particulate materials (Calvert and Pedersen, 1993). Maximum concentrations in the water column coincide with oxygen-minimum zones where the dissolution of settling Mn-oxides takes place under increasingly reducing conditions; dissolved Mn^{2+} accumulates also in the deep sulfidic waters of anoxic basins (Calvert and Pedersen, 1993). Calvert and Pedersen (1993) suggest, however, that high sedimentary concentrations of Mn in the form of Mn-carbonates (kutnahorites and rhodochrosites) indicate sediment accumulation under well oxygenated water masses; this is because Mn-oxyhydroxides must necessarily first accumulate at the sediment-water interface if subsequent burial below the redoxicline is to release enough dissolved Mn^{2+} into the sediment pore waters to exceed the solubility product of a carbonate phase. Rhodochrosite is unlikely to exist as a pure phase, however, because the range of activities of the necessary components in marine pore waters are commonly not in equilibrium with a pure form of this phase. However, this model of Mn trapping seems to pertain predominantly to clastic depositional settings (see also Tribovillard et al., 2006). Thus in Calvert and Pedersen's (1993) model, Mn-trapping occurs only once the solubility product of a carbonate phase approaching the $MnCO_3$ end-member is exceeded. In carbonate-rich sediments, however, such as those under study in the Western Canada Sedimentary Basin (Fig. 3B-1), Mn^{2+} is strongly sorbed from solution onto $CaCO_3$ (Middleburg et al., 1987). Field and laboratory simulations reported by Middleburg et al. (1987) indicate that dissolved Mn(II) concentrations in carbonate-rich sediments can be an order of magnitude lower than in carbonate-poor sediments because of this active scavenging by $CaCO_3$ and subsequent incorporation of Mn(II) into a mixed Ca-Mn carbonate phase. Thus the pore water solutions within carbonate sediments are unlikely to enter into equilibrium with pure $MnCO_3$ (rhodochrosite) (Pedersen and Price, 1982), and Mn will instead be preferentially hosted as a mixed manganoan calcium carbonate (Middelburg et al., 1987).

An Eh-pH diagram of thermodynamic phase stabilities in seawater for the system Mn-C-O-S can be used as an approximate guide for the pore water conditions required for Mn trapping in carbonates versus in sulfide form (Fig. 3B-8A-D). Simple modeling of this system indicates that the pore water activity of Mn^{2+} and of the $MnSO_4$ complex (8.63E-10) must increase by at least 3 orders of magnitude if the pore waters are to be in equilibrium with a increasingly pure Mn-carbonate phase and with the MnS (alabandite). This model assumes that the SO_4^{2-} activity is at the present seawater value of 2.66×10^{-3} and depicts three different pore water CO_2 saturation scenarios of 3, 10 and 30 times the equilibrium saturation with the present atmosphere ($10^{-3.5}$). The high-end value of 30 times saturation derives from the reporting of Ben-Yaakov (1973), whose modeling of the theoretical pH range of anoxic marine pore waters suggests values between 6.9 and 8.3 pH units, and is consistent with data from Recent anoxic sediments. The

increasing CO_2 concentration resulting from OM decomposition serves to expand the stability field of rhodochrosite, although given the arguments presented above for carbonate-rich sediments, Mn^{2+} saturation should not reach equilibrium with pure $MnCO_3$ before Mn-uptake by mixed Mn-Ca carbonate phases occurs, giving rise to Mn-calcites or pseudokutnahorites (*sensu* Mucci, 1988; see also Pedersen and Price, 1982; Middelburg et al., 1987; Mucci, 1988; Calvert and Pedersen, 1993). Spatial mapping of Mn distributions within the examined thin section points to the probable presence of a MnS phase (Fig. 3B-5); it is however also possible that the Mn-rich carbonate phase constitutes the matrix of the observed sulfide patches (Fig. 3B-6 and 7). The spatial resolution afforded by this preliminary work does not allow for a clear distinction to be made, and thus this question awaits further study. Theoretically, however, either or both phases could be present; the presence of framboidal pyrite (Fig. 3B-6 and 7) indicates strongly anoxic (sulfidic) conditions (Wignall and Newton, 1998) within the pore waters, and thermodynamic considerations (Fig. 3B-8) indicate MnS stability in the presence of increased Mn activity (at least 3 orders of magnitude above present seawater values). Such conditions are at present considered rare but are not unknown in the geologic record. Both hexagonal and cubic forms of MnS have, for example, been extensively documented from the diagenetic environments that prevail in anoxic, organic matter-rich sedimentary sequences (sapropels) of the Baltic Sea, and result in the formation and *co-occurrence* of both spherical Mn-carbonate particles and aggregates and MnS (Fig. 1 in Suess, 1979; Fig. 5 in Lepland and Stevens, 1998).

Sedimentary manganese trapping in carbonates or in sulfide phases requires a sufficient local source of this metal to raise the activity of dissolved Mn^{2+} in sediment pore waters several orders of magnitude above present seawater values (Fig. 3B-8; Lepland and Stevens, 1998). Within the framework of what is presently known about the geochemistry of Mn in the oceans (Calvet and Pedersen, 1993; Tribovillard et al., 2006), the most readily available source of this metal is the particle flux of sinking Mn-oxyhydroxides which dissolve below the redoxicline, be it in the water column, at the sediment-water interface, or below it. Mn concentration maxima in the modern ocean coincide with oxygen-minimum zones, where the dissolution of settling Mn-oxides takes place under increasingly reducing conditions (Calvert and Pedersen, 1993). Thus there are several possible explanations for the observed Mn-enrichment noted in the *punctata* Event stratigraphy at the Miette platform:

1) As originally reported in the initial *punctata* Event study in the WCSB (Chapter 3), the Mn excursion could be the basis for a distinction between benthic anoxia in a stratified water-column vs. anoxic conditions only below the sediment-water interface; the latter conditions within the depositional environment could account for concurrent enrichments

of both Mn *and* sulfide-forming metals, however only if the Mn-trapping mechanism of Tribovillard et al. (2006) is considered (Chapters 3 and 4; see also Riquier et al., 2006).

2) Because Mn concentration maxima in the Modern ocean coincide with the oxygen-minimum zone (OMZ), an expansion of a well-developed Late Devonian OMZ (Jewell, 1995; Witzke, 1987) into the epeiric seaway and extensive reef system of the WCSB during the IIc1 transgressive event at the base of the *punctata* biozone (Chapters 3 and 4) could have provided the requisite dissolved Mn^{2+} for efficient trapping under anoxic conditions in carbonate-rich sediments.

3) Similar to the model proposed for the deep sub-basins of the Baltic Sea (Lepland and Stevens, 1998), a eutrophication-induced establishment and expansion of basal anoxic water masses onto shallower slope settings at the Miette platform could have promoted the dissolution of Mn-oxyhydroxides in sediments deposited under oxic water masses; this effect could have been augmented by the IIc1 transgression, but also by the possible infringement of the oceanic OMZ into the epeiric seaways (Point 3 above). The main Mn peak does seem to lag stratigraphically behind the *initial* enrichments of the redox proxies (Peak I, Fig. 3B-1), perhaps indicating the formation of a sufficient dissolved Mn^{2+} reservoir as the transgression progressed.

4) Lastly, anoxia may have existed well above the sediment-water interface at the examined stratigraphic section on the slope of the Miette platform, with Mn supplied by the sinking particle flux of Mn-oxyhydroxides. Speculatively, slow dissolution kinetics could have allowed for continued Mn-oxyhydroxide accumulation at the sediment-water interface and eventual dissolution, although this does not seem to be supported by examinations of recent sediments (*e.g.* Fig.1 D in Calvert and Pedersen, 1993). However, much of the Mn in the Modern ocean is supplied as coatings on particulates delivered by eaolian and riverine forces. It is conceivable that much of the Mn needed to produce the observed excursion in the Section AB profile (Fig. 3B-1) could have been supplied as such coatings on the detrital material which is most abundant throughout the stratigraphic interval of trace element Peak I. Subsequent Mn release under anoxic conditions and it's trapping in carbonates and/or sulfide phases just a bit higher in the stratigraphy would constitute a 'host-phase swap,' and would effectively explain the preferential association of Mn with the redox component extracted in the factor analysis presented earlier (Section 3B.2.2.3.).

3C.2.3.3. OM-rich, anoxic sediments and Mn-carbonate precipitation

The precipitation of Mn-carbonates (*sensu* Suess, 1979) seems to be favored by an increase in the carbonate alkalinity of marine pore waters (Calvert and Pedersen, 1993; Lepland and Stevens, 1998), and such conditions can be induced by the products of sedimentary OM decomposition by heterotrophic microbes. Berner et al. (1970) found that microbial sulfate reduction has the most pronounced effect on carbonate alkalinity; if accompanied by ammonia formation, these advanced stages of OM-recyling can produce pore water alkalinities over 30 times as high as the overlying seawater and make them highly supersaturated with respect to $CaCO_3$ and apparently also with respect to Mn-carbonates (Suess, 1979, Lepand and Stevens, 1998). Such reducing conditions occur when the reactants allowing for OM consumption by aerobic respiration and denitrification become depleted, and the oxidation of Mn- and Fe- oxides has taken place. This sequence of reactions is as follows (after Tribovillard et al., 2006, using Redfield ratios of C:N:P = 106:16:1):

Aerobic respiration:

(Eq. 3B-3) $(CH_2O)_{106}(NH_3)_{16}H_3PO_4 + 138O_2 \text{ - > } H_3PO_4 + 16HNO_3 + 138CO_2 + 122H_2O$

Denitrification

(Eq. 3B-4) $(CH_2O)_{106}(NH_3)_{16}H_3PO_4 + 94.4HNO_3 \text{ - > } H_3PO_4 + 55.2N_2 + 106CO_2 + 177.2H_2O$

Mn-oxide reduction

(Eq. 3B-5) $(CH_2O)_{106}(NH_3)_{16}H_3PO_4 + 212Fe_2O_3 + 848H^+ \text{ - > } H_3PO_4 + 424Fe^{2+} + 16NH_3 +$
$+ 106CO_2 + 530H_2O$

Fe-oxide reduction

(Eq. 3B-6) $(CH_2O)_{106}(NH_3)_{16}H_3PO_4 + 236MnO_2 \text{ - > } H_3PO_4 + 236Mn^{2+} + 16NH_3 + 106CO_2 +$
$+ 366H_2O$

Sulfate reduction

(Eq. 3B-7) $(CH_2O)_{106}(NH_3)_{16}H_3PO_4 + 53SO_4^{2-} \text{ - > } H_3PO_4 + 53S^{2-} + 16NH_3 + 106CO_2 + 106H_2O$

CO_2 is a by-product in all OM-oxidation reactions above (equations 1-5), and may contribute further to increasing alkalinity in carbonate-rich sediments through the dissolution of $CaCO_3$:

(Eq. 3B-8) $CO_2 + H_2O + CaCO_3 \text{ < > } Ca^{2+} + 2HCO_3^-$

A significant alkalinity increase occurs with the reduction of Fe- and Mn-oxides and pore water sulfate (equations 3-5), producing the bases NH_3 and S^{2-} which then react with dissolved CO_2 and raise the alkalinity further by the reactions (after Berner et al., 1970):

(Eq. 3B-9) $S^{2-} + CO_2 + 2H_2O \rightarrow H_2S + CO_3^{2-}$

and

(Eq. 3B-10) $NH_3 + CO_2^{-} + H_2O \rightarrow NH_4^{+} + HCO_3^{-}$

(Eq. 3B-11) $NH_3 + HCO_3^{-} \rightarrow NH_4^{+} + CO_3^{2-}$

With H_2S released into the pore waters (Eq. 3B-9), MnS becomes stable if the activity of dissolved Mn^{2+} is sufficiently high (Section 3B.2.3.2.; Lepland and Stevens, 1998).

3C.3. References

Ben-Yaakov, S., 1973. pH buffering of pore water of recent anoxic marine sediments. *Limnology and Oceanography,* **18**(1), 86-94

Berner, R.A., Martha, R.S. and Thomlinson, C., 1970. Carbonate alkalinity in the pore waters of anoxic marine sediments. *Limnology and Oceanography*, **15**(4), 544- 549

Calvert, S.E. and Pedersen, T.F., 1993. Geochemistry of recent oxic and anoxic marine sediments - implications for the geological record. *Marine Geology*, **113**(1-2), 67- 88

Davis, J.C., 2002. *Statistics and Data Analysis in Geology (3rd ed.)*. John Wiley & Sons, New York

De Vleeschouwer, D., Whalen, M.T., Day, J.E., Philippe, C., 2012. Cyclostratigraphic calibration of the Frasnian (Late Devonian) time-scale (western Alberta, Canada). *The Geological Society of America Bulletin*. doi:10.1130/B30547.1

Jewell, P.W., 1995. Geologic consequences of globe-encircling equatorial currents. *Geology*, **23**(2), 117-120

Lepland, A. and Stevens, R.L., 1998. Manganese authigenesis in the Landsort Deep, Baltic Sea. *Marine Geology,* **151**, 1-25

Melim, L.A., Eberli, G.P., and Walgenwitz, F., 2000. Diagenesis of the Miette Buildup, Devonian, Canada – Fabrics and variability. In: Homewood, P.W., and Eberli, G.P., (Eds.), Genetic Stratigraphy on the Exploration and Production Scales— Case Studies from the Pennsylvanian of the Paradox Basin and the Upper Devonian of Alberta, Bulletin Centre Recherche Elf Exploration-Production, Memoire, **24**, 269–284

Middelburg, J.J., De Lange, G.J. and van der Weijden, C., 1987. Manganese solubility control in marine pore waters. *Geochimica et Cosmochimica Acta,* **51,** 759-763

Mucci, A., 1988. Manganese uptake during calcite precipitation from seawater: Conditions leading to the formation of a pseudokutnahorite. *Geochimica et Cosmochimica Acta,* **52,** 1859-1868

Pedersen, T.F. And Price, N.B., 1982. The geochemistry of manganese carbonate in Panama Basin sediments. *Geochimica et Cosmochimica Acta*, **46,** 59-68

Racka, M., Marynowski, L., Filipiak, P. and Sobstel, M., 2010. Anoxic Annulata Events in the Late Famennian of the Holy Cross Mountains (Southern Poland): Geochemical and palaeontological record. *Palaeogeography, Palaeoclimatology, Palaeoecology*, **297,** 549-575

Rickers, K., Thomas, R. and Heinrich, W. 2004. Trace-element analysis of individual synthetic and natural fluid inclusions with synchrotron radiation XRF using Monte Carlo simulations for quantification. *European Journal of Mineralogy*, **16,** 23-35

Riquier, L., Tribovillard, N., Averbuch, O., et al., 2006. The Late Frasnian Kellwasser horizons of the Harz Mountains (Germany): Two oxygen-deficient periods resulting from different mechanisms. *Chemical Geology*, **233**, 137-155

Sageman B.B., Murphy, A.E., Werne, J.P., Ver Straeten, C.A., Hollander, D.J., Lyons, T.W., 2003. A tale of shales: the relative roles of production, decomposition, and dilution in the accumulation of organic-rich strata, Middle–Upper Devonian, Appalachian basin. *Chemical Geology*, **195**, 229– 273

Schultz, R.B. and Rimmer, S.M. 2004. Geochemistry of organic-rich shales: new perspectives. *Chemical Geology*, **206,** 163-165

Sham, T.K. And Rivers, M.L., 2002. A brief overview of synchrotron radiation. *In:* Fenter, P.A., Rivers, M.L., Sturchio, N.C. and Sutton, S.R. (Eds.), Applications of Synchrotron radiation in low-temperature geochemistry and environmental science. *Reviews in Mineralogy and Geochemistry,* **49,** 117-147

Suess, E., 1979. Mineral phases formed in anoxic sediments by microbial decomposition of organic matter. *Geochimica et Cosmochimica Acta,* **43,** 339-352

Sutton, S.R., Bertsch, P.M., Newville, M., Rivers, M., Lanzirotti, A. and Eng, P. 2002. Microfluorescence and microtomography analyses of heterogeneous earth and environmental materials. *In:* Fenter, P.A., Rivers, M.L., Sturchio, N.C. and Sutton, S.R. (Eds.), Applications of Synchrotron radiation in low-temperature geochemistry and environmental science. *Reviews in Mineralogy and Geochemistry,* **49,** 429-483

Tribovillard, N., Algeo, T.J., Lyons, T. and Riboulleau, A., 2006. Trace metals as paleoredox and paleoproductivity proxies: An update. *Chemical Geology*, **232**, 12- 32

Wignall, P.B. And Newtron, R., 1998. Pyrite framboid diameter as a measure of oxygen deficiency in ancient mudrocks. *American Journal of Science,* **298**, 537-552

Witzke, B.J., 1987. Models for circulation patterns in epicontinental seas applied to Paleozoic facies of North America craton. *Paleoceanography,* **2**(2), 229-248

van der Weijden, C.H., 2002. Pitfalls of normalization of marine geochemical data using a common divisor, *Marine Geology*, **184**, 167-187

Veizer, J., 1983. Trace elements and isotopes in sedimentary carbonates, *Reviews in Mineralogy: Carbonates: Mineralogy and Chemistry*, **11**, 265-299

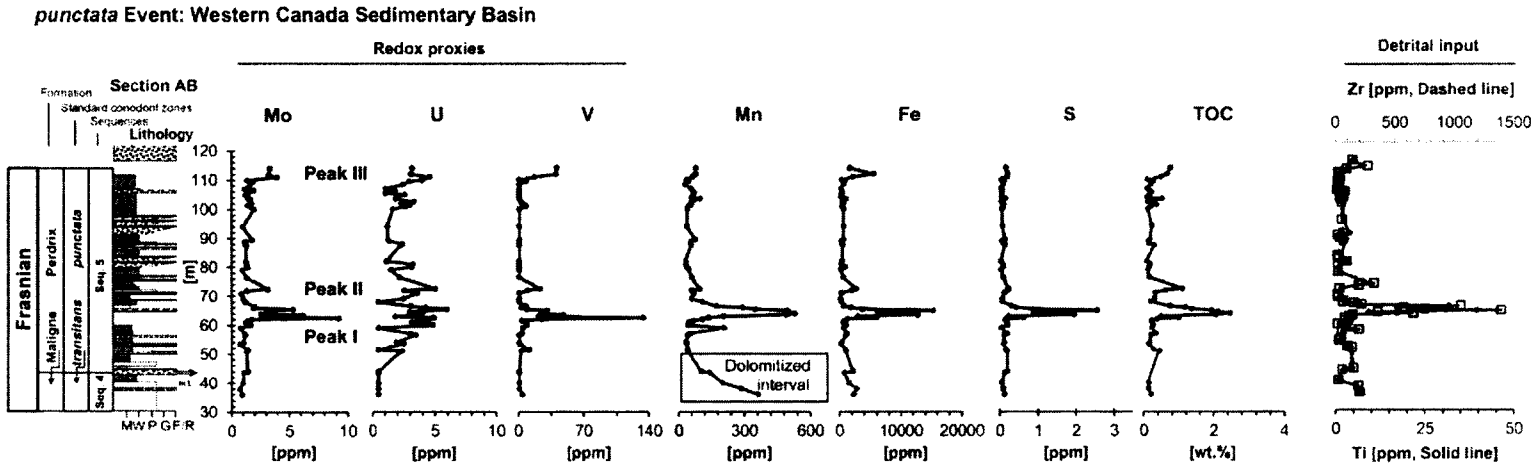

Fig. 3C-1. Chemostratigraphic distribution of 1) the redox proxies Mo, U and V; 2) Fe, Mn, S and TOC, and 3) the detrital input proxies Ti and Zr across the *punctata* Event stratigraphy in the Western Canada Sedimentary Basin.

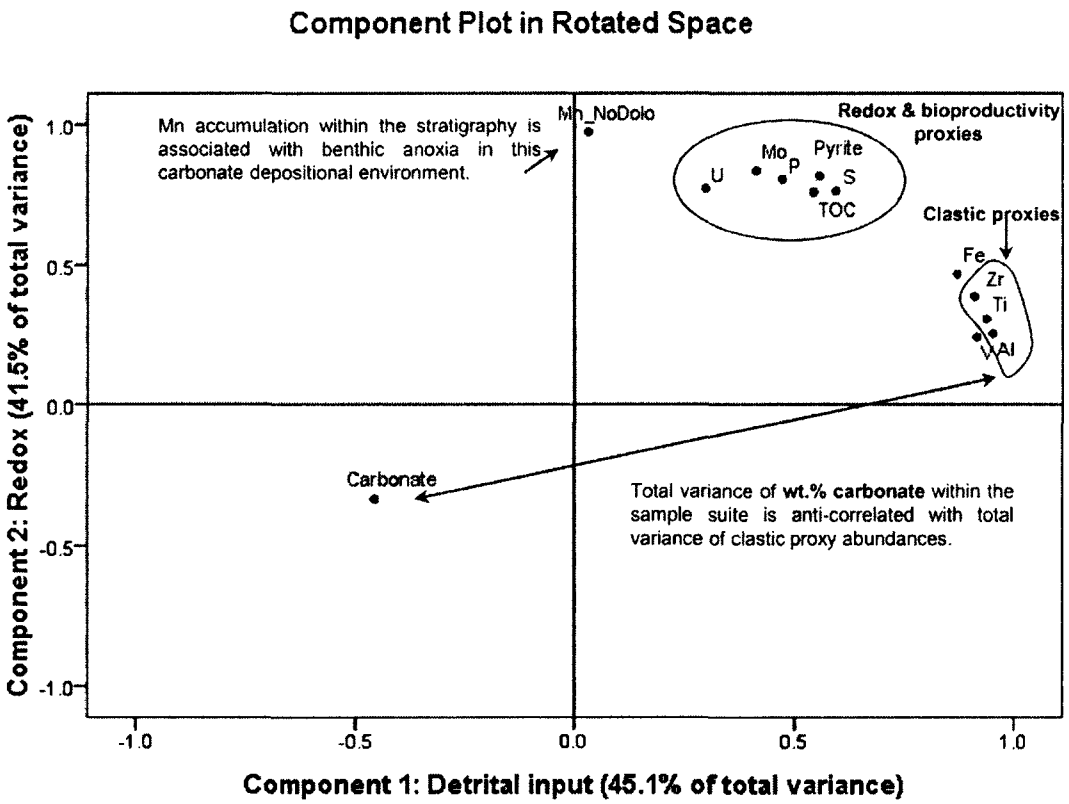

Fig. 3C-2. Results of the factor analysis used to assess the influence of detrital input (Component 1) vs. benthic anoxia (Component 2) on the accumulation of Mn and redox-sensitive proxies. Refer to Table 3C-1.

Table. 3C-1. Numerical results of the factor analysis used to asses the influence of detrital input (Component 1) vs. benthic anoxia (Component 2) on the accumulation of Mn and redox-sensitive proxies. Refer to Fig. 3B-1.

Total Variance Explained							Communalities			Rotated Component Matrix[a]	
Component	Initial Eigenvalues			Rotation Sums of Squared Loadings						Component	
	Total	% of Variance	Cumulative %	Total	% of Variance	Cumulative %	Variable	Initial	Extraction	1	2
1	**9.600**	**73.844**	**73.844**	**5.858**	**45.058**	**45.058**	**Ti**	1.000	.973	**.938**	.307
2	**1.656**	**12.735**	**86.579**	**5.398**	**41.520**	**86.579**	**Zr**	1.000	.977	**.910**	.386
3	1.051	8.083	94.661				**P**	1.000	.870	.472	**.804**
4	.451	3.467	98.128				**Mn***	1.000	.946	.032	**.972**
5	.215	1.650	99.778				**Fe**	1.000	.976	**.871**	.467
6	.029	.222	100.000				**V**	1.000	.896	**.915**	.242
							Mo	1.000	.867	.413	**.834**
							U	1.000	.681	.297	**.770**
							TOC	1.000	.871	.543	.759
							Carbonate	1.000	.320	-.456	-.335
							Pyrite	1.000	.974	.557	**.815**
							S	1.000	.934	.594	**.762**
							Al	1.000	.972	.952	.255

[a]. Rotation converged in 3 iterations.

Extraction Method: Principal Component Analysis. Rotation Method: Varimax with Kaiser Normalization.

*** = Mn data does not include datapoints from the dolomitized interval near the bottom of stratigraphic Section AB.**

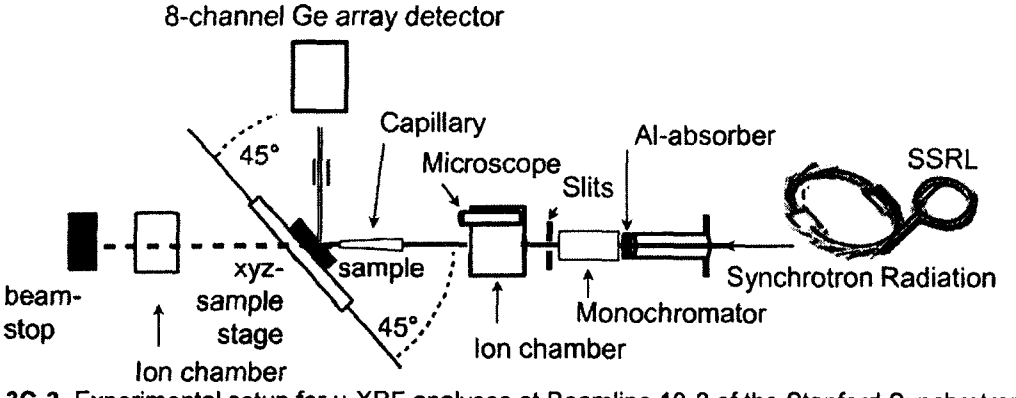

Fig. 3C-3. Experimental setup for μ-XRF analyses at Beamline 10-2 of the Stanford Synchrotron Light Source (SSRL). Modified after Fig. 4 in Rickers et al. (2004).

Sample pE 63.5

Astronomically estimated sedimentation rate: 6.3 cm/kyr = **0.064 mm/yr**
(De Vleeschouwer et al., 2012)

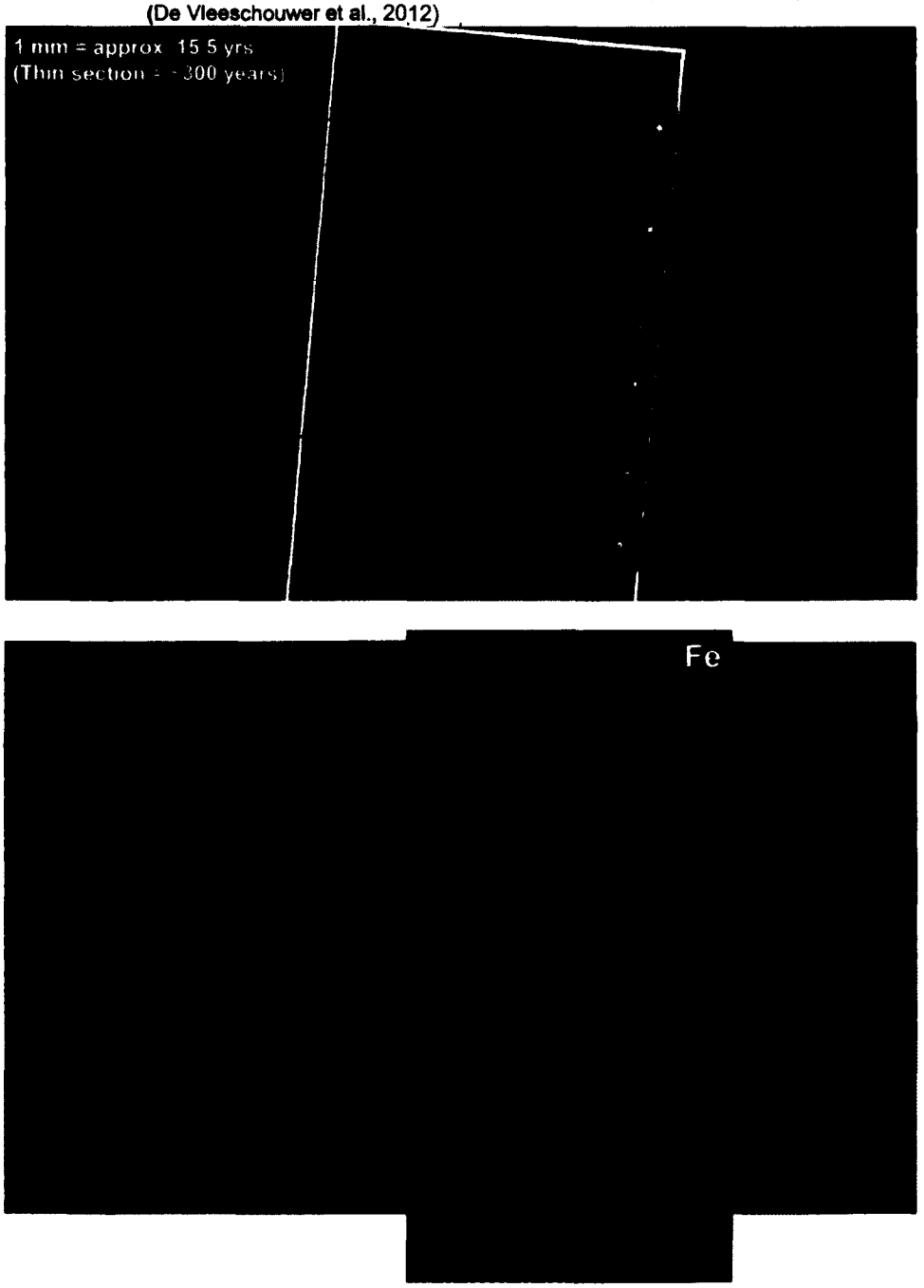

Fig. 3C-4. Thin section photograph of a sample from the main trace element anomaly of the *punctata* Event in the Western Canada Sedimentary Basin (63.5 m in Section AB stratigraphic profile). This sample was the focus of preliminary work using synchrotron μ-XRF mapping of element distributions, with the intent of determining the predominant host phases for elemental proxies of interest. Lower image shows a partial overly of an Fe map.

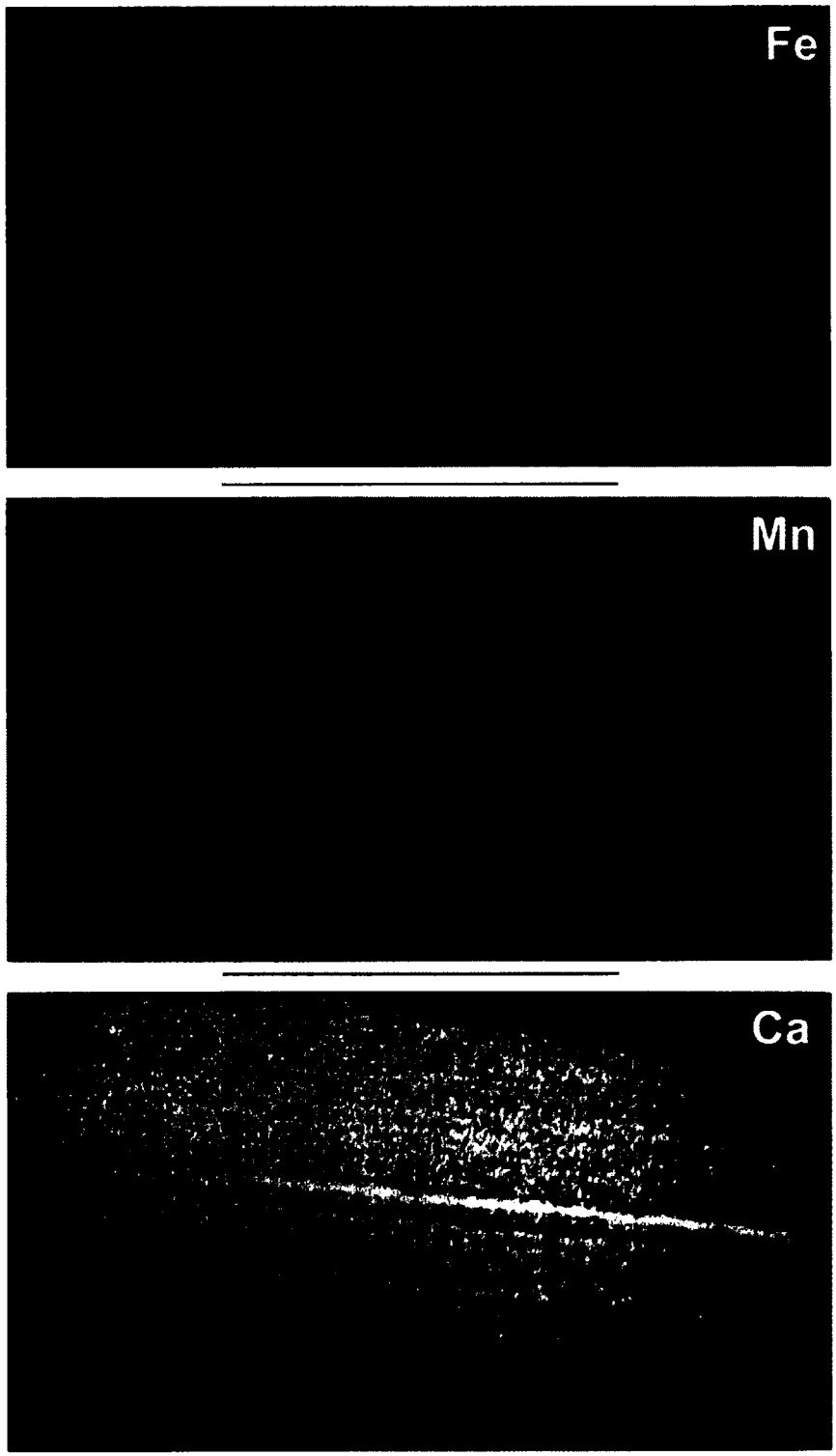

Fig. 3C-5. μ-XRF maps of Fe, Mn and Ca distributions across the thin section of sample pE 63.5 (see Fig. 3B-4).

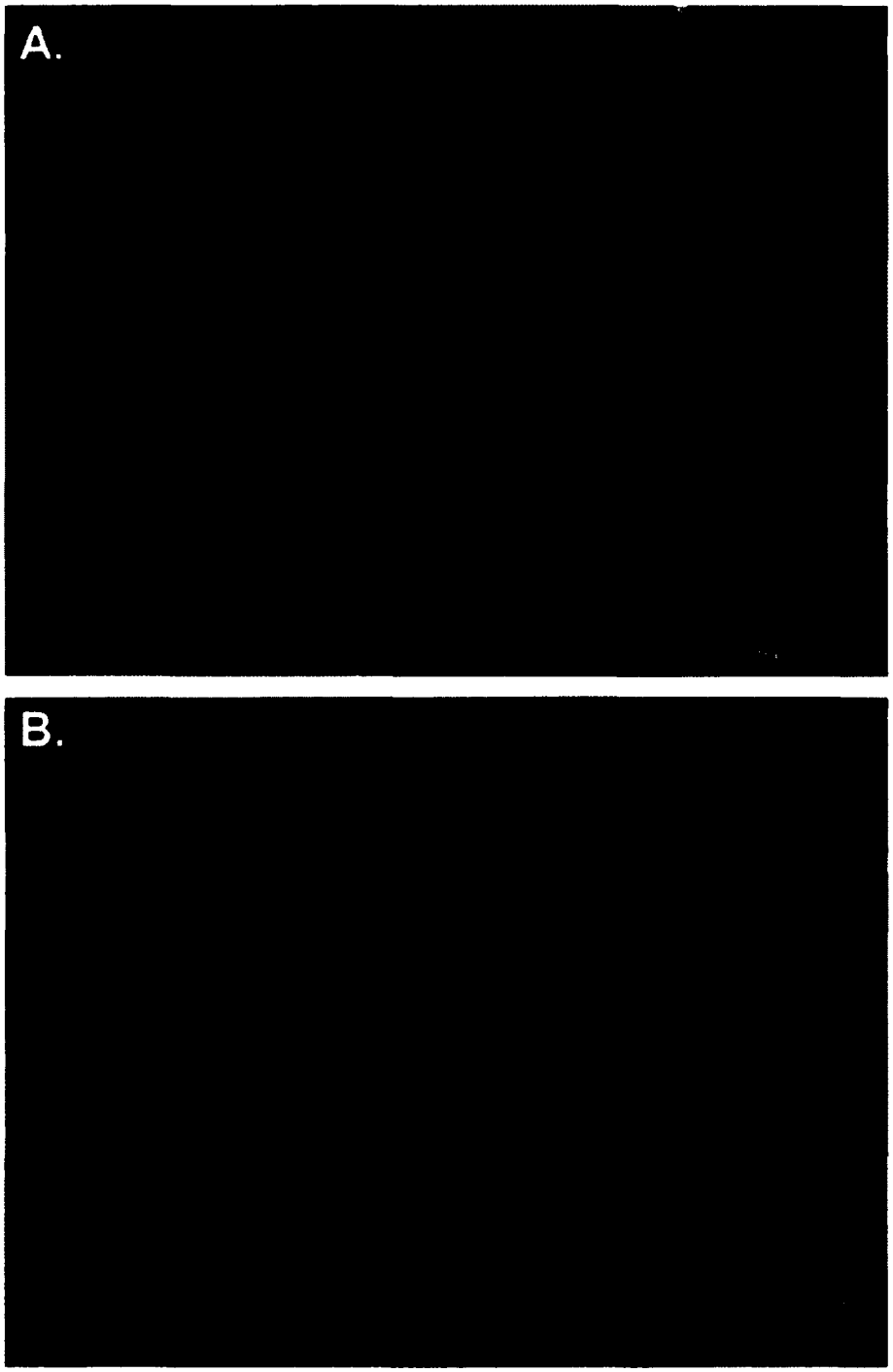

Fig. 3C-6. Sulfide morphologies found within the laminated, organic matter-rich carbonate sediment of the main trace element anomaly of the *punctata* Event in the Western Canada Sedimentary Basin (sample pE 63.5). Reflected light microscopic images (500x). **A.** Possibly mixed Fe-Mn sulfides; framboids **B.** Variable morphologies of apparently mixed Fe-Mn sulfides; refer to μ-XRF Fe-Mn distribution maps, Fig. 3B-5.

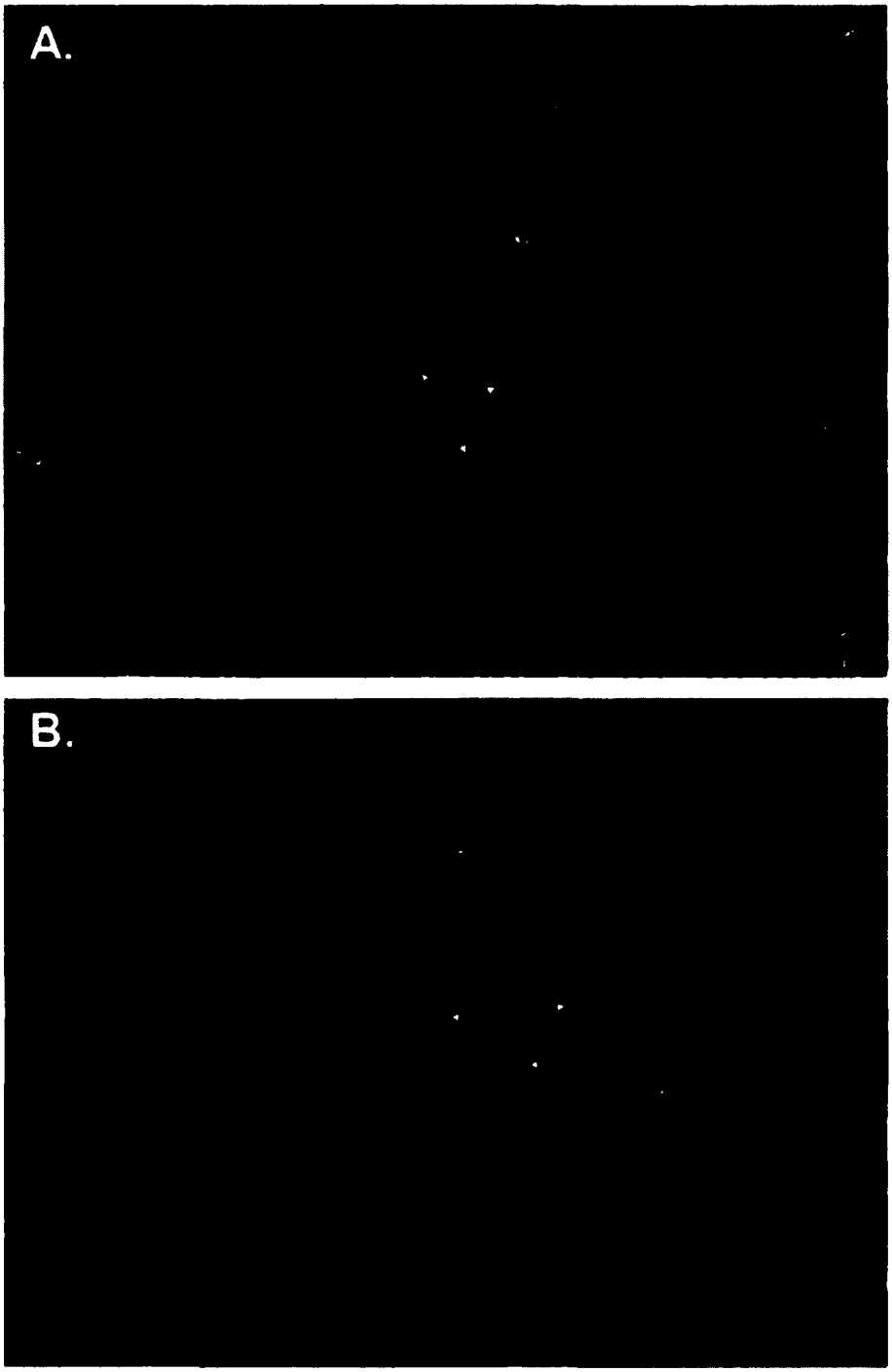

Fig. 3C-7. Association of sulfides with organic matter (OM) within the laminated, organic matter-rich carbonate sediment of the main trace element anomaly of the *punctata* Event in the Western Canada Sedimentary Basin (sample pE 63.5). Transmitted light microscopic image (cross-polarized light); low intensity of reflected light highlights the sulfides within the OM (black patches).

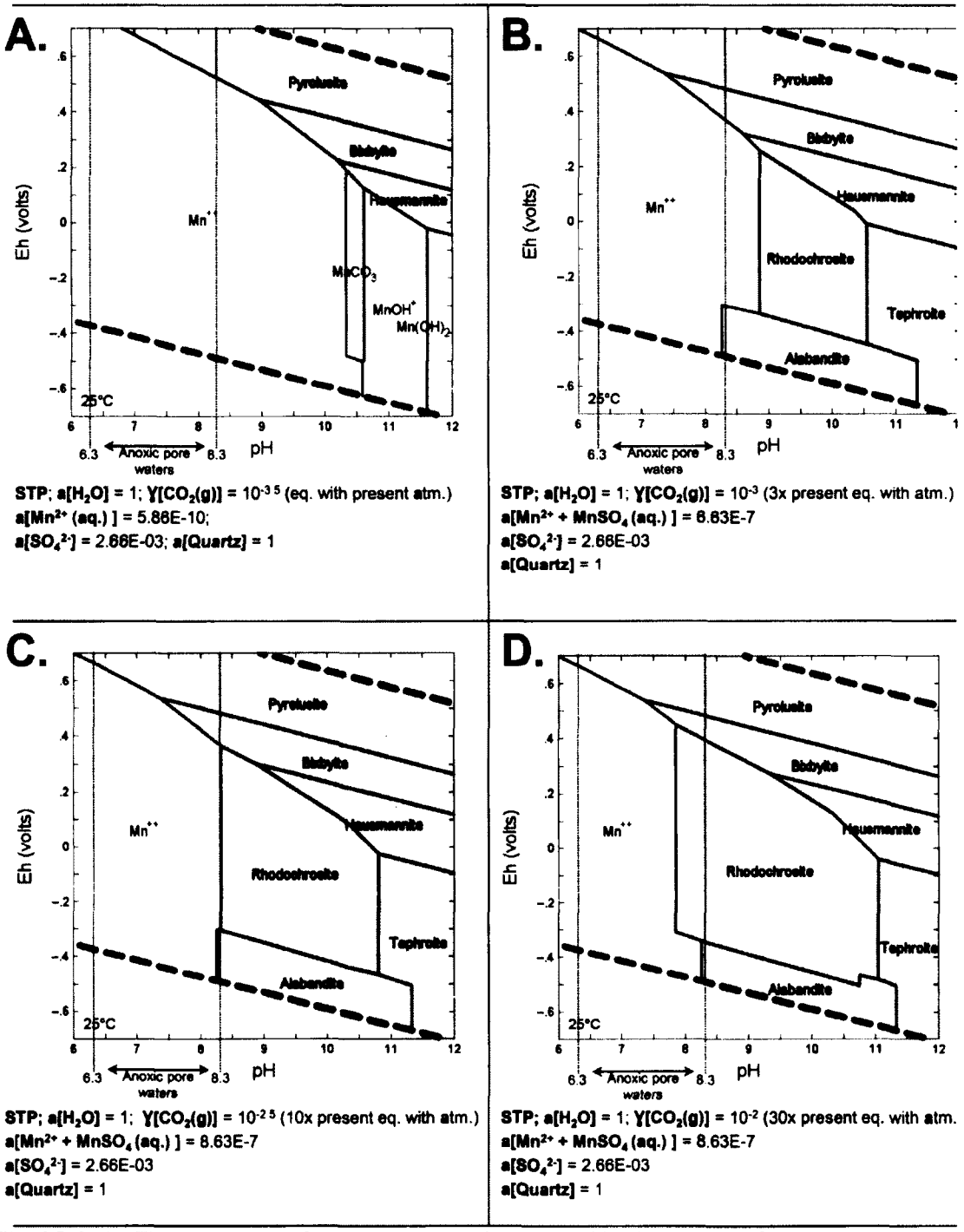

STP; a[H_2O] = 1; Σ[CO_2(g)] = $10^{-3.5}$ (eq. with present atm.)
a[Mn^{2+} (aq.)] = 5.86E-10;
a[SO_4^{2-}] = 2.66E-03; a[Quartz] = 1

STP; a[H_2O] = 1; Σ[CO_2(g)] = 10^{-3} (3x present eq. with atm.)
a[Mn^{2+} + $MnSO_4$ (aq.)] = 8.63E-7
a[SO_4^{2-}] = 2.66E-03
a[Quartz] = 1

STP; a[H_2O] = 1; Σ[CO_2(g)] = $10^{-2.5}$ (10x present eq. with atm.)
a[Mn^{2+} + $MnSO_4$ (aq.)] = 8.63E-7
a[SO_4^{2-}] = 2.66E-03
a[Quartz] = 1

STP; a[H_2O] = 1; Σ[CO_2(g)] = 10^{-2} (30x present eq. with atm.
a[Mn^{2+} + $MnSO_4$ (aq.)] = 8.63E-7
a[SO_4^{2-}] = 2.66E-03
a[Quartz] = 1

Fig. 3C-8. An Eh-pH diagram of thermodynamic phase stabilities in seawater for the system Mn-C-O-S used to approximate the pore water conditions required for the precipitation of Mn as carbonate and sulfide phases. Anoxic pore water pH range after Ben-Yaakov (1973). In carbonate-rich sediments, the rhodochrosite field more appropriately represent mixed Ca-Mn carbonates (Mucci, 1988).

4. Stable Isotope ($\delta^{13}C_{carb\ \&\ org}$, $\delta^{15}N_{org}$) and Trace Element Anomalies during the Late Devonian '*punctata* Event' in the Western Canada Sedimentary Basin[1]

Abstract

Late Devonian marine deposits in the Western Canada Sedimentary Basin were analyzed for (1) accumulations of bioproductivity and paleoredox trace element proxies and for (2) variations of $\delta^{13}C_{(carb\ \&\ org)}$ and $\delta^{15}N_{org}$ in order to understand and interpret the regional history of the global yet short-term '*punctata* Event' geochemical perturbation. Statistical correlations suggest that changes in detrital input and associated micronutrient delivery were the main driver of a eutrophication event noted early and possibly also late in the *punctata* zone around the isolated Miette platform, manifested by increased TOC, positive $\delta^{13}C$ excursions and concurrent enrichments of all elemental proxies. Evaluation of data within a regional sequence stratigraphic perspective revealed a eustatic sea level influence, with proxy accumulations associated mostly with early transgression (IIc1). Deposition and preservation of organic matter-rich facies occurred during conditions of enhanced primary production and facilitated bottom water suboxia-anoxia. Following eutrophication, lower $\delta^{15}N_{org}$ and $\delta^{13}C_{org}$ values predominated and persisted throughout much of the *punctata* zone before rebounding toward its close, suggesting a time interval of environmental stagnation and lower overall productivity during which N_2-fixing autotrophs may have had an ecological advantage under nitrate-limited conditions. The *punctata* Event approximately coincided with the advent of archaeopterid forest expansion beginning around mid-Frasnian time, which fundamentally altered the nature of continental weathering through extensive soil formation and increased nutrient delivery to the oceans. This evolutionary event may have amplified the detrital influx, already elevated by sea level lowstand and early transgression and increased denudation of rising mountain ranges in near-equatorial regions.

4.1. Introduction

The Late Devonian '*punctata* Event' was a global yet relatively short-term (0.5-1.0 Ma) perturbation of the C-cycle, associated with excursions of various geochemical proxies but without any significant faunal turnover (da Silva and Boulvain, 2008; John et al., 2008; Ma et al., 2008; Marynowski et al., 2008; Morrow et al., 2009; Pisarzowska et al., 2006; Pisarzowska, 2008;

---

[1] Śliwiński, M.G., Whalen, M.T., Newberry, R.J., Payne, J., and Day, J., 2011. Stable Isotope ($\delta^{13}C_{carb\ \&\ org}$, $\delta^{15}N_{org}$) and Trace Element Anomalies during the Late Devonian '*punctata* Event' in the Western Canada Sedimentary Basin. *Palaeogeography, Palaeoclimatology, Palaeoecology*, **307**, 245–271

Racki et al., 2008; Śliwiński et al., 2010; Yans et al., 2007). It is characterized by one of the larger positive $\delta^{13}C_{carb}$ excursions documented throughout Phanerozoic time, with a shift of up to ~5-6‰ in some depositional settings (Holmden et al., 2006; Yans et al., 2007), although more commonly reported as 4-5‰ and occurring in four distinct steps (Pisarzowska et al., 2006; Pisarzowska, 2008; Racki et al., 2004). Its casual mechanism seems to be a peculiar combination of paleobotanical developments in the terrestrial biosphere coupled with the uplift and weathering of orogens in near-equatorial settings, which would have perturbed the nutrient balance in epeiric seaways (John et al., 2008; Pisarzowska, 2008; Racki et al., 2008, Śliwiński et al., 2010). An examination of strata containing the Alamo Impact Breccia (Nevada, USA) demonstrated that an extraterrestrial impact-related trigger for this perturbation proposed earlier (Yans et al. (2007) is highly improbable (Morrow et al., 2009). This lends support and shifts focus back to Earth-bound causes, in accordance with evidence suggesting a prolonged nature of Late Devonian biosphere perturbations leading up to the Frasnian-Famennian (F/F) biotic crisis – the fifth largest extinction event of the Phanerozoic (Algeo et al., 1995; House, 2002; Racki, 2005; Sepkoski, 1984).

In this contribution we report on stable isotope anomalies of both organic and inorganic carbon ($\delta^{13}C_{carb}$, $\delta^{13}C_{org}$) and nitrogen ($\delta^{15}N_{org}$) and apply the use of bioproductivity and paleoredox trace element proxies in a dominantly carbonate depositional environment to interpret the *punctata* Event in the Western Canada Sedimentary Basin (WCSB). This data builds upon recent work documenting trace element, total organic carbon (TOC) and magnetic susceptibility (MS) variations recorded along the southeast margin of the isolated Miette carbonate platform (Śliwiński et al., 2010). Chemostratigraphic profiles were expanded for this study and aid the interpretation of isotopic histories, providing a higher resolution account of oceanographic changes in the *punctata* conodont biozone. This independent geochemical approach allowed us to make first-order distinctions in the isotopic histories between 1) those features that can be directly tied to changes in primary production and increased burial of ^{12}C-enriched organic matter (OM) and 2) those related to different phases of 3rd order relative sea level change (*i.e.* T-R cycles). From a methodological viewpoint it is assumed that a diversity of independent geochemical proxies converge on an internally consistent interpretation in terms of regional sequence stratigraphy and relative sea level change, variations in bioproductivity, detrital input and redox conditions, all set against the background of Devonian environmental and ecological changes and C-cycle perturbations.

Regional high-resolution $\delta^{13}C_{carb}$ data spanning the Upper Devonian in the WCSB were previously reported by Holmden et al. (2006); however, no organic $\delta^{13}C$ records from western Laurussia have hitherto been published for comparison with such data from European and Chinese sections (Ma et al., 2008; Pisarzowska et al., 2006; Pisarzowska, 2008). Additionally, we

report here the first record of variations in the isotopic composition of nitrogen ($\delta^{15}N_{org}$) in the *punctata* zone, which has the potential to provide insight into biotic processes associated with the marine N-cycle, mainly the extent of biological N_2-fixation and water column denitrification and their relation to paleoredox conditions. The use of the $\delta^{15}N$ proxy in Devonian paleoceanography is very limited, but has previously been employed as part of a multi-proxy approach concerned with the Earth-system perturbations at the F/F extinction event interval in the WCSB (Payne, 2009), and to help explain the eutrophication and demise of the massive carbonate buildups in this same basin later at the Devonian-Carboniferous (D-C) boundary (Caplan et al., 1996; see also de la Rue et al., 2007).

4.2. Geologic background

We examined two stratigraphic profiles within the Maligne and Perdrix Formations of the Miette carbonate platform margin that contain the *Palmatolepis punctata* conodont biozone (MN Zones 5 & 6 of Klapper, 1989) and portions of the underlying *P.transitans* (MN Zone 4) and overlying *P.hassi* zones (MN Zones 7-10) (Sections AB and K, Fig. 4.1; Whalen et al., 2000; Whalen and Day, 2008). Based on the Devonian time scale of Kaufmann (2006), each of these zones averages 0.6 Ma in duration. During Late Devonian time, the WCSB, with its system of isolated and attached platforms that developed during Frasnian time atop a preexisting carbonate ramp, was situated at near-equatorial latitudes on the west coast of Laurussia (Fig. 4.2). Miette had an aerial extent of ~165 km^2 and a thickness of 400-500 m (Geldsetzer, 1989; Mountjoy, 1989). Prior sequence and biostratigraphic work determined that platform growth kept pace with a 2^{nd} order sea level rise and nine 3^{rd} order depositional sequences spanning the Late Givetian to Early Famennian have been identified (Figs. 4.2 and 4.3; Whalen et al., 2000; Whalen and Day, 2008). Rates of platform sedimentation surpassed those of the associated basins (Whalen et al., 2000), which are filled with platform-derived carbonate sediment variably mixed with fine-grained siliciclastics sourced from the Ellesmerian Fold Belt (Canadian Arctic Archipelago) and central Laurussia (Oliver and Cowper, 1963; Stoakes, 1980; Switzer et al., 1994; Whalen and Day, 2008, 2010). Extensive reef development ceased in this region following the F/F mass extinction event which exterminated the stromatoporoid-coral frame-building fauna (McLaren, 1982; McLaren and Goodfellow, 1990; Stearn, 1987).

A rigorous conodont biostratigraphy could not be established for the upper portion of the studied interval at Section AB, where samples did not yield sufficient fossils to constrain the position of the *punctata-hassi* zonal boundary. The biostratigraphy is reinforced by sequence stratigraphic and MS correlations with well-constrained equivalent sections in an adjacent thrust sheet (Fig. 4.2), which indicates that this boundary is situated within a 28 m covered interval that

lies directly above the sampled horizons (Whalen and Day, 2008, 2010). In Section K, this same boundary is obscured by a package of coarse-grained redeposited beds (Whalen et al., 2000).

Both stratigraphic profiles are characterized by stark alternations of organic-rich carbonate mudstones-wackstones and coarser-grained redeposited carbonate lithologies (Fig. 4.4). Some basinal facies are bioturbated, while others lack benthic fauna, are laminated and contain framboidal pyrite, indicating changes in the oxygenation level of basinal waters (Whalen et al., 2000). Detailed facies descriptions of the Miette platform were reported previously by Whalen et al. (2000) and facies descriptions of the broader WCSB can be found in Klovan (1964), Stoakes (1980) and van Buchem et al. (1996), among others. The chief minerals present in the slope and basin-filling facies are calcite, dolomite, illite and fine-grained quartz (Stoakes, 1980), an observation consistent with unpublished x-ray diffraction analyses of a small sample subset from the Section AB profile.

4.3. Diagenetic background

4.3.1. Burial history

Diagenesis of carbonate sediment determines the extent to which the primary isotopic composition of C and O - that of the seawater from which carbonate precipitated either inorganically or through biological mediation - may have been altered following deposition and burial. Diagenesis of the Miette platform was previously described within a sequence stratigraphic perspective by Melim et al. (2000) (see also Mattes and Mountjoy, 1980). Deeper water slope facies, such as those of Sections AB and K, were dominantly affected by marine burial diagenesis, including fine blocky spar cementation, minor dissolution, silicification and mechanical compaction. Meteoric diagenesis, which commonly involves relatively ^{18}O and ^{13}C depleted fluids, can strongly distort the primary isotopic signal of marine precipitates, but is limited in extent and restricted to platform-top and margin facies (Meyers and Lohmann, 1985). Detailed analyses of the geochemical signatures of specific diagenetic phases is beyond the scope of this study; however, such a diagenetic analysis of the neighboring Southesk-Cairn Carbonate Complex (SCCC, Fig. 4.2) serves as a regional reference (Machel and Buschkuehle, 2008). The compositions, temperatures and flow patterns of diagenetic fluids within the SCCC were additionally constrained in the reconstruction of the burial history, demonstrating that temperatures at maximum depths of 6000-7000 m likely did not exceed 150-220°C (Fig. 19 in Machel and Buschkuehle, 2008). A comparable burial history and diagenetic evolution was determined for the Fairholme Carbonate Complex in southwest Alberta (~150 km away – Fig. 4.2; Vandeginste et al., 2009 and Fig. 15 therein). Given the proximity of the Miette platform to these

aerially extensive carbonate complexes (Fig. 4.2), it seems reasonable to presume similar diagenetic temperatures. Recovery of conodonts with a CAI of 3-3.5 (conodont alteration index – Epstein et al., 1977; Whalen and Day, 2010) further indicates that temperatures did not exceed a maximum of ~220 °C.

Diagenetic fabrics and their isotopic compositions at both the Fairholme and Southesk-Cairn Carbonate Complexes were noted to be generally similar to those that are common and widespread elsewhere in the Devonian of the WCSB, especially south of the Peace River Arch (Fig. 4.2) (Machel and Buschkuehle, 2008; Vandeginste et al., 2009). The respective diagenetic histories differ, however, in their final stages. Mainly, the Fairholme Complex was first buried to depths of ~6000 m but then largely uplifted during the Laramide Orogeny (Vandeginste et al., 2009); in contrast, much of the SCCC has remained in the Alberta Subsurface at a depth of ~3000 m (Machel and Buschkuehle, 2008). It follows then that the time interval over which diagenetic effects associated with maximum burial could be expressed was considerably shorter for all areas of platforms now exposed in the Canadian Rockies compared to those still buried.

4.3.2. Diagenetic alteration of OM $\delta^{13}C$ and $\delta^{15}N$

The isotopic composition of kerogen is a complex composite signal which reflects 1) the type and relative proportions of isotopically distinct marine vs. terrestrial OM (*e.g.* Popp et al., 1997; Hayes, 1993); 2) post depositional OM reworking by heterotrophic organisms (*e.g.* Hayes, 1993); 3) selective biodegradation of different macromolecules, which is itself a complex function of redox conditions near the sediment-water interface (SWI) and other environmental parameters; and 4) further bio- and thermodegradation effects during kerogen maturation and oil and gas generation/migration (Baxby et al., 1994; Galimov, 1980; Machel, 2005; Oldenburg et al., 2007; Popp, 1997; Rigby and Bats, 1986; Tyson 1995; Yamaguchi et al., 2010).

An assessment of the diagenetic history and kerogen type is needed in order to make reliable interpretations of isotopic data in terms of past oceanic geobiological changes. Devonian and Mississippian strata in the WCSB were previously evaluated in terms of kerogen type and regional paleogeography and paleoenvironments, revealing that rocks of the Woodbend Group of west-central Alberta, which contain the Maligne and Perdrix formations of interest herein, are dominated by marine kerogen; terrestrial OM is generally lacking except adjacent to landmasses such as the nearby Peace River Arch (Fig. 4.2; Allan and Creaney, 1991; Stasiuk and Fowler, 2004). The $\delta^{13}C_{org}$ values of modern low- to mid- latitude marine plankton fall in the range of -18 to -24‰ (Tyson, 1995) and recent marine sedimentary OM shows a nominal average of -25‰ (Holser, 1997). The range of $\delta^{15}N_{org}$ is more variable, falling between ~0 and 20‰ (*e.g.* Hoefs, 1987; Rau et al., 1987).

During its transformation to kerogen, OM initially becomes isotopically lighter as biodegradation removes ^{13}C-enriched carbohydrates and proteins while preserving ^{12}C-enriched lipids (Galimov, 1980; Hoefs, 1987). As thermal maturation progresses (T > 50°C), OM then becomes isotopically heavier as liquid and gaseous hydrocarbons and other ^{12}C-enriched organic compounds are released through bio- and thermodegradation and sulfate reduction processes (Fig. 4.5, after Machel et al., 1995 and Sassen et al., 1987; Hoefs, 1987; Hoering and Moore, 1957; Oldenburg et al., 2007; Rullkötter, 1993; Yuenian et al., 2000). Thermal alteration is thought to induce a maximum ^{12}C-enrichment of up to ~3‰ (Hoefs, 1987; Machel et al., 1995), while variations in excess of this are most probably due to changes in the dynamics of isotope exchange reactions between OM and carbonates during deposition (Hoefs, 1987).

Compounds 'cleaved' from maturing OM show the following range of $\delta^{13}C$ values: crude oil: -20 to -30‰, gas condensates: -20 to -45‰, biogenic methane: -50 to -70‰ (Machel et al., 1995; Schoell, 1983; Vandeginste et al., 2009). Based on limited studies, the $\delta^{15}N$ of crude oil falls in the 1 to ~7‰ range (*e.g.* Kerans, 1985; Hoering and Moore, 1957; Oldenburg et al., 2007), whereas that of N_2 gas depends on the degree of maturation. Low maturity corresponds to light gas with $\delta^{15}N$ in the -19 and -10‰ range, whereas mature OM yields heavier values between -10 to -2‰ range (Zhu et al., 2000).

Burial temperatures at the Miette platform and surrounding carbonate complexes (Section 3.1.) correspond to those well within the 'oil window' (Fig. 4.5). Presumably thermal alteration affected the stratigraphic sections of interest uniformly, as their thickness of <100 m is small compared to average burial depths of 6000-7000 m. The relatively low diagenetic temperature suggests that trends and magnitudes of isotopic shifts have been conserved, and it is interesting to note that if what remains preserved today is an isotopically enriched residue, then the original OM at the time of deposition must have had a bulk C and N isotopic composition more depleted than modern analogues.

4.3.3. Extent of dolomitization at the Miette platform

Dolomitization of Devonian carbonate platforms in the WCSB was described on multiple occasions and many models involving the migration of fluids proposed, albeit with no emergent consensus (see brief overview in Vandeginste et al., 2009). In contrast to most subsurface carbonate buildups, the dolomitization process at the *isolated* Miette platform might have been 'frozen' in place, leaving it only partially altered (Melim et al., 2000).

Dolomitization follows system tracts and can be ascribed to shallow burial (<260-360 m – Melim et al., 2000). Platform facies are preferentially and pervasively dolomitized within the upper TST and upper HST (Melim et al., 2000). In contrast, low permeability distal slope and basin

facies rarely contain more than 30% dolomite, commonly associated with clay and/or organic-rich horizons in the TST (Melim et al., 2000). This dolomite is calcian, suggesting that inefficient fluid movement prevented the formation of more stoichiometric varieties (Melim et al., 2000). Pumping of marine waters through the sediment at shallow burial depths during transgressive pulses likely supplied the Mg^{2+} ions needed for initial dolomitization (*c.f.* Soreghan et al., 2000). The lower permeability facies surrounding this isolated platform may have led to poor connectivity with the main diagenetic fluid 'aquifer'/conduit system during deeper burial, precluding more extensive dolomitization (*c.f.* Machel and Buschkuehle, 2008). Relatively rapid burial and uplift of the platform during the Laramide Orogeny, compared to the carbonate complexes that remain in the subsurface, may have further limited the extent of alteration. It is noteworthy, however, that the time-equivalent isolated Redwater reef complex also experienced no dolomitization, despite its subsurface location (Wendte, 1994).

4.4. Methods

4.4.1. Wave-length dispersive X-ray fluorescence (WD-XRF) spectroscopy

Minor and trace element abundances in the marine sedimentary rock record provide insight into (1) changes of oceanic bioproductivity (*e.g.* Ni, Cu, P, Ba, Zn); (2) changes in the relative fluxes of terrigenous siliciclastics entering a depositional basin (*e.g.* Al, Si, Ti, K, Cr, Zr, Co); and (3) yield a record of the dominant redox conditions near the sediment-water interface (*e.g.* U, Mo, V, Ni/Co, U/Th, V/Cr, V/(V+Ni)) (Algeo and Maynard, 2008; Calvert and Pedersen, 1993; Hatch and Leventhal, 1992; Jones and Manning, 1994; Piper and Calvert, 2009; Rimmer, 2004; Rimmer et al., 2004; Riquier et al., 2006; Tribovillard et al., 2006). We present here an expanded trace element dataset of bioproductivity (Ni, Cu, P) and paleoredox proxies (Mo, U, V, Ni/Co, U/Th, V/Cr, V/(V+Ni)) over that initially published in Śliwiński et al. *(2010)*, as continued work provides a more detailed account of the geochemical variability during the *punctata* zone Event. Following the methodology arguments laid out previously, no *Al-normalization* nor *enrichment factor* calculations were applied to raw data (Śliwiński et al., 2010).

The sampled material consists of carbonate mudstones-wackstones. Elemental abundances were measured using a *PANalytical Axios wavelength-dispersive x-ray fluorescence spectrometer* (WD-XRF) at the University of Alaska Fairbanks *Advanced Instrumentation Laboratory*. Custom trace element analytical routines were developed for this lithology and were optimized to detect low concentrations (~0-50 parts per million [ppm]) of various trace elements, with an analytical resolution capable of distinguishing concentration differences between samples down to ~0.5-1 ppm. Each analyte was calibrated against 'in-house' and certified standard

reference materials (*e.g. United States Geological Survey, United States National Institute of Standards and Technology*). The accuracy of calibration lines relative to standards is within 10%, whereas empirically determined detection limits (using 99.999% pure $CaCO_3$) and representative precisions for the elemental data presented here is reported in Table 4.1. Samples were prepared by powdering using hardened steel vials from SPEX CertiPrep Group and pressed into 35 mm diameter pellets using a polyvinyl alcohol binder.

4.4.2. Isotopic analyses ($\delta^{13}C_{carb}$, $\delta^{18}O_{carb}$, $\delta^{13}C_{org}$ and $\delta^{15}N_{org}$), TOC and Carbonate Content

Whole-rock analyses of $\delta^{13}C_{carb}$ and $\delta^{18}O_{carb}$ values (n = 59) were done using carbonate mudstones-wackstones with minimal admixture of vein calcite. Isotope ratios of subsamples of material powdered for XRF analyses were determined using continuous-flow isotope ratio mass spectrometry (CF-IRMS) at the *Alaska Stable Isotope Facility's* Delta+XP mass spectrometer interfaced with a Thermo Gasbench II carbonate analyzer. Typically, instrument precision is <0.2‰. Stable isotope abundances are expressed using delta (δ) notation measured against the Peedee belemnite (VPDB) standard.

Samples for $\delta^{15}N_{org}$ (n = 53) and $\delta^{13}C_{org}$ (n = 55) analyses were prepared by acidifying 1 gram subsamples of powdered material with an excess of 1 M HCl. The acid-insoluble residues were rinsed, freeze-dried and analyzed for their C and N contents using a Costech Elemental Analyzer (ECS 4010). Isotope ratios were then measured using a Conflo III interface with a Delta+XP Mass Spectrometer and ratios were reported using delta (δ) notation relative to the PDB and Atmospheric-air standards respectively. Typical instrumental precision is <0.2‰.

Organic C concentrations in the acid-insoluble residues were used to calculate the whole rock TOC by noting the mass lost during carbonate acidification, yielding also a total carbonate content (TCC). The analytical precision and accuracy associated with these analyses is respectively within 2% and 5% of the reported values.

4.5. Results

4.5.1. Whole rock $\delta^{13}C$ and $\delta^{18}O$ (Section AB only)

Isotope ratios of C and O in the Section AB profile oscillate between 0.19 and 4.05‰ $\delta^{13}C$ and -10.21 and -3.25‰ $\delta^{18}O$ (Appendix 4A-1). Values typical for the Late Devonian ocean have been documented in various studies (Table 4.2, *e.g.* Buggisch and Joachimski, 2006; Carpenter and Lohmann, 1989; Denison et al., 1997; Hurley and Lohmann, 1989; Kaufman, 1989; Machel and Buschkuehle, 2008; Mountjoy et al., 1999; van Geldern et al., 2006); many of

these focused on reefal carbonate cements which are regarded to yield the most accurate record of open-marine $\delta^{13}C$ and $\delta^{18}O$ (Gonzalez and Lohmann, 1985).

Cross-plotting $\delta^{13}C_{carb}$ vs. $\delta^{18}O_{carb}$ reveals that most of our data plot either near or within this published compilation and are consistent with regional data from the Devonian of the WCSB (Fig. 4.6; *e.g.* Green, 1999; Smith, 2001; Machel and Buschkuehle, 2008). Such compilations of 'typical values' together with a lack of covariance between the two geochemical properties have been previously used as a screen for diagenetic overprinting of the primary isotopic signal (*e.g.* Allan and Matthews, 1982; da Silva and Boulvain, 2008; Immenhauser et al., 2003; Morrow et al., 2009). No clear statistical covariance is evident in our data, as the R^2 of a linear regression of all results is 0.0018. Several $\delta^{18}O$ values lie outside these ranges whereas their corresponding $\delta^{13}C$ values fall within them, a likely reflection of carbonate sediment recrystallization and stabilization at elevated temperatures during shallow burial where changes in $\delta^{18}O$ are more likely due to interactions with pore fluids (Machel, 1997). It's been noted that a particular mineral phase may be modified outside its original compositional range for one geochemical property, but not for others (Machel, 1997; Machel and Buschkuehle, 2008). For example, equilibrium fractionation of C-isotopes is not temperature sensitive but that of O-isotopes is; thus diagenetic mineral stabilization at elevated burial temperatures generally leads to depleted $\delta^{18}O$ (at least in low-Mg-calcite), although the total proposed range of alteration falls mostly within ±2‰ range (Veizer, 1983).

Carbonate $\delta^{13}C$ at Section AB increase from ~0.75‰ to ~4‰ near the upper boundary of the *transitans* zone, which corresponds to sea level lowstand near the 3rd order Sequence (Seq.) 4-5 transition (Fig. 4.7). A gradual decrease to ~2.5‰ then follows throughout a ~15 meter dolomitized interval, after which values continue to fall to ~0.5‰. A positive excursion of ~2‰ is noted at the maximum flooding zone (mfz, 60-65 m in profile), with a subsequent negative shift of ~1.2‰. A second positive excursion of ~1.2‰ is observed several meters higher and is followed by a negative rebound of ~1.1‰.

Both noted positive $\delta^{13}C_{carb}$ shifts were concurrent with positive excursions of $\delta^{13}C_{org}$ and occur in horizons with elevated TOC and accumulations of bioproductivity and redox trace element proxies (Peaks I & II, Figs. 4.7 and 4.9). However, no corresponding positive $\delta^{13}C_{carb\ \&\ org}$ shifts were noted higher in the profile toward the top of the *punctata* zone in relation to a third although smaller trace element and TOC enrichment (Peak III, Fig. 4.9). Between these elevated TOC/trace element horizons in both the lower and upper portions of the zone, the $\delta^{13}C_{carb}$ trend forms a broad positive hump that reaches a high of ~3.5‰. Values then decrease again through a stepwise negative excursion reaching depletion down to ~0‰, and later rebound stepwise

toward ~3.5‰. Covered intervals and horizons disturbed by redeposition preclude extending the isotopic records further to the *punctata-hassi* boundary.

4.5.2. Vein calcite $\delta^{13}C$ and $\delta^{18}O$ (Section AB)

Isotopic analysis of the coarsest calcitic vein found in the stratigraphic section (~2 mm thick, 43.5 m in profile, Section AB) broadly constrains the composition of post-depositional fracture fill calcite and outlines how the incorporation of vein material could bias whole rock $\delta^{13}C$ and $\delta^{18}O$ values. For this vein, $\delta^{13}C$ = -9.27‰ and $\delta^{18}O$ = -15.98‰, which plots within the range of values observed in the WCSB (Fig. 4.6). Cross-plotting all $\delta^{13}C_{carb}$ vs. $\delta^{18}O_{carb}$ data revealed no trend toward the depleted composition of this diagenetic calcite (Fig. 4.6).

4.5.3. Matrix dolomite $\delta^{13}C$ and $\delta^{18}O$ and the extent of dolomitization (Section AB)

Thin section petrography shows that dolomitization is restricted only to the lower portion of the main stratigraphic profile (~34-50 m, Section AB). Two samples composed entirely of matrix dolomite that replaced original lime mud yielded $\delta^{13}C$ values of 3.88 and 3.99‰, and $\delta^{18}O$ of -5.20 and -7.75‰ (Fig. 4.6). This diagenetic phase plots above the composite field of Late Devonian seawater $\delta^{13}C$ and $\delta^{18}O$, but does not plot anomalously with respect to the limestone dataset and is well within the range of matrix dolomites reported elsewhere from the WCSB (Fig. 4.6; Green, 1999; Machel and Buschkuehle, 2008; Smith, 2001). Two other wholly dolomitized samples plot similarly, although these are not purely matrix dolomite as some coarser vein-filling dolomite is also present (Fig. 4.6).

It is noteworthy that although the range of matrix dolomite $\delta^{13}C$ values extends up to about +6‰ in the WCSB (Green, 1999), only one datapoint represents this high end (Fig. 4.6); all other measurements fall between 0-4‰. Dolomitization tends to leave C-isotope ratios unaltered (Tucker, 2001), while substantially changing $\delta^{18}O$, especially at elevated temperatures (*e.g.* Fig. 4 in Veizer, 1983). Nonetheless, theoretical fractionation calculations indicate that the $\delta^{13}C$ of dolomites should be about 2‰ heavier than cogenetic calcites (Friedman and O'Neill, 1977; Veizer, 1983). All partially or wholly dolomitized samples in the Section AB profile plot near the field of Late Devonian marine values with respect to C but also with respect to O with the exception of a single sample (Fig. 4.6), suggesting that dolomite contains only C redistributed from nearby horizons and marine pore fluids. We thus opted to retain samples from the dolomitized horizon within the chemostratigraphic profile, although the $\delta^{13}C$ trend through this thin interval should be viewed with caution.

4.5.4. $\delta^{13}C_{org}$ and $\delta^{15}N_{org}$ (Sections AB and K)

The observed range of $\delta^{13}C_{org}$ values in both stratigraphic sections falls between -25 and -30‰ (Appendix 4 A-1) and is within the bounds of Types I and II marine kerogens (-27 to -34‰ and -24 to -34‰ $\delta^{13}C$, respectively; after Tyson, 1995) and conforms well with a global Phanerozoic average range of -28 to -32‰ $\delta^{13}C$ (Cambrian- Oligocene; Hayes, 1993). $\delta^{13}C_{org}$ values at Section AB become progressively more negative towards the close of the *transitans* zone and continue decreasing into the lower *punctata* zone from approx. -25.5 to -30‰ (Fig. 4.7). A positive ~3.75‰ excursion is then noted at the mfz above the Seq. 4-5 boundary, after which values taper off and become more depleted at about -29 to -30‰. At Section K, $\delta^{13}C_{org}$ decreases from about -27‰ to approx. -29‰ following the Seq. 4-5 boundary and a positive excursion correlative with the one at Section AB is then noted, although its magnitude of only ~1.2‰ is smaller (Fig. 4.7). This is a likely reflection of poorer peak resolution, as only a single sample defines the maximum extent of the excursion over a 3-m interval. In its upper portion, however, Section K provides a more resolved record of C-isotope variability higher in the *punctata* zone than does Section AB, where numerous coarse-grained redeposited horizons made detailed sampling (0.5 m) unfeasible. Interestingly, another positive shift – similar in magnitude at ~ 3‰ – is observed. A 'splicing' of both isotope records suggests that post-excursion values taper off to about -28 to -29 ‰ (Fig. 4.7).

The range of $\delta^{15}N_{org}$ values falls between -6 to 3‰ at Section AB, but is narrower in Section K at -2 to 2‰ (Appendix 4 A-1). On average, values are slightly depleted relative to the atmospheric standard (~0‰) at -1.0 ± 1.2‰ (1σ) and -0.6 ± 1.1‰ (1σ), respectively. Similar to the broad negative $\delta^{13}C_{org}$ trend, a broad negative hump in $\delta^{15}N_{org}$ values is noted in the K-Section profile (less resolved at Section AB). It begins with a negative 2‰ shift and ends with a positive 1.7δ‰ rebound. Prior to and after this broad negative, $\delta^{15}N_{org}$ averages 0.6‰ and -0.4‰ respectively, whereas during its course values average -1.5‰. The lower shift toward more depleted values is not discernable in the Section AB profile, but a correlative positive shift (~2.3‰) is noted higher in the section.

4.5.5. Trace element proxies and TOC

Prominent excursions of TOC and of all elemental proxies for relative changes in surface water bioproductivity (Ni, Cu, P) and paleoredox conditions near the SWI (Mo, V, U, Ni/Co, U/Th, V/Cr, V/(V+Ni)) are observed within the *punctata* zone and correspond to the global $\delta^{13}C_{(carb\ \&\ org)}$ excursions noted elsewhere (Figs. 4.7, 4.8, 4.9, Appendix 4A-2; Racki et al., 2008; Morrow et al., 2009). These enrichments correlate best with '$\delta^{13}C_{carb}$ Event III' of the four designated as distinct stages of the *punctata* Event (Fig. 4.8; Pisarzowska et al., 2006; Pisarzowska, 2008). Event III is

characterized by the main positive C-isotope excursion and is near-concurrent with the onset of transgressive pulse IIc-1 and the *transitans-punctata* zonal boundary. Geochemical anomalies in the *punctata* zone at the Miette platform were previously reported to have occurred during sea level lowstand and early transgression (Śliwiński et al., 2010). However, a reevaluation of the location of the Seq. 4-5 boundary based on facies stacking patterns and correlations with the nearby and well constrained stratigraphic Section K suggests that it is situated somewhat lower down in the Section AB profile (at 43 m, rather than at 64 m as reported earlier). The trace element excursions are thus found in the TST (Seq. 5) and are strongly correlated with detrital input proxies, TOC and MS (Appendices 3 and 4; Śliwiński et al., 2010). A concurrent lithologic change is noted within this interval from a total carbonate average of ~95 wt.% to more shaley mudstones at ~70 wt.% (Fig. 4.4).

The stratigraphic distribution of Ni, Cu, P and TOC reveals prominent excursions between 61.5-66.5 and 69-76.5 meters in Section AB, and a possible third enrichment near the top of the section at 111.0-114.0 m (Fig. 4.9). Stratigraphic 'background levels' for each analyte are defined between these three peaks. Within the largest of these excursions (Peak I, Fig. 4.9), concentrations are elevated up to 21 times above stratigraphic background, and somewhat less so in the subsequent two excursions higher in the section (Fig. 4.9). TOC rises to a maximum of 2.5 wt.% concurrently with the largest of the three shifts, (stratigraphic background = 0.3 wt.%), and up to ~1 wt.% and 0.75 wt.% higher up (Fig. 4.9). Note, however, that these TOC values are likely minima due to possible OM oxidation and weathering in outcrop (see *i.e.* Lüning et al., 2004). Increases in TOC are met by positive deflections of the $\delta^{13}C_{org}$ trend (Fig. 4.7), most notably at the stratigraphic level of Peaks I and II (compare Figs. 4.7 and 4.9). Similar overall trends are observed in the distribution of the paleoredox proxies (Fig. 4.9), where the first excursion peak is characterized by a maximum of 24-fold enrichment, with lesser but still prominent deviations from stratigraphic background associated with the two other peaks. Qualitatively, values of the redox indices are also noticeably elevated at these same depositional horizons (Fig. 4.9).

4.6. Discussion

4.6.1. The *punctata* Event in the context of Late Devonian environmental and ecosystem changes

Unprecedented evolutionary changes affected the Late Devonian biosphere, with increases in the biodiversity of terrestrial habitats and in the rates of their colonization by metazoans and plants (Coates, 2001; Edwards and Burgess, 1990, 2001; Milner, 1990; Selden,

1990, 2001). Especially noteworthy was the geographic expansion and diversification of deeply-rooted vascular land floras (Algeo et al., 1995; Algeo and Scheckler, 1998; House, 2002; Joachimski et al., 2009; Scheckler, 2001; Streel et al., 2000; Wright, 1990). Current interpretations suggest that widespread anoxia and deposition of OM-rich facies were related to increased nutrient delivery to the oceans, stimulated by terrestrial afforestation, intensified pedogenesis and weathering of lands uplifted during pulses of Eovariscan and Ellesmerian orogenic activity (Algeo and Scheckler, 1998; Racki, 1998, 2005; Tribovillard et al., 2004). A warming Frasnian 'greenhouse' climate and rising sea level (2^{nd} order) were conducive to the development of vast epeiric seas and extensive reef complexes such as those of the WCSB and the Devonian "Great Barrier Reef" of Western Australia (Playford et al., 1984; Geldsetzer, 1989; Kiessling et al., 1999; Mountjoy, 1989; Mossop and Shetsen, 1994). Climatic conditions shifted towards an 'icehouse' mode near the F/F boundary interval, culminating in end Devonian glaciations (Brzezinski et al., 2008; Caputo et al., 2008). These changes and ecosystem stressors – among them multiple extraterrestrial bolide impacts, flood basalt volcanism and sea level fluctuations – eventually contributed to one of the most severe extinction events since the radiation of metazoans during the Cambrian explosion (House, 2002; Racki, 2005; Sepkoski, 1984). However, approximately twenty 'short-term' Devonian 'events' have been recognized prior to the F/F boundary; some are characterized by a distinctive 'brief' faunal perturbation and/or with the deposition of black shales and other OM-rich facies, but also major excursions or permanent shifts of various geochemical records (Algeo et al., 1995; House, 2002). It is unlikely that any one of these events will comprehensively explain the global ecosystem and environmental changes of this time interval (House, 2002).

4.6.2. The *punctata* zone $\delta^{13}C$ excursion in the WCSB and correlative records

Of particular interest in the current state of Late Devonian studies is the reconstruction of diverse geochemical records with temporal resolutions higher than individual biozones (Racki, 2005), as for example the high resolution long-term $\delta^{13}C$ stratigraphies of Europe and the WCSB (Yans et al., 2007 and Holmden et al., 2006, respectively; Fig. 4.10). While widely distant, both records show a remarkable similarity and allow the resolution of higher frequency, shorter-term geochemical events (Fig. 4.10). They thus provide the broader-scale contextual framework for interpreting such shorter-term C-cycle perturbations (e.g. the *punctata* Event), revealing long-term patterns and relationships between major isotopic shifts, sea level changes, bioevents, and the deposition of OM-rich sediments (Buggisch and Joachimski, 2006; van Geldern et al., 2006; van Geldern and Joachimski, 2001). However a larger number of such high-resolution records is needed from paleodistant depositional basins so that inter-basinal comparisons can resolve

regional versus *global* contributions in what are increasingly being recognized as complex composite geochemical signals (Racki, 2005).

The supraregional extent of the *punctata* zone anomaly establishes it as a global C-cycle perturbation (Yans et al., 2007; Racki et al., 2008). However, while isotopic histories from all basins converge on a similar overall trend, both the excursion magnitudes and the Frasnian 'baseline' values vary from study to study (Fig. 4.8), reflecting the superposition of *regional* and *global* effects contributing to the isotopic record at any one location (*c.f.* Panchuk et al., 2006; see also Ma et al., 2008). In epeiric seas, regional effects are likely nontrivial and have been regarded as 'the rule rather than the exception' (Dopieralska et al., 2006; Holmden et al., 1998; Immenhauser et al., 2003; Panchuk et al., 2006). These include 1) variable inputs of ^{13}C-depleted meteoric fluids; 2) epeiric water mass 'ageing,' whereby restricted circulation of platform-top waters and the oxidation of sedimentary OM releases ^{12}C back into the water column, lowering its overall $\delta^{13}C$; 3) variable mixing of compositionally distinct dissolved inorganic carbon reservoirs of the open ocean, epeiric seaways and terrestrial runoff, in turn controlled by regional geography, seawater circulation patterns and T-R cycles; and 4) different post-depositional diagenetic histories (Immenhauser et al., 2003; Panchuk et al., 2006). Global $\delta^{13}C$ correlations commonly show different excursion magnitudes and pre- and post-excursion isotopic baselines which, in the absence of diagenetic alteration and sedimentary hiatuses, should not be the case if epeiric sea records reflect only changes in the $\delta^{13}C$ of the surface ocean and global perturbations of the C-cycle (Panchuk et al., 2006). The magnitude of the global open-marine $\delta^{13}C$ signal that contributed to the *punctata* zone anomaly - unmodulated by regional effects - still remains uncertain and decoupling of signals awaits further study. Off-platform localities, however, are likely at present its closest approximation (Table 4.3, Fig. 4.8).

Trace element and isotopic excursions noted in the lower *punctata* zone at the Miette platform correlate with the main positive $\delta^{13}C_{carb}$ shift (compare Figs. 4.7 and 4.9) observed in the widely distant basins of Eastern and Western Laurussia and South China (Figs. 4.7 and 4.9). This main positive in the latter locality, however, was noted somewhat below both the *transitans-punctata* boundary and the IIc1 transgressive pulse than in other sections (Fig. 4.8), and one of the Eastern Laurussian records is less clear in this regard, although a positive shift of ~3.5-4‰ is evident, albeit higher above the IIc1 pulse (Yans et al., 2007; Fig. 4.8). A few studies note and emphasize the abrupt negative excursion higher in the *punctata* zone as the more noteworthy $\delta^{13}C_{carb}$ anomaly that defines the *punctata* Event (Fig. 4.8; Yans et al., 2007; da Silva et al., 2010). A comparable excursion is noted in northeastern Alberta (Holmden et al., 2006), although correlation uncertainties between sections exist due to differing biostratigraphies (ostracode-based in Holmden et al. (2006) vs. conodont-based in all other *punctata* Event studies). Yet the

striking similarity between the broad-scale $\delta^{13}C_{carb}$ trends of Yans et al. (2007) and Holmden et al. (2006) strongly suggests that they are indeed one and the same excursion (Fig. 4.10). A similar feature is noted also in the present study, although its magnitude is smaller – a likely reflection of sampling in off-platform successions as opposed to platform-top depositional settings (Figs. 4.7 and 4.8; see further discussion below).

It seems apparent that discrepancies in biostratigraphic constraints are at least partially at fault for the offsets in timing noted among different basins for the main positive $\delta^{13}C_{carb}$ shift near the IIc1 transgressive pulse and the *transitans-punctata* zonal boundary (Fig. 4.8). Variations may further be related to varying degrees of communication between platform-top water masses and the open ocean, resulting in the asynchronous arrival of the *punctata* Event $\delta^{13}C$ anomaly carried by open-marine waters (*c.f.* Dopieralska et al., 2006; Holmden et al., 1998; Immenhauser et al., 2003; Ma et al., 2008; Panchuk et al., 2006; Pisarzowska, 2008). Differences in excursion magnitude on the other hand seem to be readily explained by noting the position of each sampled profile within a basin to platform-top transect and invoking variable contributions of regional effects to each composite signal (*c.f.* Pisarzowska's, 2008 compilation for the South Polish carbonate shelf; Fig. 4.11, Table 4.3). What becomes evident is a progressively larger magnitude of the main positive C-isotope excursion (from +2-2.5‰ up to +5-6‰) but also of the negative excursion higher in the *punctata* zone (from - 2-3‰ up to – 2-7‰; Fig. 4.11).

We see the $\delta^{13}C_{carb}$ record at the Miette platform as a composite of characteristic isotopic signals, including those of 1) the global *punctata* zone C-cycle perturbation; 2) regional biological forcing due to bioproductivity blooms and increased OM preservation; 3) isotopic effects associated with 3rd and 4th order sea level cycling; and 4) related changes in the extent of carbonate weathering during sea level lowstand and platform exposure. The most readily extractable signal of isotopic forcing is that which can be directly related to trace element excursions near the mfz which suggests regional eutrophication of the platform environment (Figs. 4.7 and 4.9). In terms of sea level change and isotopic forcing, 4th-order cycles are difficult to resolve in the slope facies due to even higher frequency sedimentary cyclicity, although 3rd order trends seem apparent. For example, $\delta^{13}C_{carb}$ increases near the close of the *transitans* zone during 3rd order lowstand (Seq. 4; Fig. 4.7) and could reflect increased admixture of isotopically-heavier weathered carbonate from subaerial exposure (Kump and Arthur, 1999; Whalen et al., 2000); dolomitization in a ~15 m interval straddling the Seq. 4-5 boundary, however, offers an alternative explanation for the heavier $\delta^{13}C_{carb}$ values (Section 5.3). The subsequent $\delta^{13}C_{carb}$ decrease during transgression records the diminution of this effect and a shift toward more open marine values (Table 4.2).

The $\delta^{13}C$ of the terrestrially-derived C signal depends in large part on the relative proportions of weathered carbonate and OM which complicates a simple interpretation (Kump and Arthur, 1999). During lowstand, however, restricted circulation in the basin coupled with ^{12}C-enriched OM decomposition and a greater admixture of isotopically light meteoric fluids likely contributed to the formation of depleted platform-top water masses and the precipitation of equally depleted carbonate (*c.f.* Holmden et al., 1998; Immenhauser et al., 2003). Such processes would have acted as a buffer against any ^{13}C-enriched weathering flux affecting the Miette platform during the Seq. 4-5 transition. The isotopic effects of increased bioproductivity near the overlying *mfz* were then expressed and superimposed on the isotopic effects of T-R cycling; increased OM production, export, burial and oxidation exhausted available oxygen in basinal waters, establishing an effective mechanism for OM preservation and the removal of ^{12}C from the isotopic reservoir (Fig. 4.7).

One feature of the *punctata* zone $\delta^{13}C_{carb}$ trend at Miette that is not readily explained by the isotopic forcing processes discussed above is the stepwise negative-stepwise positive excursion near the top of Section AB, where depletion down to ~0‰ occurs. This negative excursion is apparently correlative with similar shifts observed in northeastern Alberta and Belgium (Holmden et al., 2006 and Yans et al., 2007, respectively; Figs. 4.8 and 4.10). In platform-top depositional settings, Holmden et al. (2006) interpreted this as a result of extreme sea level lowstand, subaerial exposure, pedogenetic processes and the formation or alteration of carbonates in the presence of brackish or freshwater fluids with low $\delta^{13}C$ values. Platform exposure and export of ^{13}C-depleted carbonate detritus could perhaps also account for the lower $\delta^{13}C$ values in the periplatform settings of Miette if either 1) the $\delta^{13}C$ of the weathering flux was close to 0‰, or 2) the contribution of the weathering flux was not significant relative to size of the basinal C-reservoir to impart an isotopic shift. However, while the platform top was likely exposed during lowstand, neither stratigraphic section shows any evidence of extreme subaerial exposure within these horizons (Whalen et al., 2000; Whalen and Day, 2008).

The various global *punctata* Event $\delta^{13}C_{carb\ \&\ org}$ profiles have been described in terms of a 'broad positive' excursion (Racki et al., 2008). However, a fair amount of variability and deviation from this idealized trend is noted among the various profiles and in the foreslope-to-platform transect reference sections of Pisarzowska (2008), especially in the Section AB equivalent, distal slope-basinal profile at Kostomłoty-Mogiłki (Fig. 4.8; Pisarzowska, 2008). Only a mild broad positive trend in $\delta^{13}C_{carb}$ is discernable in the record from the Miette platform, with $\delta^{13}C_{org}$ forming only a narrow positive excursion in the lower *punctata* zone (Figs. 4.7 and 4.8). It is conceivable, however, that increased bioproductivity characterized a broader portion of the *punctata* zone than is evidenced by the TOC and trace element enrichments noted especially near the mfz (Fig. 4.9).

No record in this form exists to attest for this perhaps for the simple reason that suboxic-anoxic bottom water conditions favorable to OM preservation seem not to have been prevalent throughout the entire biozone (Fig. 4.9). This in turn can be explained by the morphological development of the platform. For example, once backstepping began and a steeper margin developed (bypass margin; Fig. 4.4 in Whalen and Day, 2008), it likely created a depositional system that could episodically be oxygenated by gravity flows during platform margin bypass and slope readjustment (Whalen et al., 2000; Whalen and Day, 2008). Such a 'basinal anoxia-disturbing' mechanism, related to platform growth and development, was also proposed at the isolated Redwater platform in the WCSB (Chow et al., 1995). Variations in OM $\delta^{13}C$ and $\delta^{15}N$, however, reveal no equally broad positive trends indicative of increased primary production, but rather suggest environmental stagnation with lower overall productivity following eutrophication near the mfz (Section 6.3.2.)

4.6.3. Trace element variations and changes in organic $\delta^{13}C$ and $\delta^{15}N$: eutrophication, stagnation and intensified marine N_2-fixation?

4.6.3.1. Trace elements

Changes in the production, export and preservation of OM under oxygen-deficient bottom water conditions and its dilution by biogenic or detrital input are regarded as fundamental to the formation of OM-rich facies (Canfield, 1994; Murphy et al., 2000; Pedersen and Calvert, 1990; Sageman et al., 2003). These processes can be viewed as end-members of a continuum, along which the influence of each end-member shifts as time passes and oceanographic conditions change. Evaluation of *punctata* zone trace element variations within a sequence stratigraphic perspective reveals that T-R cycles in the WCSB likely exerted a strong control on the influx of terrestrially-derived biolimiting nutrients (Śliwiński et al., 2010; Whalen et al., 2000; Whalen and Day, 2008, 2010). Strong statistical correlations were found between variations of detrital input, bioproductivity, and paleoreodox proxies with MS and TOC (Tables 4A-3 and 4A-4; Śliwiński et al., 2010). Transient eutrophication of the regional environment was apparently in large-part detrital-driven, and increased OM export to the SWI resulted either in 1) the establishment of suboxic/anoxic conditions favorable toward OM preservation or 2) the intensification and perpetuation of such preexisting conditions due to sluggish circulation in the basin (Stoakes, 1980).

Eutrophication in the following discussion is understood as a situation where increased nutrient levels in an epeiric seaway result in phytoplankton and algal blooms, shoaling of the euphotic zone through reduced water transparency, diminished carbonate production and trophic

changes favoring a lower biodiversity dominated by generalists and opportunistic species (*c.f.* Hallock, 1988a,b; Hallock and Schlager, 1986; Wood, 1993; Brasier, 1995; Whalen et al., 2002). Contemporary examples of eutrophication in reef systems and carbonate platforms include, for example, the case of the Great Barrier Reef lagoon and reefs off the coast of Brazil (Bell, 1992; Costa Jr. et al., 2008).

Elevated concentrations of Ni, Cu, P and concurrent TOC increases in Section AB suggest episodic intensifications of primary production and OM export to the SWI in the lower and possibly also the upper *punctata* zone (Fig. 4.9). The time interval of each of the three anomalous horizons can be approximated by accepting the following constraints: 1) that the *punctata* zone was 0.6 Ma in duration (Kaufmann, 2006); 2) the measured section accounts for almost the entire zone, with the *punctata-hassi* boundary lying within just a few meters above the sampled horizons (Section 2); and 3) by subtracting out the total thickness of redeposited beds in the section to account only for background sedimentation. This yields a duration of ~40 k.y. for the lowest excursion (Peak I, Fig. 4.9), ~60 k.y. for the subsequent (Peak II, Fig. 4.9), and some 25 k.y. for the last (Peak III, Fig. 4.9).

Copper and Ni are paleoceanographic proxies for changes in primary production intensity, as primary producers actively assimilate these metals for use in the biochemical mechanisms that allow for the utilization of C, N, P, and Si (the major algal nutrients; Falkowski, 2004; Morel et al., 2004). Sinking OM further 'scavenges' these metals from the water column via passive chemical complexing, as does the redox cycling of Fe-Mn oxyhydroxides (*e.g.* Bruland and Lohan, 2004; Morel et al., 2004; Tribovillard et al., 2006). Seawater, however, has been described as the most extreme environment on Earth with respect to its paucity of essential bioactive trace metals, resulting in the evolution of highly efficient uptake systems with rates approaching the physical limits posed by kinetics and rates of diffusion of chemical species to cell surfaces (Morel et al., 2004). The rate of uptake is generally proportional to the free-metal, chemically-reactive concentration in seawater (Bruland and Lohan, 2004; Morel et al., 2004). The bulk trace elemental make-up of phytoplankton is thus reflected in the 'excess' trace element fraction of black shales and sapropels – that is, the concentration fraction that is not bound in detrital components (Falkowski, 2004).

A further mechanism for Ni and Cu accumulation in a carbonate depositional environment, however, is carbonate precipitation which is generally negligible in siliciclastic systems. A study on the incorporation of metals into foraminiferal calcite demonstrated that progressively higher concentrations of Ni and Cu in the surrounding chemical environment are reflected by a proportional increase in the biomineralized tests (Munsel et al., 2010). This is due to a general tendency of the transition metals to be preferentially partitioned into carbonate rather

than the seawater solution (Veizer, 1983; Munsel et al., 2010), suggesting in turn that in a carbonate depositional system, various trace elements will not only accumulate through delivery in association with OM and the detrital fraction, but also through incorporation into precipitated carbonate phases.

Nickel and Cu accumulations noted in the *punctata* zone stratigraphy at the Miette platform are accompanied by higher concentrations of P, which is an essential biolimiting nutrient in the oceans on geological timescales (Algeo and Ingall, 2007). The primary source of sedimentary P is sinking OM which releases PO_4^{3-} during subsequent oxic, suboxic and anoxic bacterial degradation; enrichments, however, are not necessarily *directly* indicative of intensified bioproductivity (Ruttenberg, 1990; Ruttenberg and Berner, 1993; Tribovillard et al., 2006). Both modern and ancient studies have proposed models coupling oceanic anoxia to more efficient sedimentary P recycling and thus increased primary production *(e.g.* Ingall and Jahnke, 1994; van Cappellen and Ingall, 1994; Algeo and Ingall, 2007). Phosphate is thought to be sequestered in the sediment via bioaccumulation and redox cycling of Fe-oxyhydroxides - to which it adsorbs - under *oxic* bottom waters, but also through the redox-independent precipitation of calcium-phospahte minerals (van Cappellen and Ingall, 1994). Conversely under anoxic conditions, phosphate is thought to be preferentially released and recycled back into the water column and eventually into the euphotic zone, where it can again be utilized by primary producers (van Cappellen and Ingall, 1994).

Recent findings suggest, however, that microbial sequestration of P under *anoxic* conditions may result in far more extensive P-trapping, as bacteria act to catalyze the conversion of dissolved phosphate to solid carbonate-apatite phases (Goldhammer et al., 2010; Ingall, 2010). Elevated P accumulations during the *punctata* Event in the WCSB (Fig. 4.9) can be taken to corroborate interpretations of increased OM fluxes to the sediment, with possible subsequent P-trapping through authigenic apatite formation under suboxic-anoxic water conditions (see discussion below). However, a detrital origin – that is P in the form of detrital apatite - is likewise possible given the above-mentioned statistical correlations among all proxies with the detrital input (Tablers 4A-3 and 4A-4).

Accumulations of redox sensitive trace elements above stratigraphic background levels within the three excursion horizons (Fig. 4.9) in the *punctata* zone can be taken to imply restricted circulation around the Miette platform (Stoakes, 1980) and the establishment or intensification of suboxic-anoxic conditions favorable towards OM preservation. Redox sensitive *indices* (Fig. 4.9) were used in previous studies as *collective* and *relative* indicators of *dominant* (or time-averaged) redox conditions (Rimmer, 2004; Rimmer et al., 2004; Riquier et al., 2006; Algeo and Maynard, 2008; Racka et al., 2010; Śliwiński et al., 2010). Using the oxic-suboxic-

anoxic threshold values determined by Hatch and Leventhal (1992) and Jones and Manning (1994) (Table 4.4) strengthens redox interpretations based on the more commonly employed U, Mo and V proxies (Algeo and Maynard, 2008; Calvert and Pedersen, 1993; Piper and Calvert, 2009; Tribovillard et al., 2006). Caution, however, has been advocated against strict applications of those and other redox thresholds as they have been observed to yield discrepant paleoredox interpretations (Rimmer, 2004, see also Racka et al., 2010 and references therein). A set of absolute threshold values based either on contemporary suboxic-anoxic basin analogues or thresholds determined for a particular paleobasin are likely not appropriate for depositional environments of a different age, paleogeographic setting, or different detrital provenance. Collectively, all indices in the stratigraphy at the Miette platform seem to imply a change toward oxygen-deficient conditions in the lower and upper *punctata* zone, concurrent with interpreted eutrophication (Fig. 4.9). The Mo-U-V suite of proxies likewise indicates such a change, with the accumulation of Mo possibly indicating the development of temporary euxinic (*i.e.* sulfidic) conditions (Fig. 4.9; Tribovillard et al., 2006).

Increased detrital input in the WCSB during the IIc1 transgressive pulse may have been a 'mixed-signal', influenced by regional 3rd order sea level change set against the background of global Late Devonian environmental and ecosystem changes (Śliwiński et al., 2010). In accordance with models of MS variations and regional sequence stratigraphy, enhanced delivery of terrigenous material is expected during conditions of sea level lowstand and early transgression (Ellwood et al., 1999; Whalen and Day, 2008, 2010). However, coeval developments on land conceivably acted to amplify this input, stimulating the oceanographic changes observed in the *punctata* zone (Pisarzowska et al., 2006; Racki et al., 2008). A broad climatic warming trend (up to 30-32°C) spanning most of Frasnian time (Streel et al., 2000; Joachimski et al., 2009) likely intensified the weathering of uplifted lands in the Ellesmerian fold belt which sourced the WCSB (Oliver and Cowper, 1963; Stoakes, 1980; Switzer et al., 1994; Whalen and Day, 2008; see Śliwiński et al., 2010 for broader discussion of the tectonic uplift stimulus and regional MS variability in relation to the *punctata* Event). Note however that conodont apatite $\delta^{18}O$ records from Central Europe indicate a weak although accelerated cooling trend (~28-24°C) throughout the *punctata* zone following the main positive $\delta^{13}C$ shift near the *transitans-punctata* boundary (Pisarzowska, 2008; Racki et al., 2008 and Fig. 4.1 therein), which may represent a shorter term (higher-order) climatic oscillation superimposed on the broader warming tendency of the Frasnian. Potentially far more influential, however, could have been the rapid rise and expansion of the first terrestrial forests and concurrent evolution of complex paleosols, beginning in mid-Frasnian time (Section 6.3.3.; Algeo et al., 1995; Algeo and Scheckler, 1998).

4.6.3.2. Organic $\delta^{13}C$ and $\delta^{15}N$

Stable isotope ratios of C and N change in predictable ways during cycling through the biosphere and ocean-atmosphere system (*e.g.* Altabet, 2006; Galbraith et al., 2008; Hayes, 1993; Holser, 1997; Kump and Arthur, 1999; Peterson and Fry, 1987; Popp et al., 1997; Veizer et al., 1999). A measure of trends and tendencies in the isotopic composition of bulk OM or of specific organic compounds makes stable isotope dynamics applicable to solving biogeochemical problems in the present, and by way of analogy, in ecosystems of the distant geologic past (Peterson and Fry, 1987). The integration of such isotopic trends with trace element records presents a clearer account of oceanographic changes throughout the *punctata* zone in the WCSB (Figs. 4.7 and 4.9). Regional variations in C and N cycling were likely a significant contributor to the isotopic records, as water masses in Paleozoic epeiric seaways likely experienced restriction and isotopic/compositional evolution away from the parent open marine waters through a combination of biological activity, sluggish circulation and temperature and density contrasts (by way of analogy with modern near-equatorial carbonate systems; Patterson and Walter, 1994; Holmden et al., 1998; Immenhauser et al., 2003; Ma et al., 2008; Panchuk et al., 2006).

The lower *punctata* zone at the Miette platform is characterized by concurrent positive $\delta^{13}C_{carb\ \&\ org}$ excursions near the mfz (Fig. 4.7) that correlate with a stratigraphic TOC maximum and the beginning of a broader positive $\delta^{13}C_{carb}$ trend that has been observed in other basins (Section 6.2; Fig. 4.8). Correlative positive excursions in $\delta^{13}C_{org}$ trends have also been noted in other localities, which show a similar spread of both isotopic values and of excursion magnitudes (~4‰ Ma et al., 2008; Pisarzowska et al., 2006; Racki, 2004). However, in contrast to the broad positive deviations noted in these correlative sections, a broad *negative* is observed at Miette, bounded by two narrower positive deflections in the lower *and upper* portions of the *punctata* zone (Fig. 4.7). Throughout this broad negative interval, $\delta^{13}C_{org}$ averages -29.8‰. Prior to and thereafter, values average about -28‰.

Positive excursions of organic $\delta^{13}C$ indicate 1) increases in surface water primary productivity and/or 2) increases in the amount of buried, ^{12}C-enriched OM (Kump and Arthur, 1999; Sephton et al., 2002). Integration of trends in the isotopic and trace element data indicates that both these mechanisms of ^{13}C-enrichment were expressed early in the *punctata* zone, with oxygen deficient conditions near the SWI allowing for the preservation and burial of isotopically light OM produced during eutrophication (Figs. 4.7 and 4.9).

A survey of palynofacies and organic biomarkers in correlative sections at the isolated Redwater Platform in the WCSB (Fig. 4.2) and in Central Europe revealed further evidence for enhanced bioproductivity in the lower *punctata* zone (Chow et al., 1995; Marynowski et al., 2008). During the deposition of the Duvernay Formation - a subsurface equivalent of the Perdrix Fm.

(Fig. 4.1) - at Redwater, OM-rich sediments generally accumulated during conditions of 'normal' surface water productivity but enhanced preservation under anoxic bottom waters (Chow et al., 1995). A single anomalous organic-rich horizon, however, was found to contain a high concentration of algal akinete cells that are indicative of algal blooms and anomalously high surface bioproduction (Chow et al., 1995). In Central Europe, organic geochemical proxies revealed independent but similar conclusions regarding the trends of oceanographic changes in the *punctata* zone (compare Fig. 4.9 herein and Figs. 5 and 9 in Marynowski et al., 2008). Mainly, (1) the lower *punctata* zone seems to be characterized by unusually high bioproductivity and concurrent establishment of suboxic-anoxic bottom water conditions. The characteristic biomarker isorenieratane – a compound derived from green sulfur bacteria – was recovered from platform-top depositional settings in Central Europe, suggesting temporary *photic zone* euxinia (Marynowski et al., 2008). (2) The upper *punctata* zone is then characterized by lower overall productivity and oxic conditions during sedimentation of the 3rd order regressive facies leading up to the *punctata-hassi* zonal boundary. (3) Near this boundary interval another lesser bioproductivity increase is noted, with concurrent, although again less intense, sub-photic zone suboxia-anoxia.

General increases and statistical correlations of all proxies with the detrital input and the coincidence with transgression in the WCSB point to an increased delivery of nutrients from land, perhaps initiating the '*punctata* Event'. A steadily increasing terrestrial input throughout the *transitans, punctata* and *hassi* zones is noted also in Central Europe based on characteristic palynofacies and organic biomarker assemblages (Marynowski et al., 2008).

A concurrent lithologic transition in the slope facies at the Miette platform from muddy mudstones-wackstones to black, organic-rich, shaly mudrocks near the mfz further implies an environmental shift from oligotrophic to eutrophic conditions (Brasier, 1995; Hallock, 1988a; Hallock and Schlager, 1986; Wood, 1993). The eutrophication event was likely associated with a faunal shift in which planktonic primary producers and benthic algae became temporarily dominant under 'greenwater' environmental conditions (Brasier, 1995). A scenario like this has previously been implicated for transgressive systems at the Miette platform (Whalen et al., 2002) and in the eutrophication model of Devonian carbonate ramp demise in western Alberta following the F/F events and later at the D-C boundary (Caplan et al., 1996 and Peterhänsel and Pratt, 2001, respectively). Within the bounds of the *punctata* C-isotope anomaly, Pisarzowska et al. (2006) observed a moderate biodiversity depletion and a more homogenous, impoverished fauna due to eutrophic conditions and overall ecosystem stagnation in Central Europe, although no significant extinction. Following the transgressive pulse and bioproductivity blooms, the concentration of bioavailable nutrients may have been reduced through increased consumption

and organic-C burial allowing stagnant conditions to limit the size of the biomass, thus inducing the broad negative $\delta^{13}C_{org}$ trends within the bounds of the positive excursions noted at the Miette platform (Fig. 4.7). A similar trend in $\delta^{15}N_{org}$ values also predominates throughout this interval.

Bulk sedimentary $\delta^{15}N$ measurements are being increasingly used to reconstruct past changes in the extent of (1) marine N_2 fixation; (2) water column denitrification and (3) sedimentary denitrification (Altabet, 2006; Galbraith et al., 2008). These processes have likely been the dominant input and output variables of a steady state marine N-cycle throughout geologic time (Altabet, 2006; Galbraith et al., 2008). We assume this to hold true for the Late Devonian, but assert that interpretations of $\delta^{15}N_{org}$ trends in deep time are at present only broad outlines of *conceivable* oceanographic changes. The record of past variations in the mean isotopic composition of oceanic nitrate ($\delta^{15}N_{nitrate}$) – the dominant form of fixed (bioavailable) N in the oceans and the global variable in the composite $\delta^{15}N$ signal - has not yet been resolved (Altabet, 2006; Galbraith et al., 2008). This necessitates an assumption about a global Late Devonian 'baseline value,' which can only be approximated to the first order using the modern mean oceanic $\delta^{15}N_{nitrate}$ value of 5‰ (Galbraith et al., 2008). This global average is governed by the relative proportion of sedimentary versus water column denitrification, where the former generally results in no net isotopic fractionation, whereas denitrification in the water column under suboxic-anoxic conditions induces ^{15}N-enrichments as high as 22-30‰ (Galbraith et al., 2008). Given the commonality of suboxic/anoxic events during Devonian time, however, mean oceanic $\delta^{15}N_{nitrate}$ was conceivably somewhat higher than at present. In a manner analogous to $\delta^{13}C$ records, $\delta^{15}N$ is a composite signal of 1) changes in average oceanic $\delta^{15}N_{nitrate}$; 2) regional watermass enrichments or depletions relative to mean oceanic $\delta^{15}N_{nitrate}$ through interactions with terrestrially-derived dissolved nitrate; and 3) changes in the extent to which nitrate is regionally consumed (where near full consumption equates to no expression of the metabolic fractionation effect; Galbraith et al., 2008).

The $\delta^{15}N_{org}$ signal at the Miette platform is more chaotic in the platform-margin proximal stratigraphic section (AB) than in the more basin-ward profile (Section K) (Fig. 4.7). The character of both sections differs most prominently in the relative amount of coarse-grained horizons redeposited from upslope (prevalent in Section AB), suggesting that the less noisy trend in the more basinal profile (Section K) is related to more continuous 'background' sedimentation (Fig. 4.4). The low $\delta^{15}N_{org}$ values in both profiles, however, seem to be anomalously depleted and generally outside the typical range of the modern planktonic biomass and modern marine nitrate (~5‰), and are more unusual when one considers that the kerogen analyzed likely represents an isotopically enriched residual following bio- and thermodegradation associated with petroleum and gas generation (Fig. 4.5) (Altabet, 2006; Galbraith et al., 2008; Hoefs, 1987; Libes and

Deuser 1988; Rau et al., 1987). Prominent examples of similarly ^{15}N-depleted values encountered in the rock record include the Pliocene sapropels of the Mediterranean Sea (horizons of organic-rich sediments – *e.g.* Arnaboldi and Meyers, 2006; Calvert et al., 1992, Struck et al., 2001) and Cretaceous OM-rich Atlantic sedimentary sequences (Kuypers et al., 2004; Rau et al., 1987). It was proposed in both cases that slow turnover and denitrification in the water column could have reduced the resupply of bioavailable nitrate to surface waters, resulting in nitrate-limited conditions favorable to the proliferation of the otherwise marginal N_2-fixing autotrophs - mostly cyanobacteria - which gain an ecological advantage by their unusual ability to utilize dissolved N_2 gas (Altabet, 2006; Galloway, 2003). The bulk $\delta^{15}N$ of N_2-fixing microbes is only minimally fractionated relative to atmospheric N_2 at 0 to -2‰ (Galbraith et al., 2008). Thus, if such a biomass became a regionally significant fraction of the OM exported to the sediment during more stagnant conditions following the eutrophication event early in the *punctata* zone, $\delta^{15}N_{org}$ values could conceivably have taken on the depleted character noted in both sections (Fig. 4.7). Sluggish circulation around the reef complexes in the WCSB and seawater ageing in this epeiric setting could have been pronounced, allowing for the perpetuation of such nitrate-limited conditions throughout much of the *punctata* zone (Fig. 4.7).

4.6.3.3. The punctata Event within the context of the Devonian *terrestrial-marine teleconnections* model

The rapid and geographically widespread evolution of soils and deeply-rooted, arborescent vascular land plants is likely one of the more influential factors driving the biotic and geochemical perturbations noted in the marine record of Middle-Late Devonian time (Algeo et al., 1995; Algeo and Scheckler, 1998). The *Devonian terrestrial-marine teleconnections* model (Algeo and Scheckler, 1998) proposes that this evolutionary event monumentally altered the character of continental weathering through the advent of efficient and thorough bedrock weathering in the microenvironments surrounding root systems of arborescent taxa, such as the archeopterids (see also Beerling and Berner, 2005; Berner, 1997, 1998; Wright, 1990; Scheckler, 2001). This increased the fluxes of readily available trace elements and macronutrients to the ocean, which is considered an extreme environment in terms its scarcity in essential trace elements needed for primary production and utilization of C, N, P and Si (Morel et al., 2004).

Afforestation could have been exceptionally rapid. Burnham (2008) estimates that the time needed for newly evolved and reasonably successful plant species to increase in abundance to a biomass sufficiently large so as to have a high probability of representation in the fossil record is geologically short – measured in mere thousands of years. For rocks of Devonian age, this can be thought of as near instantaneous. However a lack of suitable datable materials in

Devonian non-marine successions will likely continue to hinder a *tight* constraint and correlation between the timing of initial forest expansion with marine events in the geological record. We can speculate, however, that the *punctata* Event, temporally near the onset of archaeopterid rise to dominance, may record the geochemical consequence of one of several initial pulses of terrestrial afforestation.

A fundamental characteristic of this model is its eloquent description of a *dynamic* but *transient* response of the lithosphere-atmosphere-ocean system to a rapid and geographically expansive diversification of a terrestrial biomass capable of interacting with its substrate in an evolutionarily unprecedented way. The large atmospheric CO_2 reservoir of the pre-Devonian (4-20 PAL [present atmospheric level], Berner, 1994, 2006; Berner et al., 2007) may have allowed for a *rapid*, however pulsed, diversification and expansion of forests. 'Excess' atmospheric CO_2 – that is the amount in excess of that supplied by influxes into the atmosphere-ocean system by volcanic and metamorphic degassing - was consumed and actively pumped into soils where it stimulated a transient increase in silicate weathering. A steady-state was eventually achieved with lower overall atmospheric CO_2 levels (1 PAL during the mid-Carboniferous, Berner, 1994, 2006; Berner et al., 2007) maintained via active pumping by terrestrial vegetation and more steady rates of silicate weathering, albeit still higher than those of the pre-Devonian.

4.7. Conclusions

The application of various geochemical proxies for changing oceanic bioproductivity and redox conditions and integration with a high resolution regional sea level history provides an internally consistent account of the Late Devonian *punctata* Event in the Western Canada Sedimentary Basin (WCSB). Variations of trace element proxies in this predominantly carbonate depositional environment, together with excursions of $\delta^{13}C_{(carb\ \&\ org)}$ and $\delta^{15}N_{org}$ and increased TOC indicate eutrophication of the basin early in the *punctata* zone, but also possibly near its close. Export of organic matter to the sediment seems to have been intense enough to drive bottom water suboxia-anoxia and thus the establishment of conditions favorable to its preservation. Lower overall $\delta^{13}C_{org}$ and $\delta^{15}N_{org}$ values indicate that a stagnant period of lower overall productivity persisted following the main eutrophication event near the *transitans-punctata* boundary, during which N_2-fixing microbes may have had an ecological advantage under nitrate limited conditions. A correlative eutrophication event was also reported from Central Europe where it was followed by stagnant 'greenwater' conditions and a more impoverished biota, and organic petrography of strata at the Redwater Carbonate Complex in the WCSB revealed an anomalous organic matter-rich horizon indicative of algal blooms and higher than normal surface water productivity.

Strong statistical correlations of all proxies with the detrital input (reported previously in Śliwiński et al., 2010) suggest that eutrophication was at least partially detrital-driven during conditions of 3rd order sea level transgression, in agreement with regional sequence stratigraphy and models of MS variations during T-R cycles (Whalen and Day, 2008, 2010).

The $\delta^{13}C_{carb}$ record at the Miette buildup is a complex composite of isotopic effects associated with 1) a global C-cycle perturbation within the *punctata* biozone; 2) 3rd and 4th order sea level T-R cycles; and 3) bioproductivity blooms and the removal and burial of ^{12}C-enriched organic matter at the IIc1 mfz.

A survey of the literature reveals that the magnitude of the global *punctata* Event $\delta^{13}C_{carb}$ excursions varies among basins. This can be explained in part by noting the location of each studied profile within a platform-top to basin transect, wherein the excursion magnitudes decrease basinwards. Variable mixing of the anomalous global C-isotope signal with regional C-cycle effects may further account for the observed differences.

Given its numerous oxidation states, the pathways of $\delta^{15}N_{org}$ diagenesis are complex and at present little understood. The use of such records in studies of Devonian-aged rocks seems at best to equivocally suggest possible changes in oceanographic conditions that may have taken place, although only when interpreted in the context of other geochemical proxies. In a manner analogous to $\delta^{13}C$ records, regional N-cycling in the epeiric seaway of the Western Canada Sedimentary Basin likely heavily influenced the composite record, overshadowing the global $\delta^{15}N$ signal. This record at the Miette platform may have been complicated by bio- and thermo-degradation associated with kerogen maturation at burial temperatures reaching ~200°C. While the net effect was likely isotopic enrichment, the residual kerogen is nonetheless lighter than modern planktonic $\delta^{15}N$ and falls within the range of N_2-fixing microbes. These gain an ecological advantage when oceanic nitrate stores in surface waters become depleted and restore a balance through atmospheric N_2-fixation. Conceivably, eutrophication early in the *punctata* zone would have depleted bioavailable nitrate, giving N_2-fixers a temporary ecological advantage. Low $\delta^{15}N_{org}$ values could be a reflection of a greater contribution of such a biomass to the total organic matter exported to the sediment-water interface.

The timing of the *punctata* Event approximately coincides with the advent of archaeopterid forest expansion and rise to dominance beginning around mid-Frasnian time. This evolutionary event may have amplified the detrital flux to the oceans, which was likely already elevated by conditions of sea level lowstand, early transgression and episodes of increased weathering of rising orogens in near-equatorial regions. The *marine-terrestrial teleconnections model* of *Algeo and Scheckler (1998)* thus provides an intricate contextual framework for interpreting the *punctata* geochemical anomalies.

Acknowledgments

This work is dedicated to prof. B. Charlotte Schreiber, for her caring support. We thank K. Severin for constructive discussions and instrumental help in developing specialized XRF trace element analytical protocols and J. Addison for providing much help with data interpretation. We kindly thank T. Howe and the *Alaska Stable Isotope Facility* for help with generating isotope data, and express gratitude to the *American Association of Petroleum Geologists* for helping to offset the costs of analytical work via the *Grants-in-Aid* Program (Śliwiński 2010). We would like to acknowledge A. Fuhrman, M. Kuhn, H. Dowd, J. Morris (Illinois State U.), J. Over, A. Norton, M. Lester (SUNY Geneseo), P. Mayer (U. Wisconsin Madison), and A. Krumhardt, and R. Missler (UAF) for assistance in the field. Acknowledgement is also made to the donors of The Petroleum Research Fund, administered by the American Chemical Society (Whalen), and to the National Geographic Society-Foundation for Exploration and Research (Day) for partial support of this research. The *Geophysical Institute and Department of Geology and Geophysics, University of Alaska Fairbanks* are further acknowledged for additional financial support. This research would not have been possible but for the cooperation of Parcs Canada who provided access and permission to sample at field localities in Jasper National Park.

4.8 References

Algeo, T.J., Berner, R.A., Maynard, J.B., and Scheckler, S.E., 1995. Late Devonian oceanic anoxic events and biotic crises: "rooted" in the evolution of vascular land plants? GSA Today, **5**, 1-66

Algeo, T.J., and Ingall, E., 2007. Sedimentary Corg:P ratios, paleocean ventilation, and Phanerozoic atmospheric *p*O2: Palaeogeography, Palaeoclimatology, Palaeoecology, **256**, 130-155

Algeo, T.J., and Scheckler, S.E., 1998. Terrestrial-marine teleconnections in the Devonian: links between the evolution of land plants, weathering processes, and marine anoxic events. Philosophical Transactions of the Royal Society B-Biological Sciences, **353**, 113-128

Algeo, T.J., and Maynard, J.B., 2008. Trace-metal covariation as a guide to water-mass conditions in ancient anoxic marine environments. Geosphere, **4**, 872-887

Allan, J.R., and Matthews, R.K., 1982. Isotope signatures associated with early meteoric diagenesis. Sedimentology, **29**, 797-817

Allan, J., and Creaney, S., 1991. Oil families of the Western Canada Basin. Bulletin of Canadian Petroleum Geology, **39**, 107-122.

Altabet, M.A., 2006. Isotopic tracers of the marine nitrogen cycle: present and past. In: Handbook of Environmental Chemistry Volume 2 Part N, 251-293

Arnaboldi, M., and Meyers, P.A., 2006. Patterns of organic carbon and nitrogen isotopic compositions of latest Pliocene sapropels from six locations across the Mediterranean Sea. Palaeogeography, Palaeoclimatology, Palaeoecology, **235**, 149-167

Baxby, M., Patience, R.L. and Bartle, K.D., 1994. The origin and diagenesis of sedimentary organic nitrogen. Journal of Petroleum Geology, **17**(20), 211–230

Bathurst, R.G.C., 1982. Genesis of stromatactis cavities between submarine crusts in Paleozoic carbonate mud buildups. Journal of the Geological Society of London, **139,** 165-181

Beerling, D.J., and Berner, R.A., 2005. Feedbacks and the coevolution of plants and atmospheric CO_2. Proceedings of the National Academy of Sciences of the United States of America, **102**, 1302-1305

Bell, P.R.F., 1992. Eutrophication and coral reefs – some examples in the Great Barrier Reef Lagoon. Water Research, **26**(5), 553-568

Berner, E.K., Berner, R.A. and Moulton, K.L., 2007. Plants and mineral weathering: Present and past. In Treatise on Geochemistry, Chapter 5.06, 169-188

Berner, R.A., 1994. GEOCARB-II - A revised model of atmospheric CO_2 over Phanerozoic time. American Journal of Science, **294**, 56-91.

Berner, R.A., 1997. Paleoclimate - The rise of plants and their effect on weathering and atmospheric CO_2. Science, **276**, 544-546

Berner, R.A., 1998. The carbon cycle and CO_2 over Phanerozoic time: the role of land plants Philosophical Transactions of the Royal Society of London Series B-Biological Sciences, **353**, 75-81

Berner, R.A., 2006. GEOCARBSULF: A combined model for Phanerozoic atmospheric O_2 and CO_2. Geochimica et Comochimica Acta, **70**(23), 5653-5664

Bond, G.C., and Kominz, M.A., 1984. Construction of tectonic subsidence curves for the early Paleozoic miogeocline, southern Canadian Rocky Mountains: Implications for subsidence mechanisms, age of breakup, and crustal thinning: Geological Society of America, Bulletin,**95**, 155–173

Brasier, M.D., 1995. Fossil indicators of nutrient levels. 1: Eutrophication and climate change. *In:* Bosence, D.W.J., and Allison, P.A., eds., marine palaeoenvironmental analysis from fossils. Geological Society [London] Special Publication, **83**, 133-132

Bruland, K.W., and Lohan, M.C., 2004. Controls of Trace Metals in Seawater. In. The Oceans and Marine Geochemistry, Treatise on geochemistry volume 6, Eds. Elderfield, H., Holland, H. D., and Turekian, K. K., Elsevier, Amsterdam, Heidelberg, 23-47

Brzezinski, D.K., Cecil, C.B., Skema, V.W., and Stamm, R., 2008. Late Devonian glacial deposits from the eastern United States signal an end of the mid-Paleozoic warm period: Palaeogeography, Palaeoclimatology, Palaeoecology, **268**, 143–151.

Buggisch, W., and Joachimski, M.M., 2006. Carbon isotope stratigraphy of the Devonian of Central and Southern Europe. Palaeogeography, Palaeoclimatology, Palaeoecology, **240**, 68-88

Burnham, R.J., 2008. Hide and go seek: What does presence mean in the fossil record? Annals of the Missouri Botanical Garden, **95**, 51-71.

Calvert, S.E., Nielsen, B., and Fontugne, M.R., 1992. Evidence from nitrogen isotope ratios for enhanced productivity during formation of eastern Mediterranean sapropels. Nature 359

Calvert, S.E., and Pedersen, T.F., 1993. Geochemistry of recent oxic and anoxic marine sediments - implications for the geological record. Marine Geology, **113**(1-2), 67-88

Canfield, D.E., 1994. Factors influencing organic carbon preservation in marine sediments. Chemical Geology, **114**(3-4): 315-329

Caplan, M.L., Bustin, R.M., and Grimm, K.A., 1996. Demise of a Devonian-Carboniferous carbonate ramp by eutrophication. Geology **24**(8), 715-718

Caputo, M.V., 2008. Late Devonian and Early Carboniferous glacial records of South America. Geological Society of America Special Papers, **441**, 161-173

Carpenter, S.J. and Lohmann, K.C., 1989. $\delta^{18}O$ and $\delta^{13}C$ variation in Late Devonian marine cements from the Golden Spike and Nevis reefs, Alberta Canada: Journal of Sedimentary Petrology, **59**, 792-814

Chow, N., Wendte, J. and Stasiuk, L.D. 1995. Productivity versus preservation controls on two organic-rich carbonate facies in the Devonian of Alberta: sedimentological and organic petrological evidence. Bulletin of Canadian Petroleum Geology, **43**, 433-460.

Coates, M.I., 2001. Major Events in the History of Life: Palaeozoic Events: Origin of Tetrapods. In Briggs, D.E.G. and Crowther, P.R. (eds.), Palaeobiology II. Blackwell Science, Oxford. 74-79

Costa, Jr., O.S., Nimmo, M., and Attrill, M.J., 2008. Coastal nitrification in Brazil: a review of the role of nutrient excess on coral reef demise. Journal of South American Earth Science, **25**, 257-270

da Silva, A.C. and Boulvain, F., 2008. Carbon isotope lateral variability in a Middle Frasnian carbonate platform (Belgium): significance of facies, diagenesis and sea-level history. Palaeogeography, Palaeoclimatology, Palaeoecology 269, 189–204

Day, J., 1996. Faunal signatures of Middle-Upper Devonian depositional sequences and sea level fluctuations in the Iowa Basin: US mid-continent. Geological Society of America Special Papers, **306**, 277-300

Denison, R.E., Koepnick, R.B., Burke, W.H., Hetherington, E.A. and Fletcher, A., 1997. Construction of the Silurian and Devonian seawater 87Sr-86Sr curve. Chemical Geology, **140**, 109-121

Dopieralska, J., Belka, Z., and Haack, U., 2006. Geochemical decoupling of water masses in the Variscan oceanic system during Late Devonian times. Palaeogeography, Palaeoclimatology, Palaeoecology, **240**, 108-119

Dunn, P.A., Lohmann, K.C., and Hurley, N.F., 1985. Secular del13C and del18O variations in Devono-Carboniferous carbonates (abs.) Geological Society of America Abstracts with Programs, **17**, 569

Edwards, D., and Burgess, N.D., 1990. Major Events in the History of Life: Terrestrialization: Plants. In Briggs, D.E.G. and Crowther, P.R. (eds.), Palaeobiology. Blackwell Science, Oxford. 60-64

Edwards, D., and Burgess, N.D., 2001. Major Events in the History of Life: Palaeozoic Events: Early Land Plants. In Briggs, D.E.G. and Crowther, P.R. (eds.), Palaeobiology II. Blackwell Science, Oxford. 63-67

Ellwood, B.B., Crick, R.E., and Hassani, A.E., 1999. The magneto-susceptibility event and cyclostratigraphy (MSEC) method used in geological correlation of Devonian rocks from Anti-Atlas Morocco: AAPG, Bulletin, **83**, 1119–1134.

Epstein, A.G., Epstein, J.B., and Harris, L.D., 1977. Conodont Color Alteration – An Index to Organic Metamorphism. U.S. Geological Survey Professional Paper 995

Falkowski, P.G., 2004. Biogeochemistry of Primary Production in the Sea. *In.* Biogeochemistry, Treatise on geochemistry volume 8, Eds. Elderfield, H., Holland, H. D., and Turekian, K. K., Elsevier, Amsterdam, Heidelberg, 185-213

Friedman, L., and O'Neill, J.R., 1977. Compilation of stable isotope fractionation factors of geochemical interests. U.S. Geological Survey, Paper, 440-KK: 12 pp.

Galbraith, E. D., Sigman, D.M., Robinson, R. S., Pedersen, T. F., 2008. "Nitrogen in Past Marine Environments", in Nitrogen in the Marine Environment (2nd edition), edited by D. G. Capone, D. A. Bronk, M. R. Mulholland, and, E. J. Carpenter, Chapter 34, 1497-1535, Academic Press

Galimov, E.M., 1980. C^{13}/C^{12} in kerogen. In Kerogen, Insoluble Organic Matter from Sedimentary Rocks (ed. Durand, B.). Editions Technip. Paris

Galloway, J.N., 2003. 8.12. The Global Nitrogen Cycle. *In:*.Holland, H.D., and Turekian, K.K. (Eds.), Treatise on Geochemistry Volume. Elsevier Ltd., 557-583

Geldsetzer, H.H.J., 1989. Ancient Wall reef complex, Frasnian age, Alberta, In Geldsetzer, H.H.J., James, N.P. and Tebbutt, G.E. (eds.), Reefs, Canada and Adjacent Areas, Canadian Society of Petroleum Geologists, Memoir, **13**, 431-439

Girard, C., Klapper, G., and Feist, R., 2005. Subdivision of the terminal Frasnian linguiformis conodont Zone, revision of the correlative interval of Montagne Noire Zone 13, and discussion of stratigraphically significant associated trilobites. In Over, D.J., Morrow, J.R., and Wignall, P.B., (eds.), Understanding Late Devonian and Permian-Triassic Biotic and Climatic Events: Towards an Integrated Approach. Elsevier B.V.

Goldhammer, T., Brüchert, V., Ferdelman, T.G., and Zabel, M., 2010. Microbial sequestration of phosphorus in anoxic upwelling sediments. Nature Geoscience, **3**, 557-561

Gonzalez, L.A., and Lohmann, K.C., 1985. Carbon and oxygen isotopic composition of Holocene reefla carbonates. Geology, **13**, 811-814

Green, D.G., 1999. Dolomitization and deep burial of the Devonian of west-central Alberta deep basin (Leduc and Wabamun formations) [Unpublished Ph.D. thesis]: Montreal, McGill University, 267 p.

Hallock, P., 1988a. The role of nutrient availability in bioerosion: consequences to carbonate buildups. Palaeogeography, Palaeoclimatology, Palaeoecology, **63**, 275-291

Hallock, P., 1988b. Platforms of the Nicaraguan Rise: examples of the sensitivity of carbonate sedimentation to excess trophic resources. Geology, **16**, 1104-1107

Hallock, P., and Schlager, W., 1986. Nutrient excess and the demise of coral reefs and carbonate platforms. Palaios, **1**, 389-398

Hatch, J.R., and Leventhal, J.S., 1992. Relationship between inferred redox potential of the depositional environment and geochemistry of the Upper Pennsylvanian (Missourian) Stark Shale Member of the Dennis Limestone, Wabaunsee Country, Kansas, U.S.A. Chemical Geology, **99**, 65-82

Hayes, J.M., 1993. Factors controlling ^{13}C contents of sedimentary organic compounds: Principles and evidence. Marine Geology, **113**, 111-125

Hoefs, J., 1987. Stable Isotope Geochemistry – Minerals and Rocks. Third, Completely Revised and Enlarged Edition. Springer-Verlag

Hoering, T.C., and Moore, H.E., 1957. The isotopic composition of the nitrogen in natural gases and associated crude oils. Geochimica et Cosmochimica Acta, **13**, 225-232

Holmden, C., Braun, W.K., Patterson, W.P., Eglington, B.M., Prokopiuk, T.C., and Whittaker, S., 2006. Carbon isotope chemostratigraphy of Frasnian sequences in Western Canada. Saskatchewan Geological Survey, Summary of Investigation, **1**, 1-6

Holmden, C., Creaser, R.A., Muehlenbachs, K., Leslie, S.A. and Bergström, S.M., 1998. Isotopic evidence for geochemical decoupling between ancient epeiric seas and bordering oceans: Implications for secular curves. Geology, **26**, 567–570

Holser, W.T., 1997. Geochemical events documented in inorganic carbon isotopes. Palaeogeography, Palaeoclimatology, Palaeoecology, 132(1-4), 173-182House, M.R., 2002. Strength, timing, setting and cause of mid-Palaeozoic extinctions. Palaeogeography Palaeoclimatology Palaeoecology, **181**, 5-25

House, M.R., 2002. Strength, timing, setting and cause of mid-Palaeozoic extinctions. *Palaeogeography, Palaeoclimatology, Palaeoecology*, **181**, 5-25.

Hurley, N.F., and Lohmann, K.C., 1989. Diagenesis of Devonian reefal carbonates in the Oscar Range, Canning Basin, Western Australia. Journal of Sedimentary Petrology, **59**, 127-146

Immenhauser, A., Della Porta, G., Kenter, J.A.M., and Bahamonde, J.R., 2003. An alternative model for positive shifts in shallow-marine carbonate $\delta^{13}C$ and $\delta^{18}O$. Sedimentology, **50**, 953-959

Ingall, E.D., 2010. Phosphorus burial. Nature Geoscience, **3**, 521-522

Ingall, E., and Jahnke, R., 1994. Evidence for enhanced phosphorus regeneration from marine sediments overlain by oxygen depleted waters. Geochimica et Cosmochimica Acta, **58**, 2571-2575

Joachimski, M.M., Breisig, S., Buggisch, W., Talent, J.A., Mawson, R., Gereke, M., Morrow, J.R., Day, J., and Weddige, K., 2009. Devonian climate and reef evolution: Insights from oxygen isotopes in apatite. Earth and Planetary Science Letters, **284**, 599-609

John, E.H., Cliff, R., and Wignall, P.B., 2008. A positive trend in seawater Sr-87/Sr-86 values over the Early-Middle Frasnian boundary (Late Devonian) recorded in well-preserved conodont elements from the Holy Cross Mountains, Poland. Palaeogeography Palaeoclimatology Palaeoecology, **269**, 166-175

Johnson, J.G., Klapper, G. and Sandberg, C.A., 1985. Devonian eustatic fluctuations in Euramerica. Geological Society of America Bulletin, **96**, 567-587

Jones, B., and Manning, D.A.C., 1994. Comparison of geochemical indices used for the interpretation of paleoredox conditions in ancient mudstone. Chemical Geology, **111**, 111-129

Kaufman, J., 1989. Sedimentology and diagenesis of the Swan Hills Formation (Middle-Upper Devonian), Rosevear Field, Alberta, Canada (unpublished Ph.D. thesis): State University of New York at Stony Brook, 412 p.

Kaufmann, B., 2006. Calibrating the Devonian time scale: A synthesis of U-PbID-TIMS ages and conodont stratigraphy. Earth-Science Reviews, **76**, 175-190

Kerans, C., 1985. Petrology of Devonian and Carboniferous carbonates of the Canning and Bonaparte Basins: Western Australian Mining and Petroleum Research Institute, Report 12, 203 p.

Kiessling , W., Flugel , E., and Golonka , J., 1999. Paleoreef maps : evaluation of a comprehensive database on Phanerozoic reefs. The American Association of Petroleum Geologists, Bulletin, **83**, 1552-1587

Klapper, G., 1989. The Montagne Noire Frasnian (Upper Devonian) conodont succession. Memoirs of the Canadian Society of Petroleum Geologists, **14**, 449-459

Klapper G., and Becker, R.T., 1999. Comparison of Frasnian (Upper Devonian) conodont zonations. In Serpagli, E., and Corradini, C., (eds), *Studies on Conodonts, Proceedings of the Seventh European Conodont Symposium, Bologna-Modena, 1998,* pg. 339-348. *Bolletino della Società Paleontologica Italiana,* **37**(2/3)

Klapper, G., and Foster, C.T., 1993. Shape Analysis of Frasnian Species of the Late Devonian Conodont Genus Palmatolepis, Memoir (The Paleontological Society), Vol. 32, Supplement to Vol. 67, no. **4** of the Journal of Paleontology, 1-35

Klovan, J.E., 1964. Facies analysis of the Redwater reef complex, Alberta. Canada Bulletin of Canadian Petroleum Geology, **12**, 1-100

Kump, L.R., and Arthur, M.A., 1999. Interpreting carbon-isotope excursions: carbonates and organic matter. Chemical Geology, **161**, 181-198

Kuypers, M.M.M., and van Breugel, Y., Schouten, S., Erba, E., and Damste, J.S.S., 2004. N_2-fixing cyanobacteria supplied nutrient N for Cretaceous oceanic anoxic events. Geology, **32**(10), 853-856

Libes, S.M., and Deuser, W.G., 1988. The isotope geochemistry of particulate nitrogen in the Peru upwelling area and the Gulf of Maine. Deep Sea Research Part A. Oceanographic Research Papers, 35(4), 517-533

Lüning, S., Wendt, J., Belka, Z., and Kaufmann, B., 2004. Temporal-spatial reconstruction of the early Frasnian (Late Devonian) anoxia in NW Africa: new field data from the Ahnet Basin (Algeria). Sedimentary Geology, **163**, 237-264

Ma, X.P., Wang, C.Y., Racki, G. and Racka, M., 2008. Facies and geochemistry across the Early-Middle Frasnian transition (Late Devonian) on South China carbonate shelf: Comparison with the Polish reference succession. Palaeogeography Palaeoclimatology Palaeoecology, **269**, 130-151

Machel, H.G., Krouse, H.R., and Sassen, R., 1995. Products and distinguishing criteria of bacterial and thermochemical sulfate reduction. Applied Geochemistry, **10**, 373-389

Machel, H.G., 1997. Recrystallization versus neomorphism, and the concept of "significant recrystallization" in dolomite research. Sedimentary Geology, **113**, 161-168

Machel, H.G., 2005. Investigations of burial diagenesis in carbonate hydrocarbon reservoir rocks. Geoscience Canada, **32(3)**, 103-128

Machel, H.G., and Buschkuehle, B.E., 2008. Diagenesis of the Devonian Southesk-Cairn Carbonate Complex, Alberta, Canada: marine cementation, burial dolomitization, thermochemical sulfate reduction, anhydritization, and squeegee fluid flow. Journal of Sedimentary Research, **78**, 366-389

Marynowski, L., Filipiak, P., and Pisarzowska, A., 2008. Organic geochemistry and palynofacies of the Early-Middle Frasnian transition (Late Devonian) of the Holy Cross Mountains, Southern Poland. Palaeogeography Palaeoclimatology Palaeoecology, **269**, 152-165

Mattes, B.W., and Mountjoy, E.W., 1980. Burial dolomitization of the Upper Devonian Miette buildup, Jasper National Park, Alberta, in Zenger, D.H., Dunham, J.B., and Ethington, R.L., eds., Concepts and Models of Dolomitization, SEPM, Special Publication, **28**, 259–297

McLaren, D.J., 1982. Frasnian-Famennian extinction. Geological Society of America Special Papers, **190**, 477-484.

McLaren, D.J., and Goodfellow, W.D., 1990. Geological and biological consequences of giant impacts. Annual Review of Earth and Planetary Sciences, **18**, 123-171

Melim, L.A., Eberli, G.P., and Walgenwitz, F., 2000. Diagenesis of the Miette Buildup, Devonian, Canada – Fabrics and variability. In: Homewood, P.W., and Eberli, G.P., (Eds.), Genetic Stratigraphy on the Exploration and Production Scales—Case Studies from the Pennsylvanian of the Paradox Basin and the Upper Devonian of Alberta, Bulletin Centre Recherche Elf Exploration-Production, Memoire, **24**, 269–284

Meyers, W.J., and Lohmann, K.C., 1985. Isotope geochemistry of regionally extensive calcite cement zones and marine components in Mississippian limestones, New Mexico: Society of Economic Paleontologists and Mineralogists Special Publication, **36**, 223-264

Milner, A.C., 1990. Major Events in the History of Life: Terrestrialization: Vertebrates. In Briggs, D.E.G. and Crowther, P.R. (eds.), Palaeobiology. Blackwell Science, Oxford. 68-72

Mossop, G.D., and Shetsen, I., 1994: Geological atlas of the Western Canada Sedimentary Basin; Canadian Society of Petroleum Geologists and Alberta Research Council, Special Report 4, http://www.ags.gov.ab.ca/publications/wcsb_atlas/atlas.html

Morel, F. M. M., Milligan, A.J., and Saito, M. A. 2004. Marine bioinorganic chemistry: The role of trace metals in the oceanic cycles of major nutrients, in: The Oceans and Marine Geochemistry, Treatise on geochemistry volume 6, edited by: Elderfield, H., Holland, H. D., and Turekian, K. K., Elsevier, Amsterdam, Heidelberg, 113–143

Morrow, J.R., Sandberg, C.A., Malkowski, K., Joachimski, M.M., 2009. Carbon isotope chemostratigraphy and precise dating of middle Frasnian (lower Upper Devonian) Alamo Breccia, Nevada, USA. Palaeogeography, Palaeoclimatology, Palaeoecology, **282**, 105-118

Mountjoy, E.W., 1965. Stratigraphy of the Devonian Miette reef complex and associated strata, eastern Jasper National Park, Alberta: Geological Survey of Canada, Bulletin, **110**, 132

Mountjoy, E.W., 1980. Some questions about the development of Upper Devonian carbonate buildups (reefs) western Canada: Bulletin of Canadian Petroleum Geology, **28**, 315–344

Mountjoy, E.W., 1989. Miette Reef Complex (Frasnian), Jasper National Park, Alberta. Memoirs of the Canadian Society of Petroleum Geologists, **13**, 497-505

Mountjoy, E.W., Machel, H.G., Green, D., Duggan, J., and Williams-Jones, A.E., 1999. Devonian matrix dolomites and deep burial carbonate cements: A comparison between the Rimbey-Meadowbrook reef trend and the deep basin of west-central Alberta: Bulletin of Canadian Petroleum Geology, **42**, 487-509

Munsel, D., Kramar, U., Dissard, D., Nehrke, G., Berner, Z., Bijma, J., Reichart, G.-J., and Neumann, T., 2010. Heavy metal incorporation in foraminiferal calcite: results from multi-element enrichment culture experiments with *Ammonia tepida,* Biogeosciences, **7**, 2339–2350

Murphy, A.E., Sageman, B.B., Hollander, D.J., Lyons, D.J., and Brett, C.E., 2000. Black shale deposition and faunal overturn in the Devonian Appalachian basin: Clastic starvation, seasonal water-column mixing, and efficient biolimiting nutrient recycling. Paleoceanography, **15**, 280-291

Oldenburg, T.B.P., Larter, S.R., and Huang, H., 2007. Nitrogen isotope systematics of petroleum fractions of differing polarity – Neutral versus basic compounds. Organic Geochemistry, **38**, 1789-1794

Oliver, T.A., and Cowper, N.W., 1963. Depositional environments of the Ireton Formation, central Alberta. Bulletin of Canadian Petroleum Geology, **11**, 183-202

Panchuk, K.M., Holmden, C.E., and Leslie, S.A., 2006. Local controls on carbon cycling in the Ordovician Midcontinent region of North America, with implications for carbon isotope secular curves. Journal of Sedimentary Research, **76**, 200-211

Patterson, W.P., and Walter, L.M., 1994. Depletion of ^{13}C in seawater ΣCO_2 on modern carbonate platforms: Significance for the carbon isotopic record of carbonates. Geology, **22**, 885-888

Payne, J. H., 2009. Chemostratigraphy of the Late Devonian Frasnian-Famennian Transition in Alberta, Canada and its implications. Thesis, Dept. of Geology and Geophysics, University of Alaska Fairbanks

Pedersen, T.F., and Calvert, S.E., 1990. Anoxia vs. productivity - what controls the formation of organic carbon-rich sediments and sedimentary rocks? AAPG Bulletin-American Association of Petroleum Geologists, **74**, 454-466

Perkins, R.B., Piper, D.Z., and Mason, C.E., 2008. Trace-element budgets in the Ohio/Sunbury shales of Kentucky: Constraints on ocean circulation and primary productivity in the Devonian-Mississippian Appalachian Basin. Palaeogeography Palaeoclimatology Palaeoecology, **265**, 14-29

Peterhänsel, A., and Pratt, B.R., 2001. Nutrient-triggered bioerosion on a giant carbonate platform masking the post extinction Famennian benthic community. Geology, **29**, 1079-1082

Peterson, B.J., and Fry, B., 1987. Stable isotopes in ecosystem studies. Annual Review of Ecology and Systematics, **18**, 293-320

Piper, D.Z., and Calvert, S.E., 2009. A marine biogeochemical perspective on black shale deposition Earth-Science Reviews, **95**, 63-96

Piper, D.Z., and Perkins, R.B., 2004. A modem vs. Permian black shale - the hydrography, primary productivity, and water-column chemistry of deposition. Chemical Geology, **206**, 177-197

Pisarzowska, A., 2008. Geochemia stabilnych izotopów węgla i tlenu na pograniczu dolnego i śrdokowego franu (dewon górny) na obszarze południowego szelfu Laurussi. PhD. Thesis, Silesian University, Sosnowiec, Poland.

Pisarzowska, A., Sobstel, M., and Racki., G., 2006. Conodont-based event stratigraphy of the Early-Middle Frasnian transition on the South Polish carbonate shelf. Acta Palaeontologica Polonica, **51(4)**, 609-646

Playford, P.E., McClaren, D.J., Orth, C.J., Gilmore, J.S., and Goodfellow, W.D., 1984. Iridium anomaly in the upper Devonian of the Canning basin, Western Australia. Science, **226**, 437-439

Popp, B.N., Parekh, P., Tilbrook, B., Bidigare, R.R., and Laws, E.A., 1997. Organic carbon $\delta^{13}C$ variations in sedimentary rocks as chemostratigraphic and paleoenvironmental tools. Palaeogeography, Palaeoclimatology, Palaeoecology, **132**, 119-132

Racka, M., Marynowski, L., Filipiak, P. and Sobstel, M., 2010. Anoxic Annulata Events in the Late Famennian of the Holy Cross Mountains (Southern Poland): Geochemical and palaeontological record. *Palaeogeography, Palaeoclimatology, Palaeoecology*, **297**, 549-575

Racki, G., 1998. Frasnian-Famennian biotic crisis: undervalued tectonic control? Palaeogeography, Palaeoclimatology, Palaeoecology, **141**, 177-198

Racki, G., 2005. Toward understanding Late Devonian global events: few answers, many questions. In: Over, D.J., Morrow, J.R. and Wignall, P.B. (eds.) Understanding Late Devonian and Permian-Triassic biotic and climatic events: Towards an integrated approach. Elsevier, B.V., Chapter 2: 5-36

Racki, G., Joachimski, M.M., and Morrow, J.R., 2008. A major perturbation of the global carbon budget in the Early-Middle Frasnian transition (Late Devonian) – Preface. Palaeogeography Palaeoclimatology Palaeoecology, **269**, 127-129

Racki, G., Piechota, A., Bond, D., and Wignall, P.B., 2004. Geochemical and ecological aspects of lower Frasnian pyrite ammonoid level at Kostomłoty (Holy Cross Mountains, Poland). In: Racki, G., Narkiewicz, M. (Eds.), Multidisciplinary Event Approaches to the Devonian Stratigraphic Record. Geological Quarterly, **48** 267–282

Rau, G.H., Arthur, M., and Dean, W.E., 1987. $^{15}N/^{14}N$ variations in Cretaceous Atlantic sedimentary sequences: implication for past changes in marine nitrogen biogeochemistry. Earth and Planetary Science Letters, **82**, 269-279

Rigby, D., and Batts, B.D., 1986. The isotopic composition of nitrogen in Australian coals and oil shales. Chemical Geology, **58**, 273–282

Rimmer, S.M., 2004. Geochemical paleoredox indicators in Devonian-Mississippian black shales, central Appalachian basin (USA). Chemical Geology, **206**, 373-391

Rimmer, S.M., Thompson, J.A., Goodnight, S.A., and Robl, T.L., 2004. Multiple controls on the preservation of organic matter in Devonian-Mississippian marine black shales: geochemical and petrographic evidence. Palaeogeography Palaeoclimatology Palaeoecology, **215**, 125-154

Riquier, L., Tribovillard, N., Averbuch, O., et al., 2006. The Late Frasnian Kellwasser horizons of the Harz Mountains (Germany): Two oxygen-deficient periods resulting from different mechanisms. Chemical Geology, **233**, 137-155

Rue, de la, S., Rowe, H.D., and Rimmer, S.M., 2007. Palynological and bulk geochemical constraints on the paleoceanographic conditions across the Frasnian-Famennian boundary, New Albany Shale, Indiana. International Journal of Coal Geology, **71**, 72-84

Rullkötter, J., 1993. The Thermal Alteration of Kerogen and the Formation of Oil. In Organic Geochemistry, Principles and Applications. Eds.: Engel, M.H., Macko, S.A. Plenum Press, New York, 337-396

Ruttenberg, K.C., 1990. Diagenesis and burial of phosphorus in marine sediments: Implications for the marine phosphorus budget. Ph.D. dissertation. Yale University.

Ruttenberg, K.C., and Berner, R.A., 1993. Authigenic apatite formation and burial in sediments from non-upwelling, continental margin environments. Geochimica et Cosmochimica Acta, **57**, 991-1007

Sageman B.B., Murphy, A.E., Werne, J.P., Ver Straeten, C.A., Hollander, D.J., and Lyons, T.W., 2003. A tale of shales: the relative roles of production, decomposition, and dilution in the accumulation of organic-rich strata, Middle–Upper Devonian, Appalachian basin. Chemical Geology, **195**, 229– 273

Sandberg, C.A., Morrow, J.R., and Ziegler, W., 2002. Late Devonian sea-level changes, catastrophic events, and mass extinctions. Geological Society of America Special Papers, **356**, 473-487

Sassen, R., Moore, C.H., Nunn, J.A., Meedsen F.C., and Heydari, E., 1987. Geochemical studies of crude oil generation, migration, and destruction in the Mississippi Salt Basin. Gulf Coast Association of Geological Societies Transactions, **37**, 217-224

Scheckler, S.C., 2001. Major Events in the History of Life: Palaeozoic Events: Afforestation – The First Forests. In Briggs, D.E.G. and Crowther, P.R. (eds.), Palaeobiology II. Blackwell Science, Oxford. 67-71

Schoell M. 1983. Genetic characterization of natural gasses. American Association of Petroleum Geologists Bulletin, **67**, 2225-2238

Selden, P.A., 1990. Major Events in the History of Life: Terrestrialization: Invertebrates. In Briggs, D.E.G. and Crowther, P.R. (eds.), Palaeobiology. Blackwell Science, Oxford. 64-68

Selden, P.A., 2001. Major Events in the History of Life: Palaeozoic Events: Terrestrialization of Animals. In Briggs, D.E.G. and Crowther, P.R. (eds.), Palaeobiology II. Blackwell Science, Oxford. 71-74

Sephton, M.A., Amor, K., Franchi., I.A., Wignall, P.B., Newton, R., and Zonnenveld, J-P., 2002. carbon and nitrogen isotope disturbances and an end-Norian (Late Triassic) extinction event. Geology, **30**(12), 1119-1122.

Sepkoski, J.J., Jr., 1984. A kinetic model of Phanerozoic taxonomic diversity III. Post-Paleozoic families and mass extinctions. Paleobiology, **10**(2), 246-267

Śliwiński, M.G., Whalen, M.T., and Day, J., 2010. Trace element variations in the Middle Frasnian punctata zone (Late Devonian) in the western Canada sedimentary basin—changes in oceanic bioproductivity and paleoredox spurred by a pulse of terrestrial afforestation? Geologica Belgica, **4**, 459–482

Smith, S.G.W., 2001. The origin and timing of late-stage carbonate cements in Devonian carbonates of the deep Alberta basin: based on fluid inclusion and isotopic evidence [Unpublished M.Sc. thesis]: Montreal, McGill University, 116 p

Soreghan, G.S., Engel, M.H., Furley, R.A., and Giles, K.A. 2000. Glacioeustatic transgressive reflux: Stratiform dolomite in Pennsylvanian bioherms of the Western Orogrande Basin, New Mexico. Journal of Sedimentary Research, 70(6), 1315-1332

Stasiuk, L.D., and Fowler, M.G., 2004. Organic facies in Devonian and Mississippian strata of Western Canada Sedimentary Basin: relation to kerogen type, paleoenvironment, and paleogeography. Bulletin of Canadian Petroleum Geology, **52**(3), 234-255

Stearn, C.W., 1987. Effect of the Frasnian-Famennian extinction event on the stromatoporoids. Geology, **15**, 677-679

Stoakes, F.A., 1980. Nature and control of shale basin fill and its effect on reef growth and termination: Upper Devonian Duvernay and Ireton Formations of Alberta, Canada. Bulletin of Canadian Petroleum Geology. **28**, 345-410

Streel, M., Caputo, M.V., Loboziak, S., and Melo, J.H.G., 2000. Late Frasnian-Famennian climates based on palynomorph analyses and the question of the Late Devonian glaciations. Earth-Science Reviews, **52**, 121-173.

Struck, U., Emeis, K.C., Voss, M., Krom, M.D., and Rau, G.H., 2001. Biological productivity during sapropel S5 formation in the Eastern Mediterranean Sea: Evidence from stable isotopes of nitrogen and carbon. Geochimica et Cosmochimca Acta, **65**(19), 3249-3266

Switzer, S.B., Holland, W.G., Christie, G.S., Graf, G.C., Hedinger, A.S., McAuley, R.J., Wierzbicki, R.A., and Packard, J.J., 1994. Devonian Woodben-Winterburn strata of the western Canada sedimentary basin. In Mossop, G. and Shetsen, I. (eds.) Geological Atlas of the Western Canada Sedimentary Basin: Canadian Society of Petroleum Geologists and Alberta Research Council, 165-202

Tribovillard, N., Algeo, T.J., Lyons, T., and Riboulleau, A., 2006. Trace metals as paleoredox and paleoproductivity proxies: An update. Chemical Geology, **232**, 12-32

Tribovillard, N., Averbuch, O., Devleeschouwer, X., Racki, G. and Riboulleau, A., 2004. Deep-water anoxia over the Frasnian-Famennian boundary (La Serre, France): a tectonically induced oceanic anoxic event? Terra Nova, **16**, 288-295

Tucker, M.E., 2001. Sedimentary Petrology. Blackwell Science, Oxford.

Tyson, R.V., 1995. Bulk Geochemical Characterization and Classification of Organic Matter: Stable Carbon Isotopes ($\delta^{13}C$). *In.* Sedimentary Organic Matter - Organic facies and palynofacies. Chapman and Hall, London, 395-417

van Buchem, F.S.P., Eberli, G.P., Whalen, M.T., Mountjoy, E.W., and Homewood, P.W., 1996. The basinal geochemical signature and platform margin geometries in the Upper Devonian mixed carbonate-siliciclastic system of western Canada. Bulletin De La Societe Geologique De France, **167**, 685-699

van Cappellen, P., and Ingall, E.D., 1994. Redox stabilization of the atmosphere and oceans by phosphorus-limited marine productivity, Science, **271**, 493-496

van Geldern, R., and Joachimski, M.M., 2001. The stable isotopic composition of Devonian brachiopods. TerraNostra **4**, 76–80

van Geldern, R., Joachimski, M.M., Day, J., Jansen, U., Alvarez, F., Yolkin, E.A., and Ma, X-P. 2006. Carbon, oxygen and strontium isotope records of Devonian brachiopod shell calcite, Paleogeography, Palaeoclimatology, Paleoecology, **240**, 47–67

Vandeginste, V., Swennen, R., Gleeson, S.A., Ellam, R.M., Osadetz, K., and Roure, F., 2009. Thermochemical sulphate reduction in the Upper Devonian Cairn Formation of the Fairholme carbonate complex (SW Alberta, Canadian Rockies): evidence from fluid inclusions and isotopic data. Sedimentology, **56**, 439-460

Veizer, J., 1983. Trace elements and isotopes in sedimentary carbonates, Reviews in Mineralogy: Carbonates: Mineralogy and Chemistry, **11**, 265-299

Veizer, J., Fritx, P., and Jones, B., 1986. Geochemistry of brachiopods, oxygen and carbon isotopic records of Paleozoic oceans. Geochimica et Cosmochimica Acta **50**, 1679-1696

Veizer, J., Ala, D., Azmy, K., Bruckschen, P., Buhl, D., Bruhn, F., Carden, G.A.F., Diener, A., Ebneth, S., Godderis, Y., Jasper, T., Korte, C., Pawellek, F., Podlaha, O.G., and Strauss, H., 1999. $^{87}Sr/^{86}Sr$, $\delta^{13}C$ and $\delta^{18}O$ evolution of Phanerozoic seawater. Chemical Geology, **161**, 59-88

Walls, R.A., Mountjoy, E.W., and Fritz, P., 1979. Isotopic composition and diagenetic history of carbonate cements in Devonian Golden Spike Reef, Alberta, Canada. Geological Society of America Bulletin, **90**, 963-982

Wendte, J.C., 1994. Cooking Lake platform evolution and its control on Late Devonian Leduc reef inception and localization, Redwater, Alberta. Bulletin of Canadian Petroleum Geology, **42**, 499–528.

Whalen, M.T. and Day, J.E., 2008. Magnetic susceptibility, biostratigraphy, and sequence stratigraphy: insights into Devonian carbonate platform development and basin infilling, western Alberta, Canada. Society for Sedimentary Geology, **89**, 291-314

Whalen, M.T. and Day, J.E., 2010. Cross-basin variations in magnetic susceptibility influenced by changing sea level, paleogeography and climate, Upper Devonian Western Canada Sedimentary Basin. Journal of Sedimentary Research, **80**, 1109-1127

Whalen, M.T., Day, J., Eberli, G.P., and Homewood, P.W., 2002. Microbial carbonates as indicators of environmental change and biotic crises in carbonate systems: examples from the Late Devonian, Alberta basin, Canada. Palaeogeography, Palaeoclimatology, Palaeoecology, **18**,127-151

Whalen, M.T., Eberli, G.P., Van Buchem, F.S.P., Mountjoy, E.W., and Homewood, P.W., 2000. Bypass margins, basin-restricted wedges, and platform-to-basin correlation, Upper Devonian, Canadian Rocky Mountains: Implications for sequence stratigraphy of carbonate platform systems. Journal of Sedimentary Research, **70**, 913-936

Wood, R., 1993. Nutrients, predation and the history of reef-building. Palaios, **8**, 526-543

Wright, V.P., 1990. Major Events in the History of Life: Terrestrialization: Soils. In Briggs, D.E.G. and Crowther, P.R. (eds.), Palaeobiology. Blackwell Science, Oxford. 57-59

Yamaguchi, K.E., Ogurim K., Ogawa, N.O., Sakai, S., Hirano, S., Kitazato, H., and Ohkouchi, N., 2010. Geochemistry of modern carbonaceous sediments overlain by a water mass showing photic zone anoxia in the saline meromictic Lake Kai-ike, southwest Japan: I. Early diagenesis of organic carbon, nitrogen, and phosphorus. Palaeogeography, Palaeoclimatology, Palaeoecology, **294**, 72–82

Yans, J., Corfield, R.M., Racki, G., and Preat, A., 2007. Evidence for perturbation of the carbon cycle in the Middle Frasnian punctata Zone (Late Devonian). Geological Magazine, **144**, 263-270

Yuenian, Z., Buqing, S., and Fang, C., 2000. The isotopic composition of molecular nitrogen: implications on their origins in natural gas accumulations. Chem. Geology, **164**, 321-330

Zhu, Y., Buqing Shi, B., Fang, C., 2000. The isotopic compositions of molecular nitrogen: implications on their origins in natural gas accumulation. Chem. Geology, **164**(3-4), 321-330

Ziegler, W., and Sandberg, C.A., 1990. The Late Devonian standard conodont zonation: Courier Forschungs-Institut Senckenberg, **121**, 1-115.

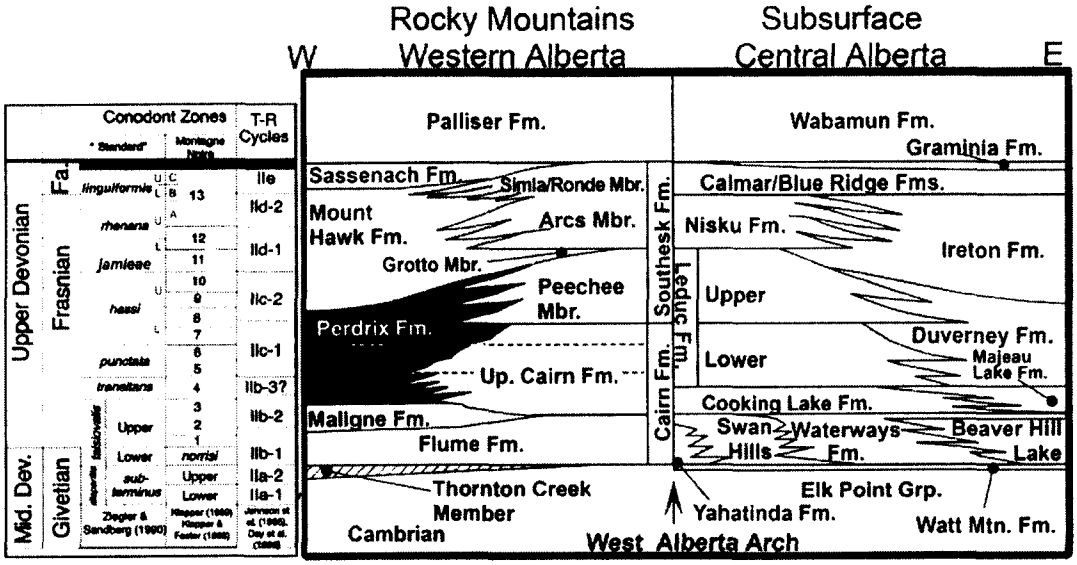

Fig. 4.1. Schematic stratigraphy of the Upper Devonian in the Rocky Mountains of Western Alberta and the central Alberta subsurface. Note the differing stratigraphic nomenclature for platform vs. basin facies and between the surface and subsurface (after Whalen et al., 2000). Conodont zonation after Ziegler and Sandberg (1990); Mongtage Noire (MN) Zones after Klapper (1989) and Klapper and Foster (1993); T-R cycles after Johnson et al., (1985) and Whalen and Day (2010).

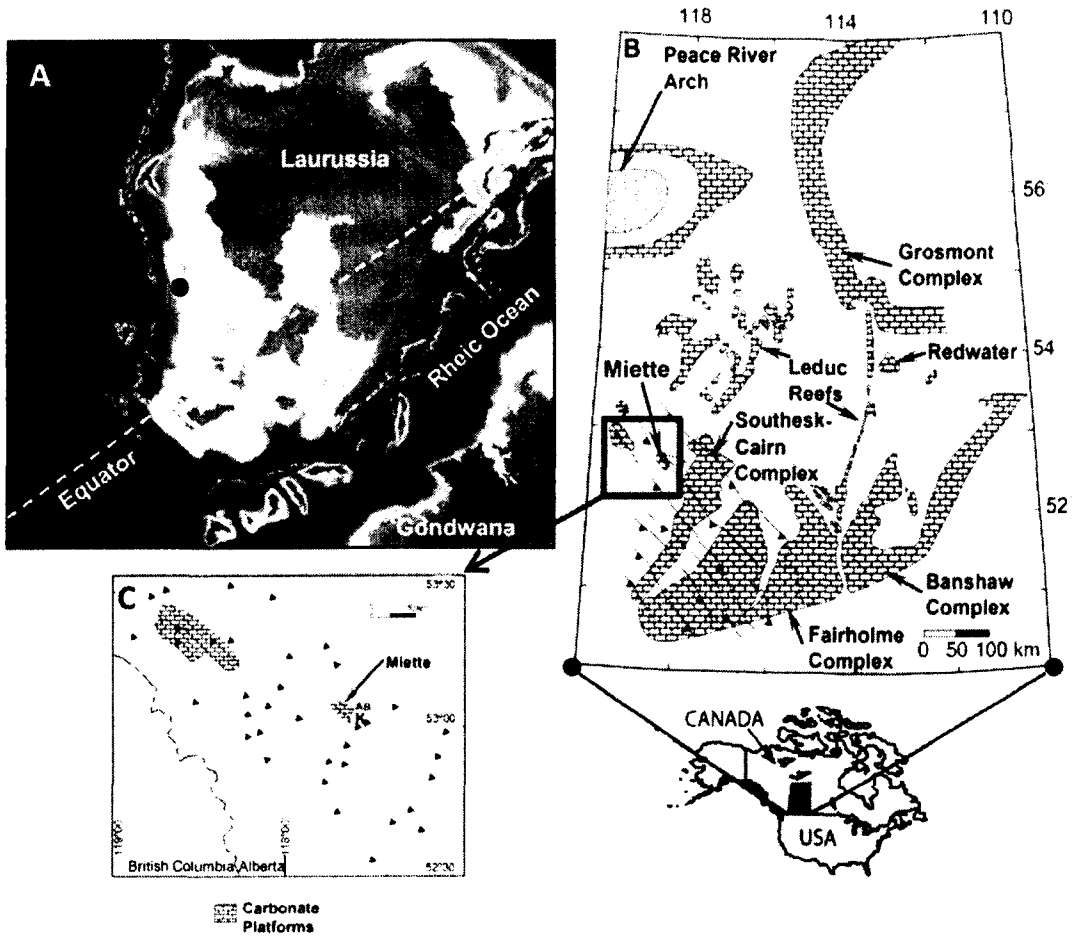

Fig. 4.2. Study area. A. Paleogeographic reconstruction of Late Devonian North America (Ron Blakey, Northern Arizona University, Geology). Location of the study area indicated by black dot. B. Location of the isolated Miette carbonate platform in relation to other platforms in the greater Western Canada Sedimentary Basin. C. Location of the Miette platform in relation to the thrust belt of Western Alberta. 'AB' and 'K' denote the positions of measured stratigraphic sections. Insets B and C modified after Mountjoy, 1965, 1980; Geldsetzer, 1989; Switzer et al., 1994; Whalen et al., 2000.

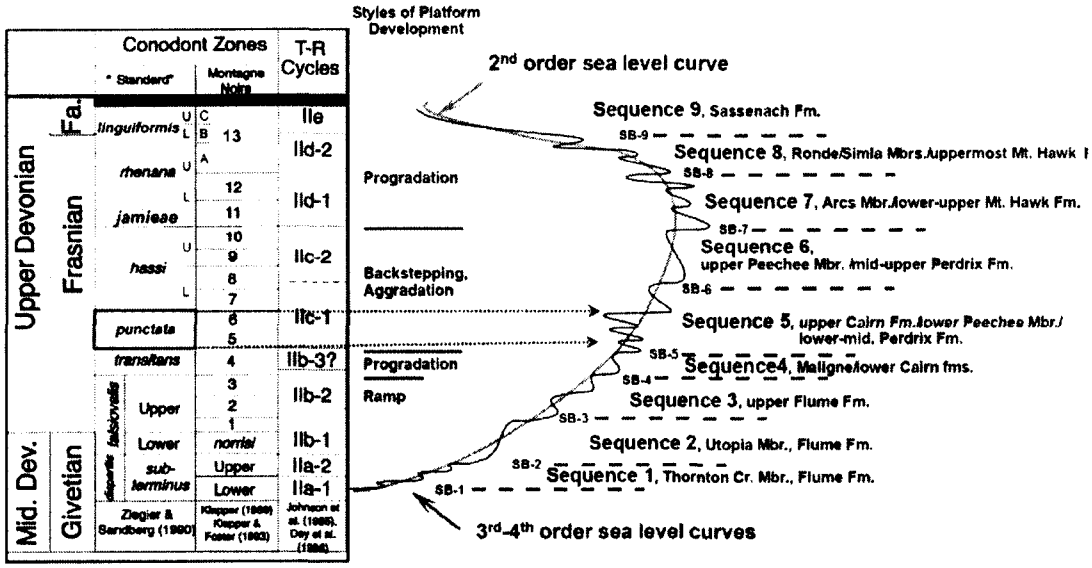

Fig. 4.3. Sequence stratigraphy (Whalen and Day, 2008), conodont zonation (Ziegler and Sandberg, 1990) and sea level history developed for the study area (after Whalen et al., 2000). The geochemical anomalies of the *punctata* Event are noted to have began early during transgressive pulse IIc1, a time interval of carbonate platform backstepping and aggradation. Mongtage Noire (MN) Zones after Klapper (1989) and Klapper and Foster (1993); T-R cycles after Johnson et al., (1985) and Day (1996).

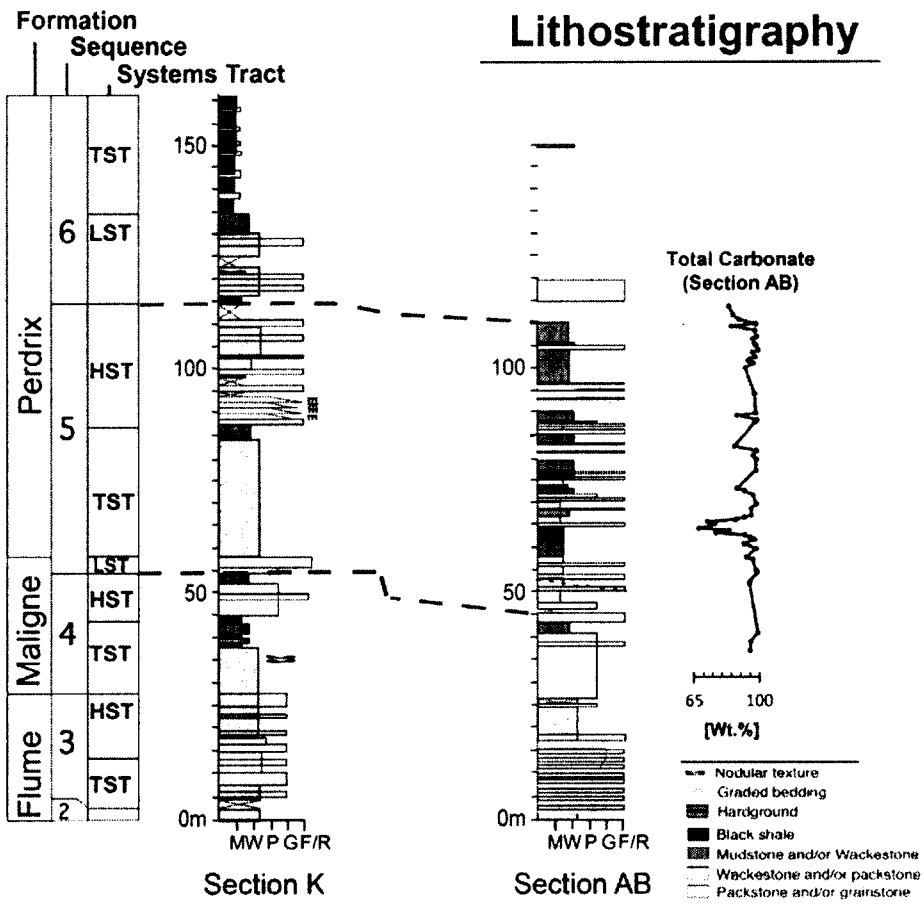

Fig. 4.4. Lithostratigraphic profiles of Sections AB and K, sequence stratigraphy and total carbonate content (Section AB only). M = mudstone, W = wackestone, P = packstone, G = grainstone, F/R = floatstone/rudstone, LST = lowstand systems tract, TST = transgressive systems tract, HST = highstand systems tract.

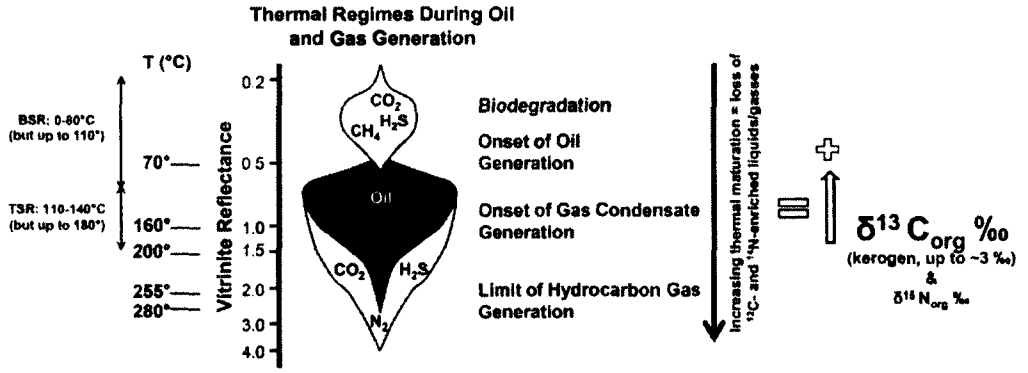

Fig. 4.5. Schematic diagram depicting the cleaving of liquid and gaseous organic compounds enriched in ^{12}C and ^{14}N during the thermal regimes of oil and gas generation. Figure modified after Sassen et al. (1987) and Machel et al (1995). Bio- and thermo-degradation of OM generally produces an isotopically enriched kerogen residue (up to ~3‰ $\delta^{13}C$ – Hoefs, 1987, Machel, 1995). The extent of $\delta^{15}N_{org}$ enrichment is not well constrained at present. BSR denotes the biochemical sulfate reduction process, whereas TSR is the process of thermochemical sulfate reduction. Vitrinite reflectance is a method in organic petrography used to assess the extent of thermal maturity of sedimentary OM.

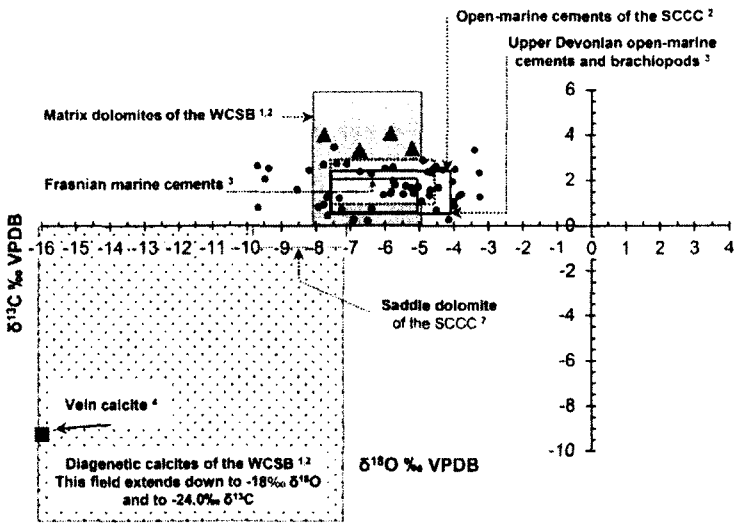

Fig. 4.6. Crossplot of $\delta^{13}C_{carb}$ vs. $\delta^{18}O_{carb}$ of all analyses. No strong covariance (R^2=0.0018) is observed, arguing against significant diagenetic alteration. Plotted for reference are ranges of isotopic values typical of Late Devonian open-marine cements, but also regional signatures of different diagenetic phases from the WCSB. SCCC = Southesk-Cairn Carbonate Complex (Fig. 4.2), located as close as 25 km to the Miette platform. Triangles denote the isotopic composition of matrix dolomite determined in the present study, whereas the larger filled circle represents the composition of vein calcite. [1] = Mattes and Mountjoy, 1980; [2] = Machel and Buschkuehle, 2008; [3] = Hurley and Lohmann, 1989; [4] = ~2 mm thick calcite vein located at 43.5 meters in the Section AB profile.

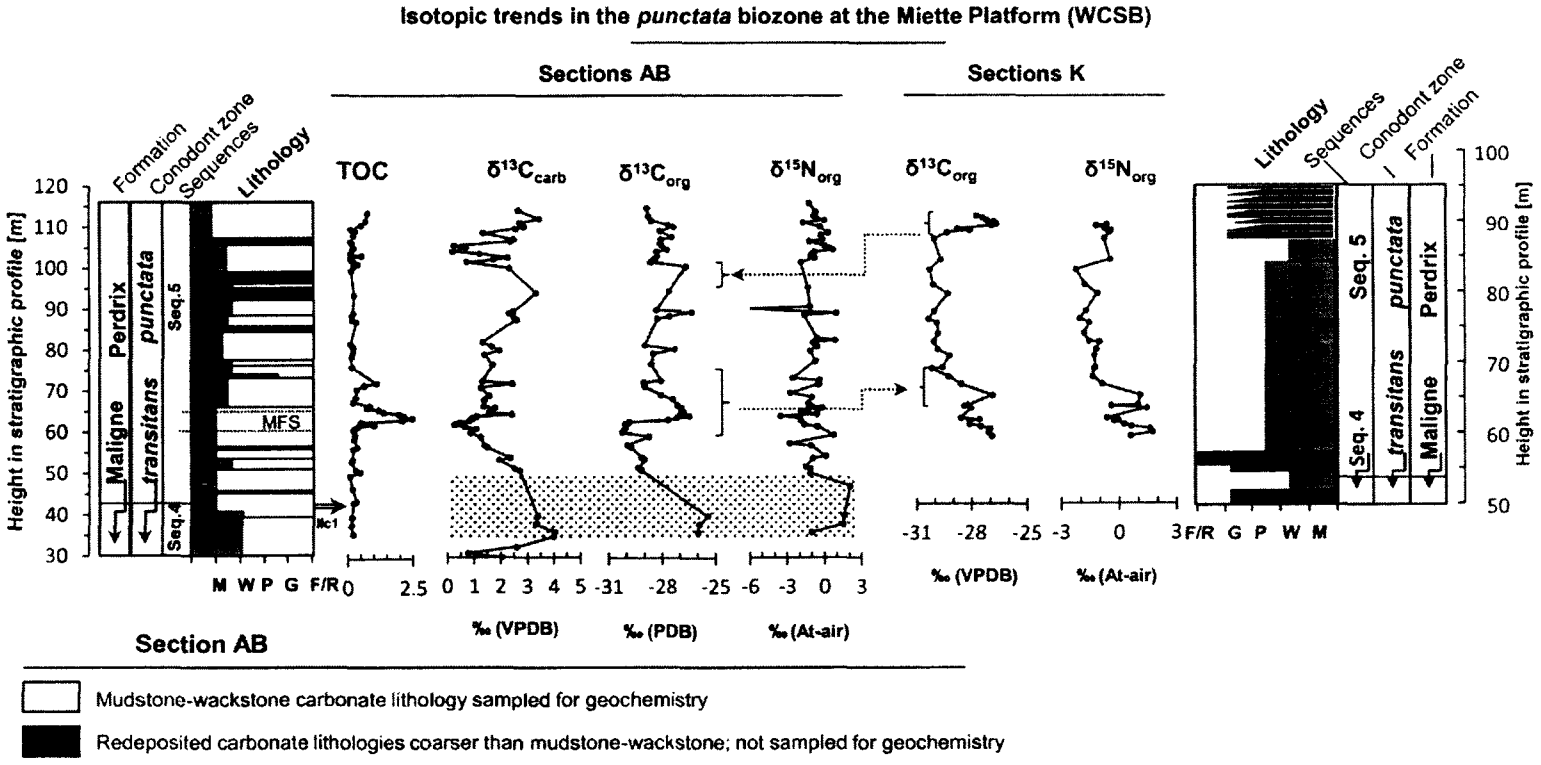

Fig. 4.7. Isotopic trends and TOC variations in the *punctata* biozone at the studied stratigraphic sections (AB and K) of the Miette platform. Note especially the concurrent excursions of TOC and $\delta^{13}C_{carb\ and\ org}$ at the mfz of Section AB, which correspond to the first two excursions of bioproductivity and redox trace element proxies (Fig. 4.9). The stepwise negative-stepwise positive $\delta^{13}C_{carb}$ excursion near the top of the AB profile is curious in that it has no corresponding strong trace element enrichment as noted near the mfz. Note also that the $\delta^{13}C_{org}$ and $\delta^{15}N_{org}$ records are clearer in the more basinal profile of Section K, where less redeposited intervals are present. Solid shaded intervals denote time-equivalent isotopic excursions in both sections (note that the K profile is more condensed). Dotted shaded region denotes the dolomitized interval at Section AB. M = mudstone, W = wackestone, P = packstone, G = grainstone, F/R = floatstone/rudstone.

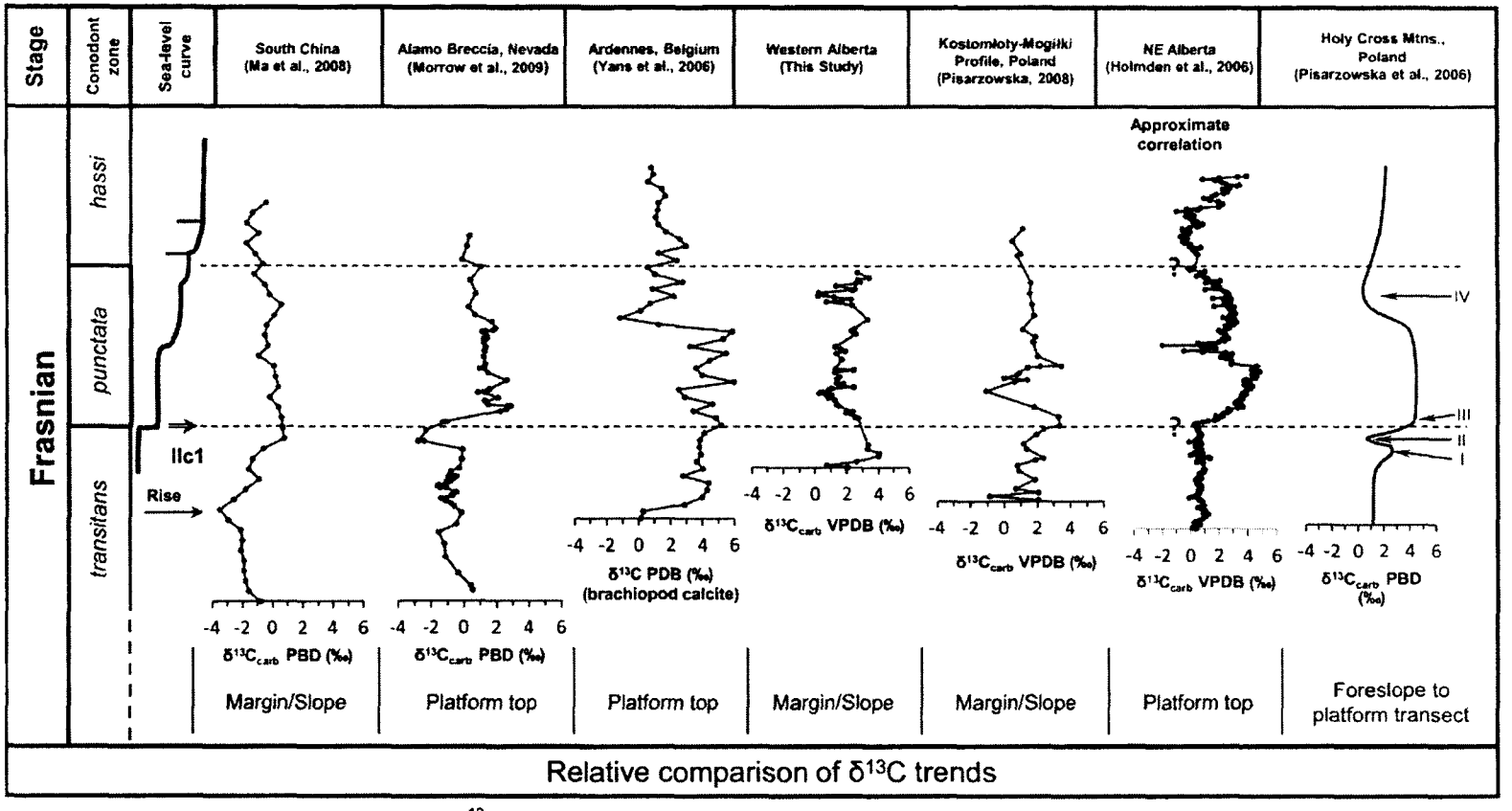

Fig. 4.8. A compilation of *punctata* Event $\delta^{13}C_{carb}$ records (modified after Morrow et al., 2009 with the addition of records from the WCSB of Holmden et al., 2006 and those of the present study). The isotopic histories are plotted against a generalized sea level curve (after Whalen et al., 2010) and the location of each profile within a basin to platform-top transect has been indicated. Note that Holmden et al. (2006) employed a ostracode-based biostratigraphy, and a more precise correlation of this dataset with the other profiles is currently not possible (the correlation above is based on comparisons of $\delta^{13}C_{carb}$ and unpublished $\delta^{13}C_{org}$ and TOC data with the records at the Miette platform – personal comm. with C. Holmden). Arrows labeled 'I, II, III, and IV' denote the four steps of the *punctata* Event (after Pisarzowska et al., 2006; Pisarzowska, 2008).

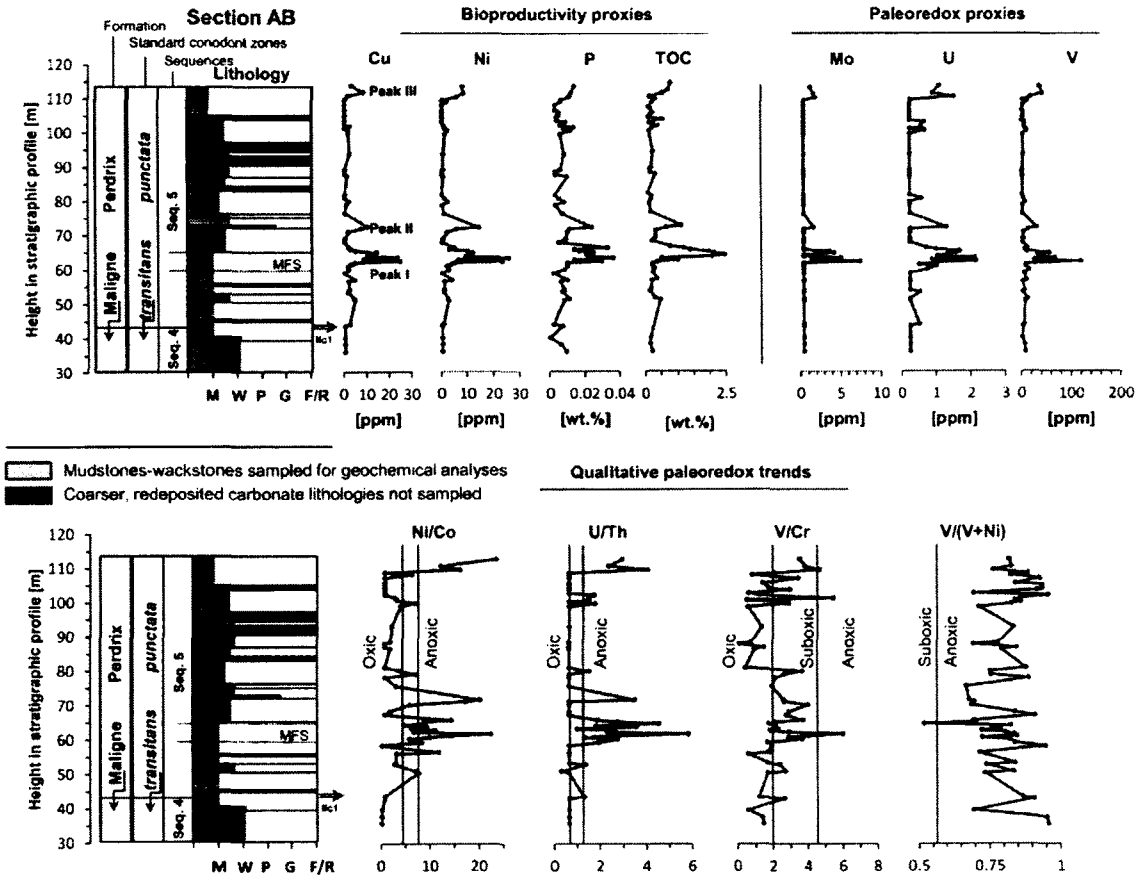

Fig. 4.9. Bioproductivity and bottom water redox trace element proxy profiles through the upper *transitans* and most of the *punctata* biozones. A 28 meter covered interval precludes extending this chemostratigraphic profile further up to the *punctata-hassi* boundary. Three excursion horizons are noted (Peaks I, II and III, shaded gray), the first two of which correspond to the transgressive phase and the mfz of 3rd order depositional Sequence 5 within the IIc-1 T-R cycle. Datapoints lying along vertical concentration lines in the trace element profiles are those that fell below analytical detection limits (DL), and were substituted with a value equal to one-half the DL for each analyte. Peak 1 ≈ Event III of Pisarzowska et al. (2006), Peak 2 has no equivalent, and Peak 3 ≈ Event IV (see Fig. 4.8). M = mudstone, W = wackestone, P = packstone, G = grainstone, F/R = floatstone/rudstone.

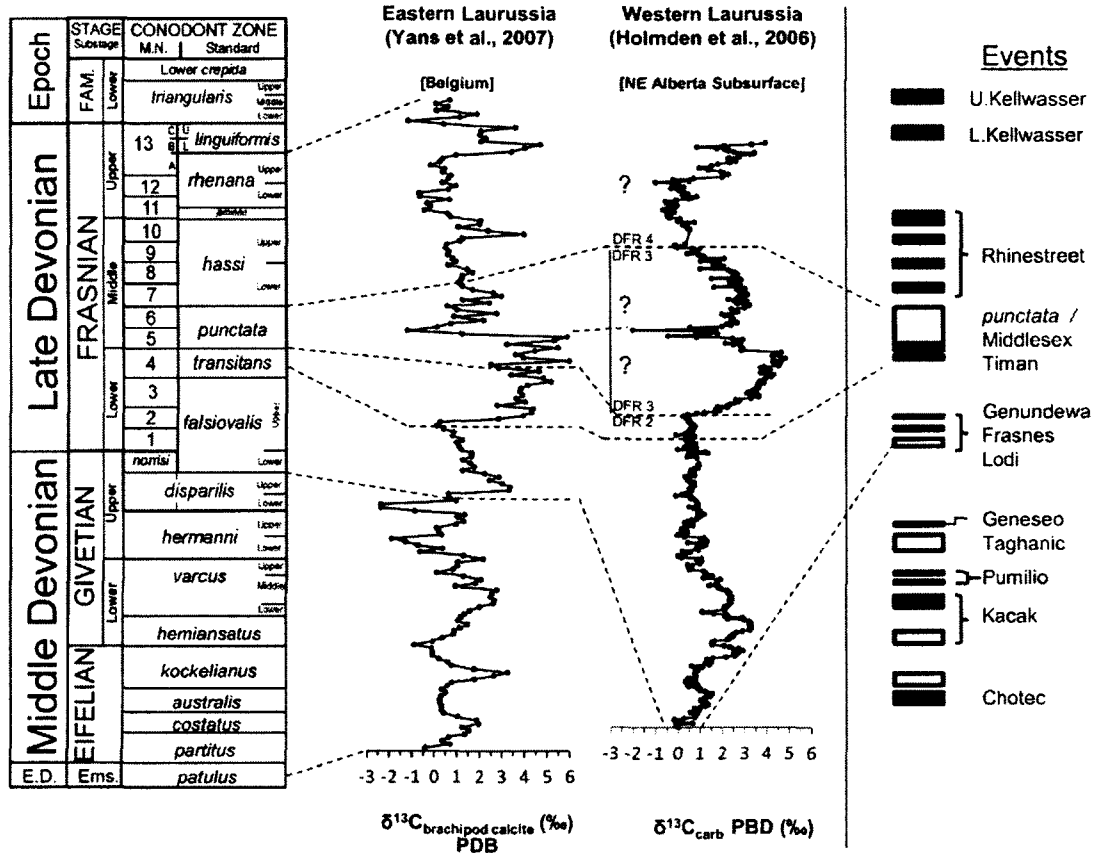

Fig. 4.10. A comparison of Middle-Late Devonian $\delta^{13}C_{carb}$ stratigraphies from Eastern and Western Laurussia (Belgium and the WCSB, Yans et al., 2007 and Holmden et al., 2006, respectively), which provide a broader context for the *punctata* Event record from the Miette platform in the WCSB (Fig. 4.7). Note that the correlation of the two broad scale records is only approximate, as two independent and uncorrelated biostratigraphic frameworks were used in constructing them. Note also that isotopic data in Yans et al., (2007) is derived from brachiopod calcite as opposed to micrite analyses in Holmden et al., (2006). Plotted for reference are global Late Devonian 'events' after House (2002), defined as sedimentological, faunal and geochemical perturbations within the marine realm. Those events associated with the deposition of OM-rich facies are denoted by solid rectangles. MN Zones after Klapper (1989), Klapper and Foster (1993), and Girard et al., (2005). Conodont zonation after Klapper and Becker (1999) and Yans et al., (2007).

Magnitude of *punctata* zone $\delta^{13}C$ excursions in relation to location in a platform-top to basin transect

Main $\delta^{13}C$ shift of the *punctata* Event – 'Event III' of IV (*Pisarzowska et al., 2006; Pisarzowska, 2008).* Near-coincident with transgressive pulse IIc.

(+) 2.5 ‰[1] **(+) 2-5‰[2]** **(+) 5-6‰[3]**

Negative C-isotopic shift noted higher in the *punctata* zone

(-) 2-3 ‰[1] **(-) 2-4 ‰[2]** **(-) 2-7‰[3]**

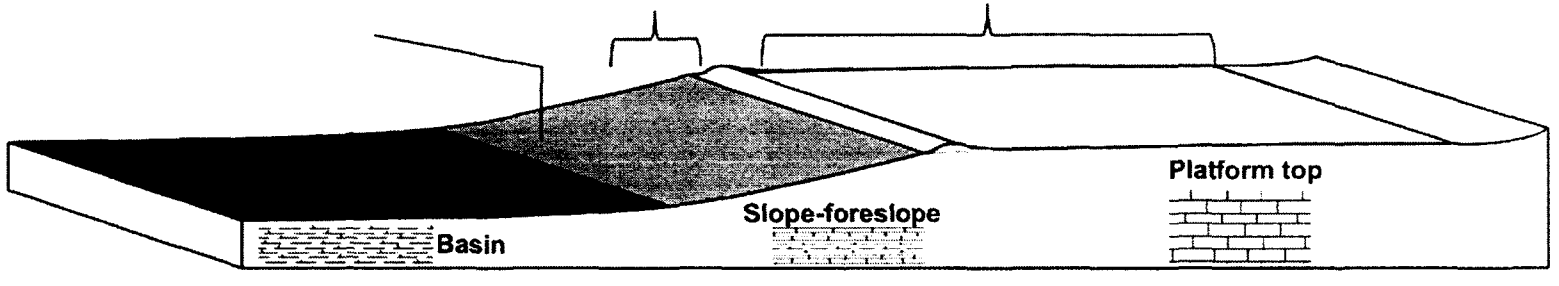

Generalized carbonate platform-top to basin transect*

Fig. 4.11. Magnitudes of *punctata* zone $\delta^{13}C_{carb}$ excursions in relation to depositional settings within a platform-top to basin transect. [1] Ma et al. (2008), Present study; [2] Racki et al., (2004), Pisarzowska et al., (2006); [3] Yans et al., (2007) – [brach. calcite used], Morrow et al., (2009), Holmden et al., (2006) .

Table 4.1. Analytical detection limits and representative precisions for each minor and trace element analyzed based on calibrations of x-ray fluorescence (XRF) analytical routines developed for this study.

Element	Ni	Cu	P	Mo	V	U	Th	Cr	Co
Units	(ppm)	(ppm)	(wt.%)	(ppm)	(ppm)	(ppm)	(ppm)	(ppm)	(ppm)
Detection Limit	0.7	1	0.001	0.9	1.4	0.4	1	2	1
Average standard deviation[1]	0.3	0.3	0.001	0.2	0.6	0.2	0.3	1.1	0.2

[1]Average standard deviation of 6 replicate analyses of two XRF pressed pellets made for sample pE44.0.

Table 4.2. Range of literature-derived $\delta^{13}C$ and $\delta^{18}O$ values representative of the Late Devonian ocean. Note the regional data from the WCSB.

Study	Material sampled	$\delta^{13}C$	$\delta^{18}O$
Hurley & Lohmann, (1989)	Frasnian marine cements	1.5 to 2.5 ‰	-5.0 to -7.5 ‰
da Silva & Boulvain, (2008)	Frasnian lagoonal carbonates	-1.75 to 2.2 ‰	-5.0 to -13.9 ‰
da Silva & Boulvain, (2008)	Frasnian biostromal carbonates	1.2 to 4.8 ‰	-5.0 to -14.2 ‰
Viezer et al., (1986)	Frasnian brachiopods	-1.0 to 2.0 ‰	-5.5 to 7.5 ‰
Viezer et al., (1999)	Late Devonian marine carbonate	0.0 to 2.0 ‰	-4.5 to -7.5 ‰
Bathurst, (1982)	Late Devonian marine cements	1.9 (±0.1) ‰	-5.0 (±0.4) ‰
Playford et al., (1984)	Late Devonian marine cements	2.0 (±1.0) ‰	-5.0 (±1.0) ‰
Kerans, (1985)	Late Devonian marine cements	1.8 (±2.0) ‰	-4.7 (±2.0) ‰
Walls et al., (1979)	Late Devonian marine cements	2.4 (±0.8) ‰	-6.5 (±0.8) ‰
Dunn et al., (1985)	Late Devonian marine cements	3.8 (±1.8) ‰	-5.0 (±1.0) ‰
Buggisch and Joachimski (2006)	Late Devonian marine carbonate of Central and Southern Europe from 'deep water settings below wave base'	Values fall in the 0.5-3.0 ‰ range[a]	Not reported
van Geldern et al., (2006)	Global compilation of Late Devonian brachiopod calcite	Values fall in the -1 to 2.5 ‰ range[b]	-4.0 to -7.0 ‰
Machel & Buschkuehle (2008)	**Late Devonian marine cements (Southesk-Cairn Carbonate Complex, western Alberta)**	2.0 (±1.0) ‰	-7.5 to -4.5 ‰
Hurley & Lohmann (1989)	**Late Devonian marine cements (average)**	**2.0 (±0.5) ‰**	**-4.5 (±0.5) ‰**
Hurley & Lohmann (1989)	**Late Devonian open marine cements, brachiopods and cyanobacterial crusts**	**~ 0.5 to 2.5 ‰**	**~ -4 to -7.5 ‰**

[a] This range excludes the major C-isotope excursions associated with the Falsiovalis, Kellwasser and Hangenberg/D-C boundary Events (see reference)

[b] This range excludes the major C-isotope excursions associated with the Kellwasser Events (see reference)

Table 4.3. A comparison of magnitudes of the main positive *punctata* Event $\delta^{13}C_{carb}$ shift near the IIc transgressive pulse and the *transitans-punctata* biozone boundary, in relation to the material sampled for $\delta^{13}C$ analyses and location of sampled profiles within a platform-top to basin transect.

Study	Material sampled:	Main +$\delta^{13}C$ shift[1]	Location in platform to basin transect:
Racki et al., (2004)	Whole rock (micrite)	~2 ‰	Foreslope
Piszrzowska et al., (2006)	Whole rock (micrite)	2-5 ‰	Foreslope to platform transect
Yans et al. (2006)	Brachiopod calcite	~5 ‰	Bank to reef successions
Ma et al. (2008)	Whole rock (micrite)	~2.5 ‰	Margin/slope
Holmden et al., (2006)	Whole rock (micrite)	~5 ‰	Platform top
Morrow et al., (2009)	Whole rock (micrite)	~6 ‰	Platform top
Present study	Whole rock (micrite)	~2.5 ‰	Margin/slope (isolated platform)

[1]'Event III' of IV (*Pisarzowska et al., 2006; Pisarzowska, 2008)* – the main $\delta^{13}C$ shift of the *punctata* Event near the *transitans-punctata* boundary. Coincident with transgressive pulse IIc.

Table 4.4. Thresholds of redox sensitive trace element ratios indicative of oxia, dysoxia and anoxia (Hatch and Leventhal, 1992; Jones and Manning, 1994).

Water column oxygenation conditions:

	Oxic	Dysoxic	Anoxic
Ni/Co[a]	< 5.00	5.00-7.00	> 7.00
V/Cr[a]	< 2.00	2.00-4.25	> 4.25
V/(V+Ni)[b]	< 0.46	0.46-0.60	0.54-0.82
U/Th[a]	< 0.75	0.75-1.25	> 1.25

[a] Jones and Manning (1994)

[b] Hatch and Leventhal (1992)

Appendix 4A

Appendix to Śliwiński et al. (2011): Geochemical Data

Table 4A-1. δ13Ccarb ‰ and δ18Ocarb ‰: Section AB

Sample		$\delta^{13}C_{carb}$ ‰ VPDB	$\delta^{13}C_{carb}$ ‰ $1\sigma^a$	$\delta^{18}O_{carb}$ ‰ VPDB	$\delta^{18}O_{carb}$ ‰ $1\sigma^a$
pE	114.0	2.68	0.39	-7.76	0.23
pE	112.0	3.45	0.44	-7.45	0.23
pE	111.0	2.73	0.41	-7.39	0.34
pE	110.0	2.88	0.18	-4.88	0.27
pE	109.5	2.57	0.28	-5.76	0.22
pE	108.5	1.34	0.63	-6.04	0.21
pE	107.0	2.51	0.37	-5.98	0.21
pE	106.5	2.37	0.16	-6.72	0.32
pE	105.5	0.24	0.79	-6.91	0.17
pE	105.0	0.68	0.66	-7.25	0.25
pE	104.0	0.19	0.77	-6.50	0.24
pE	103.5	1.21	0.43	-7.32	0.28
pE	102.5	2.28	0.27	-6.39	0.29
pE	102.0	1.72	0.15	-5.39	0.03
pE	101.5	0.72	0.73	-6.38	0.19
pE	101.0	-	-	-	-
pE	100.0	2.33	0.13	-4.65	0.10
pE	94.0	3.32	0.16	-3.40	0.06
pE	89.5	2.47	0.17	-3.96	0.10
pE	89.0	2.32	0.13	-3.26	0.08
pE	88.0	2.50	0.14	-4.61	0.09
pE	87.5	2.59	0.14	-4.52	0.08
pE	82.0	1.30	0.12	-3.86	0.08
pE	81.0	1.64	0.16	-5.24	0.09
pE	80.0	1.93	0.14	-4.03	0.07
pE	79.0	1.37	0.16	-3.79	0.09
pE	76.5	1.70	0.14	-5.03	0.09
pE	72.5	1.32	0.12	-4.72	0.12
pE	72.0	2.45	0.17	-4.31	0.07
pE	71.0	1.26	0.16	-3.25	0.09
pE	69.0	1.56	0.16	-4.69	0.08
pE	68.0	1.39	0.13	-5.16	0.07
pE	66.5	1.37	0.12	-5.46	0.06
pE	66.0	1.78	0.17	-5.71	0.07
pE	65.5	1.67	0.10	-4.45	0.05
pE	65.0	1.57	0.36	-8.54	0.24
pE	64.5	2.42	0.36	-8.18	0.26
pE	64.0	1.07	0.12	-4.94	0.06
pE	63.5	0.92	0.38	-7.75	0.30
pE	63.0	0.82	0.37	-7.92	0.25
pE	62.5	0.44	0.31	-7.65	0.23
pE	62.0	0.26	0.16	-4.15	0.08
pE	61.5	0.66	0.12	-4.52	0.08
pE	61.0	1.06	0.11	-4.00	0.04
pE	60.0	0.85	0.11	-3.98	0.08
pE	59.0	1.25	0.14	-7.67	0.05
pE	57.0	1.40	0.14	-5.83	0.09
pE	56.5	1.50	0.14	-5.81	0.06
pE	54.0	2.37	0.15	-4.74	0.07
pE	53.5	1.94	0.16	-5.75	0.08
pE	51.5	2.52	0.16	-9.36	0.10
pE	51.0	2.71	0.13	-7.10	0.07
pE	43.5v	-9.27	0.53	-15.98	0.30
pE	40.0	3.38	0.17	-5.20	0.05
pE	38.0	3.31	0.15	-6.72	0.07
pE	36.0	4.05	0.15	-5.83	0.08
pE	35.0	3.99	0.45	-7.75	0.29
pE	32.5	2.61	0.41	-9.69	0.27
pE	31.0	0.77	0.47	-9.67	0.34
pE	30.0	2.05	0.38	-9.46	0.27

[a] One standard deviation of three measurements

Table 4A-1 continued: δ13Corg ‰ and δ15Norg ‰: Section AB

Sample		Sample Wt. [mg]	Conc N [%]	Conc C [%]	$\delta^{15}N_{org}$ ‰ At-air	$\delta^{13}C_{org}$ ‰ PDB	TOC Bulk Rock
pE	114.0	2.036	0.15	4.83	-1.18	-28.85	0.76
pE	112.0	2.650	0.21	5.01	-0.67	-28.77	0.68
pE	111.0	2.136	0.15	4.92	-0.81	-28.62	0.51
pE	110.0	5.313	0.29	6.42	0.00	-27.66	0.11
pE	109.5	3.092	0.06	1.91	-1.66	-27.35	0.29
pE	108.5	2.831	0.30	8.84	-0.36	-28.12	0.21
pE	107.0	2.209	0.25	7.27	0.28	-27.44	0.10
pE	106.5	3.699	0.15	4.55	-0.29	-28.10	0.16
pE	105.5	2.789	0.37	9.22	-0.15	-28.12	0.23
pE	105.0	2.091	0.36	9.72	-1.16	-28.04	0.17
pE	104.0	2.175	0.40	14.19	0.03	-27.72	0.10
pE	103.5	2.324	0.57	16.42	0.42	-28.34	0.53
pE	102.5	6.323	0.25	5.35	-0.74	-28.31	0.11
pE	102.0	4.670	0.12	4.83	-0.92	-28.37	0.23
pE	101.5	2.258	0.16	6.63	-1.08	-28.54	3.40
pE	101.0	2.030	0.24	6.87	-0.78	-28.67	0.21
pE	100.0	6.490	0.05	1.61	-1.88	-26.68	1.41
pE	94.0	1.670	0.35	8.81	-0.87	-27.37	0.20
pE	89.5	2.361	0.29	10.15	-1.17	-28.35	0.18
pE	89.0	5.128	0.02	1.21	-6.16	-25.60	0.14
pE	88.0	3.709	0.30	12.95	0.93	-27.62	0.15
pE	87.5	1.594	0.23	14.65	-1.64	-28.30	0.31
pE	82.0	6.967	0.02	0.64	-3.70	-22.67	0.08
pE	81.0	1.620	0.41	13.85	-0.95	-29.02	0.18
pE	80.0	1.850	0.22	5.14	-0.63	-27.32	0.16
pE	79.0	1.880	0.27	7.46	-1.18	-28.54	0.12
pE	76.5	2.200	0.32	9.06	-0.74	-28.63	0.16
pE	72.5	1.680	0.29	9.96	-2.55	-28.09	1.08
pE	72.0	1.680	0.33	8.76	-0.43	-29.05	0.63
pE	71.0	2.080	0.27	10.74	-0.47	-29.00	0.32
pE	69.0	1.997	0.43	20.42	-2.77	-28.09	0.30
pE	68.0	1.740	0.21	4.99	-0.98	-27.42	0.20
pE	66.5	1.941	0.33	19.85	-1.30	-27.13	0.74
pE	66.0	1.540	0.39	17.36	-1.15	-26.96	1.17
pE	65.5	2.090	0.33	11.84	-0.22	-26.93	1.36
pE	65.0	1.816	0.24	7.49	-1.33	-26.84	1.95
pE	64.5	1.974	0.21	9.75	-1.90	-26.94	2.14
pE	64.0	1.910	0.27	10.27	-0.62	-26.48	2.46
pE	63.5	1.712	0.18	6.81	-3.54	-27.18	2.07
pE	63.0	1.823	0.12	3.21	-1.99	-27.70	0.51
pE	62.5	1.866	0.16	4.38	-1.92	-29.87	0.99
pE	62.0	1.520	0.15	5.16	-	-30.07	0.38
pE	61.5	1.700	0.18	4.82	-1.64	-30.05	0.23
pE	61.0	1.440	0.31	9.31	-0.55	-30.09	0.22
pE	60.0	1.760	0.10	3.30	-	-30.23	0.27
pE	59.0	1.947	1.04	14.43	0.72	-28.78	0.23
pE	57.0	1.970	0.14	5.40	-2.82	-29.93	0.35
pE	56.5	2.050	0.14	6.02	-1.06	-29.78	0.20
pE	54.0	1.500	0.26	10.42	0.09	-29.19	0.17
pE	53.5	1.680	0.29	12.31	-0.92	-29.04	0.13
pE	51.5	1.580	0.18	6.03	-1.53	-29.36	0.29
pE	51.0	1.720	0.25	9.57	-1.15	-29.23	0.45
pE	43.5v	-	-	-	-	-	-
pE	40.0	2.755	0.52	20.37	1.55	-25.46	0.15
pE	38.0	5.010	0.11	2.96	1.45	-25.93	0.13
pE	36.0	1.670	0.13	4.40	-1.02	-25.98	0.20

Table 4A-1 continued: δ13Corg ‰ and δ15Norg ‰: Section K

Sample	Depth	Sample Wt. [mg]	Conc N [%]	Conc C [%]	$\delta^{15}N_{org}$ ‰ At-air	$\delta^{13}C_{org}$ ‰ PDB
K17	**56.30**	10.300	0.46	8.93	1.03	-26.96
K238	**56.30**	10.189	0.48	10.85	1.09	-26.77
K18	**56.50**	10.478	0.47	10.05	0.90	-27.48
K245	**58.90**	10.532	0.47	9.31	0.58	-26.89
K246	**59.40**	10.230	0.44	8.59	1.75	-27.07
K247	**59.90**	10.260	0.41	8.33	1.62	-27.00
K248	**60.20**	10.175	0.44	7.93	0.63	-27.51
K250	**60.50**	10.576	0.42	7.21	0.27	-28.10
K251	**60.90**	10.245	0.37	6.28	-0.26	-28.11
K249	**61.10**	10.184	0.40	8.11	-0.05	-27.57
K20	**61.30**	10.455	0.39	6.62	-0.64	-28.58
K21	**62.60**	9.829	0.56	9.19	1.45	-28.03
K253A	**62.90**	10.720	0.38	6.76	-0.39	-28.40
K253B	**63.00**	9.954	0.43	6.76	0.97	-28.20
K22	**64.30**	10.939	0.02	0.80	1.10	-26.86
K256	**65.80**	10.708	0.30	5.74	-0.87	-28.58
K257	**66.80**	10.432	0.20	5.95	-1.36	-29.23
K258	**67.90**	10.749	0.33	5.40	-1.28	-30.18
K23	**68.00**	10.400	0.24	4.31	-1.22	-29.59
K260	**69.60**	10.535	0.20	2.84	-1.30	-29.22
K261	**70.40**	10.516	0.26	4.92	-1.20	-29.87
K24	**71.40**	10.680	0.28	5.12	-1.03	-30.07
K262	**71.50**	10.026	0.26	5.34	-1.59	-30.07
K263	**72.50**	10.668	0.20	4.69	-1.84	-29.85
K265	**74.00**	9.735	0.15	3.06	-1.55	-29.89
K25	**74.50**	10.170	0.15	3.31	-2.05	-30.36
K266	**75.50**	10.680	0.13	3.64	-1.72	-30.05
K267	**77.80**	10.246	0.14	1.92	-1.11	-29.29
K268	**79.00**	10.094	0.16	3.14	-1.77	-30.11
K269	**81.00**	10.712	0.14	2.12	-2.23	-30.28
K26	**82.30**	10.415	0.26	4.52	-0.47	-29.67
K270	**85.10**	10.670	0.24	3.44	-0.75	-30.04
K271	**85.90**	10.283	0.21	4.38	-0.50	-29.33
K272	**86.20**	10.156	0.11	3.50	-0.41	-28.07
K27	**86.40**	10.175	0.22	4.04	-0.70	-28.78
K273	**86.80**	10.501	0.27	5.81	-1.15	-26.90
K28	**87.00**	10.197	0.29	6.33	-0.61	-26.65
K274	**87.30**	10.374	0.28	7.09	0.45	-26.80
K275	**87.50**	9.546	0.25	5.69	0.56	-27.16
K276	**87.90**	10.504	0.32	7.10	0.83	-27.37
K29	**88.10**	10.905	0.55	9.10	-2.03	-27.70
K29A	**91.40**	9.815	0.48	9.19	0.81	-27.75
K30	**93.00**	9.987	0.16	4.75	4.45	-26.82
K31	**95.00**	10.222	0.06	2.12	3.68	-27.43

Table 4A-2. XRF trace element data (Section AB).

Sample	Cu	Ni	P	Mo	U	V	Th	Co	Cr	Ni/Co	U/Th	V/Cr	V/(V+Ni)
	[ppm]	[ppm]	[ppm]	[ppm]	[ppm]	[ppm]	[ppm]	[ppm]	[ppm]	-	-	-	-
114.0	3.3	8.1	0.014	1.1	1.1	36.6	0.4	0.3	10.4	23.6	3.0	3.5	0.8
112.0	8.4	8.6	0.012	1.5	0.9	41.1	0.4	0.7	10.7	12.4	2.4	3.8	0.8
111.0	1.9	5.6	0.011	1.7	1.5	17.9	0.4	0.3	3.8	16.3	4.1	4.6	0.8
110.0	0.5	0.3	0.006	0.4	0.2	2.3	0.4	0.3	1.1	0.9	0.6	2.1	0.9
109.5	0.5	2.2	0.006	0.4	0.2	10.3	0.4	0.3	12.9	6.4	0.6	0.8	0.8
108.5	0.5	0.3	0.003	0.4	0.2	3.9	0.4	0.3	1.1	0.9	0.6	3.4	0.9
107.0	0.5	0.3	0.003	0.4	0.2	1.6	0.4	0.3	1.1	0.9	0.6	1.4	0.8
106.5	0.5	0.3	0.005	0.4	0.2	4.2	0.4	0.3	2.7	0.9	0.6	1.6	0.9
105.5	0.5	0.3	0.005	0.4	0.2	4.4	0.4	0.3	2.5	0.9	0.6	1.8	0.9
105.0	0.5	0.3	0.004	0.4	0.2	3.3	0.4	0.3	1.1	0.9	0.6	2.9	0.9
104.0	0.5	0.3	0.004	0.4	0.2	0.7	0.4	0.3	1.1	0.9	0.6	0.6	0.7
103.5	0.5	0.3	0.009	0.4	0.6	6.4	0.4	0.3	5.3	0.9	1.8	1.2	1.0
103.0	1.5	0.3	0.004	0.4	0.2	0.7	0.8	0.3	1.1	0.9	0.3	0.6	0.7
102.5	0.5	1.0	0.006	0.4	0.6	6.2	0.4	0.3	1.1	3.0	1.5	5.5	0.9
102.0	2.8	1.2	0.014	0.4	0.6	6.2	0.4	0.3	12.1	3.4	1.5	0.5	0.8
101.5	0.5	1.5	0.008	0.4	0.2	9.3	0.4	0.3	4.2	4.5	0.6	2.2	0.9
101.0	2.0	2.4	0.012	0.4	0.7	11.4	0.4	0.3	3.9	6.9	1.8	2.9	0.8
100.0	2.0	1.4	0.006	0.4	0.2	3.5	0.4	0.3	6.1	4.2	0.6	0.6	0.7
94.0	2.7	0.8	0.008	0.4	0.2	3.9	0.4	0.3	2.9	2.3	0.6	1.3	0.8
89.5	0.5	0.7	0.006	0.4	0.2	2.5	0.4	0.3	3.3	2.0	0.6	0.8	0.8
89.0	0.5	0.3	0.003	0.4	0.2	0.7	0.4	0.3	5.8	0.9	0.6	0.1	0.7
88.0	0.5	0.3	0.003	0.4	0.2	1.7	0.4	0.3	1.1	0.9	0.6	1.5	0.8
87.5	1.6	0.7	0.010	0.4	0.2	2.5	0.4	0.3	2.7	1.9	0.6	0.9	0.8
82.0	0.5	0.3	0.003	0.4	0.2	2.2	0.4	0.3	5.1	0.9	0.6	0.4	0.9
81.5	0.5	0.3	0.003	0.4	0.6	1.8	0.4	0.3	1.1	0.9	1.5	1.6	0.9
80.0	2.3	2.5	0.008	0.4	0.2	7.6	0.4	0.3	2.9	7.3	0.6	2.6	0.8
79.0	1.2	0.3	0.003	0.4	0.2	2.4	0.4	0.3	1.1	0.9	0.6	2.2	0.9
76.5	0.5	1.1	0.007	0.4	0.2	2.2	0.4	0.3	1.1	3.2	0.6	2.0	0.7
72.5	10.6	14.4	0.024	1.6	1.3	30.4	0.4	0.7	11.7	20.3	3.5	2.6	0.7
72.0	7.8	6.0	0.011	0.4	0.2	13.7	0.4	0.3	5.2	17.4	0.6	2.6	0.7
71.0	2.0	2.1	0.010	0.4	0.2	4.5	0.4	0.3	1.1	6.0	0.6	4.0	0.7
69.0	0.5	0.6	0.009	0.4	0.2	3.3	0.4	0.3	1.1	1.8	0.6	2.9	0.8
68.0	0.5	0.3	0.005	0.4	0.2	3.1	0.4	0.3	1.1	0.9	0.6	2.8	0.9
67.0	5.5	7.4	0.019	0.4	1.9	26.5	0.4	0.3	10.2	21.6	5.1	2.6	0.8
66.5	2.1	4.9	0.033	0.4	0.7	11.4	0.4	0.3	3.1	14.4	1.9	3.7	0.7
66.0	3.1	3.0	0.014	0.4	1.0	7.3	0.4	0.3	3.4	8.9	2.7	2.1	0.7
65.5	5.0	10.2	0.017	3.7	1.7	10.9	0.4	1.1	6.2	9.0	4.6	1.8	0.5
65.0	14.5	11.9	0.025	4.1	1.6	56.0	0.9	2.5	26.2	4.7	1.8	2.1	0.8
64.5	12.0	10.4	0.021	0.4	1.3	32.5	0.4	1.1	15.4	9.5	3.6	2.1	0.8
64.0	10.5	9.6	0.023	0.4	1.0	35.5	1.0	1.5	15.7	6.3	1.0	2.3	0.8
63.5	23.7	25.6	0.036	5.0	2.1	67.1	0.8	2.3	36.4	11.1	2.6	1.8	0.7
63.0	8.9	6.4	0.014	1.4	0.9	26.9	0.4	0.9	9.2	6.8	2.4	2.9	0.8
62.5	24.7	23.2	0.030	7.3	2.1	120.8	0.4	1.0	20.2	22.5	5.8	6.0	0.8
62.0	4.7	5.0	0.010	0.4	1.0	27.9	0.4	0.3	6.9	14.5	2.7	4.0	0.8
61.5	3.3	3.4	0.010	0.4	0.5	9.1	0.4	0.3	3.2	10.0	1.3	2.9	0.7
61.0	1.9	2.0	0.010	0.4	1.0	9.3	0.4	0.3	2.5	5.9	2.7	3.7	0.8
60.0	2.2	2.9	0.008	0.4	0.7	15.2	0.4	0.3	8.9	8.4	1.9	1.7	0.8
59.0	0.5	0.3	0.002	0.4	0.2	5.5	0.4	1.1	2.8	0.3	0.6	1.9	0.9
57.0	4.6	4.1	0.010	0.4	0.2	10.2	0.4	0.3	5.8	11.9	0.6	1.8	0.7
56.5	2.3	1.1	0.006	0.4	0.2	3.1	0.4	0.3	5.2	3.3	0.6	0.6	0.7
54.0	2.3	1.1	0.008	0.4	0.2	5.7	0.4	0.3	3.4	3.2	0.6	1.7	0.8
53.5	1.8	1.0	0.007	0.4	0.5	2.7	0.4	0.3	1.1	2.8	1.4	2.4	0.7
51.5	4.5	2.4	0.011	0.4	0.2	12.6	0.8	0.3	4.6	7.1	0.3	2.7	0.8
51.0	4.7	2.7	0.008	0.4	0.2	7.4	0.4	0.3	4.3	7.8	0.6	1.7	0.7
50.0	2.9	0.3	0.012	0.4	0.2	4.4	0.4	0.3	16.7	0.9	0.6	0.3	0.9
47.0	0.5	0.3	0.003	0.4	0.2	0.7	0.4	0.8	1.1	0.4	0.6	0.6	0.7
44.0	2.5	0.7	0.002	0.4	0.5	5.0	0.4	0.9	4.2	0.8	1.3	1.2	0.9
43.5	0.5	0.3	0.007	0.4	0.2	3.0	0.4	0.3	1.1	0.9	0.6	2.7	0.9
40.0	0.5	0.3	0.000	0.4	0.2	0.7	0.4	1.1	1.1	0.3	0.6	0.6	0.7
38.0	0.5	0.3	0.006	0.4	0.2	5.9	0.4	1.2	4.3	0.2	0.6	1.4	1.0
36.0	0.5	0.3	0.009	0.4	0.2	6.9	0.4	1.2	4.7	0.2	0.6	1.5	1.0

Table 4A-3. Matrix of Pearson (parametric) correlations for the geochemical dataset (software used: Statistical Package for the Social Sciences (SPSS)). The broader geochemical dataset of Śliwiński et al., (2010) was recently expanded, although not all refined chemostratigraphic profiles are presented herein. Included for reference, however, are the statistical relationships of the detrital input proxies (Al, Si, K, Ti, Zr, Cr) mentioned in the text to the bioproductivity, redox and stable isotope data presented.

Pearson (parametric) Correlations (N=53)

	MS	Al	Si	K	Ti	Zr	Cr	Ni	Cu	Ba	P	Mo	V	U	Ni/Co	U/Th	V/Cr	V/(V+Ni)	δ13C	δ18O	δ13Corg	TOC	δ15Norg
MS	1.000	.535**	.489**	.562**	.476**	.657**	.434**	.514**	.485**	.181	.401**	.285*	.394**	.360**	.523**	.347*	.219	-.212	.092	-.108	-.272*	.273*	-.043
Al	.535**	1.000	.823**	.997**	.987**	.754**	.929**	.901**	.930**	.455**	.802**	.733**	.807**	.728**	.454**	.500**	.208	-.154	-.161	-.396**	.065	.623**	-.268
Si	.489**	.823**	1.000	.814**	.788**	.648**	.867**	.819**	.799**	.304*	.678**	.650**	.788**	.671**	.554**	.607**	.226	-.137	-.142	-.397**	.124	.626**	-.410**
K	.562**	.997**	.814**	1.000	.979**	.761**	.914**	.898**	.930**	.463**	.801**	.730**	.807**	.714**	.468**	.506**	.223	-.159	-.147	-.398**	.056	.614**	-.259
Ti	.476**	.987**	.788**	.979**	1.000	.716**	.916**	.847**	.881**	.460**	.774**	.686**	.742**	.714**	.344*	.428**	.138	-.128	-.146	-.387**	.129	.623**	-.256
Zr	.657**	.754**	.648**	.761**	.716**	1.000	.705**	.752**	.758**	.410**	.692**	.570**	.609**	.563**	.547**	.524**	.250	-.385**	-.291*	-.104	-.257	.492**	-.318*
Cr	.434**	.929**	.867**	.914**	.916**	.705**	1.000	.868**	.883**	.468**	.768**	.734**	.799**	.699**	.449**	.499**	.095	-.125	-.165	-.392**	.079	.594**	-.371**
Ni	.514**	.901**	.819**	.898**	.847**	.752**	.868**	1.000	.954**	.279*	.868**	.849**	.887**	.799**	.713**	.741**	.387**	-.324*	-.225	-.341*	-.076	.582**	-.314*
Cu	.485**	.930**	.799**	.930**	.881**	.758**	.883**	.954**	1.000	.335*	.820**	.834**	.910**	.696**	.588**	.625**	.329*	-.226	-.226	-.374**	-.065	.544**	-.313*
Ba	.181	.455**	.304*	.463**	.460**	.410**	.468**	.279*	.335*	1.000	.312*	.373**	.305*	.153	006	090	013	.018	-.061	-.274*	115	.315*	-.048
P	.401**	.802**	.678**	.801**	.774**	.692**	.768**	.868**	.820**	.312*	1.000	.669**	.733**	.742**	.644**	.647**	.359**	-.324*	-.224	-.287*	-.035	.601**	-.296*
Mo	.285*	.733**	.650**	.730**	.686**	.570**	.734**	.849**	.834**	.373**	.669**	1.000	.877**	.683**	.486**	.703**	.361**	-.180	-.211	-.347*	-.044	.381**	-.208
V	.394**	.807**	.788**	.807**	.742**	.609**	.799**	.887**	.910**	.305*	.733**	.877**	1.000	.671**	.628**	.695**	.478**	-.031	-.224	-.420**	-.141	.454**	-.227
U	.360**	.728**	.671**	.714**	.714**	.563**	.699**	.799**	.696**	.153	.742**	.683**	.671**	1.000	.538**	.791**	.308*	-.190	-.233	-.316*	-.013	.501**	-.087
Ni/Co	.523**	.454**	.554**	.468**	.344*	.547**	.449**	.713**	.588**	006	.644**	.486**	.628**	.538**	1.000	.711**	.560**	-.394**	-.126	-.177	-.358**	.322*	-.245
U/Th	.347*	.500**	.607**	.506**	.428**	.524**	.499**	.741**	.625**	.090	.647**	.703**	.695**	.791**	.711**	1.000	.524**	-.282*	-.204	-.257	-.168	.362**	-.143
V/Cr	.219	.208	.226	.223	.138	.250	.095	.387**	.329*	.013	.359*	.361**	.478**	.308*	.560**	.524**	1.000	.055	-.218	-.236	-.450**	.087	055
V/(V+Ni)	-.212	-.154	-.137	-.159	-.128	-.385**	-.125	-.324*	- 226	.018	-.324*	-.180	-.031	-.190	-.394**	-.282*	.055	1.000	.034	- 261	.028	-.227	246
$\delta^{13}C$	.092	-.161	-.142	-.147	-.146	-.291*	-.165	-.225	-.226	-.061	-.224	-.211	-.224	-.233	-.126	-.204	-.218	.034	1.000	.007	.289*	-.203	192
$\delta^{18}O$	-.108	-.396**	-.397**	-.398**	-.387**	-.104	-.392**	-.341*	-.374**	-.274*	-.287*	-.347*	-.420**	-.316*	-.177	- 257	-.236	- 261	.007	1.000	.098	-.275*	- 109
$\delta^{13}Corg$	-.272*	.065	.124	.056	.129	-.257	.079	-.076	-.085	.115	-.035	-.044	-.141	-.013	-.358*	-.168	- 450**	.028	.289*	.098	1.000	122	-.168
TOC	.273*	.623**	.626**	.614**	.623**	.492**	.594**	.582**	.544**	.315*	.601**	.381**	.454**	.501**	.322*	.362**	.087	-.227	-.203	-.275*	.122	1.000	- 181
$\delta^{15}Norg$	-.043	-.268	-.410**	-.259	-.256	-.318*	-.371**	-.314*	-.313*	-.048	-.296*	- 208	- 227	-.087	- 245	-.143	.055	246	.192	-.109	- 168	-.181	1.000

**. Correlation is significant at the 0.01 level (2-tailed).

*. Correlation is significant at the 0.05 level (2-tailed)

Appendix 4A-4. Matrix of Spearman (non-parametric) correlations for the geochemical dataset (software used: Statistical Package for the Social Sciences (SPSS)). The broader geochemical dataset of Śliwiński et al., (2010) was recently expanded, although not all refined chemostratigraphic profiles are presented herein. Included for reference, however, are the statistical relationships of the detrital input proxies (Al, Si, K, Ti, Zr, Cr) mentioned in the text to the bioproductivity, redox and stable isotope data presented.

	MS	Al	Si	K	Ti	Zr	Cr	Ni	Cu	Ba	P	Mo	V	U	Ni/Co	U/Th	V/Cr	V/(V+Ni)	δ13C	δ18O	δ13Corg	TOC	δ15Norg
MS	1.000	.752**	.472**	.737**	.764**	.709**	.484**	.645**	.653**	.625**	.572**	.460**	.677**	.416**	.545**	.400**	.285*	-.218	.090	-.106	-.212	.485**	-.107
Al	.752**	1.000	.724**	.988**	.980**	.683**	.760**	.794**	.820**	.841**	.811**	.562**	.860**	.631**	.682**	.589**	.263	-.201	-.006	-.298*	-.058	.720**	-.270
Si	.472**	.724**	1.000	.704**	.657**	.548**	.875**	.712**	.627**	.701**	.595**	.581**	.759**	.540**	.637**	.551**	.186	-.135	-.125	-.278*	.097	.646**	-.487**
K	.737**	.988**	.704**	1.000	.967**	.687**	.730**	.795**	.821**	.838**	.819**	.548**	.854**	.615**	.685**	.596**	.326*	-.194	-.019	-.318*	-.077	.696**	-.265
Ti	.764**	.980**	.657**	.967**	1.000	.655**	.715**	.766**	.796**	.842**	.801**	.551**	.835**	.639**	.637**	.583**	.248	-.220	.024	-.288*	-.037	.705**	-.227
Zr	.709**	.683**	.548**	.687**	.655**	1.000	.566**	.804**	.836**	.619**	.668**	.461**	.590**	.439**	.752**	.526**	.315*	-.436**	-.163	.014	-.245	.552**	-.356*
Cr	.484**	.760**	.875**	.730**	.715**	.566**	1.000	.721**	.715**	.662**	.652**	.542**	.743**	.558**	.615**	.525**	-.019	-.201	-.054	-.253	.078	.657**	-.472**
Ni	.645**	.794**	.712**	.795**	.766**	.804**	.721**	1.000	.894**	.752**	.871**	.632**	.834**	.611**	.940**	.684**	.451**	-.527**	-.126	-.182	-.208	.779**	-.433**
Cu	.653**	.820**	.627**	.821**	.796**	.836**	.715**	.894**	1.000	.727**	.833**	.569**	.736**	.557**	.818**	.587**	.332*	-.449**	-.103	-.155	-.211	.680**	-.385**
Ba	.625**	.841**	.701**	.838**	.842**	.619**	.662**	.752**	.727**	1.000	.765**	.591**	.831**	.673**	.642**	.695**	.367**	-.160	-.152	-.313*	-.052	.676**	-.239
P	.572**	.811**	.595**	.819**	.801**	.668**	.652**	.871**	.833**	.765**	1.000	.569**	.792**	.652**	.792**	.680**	.411**	-.388**	-.085	-.193	-.127	.778**	-.377**
Mo	.460**	.562**	.581**	.548**	.551**	.461**	.542**	.632**	.569**	.591**	.569**	1.000	.599**	.622**	.518**	.653**	.341*	-.223	-.054	-.394**	.028	.501**	-.264
V	.677**	.860**	.759**	.854**	.835**	.590**	.743**	.834**	.736**	.831**	.792**	.599**	1.000	.701**	.746**	.647**	.490**	-.074	-.144	-.407**	-.182	.771**	-.272
U	.416**	.631**	.540**	.615**	.639**	.439**	.558**	.611**	.557**	.673**	.652**	.622**	.701**	1.000	.501**	.848**	.321*	-.115	-.214	-.297*	.021	.568**	-.044
Ni/Co	.545**	.682**	.637**	.685**	.637**	.752**	.615**	.940**	.818**	.642**	.792**	.518**	.746**	.501**	1.000	.636**	.499**	-.530**	-.121	-.084	-.371**	.696**	-.437**
U/Th	.400**	.589**	.551**	.596**	.583**	.526**	.525**	.684**	.587**	.695**	.680**	.653**	.647**	.848**	.636**	1.000	.431**	-.217	-.236	-.205	-.093	.546**	-.192
V/Cr	.285*	.263	.186	.326*	.248	.315*	-.019	.451**	.332*	.367**	.411**	.341*	.490**	.321*	.499**	.431**	1.000	.009	-.264	-.205	-.381**	.321*	-.075
V/(V+Ni)	-.218	-.201	-.135	-.194	-.220	-.436**	-.201	-.527**	-.449**	-.160	-.388**	-.223	-.074	-.115	-.530**	-.217	.009	1.000	-.034	-.236	-.021	-.292*	.260
$\delta^{13}C$	.090	-.006	-.125	-.019	.024	-.163	-.054	-.126	-.103	-.152	-.085	-.054	-.144	-.214	-.121	-.236	-.264	-.034	1.000	-.019	.242	-.182	.168
$\delta^{18}O$	-.106	-.298*	-.278*	-.318*	-.288*	.014	-.253	-.182	-.155	-.313*	-.193	-.394**	-.407**	-.297*	-.084	-.205	-.205	-.236	-.019	1.000	.016	-.295*	.017
$\delta^{13}Corg$	-.212	-.058	.097	-.077	-.037	-.245	.078	-.208	-.211	-.052	-.127	.028	-.182	.021	-.371**	-.093	-.381**	-.021	.242	.016	1.000	-.056	-.032
TOC	.485**	.720**	.646**	.696**	.705**	.552**	.657**	.779**	.680**	.676**	.778**	.501**	.771**	.568**	.696**	.546**	.321*	-.292*	-.182	-.295*	-.056	1.000	-.354*
$\delta^{15}Norg$	-.107	-.270	-.487**	-.265	-.227	-.356*	-.472**	-.433**	-.385**	-.239	-.377**	-.264	-.272	-.044	-.437**	-.192	-.075	.260	.168	.017	-.032	-.354*	1.000

**. Correlation is significant at the 0.01 level (2-tailed).

*. Correlation is significant at the 0.05 level (2-tailed).

5. Constraining clastic input controls on magnetic susceptibility and trace element anomalies during the Late Devonian *punctata* Event in the Western Canada Sedimentary Basin[1]

Abstract:

Factor analyses were applied to trace element and magnetic susceptibility (MS) records of the Late Devonian paleoceanographic '*punctata* Event' perturbation in the Western Canada Sedimentary Basin to constrain the extent to which geochemical anomalies were driven by 1) changes in clastic input (Factor 1; 55.1 % of total variance) vs. 2) anoxia in the depositional environment (Factor 2; 35.2 % of total variance). MS associates only with Factor 1 (r = 0.971) and is significantly correlated (99.9 % level) with acid-insoluble limestone residues and clastic proxies (Al, Si, K, Ti, Zr; r = 0.542-0.639). Based on XRD analyses of a small subset of these residues (N = 7), a multivariate linear regression model accounts for 97.7 % of total MS variance as a function of variable admixing of illite, pyrite, quartz and feldspar, in turn variably diluted by stratigraphic changes in the total carbonate content.

5.1. Introduction

The global Late Devonian '*punctata* Event' was a pronounced paleoceanographic perturbation characterized by geochemical anomalies that arose in the chemostratigraphic record during an apparent short-term (<0.6 M.y., Kaufmann, 2006) yet wide-spread eutrophication of epicontinental seaways, resulting in the deposition of organic matter (OM)-rich facies, the development of photic zone anoxia, but curiously no significant biotic turnover (Pisarzowska et al., 2006; Racki et al., 2008 and references therein; Morrow et al., 2009; Śliwiński et al., 2010, 2011). Our current understanding of Late Devonian oceanic anoxic events (House, 2002; Racki, 2005) indicates that the Early-Middle Frasnian *punctata* Event is one of the first in a sequence of perturbations that predate the Frasnian-Famennian extinction. Within the context of Algeo and Scheckler's (2010; Figs. 1 and 2 therein) 'qualitative reading of the paleobotanic record,' the

---

[1] Śliwiński, M.G., Whalen, M.T., Meyer, F. and Majs, F., *(in press)*. Constraining clastic input controls on magnetic susceptibility and trace element anomalies during the Late Devonian *punctata* Event in the Western Canada Sedimentary Basin. *Terra Nova,* doi: 10.1111/j.1365-3121.2012.01063.x

punctata Event curiously occurred near the onset of a sharp increase in the rate of diversification and expansion of the aboriginal terrestrial forests; the resulting transient increase in the intensity of pedogenic weathering and in the flux of soil-derived nutrients to marine ecosystems provides a causal mechanism to help explain the numerous organic carbon burial events of the Late Devonian.

Evaluation of chemostratigraphic trends across the *punctata* Zone stratigraphy at the Miette carbonate platform in the Western Canada Sedimentary Basin (WCSB) revealed that eutrophication and geochemical anomalies, including positive MS excursions, associate strongly with 3rd-order transgressive strata and with increased siliciclastic input in the lower *punctata* Zone (Śliwiński et al., 2010, 2011). This contribution focuses on the use of factor analyses to constrain 1) the influence of clastic input vs. benthic anoxia on the observed trace element excursions, and to 2) assess the extent to which magnetic susceptibility (MS) records within the stratigraphy track changes in the clastic input, with mineralogical controls on MS variance assessed by XRD analyses of acid-insoluble limestone residues and multivariate regression analyses. Variations in the MS of marine sedimentary deposits are commonly interpreted in terms of climatic change and its associated effects on weathering intensity, clastic fluxes or pedogenesis (Kukla *et al.* 1988; Verosub *et al.* 1993; Shackleton *et al.*, 1999; Elwood *et al.*, 1999, 2000; Whalen and Day, 2008, 2010). MS is largely controlled by detritally-sourced paramagnetic and ferrimagnetic minerals (Ellwood, 2007), although the possibility of MS alteration during diagenesis cannot be ignored (*e.g.* Burton *et al.* 1993; Brothers *et al.*, 1996; Enkin *et al.*, 2000; Gill *et al.*, 2002; Katz *et al.* 1998; Schneider *et al.* 2004).

5.2. Geologic background

The stratigraphic profile (AB) sampled in outcrop at the Miette platform margin (Fig. 5.1) encompasses the upper Maligne and lower Perdrix formations spanning the upper *Palmatolepis transitans* and overlying *P. punctata* conodont biozones (MN Zones 4-5 of Klapper, 1989). During Late Devonian time the WCSB was situated at near-equatorial latitudes along Laurussia's western margin and was the site of extensive reef complex development (Fig. 5.1; Whalen and Day, 2010). The basin was in-filled by platform-derived carbonate sediments variably mixed with fine-grained siliciclastics sourced from the Ellesmerian Fold Belt (Canadian Arctic Archipelago) and central Laurussia (Oliver and Cowper 1963; Stoakes, 1980; 1992; Switzer *et al.*, 1994; Whalen and Day, 2008, 2010). Detailed descriptions of facies, sequence- and biostratigraphy, cross-basin MS variability and geochemical accounts of the anomalous *punctata* Event were

reported previously by Whalen *et al.* (2000, 2002), Whalen and Day (2008, 2010), and Śliwiński *et al.* (2010, 2011).

5.3. Methods

Chemostratigraphic abundances of proxy elements used to track changes in paleoceanographic conditions (detrital input: Al, Si, K, Ti, Zr, Co, Cr; bioproductivity: Ni, Cu); dominant sediment-water interface redox conditions: U, Mo, V, Ni/Co, V/Cr, U/Th; Rimmer, 2004; Tribovillard et al., 2006) were measured in carbonate mudstones-wackestones by wave-length dispersive X-ray fluorescence spectroscopy at the Advanced Instrumentation Laboratory (AIL), University of Alaska Fairbanks, following the methods in Śliwiński et al. (2012).

The mineralogy of five acid-insoluble (excess 2N HCl) carbonate residues from the highest bulk MS samples within the stratigraphy and two representative low-MS samples was semi-quantitatively determined by X-ray diffraction analyses of samples packed in 0.7-mm borosilicate glass capillaries using an X'PERT PRO Materials Research Diffractometer at the AIL. The incident beam optics were outfitted with a Cu tube (45 kV, 40 mA), Ni filter, a parabolic mirror to parallelize the diverging X-ray beam, a 1/16° divergence slit and a 15-mm mask, while the diffracted radiation was measured by a X'Celerator detector with matching 0.02-radians Soller slits. Five scans were collected per sample (3.65-90° 2θ, 0.0125° step size, 120 sec/step) with a 45° rotation of the glass capillary between subsequent measurements. Mineral abundances were calculated using mineral reference intensity ratios (RIR) and peak area integrations using PANalytical's HighScore Plus software. A multivariate regression was calculated using SPSS statistical software to explain stratigraphic MS variance in terms of variable admixing of non-carbonate mineral phases. Mass-normalized MS measurements were made thrice and averaged using samples weighed to within ±0.001 g and using a KLY-3 Kappa bridge MS-meter (B. Ellwood's Lab, Louisiana State University).

Factor analyses (Davis, 2002) were performed using SPSS software and the geochemical datasets of Whalen and Day (2008) and Śliwiński et al. (2011). Log-transforms were applied as needed to normalize data distributions before higher-level analysis. Factors were extracted based on a principal component analysis and rotated using Kaiser's varimax scheme. Only those factors with eigenvalues > 1.0 were considered relevant as only these account for a greater proportion of total variance than the original standardized variables; this approach was found to be especially useful if the original variables are highly correlated (Davis, 2002).

5.4. Results

The MS of the sample suite shows 1) a moderate correlation with variations in the abundance of acid-insoluble residues and clastic proxies (Fig. 5.2; r = 0.542-0.639, 99.9 % confidence level) and 2) generally mimics their chemostratigraphic trends, which show two excursion intervals above background levels in the lower *punctata* Zone and a third, smaller enrichment near the *punctata-hassi* zonal boundary (Peaks I-III, Fig. 5.3). However, it is important to note that 1) the primary clastic excursion interval (Peak I) corresponds to the smallest of the five positive MS peaks, whereas 2) the smallest of the three notable clastic enrichments (Peak III) correlates to the highest MS value within the stratigraphy. Similar MS highs in the lower and upper portions of the *punctata* Zone were noted also in Central Europe (Nawrocki *et al.*, 2008 and discussion in Śliwiński *et al.*, 2010).

Semi-quantitative XRD analyses indicate the presence of variably admixed abundances of feldspar, quartz, illite and pyrite within the acid-insoluble residues and whole rock samples (Table 5.1, Fig. 5.4). Following the MS assessment of typical detrital minerals expected in marine deposits, feldspars and quartz are diamagnetic if pure, but slightly paramagnetic (approx. 10^{-8}-10^{-9} m^3kg^{-1}) if they contain fine-grained ferrimagnetic or paramagnetic mineral impurities (Ellwood *et al.*, 2000). Pyrite carries the highest positive magnetic susceptibility among the phases identified (approx. 10^{-7}-10^{-6} m^3kg^{-1}; Ellwood *et al.*, 2000), and thus variations in its whole rock abundances likely exerts a significant control on the composite MS signal of the sampled deposits. A multivariate regression model accounts for r = 97.7 % of total MS variance in terms of variable mixtures of these residual minerals, which are in turn variably diluted in diamagnetic carbonate (Table 5.1, Fig. 5.5).

Factor analyses were performed to determine how the multivariate geochemical dataset partitions among the first two dominant eigenvectors extracted, which collectively account for 90.2 % of total variance (Fig. 5.6, Tables 5.2 and 5.3). Both the elemental proxies and the small subset of mineralogical analyses form a continuum between the moderate to heavy positive loading regions of Factors 1 and 2 (Fig. 5.6), along which they partition into the commonly recognized suites of elements/minerals associated with clastic input (Factor 1) and those that accumulate under suboxic-anoxic conditions (Factor 2; *e.g.* Rimmer, 2004; Tribovillard *et al.*, 2006). Factor 1 explains 55.1 % of total variance and received strong loadings from MS, acid-insoluble residues and the clastic proxies, and moderate to strong loadings from Ni, Cu, Fe and the abundances of feldspar, quartz and illite. Factor 2, which explains an additional 35.2 % of total variance, received only very weak loadings from MS and clastics, but shows a stronger tendency for explaining most of the variance noted among pyrite and proxies for paleoredox (Mo, U) and bioproductivity (Ni, P,

TOC). Variations in the total carbonate content are anti-correlated with both factors, reflecting its inverse relationship to clastic abundances within the stratigraphy (Factor 1), but also to the development of benthic anoxia (Factor 2), which is commonly associated with increases in clastic content and decreases in total carbonate as outlined in the transgressive black shale model (Wignall, 1991).

5.5. Discussion

Global Late Devonian paleoceanographic 'events' are characterized by biotic turnovers, OM-rich facies deposition and geochemical anomalies commonly attributed to benthic anoxia (House, 2002; Algeo *et al.*, 1995). They are interpreted as outcomes of peculiar combinations of stresses affecting epeiric environments, including changes in sea level and excessive nutrient availability associated with 1) the evolutionary expansion of the first terrestrial forests and complex soils (Algeo *et al.*, 1995; House, 2002; Algeo and Scheckler, 1998, 2010), and 2) the rise and efficient weathering of near-equatorial orogenic belts (*cf.* Racki, 2005; Racki *et al.*, 2008).

The results of the factor analysis allow us to better understand the nature of the cause and effect mechanisms driving the geochemical variance noted during the *punctata* Event in the WCSB. The two extracted factors account for 90.2 % of total variance and allow for 1) determining the extent to which the composite MS signal is a tracer of changes in clastic input and 2) allow for a clear distinction between redox-sensitive trace metal accumulation resulting solely from increases in the clastic content of the carbonates in question vs. accumulation associated with anoxic scavenging from the water column. Prior evaluations of the geochemical records within a sequence stratigraphic perspective indicate that increases of the clastic influx and its associated biolimiting nutrients during sea level lowstand and subsequent 3rd-order transgression (T-R IIc1, Whalen and Day, 2008) led to the eutrophication of the epeiric environment surrounding the Miette platform; a subsequent development was either the establishment or intensification of preexisting benthic anoxia and enhanced OM preservation (Śliwiński *et al.*, 2010, 2011). Within this framework, Factor 1 is most readily interpreted as the suite of physical processes responsible for fluvial and eolian clastic delivery to the WCSB (Whalen and Day, 2010; Śliwiński *et al.*, 2011). Factor 2 explains an additional 35.2 % of total variance and seems best ascribed to processes that contribute to the development of benthic anoxia, which is conducive to the excess accumulation of OM and its proxies (TOC, Ni, P), redox sensitive trace metals (U, Mo) and pyrite (Fig. 5.6). The shared weak commonality of the latter with Factor 1 is a reminder that continental weathering and sediment delivery to marine basins is a major source of trace elements in the oceans (Worsley and Davies, 1979; Bruland and Lohan,

2004). On the other hand, the slight to moderate commonalties between clastic proxies and Factor 2 are a reflection of the fact that increases in the clastic content of carbonate systems is commonly associated with transgressive phases of T-R cycles (*cf.* Wignall, 1991).

Changes in the production, export and preservation of OM under oxygen-deficient conditions and its dilution by biogenic or clastic input are regarded as fundamental to the formation of OM-rich facies (*e.g.* Murphy *et al.*, 2000; Sageman *et al.* 2003). The results of factor analyses coupled with patterns of trace metal covariability may help resolve the dominant control on OM accumulation during the *punctata* Event by explaining the degree of water mass restriction of the WCSB relative to the open ocean. Calculating Z-statistics for trace metal data (*c.f.* Algeo and Maynard, 2008) emphasizes patterns of stratigraphic variability among those elements with different oceanic residence times (Table 5.4, Fig. 5.7); restricted anoxic conditions prevent deepwater renewal and cause divergent draw-down of the basinal trace element reservoir through sedimentary uptake (compare Figs. 5.7 and 5.8 in Algeo and Maynard, 2008). This has been done for the chemostratigraphic distributions of Ni, Cu, Mo, V and U throughout the *punctata* interval at Miette and reveals covariation without any significant divergence among these elements throughout all three excursion intervals (Peak I-III, Figs. 5.3 and Fig. 5.7). This observation argues for an overall steady state of deepwater renewal with no long-term basinal restriction, allowing us to speculate that the accumulation of OM-rich facies during the *punctata* Event may have been driven by detritally-induced eutrophication and enhanced preservation under the anoxic conditions it helped bring about.

5.6. Conclusions

Three discrete pulses of increased siliciclastic input characterize the Late Devonian *punctata* Zone stratigraphy at the Miette carbonate platform in the WCSB. Excursions are noted primarily in the lower portion of the biozone , with a third smaller clastic increase near the *punctata-hassi* zonal boundary.

The MS of the sample suite shows a moderate correlation with variations in the abundance of acid-insoluble residues and clastic proxies (Al, Si, K, Ti, Zr; $r \approx 0.542$-0.639 XRD analyses of a subset of acid-insoluble limestone residues from representative high and low MS samples within the *punctata* Zone stratigraphy indicate the presence of variable proportions of quartz, feldspar, illite and pyrite. A multivariate regression based on mineral abundances accounts for $r = 97.7$ % of total MS variance.

Factor analyses extracted two primary eigenvectors that account for 90.2 % of total geochemical variance. These can be interpreted as the physical processes of 'clastic delivery

(Factor 1)' and 'transgressive anoxia (Factor 2).' Clastic proxies and MS associate almost exclusively with the former. The variance among quartz, illite and feldspar abundances is also heavily loaded onto Factor 1; a moderate commonality is shared also with Factor 2 and is interpreted in terms of the transgressive black shale model (Wignall, 1991). Redox-sensitive proxies associate primarily with Factor 2, indicating that their accumulation is not the sole result of increased clastic content within the stratigraphy but also of 'excess accumulation' resulting from anoxic scavenging processes near the sediment-water interface.

Z-scale-normalized trends of redox sensitive trace metals (Ni, Cu, Mo, V, U) with differing oceanic residence times show no significant divergent behavior within the *punctata* Zone stratigraphy, suggesting continued deepwater renewal of the slope and basinal waters surrounding the Miette platform throughout the duration of *punctata* Zone and its three anoxic intervals (Peaks I-III). This implies that accumulation of OM-rich horizons during the *punctata* Event paleoceanographic perturbation were driven by increased productivity in the euphotic zone and subsequent OM preservation under the anoxic conditions it helped induce.

Acknowledgments

We thank the University of Alaska Fairbanks Vice Chancellor of Research and the Geophysical Institute, along with the donors of The Petroleum Research Fund, administered by the American Chemical Society, for financial support. We warmly thank Parcs Canada for providing permits to sample in Jasper National Park, and the UAF Technology Advisory Board for a grant that helped AIL outfit the XRF lab with the latest trace element analytical capabilities. This work was developed in association with the IGCP 580 program.

5.7. References

Algeo, T.J., Berner, R.A., Maynard, J.B. and Scheckler, S.E., 1995. Late Devonian oceanic anoxic events and biotic crises: "rooted" in the evolution of vascular land plants? *GSA Today*, **5**, 1-66.

Algeo, T.J. and Maynard, J.B., 2008. Trace-metal covariation as a guide to water-mass conditions in ancient anoxic marine environments. *Geosphere*, **4**, 872-887.

Algeo, T.J. and Scheckler, S.E., 1998. Terrestrial-marine teleconnections in the Devonian: links between the evolution of land plants, weathering processes, and marine anoxic events. *Philos. T. R. Soc. B.*, **353**, 113-128.

Algeo, T.J. and Scheckler, S.E., 2010. Land plant evolution and weathering rate changes in the Devonian. *J. Earth. Sci.*, **21**, 75-78.

Brothers, L.A., Engel, M.H., and Elmore, R.D., 1996. The late diagenetic conversion of pyrite to magnetite by organically complexed ferric iron. *Chem. Geol.,* **130**, 1-14.

Bruland, K.W. and Lohan, M.C., 2004. Controls of Trace Metals in Seawater. In. *The Oceans and Marine Geochemistry, Treatise on Geochemistry* (H. Elderfield, H.D. Holland, H. D. and K.K. Turekian, eds), Elsevier, Amsterdam, **6**, 23-47.

Burton, E.A., Machel, H.G. and Qi, J., 1993. Thermodynamic constraints on anomalous magnetization in shallow and deep hydrocarbon seepage environments, In: *Applications of Paleomagnetism to Sedimentary Geology* (D.M. Aissaoui, D.F. McNeill and N.F. Hurley, eds). *Soc. Econ. Pa.*, **49**, 193-207.

Davis, J.C., 2002. *Statistics and Data Analysis in Geology (3rd ed.)*. John Wiley & Sons, New York

Ellwood, B.B., 2007. Magnetic Susceptibility (MS) Low Field, In: *Encyclopedia of Geomagnetism and Paleo-magnetism* (D. Gubbins and E. Herrero-Bervera, eds). Springer Dordrecht

Ellwood, B.B., Crick, R.E. and El Hassani, A., 1999. The magneto-susceptibility event and cyclostratigraphy (MSEC) method used in geological correlation of Devonian rocks from Anti-Atlas Morroco. *Am. Assoc. Petr. Geol. B.,* **83**, 1119-1134.

Ellwood, B.B., Crick, R.E., El Hassani, A., Benoist, S.L. and Young, R.H., 2000. Magnetosusceptibility event and cyclostratigraphy method applied to marine rocks: Detrital input versus carbonate productivity. *Geology*, **28**, 1135-1138.

Enkin, R.J., Osadetz, K.G., Baker, J. and Kisilevsky, D., 2000. Orogenic remagnetizations in the Front Ranges and Inner Foothills of the southern Canadian Cordillera: Chemical harbinger and thermal handmaiden of Cordilleran deformation. *Geol. Soc. Am. Bull.*, **112,** 929–942.

Faure, G., 1998. *Principles and Applications of Geochemistry (2nd Edition).* Prentice Hall, Upper Saddle River

Gill, J.D., Elmore, R.D. and Engel, M.H., 2002. Chemical remagnetization and clay diagenesis: testing the hypothesis in the Cretaceous sedimentary rocks of northwestern Montana. *Phys. Chem. Earth,* **27,** 1131-1139.

House, M.R., 2002. Strength, timing, setting and cause of mid-Palaeozoic extinctions. *Palaeogeogr. Palaeocl.*, **181**, 5-25.

Johnson, J. G., Klapper, G. and Sandberg, C. A., 1985. Devonian eustatic fluctuations in Euramerica. *Geol. Soc. Am. Bull.,* **96**, 567-587.

Katz, B., Elmore, R.D., Cogoini, M. and Ferry, S., 1998. Widespread chemical remagnitization: orogenic fluids or burial diagenesis of clays? *Geology*, **26**, 603-606.

Klapper, G., 1989. The Montagne Noire Frasnian (Upper Devonian) Conodont Succession. In: *Devonian of the World* (N.J. McMillan, A.F. Embry and D.J. Glass, eds). Canadian Society of Petroleum Geologists Memoir 14, **3**, 449-468.

Klapper, G., 1997. Graphic correlation of Frasnian (Upper Devonian) sequences in Montagne Noire, France and western Canada, In: *Paleozoic Sequence Stratigraphy, Biostratigraphy, and Biogeography: Studies in Honor of J. Granville ("Jess") Johnson* (G. Klapper, M.A. Murphy, and J.A. Talent, eds). *Geol. S. Am. S.*, **321**, 113-130.

Kukla, G., Heller, F., Liu, X.M., Xu, T.C., Liu, T.S. and An, Z.S., 1988. Pleistocene climates in China dated by magnetic susceptibility. *Geology*, **16**, 811-814.

Murphy, A.E., Sageman, B.B., Hollander, D.J., Lyons, D.J. and Brett, C.E., 2000. Black shale deposition and faunal overturn in the Devonian Appalachian basin: Clastic starvation, seasonal water-column mixing, and efficient biolimiting nutrient recycling. *Paleoceanography*, **15**, 280-291.

Nawrocki, J., Polechońska, O. and Werner, T., 2008. Magnetic susceptibility and selected geochemicalmineralogical data as proxies for Early to Middle Frasnian (Late Devonian) carbonate depositional settings in the Holy Cross Mountains, southern Poland. *Palaeogeogr. Palaeocl.*, 269, 176-188.

Oliver, T.A. and Cowper, N.W., 1963. Depositional environments of the Ireton Formation, central Alberta. *B. Can. Petrol. Geol.*, **11**, 183-202

Racki, G., 2005. Toward understanding Late Devonian global events: few answers, many questions. In:*Understanding Late Devonian and Permian-Triassic biotic and climatic events: Towards an integrated approach.* (D.J. Over, J.R. Morrow and P.B. Wignall, eds). Elsevier Amsterdam, **2**, 5-36

Racki, G., Joachimski, M.M. and Morrow, J.R., 2008. A major perturbation of the global carbon budget in the Early-Middle Frasnian transition (Late Devonian) – Preface. *Palaeogeogr. Palaeocl.*, **269**, 127-129.

Rimmer, S.M., 2004. Geochemical paleoredox indicators in Devonian-Mississippian black shales, central Appalachian basin (USA). *Chem. Geol.*, **206**, 373-391.

Sageman, B.B., Murphy, A.E., Werne, J.P., Ver Straeten, C.A., Hollander, D.J. and Lyons, T.W., 2003. A tale of shales: the relative roles of production, decomposition, and dilution in the accumulation of organic-rich strata, Middle–Upper Devonian, Appalachian basin. *Chem. Geol.*, **195**, 229– 273.

Schneider, J., Bechstadt, T. and Machel, H.G., 2004. Covariance of C- and O-isotopes with magnetic susceptibility as a result of burial diagenesis of sandstones and carbonates: an example from the Lower Devonian La Vid Group, Cantabrian Zone, NW Spain: *Int. J. Earth. Sci.*, **93**, 990-1007.

Shackleton, N.J., Crowhurst, S.J., Weedon, G.P. and Laskar, J., 1999. Astronomical calibration of Oligocene–Miocene time. *Philos. T. R. Soc. Lond.*, **A357**, 1907–1929.

Śliwiński, M.G., Whalen, M.T. and Day, J., 2010. Trace element variations in the Middle Frasnian punctata zone (Late Devonian) in the western Canada sedimentary basin—changes in oceanic bioproductivity and paleoredox spurred by a pulse of terrestrial afforestation? *Geologica Belgica*, **4**, 459–482.

Śliwiński, M.G., Whalen, M.T., Newberry, R.J., Payne, J. and Day, J., 2011. Stable Isotope ($\delta^{13}C_{carb\ \&\ org}$, $\delta^{15}N_{org}$) and Trace Element Anomalies during the Late Devonian '*punctata* Event' in the Western Canada Sedimentary Basin. *Palaeogeogr. Palaeocl.*, **307**, 245–271.

Śliwiński, M.G., Spaleta, K.J., Meyer, F.J., Hutton, E.M., Newberry, R.J., Trainor, T.P., Severin, K.P. and Whalen, M.T., 2012. Making low concentration in-house pressed briquette trace element standards for carbonate rock analyses by WD-XRF. *Chem. Geol.*, **298-299**, 97-115

Stoakes, F.A., 1980. Nature and control of shale basin fill and its effect on reef growth and termination: Upper Devonian Duvernay and Ireton Formations of Alberta, Canada. *B. Can. Petrol. Geol.*, **28**, 345-410

Stoakes, F.A., 1992. Woodbend Megasequence. In: *Devonian-Early Mississippian Carbonates of the Western Canada Sedimentary Basin: A Sequence Stratigraphic Framework* (J.C. Wendte, F.A. Stoakes and C.V. Campbell, eds). *Soc. Econ. Pa. Short Course*, **28**, 183-206.

Switzer, S.B., Holland, W.G., Christie, G.S., Graf, G.C., Hedinger, A.S., McAuley, R.J., Wierzbicki, R.A., and Packard, J.J., 1994. Devonian Woodbend-Winterburn strata of the western Canada sedimentary basin. In: *Geological Atlas of the Western Canada Sedimentary Basin* (G. Mossop and I. Shetsen, eds.): *Canadian Society of Petroleum Geologists and Alberta Research Council*, 165-202

Tribovillard, N., Algeo, T.J., Lyons, T. and Riboulleau, A., 2006. Trace metals as paleoredox and paleoproductivity proxies: An update. *Chem. Geol.*, **232**, 12-32.

Verosub, K.L., Fine, P., Singer, M.J. and TenPas, J., 1993. Pedogenesis and paleoclimate: interpretation of the magnetic susceptibility record of Chinese loess-paleosol sequences. *Geology*, **21**, 1011-1014.

Whalen, M.T. and Day, J.E., 2008. Magnetic susceptibility, biostratigraphy, and sequence ' stratigraphy: insights into Devonian carbonate platform development and basin infilling, western Alberta, Canada. *Soc. for Sed. Geol.*, **89**, 291-314.

Whalen, M.T. and Day, J.E., 2010. Cross-basin variations in magnetic susceptibility influenced by changing sea level, paleogeography and climate, Upper Devonian Western Canada Sedimentary Basin. *J. Sediment. Res.*, **80**, 1109-1127.

Wignall, P.B., 1991. Model for transgressive black shales? *Geology,* **19,** 167-170.

Worsley, T.R. and Davies, T.A., 1979. Sea-level fluctuations and deep-sea sedimentation rates. *Science,* **203**, 455-456.

Ziegler, W. and Sandberg, C.A., 1990. The Late Devonian standard conodont zonation: Courier Forschungs-Institut Senckenberg, **121**, 1-115.

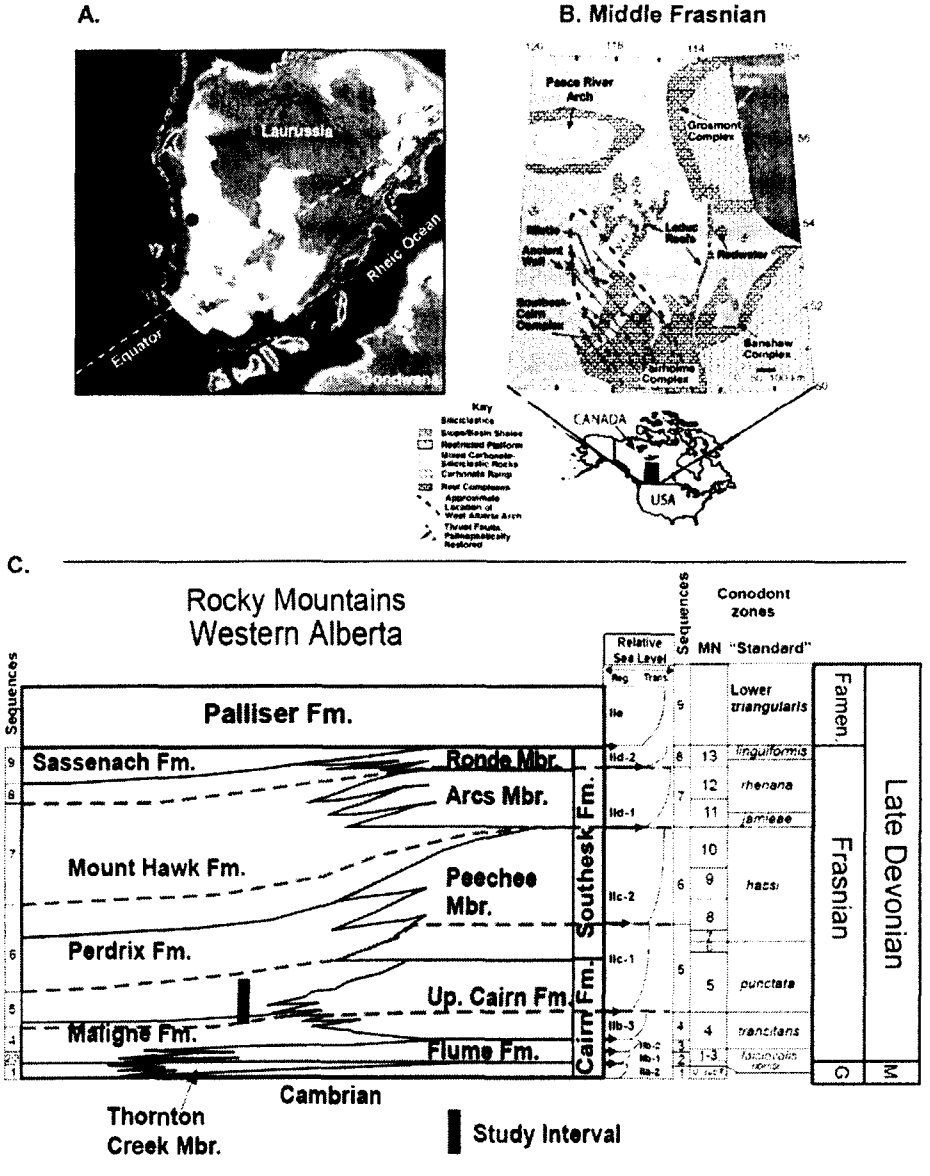

Fig. 5.1. Study area. **A.** Paleogeographic reconstruction of Late Devonian Laurussia (North America; R.Blakey, Northern Arizona University, Geology; http://www2.nau.edu/rcb7/370moll.jpg). Dot = study area. **B.** Paleogeography of the Western Canada Sedimentary Basin during mid-Frasnian time (after Whalen and Day, 2010). **C.** Stratigraphy of the Upper Devonian in the Rocky Mountains of Western Alberta (after Whalen and Day, 2010). "Standard" conodont zonation after Ziegler and Sandberg (1990); Montagne Noire (MN) conodont zonation after Klapper (1989; 1997); T-R cycles after Johnson *et al.*, (1985) and Whalen and Day (2010).

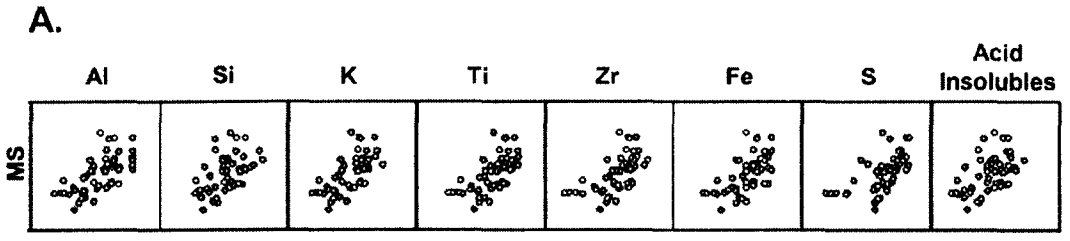

B. Parametric Correlations (N=52)

	MS	Al	Si	K	Ti	Zr	Fe	S	Acid Insolubles
MS	1.000	.635**	.525**	.627**	.839**	.606**	.594**	.574**	.542**

**. Correlation is significant at the 0.01 level (2-tailed)

C. Nonparametric Correlations (N=52)

	MS	Al	Si	K	Ti	Zr	Fe	S	Acid Insolubles
MS	1.000	.668**	.530**	.650**	.696**	.683**	.621**	.672**	.562**

**. Correlation is significant at the 0.01 level (2-tailed).

Fig. 5.2. A. Correlations of MS with clastic input proxies measured by WD-XRF throughout the entire stratigraphic profile (compare with Fig. 5.4). Log-transformed data. **B.** Parametric correlations (Pearson). **C.** Nonparametric (Spearman's rho).

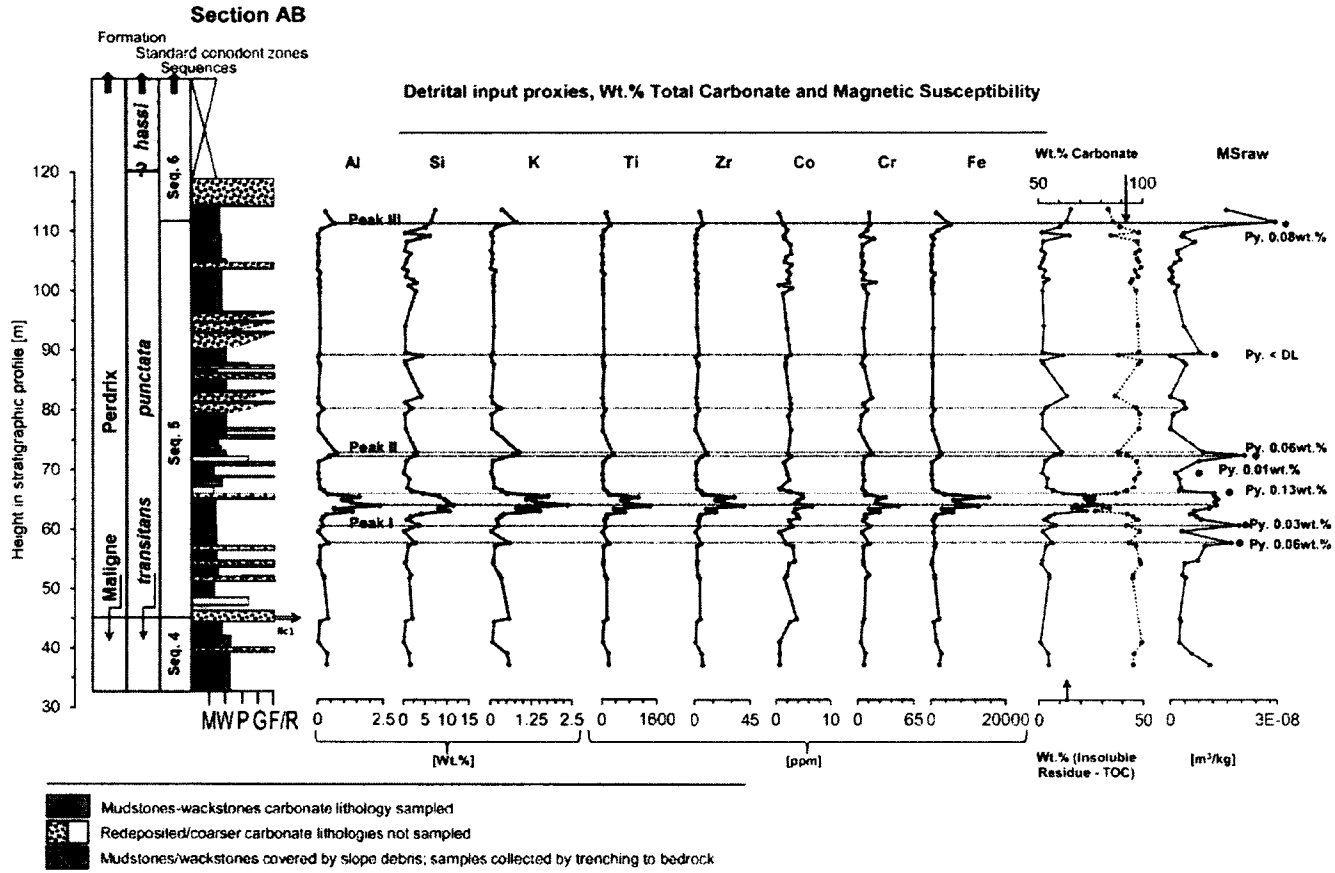

Fig. 5.3. The MS profile throughout the *punctata* Zone in the WCSB plotted against the stratigraphic distributions of clastic proxies and acid insoluble limestone residues. Circled crosses denoted samples whose acid insoluble mineralogy was determined by capillary XRD analyses. Pulses of increased clastic input (Peaks I-III) correspond to excursions of bioproductivity and paleoredox proxies (Śliwiński *et al.*, 2011). Gray stripped area indicates the lowest possible but also the most probable position of the *punctata-hassi* zonal boundary, which is situated within a 28 m covered interval (Whalen and Day, 2008, 2010).

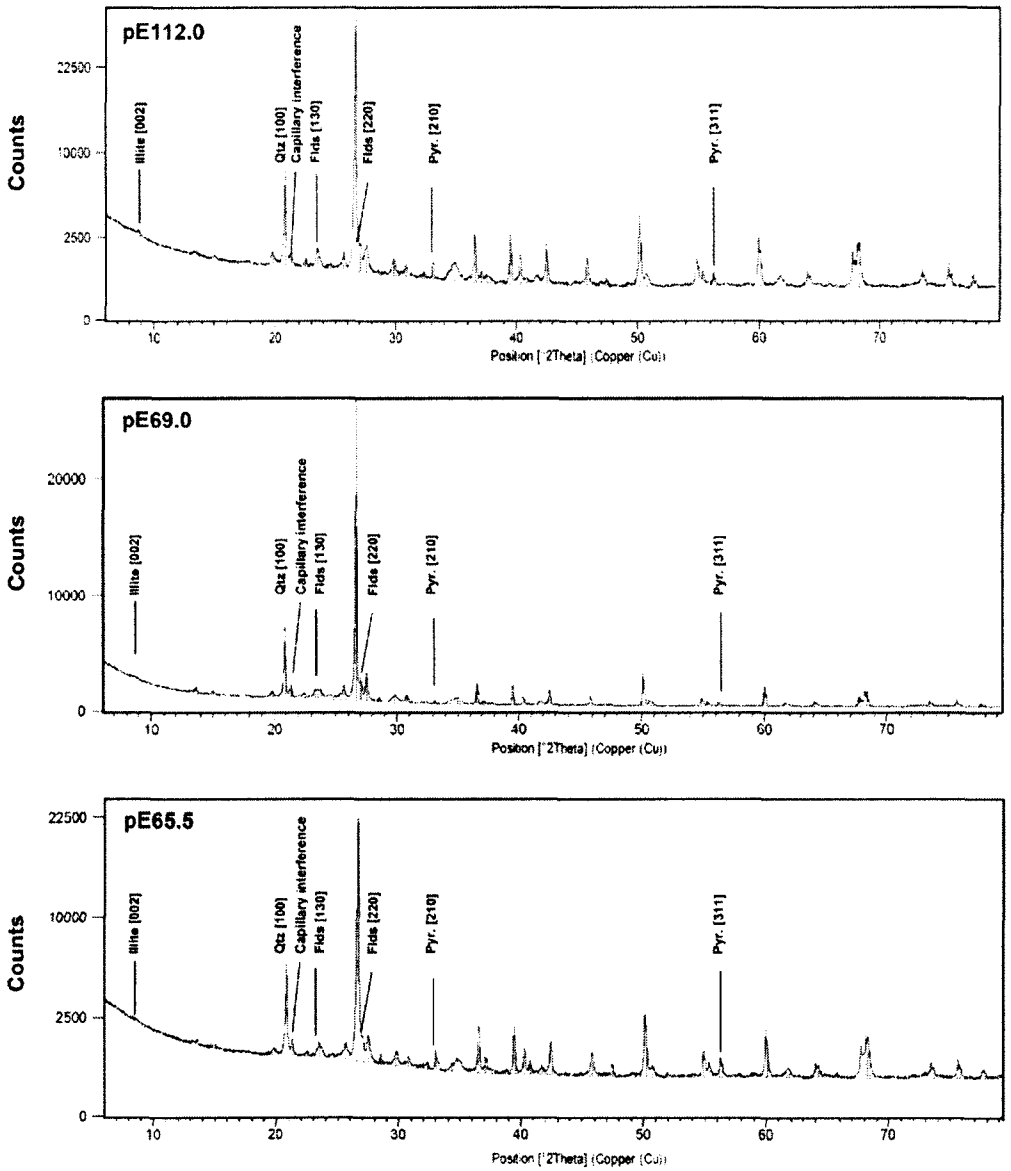

Fig. 5.4. Sample X-ray diffraction patterns of acid insoluble limestone residues from two high-MS samples (pE 65.5 and 112.0) and one low-MS sample (pE 69.0) within the stratigraphy. Extant mineral phases include quartz, feldspar (sanidine), goethite, illite and pyrite.

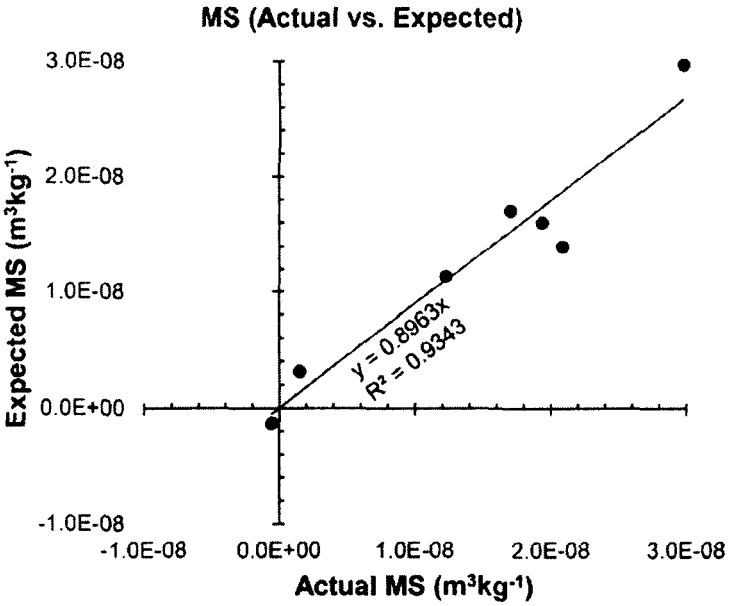

Fig. 5.5. Actual MS values vs. those predicted by a multivariate regression based on the acid insoluble mineralogy of a subset of representative high and low-MS samples within the *punctata* Zone stratigraphy (n = 7). Using the MS assessment of typical detrital minerals expected in marine deposits of Ellwood *et al.* (2000), r = 97.7 % of total MS variance can be explained in terms of variable mixtures of quartz, feldspar, illite, pyrite and geothite present in the samples analyzed and in turn variably diluted by their total diamagnetic carbonate content.

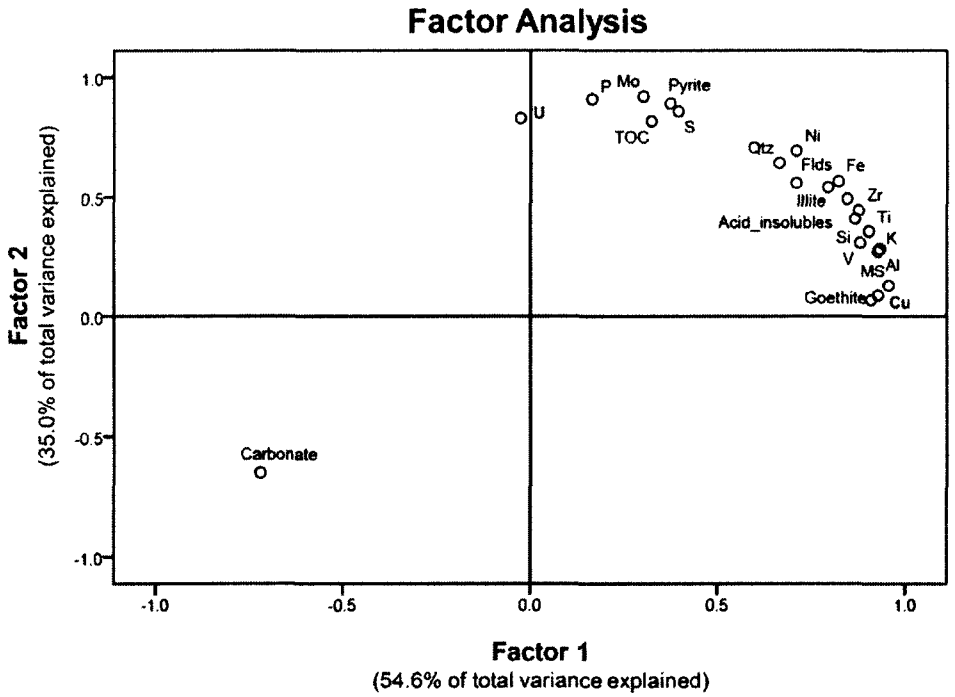

Fig. 5.6. Results of a principal component based factor analysis showing the partitioning of MS, trace element proxies and the subset of acid insoluble mineralogical data onto separate factors interpreted in terms of the physical oceanographic processes of clastic delivery (Factor 1) and the establishment of benthic anoxia (Factor 2).

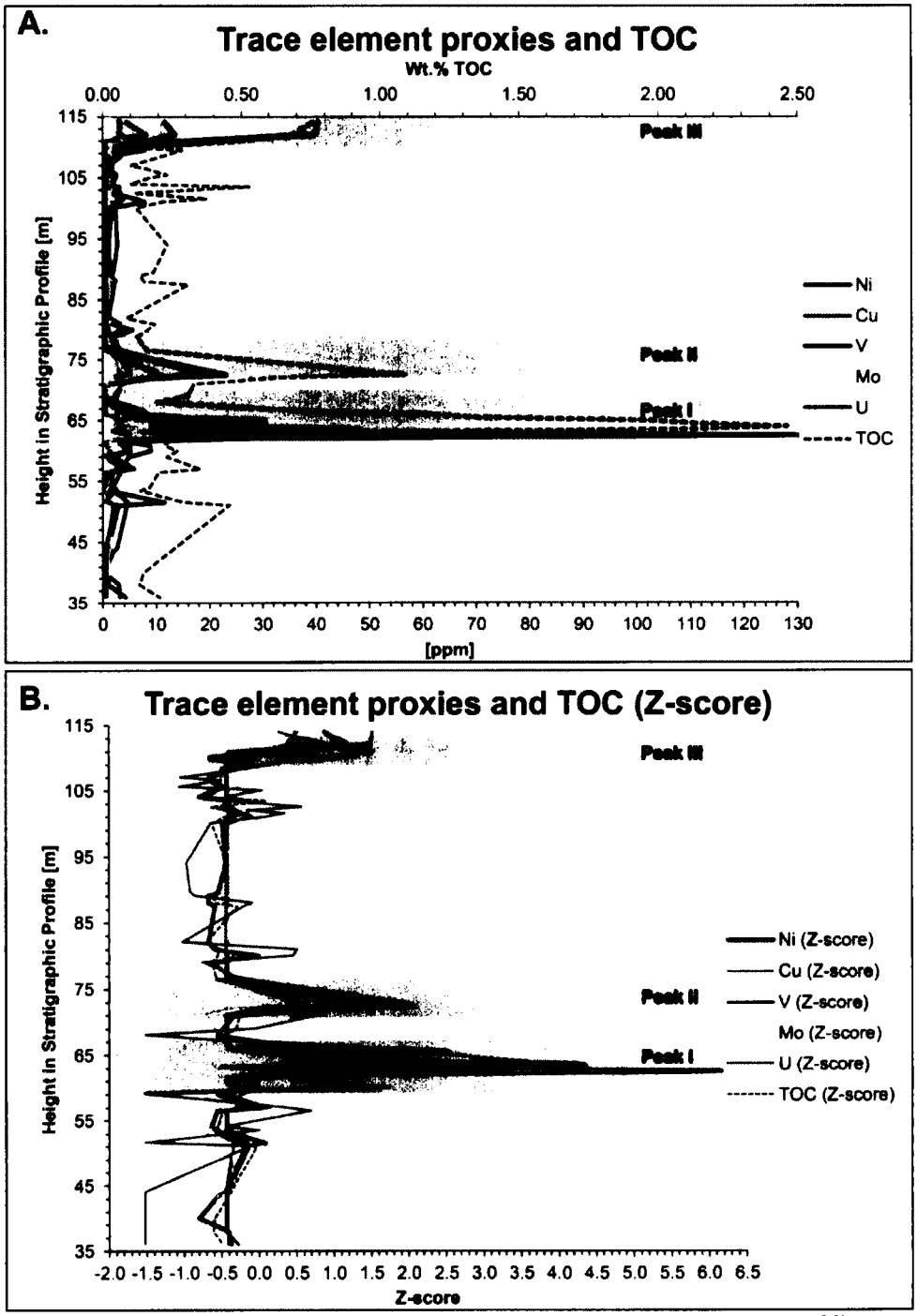

Fig. 5.7.A. Trace metal and TOC covariability throughout the *punctata* Zone at the Miette carbonate platform in WCSB. **B.** Z-scale normalized trace metal trends show no significant divergent behavior among any of the proxies with widely different oceanic residence times. This suggests a generally steady state of deep water renewal around the platform during the interpreted anoxic events within the stratigraphy (Peaks I-III, see Śliwiński *et al.*, 2011; *cf.* Algeo and Maynard, 2008).

Table 5.1. Results of semi-quantitative XRD analyses on a subset of acid insoluble limestone residues. All high-MS samples and two representative low-MS samples from the stratigraphy were analyzed using 0.7 mm borosilicate glass capillaries to circumvent the problem of small sample size.

Semi-quantitative XRD analyses

Sample	pE57.0		pE60.0		pE65.5		pE69.0 (low-MS)		pE72.0		pE89.0 (low-MS)		pE112.0	
Wt.% acid insolubles	6.54		8.10		11.49		1.49		7.23		11.76		13.48	
	A.I.R.*	Bulk rock	A.I.R.*	Bulk rock	A.I.R.*	Bulk rock	A.I.R.*	Bulk rock	A.I.R.*	Bulk rock	A.I.R.*	Bulk rock	A.I.R.*	Bulk rock
Feldspar [wt.%]	15.71	1.03	17.82	1.44	27.10	3.11	12.99	0.19	31.59	2.28	0.0	0.00	31.28	4.22
Quartz [wt.%]	45.28	2.96	48.48	3.93	41.43	4.76	50.33	0.75	35.54	2.57	100.0	11.76	36.32	4.90
Pyrite [wt.%]	0.93	0.06	0.43	0.03	1.17	0.13	0.88	0.01	0.77	0.06	0.0	0.00	0.58	0.08
Illite [wt.%]	38.08	2.49	33.27	2.70	30.30	3.48	35.80	0.53	32.11	2.32	0.0	0.00	31.83	4.29
*A.I.R = acid insoluble residue														
TOC [wt.%]		0.35		0.27		1.36		0.30		0.63		0.14		0.68
Total Carbonate [wt.%]:		93.1		91.6		87.1		98.2		92.1		88.1		85.8
Sum [wt.%]:		100.0		100.0		100.0		100.0		100.0		100.0		100.0
MS [m^3kg^{-1}]:		1.70E-08		1.94E-08		1.23E-08		1.52E-09		2.09E-08		-5.45E-10		2.98E-08
MS predicted by regression:		1.70E-08		1.60E-08		1.13E-08		3.11E-09		1.40E-08		-1.34E-09		2.97E-08

Multivariet regression: MS = (3.806E-8)Feldspar + (3.136E-8)Quartz + (2.330E-7)Pyrite + (3.282E-8)Illite + (3.186E-8)Carboante +(-3.177E-6); $R = 0.977$; $R^2 = 0.955$

Table 5.2. Components extracted in the factor analysis. The first two components (= factors) are interpreted in terms of the physical oceanographic processes of clastic delivery (Factor 1) and the establishment of benthic anoxia (Factor 2), which collectively account for 89.6 % of total geochemical variance.

Total Variance Explained						
Component	Initial Eigenvalues			Rotation Sums of Squared Loadings		
	Total	% of Variance	Cumulative %	Total	% of Variance	Cumulative %
1	**16.183**	**77.062**	**77.062**	**11.562**	**55.056**	**55.056**
2	**2.761**	**13.149**	**90.212**	**7.383**	**35.155**	**90.212**
3	1.157	5.509	95.721			
4	.790	3.761	99.481			
5	.109	.519	100.000			

Table 5.3. Loadings of all variables used in the factor analysis onto the first two extracted components (= factors).

Factor Loadings				
	Communalities		Rotated Component Matrix[a]	
Analyte	Initial	Extraction	1	2
Flds	1.000	.811	.715	.547
Qtz	1.000	.859	.707	.599
Pyrite	1.000	.930	.418	.869
Illite	1.000	.920	.822	.494
Carbonate	1.000	.939	-.738	-.628
Ni	1.000	.984	.723	.679
Cu	1.000	.831	.908	.083
V	1.000	.858	.879	.291
Mo	1.000	.941	.324	.914
U	1.000	.635	.028	.796
Al	1.000	.959	.947	.251
Si	1.000	.936	.896	.366
K	1.000	.939	.938	.244
Ti	1.000	.955	.922	.325
Zr	1.000	.970	.892	.417
Log10(MS)	1.000	.951	.971	.088
S	1.000	.886	.429	.838
Fe	1.000	.990	.831	.546
TOC	1.000	.806	.316	.840
P	1.000	.883	.175	.923
Acid insolubles	1.000	.963	.869	.456

Table 5.4. Estimated oceanic residence times for redox-sensitive trace metals. Trace element behavior in seawater described in Bruland and Lohan (2004).

Residence times of select trace elements in seawater

Element	Residence time: t x 10^3 yr			Behavior in seawater
	1	2	3	1 & 3
Ni	213	6	1.6	Micronutrient
Cu	3.1	5	1	Micronutrient
Mo	731	800	320	Conservative
V	48	50	7.9	Conservative
U	402	400	1000	Conservative

[1] *Algeo and Maynard (2008)*

[2] *Tribovillard et al. (2006)*

[3] *Mean Oceanic Residence Time from Faure (1998)*

6. Conclusions

6.1. General conclusions: the *punctata* Event in the Western Canada Sedimentary Basin

The Late Devonian '*punctata* Event' appears to have been a pronounced, global perturbation of marine biogeochemical cycles, characterized by geochemical anomalies that arose in the chemostratigraphic record during an apparent short-term (<0.6 M.y., Kaufmann, 2006; <0.8 M.y., De Vleeschouwer et al., 2012) yet wide-spread eutrophication event that affected epicontinental seaways. It resulted in 1) the deposition of organic matter-rich facies, 2) development of photic zone anoxia, yet 3) curiously no significant biotic turnover (Pisarzowska et al., 2006; Racki et al., 2008 and references therein; Morrow et al., 2009; Śliwiński et al., 2010, 2011). Our understanding of Late Devonian Oceanic Anoxic Events (House, 2002; Racki, 2005) at present indicates that the Early-Middle Frasnian *punctata* Event is one of the first in a sequence of relatively rapid (< 0.5-1.0 m.y.) perturbations that predate the Frasnian-Famennian extinction, one of the five most sever biotic crises since the Cambrian explosion. Within the context of Algeo and Scheckler's (2010; Figs. 1 and 2 therein) 'qualitative reading of the paleobotanic record,' the *punctata* Event curiously occurred near the onset of a sharp increase in the rate of diversification and expansion of the first terrestrial forests; the resulting transient increase in 1) the intensity of pedogenic weathering and 2) in the flux of soil-derived nutrients to marine ecosystems provides a causal mechanism to help explain the numerous organic carbon burial events of the Late Devonian.

The *punctata* Event is at present one of the best resolved of the Lower Paleozoic Oceanic Anoxic Events. The main eutrophication pulses in the Western Canada Sedimentary Basin unfolded over a time interval of less than approx. 400 k.y. (De Vleeschouwer et al., 2012), and thus provide insight into Earth system responses to relatively rapid nutrification episodes. The sampling strategy employed here, however (sample collection every half meter), nonetheless leaves opportunities for additional geochemical studies that could increase our temporal resolution of this peculiar paleoceanographic perturbation with the intent of better understanding Earth system responses on timescales that are more relevant to human societies – time scales on the order of 10s of thousands of years rather than hundreds of thousands of years – which would facilitate comparisons between nutrification events in the Earth's past with the increasingly rapid eutrophication of the Modern Ocean that began with the onset of the Anthropocene (Section 1.3.7.). Refining the temporal resolution in Lower Paleozoic strata, however, will require further advances in analytical methods, especially so in understanding the controls on the magnetic susceptibility of sedimentary strata (Chapter 5 herein) – a property that has recently been used in attempts to recognize orbital cyclicities in Devonian deposits and to thus refine the temporal duration of this time interval (Elwood et al., 2011; De Vleeschouwer et al., 2012). It will require

also advances in the application of micro-XRF techniques, such as those offered at synchrotron lightsources, which will facilitate the understanding of geochemical variability at the scale of individual sedimentary laminae.

General findings concerning the *punctata* Event in the Western Canada Sedimentary Basin are as follows:

- The application of various geochemical proxies for changing oceanic bioproductivity and redox conditions and integration with a high resolution regional sea level history provides an internally consistent account of the Late Devonian *punctata* Event in the WCSB. Variations of trace element proxies in this predominantly carbonate depositional environment, together with excursions of $\delta^{13}C_{(carb\ \&\ org)}$ and $\delta^{15}N_{org}$ and increased TOC indicate eutrophication of the basin early in the *punctata* Zone, but also possibly near its close. Export of organic matter to the sediment seems to have been intense enough to drive bottom water suboxia-anoxia and thus the establishment of conditions favorable to its preservation. Lower overall $\delta^{13}C_{org}$ and $\delta^{15}N_{org}$ values indicate that a stagnant period of lower overall productivity persisted following the main eutrophication event near the *transitans-punctata* boundary, during which N_2-fixing microbes may have had an ecological advantage under nitrate limited conditions. A correlative eutrophication event was also reported from Central Europe where it was followed by stagnant 'greenwater' conditions and a more impoverished biota, and organic petrography of strata at the Redwater Carbonate Complex in the WCSB revealed an anomalous organic matter-rich horizon indicative of algal blooms and higher than normal surface water productivity.
- Z-scale-normalized trends of redox sensitive trace metals (Ni, Cu, Mo, V, U) with differing oceanic residence times show no significant divergent behavior within the *punctata* Zone stratigraphy, suggesting continued deepwater renewal of the slope and basinal waters surrounding the Miette platform throughout the duration of *punctata* Zone and its three anoxic intervals (Peaks I-III). This implies that accumulation of OM-rich horizons during the *punctata* Event paleoceanographic perturbation were driven by increased productivity in the euphotic zone and subsequent OM preservation under the anoxic conditions it helped induce.
- Strong statistical correlations of all proxies with the detrital input suggest that eutrophication was at least partially detritally driven during conditions of 3rd order sea level transgression, in agreement with regional sequence stratigraphy and models of MS variations during T-R cycles (Whalen and Day, 2008, 2010).

- Three discrete pulses of increased siliciclastic input characterize the Late Devonian *punctata* Zone stratigraphy in the WCSB. Excursions are noted primarily in the lower portion of the zone, with a third lesser clastic increase near the *punctata-hassi* zonal boundary. A multivariate regression indicates that r = 67 % of total MS variance can be explained in terms of variations in clastic proxy abundances (Al, Si, K, Ti, Zr).
- XRD analyses of a subset of acid-insoluble limestone residues from representative high and low MS samples within the *punctata* Zone stratigraphy indicate the presence of variable proportions of quartz, feldspar, illite and pyrite. A multivariate regression based on mineral abundances accounts for r = 97.7 % of total MS variance.
- The $\delta^{13}C_{carb}$ record at the Miette buildup is a complex composite of isotopic effects associated with 1) a global C-cycle perturbation within the *punctata* biozone; 2) 3rd and 4th order sea level T-R cycles; and 3) bioproductivity blooms and the removal and burial of ^{12}C-enriched organic matter at the IIc1 mfz.
- A survey of the literature reveals that the magnitude of the global *punctata* Event $\delta^{13}C_{carb}$ excursions varies among basins. This can be explained in part by noting the location of each studied profile within a platform-top to basin transect, wherein the excursion magnitudes decrease basinwards. Variable mixing of the anomalous global C-isotope signal with regional C-cycle effects may further account for the observed differences.
- Given its numerous oxidation states, the pathways of $\delta^{15}N_{org}$ diagenesis are complex and at present little understood. The use of such records in studies of Devonian-aged rocks seems at best to equivocally suggest possible changes in oceanographic conditions that may have taken place, although only when interpreted in the context of other geochemical proxies. In a manner analogous to $\delta^{13}C$ records, regional N-cycling in the epeiric seaway of the Western Canada Sedimentary Basin likely heavily influenced the composite record, overshadowing the global $\delta^{15}N$ signal. This record at the Miette platform may have been complicated by bio- and thermo-degradation associated with kerogen maturation at burial temperatures reaching ~200°C. While the net effect was likely isotopic enrichment, the residual kerogen is nonetheless lighter than modern planktonic $\delta^{15}N$ and falls within the range of N_2-fixing microbes. These gain an ecological advantage when oceanic nitrate stores in surface waters become depleted and restore a balance through atmospheric N_2-fixation. Conceivably, eutrophication early in the *punctata* zone would have depleted bioavailable nitrate, giving N_2-fixers a temporary ecological advantage. Low $\delta^{15}N_{org}$ values could be a reflection of a greater contribution of such a biomass to the total organic matter exported to the sediment-water interface.

- The timing of the *punctata* Event approximately coincides with the advent of archaeopterid forest expansion and rise to dominance beginning around mid-Frasnian time. This evolutionary event may have amplified the detrital flux to the oceans, which was likely already elevated by conditions of sea level lowstand, early transgression and episodes of increased weathering of rising orogens in near-equatorial regions. The *marine-terrestrial teleconnections model* of *Algeo and Scheckler (1998)* thus provides an intricate contextual framework for interpreting the *punctata* geochemical anomalies.

6.2. General conclusions regarding XRF trace element proxy methods

The geochemical records of the numerous Oceanic Anoxic Events that have occurred throughout Phanerozoic time (Section 1.3.) is not limited to the black shale deposits which, at the present time, appear to receive a disproportionate amount of analytical and interpretive attention. These records exists also in the vast (biogenic)-carbonate deposits of the last 540 m.y. of Earth's geobiological evolution, although it's 'reading' requires modifications to some of the analytical methods commonly called upon in the study of black shales. Of particular interest is the use of suites of trace elements as proxies to understand changes in paleoceanographic bioproductivity and paleoredox conditions (Tribovillard et al., 2006). While the application of this methodology is at present well established for shale systems (Sageman et al., 2003; Algeo and Maynard, 2008), such is not the case for carbonate depositional environments, wherein the concentrations of certain key proxies (e.g. the redox indices Mo and U) are commonly near the analytical detection limits (0-5 ppm) of X-ray fluorescence spectroscopy (XRF). These difficulties seem worth overcoming, however, given the relative ease and efficiency of XRF analyses, both in terms of cost and time spent on sample processing, compared to the commonly used alternative method of liquid digestion ICP-MS. While ICP-MS offers detection limits that are well below the ppm level, it is not an efficient method for processing and analyzing the hundreds of samples that are needed to generate high-resolution chemostratigraphic profiles.

It is interesting to note that XRF was used in this work as a reconnaissance tool to identify those areas within the *punctata* Event stratigraphy in the WCSB that were most likely to host the anomalous isotopic signatures that were previously identified elsewhere around the globe (Racki et al., 2008; Morrow et al., 2009). This trace element proxy approach thus proved to be useful in deciding where in the stratigraphy to allocate most time and limited resources to documenting isotopic histories ($\delta^{13}C$ and $\delta^{15}N$). This required developing carbonate-specific XRF analytical methods:

- Low concentration (0-100 ppm) carbonate trace element standards were and can be readily prepared *in-house* by: 1) spiking ultrapure calcite powders (99.999% $CaCO_3$)

with variable volumes of single element, standard 1000 ppm ICP-MS stock solutions; 2) drying and homogenizing; 3) verifying mixture compositions by liquid digestion ICP-MS, PROTrace XRF or other independent compositional analyses; and 3) pressing into pellets of desired size for use as *in-house* standards in XRF calibrations.

- This method of *in-house* standard preparation is inexpensive, straightforward to carry out in the laboratory, and can help circumvent the general lack of certified reference materials suitable for the analysis of various trace elements that can be measured in carbonate lithologies and used as proxies of paleoceanographic changes. Further, it is easily tailored to 1) only those elements of interest, 2) to the specific calibration range desired, and 3) can help improve XRF calibrations set against other certified geologic standards that may not be optimally matched to the samples of interest.
- The precision of the XRF sample preparation procedure and analytical protocol was evaluated by replicate analyses (6x) of three pressed pellets prepared from the same representative carbonate sample. Analyses of variance reveal no significant differences at the 95% confidence level among the calculated average concentrations. The precision, expressed as a percentage of the mean, is on the order of 1) < 2.5% at the 50-100 ppm concentration level, 2) better than ± 5-10% at the 10-20 ppm level, 3) ± 5-15% near the 5 ppm level, and 4) decreases to ± 10-55% at the 1-2 ppm level which begins to overlap with analytical detection limits.

As stated above, the application of the multiproxy trace element method is well established for shale systems, and the interpretation of chemostratigraphic trends in terms of changing oceanic bioproductivity and paleoredox conditions commonly follows the reviews of trace element behavior in such systems described by Calvert and Pedersen (1993) and Tribovillard et al. (2006). However the behavior and thus interpretation of certain proxies needs to be at times reevaluated if applied to dominantly carbonate depositional environment. This is exemplified by the behavior of Mn within the *punctata* Event stratigraphy in the WCSB (Chapter 3, Appendix 3C; Section 6.4. below).

There are certain 'standard' approaches to data processing that allow for decoupling the authigenic trace element signal from that of siliciclastic detritus which is 1) a major source of trace element delivery to the oceans and 2) generally makes up the bulk of shaly sediments, thus masking the trace element signal of changing oceanic productivity and redox conditions. However, because certain elements are overwhelmingly of detrital origin (*e.g.* Al, Si, K, Ti and Zr), they can be used to ratio out the trace element contribution from the clastic content and constitute the basis of various normalization schemes, such as the often used Al-normalization and

comparisons to composite 'reference shales' (reviewed and evaluated by van der Weijden, 2002). However, the generally low abundance of admixed siliciclastics in carbonate sediments, at times near the detection limits of, for example, the Al proxy, can render such schemes useless by producing spurious correlations (van der Weijden, 2002). An alternative approach to decoupling trace element signals is through the use of factor analyses (Davis, 2002), which reduce the complexity of multivariate geochemical datasets down to just several dominant factors which explain most of the dataset variance. In the carbonate stratigraphy of the *punctata* Event in the WCSB:

- A factor analysis (Chapter 5) extracted two primary eigenvectors that account for 90.2 % of total geochemical variance. These can be interpreted as the physical processes of 'clastic delivery (Factor 1)' and 'transgressive anoxia (Factor 2).' Clastic proxies and MS associate almost exclusively with the former. The variance among quartz, illite and feldspar abundances is also heavily loaded onto Factor 1; a moderate commonality is shared also with Factor 2 and is interpreted in terms of the transgressive black shale model of Wignall (1991). Redox-sensitive proxies associate primarily with Factor 2, indicating that their accumulation is not the sole result of increased clastic content within the stratigraphy but also of 'excess accumulation' resulting from anoxic scavenging processes near the sediment-water interface.

6.3. Chemostratigraphy in the field: a look into the future

The reconstruction of chemostratigraphic trends among trace element proxies used in paleoceanography to understand changes in oceanic biogeochemical cycles should benefit greatly from the future development of handheld field XRF units capable of both accurately and precisely detecting the low concentrations of proxies commonly encountered in carbonate lithologies (0-50 ppm). Current sample preparation and analysis methods by WD-XRF spectroscopy are at present too costly, labor intensive and time consuming, thus limiting the number of samples that can be processed per stratigraphic section. Further limits are imposed by the number of samples that can be easily and inexpensively transported out of remote field locations for analysis in the laboratory. Much benefit would come from the ability to generate chemostratigraphic data out in the field – it is not inconceivable, for example, to carry a rock-grinder out into the field to prepare flat rock surface for in-situ trace element measurements once the technology of handheld XRF units achieves the necessary level of analytical sensitivity.

6.4. Developing synchrotron-based XRF methods for understanding geochemical variability during Oceanic Anoxic Events: the scale of individual sedimentary laminae

The use of synchrotron-based XRF methods of chemostratigraphic trace element analyses was introduced in Chapter 3 (Appendix 3C). These include 1) 2-dimensional composition maps generated by XRF meso-probes (analytical beam diameter of approx. 50 μm) and 2) XRF microprobes (beam diameter down to the 1-5 μm). Synchrotron radiation offers an unprecedented combination of the spatial resolution offered by EPMA (beam diameter down to 1-5 μm) with detection levels at least as low as those achievable by WD-XRF (0-5 ppm). An additional capability offered by no other analytical technique, however, is the ability to determine the oxidation state of the chemical species of interest by synchrotron-based X-ray Absorption Near Edge Structure (XANES) analyses. Recent work at the Stanford Synchrotron Radiation Lightsource (SSRL), which goes beyond the scope of this thesis, demonstrates the potential of synchrotron based-XRF analytical methods in resolving the behavior of trace element proxies at the micro-scale, and, importantly, in understanding the nature of their host-phases (Figs. 6.1. & 6.2.). XRF microprobe mapping and XANES spot analyses (Figs. 6.1. & 6.2.) confirm, for example, the existence of both MnS and Mn-carbonate phases within the most anoxic interval of the *punctata* Event stratigraphy in the WCSB (see discussion in Chapter 3, Appendix 3C), and are an encouraging step in the direction of potentially using Mn as a redox proxy in dominantly carbonate sedimentary environments. I see the use of this element for this purpose as a 'first-pass' reconnaissance tool of sorts, as Mn has the advantage of being readily measured in carbonate strata because of its generally high abundance (ave. carbonate = 1,000 ppm; Veizer, 1983) as compared to the more commonly used proxies such as V, MO and U, which pose substantial analytical difficulties for XRF instruments/methods because of their near detection-limit abundances (*e.g.* 0-10 ppm in the *punctata* Event stratigraphy in the WCSB, Chapters 3, 4 & 5). Mn could readily be detected by a hand-held XRF unit out in the field as a means of reconnaissance work that could help locate OAE-type stratigraphic intervals and facilitate a better sampling strategy.

6.5. References

Algeo, T.J. and Maynard, J.B., 2008. Trace-metal covariation as a guide to water-mass conditions in ancient anoxic marine environments. *Geosphere*, **4**, 872-887

Algeo, T.J. and Scheckler, S.E., 1998. Terrestrial-marine teleconnections in the Devonian: links between the evolution of land plants, weathering processes, and marine anoxic events. *Philosophical Transactions of the Royal Society B-Biological Sciences*, **353**, 113-128

Algeo, T.J. and Scheckler, S.E., 2010. Land plant evolution and weathering rate changes in the Devonian. *Journal of Earth Science,* **21,** 75-78.

Bardelli, F., Cattaruzza, E., Gonella, F., Rampazzo, G. and Valotto, G., 2011. Characterization of road dust collected in Fraforo del San Bernardo highway tunnel: Fe and Mn speciation. *Atmospheric Environment,* **45**, 6459-6468

Calvert, S.E. and Pedersen, T.F., 1993. Geochemistry of recent oxic and anoxic marine sediments - implications for the geological record. *Marine Geology*, **113**(1-2), 67-88

Davis, J.C., 2002. *Statistics and Data Analysis in Geology (3rd ed.)*. John Wiley & Sons, New York

De Vleeschouwer, D., Whalen, M. T., Day, J. E. and Claeys, P., 2012. Cyclo-stratigraphic calibration of the Frasnian (Upper-Devonian) time-scale (western Alberta, Canada), *Geological Society of America Bulletin*, doi:10.1130/B30547.1

Ellwood, B.B., Tomkin, J.H., El Hassani, A., Bultynck, P., Brett, C.E., Schindler, E., Feist, R. and Bartholomew, A.J., 2011. A climate-driven model and development of a floating point time scale for the entire Middle Devonian Givetian Stage: A test using magnetostratigraphy susceptibility as a climate proxy. *Palaeogeography, Palaeoclimatology, Palaeoecology*, **304**, 85-95.

House, M.R., 2002. Strength, timing, setting and cause of mid-Palaeozoic extinctions. *Palaeogeography, Palaeoclimatology, Palaeoecology*, **181**, 5-25.

Kaufmann, B., 2006. Calibrating the Devonian time scale: A synthesis of U-PbID-TIMS ages and conodont stratigraphy. *Earth-Science Reviews*, **76**, 175-190

Morrow, J.R., Sandberg, C.A., Malkowski, K., Joachimski, M.M., 2009. Carbon isotope chemostratigraphy and precise dating of middle Frasnian (lower Upper Devonian) Alamo Breccia, Nevada, USA. *Palaeogeography, Palaeoclimatology, Palaeoecology*, **282**, 105-118

Özkendir, O.M. and Ufuktepe, Y., 2005. Temperature dependent change of the MnS K-edge. *Journal of Optoelectronics and Advanced Materials,* **7**(5), 2655-2660

Pisarzowska, A., Sobstel, M., Racki., G., 2006. Conodont-based event stratigraphy of the Early-Middle Frasnian transition on the South Polish carbonate shelf. *Acta Palaeontologica Polonica*, **51(4)**, 609-646

Racki, G., 2005. Toward understanding Late Devonian global events: few answers, many questions. In: Over, D.J., Morrow, J.R. and Wignall, P.B. (eds.) Understanding Late Devonian and Permian-Triassic biotic and climatic events: Towards an integrated approach. Elsevier, B.V., Chapter 2: 5-36

Racki, G., Joachimski, M.M. and Morrow, J.R., 2008. A major perturbation of the global carbon budget in the Early-Middle Frasnian transition (Late Devonian) – Preface. *Palaeogeography Palaeoclimatology Palaeoecology*, **269**, 127-129

Ressler, T., Wong, J., Roos, J. and Smith, I.L., 2000. Quantitaitve speciation of Mn-bearing particulates emitted from autos burning (Methylcyclopentadienyl)manganese tricarbonym-added gasolines using XANES spectroscopy. *Environmental Science and Technology* **34,** 950-958

Sageman B.B., Murphy, A.E., Werne, J.P., Ver Straeten, C.A., Hollander, D.J., Lyons, T.W., 2003. A tale of shales: the relative roles of production, decomposition, and dilution in the accumulation of organic-rich strata, Middle–Upper Devonian, Appalachian basin. *Chemical Geology*, **195**, 229– 273

Śliwiński, M.G., Whalen, M.T., and Day, J., 2010, Trace element variations in the Middle Frasnian punctata zone (Late Devonian) in the western Canada sedimentary basin—changes in oceanic bioproductivity and paleoredox spurred by a pulse of terrestrial afforestation? *Geologica Belgica*, **4**, 459–482

Śliwiński, M.G., Whalen, M.T., Meyer, F. and Majs, F., *(in press).* Constraining clastic input controls on magnetic susceptibility and trace element anomalies during the Late Devonian *punctata* Event in the Western Canada Sedimentary Basin. *Terra Nova,* doi: 10.1111/j.1365-3121.2012.01063.x

Śliwiński, M.G., Spaleta, K.J., Meyer, F.J., Hutton, E.M., Newberry, R.J., Trainor, T.P., Severin, K.P. and Whalen, M.T., 2012. Making low concentration in-house pressed briquette trace element standards for carbonate rock analyses by WD-XRF. *Chemical Geology,* **298-299,** 97-115

Śliwiński, M.G., Whalen, M.T., Newberry, R.J., Payne, J. and Day, J., 2011. *Stable Isotope ($\delta^{13}C_{carb\ \&\ org}$ $\delta^{15}N_{org}$) and Trace Element Anomalies during the Late Devonian 'punctata Event' in the Western Canada SedimentaryBasin. Palaeogeography, Palaeoclimatology, Palaeoecology*, **307,** 245-271

Tribovillard, N., Algeo, T.J., Lyons, T. and Riboulleau, A., 2006. Trace metals as paleoredox and paleoproductivity proxies: An update. *Chemical Geology*, **232**, 12-32

van der Weijden, C.H., 2002. Pitfalls of normalization of marine geochemical data using a common divisor, *Marine Geology*, **184**, 167-187.

Veizer, J., 1983. Trace elements and isotopes in sedimentary carbonates, *Reviews in Mineralogy: Carbonates: Mineralogy and Chemistry*, **11**, 265-299

Webb, S. M., 2006, Sam's Microprobe Analysis Tool Kit. http://www.ssrl.slac.stanford.edu/~swebb/smak.htm:

Whalen, M.T. and Day, J.E., 2008. Magnetic susceptibility, biostratigraphy, and sequence stratigraphy: insights into Devonian carbonate platform development and basin infilling, western Alberta, Canada. *Society for Sedimentary Geology*, **89**, 291-314

Whalen, M.T. and Day, J.E., 2010. Cross-basin variations in magnetic susceptibility influenced by changing sea level, paleogeography and climate, Upper Devonian Western Canada Sedimentary Basin. *Journal of Sedimentary Research*, **80**, 1109-1127

Wignall, P.B., 1991. Model for transgressive black shales? *Geology,* **19,** 167-170.

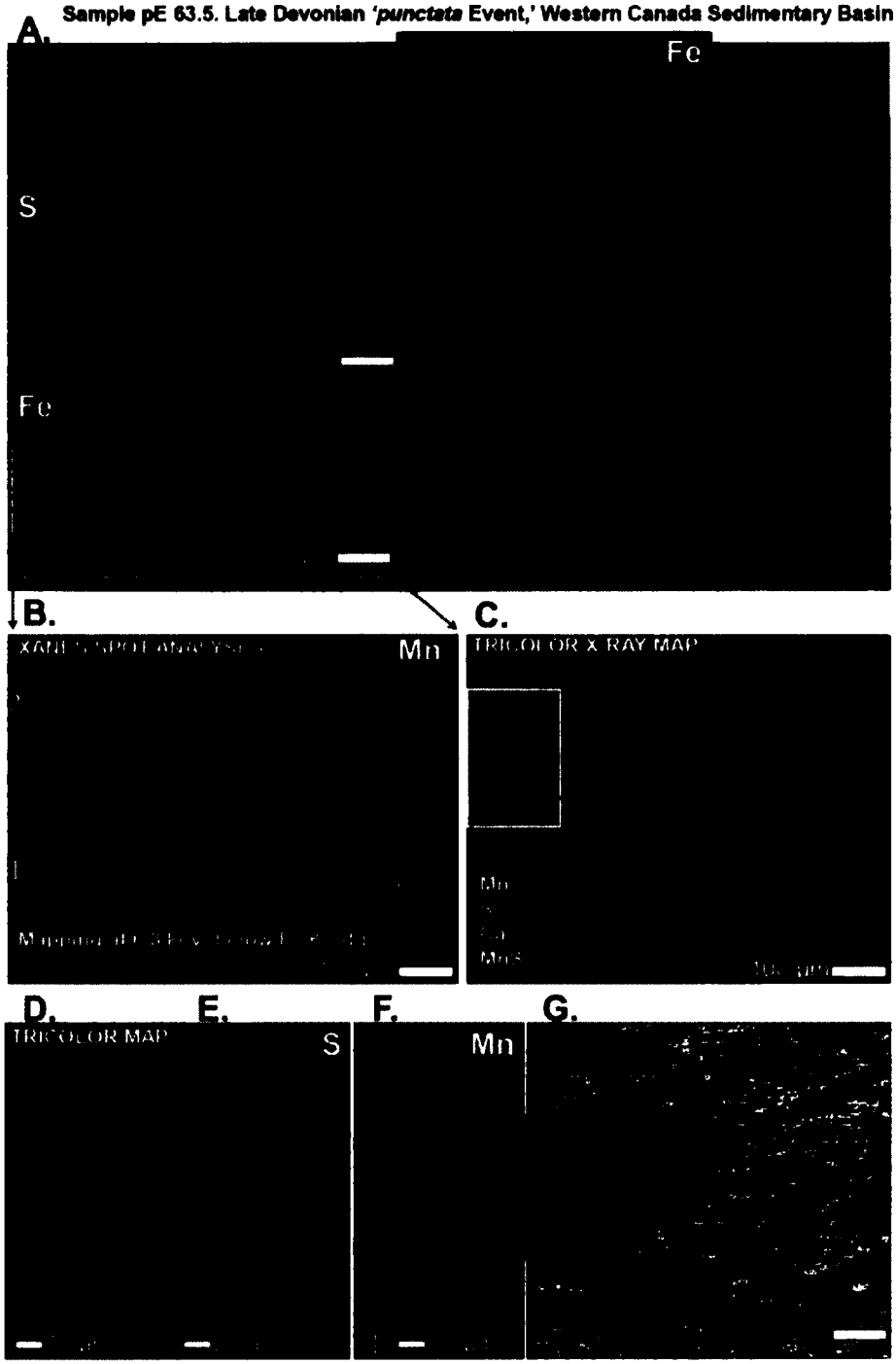

Fig. 6.1. X-ray maps of Fe, Mn, S and Ca distributions in select portions of sample pE 63.5, which represents the most anoxic interval in the *punctata* Event stratigraphy. **A:** Overview of Fe-sulfide distribution within the sample, highlighting area of interest depicted in B-G. **B:** Distribution of Mn within the sulfide patch outlined in **A. C.** Tricolor element map showing distribution of MnS vs. Fe-sulfides within the same sulfide patch. **D-F.** Detailed view of area outlined in **C.**

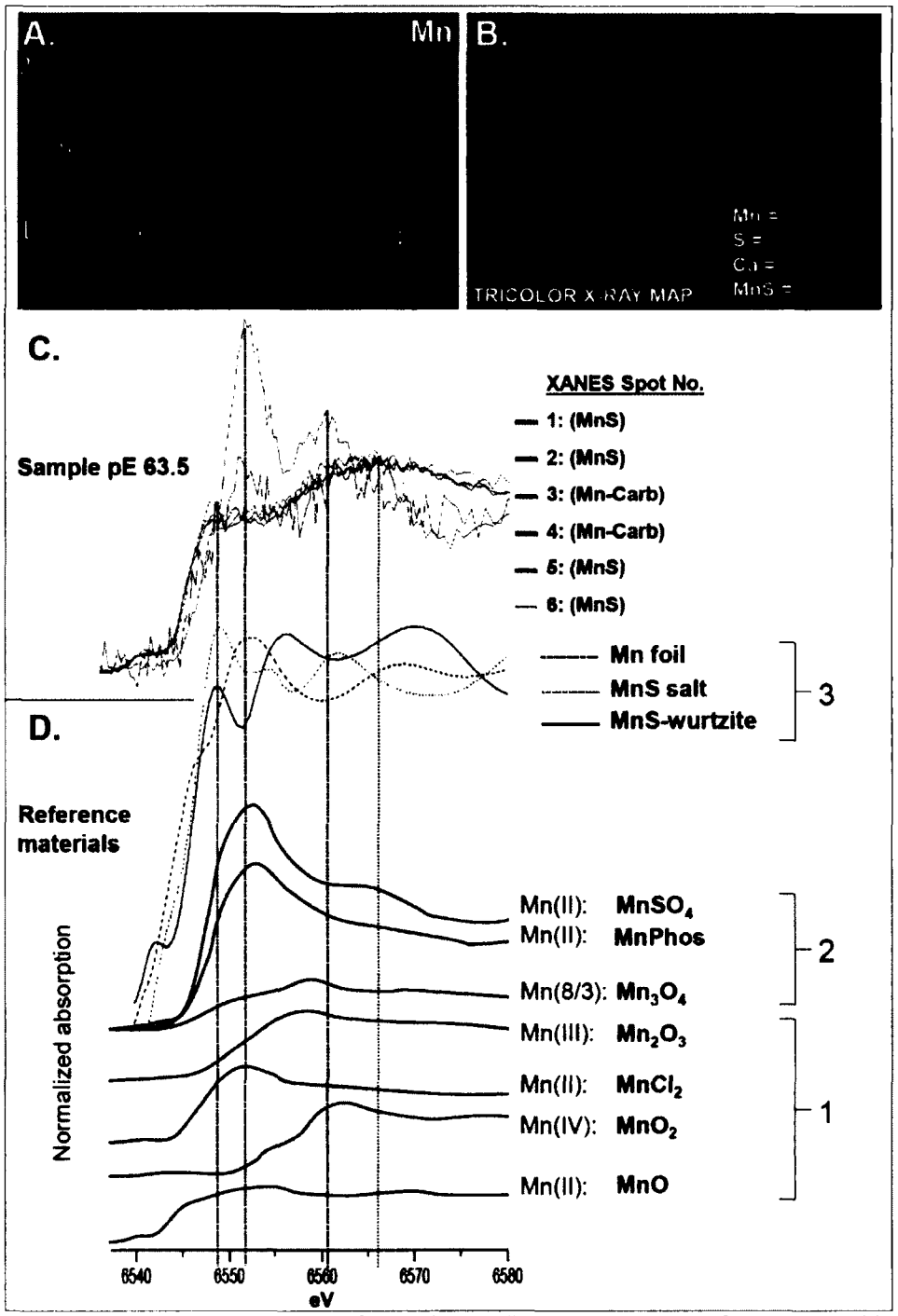

Fig. 6.2. A-B. X-ray maps of Mn, S and Ca distributions in select sulfide patch within sample pE 63.5, which represents the most anoxic intervai in the *punctata* Event stratigraphy. Refer to Fig. 6.1. A-C. **C:** XANES spectra of 6 spot analyses shown in A., revealing the presence of both MnS and Mn-carbonate phases when compared to **D.** Mn oxidation state reference spectra in the literature. **1.** Spectra after: Bardeili et al. (2011); **2:** after Ressler et al. (2000); **3**: after Özkendir and Ufuktepe (2005).